

**Late Jurassic lacustrine carbonates; a multi-scale  
analysis of the Mupe Member (Purbeck Limestone  
Group) of the Wessex Basin, U.K.**

**Arnaud Gallois**

Thesis submitted to the University of London  
for the degree of Doctor of Philosophy

Earth Sciences Department  
Royal Holloway, University of London

2016

## **Declaration of authorship**

I, Arnaud Gallois hereby declare that this thesis and the work presented in it is entirely my own. Where I have consulted the work of others, this is always clearly stated.

Arnaud Gallois  
November, 2016

## Abstract

The discovery of hydrocarbons in Lower Cretaceous, non-marine carbonates in the South Atlantic has triggered much research into understanding how such complex strata form. Sedimentary facies and basin architecture are controlled by a range of environmental parameters (*i.e.* climate, hydrology and tectonic setting) but published facies models are few and limited in their predictive value. This study develops new depositional models for non-marine microbialites and associated facies in a semi-arid climate setting in an extensional basin based on the Purbeck Limestone Group (Upper Jurassic – Lower Cretaceous) exposed in Dorset.

Outcrop studies coupled with subsurface, petrographic and petrophysical studies constrain and improve published facies models and palaeogeographical maps of the microbialites deposited in the syn-rift phase of the Wessex Basin. Two and three-dimensional seismic data imaging the Lower-Upper Jurassic in south Dorset show east-west trending south-dipping syndepositional extensional faults. These are linked via a relay ramp and new tectono-sedimentary models indicate tectonic controls on facies distribution during propagation of extensional faults. Accumulation of strata occurred in half-grabens controlled by these east-west extensional faults indicating that the facies within the Purbeck Limestone Group are, in part, controlled by this tectonic template. Outcrop study and remote sensing imaging (lidar) coupled with petrographic study is used to differentiate microbial mounds and bedded inter-mound packstone-grainstone areas and to characterise a total of 9 facies.

The limestones of the Mupe Member of the Purbeck Limestone Group represent four meter scale lacustrine cycles, deepening upwards and then shallowing upwards after a flooding surface, capped by emergent surfaces (paleosols). These sequences are characterised by accumulation of in-situ build-ups of highly porous microbial mounds that occur within less-porous bedded inter-mound packstones-grainstones. The microbial mounds are located in three stratigraphic units (“Skull”, “Hard” and “Soft Caps”) separated by three paleosols (“Basal”, “Lower” and “Great Dirt Beds”). These microbial mounds vary in thickness from about 0.2 to 3 m and preserve a high primary framework porosity. Many of the mounds developed around trees, tree trunks and branches which are preserved as moulds, or silicified wood and they comprise three sub-facies (Stromatolite, Thrombolite and Burrowed peloidal packstone). Horizontal stratification, onlapping and interdigitating of the inter-mound facies with the mounds suggest that deposition occurred contemporaneously with the development of the mounds and that they were low relief structures on the lake floor. Interpretation of high resolution ground-based lidar data collected from seven quarries in the Isle of Portland,

together with some 3-D outcrops enables a quantitative description of the morphology of the mounds and their relationship with the packstone-grainstone inter-mound facies. Most of the facies are weakly porous at micro and macroscales apart from microbial mounds. These exhibit a rather high micro and macro-porosity and the best potential reservoir unit, however as they are disconnected spatially and bounded by paleosols, the quality of the overall potential reservoir remains poor.

The main goals of this project are to predict the controls on the location, shape and the size of microbial mounds and to constrain the facies models and palaeogeographies of the Mupe Member within the Wessex Basin. The main conclusions of this multi-scale study are (1) that the two main extensional faults in this part of the Wessex Basin were active during Purbeck time; (2) that the development of microbial mounds is tectonically controlled as indicated by their relationship with the relay ramp; (3) mound occurrence is controlled by palaeotopography generated on sub-aerial exposure surfaces, fossil soils and early conifer trees; (4) mounds are developed mainly on the shallowest area of the lake as indicated by their rounded to tabular shapes, and their relationship with the packstone-grainstone inter-mound facies and the paleosols; (5) petrographic, palaeontological and isotopic data indicate an open, through-flowing brackish water lacustrine system in a semi-arid, Mediterranean-type climatic setting; and the characterisation of potential reservoir shows (6) that reservoir qualities are overall relatively poor.

## Acknowledgements

The past four years at Royal Holloway University of London have been an amazing journey where I met lots of new persons, that I worked with and/or shared lots of good memories. It is going to be difficult for me to not forget anyone, but if I do, please accept my sincere apologies.

I want to thank Dan Bosence although just “thanks” is not strong enough to express all my gratitude. I have learned (and still learning) so much with him during the last four years, not only in geology but I also improved my English (I hope) although I cannot get rid of my French accent, and in my gardening skills. I would also like to thank Peter Burgess for his enthusiasm, humour and professional advices he gave to me during this project. Working with them was (and I hope will be in the future) an amazing experience.

I wish to thank BP and Baker Hughes for funding this project that allowed me to do intensive fieldworks in Dorset and in Mexico, all my research and numerous conferences worldwide.

I want to express all my recognition to Bernie Vining for all the valuable advices all along the project and more importantly during the writing up of this thesis with our monthly meetings. I would also like to thank Ian Billing for his enthusiasm and advices during our annual meetings and in the field even under -10°C with the blizzard along the Dorset coast! I also wish to thank Anna Matthews (BP), Mary Raigosa (Baker Hughes) and Marianna Bressan (Baker Hughes) for their constructing helps and implications during this project.

Thanks to Ken McCaffrey and Vishal Bandugula (Durham University) for the week we spent in Portland for the lidar surveys; Julien Moreau and Johanna Keskinen (Copenhagen University) for the day we spent to try GPR surveys; and Rudy Swennen, Steven Claes and Eva DeBoer for their helps with the CT scans and for welcoming me in Leuven University. I would like to thank Mark Godden (Albion Stone) and Andrew Jackson (Portland Stonefirms) for always allowing me to access the active quarries on the Isle of Portland.

I wish to thank all the researchers, experts and staffs that helped me and discussed with me about the Purbeck microbialites with Howard Falcon-Lang, David Waltham, Ian Watkinson, Margaret Collinson, Trevor Burchette, Nicola Scarselli, Jürgen Adam, Chris Elders, Kevin D’Souza, Dan Parsonage, Neil Holloway and Sharon Gibbons.

I wish to thank Peter and Rachel Brachi for welcoming me in their Bed and Breakfast in Dorset and for always arranging me my stay during the field campaign.

I also want to thank all the post-graduate students with special mention to the Zorras with Silvia, Albert, Jorge 1, Jorge 2.0, Elena, Giovanni, Azad, and the recently graduated doctors Erwan, Miguel, Dami, Giulia, Serena, Sila, Seb, Oris, Ivan, Eldert, Sammia, Gerd, Celine and Laura. It was so good to meet all of them and I hope (and I am pretty sure) our ways will cross in a near future. My special thanks go to Estani with whom I shared very good moments in the office obviously but especially in the field in Dorset and in Mexico; and Erwan, Sila and Adam for their helps and discussions in the field.

I wish to thank important persons for me with all the geologists and collègues from Marseille with Emilio, Nono and Aurore, Frankov and Fanny, Pobinou and Flo, Issautche and Juliette, Arthur and Amadine, Richet and Emilie, Blénouille and himself, François, Philippe, Lisa, Cécile, Justine and all the others. Thanks for being there and for everything since 2005 for some (hein Christophe!). Special thanks go to even older friends with Romain and Aurélie, Cédric and Méryll, Pierre and Marie, Sylvain and Mylène, Guillaume and Fred and Lise.

I wish to thank my parents, Patrick and Josiane, my grand-parents, Yvette, François, Micheline and Michel, my uncle, Bruno and my sister, Auriane to support me ever and ever, even when I decided to leave France, who knows for how long. I also wish to thank the family/friends with the Francavilla, Prost, Prieur, Calvini with a special mention to Flo, Nadège and Eden, Théo, Manon and Corentin. Finally I want to thank Mersiye Bora for her constant supports and encouragements during the last years, without her it would have been much more difficult for me.



*The Purbeck limestones team on a sunny April day 2015 enjoying the Purbeck microbialites at God Nore on the Isle of Portland. (photo courtesy of Ian Billing).*

This thesis is dedicated to the memory of my grand-father,  
François Guillaume (1933-2013).

## Table of contents

<b>ABSTRACT</b>	<b>3</b>
<b>ACKNOWLEDGMENTS</b>	<b>5</b>
<b>CHAPTER 1: GENERAL INTRODUCTION</b>	<b>22</b>
1. RESEARCH PROJECT OVERVIEW	23
2. PROBLEMS TO BE ADDRESSED IN THIS THESIS	23
3. OVERVIEW OF METHODS	25
4. OUTLINE OF THE THESIS	26
<b>CHAPTER 2: THE PURBECK LIMESTONES</b>	<b>27</b>
1. INTRODUCTION	28
2. WESSEX BASIN	29
3. REVIEW OF THE PURBECK LIMESTONE GROUP	33
3.1. EXPOSURES IN SOUTH DORSET	33
3.2. LITHOSTRATIGRAPHY	36
3.2.1. <i>Group</i>	36
3.2.2. <i>Formations</i>	37
3.2.3. <i>Members</i>	37
3.2.4. <i>Beds</i>	37
3.3. BIOSTRATIGRAPHY	41
3.4. CHRONOSTRATIGRAPHY	48
3.5. FACIES	51
3.5.1. <i>Facies of the Lulworth Formation</i>	51
3.5.1.1. Facies of the Mupe Member	51
3.5.1.1.1. Facies of the Transition Bed	51
3.5.1.1.2. Facies of the Skull, Hard and Soft Cap beds	52
3.5.1.1.3. Facies of the Basal, Lower and Great Dirt Beds	58
3.5.1.1.4. Facies of the Broken Beds and Cypris Freestone	59
3.5.1.1.5. Fossils of the Mupe Member	61
3.5.1.1.6. Lateral thickness and facies variations	64
3.5.1.2. Facies of the Ridgeway Member	70
3.5.1.3. Facies of the Worbarrow Tout Member	70
3.5.2. <i>Facies of the Durlston Formation</i>	70
3.5.2.1. Facies of the Stair Hole Member	71
3.5.2.2. Facies of the Peveril Point Member	71
3.6. TECTONIC SETTING	72
3.7. PALAEOENVIRONMENTS AND PALAEOGEOGRAPHIES IN THE EARLY PURBECK TIME	75
3.7.1. <i>Palaeoenvironments in the early Purbeck time</i>	75
3.7.2. <i>Palaeogeographies in the early Purbeck time</i>	86



## **CHAPTER 3: SUBSURFACE ANALYSIS OF STRATIGRAPHIC AND TECTONIC SETTING OF THE PURBECK LIMESTONE GROUP IN THE SOUTH-WEST WESSEX BASIN** **96**

<b>1. INTRODUCTION</b>	<b>97</b>
<b>2. METHODOLOGY</b>	<b>97</b>
2.1. INTRODUCTION	97
2.2. DETAILS OF 2-D SEISMIC PROFILES	98
2.3. DETAILS OF THE 3-D BLOCK	102
2.4. DETAILS OF WELLS	103
2.5. MAPPING OF HORIZONS IN PETREL	104
2.5.1. <i>Top Portland</i>	106
2.5.2. <i>Top Purbeck</i>	106
2.6. SEISMIC AND WIRELINE LOG CHARACTERISTICS OF THE PURBECK INTERVAL	107
<b>3. INTERPRETATION OF WELL AND SEISMIC DATA</b>	<b>115</b>
3.1. THICKNESS VARIATIONS IN THE PURBECK LIMESTONE GROUP	115
3.2. FAULTS	123
3.2.1. <i>Ridgeway Fault</i>	123
3.2.2. <i>Purbeck Fault</i>	123
3.2.3. <i>Relay ramp area</i>	124
3.2.4. <i>Subsidiary faults</i>	126
<b>4. TECTONIC SETTINGS AND STRATIGRAPHY</b>	<b>130</b>
4.1. EXTENSIONAL SETTINGS	130
4.2. INVERSION SETTING	130
4.3. STRATIGRAPHIC FEATURES	131
<b>5. DISCUSSION</b>	<b>133</b>
<b>6. CONCLUSION</b>	<b>134</b>

## **CHAPTER 4: FACIES OF THE MUPE MEMBER, PURBECK LIMESTONE GROUP** **136**

<b>1. INTRODUCTION</b>	<b>137</b>
<b>2. MICROBIALITE FACIES</b>	<b>139</b>
2.1. THROMBOLITE SUB-FACIES	142
2.1.1. <i>Description</i>	142
2.1.2. <i>Interpretation</i>	146
2.1.2.1. Clotted macrofabric	146
2.1.2.2. Micritic walled tubes	146
2.1.2.3. Chalcedony spherules	152
2.1.2.4. Barite crystal aggregates	153
2.2. STROMATOLITES	156

2.2.1.	<i>Description</i>	156
2.2.2.	<i>Interpretation</i>	158
2.3.	BURROWED PELOIDAL PACKSTONE SUB-FACIES	159
2.3.1.	<i>Description</i>	159
2.3.2.	<i>Interpretation</i>	163
2.4.	FORMATION OF THE MICROBIAL MOUNDS	165
<b>3.</b>	<b>INTRACLASTIC PELOIDAL PACKSTONE-GRAINSTONE FACIES</b>	<b>171</b>
3.1.	DESCRIPTION	171
3.2.	INTERPRETATION	175
3.2.1.	<i>Peloids</i>	175
3.2.2.	<i>Intraclasts</i>	176
3.2.3.	<i>Ostracods</i>	177
3.2.4.	<i>Molluscs</i>	178
3.2.5.	<i>Gypsum pseudomorphs</i>	179
3.2.6.	<i>Ooids</i>	180
3.2.7.	<i>Fish scales</i>	185
3.2.8.	<i>Foraminifers</i>	185
3.2.9.	<i>Palaeocurrents</i>	185
3.2.10.	<i>Summary</i>	186
<b>4.</b>	<b>CROSS-BEDDED PELOIDAL PACKSTONE-GRAINSTONE FACIES</b>	<b>186</b>
4.1.	DESCRIPTION	186
4.2.	INTERPRETATION	191
4.2.1.	<i>Peloids</i>	191
4.2.2.	<i>Ostracods</i>	191
4.2.3.	<i>Ooids</i>	192
4.2.4.	<i>Intraclasts</i>	194
4.2.5.	<i>Molluscs</i>	194
4.2.6.	<i>Foraminifers</i>	195
4.2.7.	<i>Halite pseudomorphs</i>	195
4.2.8.	<i>Quartz grains</i>	196
4.2.9.	<i>Palaeocurrents</i>	197
4.2.10.	<i>Summary</i>	198
<b>5.</b>	<b>WACKESTONE TO FINE GRAINSTONE FACIES</b>	<b>198</b>
5.1.	DESCRIPTION	198
5.2.	INTERPRETATION	202
5.2.1.	<i>Peloids</i>	202
5.2.2.	<i>Ostracods</i>	202
5.2.3.	<i>Molluscs</i>	203
5.2.4.	<i>Ooids</i>	204
5.2.5.	<i>Solenopora fragments</i>	205
5.2.6.	<i>Echinoderm plates</i>	206
5.2.7.	<i>Bryozoan fragment</i>	207
5.2.8.	<i>Intraclasts</i>	208
5.2.9.	<i>Summary</i>	208
<b>6.</b>	<b>GYPSIFEROUS PELOIDAL PACKSTONE FACIES</b>	<b>209</b>

6.1.	DESCRIPTION	209
6.2.	INTERPRETATION	212
<b>7.</b>	<b>CALCAREOUS SANDSTONE FACIES</b>	<b>215</b>
7.1.	DESCRIPTION	215
7.2.	INTERPRETATION	217
<b>8.</b>	<b>CONGLOMERATE FACIES</b>	<b>218</b>
8.1.	DESCRIPTION	218
8.2.	INTERPRETATION	219
<b>9.</b>	<b>CARBONACEOUS MARL FACIES</b>	<b>219</b>
9.1.	DESCRIPTION	219
9.2.	INTERPRETATION	220
<b>10.</b>	<b>EVAPORITE FACIES</b>	<b>220</b>
10.1.	VUGGY SUB-FACIES	221
10.1.1.	<i>Description</i>	221
10.1.2.	<i>Interpretation</i>	222
10.2.	BRECCIA SUB-FACIES	226
10.2.1.	<i>Description</i>	226
10.2.2.	<i>Interpretation</i>	228
<b>11.</b>	<b>SUMMARY</b>	<b>230</b>
<b>CHAPTER 5: MICROBIAL MOUNDS; OCCURRENCE, SIZE, SHAPE, AND RELATION TO INTER-MOUND FACIES</b>		<b>231</b>
<b>1.</b>	<b>INTRODUCTION</b>	<b>232</b>
<b>2.</b>	<b>METHODOLOGY</b>	<b>234</b>
2.1.	LIGHT DETECTION AND RANGING (LIDAR) PRINCIPLE	234
2.2.	POINT CLOUDS	237
2.2.1.	<i>Acquisition with Leica ScanStation C10</i>	237
2.2.2.	<i>Workflow for interpretation</i>	239
2.3.	ADDITIONAL COMBINED TECHNIQUES	242
<b>3.</b>	<b>MICROBIAL MOUND SHAPES AND SIZES AND INTER-MOUND FACIES RELATIONSHIPS</b>	<b>243</b>
3.1.	MICROBIAL MOUNDS	243
3.1.1.	<i>Size</i>	244
3.1.2.	<i>Morphologies</i>	247
3.2.	INTER-MOUND FACIES	252
3.3.	RELATIONSHIP BETWEEN MOUND AND INTER-MOUND FACIES	252
3.3.1.	<i>Mounds vs. inter-mounds coverage</i>	252
3.3.2.	<i>Relationships between mound and inter-mound sediments</i>	253
3.3.3.	<i>Distribution of microbial mounds</i>	257
3.3.3.1.	Regional scale	257

3.3.3.2.	Local scale	260
3.3.3.3.	Controls on mound morphologies	261
<b>4.</b>	<b>CONCLUSION</b>	<b>266</b>

## **CHAPTER 6: PALAEOENVIRONMENTS OF THE MUPE MEMBER: LOGS, FACIES ASSOCIATIONS AND FACIES MODELS** **268**

<b>1.</b>	<b>INTRODUCTION</b>	<b>269</b>
<b>2.</b>	<b>SEDIMENTARY LOGS</b>	<b>269</b>
<b>3.</b>	<b>FACIES SUCCESSION AND BED TRANSITION</b>	<b>272</b>
3.1.	QUALITATIVE DESCRIPTION	272
3.2.	QUANTITATIVE ANALYSIS	275
<b>4.</b>	<b>FACIES ASSOCIATIONS</b>	<b>277</b>
4.1.	DEEP LACUSTRINE	278
4.2.	EMERGENT	279
4.3.	MOUNDED MARGINAL LACUSTRINE	279
4.4.	HYPERSALINE LACUSTRINE	280
4.5.	BEDDED MARGINAL LACUSTRINE	280
4.6.	FACIES ASSOCIATION SUCCESSIONS	281
<b>5.</b>	<b>SEDIMENTARY LOG CORRELATIONS</b>	<b>282</b>
5.1.	ISLE OF PORTLAND CORRELATION	283
5.2.	RIDGEWAY CORRELATION	285
5.3.	PURBECK CORRELATION	287
5.4.	SUMMARY	290
<b>6.</b>	<b>SEQUENCE STRATIGRAPHY OF THE MUPE MEMBER</b>	<b>292</b>
<b>7.</b>	<b>FACIES MODELS</b>	<b>303</b>
7.1.	ANALOGUES	307
7.1.1.	<i>Introduction</i>	307
7.1.2.	<i>Laguna Bacalar, Mexico</i>	307
7.1.3.	<i>Great Salt Lake, Utah, USA</i>	310
7.1.4.	<i>Hamelin Pool, Shark Bay, Australia</i>	313
7.1.5.	<i>Rottnest Island, Australia</i>	316
7.1.6.	<i>Lake Thetis, Australia</i>	318
7.1.7.	<i>Lake Clifton, Australia</i>	320
7.1.8.	<i>Lake Richmond, Australia</i>	322
7.1.9.	<i>Green River Formation (Piceance Basin) from Utah, USA</i>	324
7.1.10.	<i>Summary</i>	327
7.2.	FACIES MODELS FOR THE MUPE MEMBER	328
<b>8.</b>	<b>CONCLUSION</b>	<b>333</b>

<b>CHAPTER 7: TECTONO-SEDIMENTARY MODELS FOR THE MUPE MEMBER</b>	<b>335</b>
1. INTRODUCTION	336
2. CONTROLS ON NON-MARINE CARBONATE SEDIMENTATION	336
3. TECTONO-SEDIMENTARY MODELS OF THE MUPE MEMBER	341
3.1. SCENARIO 1	341
3.1.1. <i>Models</i>	341
3.1.2. <i>Validity of the scenario 1 models</i>	345
3.2. SCENARIO 2	348
3.2.1. <i>Models</i>	348
3.2.2. <i>Validity of the scenario 2 models</i>	352
4. SUMMARY AND CONCLUSION	353
<b>CHAPTER 8: SYNTHESIS AND CONCLUSIONS</b>	<b>355</b>
1. INTRODUCTION	356
2. SYN-RIFT SETTING OF THE WESSEX BASIN	356
3. NON-MARINE CARBONATES OF THE MUPE MEMBER	357
4. MICROBIAL MOUNDS	358
5. LACUSTRINE SEQUENCES IN THE MUPE MEMBER	359
6. CONTROLS ON FACIES DISTRIBUTION	361
6.1. BASIN-SCALE	361
6.2. SMALL-SCALE	362
7. POTENTIAL PETROLEUM SYSTEM	364
8. ANALOGUE OF SOUTH ATLANTIC RESERVOIRS	366
<b>REFERENCE LIST</b>	<b>371</b>
<b>APPENDIX 1: MODERN ANALOGUE: LAGUNA BACALAR. YUCATAN PENINSULA, QUINTANA ROO, MEXICO</b>	<b>400</b>
1. INTRODUCTION	401
2. GEOLOGICAL CONTEXT	403
3. LAKE SETTINGS	405
3.1. CLIMATE, HYDROLOGY AND WATER CHEMISTRY	405

3.2.	BATHYMETRY, LAKE FLOOR TOPOGRAPHY AND CURRENTS	407
3.3.	FAUNAS AND FLORAS	408
3.4.	SEDIMENTS	409
<b>4.</b>	<b>MICROBIAL DEPOSITS</b>	<b>412</b>
4.1.	ENVIRONMENTAL CONTROLS ON MICROBIAL GROWTH	412
4.2.	MICROBIAL DEPOSIT MORPHOLOGIES	413
4.2.1.	<i>Flat microbial crusts</i>	413
4.2.2.	<i>Encrustations</i>	415
4.2.3.	<i>Low relief mounds</i>	417
4.2.4.	<i>Tall mounds</i>	419
4.3.	MICROBIAL DEPOSITS DISTRIBUTION	421
4.3.1.	<i>Windward and leeward deposition</i>	421
4.3.2.	<i>Bathymetry, microbial types and concentrations</i>	423
<b>5.</b>	<b>CONCLUSION</b>	<b>424</b>
<b>6.</b>	<b>REFERENCE LIST</b>	<b>424</b>
	<b>APPENDIX 2: IMAGING TECHNIQS</b>	<b>426</b>
	APPENDIX 2.1.LIDAR DATASET	427
	APPENDIX 2.2.HYPERSPECTRAL IMAGING	455
	APPENDIX 2.3.GROUND PENETRATED RADAR (GPR)	460
	<b>APPENDIX 3: SEDIMENTARY LOGS</b>	<b>465</b>
1.	SEDIMENTARY LOGS	466
2.	FACIES TRANSITION ANALYSIS	490
3.	STABLE ISOTOPE (CARBON AND OXYGEN) DATA	492

## List of figures

### Chapter 2: The Purbeck Limestones

<b>Figure 2.1</b> Purbeck exposures in Europe (France, Switzerland, Germany and UK)	<b>29</b>
<b>Figure 2.2</b> Structural map of the Channel and Wessex Basins	<b>31</b>
<b>Figure 2.3</b> Lithostratigraphic column for the Wessex Basin	<b>32</b>
<b>Figure 2.4</b> Purbeck exposures in south Dorset	<b>35</b>
<b>Figure 2.5</b> Magnetostratigraphy and interval dating of the Purbeck Limestone Group	<b>50</b>
<b>Figure 2.6</b> “Burrs” of the Soft Cap bed first description	<b>52</b>
<b>Figure 2.7</b> Facies thickness variation on an East-West section of the lower Mupe Member with inferred palaeosalinities	<b>65</b>
<b>Figure 2.8</b> Log correlation of the lower part of the Mupe Member on the Isle of Portland	<b>68</b>
<b>Figure 2.9</b> Log correlation panel of the lower part of the Mupe Member across south Dorset	<b>69</b>
<b>Figure 2.10</b> Structural map of the western margin of the Wessex Basin	<b>72</b>
<b>Figure 2.11</b> Sketch north-south cross-sections showing the structural evolution of the Purbeck and Ridgeway Faults	<b>74</b>
<b>Figure 2.12</b> Palaeoenvironmental reconstructions, artistic views of the Dorset Coast and early Purbeck time	<b>75</b>
<b>Figure 2.13</b> Depositional environment reconstructions of the Dorset Coast during the deposition of the lower part of the Mupe Member	<b>77</b>
<b>Figure 2.14</b> Sequence of events involved in the drowning of the Purbeck forests and the formation of algal limestones	<b>80</b>
<b>Figure 2.15</b> Sequence of events explaining the deposition of tufa stromatolites	<b>83</b>
<b>Figure 2.16</b> Inferred palaeosalinity fluctuations of the Purbeck Limestone Group	<b>84</b>
<b>Figure 2.17</b> Cross-plot of carbon and oxygen isotope from the Skull and Hard Caps of the Mupe Member	<b>85</b>
<b>Figure 2.18</b> Depositional model for the Caps Beds of the Mupe Member	<b>86</b>
<b>Figure 2.19</b> Palaeogeographical reconstruction of the Wessex Basin at the time of the deposition of the Purbeck Limestone Group	<b>88</b>
<b>Figure 2.20</b> Palaeogeography of the Dorset Coast at the time of deposition of the Mupe Member	<b>90</b>
<b>Figure 2.21</b> Schematic palaeogeographic reconstructions of the Dorset coast area during deposition of the Caps and Dirt Beds	<b>93</b>
<b>Figure 2.22</b> Depositional environment reconstructions	<b>94</b>
<b>Figure 2.23</b> Depositional model for the Mupe Member	<b>95</b>

### **Chapter 3: Subsurface study of stratigraphic and tectonic setting of the Purbeck Limestone Group in the south-west Wessex Basin**

<b>Figure 3.1</b> Location map of wells and seismic profiles interpreted in this study	<b>98</b>
<b>Figure 3.2</b> Location map of the 2-D seismic profiles both onshore and offshore	<b>100</b>
<b>Figure 3.3</b> Example of 2-D profiles showing the quality of the seismic data	<b>101</b>
<b>Figure 3.4</b> Details of the 3-D seismic block	<b>102</b>
<b>Figure 3.5</b> Illustration of the interpretation method	<b>105</b>
<b>Figure 3.6</b> Interpreted seismic profile from the 3-D block	<b>108</b>
<b>Figure 3.7</b> Well correlation panel 1	<b>109</b>
<b>Figure 3.8</b> Well correlation panel 2	<b>110</b>
<b>Figure 3.9</b> Well correlation panel 3	<b>111</b>
<b>Figure 3.10</b> Coverage of the identified tops of the Portland and Purbeck	<b>112</b>
<b>Figure 3.11</b> Surface maps following the seismic interpretation and tie with borehole data	<b>114</b>
<b>Figure 3.12</b> Well correlation panel 1 flattened at the top Purbeck horizon	<b>117</b>
<b>Figure 3.13</b> Well correlation panel 2 flattened at the top Purbeck horizon	<b>118</b>
<b>Figure 3.14</b> Well correlation panel 3 flattened at the top Purbeck horizon	<b>119</b>
<b>Figure 3.15</b> Thickness map of the Purbeck interval. Contour line each 20ms	<b>122</b>
<b>Figure 3.16</b> Location map showing the faults interpreted from the seismic profiles	<b>124</b>
<b>Figure 3.17</b> Relay ramp	<b>125</b>
<b>Figure 3.18</b> Geometry and occurrence of Ridgeway Fault following the seismic interpretation	<b>127</b>
<b>Figure 3.19</b> Geometry of Purbeck Fault and Purbeck fault zone as seen in north-south profiles	<b>128</b>
<b>Figure 3.20</b> Subsidiary faults interpreted from seismic profiles	<b>129</b>
<b>Figure 3.21</b> MBES (Multi-Beam Echo Sounder) data also known as DORIS data	<b>130</b>
<b>Figure 3.22</b> Seismic profile GC822-27	<b>132</b>

### **Chapter 4: Facies of the Mupe Member, Purbeck Limestone Group**

<b>Figure 4.1</b> Classification of microbialites	<b>140</b>
<b>Figure 4.2</b> Mounds as seen in the field	<b>141</b>
<b>Figure 4.3</b> Macroscale thrombolite sub-facies	<b>143</b>
<b>Figure 4.4</b> Microphotographs of the thrombolite sub-facies	<b>145</b>
<b>Figure 4.5</b> Schematic diagram of microbial filament organisation and calcification types and results	<b>147</b>
<b>Figure 4.6</b> Clotted microfabrics	<b>148</b>
<b>Figure 4.7</b> Microbial filaments taxonomy	<b>149-150</b>
<b>Figure 4.8</b> Growth direction and clots	<b>151</b>
<b>Figure 4.9</b> Microphotographs of chalcedony nodules	<b>153</b>
<b>Figure 4.10</b> Barite crystals and aggregates	<b>155-156</b>
<b>Figure 4.11</b> Stromatolite facies in the field	<b>157</b>
<b>Figure 4.12</b> Stromatolite microfacies	<b>158</b>



<b>Figure 4.13</b> Burrowed peloidal packstone macrofacies	<b>160</b>
<b>Figure 4.14</b> Burrowed peloidal collar microfacies	<b>162</b>
<b>Figure 4.15</b> Microbial mounds	<b>166</b>
<b>Figure 4.16</b> Schematic model for the origin of the silicified plants on the western marginal slope of the Ngakoringora Ridge	<b>168</b>
<b>Figure 4.17</b> Reconstruction of events at the origin of the formation of the microbial mounds	<b>170</b>
<b>Figure 4.18</b> Intraclastic peloidal packstone-grasinstone macrofacies	<b>173</b>
<b>Figure 4.19</b> Intraclastic peloidal packstone-grainstone microfacies	<b>174-175</b>
<b>Figure 4.20</b> Intraclasts of the Intraclastic peloidal packstone-grainstone facies	<b>177</b>
<b>Figure 4.21</b> Gypsum pseudomorphs of the Intraclastic peloidal packstone-grainstone facies	<b>180</b>
<b>Figure 4.22</b> Ooids of the Intraclastic peloidal packstone-grainstone facies	<b>184-185</b>
<b>Figure 4.23</b> Cross-bedded peloidal packstone-grainstone facies in the field	<b>188</b>
<b>Figure 4.24</b> Orientation and direction measurements of the cross-laminations of the Cross-bedded peloidal packstone-grainstone facies	<b>189</b>
<b>Figure 4.25</b> Cross-bedded peloidal packstone-grainstone microfacies	<b>190</b>
<b>Figure 4.26</b> Ooids of the Cross-bedded peloidal packstone-grainstone facies	<b>193</b>
<b>Figure 4.27</b> Intraclasts of the Cross-bedded peloidal packstone-grainstone facies	<b>194</b>
<b>Figure 4.28</b> Hopper halite of the Cross-bedded peloidal packstone-grainstone	<b>196</b>
<b>Figure 4.29</b> Wackestone to fine grainstone facies in the field	<b>200</b>
<b>Figure 4.30</b> Wackestone to fine grainstone microfacies	<b>200</b>
<b>Figure 4.31</b> Clasts and fossils of the Wackestone to fine grainstone facies	<b>201-202</b>
<b>Figure 4.32</b> Mixed ooids of the Wackestone to fine grainstone facies	<b>204</b>
<b>Figure 4.33</b> <i>Solenopora?</i> of the Wackestone to fine grainstone	<b>206</b>
<b>Figure 4.34</b> Echinoderm clasts of the Wackestone to fine grainstone facies	<b>207</b>
<b>Figure 4.35</b> Bryozoan clasts of the Wackestone to fine grainstone facies	<b>207</b>
<b>Figure 4.36</b> Intraclasts of the Wackestone to fine grainstone facies	<b>208</b>
<b>Figure 4.37</b> Gypsiferous peloidal packstone macrofacies	<b>210</b>
<b>Figure 4.38</b> Gypsiferous peloidal packstone microfacies	<b>211</b>
<b>Figure 4.39</b> PPL and CL microphotographs of the calcite crystals	<b>212</b>
<b>Figure 4.40</b> Calcareous sandstone macrofacies	<b>216</b>
<b>Figure 4.41</b> Calcareous sandstone microfacies	<b>216</b>
<b>Figure 4.42</b> Conglomerate macrofacies	<b>218</b>
<b>Figure 4.43</b> Carbonaceous marl macrofacies	<b>220</b>
<b>Figure 4.44</b> Evaporite vuggy macrofacies	<b>221</b>
<b>Figure 4.45</b> Evaporite vuggy microfacies	<b>223</b>
<b>Figure 4.46</b> CL images of Evaporite vuggy sub-facies	<b>225</b>
<b>Figure 4.47</b> Evaporite Breccia sub-facies	<b>226</b>
<b>Figure 4.48</b> Evaporite breccia microfacies	<b>227</b>
<b>Figure 4.49</b> Large scale field view of the Evaporite breccia sub-facies	<b>239</b>

## **Chapter 5: Microbial mounds; Occurrence, size, shape, and relation to inter-mound facies**

<b>Figure 5.1</b> Location map of the lidar surveys acquired on the Isle of Portland	<b>233</b>
<b>Figure 5.2</b> Comparison of size of geological objects, processes and imaging technologies	<b>235</b>
<b>Figure 5.3</b> Main characteristics of laser light	<b>236</b>
<b>Figure 5.4</b> Lidar scanner characteristics	<b>238</b>
<b>Figure 5.5</b> Tracing out white chalk lines to indicate boundary between mound and inter-mound facies at God Nore	<b>239</b>
<b>Figure 5.6</b> Workflow applied to interpret lidar point clouds	<b>241</b>
<b>Figure 5.7</b> Widths and heights measurements of all the mounds	<b>245</b>
<b>Figure 5.8</b> Distribution of areas and perimeters of all the mounds	<b>246</b>
<b>Figure 5.9</b> Relationship between mound heights and widths	<b>248</b>
<b>Figure 5.10</b> Roundness parameter plots for the Skull Cap and Hard Cap	<b>250</b>
<b>Figure 5.11</b> Relationships between perimeters and areas and roundness for both Skull and Hard Caps, Skull Cap only and Hard Cap only	<b>251</b>
<b>Figure 5.12</b> Proportions of mounds and inter-mound facies over the Isle of Portland from the north to the south	<b>253</b>
<b>Figure 5.13</b> Example of heights of top surfaces of tabular mound and interdigitations of complex mound	<b>254</b>
<b>Figure 5.14</b> Relationships between mounds and inter-mound facies	<b>256</b>
<b>Figure 5.15</b> Views of mounds in 3-D in the field	<b>259</b>
<b>Figure 5.16</b> Mound sizes (width and heights), areas and perimeters distributions over the Isle of Portland from the north to the south	<b>261</b>
<b>Figure 5.17</b> Irregularities on the top surface of the Portland Formation	<b>262</b>
<b>Figure 5.18</b> Small-scale 3-D forward numerical model	<b>263</b>
<b>Figure 5.19</b> Lateral extent of mounds in the Hard Cap illustrated from the interpretation of the lidar point clouds at King Barrow Quarries	<b>265</b>

## **Chapter 6: Palaeoenvironments of the Mupe Member: logs, facies associations and facies models**

<b>Figure 6.1</b> Simplified geological map of South Dorset with locations of sedimentary logs measured in this study	<b>271</b>
<b>Figure 6.2</b> Idealised log for the lower Mupe Member of the study area with average thickness of each bed	<b>274</b>
<b>Figure 6.3</b> Facies relationship diagram for the Mupe Member in south Dorset	<b>277</b>
<b>Figure 6.4</b> Facies relationship diagram with facies association and depositional environments together with the generalised log	<b>282</b>
<b>Figure 6.5</b> North to south Isle of Portland correlation panel of sedimentary logs	<b>284</b>
<b>Figure 6.6</b> Ridgeway correlation of sedimentary logs both recorded and from the literature	<b>286</b>

<b>Figure 6.7</b> Purbeck correlation of sedimentary logs both recorded and from the literature	<b>289</b>
<b>Figure 6.8</b> Fence diagram of the facies associations throughout the studied area	<b>291</b>
<b>Figure 6.9</b> Hypothetical model to illustrate how depositional systems can be related to cyclic changes in water depth	<b>293</b>
<b>Figure 6.10</b> Idealised log with interpretation of depositional cycles	<b>295</b>
<b>Figure 6.11</b> Cartoons depicting the transgressive and highstand deposits	<b>299</b>
<b>Figure 6.12</b> Generalised depositional reconstruction and lake level fluctuations	<b>302</b>
<b>Figure 6.13</b> Characteristics of lake types	<b>304</b>
<b>Figure 6.14</b> Lake type models	<b>306</b>
<b>Figure 6.15</b> Laguna Bacalar, Yucatan Peninsula, Mexico	<b>309</b>
<b>Figure 6.16</b> Great Salt Lake, Utah, USA	<b>312</b>
<b>Figure 6.17</b> Hamelin Pool, Shark Bay, Australia	<b>315</b>
<b>Figure 6.18</b> Rottneest Island, western Australia	<b>317</b>
<b>Figure 6.19</b> Lake Thetis, Cervantes, western Australia	<b>319</b>
<b>Figure 6.20</b> Lake Clifton, western Australia	<b>321</b>
<b>Figure 6.21</b> Lake Richmond, Rockingham, western Australia	<b>323</b>
<b>Figure 6.22</b> Piceance Basin, Eocene Green River Formation, Utah, USA	<b>326</b>
<b>Figure 6.23</b> Facies model for prograding brackish water open lake margin for the lower Mupe Member	<b>328</b>
<b>Figure 6.24</b> Plot diagram of the $\delta^{18}\text{O}$ vs. $\delta^{13}\text{C}$ stable isotope data of the Intraclastic peloidal packstone-grainstone facies	<b>331</b>
<b>Figure 6.25</b> Facies model for regressive hypersaline water lake margin for the upper part of the Mupe Member	<b>332</b>

## **Chapter 7: Tectono-sedimentary models for the Mupe Member**

<b>Figure 7.1</b> General tectono-sedimentary models in rift settings	<b>338</b>
<b>Figure 7.2</b> Lacustrine carbonate facies in a half-graben system	<b>339</b>
<b>Figure 7.3</b> Relay ramp depositional zones and main drainage routes	<b>340</b>
<b>Figure 7.4</b> Tectono-sedimentary models of the Mupe Member following scenario 1 with the Deep lacustrine facies association	<b>343</b>
<b>Figure 7.5</b> Tectono-sedimentary models of the Mupe Member following scenario 1 without the Deep lacustrine facies association	<b>344</b>
<b>Figure 7.6</b> Palaeoenvironmental reconstruction of the uppermost part of the Freestone Beds of the Portland Group	<b>347</b>
<b>Figure 7.7</b> Tectono-sedimentary models of the Mupe Member following scenario 2 with the Deep lacustrine facies association	<b>350</b>
<b>Figure 7.8</b> Tectono-sedimentary models of the Mupe Member following scenario 2 without the Deep lacustrine facies association	<b>351</b>

## Chapter 8: Synthesis and conclusions

<b>Figure 8.1</b> Size comparison between the Wessex Basin and South Atlantic	<b>366</b>
<b>Figure 8.2</b> Comparison of basin evolutions between Brazilian margin basins, the Wessex Basin of southern England and West African margin basins	<b>367</b>
<b>Figure 8.3</b> Macrofacies comparison between one microbial mound of the Purbeck Limestone Group of the Wessex Basin and the South Atlantic microbialites	<b>368</b>
<b>Figure 8.4</b> Microfacies comparison between the lacustrine Purbeck Formation of the Wessex Basin and the lacustrine facies of the Kwanza Basin	<b>369</b>

## List of tables

### Chapter 2: The Purbeck Limestones

<b>Table 2.1</b> Purbeck Limestone Group exposures in south Dorset	34
<b>Table 2.2</b> Lithostratigraphical classification and comparison over time	39-40
<b>Table 2.3</b> Ostracod biostratigraphy of the Purbeck Limestone Group	42
<b>Table 2.4</b> Miospore biostratigraphy	44
<b>Table 2.5</b> Correlation of ostracod biostratigraphy and miospore biostratigraphy for the Mupe Member of the Purbeck Limestone Group of Dorset	47
<b>Table 2.6</b> Salinity tolerance and lake systems interpreted from gastropod species of the Mupe Member	63

### Chapter 3: Subsurface study of stratigraphic and tectonic settings of the Purbeck Limestone Group in the south-west Wessex Basin

<b>Table 3.1</b> List of the 2-D seismic profiles studied with source types used during acquisition	99
<b>Table 3.2</b> Location, depth and depth of tops interpreted of wells in South Dorset	103

### Chapter 4: Facies of the Mupe Member, Purbeck Limestone Group

<b>Table 4.1</b> Facies classification of the lower part of the Mupe Member of the Purbeck Limestone Group	138
--	-----

### Chapter 5: Microbial mounds; Occurrence, size, shape, and relation to inter-mound facies

<b>Table 5.1</b> Locations and characteristics of lidar point clouds from north to south	232
<b>Table 5.2</b> Mean size of Skull and Hard Cap mounds measured from the lidar point clouds over the Isle of Portland (from north to south)	244

### Chapter 6: Palaeoenvironments of the Mupe Member: logs, facies associations and facies models

<b>Table 6.1</b> Main characteristics of sedimentary logs undertaken for this study	270
<b>Table 6.2</b> Main characteristics of facies associations in stratigraphic order from base to top	278

# Chapter 1

## General introduction

## 1. Research project overview

Following the discovery of extensive hydrocarbon reservoirs in Lower Cretaceous non-marine carbonate deposits in the South Atlantic, interest in improving our understanding of such complex systems have significantly increased. Triggered by these discoveries, this project has been funded by BP and Baker Hughes to study a possible outcrop analogue to these South Atlantic reservoirs: the Mupe Member of the Purbeck Limestone Group deposited during the syn-rift setting of the Wessex Basin and exposed in south Dorset, U.K.

This research project involves the integration of traditional outcrop-based geological study and stratigraphic numerical forward modelling study involving two inter-related PhD studies. The outcrop-based study is presented in this thesis supervised by Dan Bosence and the modelling-based study is being undertaken by Estanislao Kozlowski (Kozlowski, *in prep.*) supervised by Pete Burgess. Although inter-related, the two theses have been written independently with the exception of Appendix 1 where joint field work on a modern analogue is presented. Where data or concepts from the inter-related PhD are used in this work then these are referred to as Kozlowski (*in prep.*). An overall aim of these PhD projects is to improve the predictive value of traditional studies on facies distribution and volume quantification of non-marine carbonates in extensional settings.

In addition to the two PhD theses three independent MSc research projects supervised by Dan Bosence and Arnaud Gallois were undertaken by Royal Holloway MSc Petroleum Geoscience students, Fleckner (2014), Shigwedha (2014) and Dharmarajah (2015) and integrated into and referenced in this study where relevant.

## 2. Problems to be addressed in this thesis

Although the Purbeck Limestone Group outcrops of south Dorset are well known and have been visited by many geologists from the U.K. and abroad for more than 200 years (since Woodward, 1729), most of the published studies focus on the facies description (West, 1975; Francis 1982, 1986), fossil biotas (Anderson, 1973; Clements, 1973; Francis, 1983; Perry, 1994; Horne, 1995, 2002) and palaeoenvironmental reconstructions (West, 1975; Francis, 1984). However, little is known about the processes and controls involved in the deposition and distribution of these non-marine carbonates. As a consequence this thesis deals with and answers a broad range of research problems from basin-scale to micro-scale:

- Tectonics plays an important role in extensional basin settings and non-marine carbonate facies distribution. However, few studies are published on this topic, compared to facies in marine settings. This thesis documents if there were tectonic controls on the non-marine carbonate facies distribution in this extensional basin; and if there were, then how lacustrine carbonate deposits might evolve in this basin.
- Syn-rift setting of the Wessex Basin is very well documented from the Permian to the mid-Cretaceous, and in particular in south Dorset where two extensional faults are known to be active during the deposition of the Jurassic rocks in general (Underhill, 1998). This thesis investigates these two extensional faults to see if they may have been active at Purbeck time; and if they were controlling the palaeotopographies, the palaeolandscapes and/or the palaeogeographies.
- Non-marine carbonates have been previously described in the Mupe Member (see above), however little has been published on the controls on their deposition and distribution. This thesis reinvestigates the facies and the environments that they represent; and what the controls were on the facies deposition and distribution in this lacustrine basin.
- Microbial mounds were previously described as stromatolites in the lower part of the Mupe Member (Webster, 1826; Pugh, 1968; West, 1975; Francis, 1982; Perry, 1994) however the scale of these structures had not been appreciated and no studies were undertaken to assess the processes involved in their formation and distribution. This thesis reveals that microbial mounds were deposited in lacustrine sequences and describes how mounds develop in such sequences with a range of morphologies and sizes. These help to document the possible controls on the microbial growth and mound distribution and how they relate to bounding paleosols and evaporites.
- Petrophysical characterisation of these limestones has not been previously undertaken. This thesis describes the different pore types and their connectivity and which units could potentially be reservoir or seal in the Mupe Member with an appraisal of the effectiveness of the reservoir units.



### 3. Overview of methods

In this section only a brief overview of all the methods used in this study is provided as this study involves a wide range of methods that are detailed in each corresponding chapters.

2-D seismic profiles (35 offshore and 22 onshore) and one 3-D block offshore were interpreted with Petrel© and calibrated with borehole data with the aim of characterising possible tectonic movements during the deposition of the Purbeck Limestone Group.

22 sedimentary logs were recorded from outcrops with more than 300 samples collected. Classic microscopy (plain polarised light, cross polarised light and gypsum plate) and cathode-luminescence are used to characterise each facies at micro-scale. These result in the definition of 9 facies into a new facies classification and 5 facies associations for the Mupe Member. These are then used to create two facies models that are integrated at a more regional scale to propose three tectono-sedimentary models for the Skull, Hard and Soft Cap beds within the Mupe Member.

In this thesis salinity values are given in parts per thousand or ppt of total dissolved solids (TDS) following the Venice System (Oertli, 1964). This Venice System defines freshwater below 0.5 ppt; brackish water between 0.5 and 30 ppt; saline (marine) between 30 and 40 ppt; and hypersaline over 40 ppt (Oertli, 1964).

Lidar surveys were undertaken in 7 quarries on the Isle of Portland with Dr. Ken McCaffrey from Durham University (U.K.) and interpreted by the author with RiscanPro software. These 2-D high-resolution surveys were used to characterise microbial mound morphologies and sizes and their relationships with the inter-mound facies. This method is also used to quantify microbial mound volumes versus inter-mound facies volumes.

In addition two combined techniques were tested in order to assess their effectiveness in characterising these mounds in 3-D. Ground Penetrating Radar (GPR) surveys were undertaken with Dr. Julien Moreau from the University of Copenhagen (Denmark) in one quarry on the Isle of Portland; and hyperspectral imaging with Dr. Tobias Kurz from the University of Bergen (Norway) was tested on 5 samples sent to Bergen. However these two techniques were not used further in this study because in both cases the outcrops conditions were not good enough to obtain interpretable images.

## 4. Outline of the thesis

Following the introduction of the project and the research questions posed in the **Chapter 1** (this chapter), **Chapter 2** summarises published works available in the literature on the Purbeck Limestone Group. In subsequent chapters many of these aspects are referred back to and incorporated into discussions.

The next chapters (**Chapters 3 to 6**) constitute the main part of the thesis and present from large-scale (basin evolution) to small-scale (micro-facies and porosity) the data acquired and interpretations undertaken during this project. **Chapter 3** presents the new results and interpretations of sub-surface data (2-D and 3-D seismic and borehole) to document the stratigraphic and tectonic setting of the western part of the Wessex Basin during Purbeck time. **Chapter 4** focuses on the description of new macro- and micro-facies identified in the field and after thin section petrographic studies for the Mupe Member of the Purbeck Limestone Group. This chapter also proposes preliminary interpretation of palaeoenvironments for each defined facies. **Chapter 5** concentrates on the work undertaken on microbial mounds and associated facies from the 3-D lidar surveys undertaken in quarries on the Isle of Portland. This chapter characterises microbial mound morphologies and sizes; relationships with the surrounded inter-mound facies; and establishes possible controls on the microbial growth. The lidar surveys and associated imaging techniques are presented in **Appendix 2**. **Chapter 6** defines facies associations and presents vertical and lateral facies succession analyses qualitatively and quantitatively. Lateral correlations of the sedimentary logs recorded in the field provide valuable information of the facies distribution and help to define new palaeoenvironmental reconstructions after comparison with modern and ancient analogues. One modern analogue of the Purbeck, the freshwater lake of Laguna Bacalar in Mexico was visited in March 2015 and the main observations made during this trip are presented in **Appendix 1**. The measured sedimentary logs recorded along the Dorset coast in this project are presented in **Appendix 3**.

**Chapter 7** presents the integration of all the data acquired and interpreted in this study and proposes three tectono-sedimentary models corresponding to the three units (Skull, Hard and Soft Cap beds) of the Mupe Member where microbial deposits are identified. These are subsequently compared and discussed with general models for lacustrine carbonates from the literature.

Finally, **Chapter 8** summarises the main outcomes of this study in answering the research questions posed in Chapter 1 and emphasises the main advances of this study for each aspect presented in this thesis.

# Chapter 2

## The Purbeck limestones

## 1. Introduction

The Purbeck Limestone Group has been quarried (and exported to Europe) since Roman times (Dunning, 1949; Calkin, 1968; Edgar and Hinde, 1999) for walls, roofs, burial cists, loomweights and querns (Calkin, 1968). However it was first studied scientifically at the beginning of the 18<sup>th</sup> century by Woodward (1729) in his *“Attempt towards a natural history of the fossils of England”* where he recorded *“sea-shells in Purbeck-Stone”*. Since then it has been of importance for geological research and teaching by geologists from Great Britain and abroad who organise field trips to southern Dorset to explore the Fossil Forest area (next to Lulworth Cove). Here exceptionally well preserved, sometimes silicified cycads and tree trunks (Woodward, 1729) are found surrounded by microbialites. This was suggested for the first time by Arkell (1947) when he writes that *“the tufa...may have been due to freshwater algae”* and this aspect is described and discussed in detail in Chapter 4 of this thesis. These structures had already been described at the beginning of the 19<sup>th</sup> century as *“burr stone”* by Webster (1826) and later as *“tufaceous and botryoidal limestone”* by Arkell (1933). This chapter aims to give an overview of the state-of-the-art of the published information on the Purbeck Limestone Group of southern England (Fig. 2.1). In England the Purbeck Limestone Group is exposed in Wiltshire (Vale of Wardour near Swindon), south-west of England (Figs. 2.1 and 2.2; Sylvester-Bradley, 1940; Needham, 2011), in south Dorset (detailed in the second section of this chapter) and in Kent, north-west of Hastings (Edmunds, 1938; Crosby and Fletcher, 1988).

The equivalent of the Purbeck Limestone Group is also exposed in Germany, Switzerland and France (Fig. 2.1). In Germany the Purbeck deposits constitute the upper part of the Münders Formation with a Berriasian age (Elstner and Mutterlose, 1996; Arp and Mennerich, 2008). These Purbeck deposits are exposed in the Lower Saxony Basin (Hils Syncline, northern Germany, Fig. 2.1), and are described as non-marine ostracod-rich limestone and marl deposits (Hoyer, 1965; Schönfeld, 1979; Schudack, 1994; Elstner and Mutterlose, 1996; Gramann *et al.*, 1997; Arp and Mennerich, 2008). In the Swiss and French Jura the Purbeck deposits are referred as Purbeckian or Purbeck limestones and constitute the Goldberg Formation, early Berriasian (Strasser and Davaud, 1983; Strasser, 1986, 1988). These deposits are described as non-marine carbonates with sequences or cycles capped by paleosols (Strasser and Davaud, 1983; Strasser, 1986, 1988). In France the Purbeck deposits are exposed in three locations in the Charente region, western France (Fig. 2.1; Bousquet, 1967; Colin *et al.*, 2004; Schnyder *et al.*, 2012), in the Boulonnais region, northern France (Fig. 2.1; Jones, 1883; Ager and Wallace,

1966; Townson and Wimbledon, 1979; Deconinck *et al.*, 2000) and in the Jura Mountains as described previously (Fig. 2.1).



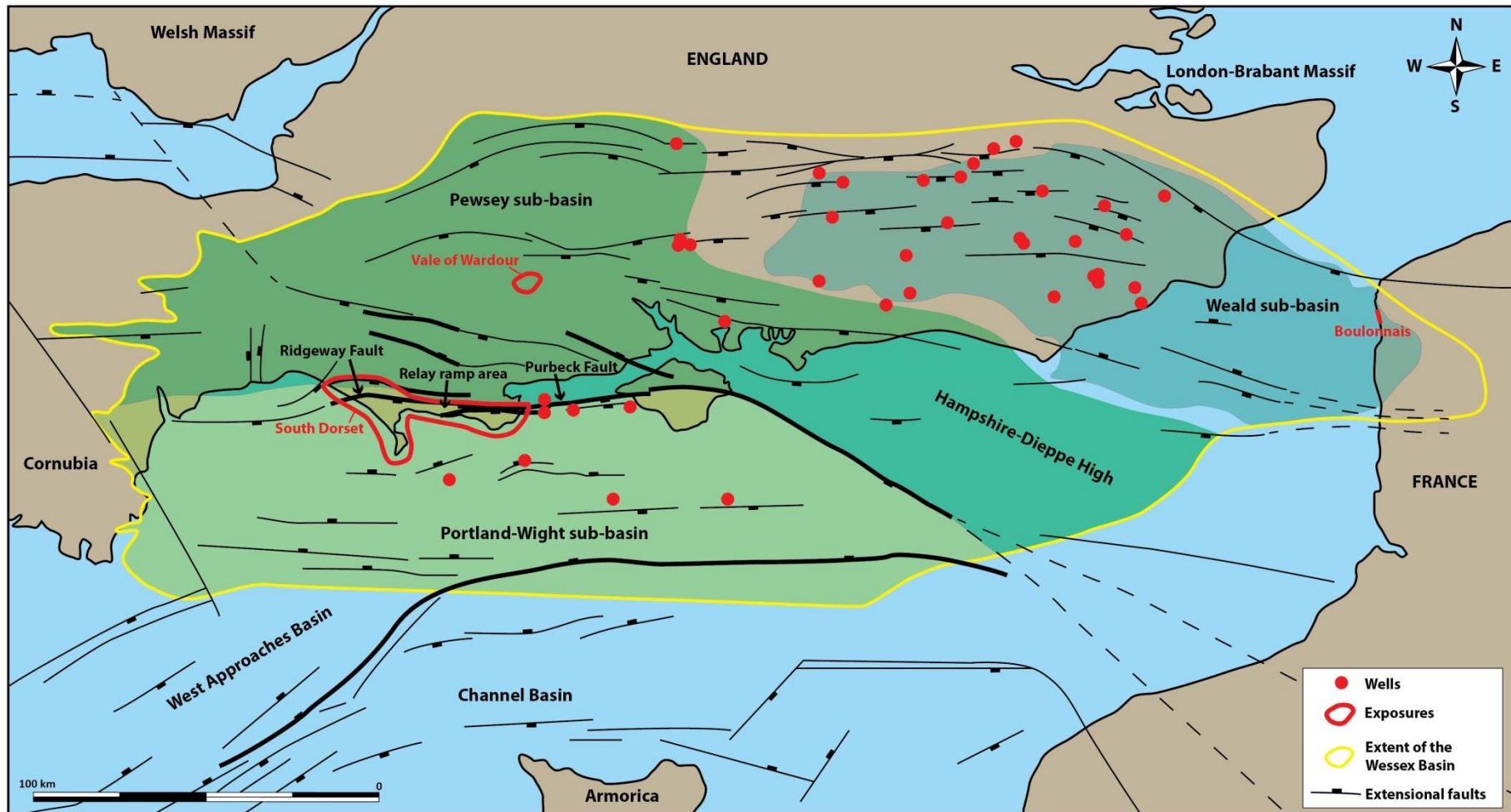
**Figure 2.1** Purbeck exposures in Europe (France, Switzerland, Germany and U.K.).

## 2. Wessex Basin

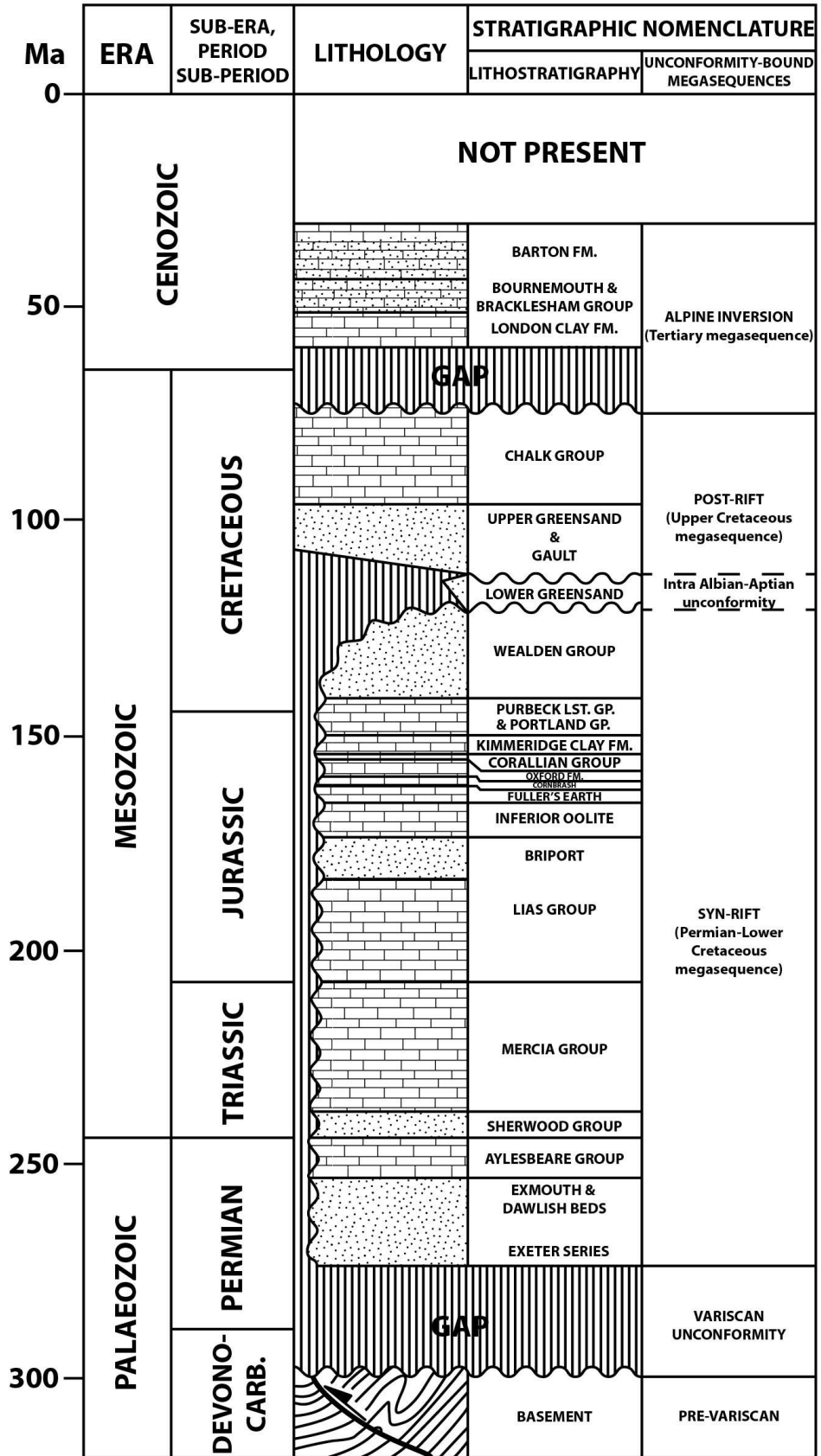
The Wessex Basin is located in southern England and northern France (Figs. 2.1 and 2.2). This basin is considered as an extensional sub-basin of a much larger system of intracratonic Mesozoic basins that covered north-western Europe (Ziegler, 1982; Underhill and Stoneley, 1998). The possible extent of the basin during Purbeck time has been suggested by several authors but still remains unclear. The extent presented in figures 2.1 and 2.2 are a compilation of information from Lake (1985), Cope *et al.* (1980), West (1992) and Underhill (2002), following intense sub-surface data analysis and fieldwork in southern England and northern France. Most of published studies (Stoneley, 1982; Allen and Wimbledon, 1991; Hamblin *et al.*,

1992; Allen *et al.*, 1998; Hawkes *et al.*, 1998; Underhill and Stoneley, 1998; Newell, 2000; Underhill, 2002) distinguished the Weald Basin from the Wessex Basin; the latter divided into two sub-basins, the Portland-Wight sub-basin to the south and Pewsey sub-basin to the north. The Weald and Wessex Basins were probably separated by the Hampshire-Dieppe High (Fig. 2.2). Some authors (Howitt, 1964; Lake, 1985; Chadwick, 1986; Cope *et al.*, 1992; Hopson *et al.*, 2008) integrate the Weald Basin as a sub-basin of the Wessex Basin (Fig. 2.2). In this study the Wessex Basin will be considered as being formed of three sub-basins; the Portland-Wight to the south-west (the subject of the thesis), the Pewsey to the north-west and the Weald to the east. This definition results from the integration and initial correlation of fieldwork studies (refer to Chapter 6 and Appendix 3) and sub-surface data interpretation (refer to Chapter 3).

Deposition in the Wessex Basin is recorded from the Permian, until the Cenozoic where deposits occur in the successor, Hampshire Basin, following Cenozoic inversion (Fig. 2.3; Underhill and Stoneley, 1998). The basin evolution can be deduced from tectonic and depositional settings recorded in these sedimentary rocks and Underhill and Stoneley (1998) defined three megasequences; the Permian-Lower Cretaceous, Upper Cretaceous and Tertiary megasequences (Fig. 2.3). The Permian-Lower Cretaceous megasequence corresponds to the syn-rift phase of the Wessex Basin and is bounded by the Variscan unconformity at the base and the Intra Aptian-Albian unconformity at the top (Fig. 2.3). This syn-rift phase is fault-controlled (faults indicated in figure 2.2) and accommodated by regional flexural subsidence (Barton *et al.*, 2011). The Upper Cretaceous megasequence corresponds to the post-rift phase of the Wessex Basin and is bounded by the Intra Albian-Aptian unconformity at the base and an Upper Cretaceous unconformity at the top (Fig. 2.3). This post-rift phase is controlled by regional flexural subsidence due to active seafloor spreading in the North Sea area (Barton *et al.*, 2011). The Cenozoic megasequence corresponds to the Alpine Inversion phase of the Wessex Basin and is bounded by an Upper Cretaceous unconformity at the base (the uppermost half of the Oligocene and Neogene are not present in the Wessex Basin, Fig. 2.3). This inversion phase is due to the distant collision of the African and European plates inverting Mesozoic extensional structures (Fig. 2.2; Barton *et al.*, 2011).



**Figure 2.2** Structural map of the Channel and Wessex Basins. The Wessex Basin is located in southern England and northern France. Extent of the Wessex Basin after Lake (1985), Cope *et al.* (1980), West (1992) and Underhill (2002). Note the thick lines identify the inverted extensional faults during the Alpine inversion (Cenozoic).



**Figure 2.3** Lithostratigraphic column for the Wessex Basin. Modified after Underhill and Stoneley (1998). Note that the Purbeck Limestone Group is grouped with the Portland Group.



### 3. Review of the Purbeck Limestone Group

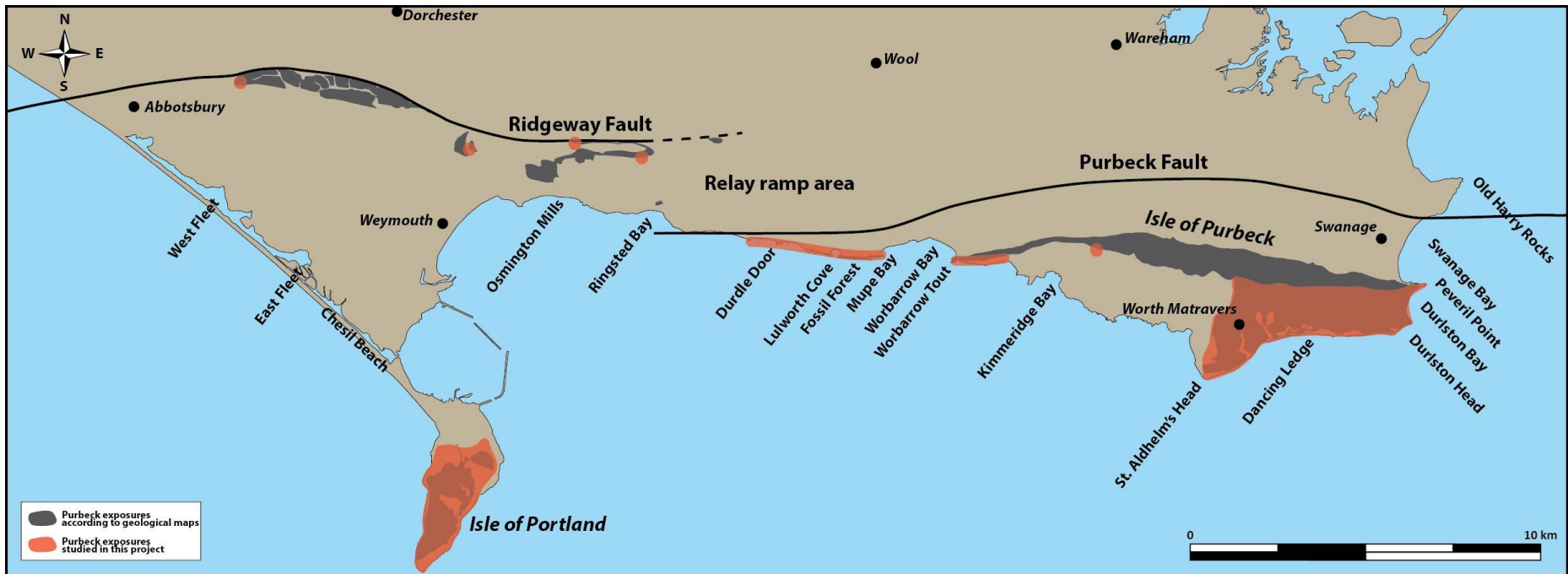
#### 3.1. Exposures in south Dorset

In this chapter, only the exposures of south Dorset (SW England) will be detailed as they are the topic of this thesis and considered as the best and most complete exposures of the Purbeck Limestone Group found in England with the type-section located in Durlston Bay (Tab. 2.1; Fig. 2.4; Clements, 1993).

Table 2.1 summarises, and figure 2.4 locates, the exposures of the Purbeck Limestone Group in south Dorset, southern England. The Purbeck rocks are particularly well exposed in south Dorset between Abbotsbury to the west and Swanage to the east (Tab. 2.1; Fig. 2.4). Although the south Dorset region is considered the best location to study the Purbeck Limestone Group, it is not continuously exposed. The accessible cliff exposures mainly result from erosion (*i.e.* cliff landslides) along the coast which has been classified as a World Heritage Site in 2001 (Dorset City Council, 2001). Apart from cliff exposures, most of the inshore outcrops are the result of quarrying either still active or at different periods in the past. Quarrying in south Dorset has occurred since Roman times (Dunning, 1949; Calkin, 1968; Edgar and Hinde, 1999; Godden, 2012) with very intense quarrying during the last millennium mainly of the underlying Portland Group (Freestone Member) for construction materials (Calkin, 1968; Godden, 2012). This quarrying provides relatively fresh surfaces through the Purbeck Limestone Group. These exposures are classified in four areas from east to west: Isle of Purbeck, Lulworth, Isle of Portland and north of Weymouth (Tab. 2.1). As a consequence the exposures studied in this project are for most of them either disused quarries or cliff faces (refer to Appendix 3 for more details).

Areas	Exposure names	Exposure types	Latitude	Longitude
North of Weymouth	Chalbury	Disused quarry	50°39'9.54"N	2°26'6.58"W
	Portesham Quarry	Disused quarry	50°40'18.03"N	2°33'8.62"W
	Poxwell Quarry	Disused quarry	50°39'3.84"N	2°21'52.12"W
	Ridgeway Road Cutting	Road cutting	50°40'7.50"N	2°27'50.03"W
Isle of Portland	Admiralty Quarry	Active quarry	50°33'22.14"N	2°25'54.17"W
	Bowers Quarry	Active and disused quarry	50°32'46.78"N	2°26'44.78"W
	Broadcroft Quarry	Active quarry	50°32'53.74"N	2°25'35.74"W
	Coombefield Quarry	Disused quarry	50°31'58.25"N	2°26'33.65"W
	Freshwater Bay	Disused quarry	50°31'51.24"N	2°26'14.83"W
	King Barrow Quarries	Disused quarry	50°33'18.61"N	2°26'10.23"W
	Mutton Cove	Disused quarry	50°32'24.90"N	2°27'11.52"W
	Penn's Weare	Disused quarry	50°32'27.46"N	2°25'35.13"W
	Perryfield Quarry	Active quarry	50°32'20.56"N	2°26'6.30"W
	Portland Bill	Disused quarry	50°30'53.20"N	2°27'31.43"W
	Sand Holes	Disused quarry	50°31'22.42"N	2°26'34.58"W
	Tout Quarry	Disused quarry	50°33'11.57"N	2°26'36.83"W
	Wallsend Cove	Cliff	50°32'2.75"N	2°27'14.87"W
Lulworth area	Dungy Head	Cliff	50°37'8.92"N	2°15'43.10"W
	Durdle Door	Cliff	50°37'16.81"N	2°16'32.01"W
	Fossil Forest	Cliff	50°36'58.37"N	2°14'23.09"W
	Lulworth Cove	Cliff	50°37'6.32"N	2°14'49.05"W
	Mupe Rocks Bay or Bacon Hole	Cliff	50°36'58.37"N	2°13'42.20"W
	Pondfield Cove	Cliff	50°36'57.12"N	2°11'4.11"W
	Worbarrow Tout	Cliff	50°36'55.95"N	2°11'11.70"W
Isle of Purbeck	Anvil Point	Disused quarry	50°35'31.77"N	1°57'29.00"W
	California Barn Quarry	Active quarry	50°35'47.71"N	1°58'31.56"W
	Dancing Ledge	Disused quarry	50°35'31.33"N	2°0'17.48"W
	Durlston Bay	Cliff	50°36'6.91"N	1°57'7.01"W
	Durlston Head	Cliff	50°35'43.58"N	1°57'3.73"W
	Fishermen's Ledge	Cliff	50°35'27.11"N	2°59'7.26"W
	Hell's Bottom	Disused quarry	50°37'11.60"N	2°6'54.88"W
	Pevenil Point	Cliff	50°36'26.24"N	1°56'39.44"W
	Seacombe Cliff	Disused quarry	50°35'22.17"N	2°1'24.78"W
	St Aldhelm's Point or Head	Cliff	50°34'43.79"N	2°3'22.29"W
	Swanworth Quarry	Active quarry	50°36'18.15"N	2°2'29.13"W
Winspit Quarry	Disused quarry	50°35'1.62"N	2°2'4.89"W	

**Table 2.1** Purbeck Limestone Group exposures in south Dorset (southern England) studied in this thesis.



**Figure 2.4** Purbeck exposures in south Dorset with location of the Ridgeway and Purbeck extensional Faults and the relay ramp area. Dark zones are after 1:50000 Geological Survey sheets 327 (Bridport), 328 (Dorchester), 341 and part of 342 (West Fleet and Weymouth) and 342 east and 343 (Swanage).

### 3.2. Lithostratigraphy

Many geologists have defined stratigraphic units of the Purbeck rocks (Tab. 2.2) since the beginning of 19<sup>th</sup> century. Woodward in 1729 was the first to label these rocks as Purbeck Stone but without a description (Tab. 2.2). The very first time the Purbeck rocks were described was in 1811 by Thomas Webster in a letter he addressed to Sir Henry Englefield in 1816 (republished and in more detail in 1826) and using some of the quarrymen's terms. These were used in later work by Fitton (1836) and Buckland and De la Bèche (1836) with some modifications. Forbes (1850) was the first to define the Purbeck sub-divisions lower, middle and upper based on the biostratigraphy of ostracods and Austen (1852) was the very first one to define the lithostratigraphy based on lithology and fossils (mainly ostracods). This scheme was slightly modified by Bristow in 1857 and is still commonly used today (Tab. 2.2; Francis, 1982, 1983, 1984, 1986; Ensom, 2010; Cope, 2012; West, 2013a).

#### 3.2.1. Group

In the 19<sup>th</sup> century the Purbeck rocks were part of the Oolitic series or Portland Oolite or Portland Purbeck (Webster, 1811 in Englefield, 1816, 1826; Damon, 1860). Later the "Purbeck Strata" were defined as the base of the Wealden Group (Fitton, 1836; Lyell, 1855). It is only in 1836 that Buckland and De la Bèche defined for the first time the Purbeck Beds as a separate stratigraphic unit. Since then the Purbeck rocks were defined either as a series as the "Purbeck" (Forbes, 1850; Brown, 1964) or the "Purbeck Beds" (Webster, 1826; Buckland and De la Bèche, 1836; Austen, 1852; Lyell, 1855; House, 1969, 1989) or the Purbeck Strata (Fitton, 1836; Fisher, 1856; Bristow, 1857; or the Purbeck Limestone (Forbes, 1850); or as a stratigraphic unit as the Purbeck Formation (Damon, 1860; Francis, 1983, 1984, 1986) or Purbeck Limestone Formation (Ensom, 1985; Cope *et al.*, 1992); or as a lithostratigraphic group as the Purbeck Group (Strahan, 1898; Arkell, 1933, 1947; Townson, 1975; Anderson, 1985; Allen *et al.*, 1998) or Purbeck Limestone Group (Clements, 1993; Westhead and Mather, 1996; Allen *et al.*, 1998; Hopson *et al.*, 2008; Ensom *et al.*, 2009; Ensom, 2010; Cope, 2012). The latest review of lithostratigraphy of this unit is by Westhead and Mather (1996) who, following Clements (1993), used the term Purbeck Limestone Group and their lithostratigraphic terms are used in this thesis (Tab. 2.2).

### **3.2.2. Formations**

Casey (1963) defined the two main sub-divisions based on the position of the Jurassic-Cretaceous boundary at the base of the Cinder Bed. The Lulworth Beds in the lowermost half and in the Jurassic part and the Durlston Beds in the uppermost half and in the Cretaceous part (Tab. 2.2). These were relabelled later by Townson (1975) as Lulworth Formation and Durlston Formation. The exact location of this boundary between the systems remains an important debate since the beginning of the 19<sup>th</sup> century. This is mainly due to the absence of biostratigraphically useful fossils (such as ammonites or brachiopods). The only fossils found in the Purbeck rocks are ostracods and molluscs, characteristic of Late Jurassic – Early Cretaceous times (refer to section 3.3 of this chapter for more detailed about Jurassic-Cretaceous boundary). The type-section is located in Durlston Bay and was described for the first time in details by Clements (1993) focusing on the middle and upper parts of the Purbeck rocks.

### **3.2.3. Members**

Westhead and Mather (1996) defined five members (Tab. 2.2), three in the Lulworth Formation and two in the Durlston Formation, and based on lithological and palaeontological content to simplify correlation from the west to the east side of all of the Wessex Basin. The Lulworth Formation is divided into the Mupe Member, Ridgeway Member and Worbarrow Tout Member while the Durlston Formation is divided into the Stair Hole Member and the Peveril Point Member (Tab. 2.2).

### **3.2.4. Beds**

Bristow (1857) was the first to name the individual beds, many of which are still in use today and in this study (Tab. 2.2). The integration of those bed names in Westhead and Mather's (1996) Members is described here. The Mupe Member groups the Caps and Dirt Beds, Broken Beds and the lowermost half of the Cypris Freestone. The Ridgeway Member groups the uppermost half of the Cypris Freestone. The Worbarrow Tout Member groups the Hard Cockle Beds, Soft Cockle Beds, Marly Freshwater Beds and Cherty Freshwater Beds. The Stair Hole Member groups the Cinder Bed, Intermarine Beds, Scallop Beds, Corbula Beds and Chief Beef Beds. The Peveril Point Member regroups the Broken Shell Limestone, Unio Bed and Upper Cypris Clays and Shales. This scheme is followed in this thesis with integration of

Francis' work (1982, 1983, 1984, 1986) on palaeosols of the lower part of the Mupe Member and West (2016) on the identification and definition of a Transition Bed located directly above the Portland Group and at the very base of the Purbeck Limestone Group. Francis (1982) defines for the lower part of the Mupe Member the Lower Skull Cap (Basal Cast Bed of Arkell, 1941 and Transition Bed of West, 2013*a*), Basal Dirt Bed, Upper Skull Cap, Lower Dirt Bed, Hard Cap, Great Dirt Bed and Soft Cap (Tab. 2.2). Later Francis (1983, 1984, 1986) grouped the three first beds into the Skull Cap.

Period	Webster 1811	Webster 1826	Fitton 1827	Buckland and De la Beche 1836	Forbes 1849	Austen 1852	Lyell 1855	Fisher 1856	Bristow 1857	Damon 1860	Strahan (with Wallis) 1898	Arkell 1933, 1947	Casey 1963	Brown 1964 (a & b)	House 1969, 1989	Townson 1975	Cope et al. 1980
Cretaceous	Purbeck Shell Limestone	Purbeck marble			Upper	Cypris Shales		Paludina clays	Paludina Clays	Upper Purbeck	Upper Purbeck	Upper Purbeck		Upper Purbeck			
	Purbeck stone					Marble Bands		Cypris shales & clays	Upper Cypris Clays & shales	Upper Purbeck	Marble Beds	Viviparus Clays		Upper Purbeck			
Jurassic	Portland Oolite or Purbeck Portland	Portland Formation			Middle	Unio beds		Marble Bands	Unio Beds with Crocodile Bed	Upper Purbeck	Unio-bed	Marble Shales and Ostracod Shales		Unio Beds			
	Clay with Gypsum					Comminuted Shell limestone		Unio beds	Upper Broken Shell Limestone (Soft Burr)	Upper Purbeck	Broken shell limestone (Burr)	Broken Shell Limestone		Upper Broken-shell Limestone			
						Beef beds		Chief Beef Beds	Chief Beef Beds	Middle Purbeck	Chief Beef Beds	Chief Beef Beds		Chief Beef Beds			
						Corbula Beds		Corbula Beds	Corbula Beds	Middle Purbeck	Corbula Beds	Corbula Beds		"Corbula" Beds			
						Pecten beds		Scallop Beds (White Roach)	Scallop Beds	Middle Purbeck	Scallop Beds	Scallop Beds		Scallop Beds			
						Turtle beds		Intermarine Lining or Leaning Vein Royal Freestone Vein Downs Vein	Intermarine Beds	Middle Purbeck	Intermarine Beds	Intermarine Beds		Intermarine Beds			
						Cinder		Cinder Bed	Cinder	Middle Purbeck	Cinder	Cinder Bed		Cinder Bed			
						Chert Beds		Cherty Freshwater	Feather Quarry New Vein	Middle Purbeck	Cherty Freshwater	Cherty Freshwater Beds		Cherty Freshwater Beds			
						Marly Beds		Marly Freshwater	Marly Freshwater	Middle Purbeck	Mammal Bed	Mammal Bed		Marly Freshwater Beds			
						Insect beds		Upper Insect beds	Upper Insect beds	Middle Purbeck	Insect Beds	Insect Beds		Soft Cockle Beds			
								Soft cockle beds	Soft Cockle Beds	Middle Purbeck	Soft-Cockle Beds	Soft-Cockle Beds		Hard Cockle Beds			
								Hard cockle beds	Hard Cockle Beds	Middle Purbeck	Hard-Cockle Beds	Hard-Cockle Beds		Hard Cockle Beds			
								Lower Insect beds	Lower Insect beds	Middle Purbeck	Lower Insect-bed	Lower Insect-bed		Hard Cockle Beds			
								Cypris Freestone	Cypris Freestone	Middle Purbeck	Cypris Freestone	Cypris Freestone		"Cypris" Freestones			
								Broken bands	Broken bands	Middle Purbeck	Broken bands	Broken Bands		Broken Beds			
								Cypris Limestone	Cypris Limestone	Middle Purbeck	Cypris Freestone Sandy Partings	Cypris Freestone		Broken Beds			
								Chert beds	Chert beds	Middle Purbeck	Soft Burr or Soft Cap	Soft Burr		Marls and Slatts			
								Dirt-bed	Dirt-bed	Middle Purbeck	Soft Cap or Burr	Aish		Bacon Tier			
								Great dirt-bed	Great Dirt-Bed	Middle Purbeck	Great Dirt-Bed	Great Dirt Bed		Aish			
								Cap	Cap or Top cap or Hard Cap	Middle Purbeck	Hard Cap or Top cap	Top Cap or Hard Cap		Soft Burr			
									Lower Dirt-Bed	Middle Purbeck	Lower Dirt Bed	Lower Dirt Bed		Great Dirt Bed			
									Skull Cap	Middle Purbeck	Skull Cap	Skull Cap		Top Cap or Hard Cap			
									Dirt bed	Middle Purbeck	Dirt bed	Skull Cap		Lower Dirt Bed			
										Middle Purbeck				Basal Beds			
										Middle Purbeck				Hard Cap			
										Middle Purbeck				Dirt Bed			
										Middle Purbeck				Bottom Rubble			
										Middle Purbeck				Black Dirt Bed			
										Middle Purbeck				Top Cap			
										Middle Purbeck				Black Dirt			
										Middle Purbeck				Skull Cap			

**Table 2.2** Lithostratigraphical classification and comparison over time since the 19<sup>th</sup> century until today. Note that the Purbeck Limestone Group was primarily divided into lower, middle and upper until Casey (1963), and considered to be part of the Portland Oolite (Webster, 1811 in Englefield, 1816) or Portland Group (Webster, 1826) and then part of the Wealden Group (Fitton, 1827 in Fitton, 1836; Lyell, 1855) until Fisher (1856) who defined the Purbeck Strata as a different unit.

Francis, 1982, 1983, 1984, 1986		Anderson 1985		Ensom 1985		Clements 1993		Wimbledon 1995		Westhead & Mather 1996		Allen 1998		Hopson <i>et al.</i> 2008		Ensom <i>et al.</i> 2009 & Ensom 2010		Cope 2012		This study			
Purbeck Formation	Upper Purbeck Formation?	Upper Purbeck		Upper and upper Middle Purbeck Beds		"Upper" Purbeck		Upper Purbeck		Peveril Point Member		Upper Purbeck		Peveril Point Member		Upper Purbeck Beds		Upper Purbeck		Peveril Point Member			
	Middle Purbeck Formation?																					Middle Purbeck	Middle Purbeck
Purbeck Formation	Lower Purbeck Formation or Basal Purbeck Formation	Lower Purbeck		Lower Middle and Lower Purbeck Beds		"Lower" Purbeck		Lower Purbeck		Lulworth Formation		Lower Purbeck		Lulworth Formation		Lower Purbeck Beds		Lower Purbeck		Lulworth Formation			
	Beds above not described																					Upper Cypris Clays and shales, with Marbles	Upper "Cypris" Clays and Shales Member
Purbeck Formation	Soft Cap	Hard and Soft Caps		Caps, Broken and Dirt Beds		"Cypris" Freestone and Hard Cockle Member		Broken Beds Member		?		Mupe Member		Mupe Member		Dirt beds		Caps Member		Broken beds and Caps		Mupe Member	
	Great Dirt Bed																						
Purbeck Formation	Hard Cap	Hard and Soft Caps		Caps, Broken and Dirt Beds		"Cypris" Freestone and Hard Cockle Member		Broken Beds Member		?		Mupe Member		Mupe Member		Dirt beds		Caps Member		Broken beds and Caps		Mupe Member	
	Lower Dirt Bed																						
Purbeck Formation	Upper Skull Cap	Hard and Soft Caps		Caps, Broken and Dirt Beds		"Cypris" Freestone and Hard Cockle Member		Broken Beds Member		?		Mupe Member		Mupe Member		Dirt beds		Caps Member		Broken beds and Caps		Mupe Member	
	Basal Dirt Bed																						
Purbeck Formation	Lower Skull Cap	Hard and Soft Caps		Caps, Broken and Dirt Beds		"Cypris" Freestone and Hard Cockle Member		Broken Beds Member		?		Mupe Member		Mupe Member		Dirt beds		Caps Member		Broken beds and Caps		Mupe Member	
	Basal Dirt Bed																						
Purbeck Formation	Lower Skull Cap	Hard and Soft Caps		Caps, Broken and Dirt Beds		"Cypris" Freestone and Hard Cockle Member		Broken Beds Member		?		Mupe Member		Mupe Member		Dirt beds		Caps Member		Broken beds and Caps		Mupe Member	
	Transition Bed																						

Table 2.2 Continued. Note the bed names to be used in this study are in the last column on the right.



### 3.3. Biostratigraphy

The biostratigraphy of the Purbeck Limestone Group is mainly based on ostracods as they represent the more abundant microfossils identifiable in these beds with biostratigraphic value (Anderson and Bazley, 1971; Anderson, 1985; Clements, 1993; Horne, 1995, 2002). However other studies proposed biostratigraphy of the Purbeck Limestone Group based on less abundant fossils such as palynomorphs (Norris, 1969, 1970; Hunt, 1985, 2004).

Ostracod biostratigraphy has been recognised for over more than a century with the first ostracods identified in the Purbeck limestones by Forbes (1850). More recent studies, by Anderson (1985) and later revised by Horne (1995, 2002), defined more precisely the biostratigraphy of the Purbeck Limestone Group (Tabs. 2.3, 2.4 and 2.5). Anderson (1985) is the most prolific contributor with the definition of 4 ostracod zones, 6 assemblages and 40 faunicycles for the Purbeck Limestone Group. Although this classification is strongly criticised by Horne (1995) due to the difficulty in identifying the stratigraphic horizons these assemblages and faunicycles correspond to, this scheme remains the most complete. Anderson's (1985) ostracod zones are based on the dominant species found with, from bottom to top, the *Cypridea dunkeri*, *Cypridea granulosa*, *Cypridea vidana* and *Cypridea setina* zones (Tab. 2.3). Horne (1995) revised the ostracod biostratigraphy and defined new zones and subzones for the Purbeck-Wealden of England (Tab. 2.3). Horne's (1995) biostratigraphy for the Purbeck consists of the *Theriosynocum forbesi* zone divided into three subzones from bottom to top: *Cypridea dunkeri* (Tab. 2.3; same as Anderson, 1985); *Cypridea granulosa* (Tab. 2.3; comprises *Cypridea granulosa* and the lowermost part of the *Cypridea vidrana* zone of Anderson, 1985); and *Cypridea propunctata* (Tab. 2.3; comprises uppermost part of *Cypridea vidrana* and *Cypridea setina* zones of Anderson, 1985). The assemblages are based on similar ostracod assemblages and are simply numbered from 1 for the lowermost to 7 for the uppermost (Tab. 2.3). The faunicycles are based on the association of Anderson's definition of C-phase (for *Cypridea* species) and S-phase ostracods (for non-*Cypridea* species), and are both named and numbered (Tab. 2.3). According to Anderson (1985) the C-phase corresponds to a group of ostracod species living in mainly freshwater conditions (however not pure freshwater), while the S-phase corresponds to a group of ostracod species living rather more saline water conditions (however not fully marine). Even if not stated clearly by Anderson, the names given to each faunicycle seem to correspond to the place where the greatest quantity of ostracod carapaces was collected. The exact boundaries of stratigraphic horizons for each faunicycle remain unclear as no thickness or detailed lithostratigraphy are defined by

Anderson (1985). More recently Horne (2002) shows that the Purbeck ostracod faunas have modern day equivalents living in non-marine settings: the superfamilies Cypridoidea (*Cypridea sensu lato* and *Mantelliana*), Cytheroidea (*Theriosynoecum* and *Timiriasevia*) and Darwinuloidea (*Darwinula*). The Purbeck ostracods are since considered as non-marine species (Horne, 2002).

Ostracod zones (Anderson, 1985)	Ostracod zones and subzones (Horne, 1995)		Assemblages (Anderson, 1985)	Main species in assemblages	Faunicycles (Anderson, 1985)	Lithostratigraphy	
	Zone	Subzones					
<i>Cypridea setina</i>		<i>Cypridea propunctata</i>	7 up		Battle <sup>40</sup>	Upper Cypris Clays and Shales	
			6	<i>Cypridea propunctata</i> <i>Cypridea setina</i> <i>Cypridea wicheri</i>	Tyneham <sup>39</sup>		Upper Broken Shell Limestone
					Durdle <sup>38</sup>		
					Tisbury <sup>37</sup>		
					Brede <sup>36</sup>		
					Mupes <sup>35</sup>		
					Lulworth <sup>34</sup>		
<i>Cypridea vidrana</i>			5	<i>Cypridea amisia</i> <i>Cypridea vidrana</i>	Greenwood <sup>33</sup>	Chief Beef Beds	
					Poxwell <sup>32</sup>		? — — ? — — ? —
					Bacon <sup>31</sup>		Corbuja Beds
					Studland <sup>30</sup>		? — — ? — — ? —
					Scallop <sup>29</sup>		Scallop Beds
					Langton <sup>28</sup>		Intermarine Beds
					Worth <sup>27</sup>		
Corfe <sup>26</sup>							
<i>Cypridea granulosa</i>	<i>Theriosynoecum forbesi</i>	<i>Cypridea granulosa</i>	4	Maximum of <i>Cypridea granulosa</i>	Royal <sup>25</sup>	Cinder Bed	
					Croydon <sup>24</sup>		
					Nothe <sup>23</sup>		
					Cinder Beds <sup>22</sup>		
					Peveril <sup>21</sup>		Cherty Freshwater Beds
					Durlston <sup>20</sup>		? — — ? — — ? —
					Netherfield <sup>19</sup>		
<i>Cypridea dunkeri</i>			3	<i>Cypridea dunkeri</i> <i>Cypridea granulosa</i>	Swanage <sup>18</sup>	Marly Freshwater Beds	
					Ashdown <sup>17</sup>		
					Goldspur <sup>16</sup>		
					Mountfield <sup>15</sup>		
					Burwash <sup>14</sup>		
					Robertsbridge <sup>13</sup>		
					Ringstead <sup>12</sup>		
<i>Cypridea dunkeri</i>			2	<i>Cypridea dunkeri</i> dominant in C-phase <i>Fabarella boloniensis</i> dominant in S-phase	Penshurst <sup>11</sup>	Soft Cockle Beds	
					Upper Soft Cockle <sup>10</sup>		
					Lower Soft Cockle <sup>9</sup>		
					Wardour <sup>8</sup>		
					Hard Cockle <sup>7</sup>		Hard Cockle Beds
					Upwey <sup>6</sup>		Cypris Freestone
					Swindon <sup>5</sup>		
			1	<i>Cypridea</i> sp. rare, mainly S-phase species	Stair <sup>4</sup>	Broken Beds ? — — ? — — ? —	
					Ridgeway <sup>3</sup>		
					Warren <sup>2</sup>		
					Quinton <sup>1</sup>		Caps and Dirt Beds

**Table 2.3** Ostracod biostratigraphy of the Purbeck Limestone Group. Lithostratigraphy following the definition in table 2.1 and in use in this study.

Following Anderson's (1985) definition, the assemblage and faunicycles corresponding to the Mupe Member, and of interest for this study, is the assemblage number 1 composed of the faunicycles 1 to 4 and the lower part of the assemblage number 2 with the faunicycle 5 (Tabs. 2.3 and 2.5). The assemblage 1 is mainly characterised by S-phase species such as *Macrodentina* and *Wolburgia* and rare occurrence of C-phase species such as *Cypridea dunkeri*, *Cypridea primavera* and *Cypridea tumescens* (Tabs. 2.3 and 2.5; Anderson and Bazley, 1961; Anderson, 1985). One of the main problems with Anderson's faunicycle for this study is that the collected ostracods come mainly from locations outside of Dorset (see details below for each faunicycle relevant to this study). Even when ostracods constituting a faunicycle were collected from Dorset there is no quantitative indication on sampling locations. The faunicycle 1 (Quinton) corresponds in the stratigraphy to the lowermost beds of the Mupe Member comprising the lowermost part of the Caps and Dirt Beds but there is no precision as to the exact beds considered (Tab. 2.3). This first faunicycle is based on collection and identification of 5485 specimens from the Wiltshire at Swindon and in the Buckinghamshire at Aylesbury (Anderson, 1985). The faunicycle 2 (Warren) comprises the uppermost Caps and Dirt Beds but again there is no exact location of the beds considered (Tabs. 2.3 and 2.5). This second faunicycle is based on collection and identification of 2814 specimens from Wiltshire at Swindon, Buckinghamshire at Aylesbury and Dorset at Poxwell Quarry and White Nothe (Tab. 2.5; Anderson, 1985). The faunicycle 3 (Ridgeway) comprises the lowermost part of the Broken Beds (Tabs. 2.3 and 2.5). This third faunicycle is based on collection and identification of 1107 specimens from Wiltshire at Swindon, Buckinghamshire at Aylesbury and Dorset at Poxwell Quarry (Anderson, 1985). The faunicycle 4 (Stair) comprises the uppermost part of the Broken Beds (Tab. 2.3). This fourth faunicycle is based on collection and identification of 72 specimens from Wiltshire at Swindon, Sussex at Henfield borehole and Dorset at Poxwell Quarry, Portesham Quarry and White Nothe (Anderson, 1985). The assemblage 2 is mainly characterised by S-phase species and is made of 7 faunicycles (of which only the first one will be described here as it probably corresponds to the top of the Mupe Member; Tab. 2.3). The faunicycle 5 (Swindon) comprises the lowermost part of the Cypris Freestone. This faunicycle is made of S-phase species such as *Fabanella boloniensis* and *Mantelliana purbeckensis* (constituting 75% of the fauna) and rare occurrence of C-phase species such as *Cypridea dunkeri*, *Cypridea primavera* and *Cypridea tumescens* (Tab. 2.3; Anderson and Bazley, 1961; Anderson, 1985). This fifth faunicycle is based on collection and identification of 32 specimens from Sussex at Mountfield, Henfield borehole, Broadoak borehole and Fairlight borehole, and Dorset at Durlston Bay (Anderson, 1985).

Palynomorph studies and identification were first conducted by Couper (1958) and Lantz (1958) but their biostratigraphic value was first recognised by Norris (1969, 1970). Norris (1969) defined for the Upper Jurassic and Lower Cretaceous of southern England several assemblages, within three biozone suites named A, B and C (Tab. 2.4). Each suite is defined by appearance of a new species and these suites are recorded from the upper part of the Kimmeridge Clay Formation until the top of the Purbeck Limestone Group in Dorset. A limitation of this classification is in the difference between suites and assemblages. In fact Norris (1969, 1970) does not detail what assemblages are compared to suites as both are characterised by groups of palynomorph species. The only difference seems to lie in the number of species that is lower in the assemblages than in the suites.

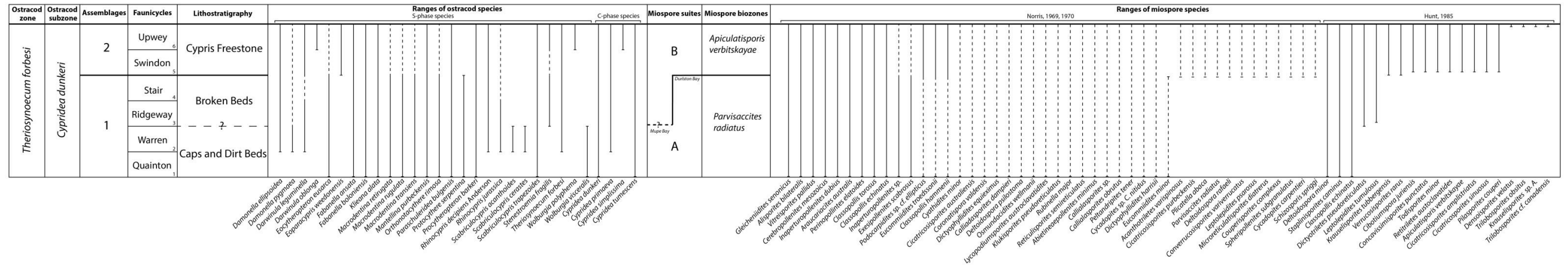
Lithostratigraphy			Miospore suites after Norris (1969)	Miospore biozones after Hunt (1985)	
Purbeck Limestone Group	Durlston Formation	Peveril Point Mb.	C		
		Stair Hole Mb.		B	<i>Matonisporites elegans</i>
	Lulworth Formation	Worbarrow Mb.	A		<i>Apiculatisporis verbitskayae</i>
		Ridgeway Mb.			A
	Mupe Mb.	- ? - Mupe Bay	Durlston Bay		
Portland Group			A		

**Table 2.4** Miospore biostratigraphy after Norris (1969, 1970) and Hunt (1985). Lithostratigraphy as defined in table 2.2. Note the boundary between suites A and B is well defined in Durlston Bay while in Mupe Bay the base of the suite B was not found due to rare occurrence of misopores (Norris, 1969). This boundary seems to be younger in Mupe Bay than in Durlston Bay.

The Purbeck Limestone Group comprises the very uppermost part of suite A and the whole suites B and C (Tab. 2.4; Norris, 1969). The relative abundance of palynomorph species in each suite is defined as *persistent* when a species constitutes more than 50% of the constituent samples in a suite; and *spasmodic* when a species constitutes less than 50% of the constituent samples in a suite (Norris, 1969, 1970). The samples studied by Norris (1969) are dominated by *Classopollis torosus* or *Inaperturopollenites dubius* that constitute together more than 70% of the total spore-pollen flora (Norris, 1969, 1970). These two species are recorded to dominate (up to 90%) of the assemblages in the lower part of the Mupe Member (*i.e.* gypsiferous beds according to Norris, 1970 lateral equivalent of the Caps and Dirt Beds in this study). The suite A is made of 32 species (11 persistent and 21 spasmodic) listed in table 2.5 with assemblages containing between 10 and 15 species (Norris, 1969). This first suite is characterised essentially by coniferalean miospores with few occurrence of filicalean, lycopsid and petridophytic species (Norris, 1969, 1970). The suite B is made of 44 species (12 persistent and 32 spasmodic) listed in table 2.5 with assemblages containing normally less than 10 species but can be up to 22 species (Norris, 1969). This second suite is essentially characterised by coniferalean spores still abundant, pteridophytic spores becoming more abundant and bryophytic spores decreasing (Norris, 1969, 1970). This reflects restricted flora diversity developing around lagoons and/or along coastal environments (Norris, 1969, 1970). This suite B differs from suite A with the appearance of rarely occurring 10 species also listed in table 2.5 (Norris, 1969). The suite C is made of 77 species (24 persistent and 53 spasmodic) with assemblages containing normally between 15 and 30 species and can be down to 4 or up to 42 species (Norris, 1969). This third suite is still essentially characterised by coniferalean, and pteridophytic spores remaining important as well (Norris, 1969, 1970). This suite differs from suite B with the appearance of rarely occurring 32 species also listed in table 2.5 (Norris, 1969). The other limitation of this classification concerns the palaeoecological value of these suites or assemblages. Norris (1969, 1970) did not detail palaeoenvironments where the plants were living that produced the pollen and spore.

Norris' classification was later revised, completed with new species and interpreted in terms of palaeoecology by Hunt (1985). Hunt defined three new biozones slightly different to that of Norris (1969, 1970) and based on first occurrence of taxa (Tab. 2.5). This was possible, due to low diversity of incoming taxa (Hunt, 1985). These are the *Parvisaccites radiatus* Biozone replacing suite A of Norris (1969), the *Apiculatisporis verbitskayae* Biozone and the *Matonisporites elegans* Biozone together replacing suite B of Norris (1969) (Hunt, 1985) and the characteristic taxa constituting these biozones are listed in table 2.5. The dominated

miospores in the upper part of the *Parvisaccites radiatus* Biozone (*i.e.* the Mupe Member, Tabs. 2.4 and 2.5) and the *Apiculatisporis verbitskayae* Biozone is *Classopollis* with the appearance of bisaccates in *Apiculatisporis verbitskayae* Biozone (Hunt, 1985). In the *Matonisporites elegans* Biozone the miospore diversity increases and is dominated by bisaccates, *Inaperturopollenites*, *Spheripollenites*, *Classopollis*, *Cerebropollenites* and spores (Hunt, 1985). According to Hunt (1985) assemblages dominated by *Classopollis* microfloras (in the Lulworth Formation) reflecting a regional xerophytic (*i.e.* semi-arid to arid) vegetation dominated by Cheirolepidiaceae (*i.e.* ancient conifers). This was also suggested by the identification of semi-arid climate sedimentological (West, 1975) and palaeontological features (Francis, 1983) in the lower part of the Muper Member. West (1975) interpreted semi-arid conditions with the formation of gypsum and halite from hypersaline brines (refer to section 3.7.2 of this chapter for complete description). Francis (1983) identified the ancient conifers *Protocupressinoxylon purbeckensis* and interpreted their growth to have occurred under arid to semi-arid climate (refer to sections 3.5.1.1.3 and 3.7.1 of this chapter for complete description). Similarly Hunt (1985) interpreted assemblages dominated by *Spheripollenites* and *Inaperturopollenites* microfloras (in the Durlston Formation) to reflect still semi-arid conditions but more humid than the Lulworth Formation. This was suggested due to the concomitance of freshwater mollusca together with halite pseudomorphs and mudcracks (Hunt, 1985). This change from arid to semi-arid climate in the Lulworth Formation to arid but more humid climate in the Durlston Formation (Hunt, 1985) was previously suggested by Vakhrameev (1970) and Sladen and Batten (1984).



**Table 2.5** Correlation of ostracod biostratigraphy and miospore biostratigraphy for the Mupe Member of the Purbeck Limestone Group of Dorset. Ostracod zones after Horne (1995) and ostracod subzones after Anderson (1985) and Horne (1995). Ostracod assemblages and faunicycles after Anderson (1985). Ranges of ostracod species after compilation of Anderson (1985) and Horne (1995) ostracod identification. Miospore suites after Norris (1969, 1970). Miospore biozones after Hunt (1985). In the ranges of ostracod species plain lines illustrate occurrence of the species while dashed lines correspond to likely occurrence. In the ranges of miospore species plain lines correspond to *persistent* species and dashed lines correspond to spasmodycally occurring species (see text for details).

### 3.4. Chronostratigraphy

The dating of the deposition time of the Purbeck Limestone Group is still controversial mainly due to the low faunal diversity with biostratigraphic value (ostracods, molluscs gastropods and bivalves, trees, cycads, and pollens). The top of the underlying Portland Group is dated from the Tithonian with *Titanites giganteus* ammonites (Spath, 1931) and the base of the overlying Wealden Group in the past was dated as Berriasian because of transgression recorded in Europe at that time (Kirkaldy, 1937; Arkell, 1947). This gives a Tithonian-Berriasian age for the deposition of the Purbeck rocks, and consequently somewhere within this Group lies the Jurassic-Cretaceous boundary. This boundary was long considered to be located at the base of the Cinder Bed, an oyster-rich deposit marking an important marine incursion in southern England into otherwise non-marine strata (Casey, 1963; Cope and Clements, 1969; Cope *et al.*, 1980). This Cinder Bed is considered as synchronous to the deposition of nodule-bed in Lincolnshire and East Anglia, the deposition of the Speeton Clay in Yorkshire, the Serpulite transgression in Poland and Germany and Ryazanian transgression of Russia (Casey, 1963). However numerous authors during the colloquium on the Jurassic-Cretaceous boundary in 1973 (Mémoires du BRGM no.86, Anon, 1975) stated that the Jurassic-Cretaceous boundary should be approximately at the base of the *Berriasella jacobi* ammonite zone of the Berriasian as equivalent in Durlston Bay to the Cypris Freestone because palynomorphs and ostracods are equivalent of the *Pseudosubalpines grandis* ammonite subzone (at the base of the *Berriasella jacobi* zone). Allen and Wimbledon (1991) used this definition and showed that the deposition of the Purbeck rocks occurred mainly during the Berriasian, lowering significantly the Jurassic-Cretaceous boundary to the lower part (base of the Cypris Freestone) of the Purbeck Limestone Group. This is partly confirmed by Hunt (1985) and Wimbledon and Hunt (1983) with palynological studies that place the Berriasian-Valanginian boundary at the top of the Purbeck.

The most recent studies were compiled by Wimbledon (2008) and Grabowski (2011) integrating magnetostratigraphy, palynomorphs and ostracod assemblages. The magnetostratigraphy of the Jurassic-Cretaceous boundary is defined in Berrias (Ardèche, France) to be between the M19r and M18n magnetic polarity zones (Galbrun *et al.*, 1986). Palaeomagnetic measurements on samples from the type-section in Durlston Bay indicate that the M18n level (base of Berriasian) is located in the Worbarrow Tout Member in the lower part of the Soft Cockle Beds (Fig. 2.5; Wimbledon, 2008). The base of the Berriasian remains in the lower part of the Purbeck Limestone Group but moves the previous Jurassic-Cretaceous



boundary proposed by Allen and Wimbledon (1991), defined at the base of the Cypris Freestone, up to the lower part of the Soft Cockle Beds (Fig. 2.5).

This study focuses on the lower part of the Mupe Member, consequently the determination of the time interval for deposition was done for the Mupe and Ridgeway Members (Tab. 2.2) because Wimbledon's (2008) magnetostratigraphy takes into account the beds rather than the members (Fig. 2.5). Wimbledon's (2008) magnetostratigraphy coupled with Grabowski's (2011) detailed palaeomagnetic polarities for the western Tethys, and the Channell *et al.* (1995), Gradstein *et al.* (2004) and Tominaga and Sager (2010) dating of magnetic sequence intervals is presented in figure 2.5. This allows determination of deposition periods for the Purbeck Limestone Group of about 8 My (minimum of 6.7 My and maximum of 9 My with a standard deviation of about 1.1 My, Fig. 2.5); the Caps and Dirt Beds together of about 415,000 years (minimum of 350,000 years and maximum of 515,000 years with a standard deviation of about 88,500 years, Fig. 2.5); the Cypris Freestone beds of about 465,000 years (minimum of 300,000 years and maximum of 620,000 years with a standard deviation of about 160,000 years, Fig. 2.5); and the Mupe and Ridgeway Member together of about 880,000 years (minimum of 650,000 years and maximum of 1.1 My with a standard deviation of about 245,00 years, Fig. 2.5).

		Stratigraphy		Polarity		Numerical time scale (My)			Average deposition times (years)																						
						CENT95	GR2004	TS2010																							
Cretaceous	Val.	Wealden Group		M12A	n	133.73	138.78	137.53	Purbeck Limestone Group: 7,960,904 (σ=1,122,141)																						
					r	133.99	139.03	137.75																							
					n	134.08	139.12	137.87																							
					r	134.27	139.29	138.04																							
		Peveril Point Member		Upper Cypris Shales	M14	n	134.53	139.53				138.40																			
					r	134.81	139.77	138.57																							
				Unio Beds		n	135.57	140.36				139.13																			
				Broken Shell Limestone	M15	r	135.96	140.66				139.49																			
				Chief Beef Beds		n	136.49	141.05				139.94																			
				Corbula Beds	M16	r	137.85	142.06				141.75																			
Jurassic	Berriasian	Purbeck Limestone Group				138.50	142.55	142.32	Purbeck Limestone Group: 7,960,904 (σ=1,122,141)																						
						138.89	142.84	142.73																							
		Stair Hole Member		Intermarine Beds	M17	n	138.89	142.84				142.73																			
				Cinder Bed		r	140.51	144.04				144.13																			
				Cherty Freshwater Beds	M18	n	141.22	144.57				144.64																			
				Marly Freshwater Beds		r	141.63	144.88				145.20																			
				Soft Cockle Beds		n	141.78	144.99				145.43																			
				Hard Cockle Beds	M19	r	141.88	145.06				145.60																			
				Cypris Freestone		n	143.07	145.95				146.18																			
				Cap beds & Dirt Beds		r	143.36	146.16				146.42																			
Jurassic	Tithonian	Purbeck Limestone Group				143.77	146.47	146.87	<b>CF: 463,323</b> (σ=159,384) <b>MRM: 877,910</b> (σ=243,954) <b>CDB: 414,587</b> (σ=88,451)																						
						143.84	146.52	147.02																							
		Ridg. Mb.				143.84	146.52	147.02																							
		Mupe Mb.				143.84	146.52	147.02																							
						144.70	147.16	147.46																							
		Portland Group		M20	n	143.84	146.52	147.02	<table border="1"> <thead> <tr> <th></th> <th>CENT95</th> <th>GR2004</th> <th>TS2010</th> </tr> </thead> <tbody> <tr> <td>Purbeck LG</td> <td>8,951,750</td> <td>6,742,385</td> <td>8,188,577</td> </tr> <tr> <td>Mupe+Ridgeway</td> <td>1,137,196</td> <td>843,617</td> <td>652,918</td> </tr> <tr> <td>Cypris Freestone</td> <td>621,829</td> <td>465,065</td> <td>303,076</td> </tr> <tr> <td>Cap beds &amp; Dirt Beds</td> <td>515,367</td> <td>378,552</td> <td>349,842</td> </tr> </tbody> </table>				CENT95	GR2004	TS2010	Purbeck LG	8,951,750	6,742,385	8,188,577	Mupe+Ridgeway	1,137,196	843,617	652,918	Cypris Freestone	621,829	465,065	303,076	Cap beds & Dirt Beds	515,367	378,552	349,842
	CENT95	GR2004	TS2010																												
Purbeck LG	8,951,750	6,742,385	8,188,577																												
Mupe+Ridgeway	1,137,196	843,617	652,918																												
Cypris Freestone	621,829	465,065	303,076																												
Cap beds & Dirt Beds	515,367	378,552	349,842																												

**Figure 2.5** Magnetostratigraphy and interval dating of the Purbeck Limestone Group. Stratigraphy and correlation with polarity after Wimbledon (2008); polarities after Grabowski (2011); and numerical time scales: CENT95 after Channell *et al.* (1995), GR2004 after Gradstein *et al.* (2004) and TS2010 after Tominaga and Sager (2010). Note on the bottom right a table summarising calculation of deposition times depending on the three timescales and used to calculate the averages in the column average deposition times. CDB: Cap beds and Dirt Beds, CF: Cypris Freestone, MRM: Mupe and Ridgeway Members and σ: standard deviation, Val.: Valanginian. Note that the periods and stages on the left are according to Wimbledon's (2008, figure 1) magnetostratigraphy correlation.

### **3.5. Facies**

Facies in the Purbeck Limestone Group evolve generally from more marginal in the lower part to more basinal in the upper part of the succession. The previous descriptions of facies in these rocks are mainly based on the detailed studies by West (1975) along the south Dorset coast, Ensom (1985) at Worbarrow Tout, Clements (1993) in Durlston Bay, Westhead and Mather (1996) along the south Dorset coast and Ensom (2010) on the Isle of Purbeck and at Bacon Hole (Mupe Bay).

#### **3.5.1. Facies of the Lulworth Formation**

Facies in the Lulworth Formation were studied in details by many authors. The most detailed studies were done by West (1975) on the Skull, Hard and Soft Caps and the Cypris Freestone; and Francis (1982, 1983, 1984, 1986) on the paleosols (Basal, Lower and Great Dirt Beds) in between the Caps with the identification of ancient conifers and cycads. Concerning the biotas, Arkell (1941) remains the most detailed study on mollusc gastropods later revised by Clements (1973) and Radley (2002). Ostracods were very well described by Anderson (1985) later revised by Horne (1995, 2002), and Barker *et al.* (1975) although this study only focused on Portesham Quarry. Overall the facies and biotas found in the Lulworth Formation reflect hypersaline conditions (West, 1975) in shallow lakes or swamps (Arkell, 1933) or a large shallow lagoon (Strahan, 1898; Davies, 1935; West, 1975).

##### **3.5.1.1. Facies of the Mupe Member**

Westhead and Mather established this member in 1996 and summarised the lithologies to be mainly micritic algal limestones at the base and passing up to bedded coarse-grained ostracod-rich limestones that are locally brecciated.

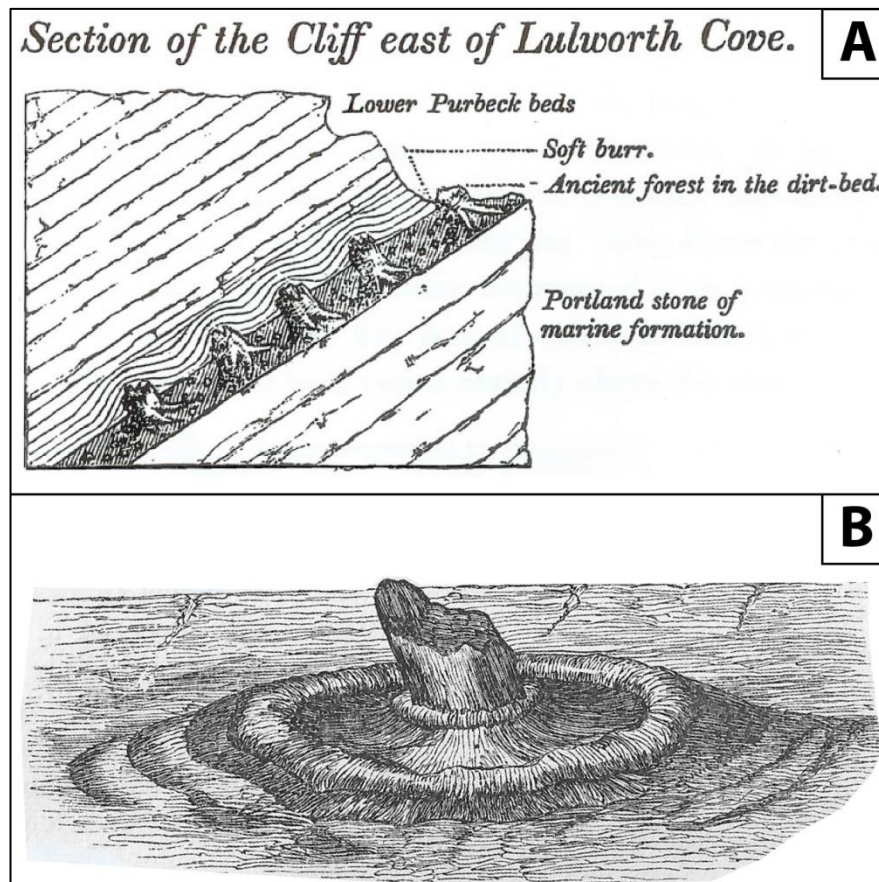
##### **3.5.1.1.1. Facies of the Transition Bed**

Few authors described the facies of this bed located at the base of the Purbeck Limestone Group. Francis (1982) named this bed the lower part of the Skull Cap and described the facies as fossiliferous micrites, biopelmicrites and biopelsparites containing ostracods, foraminifers,

bivalves and turreted gastropods. West (2013a) named this bed the Transition Bed and described thin-bedded pelletoidal limestones.

### 3.5.1.1.2. Facies of the Skull, Hard and Soft Cap beds

The first time these beds were described was in 1826 by Webster who recognised tufas and called them “*burrs*” (named after quarrymen names of the bed encasing the tree trunks, Fig. 2.6A). These were later compared by Fitton (1835) to Italian travertines. In 1836, Buckland and De La Bèche described these “*burrs*” as “*hemispherical concretions*” but without giving any further explanations. Henslow (1835 in Buckland and De La Bèche, 1835) noticed that the “*burr stone*” was protruding through the Aish (first bed of the Cypris Freestone) and that the “*burr stone*” was made of “*two circular ridges with intermediate circular depressions*” (Fig. 2.6B). He interpreted these ridges and depressions to record waves in very shallow water (Henslow, 1835 in Buckland and De La Bèche, 1835). In 1856 Fisher noticed that the surfaces of the Caps are very irregular and resemble “*deposits from a petrifying spring on moss*”.



**Figure 2.6** “*Burrs*” of the Soft Cap bed first description. A – The Soft Burr bed encasing the *in-situ* tree stumps at Lulworth Cove (drawing from Webster, 1826). B – “*Burr stone*” around an *in-situ* stump with the ridges and depressions from the Isle of Portland (drawing from Henslow, 1835 in Buckland and De La Bèche, 1835).

The first detailed study of these beds was made by Strahan in 1898 where he described granular limestones with pellets, oolitic grains and calcareous tufas (later revised by Arkell in 1947, as pelletoidal to oolitic limestones). Strahan (1898) showed that such calcareous tufas are common in petrifying springs where calcification occurs preferentially around plant remains than around pebbles. He also demonstrated that these tufas of the Mupe Member were deposited contemporaneously with the surrounding “*laminated Cyprid-limestones*”. Although Strahan compared the Purbeck tufas to calcite coating in petrifying springs, he also inferred a possible filamentous freshwater algal origin due to circular ridges discovered by Buckland and De la Bèche (1836) on the surface.

Pugh (1968) remains the most complete and detailed work done so far on the Cap deposits. Pugh (1968) focused on the algae found in the Hard Cap bed. She documented occurrence of filamentous red algae (Rhodophycophyta), green algae (Chlorophycophyta) and blue-green algae (Schizophyta). The red algae were the less common and only represented by one Genus *Solenopora dybowski* and found only at the base of the Hard Cap at Worbarrow Bay (Pugh, 1968). The green algae were represented by three genera from the same Family *Codiaceae*; *Ortonella garwood* (found at the base of the Hard Cap and in the Cypris Freestone between Mupe and Worbarrow Bays); *Cayeuxia frolo* found in the upper part of the Hard Cap at Perryfield Quarry); and *Hedströemia rothpletz* (found in the Hard Cap at Stair Hole; Pugh, 1968). The most common were the blue-green algae (reinterpreted recently as cyanobacteria, Riding, 1991) represented by two Families Porostromata and Spongiosstromata (Pugh, 1968). The former were represented by one Genus *Girvanella Nicolson & Etheridge* and found in the Cypris Freestone at Lulworth and in the Hard Cap at St. Aldhelm’s Head and Portesham; the latter were classified by their macro-morphologies because Spongiosstromata grow in colonies (Pugh, 1968). Pugh (1968) defined three classes, Laterally Linked Hemispheres (LLH), Stacked Hemispheres (SH) and Spherical Structures (SS). The LLH are found mainly in the Hard Cap but can also be encountered in the Soft Cap (particularly abundant in the lower part) and are comparable as algal mats (Pugh, 1968). These algal mats are inter-bedded with pellet limestones or horizons with a clotted texture (Pugh, 1968). These LLH correspond to the tufaceous limestones described by earlier workers and abundant in the Hard Cap on the Isle of Portland and their surfaces are compared to cauliflowers (Pugh, 1968). At microscale these LLH are micritic with algal filaments (made of dense micritic walls with a diameter of about 80 µm) and/or patches of brown radial calcite of a diameter between 115 and 230 µm and that can be replaced by siliceous spherulites (Pugh, 1968). The SH compose algal colonies or burrs from earlier workers and can be found in the Soft Cap at Portesham, Mupe Bay and Fossil Forest as

well as at the base of the Hard Cap at Portland Bill (Pugh, 1968). At macro-scale these SH are found encrusting tree stumps, resulting in a depression in the centre of the hemispheres (Pugh, 1968). At micro-scale, textures are similar to LLH although clots are better defined between 60 and 200  $\mu\text{m}$  organised in clusters within a micrite or microsparite (Pugh, 1968). The SS are found at the base of the Cypris Freestone at Mupe and Worbarrow Bays and organised nodules interpreted to be small isolated colonies of encrusting algae (Pugh, 1968). These colonies are between 114 and 850  $\mu\text{m}$  in diameter with laminations of sparite or clotted micrite between 30 and 140  $\mu\text{m}$  thick and the centre part of the nodules is made of either a pellet or a shell fragment (Pugh, 1968).

West (1975) revised and updated by West (2016) presented a study of facies of the lower part of the Mupe Member and defined four facies associations separated by paleosols (dirt beds). West (1975) also inferred palaeosalinities for each facies based on biotas (molluscs and ostracods mainly) and quantity of evaporite pseudomorphs (presented in section 3.5.1.1.6 of this chapter). The facies associations are stratigraphically classified from base to top as facies A, B, C and D (Fig. 2.7). Facies A is a thin bedded fine grained pelletoidal or peloidal limestone with stromatolites (Spongiostromata-type), peloids, molluscs (bivalves, and *Hydrobia* and *Valvata* gastropods), foraminifera, crustaceans (*Archaeoniscus*), fish, calcispheres, ostracods (West, 1975) and also a red alga (*Solenopora*) documented by Pugh (1969, in West, 1975). This facies A is found in the Skull Cap and the first half of the Hard Cap beds (until appearance of evaporites) (West, 1975). Facies B is a pelletoidal limestone with stromatolites (Spongiostromata-type), small replaced lenticular gypsum, ooids, and few ostracods and bioclasts and is found in the second half of the Hard and Soft Cap beds (West, 1975). Facies C is a calcitised evaporite (secondary anhydrite), unfossiliferous and is found at the base of the Cypris Freestone beds (West, 1975). Rare and thin horizons of calcareous shales or pelletoidal limestones are found and chert nodules are commonly replacing calcium sulphate (West, 1975). Facies D is a limestone with ostracods, molluscs (*Hydrobia* and *Valvata* molluscs), crustaceans (*Archaeoniscus*), fish (*Ichthyokentema purbeckensis*, according to Griffith and Patterson, 1963), ooids, peloids and locally halite pseudomorphs filled with surrounding pelletoidal limestones (West, 1975). This facies is also characterised by sedimentary structures such as wave ripples and is only found in the Cypris Freestone beds (West, 1975).

Francis (1982) described and detailed two facies for the Skull, Hard and Soft Cap beds, the algal limestones and the pelletoid limestones. Francis (1982) showed that these beds are mainly made of the algal limestones and sub-divided these into Porostromate (microbial filaments preserved) and Spongiostromate (microbial filaments not preserved)

microstructures. This classification is based on Pugh (1968) described above. However Francis (1982) determined that because of a lack of filamentous structures in the algal limestones of the Caps beds, those are mainly made of Spongiostromata-type stromatolites. Francis (1982) described the stromatolites of the Hard and Soft Cap as “*hemispherical mounds linked by flat-lying algal mat*” and noticed that they form circular “burrs” in the Soft Cap while they form large mounds in the Hard Cap. These are surrounding silicified in-situ tree stumps in the Soft Cap and moulds of former tree trunks and branches in the Hard Cap (Francis, 1982). She described in the burrs of the Soft Cap to have, in addition to the bandings, circular concentric ridges about 10-20 cm wide that she interpreted to be due to an increasing growth of the algal colonies during their formation. The doming typical of the Soft Cap bed is said to be not very well understood although in Independent Quarry (Isle of Portland) and at Fossil Forest, burrs are found respectively doming on top of a short fossil tree stump and a boulder (Francis, 1982). In between the domes the stromatolites form horizontal structures (Francis, 1982). Fish scales and ostracods are often found in voids that are sometimes filled with geopetal pelletoid sediments within these mounds (Francis, 1982). At Mupe and Worbarrow Bays stromatolites are present in the Hard Cap but as algal mats (laminated micritic and pelletoidal layers) and often associated with calcitised gypsum pseudomorphs (Francis, 1982). The pelletoid limestones are closely associated with the algal limestones (Francis, 1982). The pellets are micritic rounded aggregates between 30 and 200  $\mu\text{m}$  in diameter, when over 200  $\mu\text{m}$  they are described as intraclasts of micritic algal limestones broken off from the stromatolites (Francis, 1982). These were classified as inorganic pellets due to the wide range of sizes and can be originated from inorganic precipitation or micritisation of organic material (Francis, 1982). These can be a component of the stromatolitic laminae as well as infilling voids within the mounds or covering mounded structures (Francis, 1982). When the pellets were found in the algal mats, Francis (1982) described them as “mottled” or “clotted” because pelletoids have merged and formed clots of micrite. Francis (1982) interpreted the formation of these clots to be due to recrystallisation of the micritic matrix into spar cement leaving micritic patches (or clots) isolated; or due to patchy recrystallisation of the micritic matrix. Francis (1982) identified only in the clotted texture, pale brown calcite spherulites (radial calcite) of about 200  $\mu\text{m}$  in diameter forming patches or replacing the micritic matrix, and their origin remains unknown.

Bosence (1987) described and detailed two facies for the Skull, Hard and Soft Cap beds exposed on the Isle of Portland, bedded peloidal packstones to grainstones (depending on the bed) and tufas. The bedded peloidal packstones to grainstones contain ostracods, molluscs and ellipsoidal peloids (90 to 120  $\mu\text{m}$ ) cemented by a fine calcite spar cement (Bosence, 1987).

Locally this facies can be ostracod-rich or bivalve-rich (of *Neomiodon*) with intraclasts of tufas and *Cayeuxia* alga (Bosence, 1987). The tufas are composed of different facies and structures and divided into four components, framework, syndepositional cements, internal cements and post-depositional cements (Bosence, 1987). As also described by Francis (1982), tufas are found either around the base of former trees or around tree trunks and branches of fallen trees (Bosence, 1987). The framework is divided into burrowed thrombolites and skeletal stromatolites (Bosence, 1987). The burrowed thrombolites are found encasing the trees and form cauliflower-like buildups made of peloidal and clotted micrites (Bosence, 1987). These expand upwards and outwards concentrically from the trees and contain irregular and sinuous burrows of about 1 mm in diameter (Bosence, 1987). These burrows are compared to modern-day chironomid larvae burrows and the Purbeck burrowed tufas are compared to chironomid tufas of Schwabisch Alps (Irion and Muller, 1968; Bosence, 1987). The skeletal stromatolites are part of the buildups but remain an occasional component (Bosence, 1987). These form small columns (up to 100 mm high) of *Pycnoporidium* and *Cayeuxia* filamentous algae and are found interbedded with the burrowed thrombolites (Bosence, 1987). The filaments are between 22 and 60  $\mu\text{m}$  in diameter with micritic walls between 7 and 20  $\mu\text{m}$  thick (Bosence, 1987). The syndepositional cements are found either as a thick fringe of brown fibrous calcite (between 100 and 200  $\mu\text{m}$  thick) around thrombolites, stromatolites, reworked clasts and in cavities in tufas; or as an early coarse calcite spar in the tufas (Bosence, 1987). The internal sediments are found in the cavities of the tufas and after the syndepositional cements (Bosence, 1987). These are made either of the surrounding bedded peloidal packstones to grainstones with tufa intraclasts and ostracod debris; or calcisiltite forming laminated and inclined laminae infilling cavities within the tufas and similar to vadose silts of Dunham (1969), Grover and Read (1978) or Longman (1980) (Bosence, 1987). The postdepositional cements consist of gypsum pseudomorphs in the tufas and are thought to be formed after the deposition (Bosence, 1987). Other cements are blocky calcite spars present in all the facies described and barite crystals within cavities of the tufas (Bosence, 1987).

Perry (1994) defined 3 facies occurring in the Cap beds based on locations on the Isle of Portland, those are subaerial stromatolites, tufaceous limestones (sub-divided into micro-porous and macro-porous textures) and littoral grainstones. The subaerial stromatolite facies was found locally at the base of the Lower Dirt Bed and present a laminated texture with columnar structures. At microscale this facies have an alternance of light and dark micritic layers of about 100  $\mu\text{m}$  thick (Perry, 1994). These bands overlie a micritic to peloidal sediment separated by a calcite fringe up to 400  $\mu\text{m}$  thick (Perry, 1994). The tufaceous limestones were



found in the Skull, Hard and Soft Cap beds coarsely laminated (Perry, 1994). Those were found (as described by previous authors, see above) around former tree trunks and branches forming a micro-porous texture encasing the bores and a macro-porous texture encasing the micro-porous texture (Fig. 2.14; Perry, 1994). The micro-porous texture of the tufaceous limestones is mainly made of tubules and of three fabrics (Perry, 1994). The first fabric is a micritic matrix containing the randomly distributed tubules up to about 2 mm in diameter (Perry, 1994). Because these tubules are very tortuous and cross-cut the micritic matrix, Perry (1994) interpreted them to be due to microphytic or macrophytic growths, rather than larvae burrows as suggested by Bosence (1987, see above). These were later coated by micritic fringe cements (up to 100  $\mu\text{m}$  thick) themselves coated by calcite fringe cements (up to 300  $\mu\text{m}$  thick) and associated with peloids (up to 80  $\mu\text{m}$  in diameter) and peloid aggregates (Perry, 1994). The second fabric is a white cement (up to 400  $\mu\text{m}$  thick) coating the first fabric but not always present (Perry, 1994). The third fabric consists of the micritic to dense peloidal matrix surrounding the two previous fabrics (Perry, 1994). The macro-porous texture encases the micro-porous texture, presents a rather nodular structure and appears to be made of micritic to peloidal sediments coated by radiating calcite cements (up to 2 mm thick; Perry, 1994). The littoral grainstones were said to be overlying the tufaceous limestones in the Skull and Hard Cap beds although in the Skull Cap they were only found on the eastern side of the Isle of Portland (Perry, 1994). These lithologies were reported to contain of hypersaline to brackish water ostracods, isolated brackish water bivalves and freshwater gastropods, micrites, peloids and peloid aggregates (Perry, 1994).

The latest study on the Caps beds of the Mupe Member was conducted by an MSc student Victoria Dharmarajah in Royal Holloway in September 2015. She studied the facies of the Skull and Hard Cap beds at Bowers, Perryfield and Broadcroft Quarries. Dharmarajah (2015) defined 6 facies grouped into 2 facies associations; the bedded lacustrine marginal carbonates facies association containing the peloidal bioclastic packstone to grainstone, bioclastic peloidal packstone, peloidal wackestone to grainstone, and peloidal bioclastic wackestone facies; and the mounded lacustrine marginal carbonates facies association containing the thrombolite mounds and intraclastic rudstone facies. All these facies contain similar components although in different quantities as indicated by their respective names. The components are ostracods, mollusc fragments, peloids, intraclasts of thrombolite mounds and micritic matrix (Dharmarajah, 2015). She used the facies analysis to interpret shallowing-upward sequences in the Skull Cap at the three locations studied and in the Hard Cap at Bowers and Perryfield Quarries; and a deepening upwards sequence in the Hard Cap at

Broadcroft Quarry. In addition to she performed stable isotope analyses (C and O) to decipher the palaeoenvironments which are presented in section 3.7.1 of this chapter.

### 3.5.1.1.3. Facies of the Basal, Lower and Great Dirt Beds

Identically, although the Basal, Lower and Great Dirt Beds were identified for the first time by Fitton in 1827 (in Fitton, 1836) and already thought to be “*earthly*”, it was only in 1982 that Francis studied these dirt beds in detail (and later in 1983, 1984 and 1986). These dirt beds are interpreted to be paleosols (Francis, 1982, 1986) and interbedded with the Skull, Hard and Soft Cap beds. These paleosols are made of carbonaceous marls either with limestone pebbles (Great Dirt Bed) or without limestone pebbles (Basal and Lower Dirt Beds; Francis, 1982, 1986). The Great Dirt Bed is made of black carbonaceous marls with black and white limestone pebbles which accumulated alongside *in-situ* silicified tree trunks, stumps (Francis, 1982, 1983, 1986) and roots (first observed by Fitton, 1836), and cycadophytes (Fitton, 1836; Buckland and De la Bèche, 1836). Francis (1982, 1986) determined that this palaeosol is a well-developed carbonaceous A/C rendzina profile following the New Soil Classification of England and Wales (Curtis *et al.*, 1976) and in the Mollisol Order (dark colour and organic-rich), Rendoll sub-order due to calcareous parent rocks following the US Comprehensive Soil Classification System (Soil Survey Staff, 1975; Francis, 1982, 1986). Strahan (1898) and Arkell (1947) had proposed earlier that the trees were coniferous but Francis (1982, 1983) demonstrated that the trees are *Protocupressinoxylon purbeckensis* wood, *Cupressinocladus valdensis* foliage, *Classostrobus* and *Pararaucaria collinsonae* cones and *Classopollis* pollen (also documented by Philippe & Bamford, 2008 and Philippe *et al.*, 2010). The black and white limestone pebbles are reworked materials from the underlying Hard Cap during pedogenesis as they have the same composition as the lithologies found in the Hard Cap (peloidal packstone-grainstone and microbialites; Francis, 1982, 1986). The presence of these pebbles indicates also that the underlying beds were lithified before the pedogenesis (Francis, 1982, 1986). This was also noticed by West (1975) and Francis (1983). The white pebbles show interlocking, or fitted, shapes previously described by Francis (1982, 1983, 1986) and are due to the *in-situ* weathering of carbonate parent rocks. The black pebbles constitute 30-40% of all the pebbles (Francis, 1982, 1986) and their colour is due to incorporation of organic matter (Francis, 1982, 1986). Black pebbles are often associated with calcrete deposits (Multer and Hoffmeister, 1968; Ward *et al.*, 1970; Wilson, 1967; Riding and Wright, 1981; Strasser and Davaud, 1983; Strasser, 1984) and are evidence of sub-aerial exposure, confirming the paleosol

interpretation. Similarly Francis (1982, 1986) described the Basal and Lower Dirt Beds to be made of brown carbonaceous marls with rare rooted tree stumps (although these were never found in the Basal Dirt Bed). The absence of large pebbles suggests that the underlying beds were not totally lithified before the pedogenesis (Francis, 1982, 1986). The occurrence of trees together with the high carbonate ( $\text{CO}_3^{2-}$ ) content and the calcareous parent rocks confirmed the interpretation of paleosols and showed that these paleosols were immature rendzina soil profiles (Francis, 1982, 1986). Because these paleosols are rendzina soil profiles but are thinner than the Great Dirt Bed, Francis (1982, 1986) suggested that they were most probably compacted or eroded after deposition. This can also be explained by the fact that trees stumps are rooted into the Lower Dirt Bed and a rather thick paleosol is needed to provide support for these trees. The integration of all these elements and features led Francis (1982, 1984, 1986) to interpret these paleosols as having been formed under a semi-arid climate of Mediterranean type.

#### **3.5.1.1.4. Facies of the Broken Beds and Cypris Freestone**

Above these cap and dirt beds are the Broken Beds (Tab. 2.2) which have been the centre of discussions about their formation since the beginning of the 19<sup>th</sup> century. The first time the Broken Beds were described was in 1811 by Webster (in Englefield, 1816) in Durlston Bay where he saw *“the contorted and broken fragments of the series of Purbeck beds, as one would build a wall over rugged rocks”*. After observing that laterally these contorted beds correspond to clays with gypsum, Webster (1811 in Englefield, 1816) proposed that the formation of the Broken Beds could be due to the dissolution of such clays where the *“Purbeck beds”* would have *“fallen into their present position”*. Forbes (1850) noticed similar features in Lulworth area where he saw that *“the Cypridiferous shales [...] are strangely contorted and broken up [...] at the west end of the Isle of Purbeck”* but no further explanations were given. The first interpretation for the possible origin of these Broken Beds was done by Fisher in 1854 (in Fisher, 1856) where he proposed an accumulation in a lake of calcareous muds and sands above dead vegetation (trees and branches). The decay of this vegetated layer would have created voids and collapse of the carbonate muds and sands and resulted in the facies found today (Fisher, 1856). This idea was later supported by Strahan (1898) as the Broken Beds were identified, although much thinner than in Lulworth, on the Isle of Portland and as far as the Vale of Wardour (identified there by Andrews and Juke-Brown, 1894). The widespread occurrence led Strahan (1898) to conclude that the Broken Beds were formed during the

deposition through collapsing of a cavity that resulted from the decay of plant remains. Woodward in 1895 proposed a different interpretation than Fisher (1856) due to his belief that if forest decay (that developed in the Great Dirt Bed) caused the formation of the Broken Beds, on the Isle of Portland the Broken Beds are not found even though the Great Dirt Bed is much thicker than in Lulworth. Woodward (1895) proposed that the fragmentation of the limestones might have occurred long after the deposition contemporaneously to the formation of the Purbeck Anticline and the inversion of the Purbeck Fault. This was suggested because the breccia is made of broken consolidated strata and especially that the brecciation is not confined to one particular bed but affects stratigraphically higher beds locally (Woodward, 1895). Following this observation Woodward (1895) proposed a tectonic origin of the breaking up of the Cypris Freestone related to the "*tilting of the strata*" orientated NNW with dip angles of 20° to 40°. This tilting accompanied with dissolution of calcite cement of sandstones, allowed bed-over-bed sliding of the weak carbonate layers, the toughness of the surface of the Soft Cap providing a *décollement* surface (Woodward, 1895). The irregular distribution of the Broken Beds is described by Woodward (1895) to be the result of irregular accumulation "*over the terrestrial surfaces and hummocky burrs*". Following Woodward's (1895) work, Arkell (1938) presented new interpretations of the formation of the Broken Beds. He agreed with Woodward's explanation for a tectonic origin as no clear evidence has been found in support of the vegetation decay origin (Arkell, 1938). He emphasised that no remains of organic matter or plant moulds on blocks composing the Broken Beds had been found, the thicknesses of non-deformed and deformed units are laterally the same, the folds found in the Broken Beds could not have been formed by collapsing beds, and no Broken Beds were actually identified in the Vale of Wardour (Arkell, 1938). However Arkell (1938) brought new data of the direction of tectonic forces, showing that northerly verging asymmetric folds are present on the beds of the Cypris Freestone (above the Broken Beds). According to Arkell (1938) this indicates a southward movement of the overlying beds and in accordance with the regional strike of Cenozoic folding. However a more recent study by Phillips (1964) disproved Arkell's southerly dipping argument and said the opposite that the overturning of the northerly dipping limbs shows clearly northerly movement (*i.e.* towards the Purbeck Fault). Arkell (1938) concluded that the Broken Beds are an example of drag-folding structures related to the formation of the Purbeck Anticline. Later the same year Hollingworth (1938) commented on Arkell's (1938) work highlighting that laterally in the same stratigraphic unit the occurrence of "*botryoidal masses of gypsum*" in Durlston Bay and thick anhydrite deposits in Portsdown and Henfield boreholes (East of Bournemouth). Following these facts Hollingworth (1938) proposed an

influence of the hydration of anhydrite and the solution of gypsum on the formation of the Broken Beds (this hypothesis was accepted by Arkell on a reply to Hollingworth's correspondence, 1938). This last interpretation was supported by West (1975) after the discovery and detailed study of evaporite facies and their diagenesis at the base and below the Broken Beds (West, 1961, 1964). West proposed that the formerly interbedded evaporites at the base of the Broken Beds could be the cause of a collapse breccia, and that the plastic evaporite facies below the Broken Beds could have acted as an incompetent bed that was subsequently tectonically deformed and brecciated (West, 1975).

Brown in 1961 and 1964 presented for the first time evidence of algal influence in the deposition of the Broken Beds and Cypris Freestone. Brown (1961, 1964) demonstrated that at macroscale, lumps of algal limestones are presents in the Broken Beds and that the Cypris Freestone preserve algal filaments at the microscale (*Ortonella* and *Girvanella*).

#### **3.5.1.1.5. Fossils of the Mupe Member**

In addition to Anderson (1985) and Horne (1995, 2002) biostratigraphic studies on ostracods presented in section 3.3 of this chapter, other authors identified and described ostracod species without a biostratigraphical value. Strahan (1898) identified three species in the "Lower Purbeck Beds": *Cypris purbeckensis*, *Candonna ansata* and *Candona bononiensis*. These species were previously described by Forbes (1850) however no interpretation in terms of palaeoenvironmental tolerance was ever provided. The only interpretation to determine the Purbeck beds of a freshwater origin is due to the change from the marine Portland Group to the fossil-poor Purbeck Limestone Group and the association with other freshwater animals (vertebrates and invertebrates; Webster, 1826; Forbes, 1850; Strahan, 1898). Barker *et al.* (1975) conducted a detailed palaeoenvironmental study on ostracods of the Mupe Member in Portesham Quarry. In this study they collected and identified ostracods in the Hard Cap bed and in the equivalent of the Great Dirt Bed, and used them to determine palaeosalinities rather than for their biostratigraphical value. They identified three ostracod groups based on the salinity preference: marine (*Macrocypris* sp., *Macrodentina retirugata*, *Macrodentina rugulata*, *Paraschuleridea bulgensis*, *Wolbergia visceralis*, *Protocythere serpentine* and *Othonotacythere rimosa*); euryhaline (*Fabanella ansata*, *Fabanella polita* and *Mantelliana purbeckensis*); and oligohaline (*Klieana alata*, *Scabriculocypris acanthoides*, *Cypridea tumescens praecursor*, *Cypridea dunjkeri papulata* and *Theriosynoecum forbesii*). The recognition of these groups lead to the conclusions that because of a mixture of all the species

in all the beds (apart from bed 1 where marine ostracods were found and bed 19 where only *Cypridea dunkeri papulata* was found, Barker *et al.*, 1975), 1) marine ostracods were most likely transported from the sea nearby (Barker *et al.*, 1975) and 2) that the water of the lake was brackish. Similarly they identified three euryhaline species: *Fabanella ansata*, *Fabanella palita* and *Mantelliana purbeckensis* in an equivalent bed of the Broken Beds (because absent in this area). Dharmarajah (2015) tried to collect and identify ostracods from selected locations from the Cap beds on the Isle of Portland. To identify the species, genera or family of an ostracod a preserved and unbroken shell is needed (David Horne, pers. comm., March 2015). The extraction of such preserved shells proved extremely difficult for this facies due to the hardness of the limestone and no clear conclusions could be drawn.

Although mollusc gastropods are very well documented for the upper part of the Lulworth Formation and the Durlston Formation (J. de C. Sowerby, 1836; Arkell, 1941, Casey, 1955; Clements, 1973; Morter, 1978; Kelly, 1988; Cleevely and Morris, 1988; Radley, 2002); only a few authors documented gastropods from the Mupe Member of Dorset (Arkell, 1941; Clements, 1973; Radley, 2002). This is mainly due to the difficulty of collecting identifiable shells from such well lithified limestones. Strahan (1898) described an association for the "Lower Purbeck" (but unlocated) made of three oligohaline gastropods; *Hydrobia*, *Limaea* and *Planorbis*. Arkell (1941) described four gastropods species from Dorset: *Valvata helicoides* (Transition, Caps and Broken Beds, Ridgeway), *Hydrobia chopardiana* (Transition Bed, Osmington and Ringstead), *Hydrobia forbesi* (Transition Bed, Osmington reservoir) and *Lymea physoides* (Broken Beds, Upwey). Clements (1973) remains the most detailed study of gastropods of the Mupe Member. He studied three locations in south Dorset, Poxwell Quarry, Upwey Quarry and Durlston Bay, and found similar gastropod species. Clements (1973) identified the following in the Transition Bed *Hydrobia*, *Loriolina*, *Valvata helicelloides* and hydrobiid gastropods; in the Skull Cap *Valvata sabaudiensis* and *Valvata helicelloides*; in the Lower Dirt Bed *Valvata sabaudiensis*, *Viviparus "inflatus"*, *Loriolina*, *Ceritella*, *Delphinula*, *Coelodiscus swindonensis*, *Procerithium* and hydrobiids; in the Hard Cap *Valvata helicelloides*, *Valvata sabaudiensis*, *Physa bristovii*, gastropod *sp.*, *Hydrobia* and *Hydrobiidae*; and in the Broken Beds *Valvata sabaudiensis*, *Hydrobia* and *Coelodiscus swindonensis*. Following this identification and description, Clements (1973) determined salinity tolerances for each gastropod species (apart from *Loriolina* due to a lack of data) and if they were living in either open or closed lacustrine systems presented in table 2.6.

	<b>Freshwater</b>	<b>Brackish</b>	<b>Hypersaline</b>
<b>Open system</b>	<i>Viviparus</i>	<i>Hydrobia</i>	No species identified
		<i>Valvata helliceloides</i> Gastropod sp.	
<b>Closed system</b>	<i>Physa bristovii</i>	<i>Valvata sabaudiensis</i> <i>Procerithium</i>	<i>Ceritella</i> <i>Coelodiscus swindoniensis</i> <i>Delphinula</i>

**Table 2.6** Salinity tolerance and lake systems interpreted from gastropod species of the Mupe Member (data from Clements, 1973).

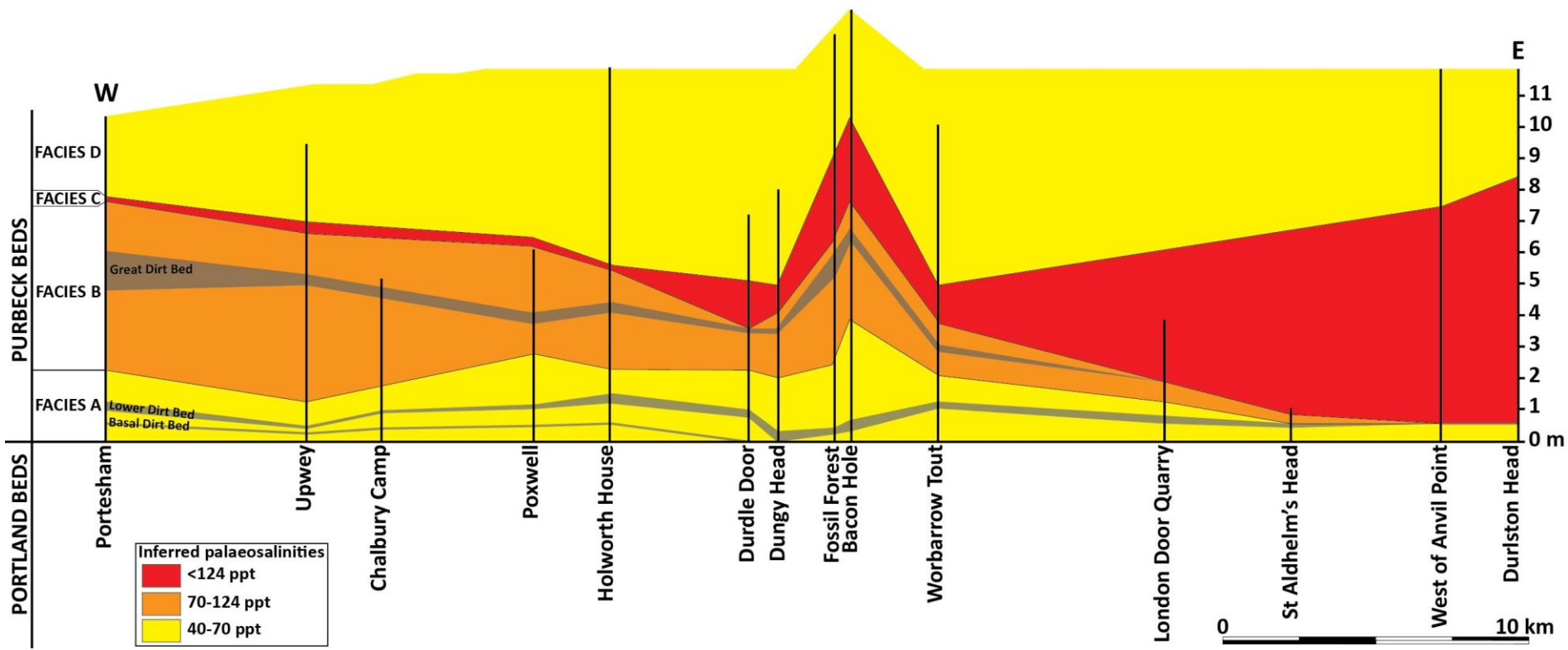
Radley (2002) summarised Arkell's (1941) work incorporating West's (1961), Clements' (1973) and Barker et al.'s (1975) studies and described two main assemblages. The first assemblage is made of Arkell's (1941) *Proauricula jaccardi* (Maillard), *Gyraulus loyri* (Coquand), *Prophysa bristovii* (de Loriol) and *Proauricula jaccardi* (de Loriol), and Clement's (1973) viviparids and hydrobiids. The second assemblage is made of Arkell's (1941) *Provalvata helicoides*, *Coelodiscus swindonensis* and Clement's (1973) hydrobiids and an unidentified spired taxon. Those assemblages helped Radley to determine variations of salinities and open/closed systems for and within each bed (detailed in section 3.7.1 of this chapter). However Clements (1973) also identified *Delphinula* sp., *Turritella*-like, procerithiids and ceritallids that are marine species. He considered that these marine species could be reworked from the underlying Portland Group.

The bivalve molluscs are very poorly documented for the Mupe Member. Strahan (1898) described only one species: *Cyrena* or *Cyclas media* for the "Lower Purbeck" of Dorset. He noticed possible occurrences of this bivalve in the first bed of the Purbeck at Upway Quarry and Holworth House. West (1975) defined four facies in the lower part of the Mupe Member of Dorset and only cited occurrence of bivalves in his facies A although without descriptions. Similarly Radley (2002) described bivalves encountered in the same unit from Portesham Quarry. Even though he described one taxa (*Corbula* sp.) from the Cypris Freestone at Swanworth Quarry and Worth Matravers, he notified "*the bivalves await documentation*" for the Cap beds and Dirt Beds.

#### **3.5.1.1.6. Lateral thickness and facies variations**

West (1975) defined four facies associations (refer to section 3.5.1.1.2 of this chapter) and inferred palaeosalinities based on comparison with modern environment salinities. The palaeosalinity of the facies A was compared to modern day Shark Bay and Persian Gulf lagoons presenting similar configurations (West, 1975) and was interpreted to have been deposited in moderately hypersaline water of about 50 to 70 part per thousands (ppt). The inferred palaeosalinity of the facies B was also deduced from Shark Bay and Persian Gulf modern day salinities of about 70 to 124 ppt (West, 1975; 2013*b*). This value was deduced from the absence of fauna and the precipitation of gypsum which, according to Friedman *et al.* (1973), reflects supersaturation around 124 ppt regarding gypsum (West, 1975; 2013*b*). The facies C was thought to be formed from nodular anhydrite as found in modern day sabkhas from the Persian Gulf (West, 1975) and was interpreted to reflect palaeosalinities of more than 124 ppt (West, 1975; 2013*b*). The facies D, as for facies A, was compared to modern day Shark Bay and Persian Gulf and was interpreted to represent paleosalinities of about 50 to 70 ppt (West, 1975). West (1975) correlated those facies associations following an East-West sedimentary log panel (Fig. 2.7). The main features recognised from this log correlation panel are that facies A and B thin considerably eastward while thickness of facies C is very thin to the West and increases consequently eastward, basinward (West, 1975).





**Figure 2.7** Facies thickness variation on an east-west section of the Mupe Member with inferred palaeosalinities. Each plain vertical line represents a log. Redrawn after West (1975).

Similarly Francis (1982) illustrated two log correlation panels showing lateral thickness and facies variations of the Cap beds and Dirt Beds north to south over the Isle of Portland (Fig. 2.8) and west to east over south Dorset coast (Fig. 2.9). Francis (1982) distinguished a lower and an upper part of the Skull Cap separated by the Basal Dirt Bed (refer to section 3.2.4 of this chapter). According to Francis (1982), the lower part of the Skull Cap is characterised by mudstones to wackestones with ostracods, foraminifers, bivalves and turreted gastropods between Portesham and Holworth House. This bed changes laterally into algal stromatolitic limestones at Lulworth area that are replaced by radial calcite in Bacon Hole (*i.e.* Mupe Bay) and disappears eastwards Worbarrow due the absence of the Basal Dirt Bed (Fig. 2.9; Francis, 1982). The Basal Dirt Bed is characterised by thin and persistent carbonaceous marls best developed over the Isle of Portland, found from Portesham to Worbarrow with the exception of Durdle Door and Lulworth (Fig. 2.9; Francis, 1982). The upper part of the Skull Cap is characterised by micritic algal limestones with abundant fish bones, ostracods and algal intraclasts (Fig. 2.9; Francis, 1982). This upper part was found all along the studied area as an algal limestone and becoming slumped and brecciated at Mupe Bay and Worbarrow (Fig. 2.9; Francis, 1982). Francis (1982) also noted that the whole Skull Cap disappears at Dungy Head as the Lower Dirt Bed is resting directly on the Portland Group. The Lower Dirt Bed consists of persistent carbonaceous marl between Portesham and Mupe Bay (including the Isle of Portland) passing laterally to impersistent black and white shale from Worbarrow eastwards (Fig. 2.9; Francis, 1982). Silicified trees (ancient conifers), cycadophytes and lignitic material were found only on the upper part of this bed and mainly on the Isle of Portland (Fig. 2.9; Francis, 1982). The thickness of this Lower Dirt Bed changes rapidly (distances of few centimeters) thickening in depressions and thinning over highs (particularly over stromatolitic mounds of the Skull Cap; Francis, 1982). Francis (1982) noted a major change from carbonaceous marl in the west to shale to the east (from Worbarrow eastwards). The black laminae in the shales preserved fish remains, ostracods, vertebrate bones and carapaces of conchostracan branchiopods on the surfaces while the white laminae are coarser-grained (Francis, 1982). This suggested river or pond sediments rather than a true paleosol (Francis, 1982; refer to section 3.7 of this chapter for reconstruction of palaeoenvironments). Between Portesham and Holworth House the upper limit of the Hard Cap bed was difficult to identify due to the poor exposures or the absence of the Great Dirt Bed (Fig. 2.9; Francis, 1982). Eastwards at Mupe Bay and Worbarrow, the stromatolitic mounds change for even stromatolitic pustular mats (Fig. 2.9; Francis, 1982). Further east stromatolitic limestones disappear because they are replaced by evaporites and correlation with western deposits was

more uncertain (Francis, 1982). The Great Dirt Bed is present and was interpreted as a paleosol only on the Isle of Portland and Lulworth area (Figs. 2.8 and 2.9; Francis, 1982). In all the other locations this bed is made of thin bands of clay locally with nodules of silicified woods such as at Upwey (Fig. 2.9). This bed was difficult to identify eastwards as most of the deposits are replaced by evaporites (Francis, 1982). The Soft Cap was described with algal stromatolites that are thicker in the Lulworth area and north of Portland (about 50 cm thick) while thinner to the south of the Isle of Portland (Fig. 2.8; Francis, 1982). To the west those “algal burrs” were described to become algal mats interbedded with wackestones with gypsum pseudomorphs while to the east of Lulworth area stromatolitic limestones were replaced by evaporites (up to Mupe Bay) and not recognisable further east (Fig. 2.9; Francis, 1982).

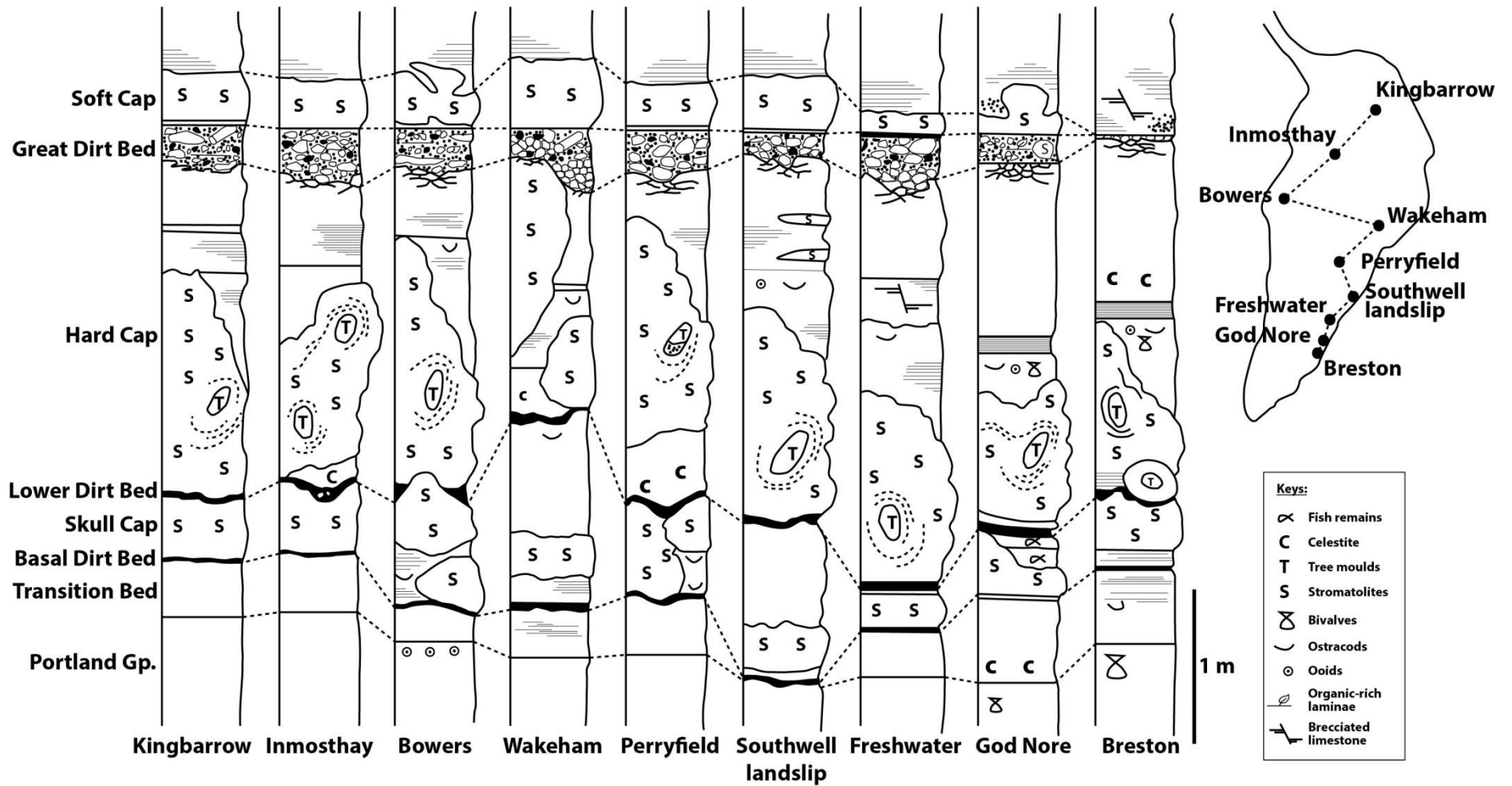


Figure 2.8 Log correlation of the lower part of the Mupe Member on the Isle of Portland, modified after Francis (1982).

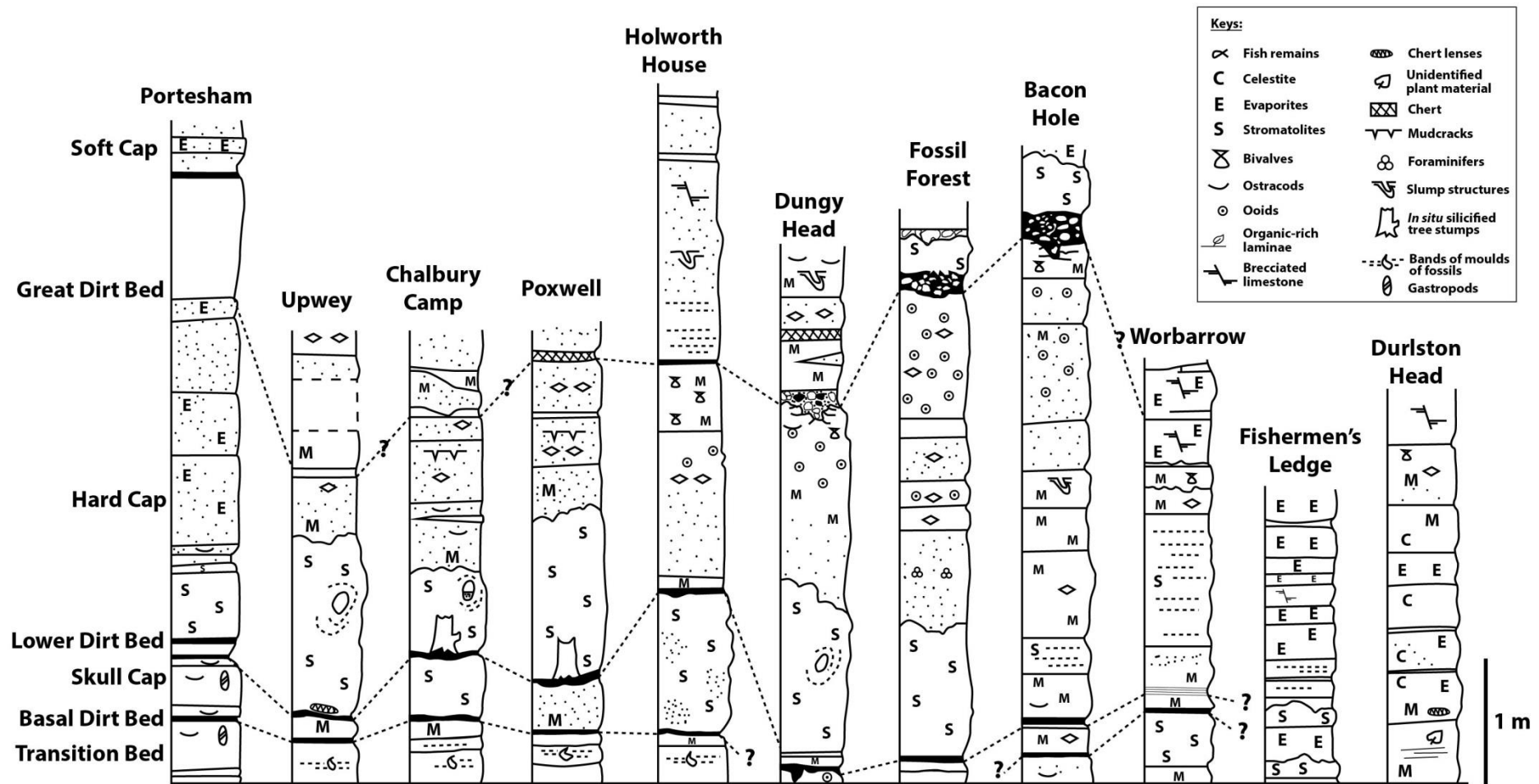


Figure 2.9 Log correlation panel of the lower part of the Mupe Member across south Dorset, modified after Francis (1982).

### **3.5.1.2. Facies of the Ridgeway Member**

The Ridgeway Member is made of bedded ostracod-rich limestones and corresponds to the uppermost half of the Cypris Freestone (Tab. 2.2) containing the same fossil assemblages as the lowermost half of the Cypris Freestone described in the previous section. The separation from the Mupe Member was made by Westhead and Mather (1996) because of significant appearance of dark grey and brown mudstone.

### **3.5.1.3. Facies of the Worbarrow Tout Member**

The Worbarrow Tout Member comprises micritic limestones with detrital quartz passing up to interbedded clays and shales (Westhead and Mather, 1996). The Hard and Soft Cockle Beds consist of bedded micritic limestones containing evaporite pseudomorphs and detrital quartz (Westhead and Mather, 1996). The non-marine molluscs *Protocardia purbeckensis*, *Provalva helicoides* and *Hydrobia* sp. gastropods are recorded by Radley (2002) occurring in coquinas, and neomiodonid and corbulid bivalves are also found (Arkell, 1933). The Marly Freshwater Beds are made of interbedded calcareous clays and shales containing *Hydrobia* sp. and *Provalvata helicoides* (Clements, 1973). The last bed of this member, the Cherty Freshwater Bed is made of micritic limestones with cherts, charophytes, *Ptychostylus harpaeformis* (Koch and Dunker, 1837), *Proauricula jaccardi*, *Ellobium* sp. gastropods, neomiodontid and unionoid bivalves and ostracods (Arkell, 1933, 1941, 1947; Clements, 1969; Batten, 2002; Radley, 2002).

### **3.5.2. Facies of the Durlston Formation**

The facies and biotas found in the Durlston Formation reflect a freshwater environment relatively stable with some marine incursions from time to time such as the deposition of the Cinder Bed (Arkell, 1947; Casey, 1963, 1973; Wimbleton and Hunt, 1983; Morter, 1984). The deposition occurred in a rather shallow lacustrine environment (Arkell, 1933), lagoon (Chadwick, 1985) or estuarine system (Strahan, 1898; Davies, 1935; Arkell, 1947). In addition Anderson (2004) provided a cyclostratigraphy study of the Durlston Formation with the recognition of four third-order sequences that comprise fourth- and fifth-order sequences.

### 3.5.2.1. Facies of the Stair Hole Member

The lowermost unit, the Stair Hole Member comprises interbedded bioclastic with micritic limestones that are locally fossil-rich and forming coquinas, that have named beds, and shales towards the top (Tab. 2.2; Westhead and Mather, 1996). The Cinder Bed is an oyster-rich (*Praeexogyra distorta*, J. de C. Sowerby) blue-grey limestone (Morter, 1984; Batten, 2002). The Intermarine Beds are made of bioclastic (biosparudite to biomicrudite) limestones containing freshwater *Viviparus* gastropods and euryhaline *Neomiodon* bivalves (El Shahat and West, 1983; Westhead and Mather, 1996), dinosaur footprints, reptile eggshells and crocodiles, turtles, shark and fish bones (West, 1979; Batten, 2002; Ensom, 2002; Evans and Searle, 2002; Norman and Barrett, 2002; Milner, 2002; Salisbury, 2002). The Scallop Beds are made of bioclastic limestones containing mainly *Chalmys* sp., pectinids, *Modiolus* sp., *Gervillia obtusa* Roemer, *Praeexogyra distorta*, *Protocardia* sp. and *Corbula* sp. bivalves (Arkell, 1933, 1947; Kelly, 1983; Radley, 2002); and *Theodoxus fisheri*, *Ptychostylus harpaeformis*, *Hydrobia*, *Procerithium*, *Peperilia perisphincta* Arkell and *Viviparus* sp. (Clements, 1969). The *Corbula* Beds consist of bioclastic limestones with *Corbula* sp., *Isognomon* sp., *Thracia* sp., *Protocardia purbeckensis*, mytilid, pectinid and oyster bivalves (Arkell, 1933, 1947; Radley, 2002); and *Theodoxus fisheri*, *Procerithium* sp., *Paraglauconia tricarinata* (J. de C. Sowerby), *Promathilda microbinaria* Arkell, *Juramarinula durlstonense*, *Ptychostylus harpaeformis*, *Viviparus* sp. and *Hydrobia* sp. gastropods (Clements, 1969; Cleevely and Morris, 1988; Radley, 2002). The last bed in this member, the Chief Beef Member, is made of organic shales with fibrous calcite and bioclastic limestone bands containing neomiodontid and unionid bivalves; and the gastropods *Viviparus* sp., *Hydrobia* sp. and *Gyraulus loryi* (Arkell, 1933; Radley, 2002).

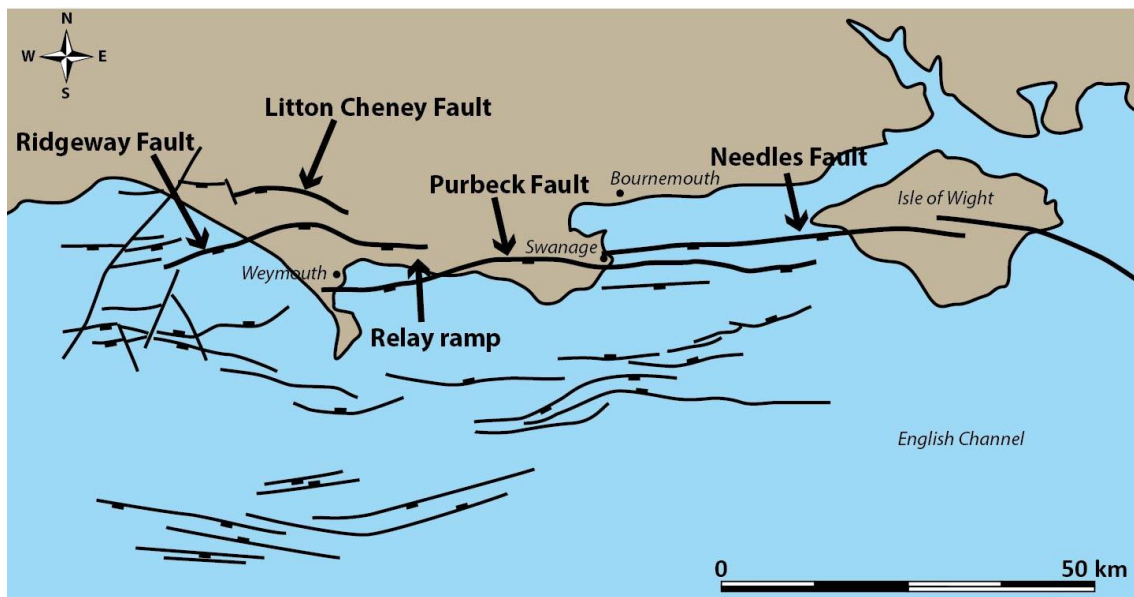
### 3.5.2.2. Facies of the Peveril Point Member

The Peveril Point Member comprises bioclastic limestones passing up to bioclastic marls and shales. The Broken Shell Limestone consists of bioclastic limestones with unionid and *Neomiodon* bivalves (Westhead and Mather, 1996; Batten, 2002) and *Theodoxus fisheri* and *Viviparus* sp. gastropod fragments (Radley, 2002). The Unio Bed is also a bioclastic limestone made of accumulation of freshwater *Unio* bivalves (Westhead and Mather, 1996; Batten, 2002). The Upper Cypris Clays and Shales are made of bioclastic marls and shales containing mainly freshwater *Viviparus* gastropods and *Unio* bivalves, and euryhaline *Cypridea* ostracods (Ensom, 1985; Batten, 2002). The Purbeck Marble, well known in UK for being a renowned

ornamental building stone, is included in the Upper Cypris Clays and Shales and comprises a *Viviparus* biomicrite (Batten, 2002).

### 3.6. Tectonic setting

As described previously (refer to section 2), the Purbeck Limestone Group was deposited during the latest stage of the syn-rift phase of the Wessex Basin (Fig. 2.3). Although syn-depositional tectonic features are very well documented for the entire Jurassic deposits (Stoneley, 1982; Chadwick, 1986; Hamblin *et al.*, 1992; Butler, 1998; Newell, 2000), no clear evidence has yet been documented for tectonic movements during the deposition of the Purbeck strata (refer to Chapter 3 for more details). Classical fieldwork on the coast of south Dorset since the 19<sup>th</sup> century (Buckland and De la Bèche, 1835; Strahan, 1898; Arkell, 1936, 1947, Phillips, 1964; Cosgrove and Hearn, 1966), and more recent sub-surface data analysis (Stoneley, 1982; Lake, 1985; Hamblin *et al.*, 1992; Butler, 1998; Harvey and Stewart, 1998; Underhill and Paterson, 1998; Underhill and Stoneley, 1998; Newell, 2000) both onshore south Dorset and offshore in Weymouth Bay and Bournemouth Bay documented tectonic features for the western margin of the Wessex Basin.

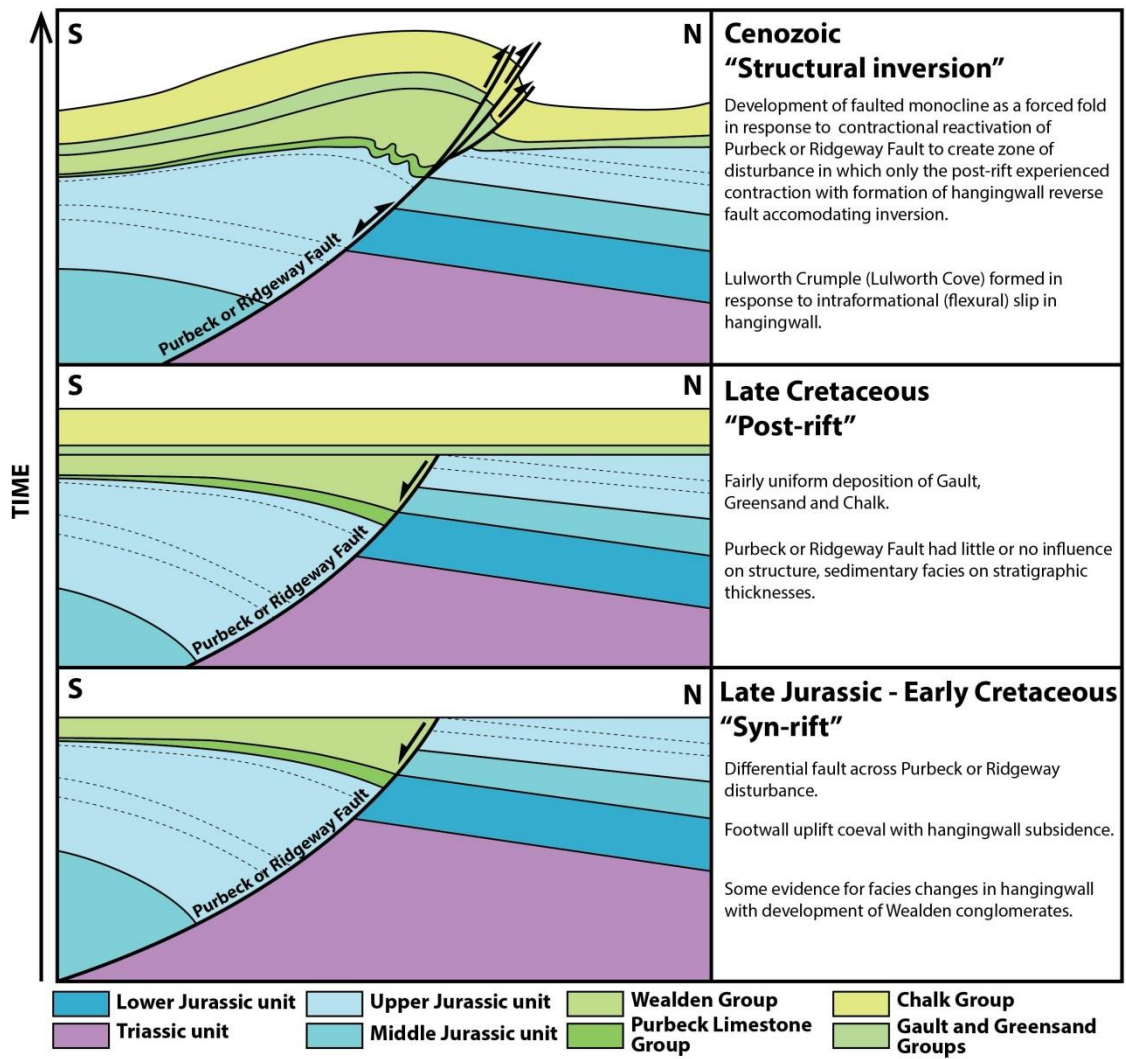


**Figure 2.10** Structural map of the western margin of the Wessex Basin showing the main extensional faults that affected Jurassic deposits (modified after Harvey and Stewart, 1998).

Two important extensional faults that were subsequently inverted have been identified in south Dorset; the Purbeck Fault to the east and the Ridgeway or Abbotsbury-Ridgeway Fault to the west (Fig. 2.10; Underhill and Stoneley, 1998; Underhill, 2002). Sub-surface data image the type of faults (shape and length) and also show the tectonic history along these faults. The



Ridgeway Fault is about 4 km long, curvilinear and rooted in Triassic salt deposits (Fig. 2.10; Darton *et al.*, 1981; Harvey and Stewart, 1998; Barton *et al.*, 2011). The Purbeck Fault is much longer (about 60 km) finishing its onshore expression on the Isle of Wight and comprises several sub-planar *en échelon* faults (such as the Needles Fault, Fig. 2.10) that cut the Variscan basement (Fig. 2.10; Butler, 1998; Barton *et al.*, 2011). These two fault systems are linked by a relay ramp area in the central part of the study area (Fig. 2.10). Their syn-depositional nature in the Jurassic was interpreted on the basis of the thickness increase of lithostratigraphic units in the hanging-wall block towards the faults than in the footwall blocks (Fig. 2.11; Colter and Havard, 1981; Stoneley, 1982; Hamblin *et al.*, 1992; Harvey and Stewart, 1998; Hawkes *et al.*, 1998). After the syn-rift phase or prior to the deposition of the Gault Formation, there occurred an erosion phase creating an unconformity reaching locally down to Permian deposits (Fig. 2.11; Butler, 1998; Underhill and Stoneley, 1998). The post-rift phase of basin evolution started with the deposition of the Gault Formation and continued through the Chalk Group (Fig. 2.11; Butler, 1998; Underhill and Stoneley, 1998). The inversion of the extensional faults was interpreted from the reactivation of the faults into reverse faults and the formation of anticlines in the hanging-wall blocks of each fault with the Weymouth Anticline south of the Ridgeway Fault and the Lulworth Bank Anticline and the Purbeck Anticline south of the Purbeck Fault (Fig. 2.11; Chadwick, 1993; Harvey and Stewart, 1998; Smith and Hatton, 1998; Underhill and Paterson, 1998).

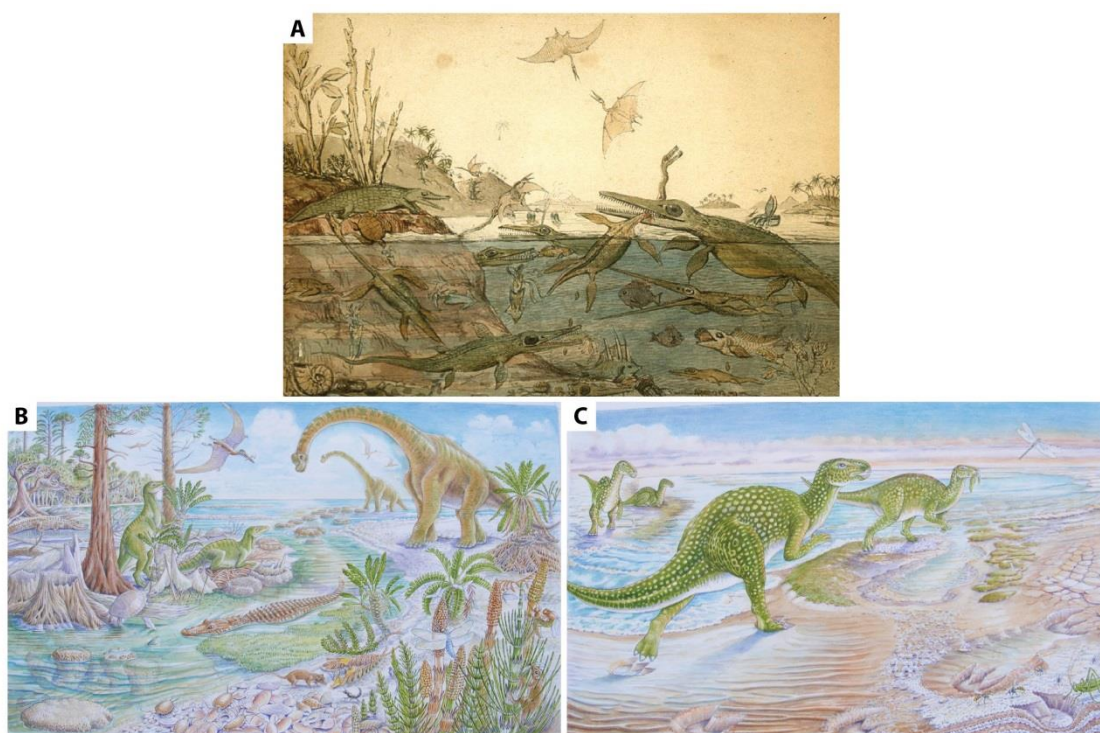


**Figure 2.11** Sketch north-south cross-sections showing the structural evolution of the Purbeck and Ridgeway Faults, redrawn after Underhill and Paterson (1998).

### 3.7. Palaeoenvironments and palaeogeographies in the early Purbeck time

#### 3.7.1. Palaeoenvironments in the early Purbeck time

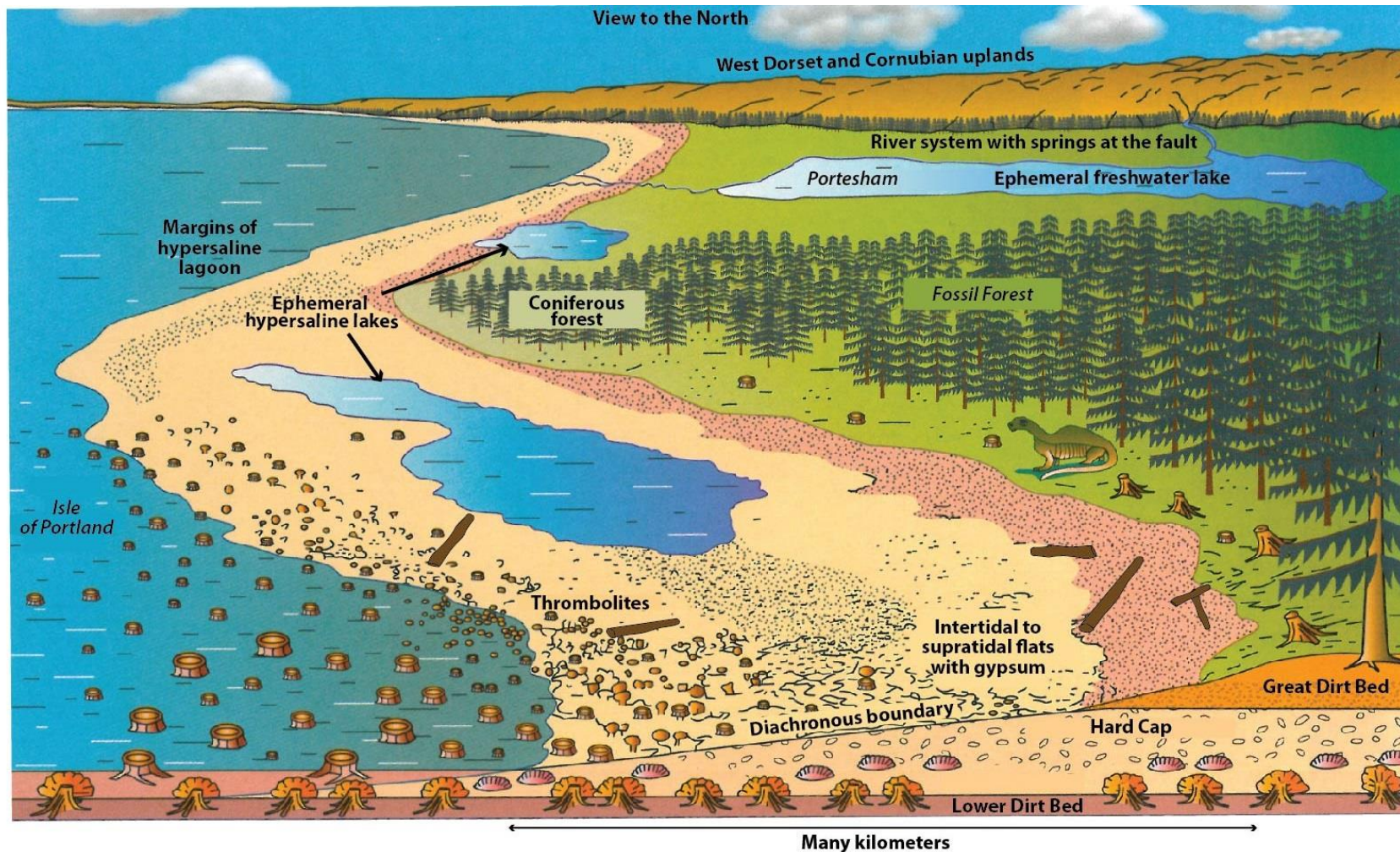
Palaeoenvironments of the Purbeck Limestone Group have been debated since De la Bèche's (1830) famous reconstruction of the environment for the Dorset Coast with all the fossils found along the Devon and Dorset coasts (Fig. 2.12A). Carol Roberts, a freelance artist from Dorset proposed two views for the lower and the upper part of the Mupe Member (Fig. 2.12B-C) based on fossils recorded from these units (<http://carolrobertsillustration.co.uk/>).



**Figure 2.12** Palaeoenvironmental reconstructions and artistic views of the Dorset Coast in early Purbeck time. A – “*Duria Antiquior* – a more ancient Dorsetshire” (De la Bèche, 1830). The Dorset Coast, note the cycads, turtles and crocodile on the left hand side as the only reported fossils to occur in the Purbeck Limestone Group (Durlston Formation). B – “*Lacustrine*” (© Carol Roberts). The lower part of the Mupe Member. Note the presence of the microbial mounds, cycads, ancient coniferous and mollusc shells however mixed with insects and dinosaurs recorded from the Durlston Formation. C – “*Evaporite*” (© Carol Roberts). The upper part of the Mupe Member where three-toes dinosaurs were living on shores of a hypersaline lake.

West (1979) and later modified by Sellwood and Wilson (1990) proposed a palaeoenvironmental reconstruction for the lower part of the Mupe Member for the south Dorset area (Fig. 2.13). This palaeoenvironmental reconstruction is based on field data recorded by West (1979) taking into account the facies distribution both vertically and laterally at the location of the modern Isle of Portland looking North (Fig. 2.13). Concerning the lateral facies distribution, West (1979) locates the possible extent of the coniferous forest and the

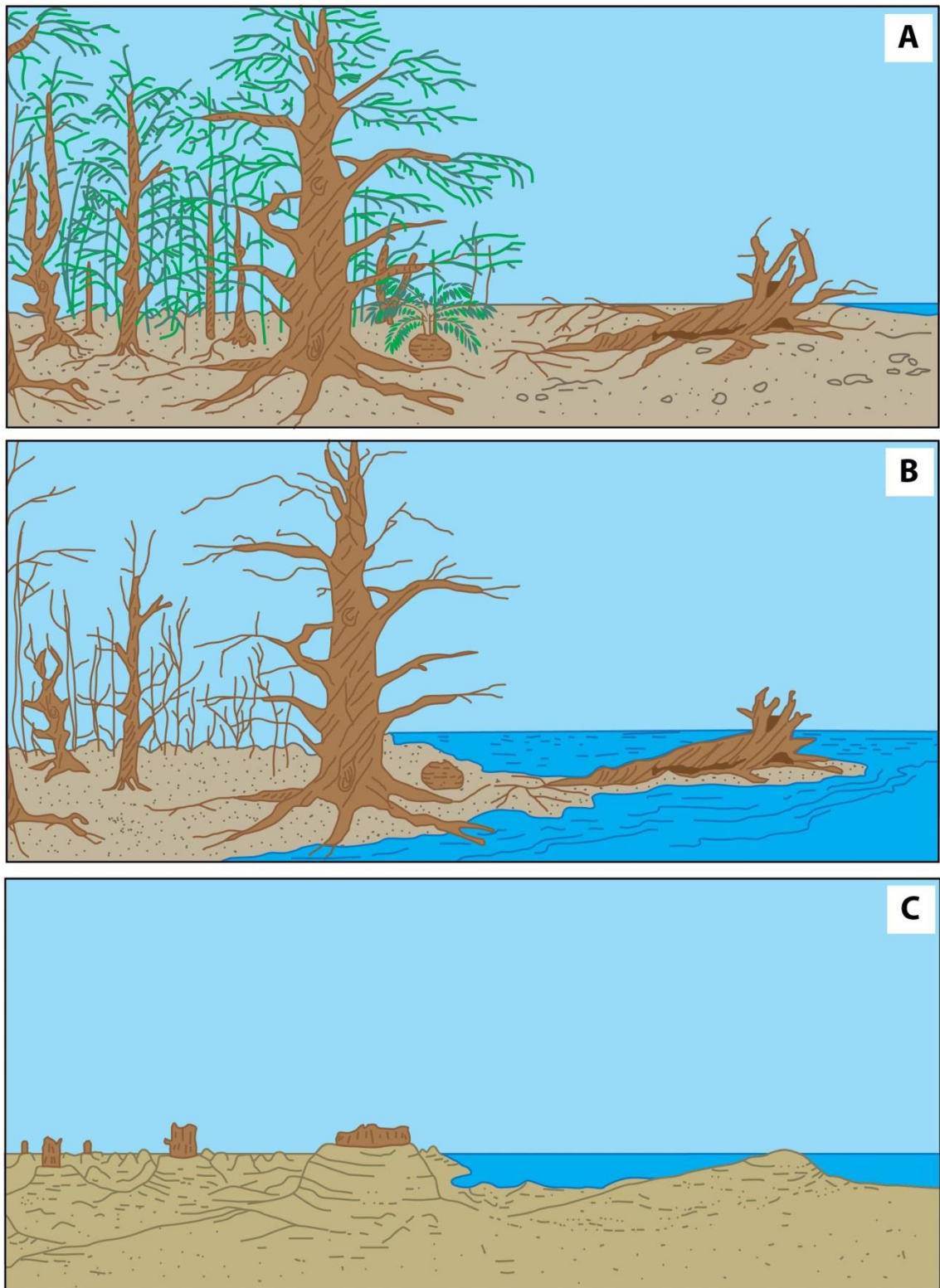
distribution of the stromatolites around tree stumps and fallen trees on the shallow margins of a hypersaline lagoon (Fig. 2.13). Ephemeral coastal lakes either hypersaline or freshwater are depicted between the forest and the shore. Hypersaline lakes host precipitation of salt and gypsum and suggest a rather closed system (in the centre of figure 2.13). Freshwater lakes with insects and charophytes (discovered in Portesham Quarry, West, 1979) suggest both input via river systems or springs and output into the lagoon (on the top of figure 2.13). Concerning the vertical facies succession, at the bottom of figure 2.13, West (1979) proposed a facies model to document the relationship between the paleosols (*i.e.* Lower and Great Dirt Beds) and the Hard Cap bed. Both rendzina paleosols supported the ancient conifers identified by Francis (1982, 1983, 1984, 1986) and in between these paleosols, the peloidal limestones of the Hard Cap bed with stromatolites and lenticular gypsum (Fig. 2.13; West, 1979). In the background West (1979) positioned a slightly higher massif, the West Dorset and Cornubian uplands named by Sellwood and Wilson (1990), to document the initial inversion activity of the Ridgeway Fault (Fig. 2.13; West, 1979, 2013*b*). West (2013*a*) mentions the rare occurrence of dinosaurs (pteropauds and sauropods) because of harsh climate (dry and warm) that was present at that time. However there are no papers in the literature describing dinosaurs living at that time such as bone remains or footprints. West (2013*a*) had inferred the dinosaurs' presence because of their occurrence in underlying and overlying beds of the Lulworth and Durlston Formations of the Purbeck limestones.



**Figure 2.13** Depositional environment reconstructions of the Dorset coast during the deposition of the lower part of the Mupe Member, modified after West (1979) and Sellwood and Wilson (1990). The dinosaurs (pterosaurs and sauropods) are inferred as they are found in the underlying and overlying deposits, but no direct evidence (bones or footprints) of such organisms living at that time was found yet in the Mupe Member deposits. Note occurrence of modern exposures in italics.

Francis (1982) worked at smaller scale and reconstructed possible series of events involved in the drowning of the forests and the formation of the algal limestones. Although Francis (1982) illustrated three steps, she provides a very brief explanation for each step (Fig. 2.14). The first step (Fig. 2.14A) illustrates the forests (associated with the Lower and the Great Dirt Beds) where ancient conifers (*Protocupressinoxylon purbeckensis*) formed a dense forest with some cycadophytes on the shores of a hypersaline lake (Francis, 1982). The second step (Fig. 2.14B) illustrates the deepening of the lake level (saline water) drowning the forest and killing the conifers and cycadophytes (Francis, 1982). The third step (Fig. 2.14C) illustrates post-deposition and after falling lake levels and the formation of algal-bound sediment over the remaining conifer trunks and fallen trees (Francis, 1982). In addition, Francis (1982) conducted a detailed study of the tree moulds left after the decay of the conifers in the algal limestones both of the Hard and Soft Cap beds. She measured the lengths, extents, aperture sizes and orientations of 58 tree holes in the Hard Cap (57 on the Isle of Portland and 1 in Chalbury Camp) and lengths and orientations of 99 burrs in the Soft Cap (28 on the Isle of Portland and 71 at Fossil Forest; Francis, 1982). In the Hard Cap, the average lengths of the tree holes were measured about 53 cm although most commonly they were 10 to 20 cm long and were found between 20 cm and 2 m high from the Lower Dirt Bed (Francis, 1982). The tree hole apertures were measured on average about 9 x 11 cm (height x width) and ranging between 2.5 and 36 cm in diameter (Francis, 1982). The average dip of the tree holes was 20° but most commonly less than 5° with dip directions between N240 (south-west) and N100 (south-east) with a more prominent direction at N190 (south) (Francis, 1982). However she demonstrated that only one tree trunk hole was found (in Portesham Quarry) as all the tree holes are rather small (9 x 11 cm) to be from a trunk. She considered the dip and dip direction measurements to correspond to branches and compared with modern conifers that have their branches with a 40° angle with the trunk. Subsequently she determined that with a main southerly dip direction of the holes, it reflected a north-south direction of the tree trunks. In the Soft Cap, the burr apertures were measured in average 46 cm ranging between 10 cm and 1.02 m while silicified logs were between 5 and 30 cm in diameter (Francis, 1982). The length of these logs was measured in average about 10-15 cm ranging between 7 and 54 cm when exposed (Francis, 1982). Both logs and few burrs were preferentially orientated along a N000-N005 (north-south) direction (Francis, 1982 as previously noted by Gray, 1861 and Hardy, 1897). Francis (1982) interpreted this common preferential orientation north-south of tree holes of the Hard Cap and logs and burrs of the Soft Cap to indicate a northerly blowing wind. However she proposed different interpretations in the occurrence of conifers in the Hard and

the Soft Cap beds (Francis, 1982). Concerning the Hard Cap, one hypothesis was that the trees were growing in the Lower Dirt Bed (Francis, 1982). They were transported by floods or storms from a northern forested area in the lagoon and algal bounded on the floor of this lagoon at the location of the Isle of Portland today (Francis, 1982). This hypothesis was mainly driven by the non-occurrence of rooted trees in the Lower Dirt Bed (Francis, 1982). Alternatively she proposed that the trees did grow in the Lower Dirt Bed and were later affected by a strong northerly blowing wind or storm (Francis, 1982). The hypothesis originated from the recording of the north-south orientations of the tree holes (Francis, 1982). Concerning the Soft Cap and the Great Dirt Bed forest, the hypothesis was that the sudden flooding of the forest by hypersaline waters killed the trees (Francis, 1982). Algal-boundstones were then deposited around the in-situ trees consolidating the base while the rest of the trees outside of the waters were rotten and fallen off due to strong northerly winds before they were encased with algal deposits (Francis, 1982).



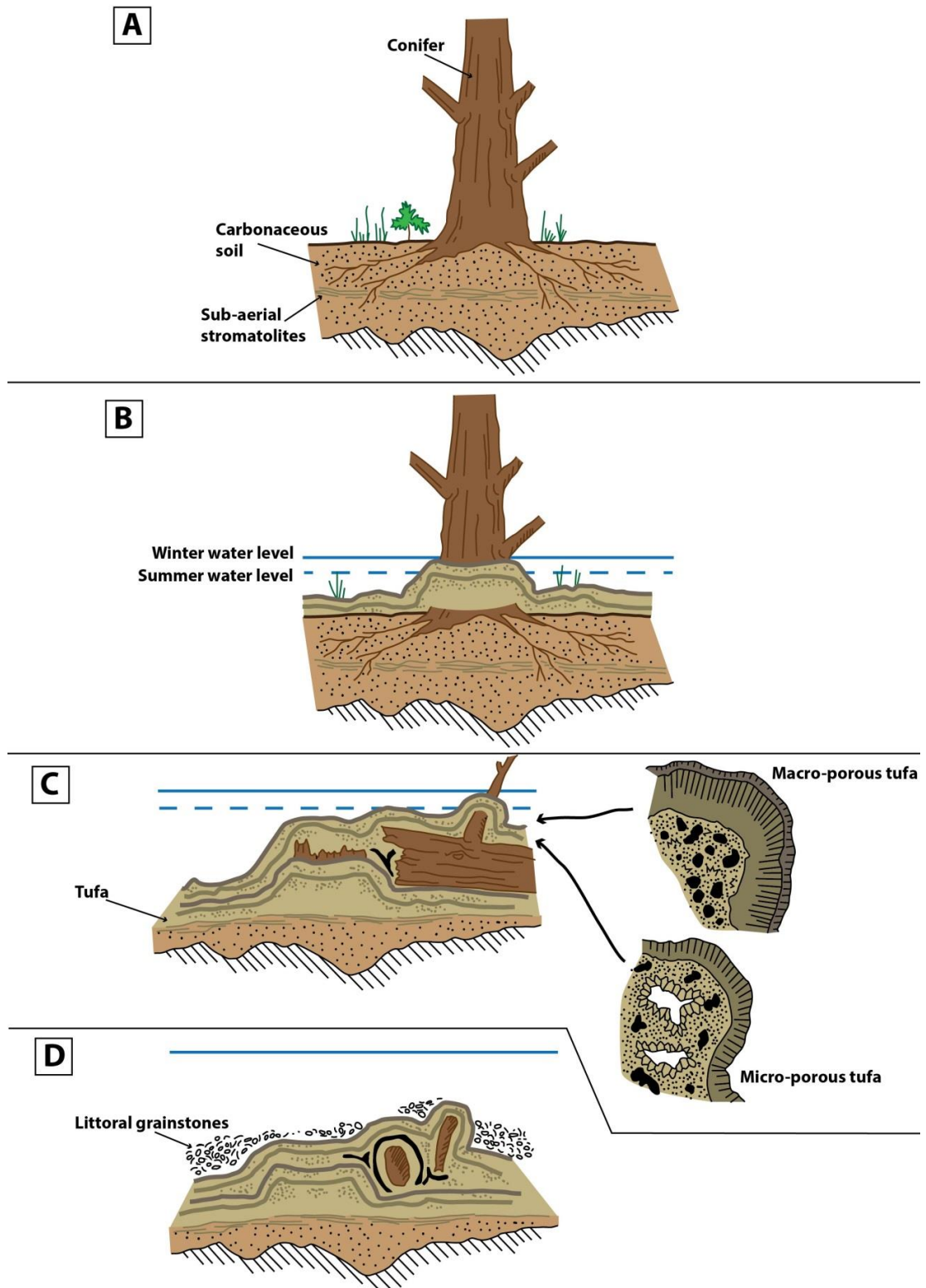
**Figure 2.14** Sequence of events involved in the drowning of the Purbeck forests and the formation of algal limestones (modified after Francis, 1982). A – Ancient conifers forming a dense forest. B – Hypersaline to saline water rising drowning the forest. C – Post-deposition of the algal limestones covering in-situ conifer stumps and fallen trees in falling lake level.



In contrast Bosence (1987) interpreted the tufa deposits (as presented earlier in section 3.5.1.1.2 of this chapter) as having formed in freshwaters as they are not associated with evaporites on the Isle of Portland. He also proposed a possible sequence of events involved in the formation of the mounds deposited around the trees. This interpretation is based on sedimentology of the mounds and associated facies. The concentric burrowed thrombolites all around the trees and with a rather similar thickness indicates that the trees were in upright position during the deposition (Bosence, 1987). The thrombolitic framework continued upwards mainly after the trees collapsed as indicated by the asymmetrical and greater thickness of the thrombolite on the upper surfaces (Bosence, 1987). The local fracturing of the burrowed thrombolite indicates that this facies was consolidated before collapsing (Bosence, 1987). This sequence of events is also confirmed by geopetal infills in the growth cavities (Bosence, 1987). The inner burrowed thrombolites comprise two geopetal infills at right angle while the outer tufa frameworks comprise only one geopetal infill concordant with the sub-horizontal position of the tree holes at present day (Bosence, 1987). Bosence (1987) noticed as well that tufas can be amalgamated and form a bioherm up to 5 m x 2 m high above the surrounding peloidal grainstones.

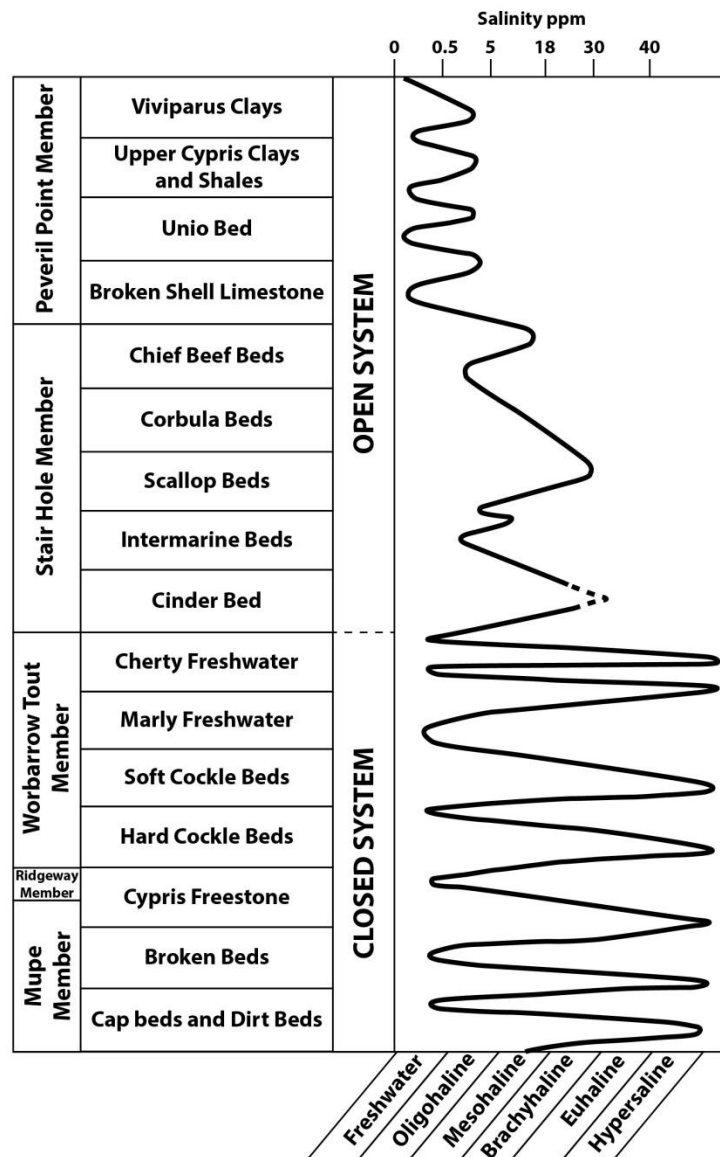
Subsequently Perry (1994) proposed a reconstruction of events for the formation of the tufa stromatolites. Following the description of the different facies (refer to section 3.5.1.1.2 of this chapter) Perry (1994) concurred with Bosence's view that the tufa stromatolites were of lacustrine freshwater origin. This was interpreted from the fabrics, the high porosity of the Purbeck tufas (typical from freshwater tufas, Pedley, 1990), the absence of evaporites and of intertidal sediments (specific of marine intertidal zone, Perry, 1994) and the fact that the trees were preserved at least during the deposition of the tufas (Perry, 1994). According to Perry (1994) if the environment was hypersaline or saline the trees would have been rotted away rapidly after the drowning and before the tufas could form around them. All this helped Perry (1994) to interpret a series of possible events in the deposition of the tufas stromatolites (Fig. 2.15). The first step (Fig. 2.15A) illustrates the paleosols forming on top of a sub-aerial exposure, containing sub-aerial stromatolites that shows the influence of biogenic processes and supporting conifer forest and other vegetation (Perry, 1994). The second step (Fig. 2.15B) illustrates the rising of freshwater lake level drowning the forest and killing the conifers and associated vegetation (Perry, 1994). The high concentration of carbonate ions in the water together with the nutrients provided by the former vegetation helped the formation of a biofilm at the base of the trees and surrounding areas (Perry, 1994). The photosynthetic activity increased the carbon dioxide content of the water and triggered the precipitation of

carbonate (Fig. 2.15B; Perry, 1994). The third step (Fig. 2.15C) illustrates the deposition of the micro- and macro-textures subject to water level fluctuations (Perry, 1994). The micro-texture tufas was formed during the wet winter season when lake level was at its highest and was burrowed during the dry summer season when emergent and lake level at its lowest (Fig. 2.15C; Perry, 1994). Similarly the macro-porous tufas were predominantly formed during the dry summer season (Fig. 2.15C; Perry, 1994). Their lack of burrows and high porosity were explained by the fact that they were never emergent (Perry, 1994). The fourth step (Fig. 2.15D) illustrates the rising of lake level, drowning of the tufas and the deposition of the littoral grainstones (Perry, 1994).



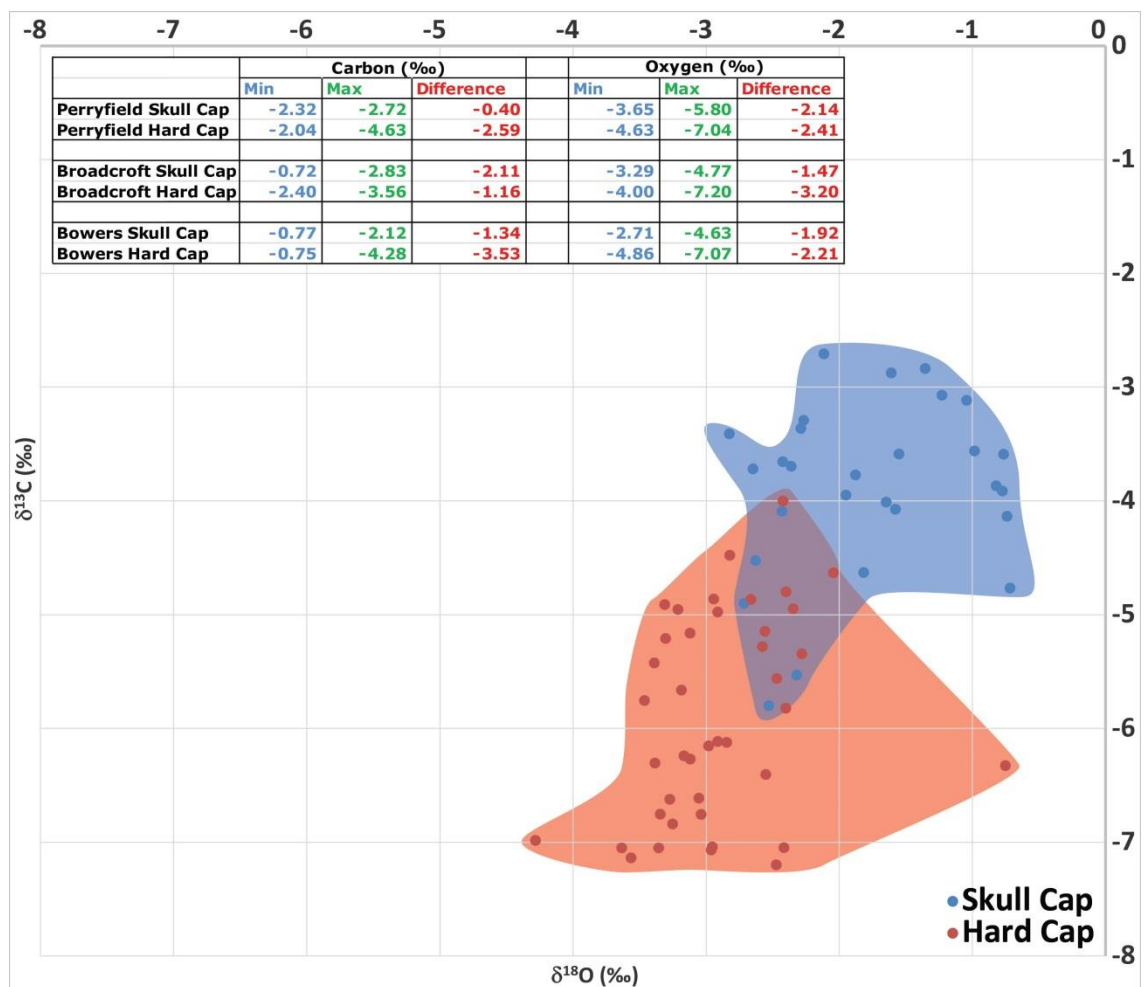
**Figure 2.15** Sequence of events explaining the deposition of tufa stromatolites (modified after Perry, 1994). A – Ancient conifers growing on carbonaceous soil with sub-aerial stromatolites in the soil. B – Rising of the freshwater lake drowning the forest and offering conditions for tufa deposition seasonally. C – The lake level continues to rise causing the death of the conifers and to break down followed by a second generation of tufa deposition. D – The transgression of marine or saline waters drown the tufas that stopped their deposition and allowed sedimentation of the littoral grainstones facies with ostracods.

Radley's (2002) review of the mollusc assemblages of the Purbeck Limestone Group of Dorset (refer to section 3.5.1.1.5 of this chapter) enabled him to infer palaeosalinities from gastropod assemblages mainly based on Fürsich's (1994) work on salinity-controlled benthic macroinvertebrates. Radley (2002) compiled data from Arkell (1941), West (1961), Clements (1973), Barker *et al.* (1975) and his own work to interpret salinity fluctuations of the Purbeck Limestone Group (Fig. 2.16). During the deposition of the Cap beds and Dirt Beds, he inferred the low diversity of fresh- to brackish water (low-salinity) species to indicate a closed lake system. The mixing of low-salinities and marine species to indicate possible periodic marine input although Radley (2002) specified that the "*precise environments remain unclear*". The low diversity of low-salinities species in the Broken Beds and Cypris Freestone to indicate a closed lake system with periodic hypersaline conditions (Fig. 2.16; Radley, 2002).

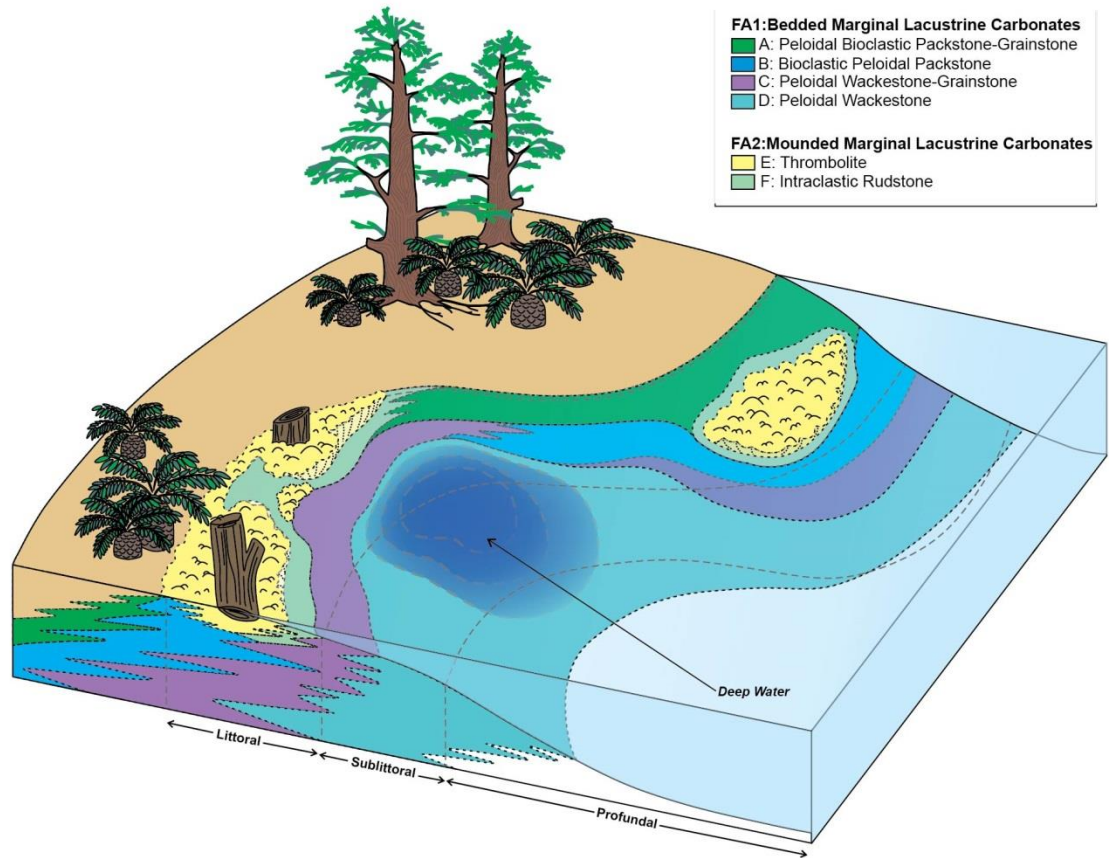


**Figure 2.16** Inferred palaeosalinity fluctuations of the Purbeck Limestone Group (modified after Radley, 2002).

As well as studying the facies, Dharmarajah (2015) conducted stable isotope (carbon and oxygen) analyses at three locations (Bowers, Perryfield and Broadcroft Quarries on the Isle of Portland) and in both the Skull and Hard Cap beds (Fig. 2.17). She compared these data to Talbot's (1990) and Leng and Marshall's (2004) general freshening trends from the Skull to the Hard Cap beds for lacustrine and open lake system. Altogether, facies and stable isotope data helped Dharmarajah (2015) to propose a depositional model for the lower part of the Mupe Member (Fig. 2.18). This depositional model presents an interpretation of facies distribution on a prograding margin of an open brackish water lake system with the coarser facies in the shallowest areas, the finer facies in the deepest areas and associated with thrombolite mounds (Fig. 2.18; Dharmarajah, 2015).



**Figure 2.17** Cross-plot of carbon and oxygen isotope from the Skull and Hard Cap beds of the Mupe Member (modified after Dharmarajah, 2015). Values in the table on the top left corner are the average values for each bed and at each location.



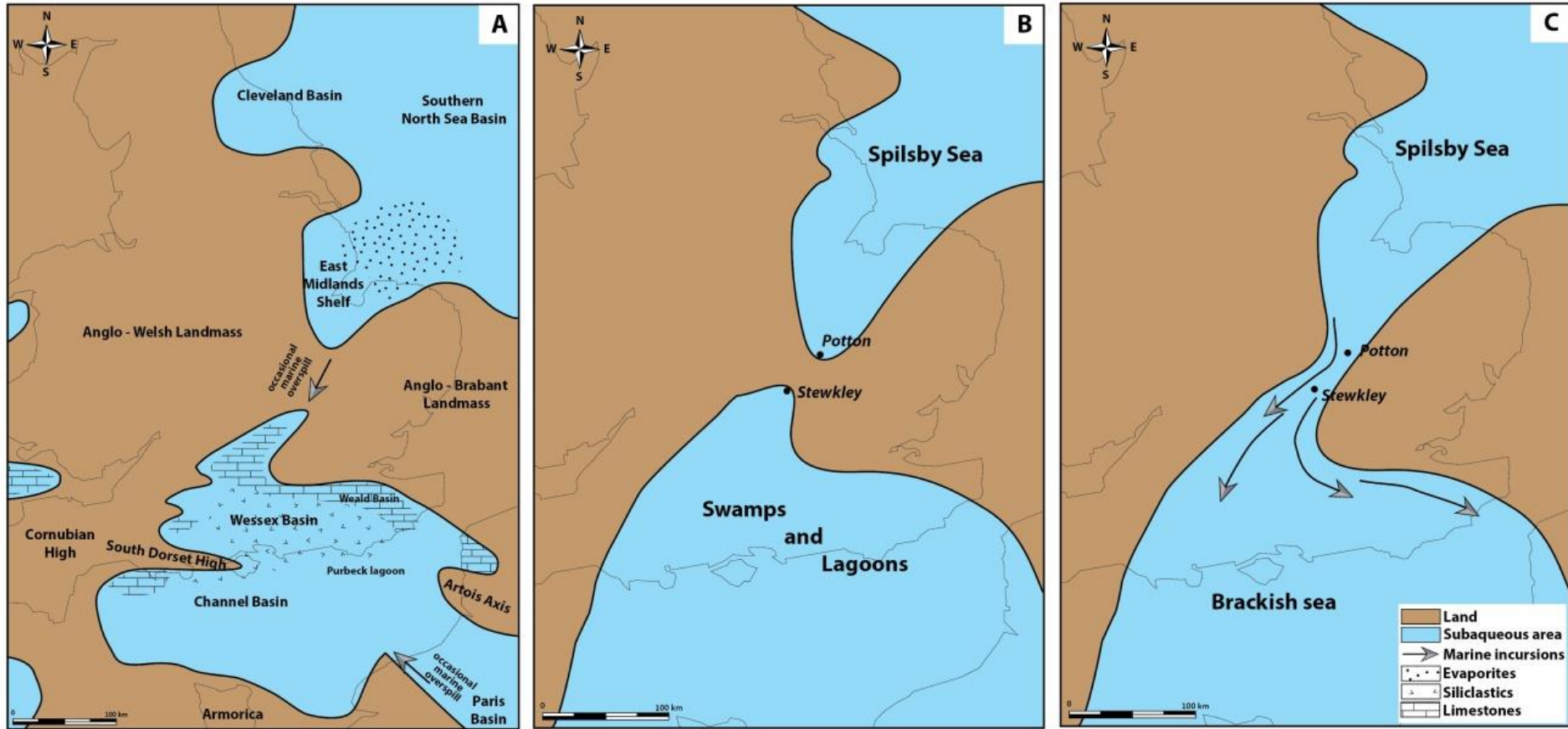
**Figure 2.18** Depositional model for the Cap beds of the Mupe Member (modified after Dharmarajah, 2015).

### 3.7.2. Palaeogeographies in the early Purbeck time

Palaeogeographical reconstructions for the Purbeck Limestone Group are of two scales, Wessex Basin scale (Fig. 2.19) and more local (*i.e.* Dorset) scale (Figs. 2.20 and 2.21).

At the basin-scale, studies show facies distribution at the time of the *Cypridea dunkeri* ostracod biozone (Fig. 2.19A-B; Casey, 1963; Lake, 1985; Cope *et al.*, 1992) and the *Cypridea granulosa* ostracod biozone (Fig. 2.19C; Casey, 1963). Figure 2.19A presents a palaeogeographical reconstruction of the south of England and north of France basins for the *Cypridea dunkeri* biozone after Cope *et al.* (1992). They showed that the margins of the basin were dominated by carbonates; while in the centre part of the basin, were deposited sulphate evaporites (Fig. 2.19A). What were likely to be present are the South Dorset High location and its influence on the deposition and facies distribution; and the occasional marine overflows from the Paris Basin to the south-east (Cope *et al.*, 1992). Cope *et al.* (1992) showed that this palaeogeographical reconstruction is nevertheless partially based on speculations. The first main speculation they made concerned the occasional connection of the southern part of the

North Sea Basin to the Wessex Basin via marine overspill that was assumed from underlying Portland deposit settings (Fig. 2.19A). The second main speculation they made concerned the extent of the Channel Basin to the south due to a lack of data available (such as well data or seismic images) from the English Channel (Fig. 2.19A). Reconstructions B-C are from Casey (1963) and explain the separation between the freshwater deposits of a southern basin (*i.e.* Wessex Basin) and the marine deposits from a northern sea basin (*i.e.* Spilsby Sea; Fig. 2.19B); and to explain the deposition of the Cinder Bed (Fig. 2.19C). The northernmost exposures of the Wessex Basin located at Stewkley are about 25 miles away from the southernmost exposures of the Spilsby Sea at Potton (Fig. 2.19B-C). The proximity of these basin margins together with the increase of molluscs at the base of the Durlston Formation helped Casey (1962, 1963) to correlate the Cinder Bed with the marine mid-Spilsby nodule-bed deposited in the Spilsby Sea (Casey, 1963). Subsequently, this correlation helped him to propose the marine incursions from the Spilsby Sea into the Wessex Basin (Casey, 1962, 1963; Fig. 2.19C).

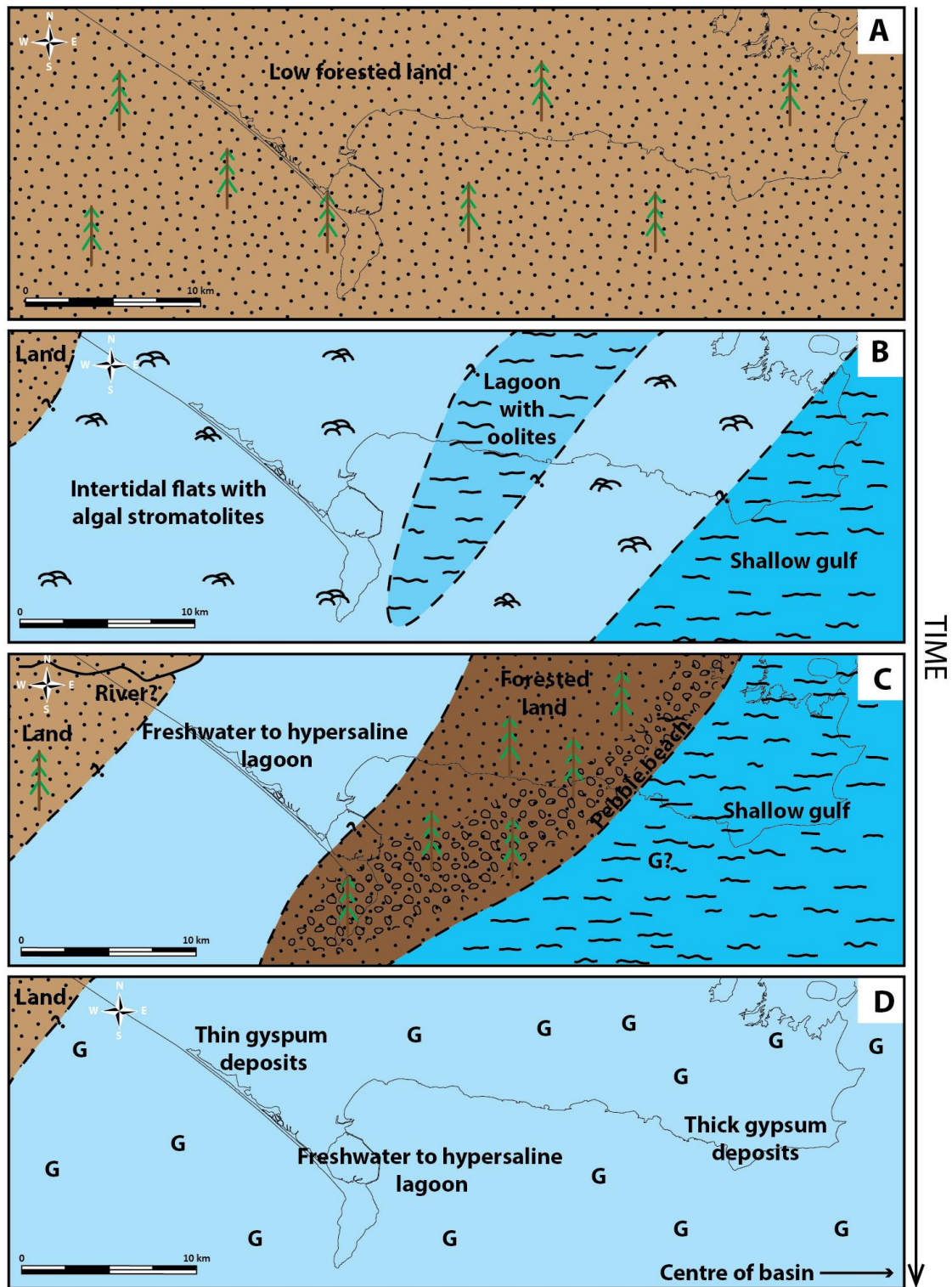


**Figure 2.19** Palaeogeographical reconstructions of the Wessex Basin at the time of the deposition of the Purbeck Limestone Group. A – For the *Cypridea dunkeri* biozone of the lower Mupe Member, redrawn after Cope *et al.* (1992). B – At the end of the Jurassic Period (probably *Cypridea dunkeri* biozone, redrawn after Casey, 1963). C – At the beginning of the Cretaceous Period at the time of the Cinder Bed deposition (probably *Cypridea granulosa* biozone, redrawn after Casey, 1963).



Despite the intensive study of the Dorset area since the 19<sup>th</sup> century, there are only a few palaeogeographical reconstructions of the lower Purbeck Limestone Group in the literature (Figs. 2.20 and 2.21; West, 1975, 1979; Francis, 1982; Sellwood and Wilson, 1990; Underhill, 2002).

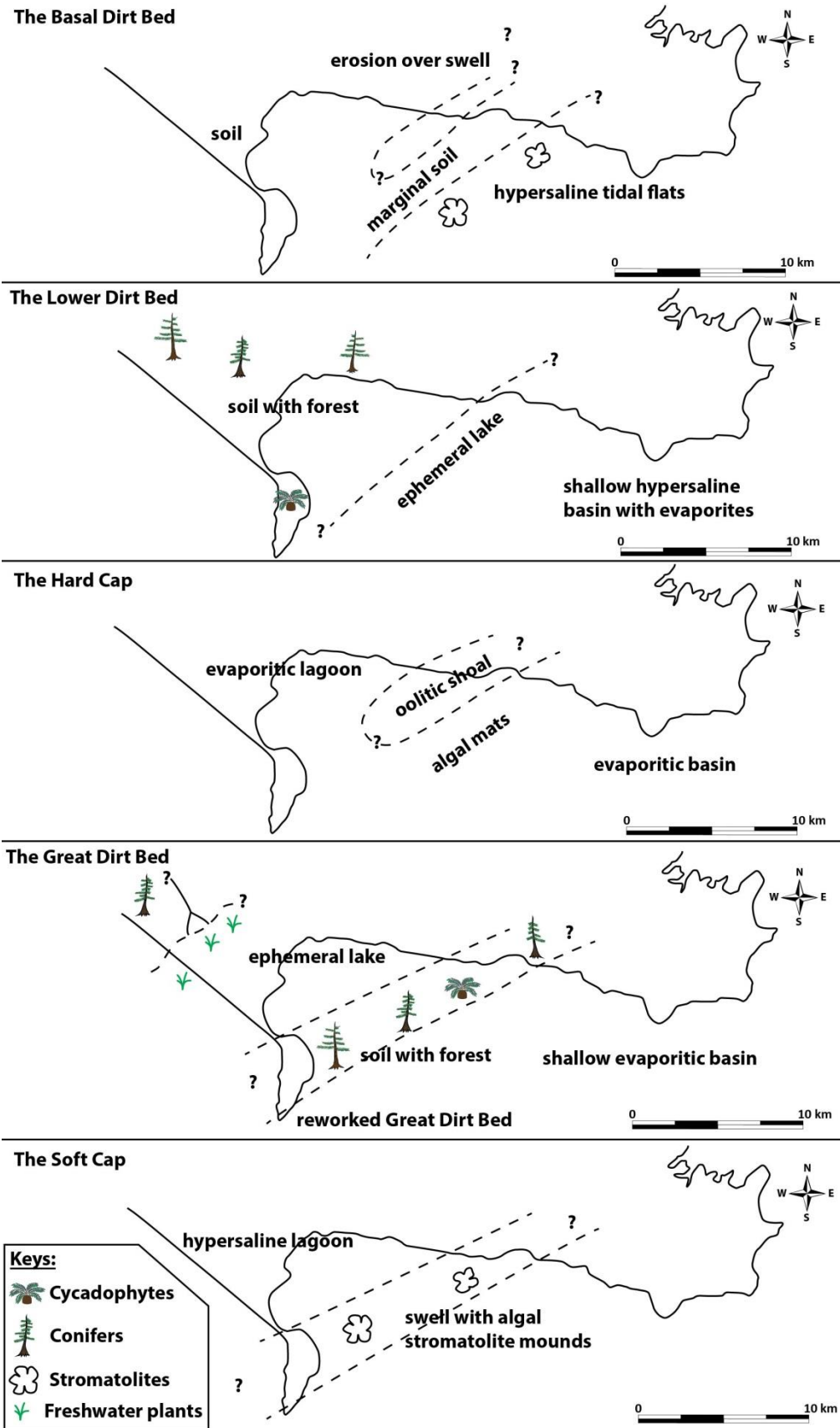
West (1975) proposed four palaeogeographies (Fig. 2.20) for the marginal facies at the time of the deposition of the Lower Dirt Bed (Fig. 2.20A), of the Hard Cap (Fig. 2.20B), of the Great Dirt Bed (Fig. 2.20C) and of the evaporites above the Soft Cap (Fig. 2.20D). In these palaeogeographies, West (1975) showed the facies distribution based on fieldwork on south Dorset Coast. The Lower Dirt Bed was interpreted by West (1975) to be deposited synchronously all along the Dorset coast (Fig. 2.20A). The Hard Cap was interpreted to be deposited in transgressive intertidal flats with algal stromatolites and an oolitic lagoon in the centre part with a NE-SW facies trend (Fig. 2.20B). The Great Dirt Bed was not deposited everywhere, but followed the same NE-SW trend of the underlying oolitic lagoon that formed a forested land with ancient coniferous trees and cycads surrounded by pebbly beaches (Fig. 2.20C). This paleosol was interpreted to be surrounded with a freshwater to hypersaline lagoon to the west and a shallow gulf to the east with possible evaporite precipitation (Fig. 2.20C). West (1975) showed that the evaporites (above the Soft Cap) were deposited synchronously in one regressive event with strata thickening to the east, to the centre of the basin (Fig. 2.20D). West (1975) proposed that the facies were organised in cycles, the base of each cycle being a paleosol (*i.e.* Lower Dirt Bed and Great Dirt Bed), overlain by stromatolitic and pelletoid limestones and capped by gypsum and limestone deposits.



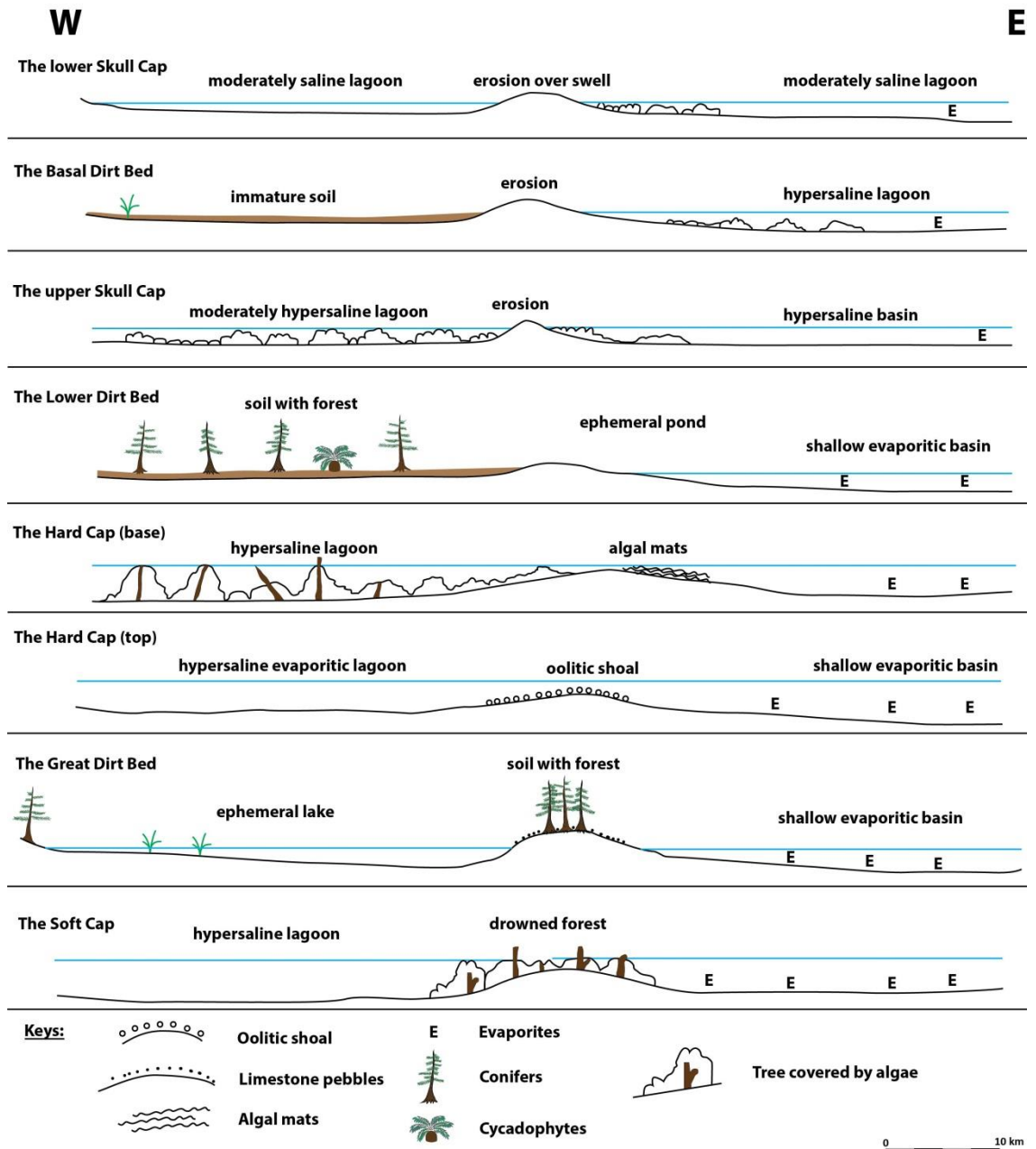
**Figure 2.20** Palaeogeography of the Dorset coast at the time of deposition of the Mupe Member modified after West (1975). A – During the deposition of the Lower Dirt Bed. B – During the deposition of the Hard Cap. C – During the deposition of the Great Dirt Bed. D – During the deposition of the evaporites just above the Soft Cap. G stands for Gypsum deposit.

Francis (1982) remains the most detailed study and reconstructions of depositional environments and palaeogeographies for the time of deposition of the lower part of the Mupe Member (Fig. 2.21). Following log correlation panels and comparison with modern day environments, Francis (1982) proposed a reconstruction of depositional environments for each bed (Fig. 2.22). The Skull Cap was interpreted to be formed during regression of sea level due to the change from marine environments (Portland Group) to non-marine determined by the appearance of stromatolites and non-marine fauna (Francis, 1982). Comparison of the lower part of the Skull Cap stromatolites to those of Shark Bay in Australia helped Francis (1982) to interpret moderately (because gypsum is absent) hypersaline lagoons to the west and the east separated by a swell. This swell passed through the Lulworth area with a NE-SW trend but its extent was difficult to determine due to lack of exposures beyond this area (Figs. 2.21 and 2.22; Francis, 1982). The persistence of this regressive phase led to the formation of the Basal Dirt Bed to the west of the swell and a thinning and reduction of plant remains at Mupe Bay and Worbarrow suggests that this area was near the margin of a much denser forest to the north (Figs. 2.21 and 2.22; Francis, 1982). However to the east remained a hypersaline lagoon with stromatolites on the margins (Figs. 2.21 and 2.22; Francis, 1982). This was followed by a transgression and the Basal Dirt Bed was covered by a moderately hypersaline lagoon to the west and a hypersaline basin to the east (Figs. 2.21 and 2.22; Francis, 1982). The western lagoon was considered by Francis (1982) as part of an intertidal zone of the hypersaline basin with stromatolite developments (Figs. 2.21 and 2.22). The Lower Dirt Bed was the result of another rapid regression that led to a sub-aerial exposure and later development of a soil (Francis, 1982). To the west of Worbarrow the paleosol supported cycadophytes and ancient conifer trees, while to the east the paleosol disappeared and was replaced by evaporite deposits suggesting a hypersaline basin (Figs. 2.21 and 2.22; Francis, 1982). At Worbarrow this paleosol was replaced by shale suggesting an ephemeral pond on the margin of a saline basin that periodically dried up (Figs. 2.21 and 2.22; Francis, 1982). The depositional setting of the Lower Dirt Bed indicates a transition from a hypersaline basin to the east passing gradually to a landed area to the west as observed in the modern day Persian Gulf (Figs. 2.21 and 2.22; Francis, 1982). The Hard Cap was the result of a rapid transgression that drowned the Lower Dirt Bed forest (Francis, 1982). The base of the Hard Cap was characterised to the west by large stromatolitic mounds that developed around tree stumps in an intertidal zone of a hypersaline lagoon (Figs. 2.21 and 2.22; Francis, 1982). The stromatolitic mounds were replaced by algal mats over the Lulworth area suggesting a high in the topography of the lagoon and separated it from a shallow evaporitic basin to the east (Figs. 2.21 and 2.22;

Francis, 1982). The top of the Hard Cap was characterised by an intertidal hypersaline evaporitic lagoon all along the studied area as suggested by the presence of evaporites (Francis, 1982). Evidence of exposure (calcrete textures and polygonal desiccation in algal mats) and deposition of oolitic shoal were found along a NE-SW trend between Lulworth area and the Isle of Portland (Figs. 2.21 and 2.22; Francis, 1982). This indicates that the swell identified in the previous reconstructions was still present and was influencing the deposition (Figs. 2.21 and 2.22; Francis, 1982). The Great Dirt Bed was the result of a regression that lasted longer than for previous soils (Francis, 1982). This led to the formation of a thick soil with large ancient conifers and pebbles derived from the underlying Hard Cap (Francis, 1982). However this soil developed only between Lulworth area and the Isle of Portland (Figs. 2.21 and 2.22; Francis, 1982). To the west dark clays with plant material, freshwater fauna, land plants and evaporites indicated an ephemeral lake drying out in summer as per modern day coastal lagoons in South Australia (Figs. 2.21 and 2.22; Francis, 1982). To the east evaporite deposits suggested a hypersaline evaporitic basin (Figs. 2.21 and 2.22; Francis, 1982). The Soft Cap was the result of another rapid transgression that drowned the Great Dirt Bed forest (Francis, 1982). The soil and the *in-situ* conifer stumps were covered by algal-bound sediment in an intertidal hypersaline lagoon (Figs. 2.21 and 2.22; Francis, 1982). Thinner deposits on the south of the Isle of Portland where only algal mats with pelletoid silts were deposited, suggested shallower conditions (Francis, 1982). To the east this bed was characterised by evaporite deposits indicating the continuation of the transgression of the evaporitic basin triggered during the Skull Cap deposition (Figs. 2.21 and 2.22; Francis, 1982).

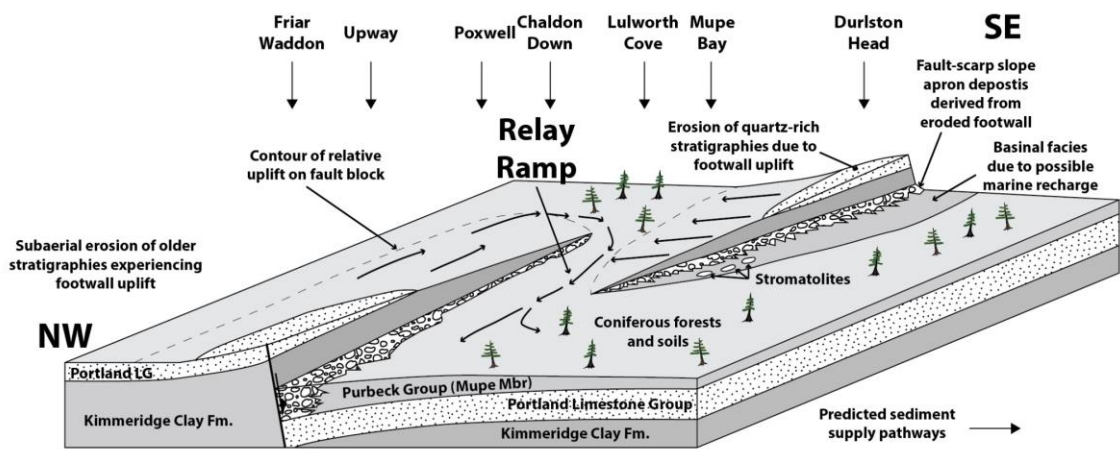


**Figure 2.21** Schematic palaeogeographic reconstructions of the Dorset coast area during deposition of the Cap beds and Dirt Beds, redrawn after Francis (1982).



**Figure 2.22** Depositional environment reconstructions, redrawn after Francis (1982).

Underhill and Paterson's (1998) regional study of onshore outcrops and offshore and onshore subsurface data provides the main depositional and tectonic settings of the Purbeck Limestone Group (Fig. 2.11). Underhill (2002) proposed a syn-sedimentary tectonic control on the facies distribution of the Mupe Member (Fig. 2.23). The facies were based on West's (1975) facies belts and "other workers" together with generalised models for sedimentation around relay ramp zones to propose a structural and depositional model for the Mupe Member. He proposed that the Abbotsbury-Ridgeway and Purbeck Faults were linked by a relay ramp area to accommodate the displacement along the faulted zone (Fig. 2.23; Underhill, 2002). He interpreted the relay ramp area to be the main pathway for sediment supply into the basin (Fig. 2.23; Underhill, 2002). He showed in his model syn-sedimentary faults active during the deposition of the Mupe Member deposits (as indicated with the thickness increasing towards the faults in figure 2.23). He inferred from published models that the deposition of a conglomeratic facies in the footwall blocks in the vicinity of the fault scarps surrounded by paleosols where the ancient cypress trees were rooted (Fig. 2.23). In addition he interpreted deeper facies to be deposited only on the eastern part of the studied area to be due to occasional marine incursions (Fig. 2.23; Underhill, 2002).



**Figure 2.23** Depositional model for the Mupe Member (redrawn after Underhill, 2002).

## Chapter 3

Subsurface study of  
stratigraphic and tectonic  
setting of the Purbeck  
Limestone Group in the  
south-west Wessex Basin



## 1. Introduction

Generations of geologists have studied the complexity of the structural evolution of the Wessex Basin (Bristow, 1889; Strahan, 1898; West, 1975; Lake, 1985; Butler, 1998; Underhill and Stoneley, 1998). This study examines the structural evolution for the western part of the Wessex Basin based on a new seismic interpretation of a 3-D block seismic data as well as 2-D seismic profiles onshore and from Bournemouth and Weymouth Bays. The main aim of this study is to identify the possible tectonic control of two main extensional faults on the deposition of the Purbeck Limestone Group (Late Jurassic-Early Cretaceous). Previous studies (Colter and Harvard, 1981; Stoneley and Selley, 1986; House, 1989; Butler and Pullan, 1990; Chadwick, 1993; Butler, 1998; Harvey and Stewart, 1998; Underhill and Stoneley, 1998; Underhill and Paterson, 2002) present clear evidence for synsedimentary tectonic structures during the Jurassic and the Early Cretaceous however it is still unclear whether the faults were active or not during Purbeck time (Tithonian-Berriasian). The seismic interpretation presented here indicates east-west syndepositional extensional faults (the Ridgeway and Purbeck Faults) with preferential accumulation in half grabens to the south that are linked by a relay ramp, emphasising a structural control on sediment accumulation during Purbeck time.

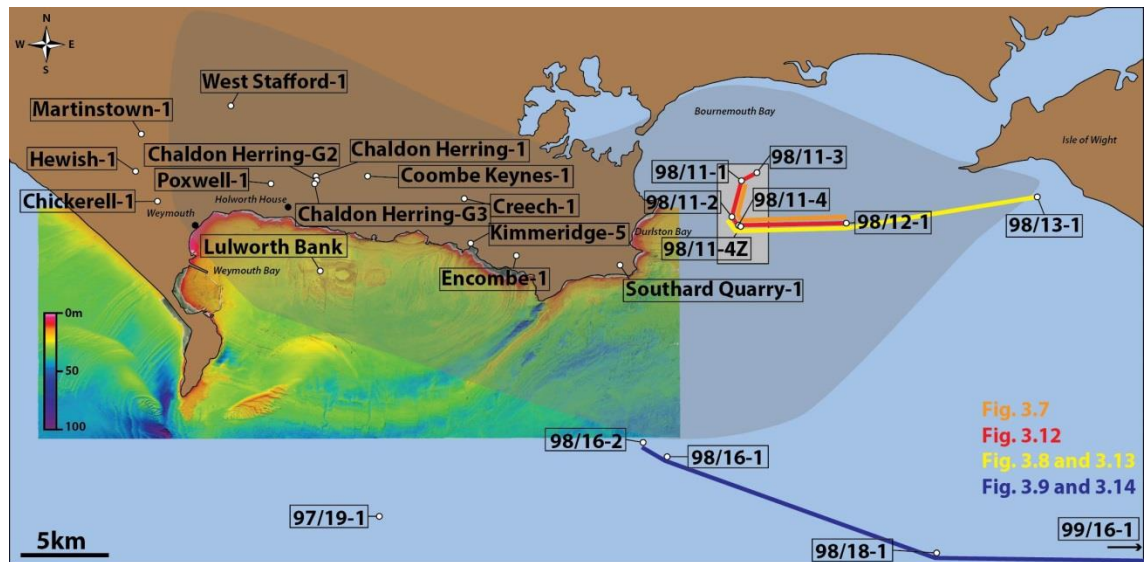
## 2. Methodology

### 2.1. Introduction

In this project 2-D seismic profiles (onshore and offshore), a 3-D block offshore and wells with borehole data (Fig. 3.1) have been interpreted with the aim of understanding the relationship between the accumulation of strata and the structural evolution of the Wessex Basin.

The geological interpretation has been carried out with Petrel™ Software (Schlumberger, version 2011). In addition a multi-beam radar acoustic survey of Weymouth Bay seafloor, the Dorset Integrated Seabed Study (DORIS, Figs. 3.1; 3.2 and 3.21) acquired in 2008 acquired by Dorset Wildlife Trust, the Maritime and Coastguard Agency and Channel Coastal Observatory (with less than 1 m resolution) as well as the British Geological Survey geological map 1:50000 onshore (1949) and the National Geographic world topographic map (public domain) have been combined within Petrel to tie the subsurface with surface data. All these data were georeferenced under ED50-UTM30 ("MENTOR: ED50-UTM30: European 1950 Based UTM, Zone 30 North, Meter") coordinate reference.

Two horizons have been interpreted in detail, Top Purbeck and Top Portland as well as a total of twenty-eight faults. Four correspond to the Ridgeway fault (named Ridgeway Faults 1; 2; 3 and 4), one to the Purbeck fault (named Purbeck Fault) and twenty-three to subsidiary faults (named Subsidiary Faults 1 to 23) created either during the rifting phase or the inversion phase of the Wessex Basin.



**Figure 3.1** Location map of wells and seismic profiles interpreted in this study. Dark grey area is the area covered by the 2-D seismic profiles (detailed in Fig. 3.2) and the light grey box corresponds to the 3-D block (detailed in Fig. 3.4). DORIS seafloor data from Weymouth Bay and Portland area detailed in figure 3.21. Orange line locates well correlation of figure 3.7. Red line locates well correlation of figure 3.12. Yellow line locates well correlation of figures 3.8 and 3.13. Blue line locates well correlation of figures 3.9 and 3.14.

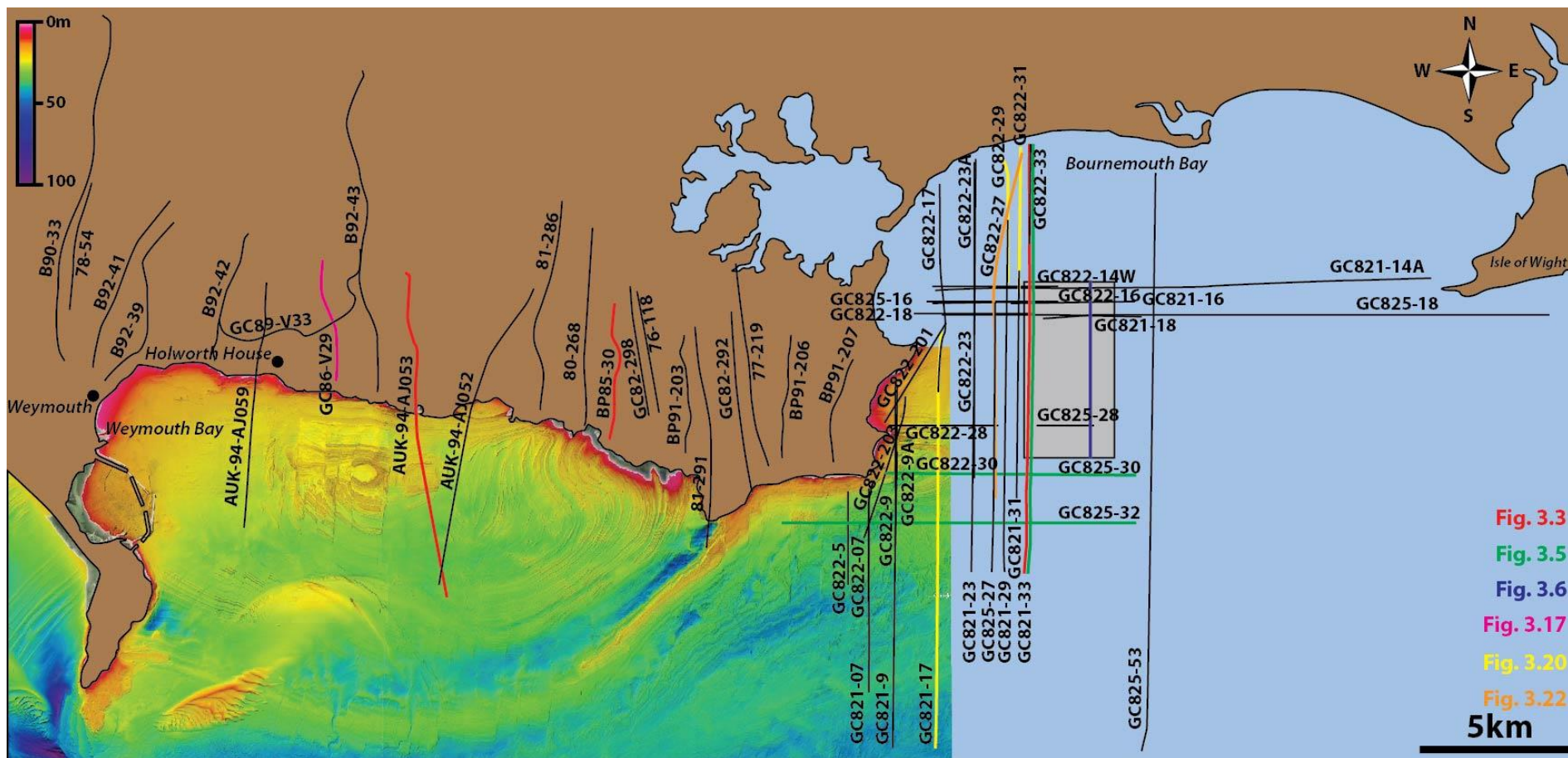
## 2.2. Details of 2-D seismic profiles

Twenty-two 2-D profiles (178.36 km in total) located onshore (between Weymouth and Durlston Bays, Figs. 3.1 and 3.2; Tab. 3.1) have been obtained from the UK Onshore Geophysical Library (UKOGL) as well as thirty-five 2-D profiles (327.04 km in total) located offshore in Bournemouth Bay (Figs. 3.1 and 3.2; Tab. 3.1; public domain) have been studied. Different source types were used during the seismic acquisition such as dynamite, vibroseis, explosive powergel (for the onshore acquisition) and airgun (for the offshore acquisition) and these are summarised in Table 3.1. The frequency ranges between 10 and 85 Hz and the interval between two stations varies from 15 m to 61 m. This information is only available for the seismic profiles acquired partly or totally onshore and not for those acquired offshore. The quality of the profiles depends on the location of their acquisition either onshore or offshore. The seismic profiles acquired offshore in Bournemouth Bay are generally of good quality (Fig. 3.3C). The seismic profiles acquired onshore have a poorer quality but improve away from the

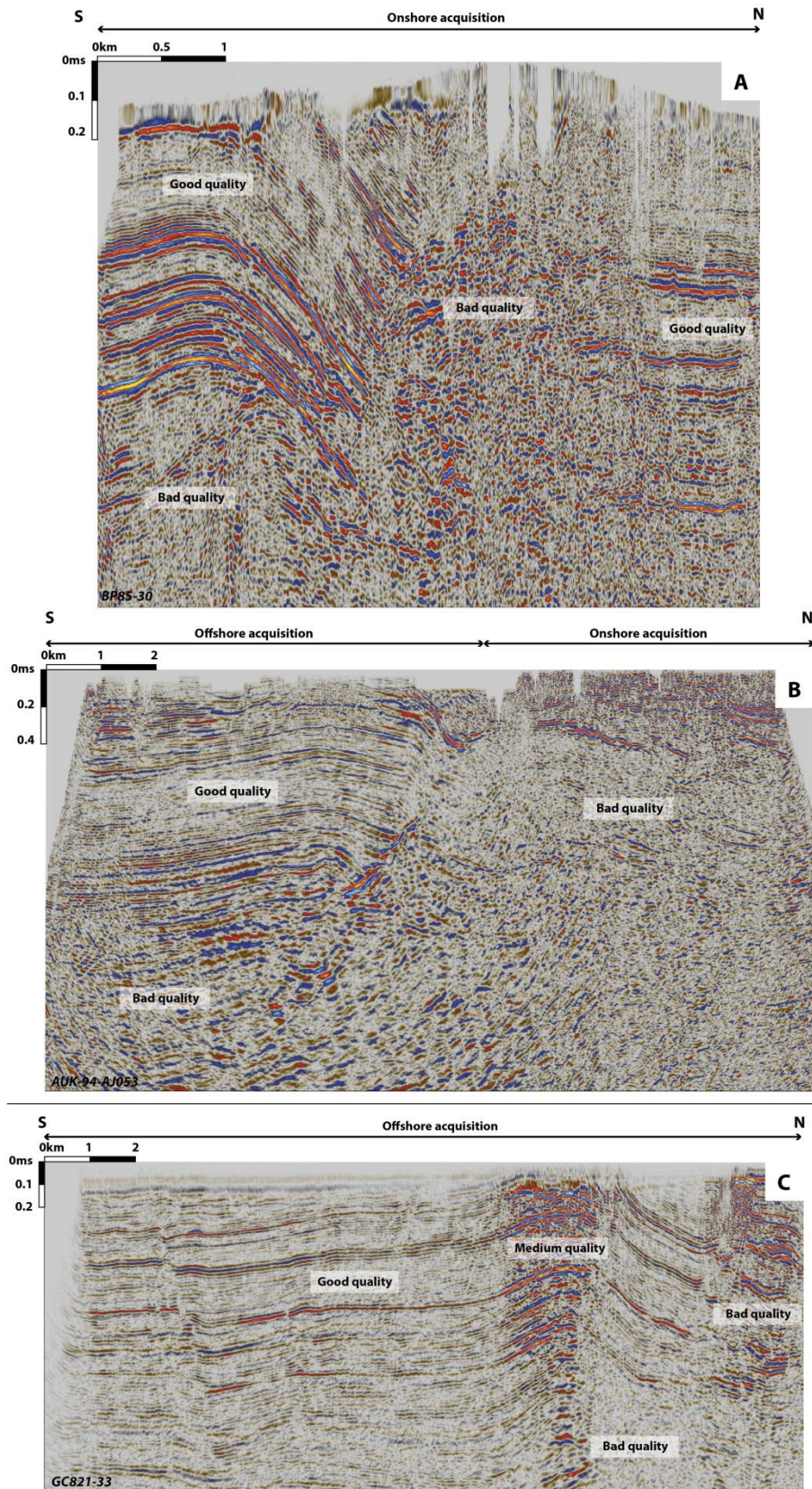
fault zones, where the quality is poor (Fig. 3.3A). Four seismic profiles are of varying quality due to their position both onshore and offshore (*i.e.* AUK-94-AJ052, AUK-94-AJ053, AUK-94-AJ059 and 81-291, Figs. 3.2 and 3.3B).

	Seismic line names	Length (km)	Source type	Station interval (m)	Frequency (Hz)	
Onshore	76-118	10	Dynamite	61		
	77-219	8.42	Dynamite	30		
	78-54	5.25	Dynamite	70		
	80-268	5	Dynamite	35		
	81-286	4.5	Dynamite	35		
	81-291	7.15	Dynamite	17.5/35		
	AUK-94-AJ052	13.20	Vibroseis	25	10-80	
			Airgun: Sleeve Type	25		
	AUK-94-AJ053	13.60	Vibroseis	25	10-80	
			Explosive - Powergel	25		
	AUK-94-AJ059	10.20	Airgun: Sleeve Type	25		
			Vibroseis	25	10-80	
			Explosive - Powergel	25		
	B90-33	15	Vibroseis	25	14-85	
	B92-39	8.20	Vibroseis	20	12-80	
	B92-41	8	Vibroseis	20	12-80	
	B92-42	6.30	Vibroseis	20	12-80	
	B92-43	13.50	Vibroseis	20	12-80	
	BP85-30	7.15	Vibroseis	15/30	10-100	
	BP91-203	4.82	Vibroseis	20	10-80	
	BP91-206	5.10	Vibroseis	20	10-80	
	BP91-207	4.57	Vibroseis	20	10-80	
	GC82-292	7.80	Dynamite	50		
	GC82-298	5.90	Dynamite	50		
	GC86-V29	5.20	Vibroseis	15	13.5-81	
	GC86-V33	9.50	Vibroseis	15	13.5-81	
	Offshore	GC821-07	6.31			
		GC821-14A	22.4			
		GC821-16	5.6			
		GC821-17	17.5			
GC821-18		8.85				
GC821-23		9				
GC821-29		14.54				
GC821-31		11.2				
GC821-33		17.5				
GC821-9		15.22				
GC822-07		3.57				
GC822-14W		5.60				
GC822-16		3.55				
GC822-17		9				
GC822-18		5.40				
GC822-201		4.85				
GC822-203		6				
GC822-23		10				
GC822-23A		7				
GC822-27		14.3				
GC822-28		5				
GC822-29		5.3				
GC822-30		3.70				
GC822-31		5.72				
GC822-33		3.90				
GC822-5		4.12				
GC822-9		3.85				
GC822-9A		4				
GC825-16		5.5				
GC825-18		23.3				
GC825-27		11.25				
GC825-28		2.55				
GC825-30		11.30				
GC825-32		16.20				
GC825-53		24				

**Table 3.1** List of the 2-D seismic profiles studied with source types used during acquisition. Empty cells: information unavailable.



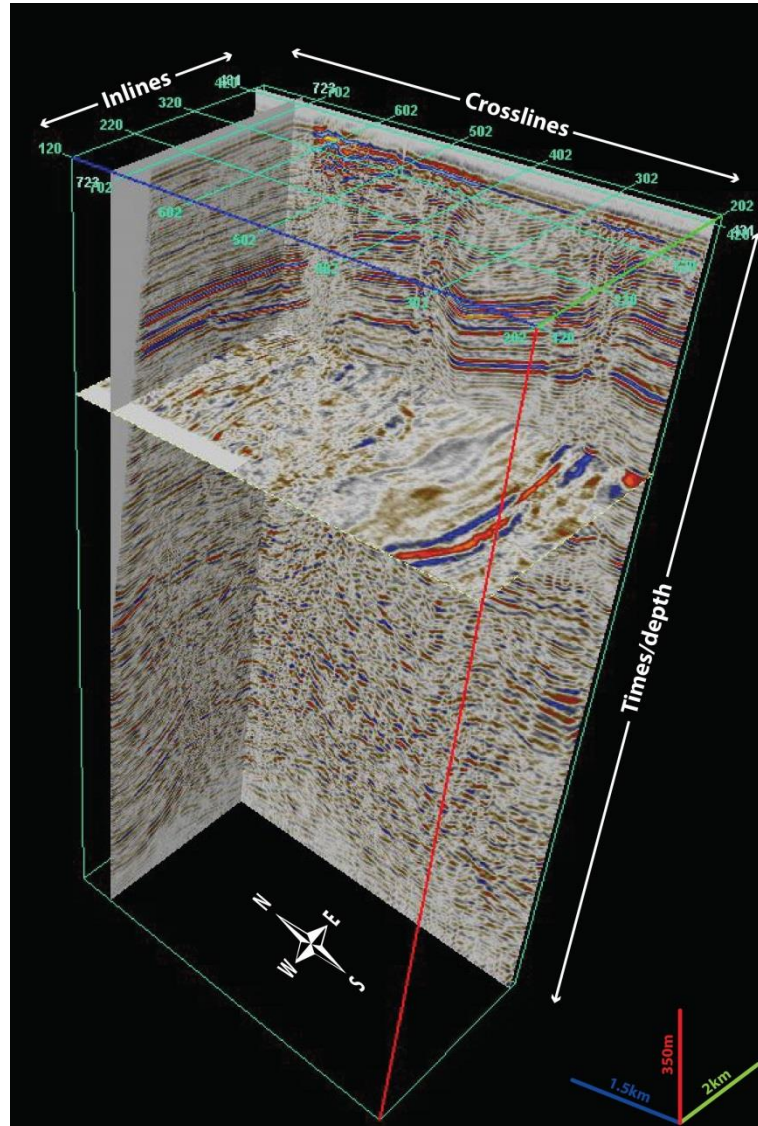
**Figure 3.2** Location map of the 2-D seismic profiles both onshore and offshore. Coloured lines locate seismic profiles presented in detail in this chapter. Grey box locates the 3-D block. DORIS seafloor data located in Weymouth Bay and Portland area detailed in figure 3.21.



**Figure 3.3** Example of 2-D profiles showing the quality of the seismic data. A – BP85-30 acquired onshore only. B – AUK-94-AJ053 acquired both offshore and onshore. C – GC821-33 acquired offshore only. Locations in figure 3.2.

### 2.3. Details of the 3-D block

A 3-D seismic survey, 4 km wide, 7.3 km long, 3 km deep and with 12.5 m line spacing (inlines and crosslines), located offshore in Bournemouth Bay (Figs. 3.1, 3.2 and 3.4; public domain) has been studied. The quality of the profiles is relatively good (Fig. 3.4). The 3-D block consists of 582 in-lines, 325 cross-lines and 3000 time slice profiles. The source types and frequency of acquisition information are not available.



**Figure 3.4** Details of the 3-D seismic block. Numbers in turquoise are the numbers of each profile studied (inlines from 202 to 784 and crosslines from 120 to 445).

## 2.4. Details of wells

Thirteen offshore wells (Tab. 3.2) with borehole data have been purchased from Information Handling Service (IHS) and thirteen onshore wells (Tab. 3.2) have been gathered from the UKOGL website (public domain and without borehole data, just formation tops are available). The wells purchased came with the checkshot point files making their importation into Petrel© relatively straightforward. However, for the wells available from the public domain, the creation of the checkshot point files was needed before their importation into Petrel©.

	Well names	X	Y	KB (m)	Depth (m)	Top Portland		Top Purbeck		Thickness Purbeck interval	
						TWT (s)	Depth (m)	TWT (s)	Depth (m)	TWT (s)	Thickness (m)
Offshore	97/19-1	554010	5586899	111.55	3474.72	NI	NI	NI	NI	–	–
	98/11-1	582568	5612081.2	29.4	2182.37	0.477	750.68	0.454	710.12	0.023	40.56
	98/11-2	581953.9	5609487.9	32.7	3472	0.397	532.88	0.349	457.2	0.048	75.68
	98/11-3	583972.8	5612835.3	32.6	2109.22	NI	NI	NI	NI	–	–
	98/11-4	582610.7	5609066.8	34.4	2119.57	0.420	574.65	0.360	477.08	0.060	97.57
	98/11-4Z	582610.8	5609066.8	34.44	2218.95	0.428	589.12	0.360	477.09	0.068	112.03
	98/12-1	591057.4	5609370.8	33.5	2389.39	0.473	652.19	0.395	511.16	0.078	141.03
	98/13-1	605524	5611204	36.42	2259.5	0.514	753.8	0.391	541	0.123	212.8
	98/16-1	577220	5591770	34.75	2490.22	0.621	840	0.577	762	0.044	78
	98/16-2	575305	5591770	39.01	2638.96	0.663	983	0.574	825.61	0.089	157.39
	98/18-1	599509	5584738	39.01	2620.98	0.509	662.9	0.467	594.4	0.042	68.5
	99/16-1	644804	5583545	36.27	2041.55	0.680	951.6	0.641	885.4	0.039	66.2
	Lulworth Banks 1	549286.5	5605038.4	15.7	762	NI	NI	NI	NI	–	–
Onshore	Chaldon Herring 1	549088.9	5611825.5	87.2	574.5	NI	39.3	NI	4.6	–	34.7
	Chaldon Herring G2	549019	5611515.5	91.1	179.2	NI	NI	NI	157	–	–
	Chaldon Herring G3	549048	5611963	79.2	574.5	NI	56.4	NI	4.6	–	51.8
	Chickerell 1	536447.6	5609984.7	22.5	2176	NI	NI	NI	NI	–	–
	Coombe Keynes 1	553091.4	5612110.6	98.4	2499.2	NI	NI	NI	NI	–	–
	Creech 1	560756.2	5610577.8	56.4	2291.1	NI	NI	NI	NI	–	–
	Encombe 1	564892.1	5606465	81.9	872.3	NI	NI	NI	NI	–	–
	Hewish 1	534975.4	5612140	31.7	2099.7	NI	NI	NI	NI	–	–
	Kimmeridge 5	561188.6	5607428.2	32.6	2923	NI	NI	NI	NI	–	–
	Martinstown 1	535459.9	5614767.8	153.3	2455	NI	NI	NI	NI	–	–
	Poxwell 1	545488.8	5611507.9	134.4	507.8	NI	0	NI	NI	–	–
	Southard Quarry 1	573116.9	5606009.9	89.1	2894	NI	148.1	NI	0	–	148.1
	West Stafford 1	542533.4	5616917.5	56.1	2054.3	NI	NI	NI	NI	–	–

**Table 3.2** Location, depth and depth of tops interpreted of wells in south Dorset. KB: Kelly Bushing. TWT: Two Way Time. NI: Not identified. 0 value means that the Formation is exposed at the surface. Formation tops as recorded on the wireline logs.

Borehole data are available only for the wells purchased, *i.e.* 97/19-1, 98/11-1, 98/11-2, 98/11-4, 98/11-4Z, 98/12-1, 98/13-1, 98/16-1, 98/16-2, 98/18-1 and 99/16-1. For all of these wells caliper, gamma ray and sonic velocity logs are available, however the neutron/density log is only available for the 98/12-1, 98/16-1, 98/18-1 and 99/16-01 wells, the resistivity log only for the 98/12-01, 98/13-01, 98/16-01, 98/16-02, 98/18-01 and 99/16-01 wells and the cuttings were recorded only on the 97/19-1, 98/11-2, 98/12-1, 98/13-1, 98/16-1, 98/16-2, 98/18-1 and 99/16-1 wells. In order to tie these with the seismic lines, each top interpretation done by operators was checked. The comparison of the wireline logs available for each well (Figs. 3.7;

3.8 and 3.9) allowed the identification of minor mistakes on the interpretation of the top Portland and Purbeck horizons and their correction in the checkshot point lists.

The importation of stratigraphic surfaces or tops into Petrel© needed to be done by hand by entering the TWT value top by top (this information was obtained after identification of alteration required provided in the well data and described in sections 2.5 and 2.6 of this chapter).

The identification of the horizons corresponding to the top of the Portland and Purbeck Limestone Groups was possible only in some wells. Top Portland was found in 98/11-1, 98/11-2, 98/11-4, 98/11-4Z, 98/12-1, 98/13-1, 98/16-1, 98/16-2, 98/18-1, 99/16-1, Southard Quarry 1, Chaldon Herring 1 and Chaldon Herring G3 wells (Tab. 3.2). Top Purbeck was found in 98/11-1, 98/11-2, 98/11-4, 98/11-4Z, 98/12-1, 98/13-1, 98/16-1, 98/16-2, 98/18-1, 99/16-1, Chaldon Herring 1, Chaldon Herring G3 and Chaldon Herring G2 wells (Tab. 3.2). In the others wells, 98/11-3, 97/19-1, Lulworth Banks 1, Chickerell 1, Encombe 1, Kimmeridge 5, Creech 1, Hewish 1, Martinstown 1, West Stafford 1 and Coombe Keynes 1 (Tab. 3.2), none of the horizons have been identified and could be used in this study to calibrate the seismic profiles. Unfortunately the Purbeck interval was never cored, presumably because the Purbeck is not considered as a reservoir interval.

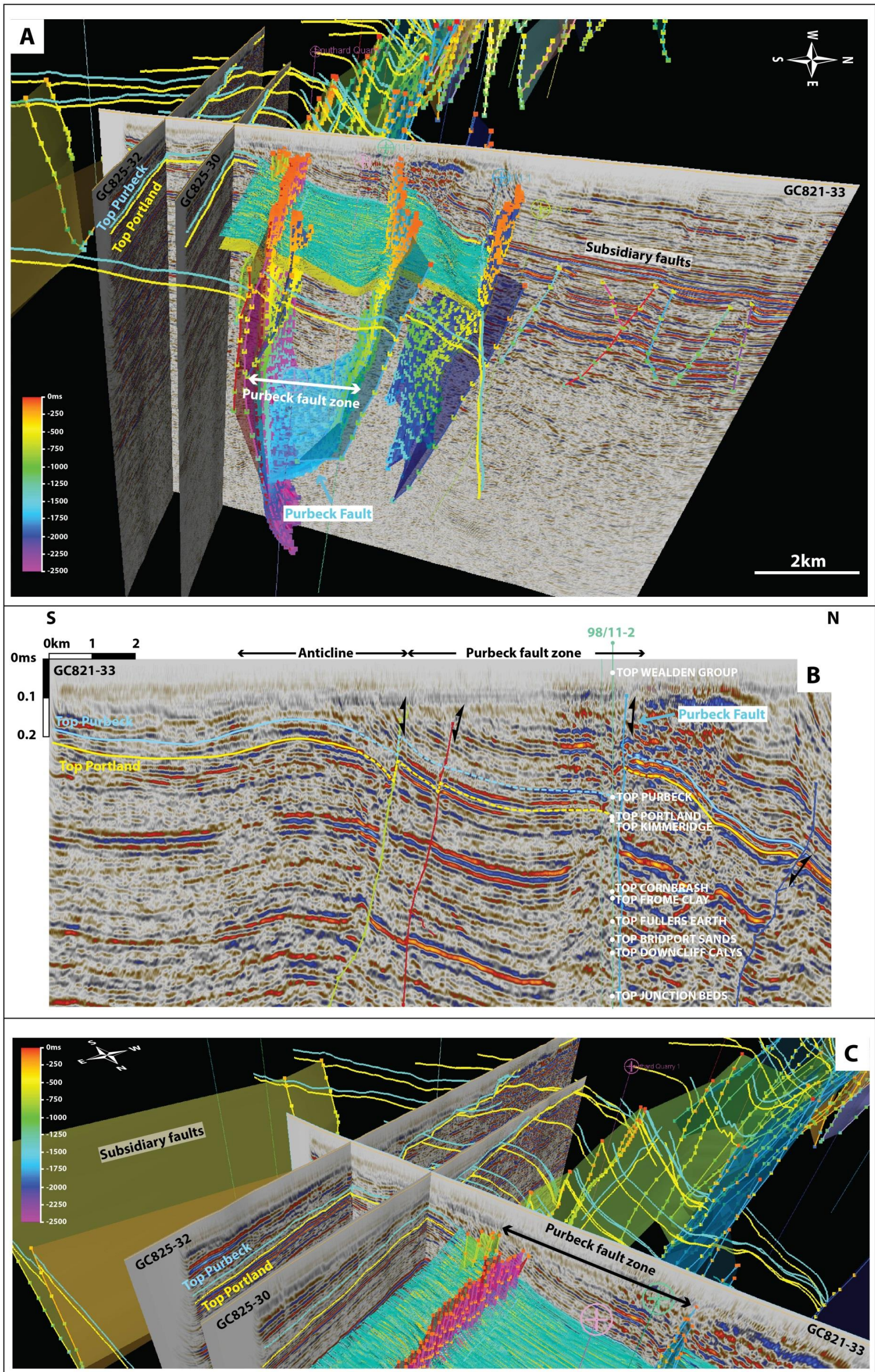
## **2.5. Mapping of horizons in Petrel**

The interpretation started from the 3-D block in Bournemouth Bay where the recognition of the tops was easier due to the good quality of the seismic profiles and because it is constrained by five wells (98/11-1, 98/12-1, 98/12-4, 98/12-4Z and 98/13-1, Figs. 3.1; 3.5 and 3.11). The interpretation started with every 10th crossline and inline profiles followed by a 3-D autotracking (relatively good due to the continuity of the markers) in between them. Finally the verification of the autotracking (correction of the possible mistakes) resulted in a complete interpretation of the studied interval in all the profiles of the 3-D block.

These surfaces have been extended to the 2-D offshore profiles in Bournemouth Bay on the GC821-33 profile (orientated N-S, Fig. 3.5) as it cross-cuts the 3-D block. Following this the surfaces are extended to the other offshore profiles and finally to the onshore profiles.

The picking of top Portland and top Purbeck horizons in the wells has been done with a combination of historically interpreted tops, cuttings and comparison of the different wireline logs (caliper, sonic velocity, gamma ray, neutron density and/or resistivity logs).





**Figure 3.5** Illustration of the interpretation method. A – 2-D profile (GC821-33) crosscutting the 3-D block, allowing the link between the 3-D block and the 2-D seismic profiles. B – GC821-33 profile illustrating the method used for the interpretation. Dashed lines are the projection of the interpretation of the 3-D block onto the 2-D profile. Blue line is the interpretation done on the 2-D lines for top Purbeck and yellow line for top Portland. C – Zoom in A illustrating how the interpretation has been extended to the other 2-D profiles. GC821-30 and GC821-32 crosscutting GC821-33 profile. Location in figure 3.2.

### **2.5.1. Top Portland**

In order to identify the Purbeck Limestone Group and to map possible thickness variations (Tab. 3.2), the top Portland pick has been identified on borehole data with the two way times. The boundary between the Portland and Purbeck Limestone Groups (*i.e.* top Portland horizon) is considered to be located at the base of the anhydrite unit (Figs. 3.7; 3.8 and 3.9) known inland to be located in the lower part of the Cypris Freestone of the Purbeck Limestone Group (such as the Broken Beds). The signals in the wireline logs are sharp and easily identifiable (Figs. 3.7; 3.8 and 3.9). The Gamma-ray log presents a decrease to lower value characteristic of anhydrite values. The sonic velocity log presents a drop to weaker values (less porous interval). The resistivity log presents an increase towards greater values, suggesting a change to less porous and less permeable interval. The density log presents higher values with a change from 2.7 to 3. The combination of all these logs is consistent with a change from limestone (Freestone member of the Portland Group) to an evaporitic interval (anhydrite present in the lower part of the Purbeck). This marker appears in blue and is continuous. It is present all across the area south of the main faults apart from in the centre part of the Weymouth anticline (Fig. 3.10B) where its absence is due to post-inversion erosion in the core of the anticline.

### **2.5.2. Top Purbeck**

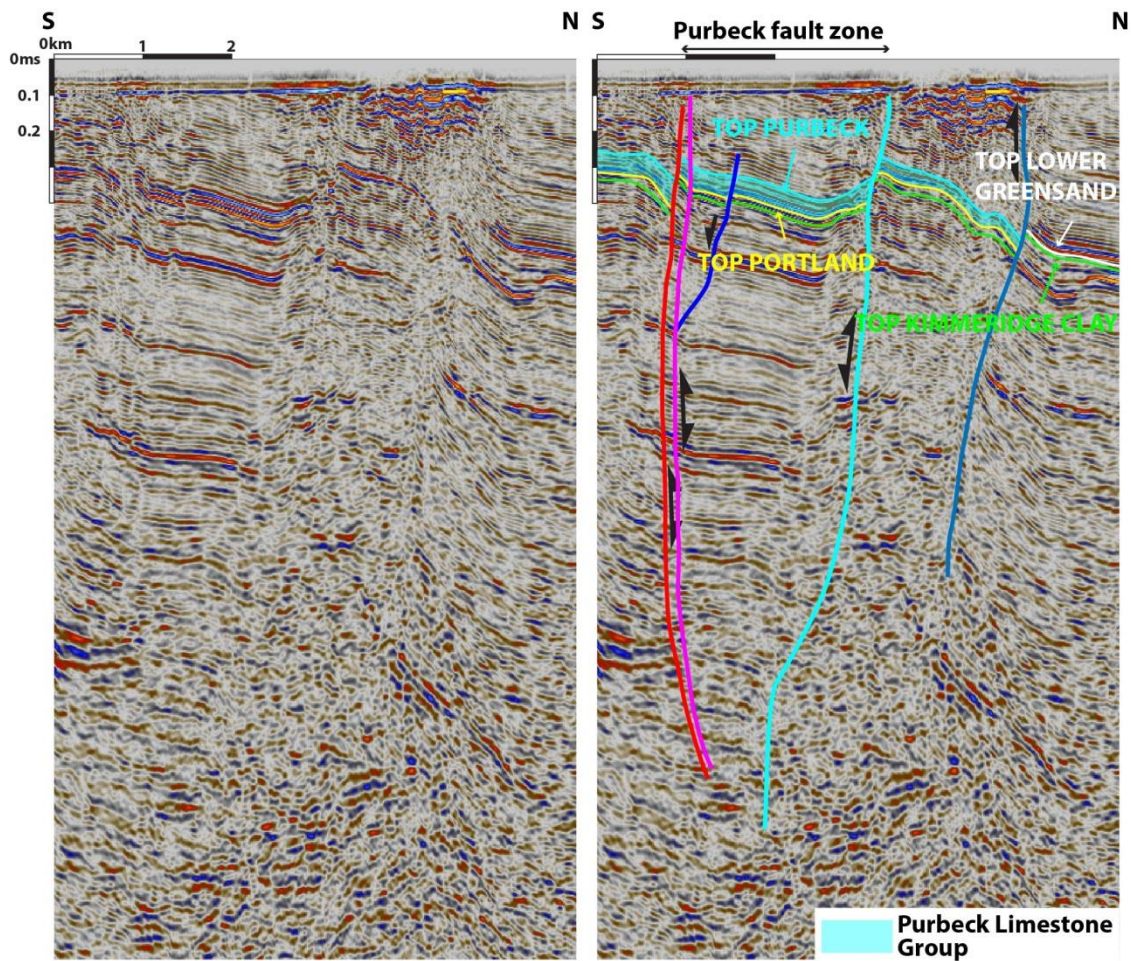
The identification of the boundary between Purbeck Limestone and Wealden Groups (*i.e.* top Purbeck horizon) is clear and sharp (Figs. 3.7; 3.8 and 3.9) due to the change from limestone in the upper part of the Purbeck Limestone Group to claystones or sandstones typical of the lower part of the Wealden Group. The gamma-ray log shows an increase to higher value reflecting an increase in the argillaceous content. The sonic velocity log presents an increase to higher value (more porous interval) and a less stable signal (alternation between porous and less porous beds). The neutron-density log presents a decrease towards lower values down to 1.9 g/cm<sup>3</sup> specific for claystone signature. However the resistivity log does not show any particular change in the signal data. This marker appears in blue and is continuous. It has been identified more or less everywhere across the area apart from the northern part of the 3-D block (Bournemouth Bay) and in the centre part of the Weymouth anticline (Weymouth Bay, Fig. 3.13A). As with the top Portland pick, its absence is mainly due to post-inversion (Cenozoic) erosion of the core of the anticline and non-deposition or erosion north of

the main west-east faults prior to the deposition of the Lower Greensand Formation (Upper Cretaceous).

## **2.6. Seismic and wireline log characteristics of the Purbeck interval**

Top Purbeck and top Portland horizons were well constrained on the wireline logs in order to tie the borehole data with the seismic lines. These horizons constrain the Purbeck interval defined by a seismic facies unit corresponding to the Purbeck Limestone Group (from the anhydrite unit upwards, see above). This facies is continuous, with a low frequency (defining the vertical space between two reflectors), a medium to high amplitude and a parallel configuration (Fig. 3.6; following concepts in Veeken, 2008). This interval is characterised by moderately serrate wireline log motifs, with three main signatures characterising three main intervals (Figs. 3.7; 3.8 and 3.9). It starts at the bottom with low gamma-ray values (anhydrite) associated with high resistivity (low water content), low value on the sonic velocity (low porosity) and density around 3 (anhydrite signature); consistent with an anhydrite rich interval characteristic of the base of the lower part of the Purbeck Limestone Group as seen in exposures on the coast and recording in the Portsdown well (West, 1975). In the wells, gamma-ray values become slightly higher (calcareous enrichment characteristic of limestone signature) associated with low resistivity (higher water content), higher values on the sonic velocity (higher porosity) and density fluctuating between 2.6 and 2.7 (calcite signature); consistent with a limestone interval. The third main interval is characterised by slightly higher gamma-ray values (argillaceous enrichment) associated with low resistivity (high water content), high sonic velocity values (higher porosity) and density fluctuating between 2.2 and 2.5 (clay signature); consistent with a claystone interval, characteristic facies of the upper part of the Purbeck Limestone Group.

Once the top Purbeck and top Portland horizons were identified on the wireline logs, the interpretation of the seismic profiles was possible and detailed in section 3 of this chapter. Even if the Purbeck Limestone Group looks thicker in the hanging-wall block of the Purbeck Fault on the seismic profiles (Fig. 3.7) the quality is not always good enough (refer to sections 2.2 and 2.3 of this chapter) to draw conclusions concerning a possible lateral variation in thickness or in lithology of the Purbeck Limestone Group just from the seismic data. The combination with borehole data is clearly needed.



**Figure 3.6** Interpreted seismic profile from the 3-D block (crossline 374). Location in Fig. 3.2.

Well correlation panels were created to identify possible thickness and lithology variations and are presented in figures 3.7 (north-south transect), 3.8 and 3.9 (west-east transects). The three intervals defined with the wireline logs above (anhydrite, limestone and claystone) are all present and all along the studied area either on the north-south transect (Fig. 3.7) or on the west-east transects (Figs. 3.8 and 3.9). This shows that the entire Purbeck Limestone Group had been deposited everywhere and preserved (*i.e.* no erosion) at least across the area covered by the correlation panels (Fig. 3.1). Laterally the Purbeck Limestone Group and each interval change in thickness but this characteristic will be described and detailed in section 3.1 of this chapter with the interpretation of these well correlation panels.

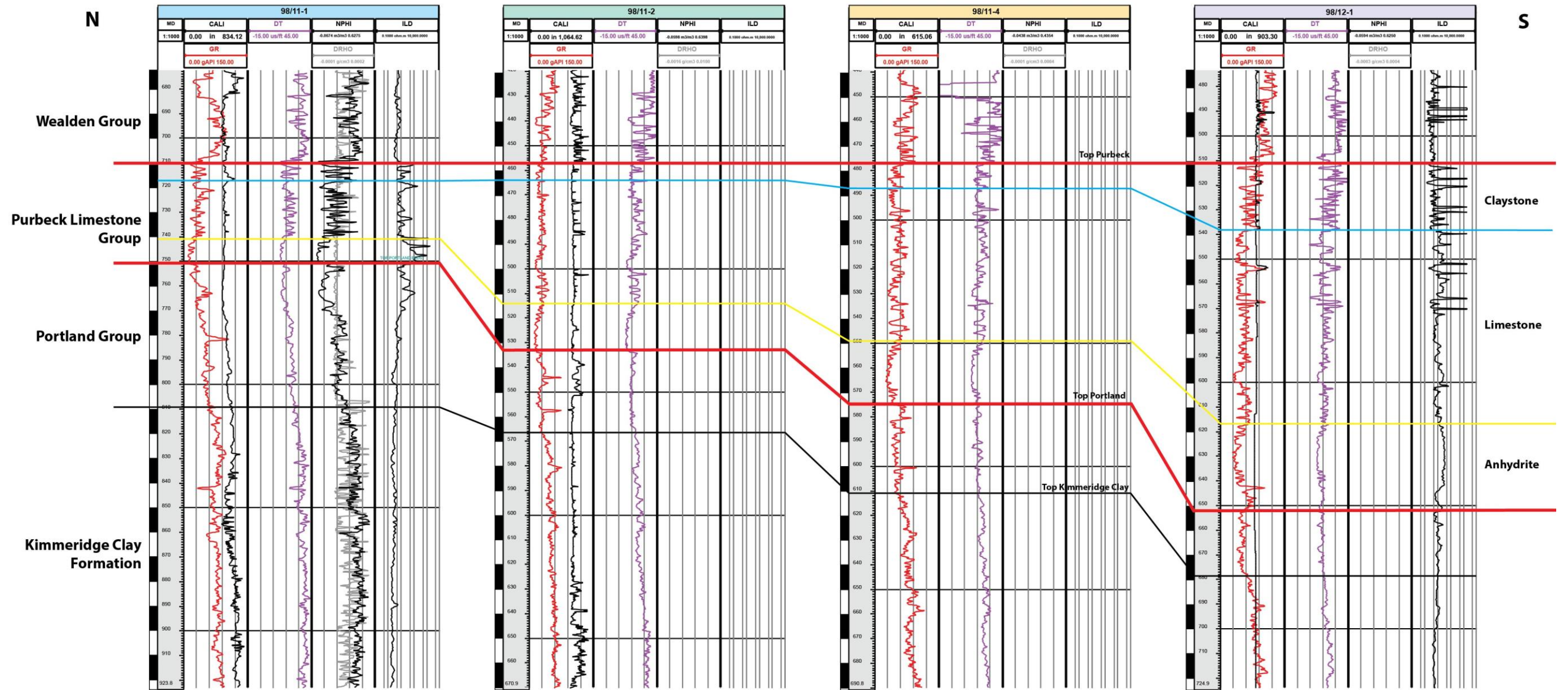


Figure 3.7 Well correlation panel 1 illustrating the succession of lithologies within the study area of the Purbeck interval flattened at the top Purbeck horizon. CALI: caliper, GR: gamma-ray, ILD: resistivity, DT: sonic velocity, NPHI: neutron, DRHO: density. Fence location in figure 3.1.

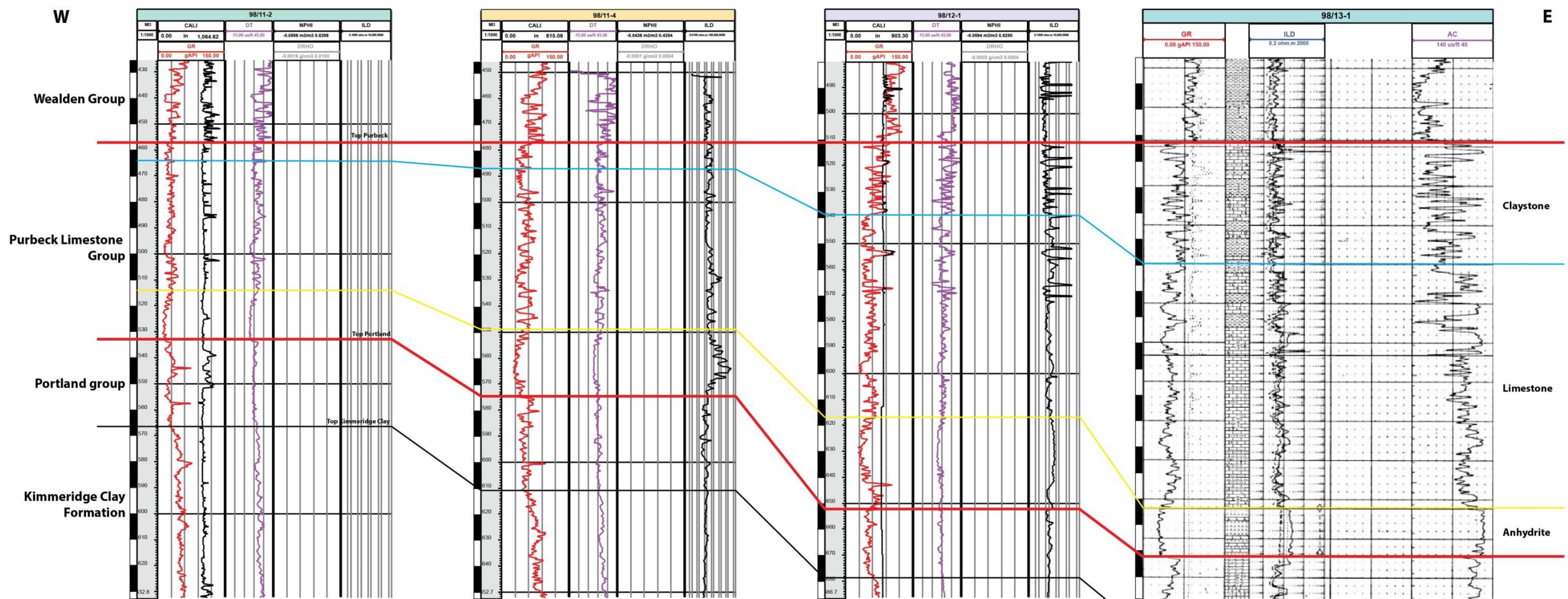


Figure 3.8 Well correlation panel 2 illustrating the succession of lithologies within the study area of the Purbeck interval flattened at the top Purbeck horizon. CALI: caliper, GR: gamma-ray, ILD: resistivity, DT: sonic velocity, NPHI: neutron, DRHO: density. Fence location in figure 3.1.

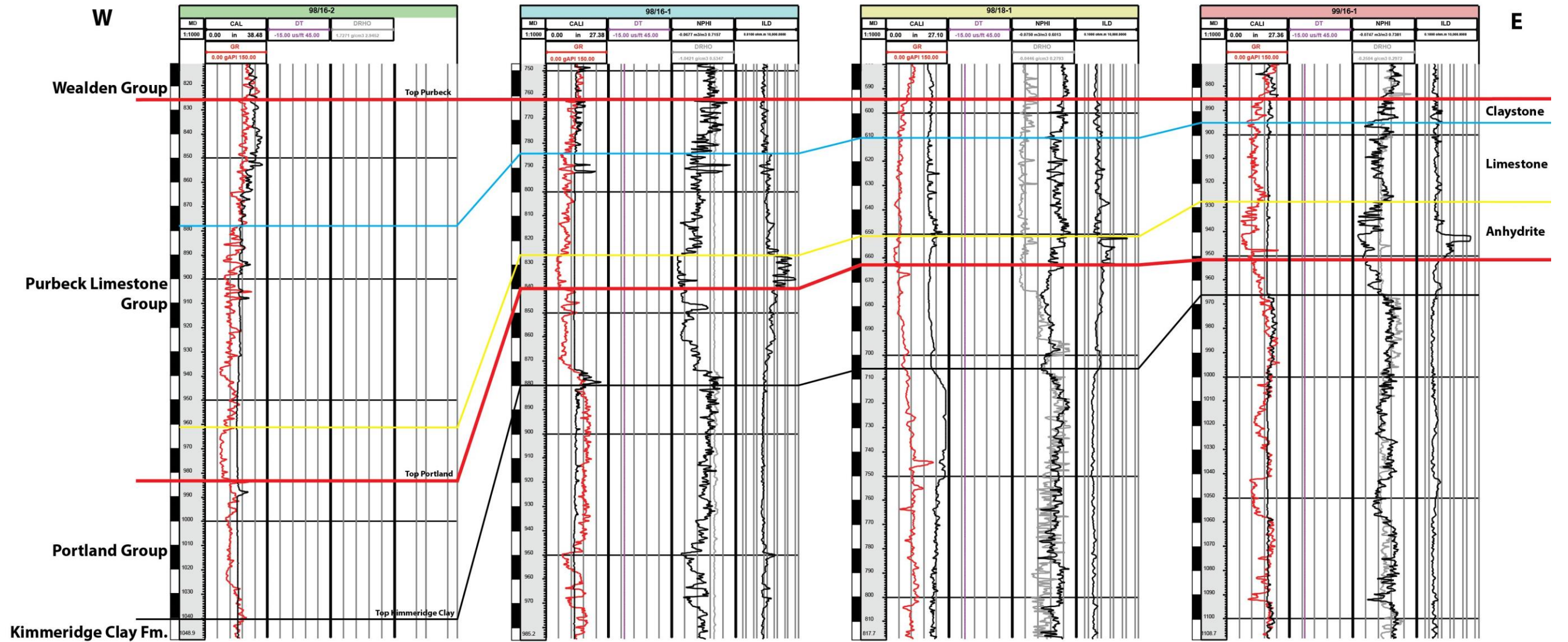
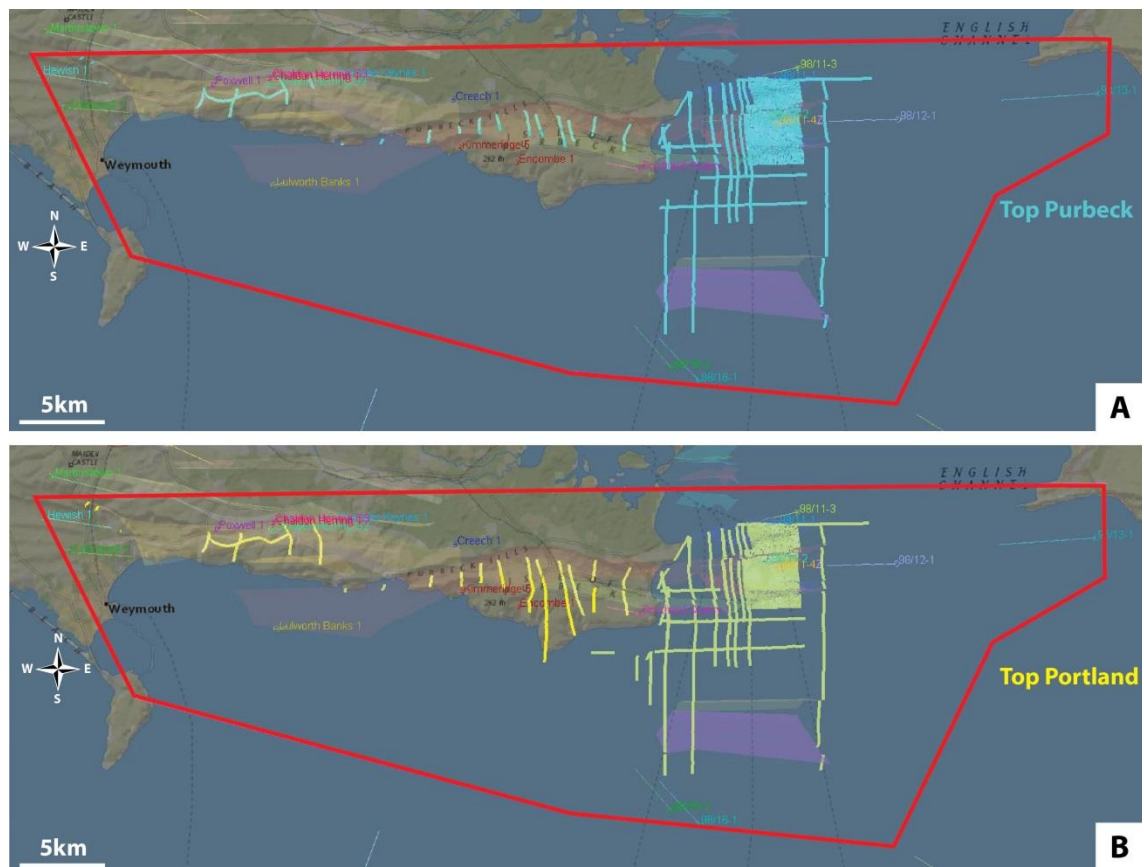


Figure 3.9 Well correlation panel 3 illustrating the succession of lithologies within the study area of the Purbeck interval flattened at the top Purbeck horizon. CALI: caliper, GR: gamma-ray, ILD: resistivity, DT: sonic velocity, NPHI: neutron, DRHO: density. Fence location in figure 3.1.

In order to create and to interpret a time thickness map to constrain any thickness variations (in time values) of the Purbeck interval, the construction of top Portland and top Purbeck surface maps was carried out with Petrel© (Figs. 3.10 and 3.11). Each surface map takes into account the occurrence of top Portland and top Purbeck picks within the wells (identified on the wireline logs of the borehole data) and is tied with the interpretation of the seismic profiles (refer to previous sections of this chapter).

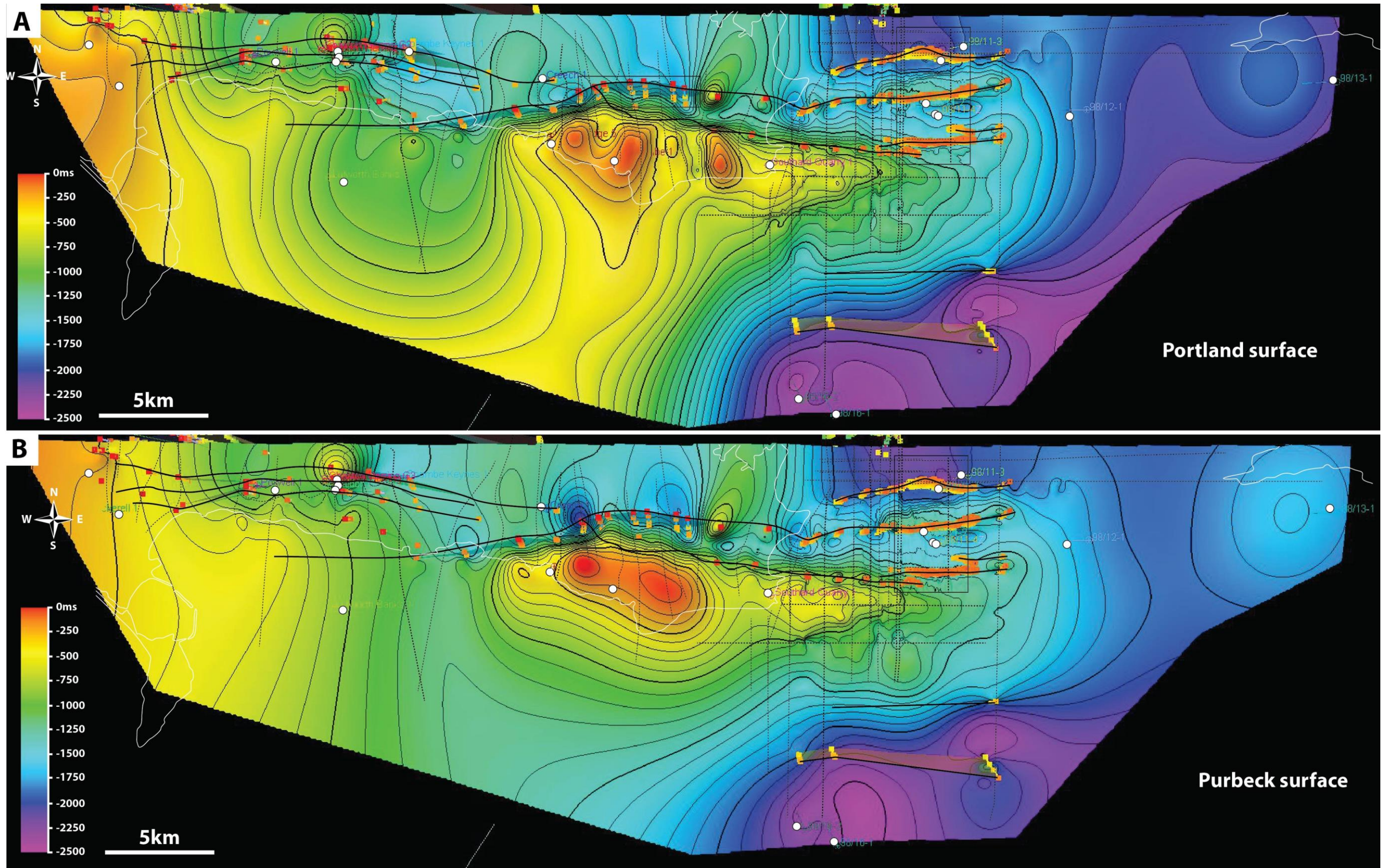


**Figure 3.10** Coverage of the identified tops of the Portland and Purbeck. A – Top Purbeck: interpreted surface appears in light blue. B – Top Portland: interpreted surface appears in yellow. Red boxes locate the area used to create the surface maps (Fig. 3.11) and the time thickness map (Fig 3.15).

To create the time thickness map the software calculates the difference between Portland and Purbeck surface maps (Figs. 3.11 and 3.15) in time values (because the depth/time conversion was not available for the seismic profiles studied). If horizons merge, the software simply allocates a value below 0 ms to the point, or the area, on the time thickness map. The red zones correspond to time value of 0 ms and below (due to surface overlaps) and the purple zones to time value of 2500 ms. When top Purbeck is absent the software will extrapolate a surface where it is lacking and it will result in a thick Purbeck interval. When both horizons are absent a 0 ms value will be attributed to the zone.



To solve those problems of interpolation, the time thickness map calculated by the software was edited manually. The integration of the onshore geological map together with interpreted MBES (Multi-Beam Echo Sounder, known as well as DORIS) data in Weymouth Bay (Fleckner, 2014) and the time thickness of the Purbeck Limestone Group on each seismic profile, helped to better constrain the time thickness map (Fig. 3.15). This resulted in a more geologically realistic map that takes into account field and borehole data. The edited map was also cropped to avoid any mis-interpolation to the area covered by seismic profiles, borehole data, geological maps and the MBES data of Weymouth Bay seafloor (Fig. 3.15).



**Figure 3.11** Surface maps following the seismic interpretation and tie with borehole data. A – Portland surface map. Contour line each 30 ms. B – Purbeck surface map. Contour line each 30 ms. Red colour corresponds to shallow values (compare to the sea bed surface) and purple colour corresponds to deep value (value ranging from 0 to 2500 ms). Dashed lines position 2-D seismic profiles and black box positions the 3-D block.

### 3. Interpretation of well and seismic data

#### 3.1. Thickness variations in the Purbeck Limestone Group

The interpretation of the well correlation panels is presented in figures 3.12 (north-south transect), 3.13 and 3.14 (west-east transects) and show lateral variations in thickness of the Purbeck Limestone Group across the area. In the first correlation panel (Fig. 3.12) a change from the north to the south with an increase in thickness can be seen from 40 m in 98/11-1 well, 75 m in 98/11-2 well, 97 m in 98/11-4 well and up to 141 m in 98/12-1 well (Tab. 3.2). In the 98/13-1 well (located north of the Purbeck Fault) the Purbeck Limestone Group is absent as the Gault Formation is in contact with the Portland Group (Figs. 3.7 and 3.12). This highlights erosion prior to the deposition of the Gault Formation, known as the Albian unconformity (described in section 4.3 of this chapter). In the other wells (98/11-1, 98/11-2, 98/11-4 and 98/12-1, located south of the Purbeck Fault) of this transect north-south the Purbeck Limestone Group is present and its thickness increases southwards (Tab. 3.2; Figs. 3.7 and 3.12). Each well is located in a different fault block (three fault blocks in total, 98/13-1 in the footwall block, 98/11-1 in intermediate fault block and 98/11-4, 98/11-2 and 98/12-1 in the hanging-wall block of the Purbeck fault zone) and these are separated by three faults (which constitute the Purbeck fault zone). The 98/13-1 well is located in the footwall block and the 98/11-2, 98/11-4 and 98/12-1 wells in the hanging-wall block of the Purbeck fault zone (98/11-1 well is located in an intermediate fault block). The fact that the Purbeck Limestone Group is thicker in the hanging-wall block than in the footwall block (40 m in the footwall against 141 m in the hanging-wall) highlights fault activity during Purbeck time and the syndepositional setting of the Purbeck Fault.

The second well correlation panel (Figs. 3.8 and 3.13) shows an increase in thickness of the Purbeck Limestone Group from the west to the east between Bournemouth Bay and the Isle of Wight (north of the studied area, Fig. 3.1). The thickness increases from 75 m in 98/11-2 well in the northwest, 97 m in 98/11-4 well, 141 m in 98/12-1 well and up to 212 m in 98/13-1 well in the southeast (Tab. 3.2). In this case the wells are not located in fault blocks separated by faults. This variation can reflect a basin profile with proximal areas in the west (*i.e.* littoral zone) and distal in the east (*i.e.* more basinal zone) of the studied area. It can also be interpreted as an increase in subsidence rate towards the east linked to active tectonics during the deposition.

The third well correlation panel (Figs. 3.9 and 3.14) shows also an increase in thickness of the Purbeck Limestone Group but this time from the east to the west, south of Weymouth Bay

and the Isle of Wight (south of the studied area, Fig. 3.1). The thickness increases from 66 m in 99/16-1 well in the southeast, 68 m in 98/18-1, 78 m in 98/16-1 and up to 157 m in 98/16-2 in the southwest (Tab. 3.2). In this case the wells are not located in different fault blocks separated by faults. This variation can reflect a basin profile with proximal areas in the east (*i.e.* littoral zone) and distal in the west (*i.e.* more basinal zone) of the studied area. This can also be interpreted as an increase in subsidence rate towards the west linked to active tectonics during the deposition.

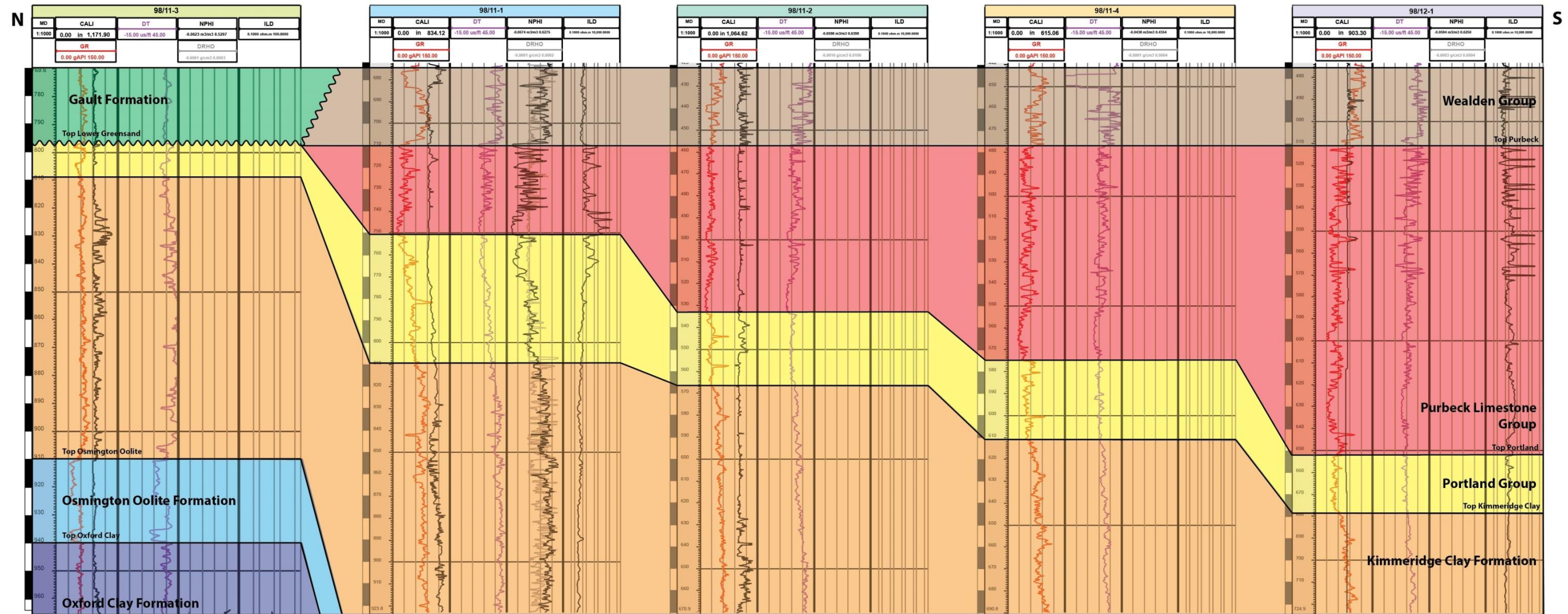


Figure 3.12 Well correlation panel 1 flattened at the top Purbeck horizon. CALI: caliper, GR: gamma-ray, ILD: resistivity, DT: sonic velocity, NPHI: neutron, DRHO: density. Fence location in figure 3.1. Each division of scale is 10 m.

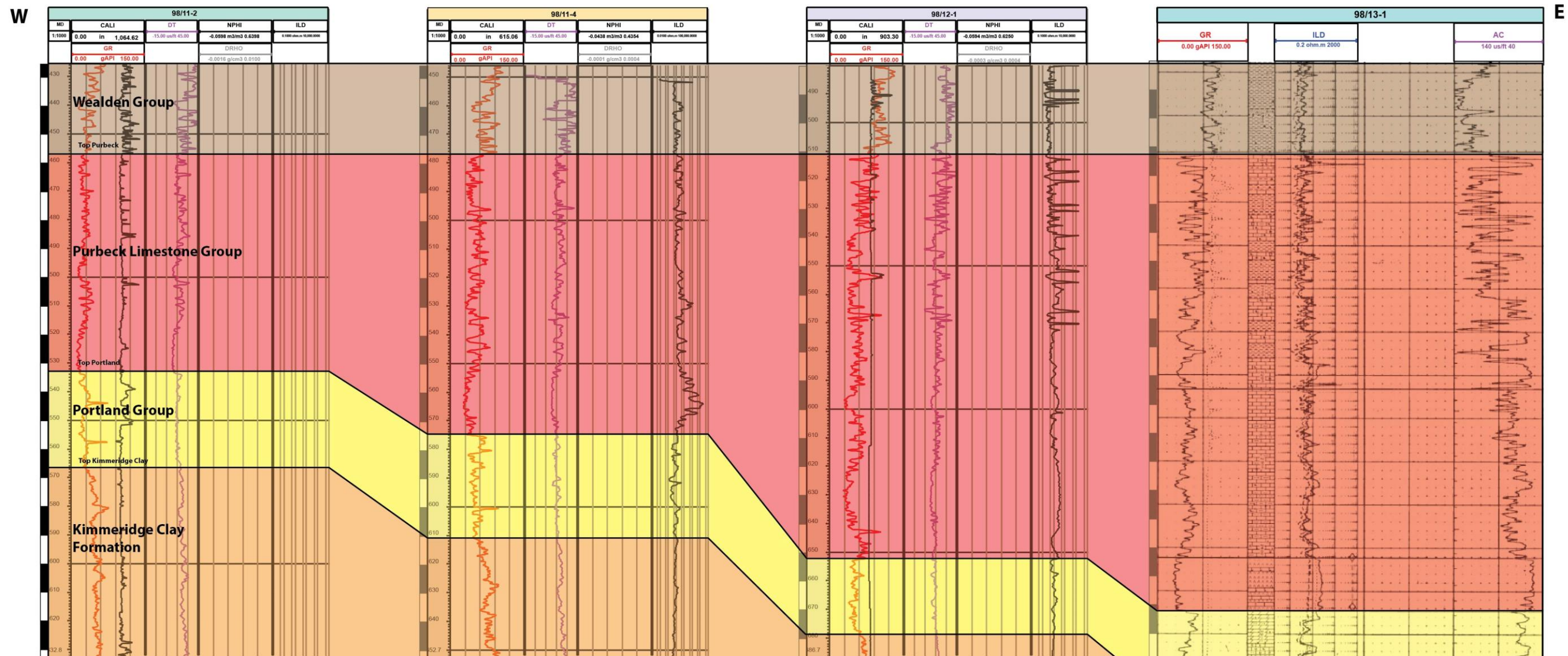


Figure 3.13 Well correlation panel 2 flattened at the top Purbeck horizon. CALI: caliper, GR: gamma-ray, ILD: resistivity, DT: sonic velocity, NPHI: neutron, DRHO: density. Fence location in figure 3.1. Each division of scale is 10 m.

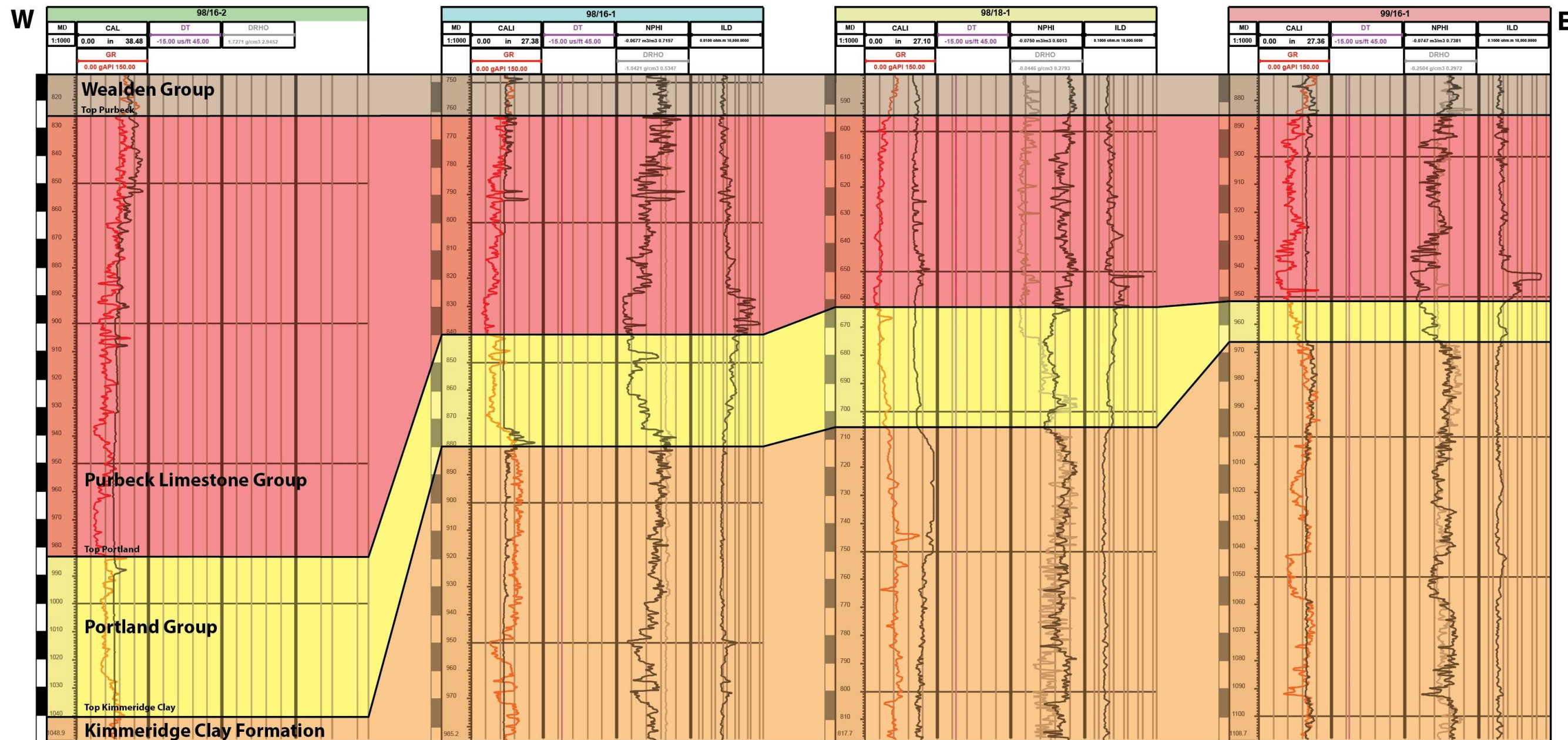


Figure 3.14 Well correlation panel 3 flattened at the top Purbeck horizon. CALI: caliper, GR: gamma-ray, ILD: resistivity, DT: sonic velocity, NPHI: neutron, DRHO: density. Fence location in figure 3.1. Each division of scale is 10 m.

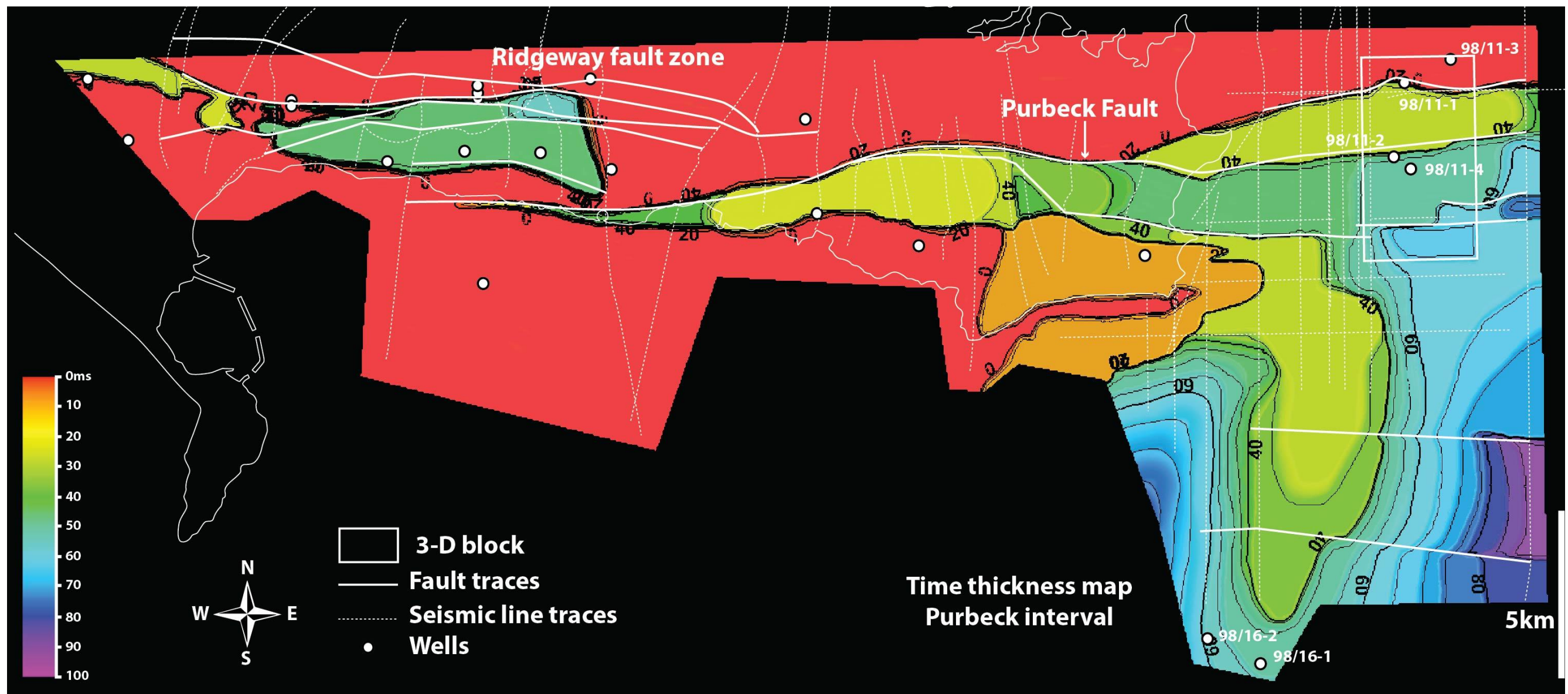
The time thickness map (Fig. 3.15) presents also variations in thickness of the Purbeck Limestone Group across the studied area however at a bigger scale (from Weymouth area to the Isle of Wight) than the well correlation panels (values range in general from 0 to 100 ms, from red to blue colour in figure 3.15). The Purbeck Limestone Group is absent in places as a result of an erosion or non-deposition. This is the case north of the Purbeck and Ridgeway Faults (Fig. 3.15), in the core of the Weymouth anticline (Figs. 3.10; 3.15) and south of Dancing Ledge cliffs (Durlston area, Fig. 3.15), where the map exhibits red colour. The absence of the Purbeck Limestone Group has been identified in the borehole data and especially with the 98/11-3 well (north of Purbeck Fault, Figs. 3.1 and 3.15) where it is recorded that the Gault Formation is in contact with Portland Group (Figs. 3.7 and 3.12). This unconformity will be documented and described in section 4.3 of this chapter.

The integration of the borehole data (well correlation panels described above and in section 2.6 of this chapter, Figs. 3.7; 3.8; 3.9; 3.12; 3.13 and 3.14) with the time thickness map (Fig. 3.15) highlights depositional and tectonic settings. The increase in thickness of the Purbeck Limestone Group in the first well correlation panel (Figs. 3.7 and 3.12) together with the location of the wells in different blocks separated by faults (Fig. 3.15) document the syndepositional setting of the Purbeck Fault during Purbeck time. The second (Figs. 3.8 and 3.13) and the third (Figs. 3.9 and 3.14) well correlation panels combined with the time thickness map (Fig. 3.15) highlight two different orientations of thickness variations. This can document the possible location and orientation of the basin during the deposition of the Purbeck Limestone Group. The thinner areas were located in the shallowest part of the basin and the thickest areas in the deepest part of the basin (northeast-southwest orientation) and this can be accentuated with a more important subsidence in the centre part of the basin than in the borders.

In addition, four possible depocentres can be identified in figure 3.15 where the thickness of the Purbeck Limestone Group is greater (blue to purple colours). One in the hanging-wall block of the Ridgeway Fault to the west, one in the hanging-wall block of the Purbeck Fault to the east, one south of Weymouth Bay with a NE-SW axis to the south and a last one south of Bournemouth Bay with a NW-SE axis to the south-east (Fig. 3.15). The depocentres located in the hanging-wall blocks of the faults with a thinner Purbeck Limestone Group laterally highlight syndepositional activity of the Purbeck and Ridgeway Faults. This lenticular depositional feature (more developed in the hanging-wall block of the Ridgeway Fault, Fig. 3.15) is very well documented in the literature where the deposition occurs preferentially in the centre part in the hanging-wall block of the fault (Schlische, 1991; Withjack *et al.*, 2002). The depocentres



located to the south of the studied area position two sub-basins, one towards the English Channel Basin to the south-west and another one towards the centre of the Wessex Basin to the south-east. These depocentres to the south are separated by a thinner Purbeck Limestone Group (greenish colours) south of Bournemouth Bay indicating a high in the palaeotopography possibly due to less subsidence than in the sub-basins (Fig. 3.15).



**Figure 3.15** Thickness map of the Purbeck interval. Contour line each 20ms. Red colour corresponds to the absence of the Purbeck interval (either due to deposition and erosion or non-deposition) and purple colour to a thick Purbeck interval (values ranging from 0 to 100 ms). Dashed lines position 2-D seismic profiles and white box positions the 3-D block.

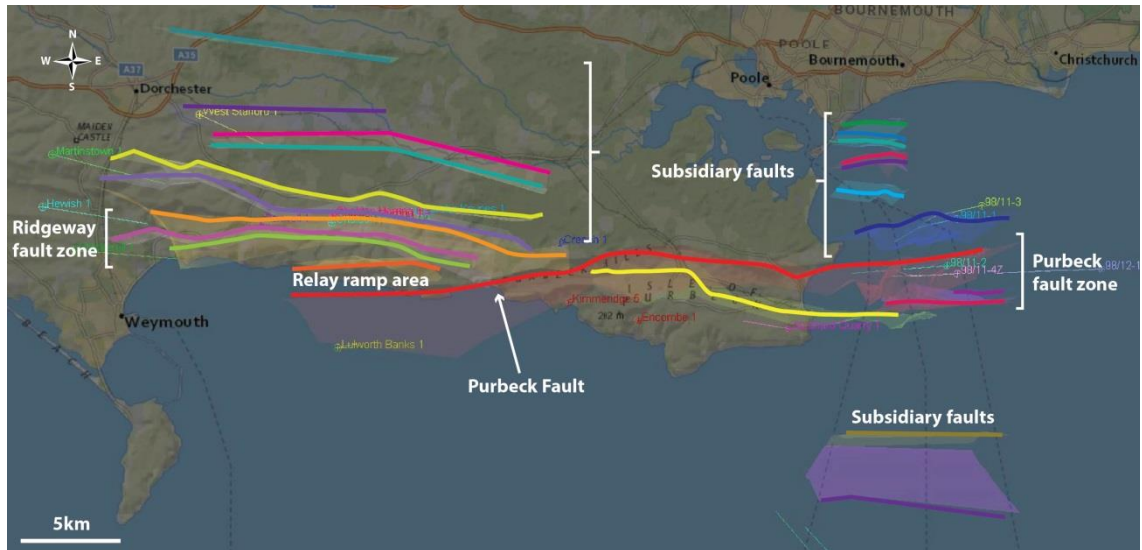
## **3.2. Faults**

### **3.2.1. Ridgeway Fault**

The Ridgeway Fault (also known as the Abbotsbury-Ridgeway Fault; Buchanan, 1998; Butler, 1998; Harvey and Stewart, 1998; Underhill and Paterson, 1998; Underhill and Stoneley, 1998; Underhill, 2002; Barton *et al.*, 2011) is an east-west trending fault and appears on the seismic profiles to be composed of four faults (Figs. 3.16, 3.18 and 3.19). These faults form a fault zone where the main fault is divided into two parallel east-west faults. They are sub-vertical with an overall normal sense of movement, dipping south and tend to become more listric with depth with detachment in the Triassic salt décollement surface (Fig. 3.22; Butler, 1998). The normal sense of movement (the hanging-wall block has moved downwards) of these faults shows their net extensional nature (Figs. 3.18 and 3.19). Associated with them, are two minor faults dipping north and forming a small graben structure (Figs. 3.18 and 3.19). Major (Fig. 3.19) and minor folds (Fig. 3.18) located in the hanging-wall block and close to the fault plans highlight a reverse displacement due to a later inversion phase on this fault following a north-south post-Cretaceous compression affecting the whole succession (Chadwick, 1993; Ziegler *et al.*, 1995; Smith and Hatton, 1998; Blundell, 2002; Mansy *et al.*, 2003).

### **3.2.2. Purbeck Fault**

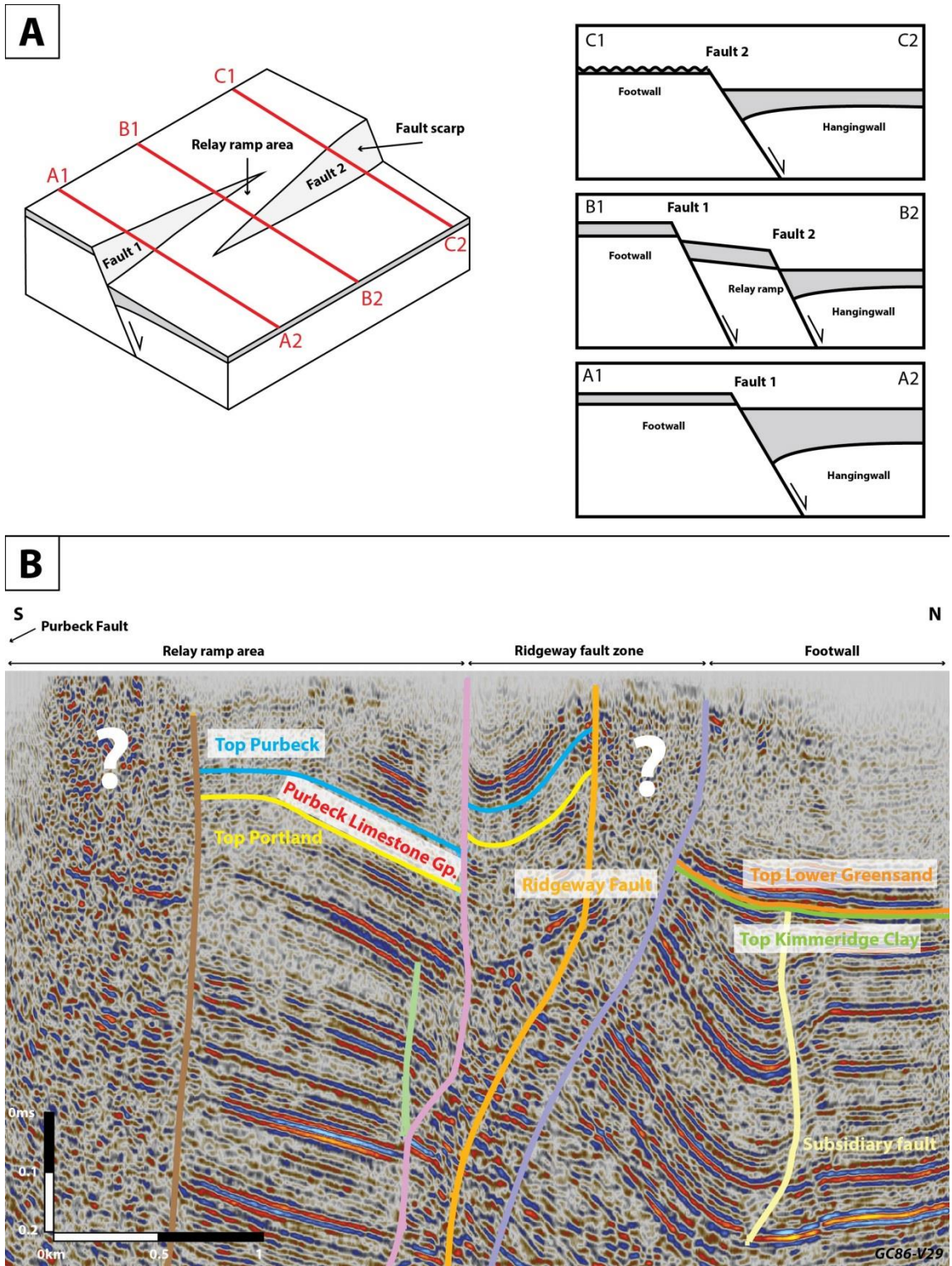
The Purbeck Fault (also known as the Purbeck-Wight Fault, Buchanan, 1998; Butler, 1998; Harvey and Stewart, 1998; Underhill and Paterson, 1998; Underhill and Stoneley, 1998; Barton *et al.*, 2011) is also east-west trending and four extensional faults have been identified (Figs. 3.6; 3.18; 3.19 and 3.22). The main fault is more or less vertical, dipping south with an overall normal component. It seems to affect the deposition (syndepositional setting) from the Permian with roots in the basement (Figs. 3.18 and 3.19; Butler, 1998). Eastwards, the association with two parallel normal faults dipping north and a shorter fault dipping south form the Purbeck fault zone (Figs. 3.6; 3.18; 3.19 and 3.22) also known as the Purbeck Disturbance in the literature (Underhill and Paterson, 1998). As with the Ridgeway Fault, the faults are extensional and the folds located in the hanging-wall block and close to the fault plans highlight a later reverse displacement due to an inversion phase following a north-south post-Cretaceous compression affecting the whole succession (Underhill and Paterson, 1998).



**Figure 3.16** Location map showing the faults interpreted from the seismic profiles.

### 3.2.3. Relay ramp area

A relay ramp area is a zone located between two normal faults, linking the footwall block of one fault with the hanging-wall block of another fault and accommodating the displacement transfer of two segments of each fault (Chadwick, 1986; Ramsay and Huber, 1987; Larsen, 1988; Peacock and Sanderson, 1991, 1994). The Ridgeway and Purbeck Faults are likely to be connected by a relay ramp area in Dorset as indicated with the offset of the faults and the area of low dips and broad outcrop in the relay ramp area (Underhill and Paterson, 1998; Underhill, 2002). In order to identify a relay ramp area between two extensional faults, it is expected on a north-south transect through the relay ramp to find a thin interval in the footwall block, slightly thicker in the relay ramp area and tilted perpendicularly to the orientation of the faults (Peacock and Sanderson, 1991, 1994) and an increase in thickness towards the fault in the hanging-wall block (cross-section B1-B2 in Fig. 3.17A). On a transect north-south and ahead of the relay ramp it is expected to find an unconformity on the footwall block and an increase in thickness in the hanging-wall towards the fault (cross-section A1-A2 in Fig. 3.17A). On a transect north-south and at the start of the relay ramp it is expected to find a thin interval on the footwall block and a thick interval with an increase in thickness towards the fault in the hanging-wall block (cross-section C1-C2 in Fig. 3.17A).



**Figure 3.17** Relay ramp. A – Simplified and idealised deposition model schemes in a relay ramp. B – GC86-V29 profile interpreted. Note the preservation of Purbeck Limestone Group in the relay ramp area. Location in figure 3.2.

The deposition of the Purbeck Limestone Group seems to have occurred in between Ridgeway and Purbeck Faults as it has been recognised on GC86-V29M and B92-43 profiles (Fig. 3.17B). It is difficult to see if the bedding is accentuated and tilted due the tectonic inversion (Cenozoic). Due to the poor quality of areas south of the relay ramp and north of the Ridgeway Fault on the seismic profiles (Fig. 3.17B), it has not been possible to identify (presence or absence) the Purbeck Limestone Group in the footwall block (as other top Formations, Fig. 3.17B). It is absent eastwards of the relay ramp area due to an unconformity (known as the Albian unconformity and detailed in section 4.3 of this chapter) as well as south of the Purbeck Fault (*i.e.* in the hanging-wall block, Fig. 3.17B) because of erosion post-inversion (Cenozoic) of the Weymouth anticline or non-deposition within Weymouth Bay (Figs. 3.10; 3.15 and 3.22).

#### **3.2.4. Subsidiary faults**

These faults are shorter than the Purbeck and Ridgeway Faults and affect only part of the Jurassic and/or younger deposits (but not the Purbeck Limestone Group). They are twenty-three in total and located both to the north and to the south of the two main inverted extensional faults (Figs. 3.18; 3.19 and 3.20). They developed under extensional settings highlighted by their normal component and were active only during Jurassic and Early Cretaceous as they do not affect Upper Cretaceous deposits (Fig. 3.20).

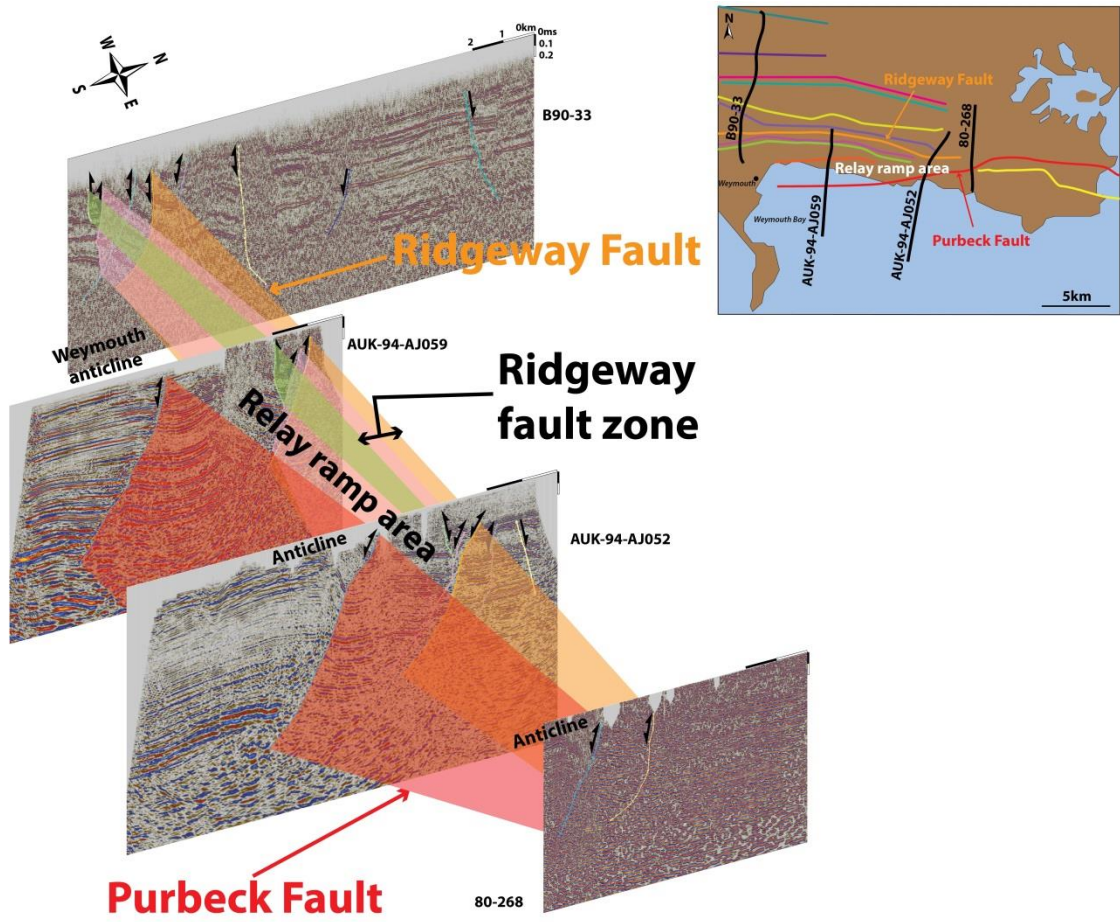


Figure 3.18 Geometry and occurrence of Ridgeway Fault following the seismic interpretation.

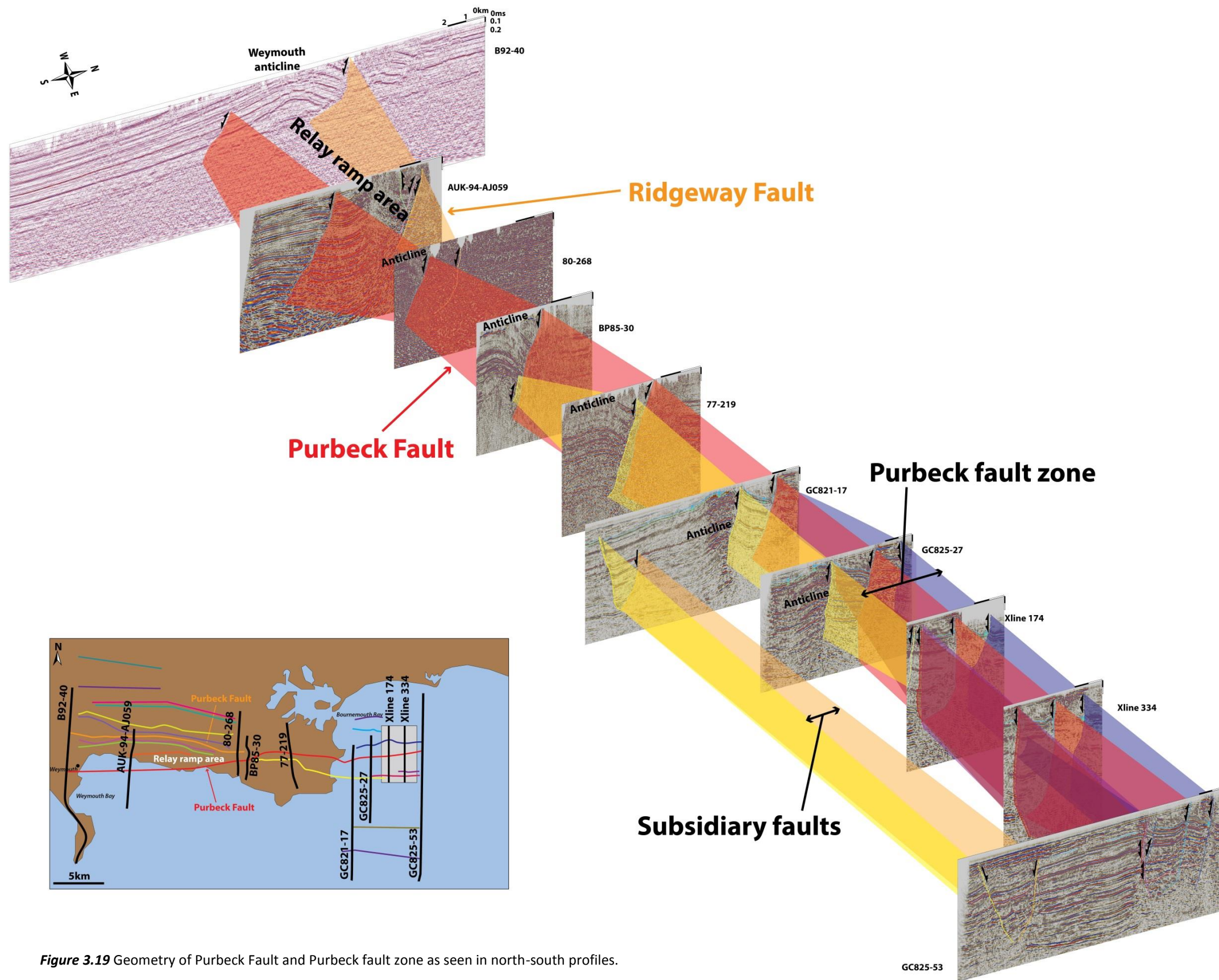
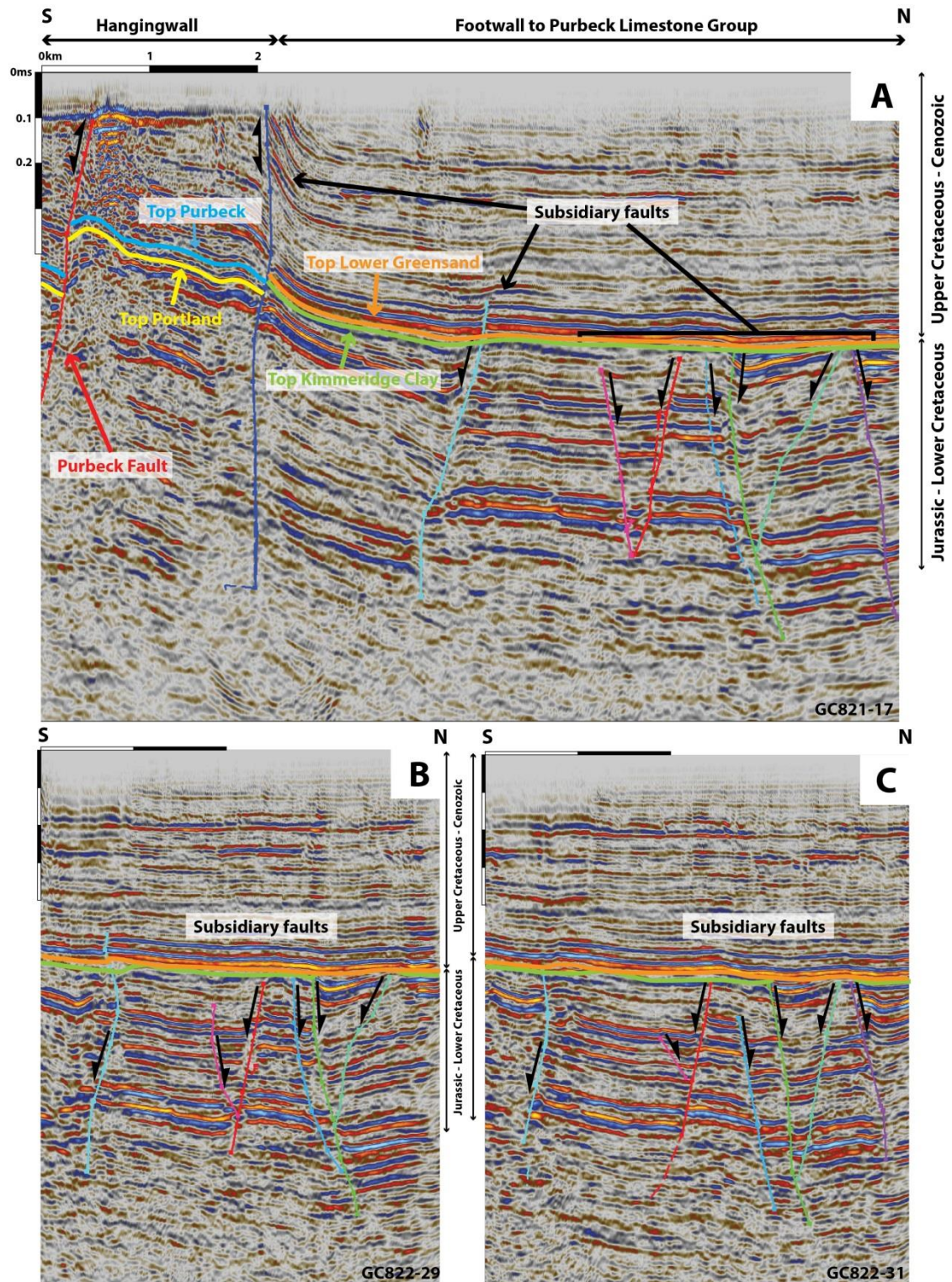


Figure 3.19 Geometry of Purbeck Fault and Purbeck fault zone as seen in north-south profiles.





**Figure 3.20** Subsidiary faults interpreted from seismic profiles. A - GC821-17 profile illustrated the stratigraphy in hanging-wall and footwall blocks of the Purbeck Fault. B - GC822-29 profile illustrating the stratigraphy in footwall block of the Purbeck Fault. C - GC821-31 profile illustrating the stratigraphy in the footwall block of the Purbeck Fault. Subsidiary faults only affect the deposition during the Jurassic and Early Cretaceous. Arrows show movement of the faults. They are normal and only the Purbeck Fault is inverted. Locations in figure 3.2.

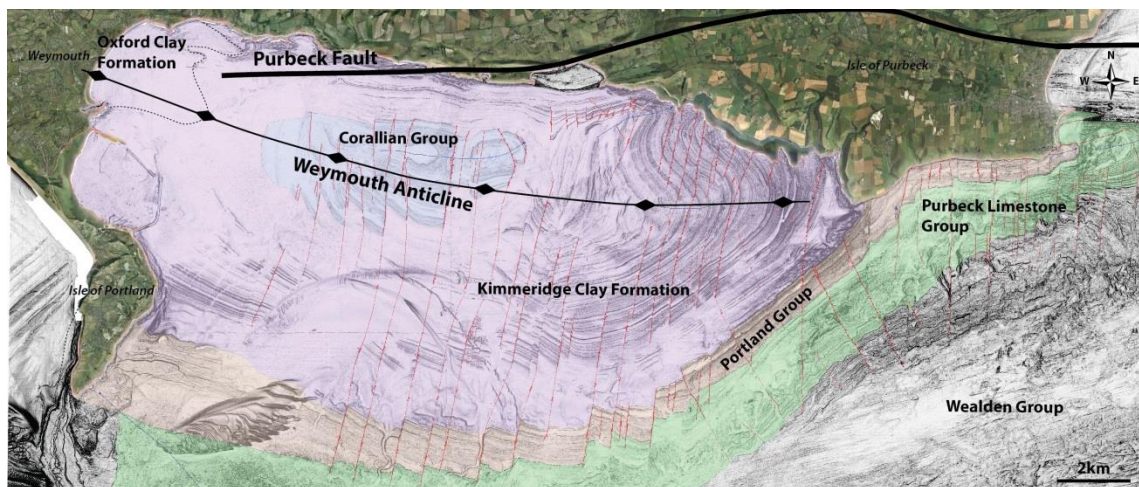
## 4. Tectonic settings and stratigraphy

### 4.1. Extensional settings

Figures 3.5B; 3.6; 3.17B; 3.18; 3.19; 3.20 and 3.22 image the geometries of the Purbeck and Ridgeway Faults based on the seismic interpretation. Formation of tilted blocks associated with extensional faults affecting the Mesozoic strata has been previously identified (Butler, 1998; Harvey and Stewart, 1998; Underhill and Stoneley, 1998) and they are the main characteristics of half-graben development in a rift setting (Gibbs, 1984; Wernicke, 1985; Davison and Underhill, 2012). This feature is also identified for the Purbeck interval, the increasing thickness on the well correlation panels (Figs. 3.7; 3.8; 3.9; 3.12; 3.13 and 3.14) from the footwall to the hanging-wall block documents the syndepositional setting of the Purbeck Fault.

### 4.2. Inversion setting

The tectonic inversion of the two main faults is highlighted by the formation of anticlines (possible reactivated roll-over anticlines) near and towards the faults (*e.g.* at a bigger scale: the Weymouth Anticline in Weymouth Bay, Figs. 3.5B; 3.18; 3.19; 3.21 and 3.22). The timing of this inversion is thought to have occurred from the Late Cretaceous to mid-Cenozoic with a maximum peak during the Miocene (Ziegler, 1981; Stoneley, 1982; Butler and Pullan, 1990; Chadwick, 1993; Butler, 1998; Underhill and Stoneley, 1998) and is linked to the regional alpine inversion phase recorded elsewhere in Europe (Phillips, 1964; Stoneley, 1982; Butler, 1998; Harvey and Stewart, 1998; Smith and Hatton, 1998; Underhill and Stoneley, 1998).



**Figure 3.21** MBES (Multi-Beam Echo Sounder) data also known as DORIS data interpreted after Fleckner (2014). Note the Weymouth Anticline within Weymouth Bay with erosion down to the Corallian Group (Oxfordian) in the core of the anticline.

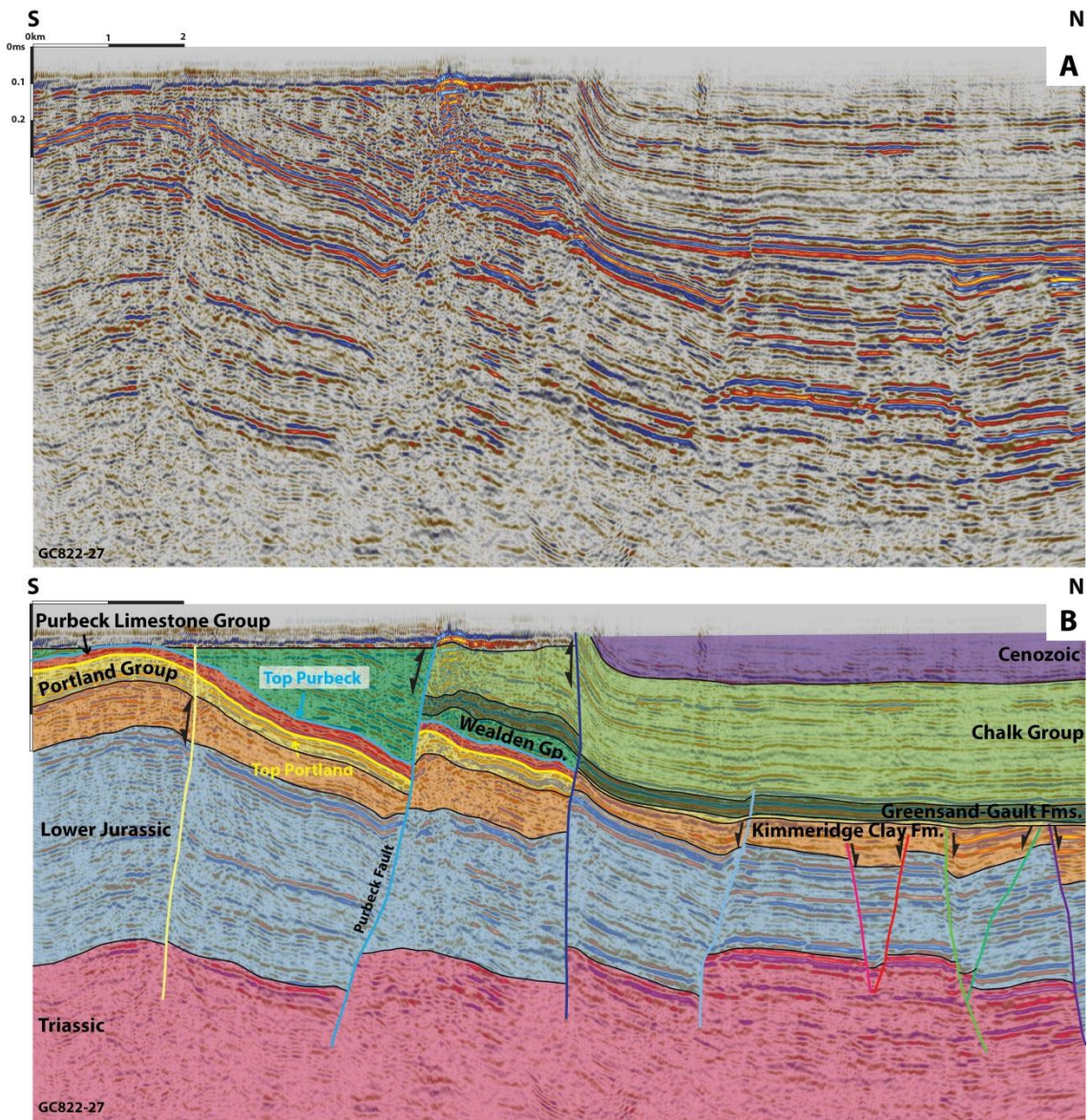
### 4.3. Stratigraphic features

The focus of this study was the identification and interpretation of the Purbeck interval, therefore only the top surfaces of the Portland and Purbeck were interpreted. However other stratigraphic features can be extracted from the seismic profiles and the borehole data and are illustrated with the interpretation of the seismic profile presented in figure 3.22.

The first feature identifiable is the syndepositional nature of the Purbeck Fault from the Early Jurassic until the Early Cretaceous (pre-Albian when the deposition of the Wealden Group occurred). This is highlighted by the extensional sense of movement on the fault (displacement downwards and to the south in the hanging-wall block of the faults).

The second feature recognisable is an unconformity that occurred from the Early Cretaceous (Albian) until the Late Cretaceous (Campanian). This has been identified by previous authors (House, 1958; Lake, 1985; Garden, 1987, 1991; Butler, 1998; Hawkes *et al.*, 1998, McMahon and Turner, 1998; Underhill and Paterson, 1998; Underhill and Stoneley, 1998) and the interpretation presented here brings more data to illustrate it. The unconformity (known as the Albian unconformity) can be seen prior to deposition of the Gault Formation (Albian) as the underlying beds (from the Kimmeridge Clay Formation to the Wealden Group) are eroded. Figure 3.22 shows two cases of erosion creating this unconformity. North of the Purbeck Fault, on the footwall block, the Lower Greensand Formation is in contact with the Kimmeridge Clay Formation while to the south it is in contact with the Wealden Group and even more south it is absent. This can be interpreted as an exposure or erosion of the footwall block down to the Kimmeridge Clay Formation after the deposition of the conglomeratic Wealden Group and prior to the deposition of the Greensand Formation. Garden (1987, 1991) studied the provenance of pebbles found in pebbly beds deposited during Early Jurassic to Late Cretaceous. He determined that most of the pebbles deposited during Albian and Aptian were detritus eroded mainly from Jurassic deposits exposed on the Cornubian massif and reworked into the Wessex Basin. Lake and Karner (1987) related this Albian unconformity to a major extension phase associated with thermal effects. The combination of these previous studies (Lake and Karner, 1987; Garden, 1991) and the seismic interpretation presented here indicates that this unconformity resulted most probably from an activity of the main faults during the Albian and Aptian. The footwall area was exposed to the north leading to erosion of rocks from the Wealden Group to locally the Kimmeridge Clay Formation while on the hanging-wall block to the south the erosion was less significant (Fig. 3.22). However no derived and reworked clasts from these Groups and

Formations were ever identified in the Purbeck Limestone Group deposits (refer to Chapters 2 and 4).



**Figure 3.22** Seismic profile GC822-27. A: uninterpreted. B: interpreted. Note thickening of Purbeck Limestone Group in hanging-wall block of the Purbeck Fault, to the south and significant erosion/non deposition in footwall block of the Purbeck Fault, to the north (see text for description). Arrows show direction of movement of the faults. Location in figure 3.2.

## 5. Discussion

The tectonic evolution of the Wessex Basin has been studied since the end of the 19th century (Bristow, 1889; Strahan, 1898), and more intensively using subsurface data since the discovery of the Wytch Farm oil field (located in Poole Harbour and Bournemouth Bay) in 1973 (Hinde, 1980; Colter and Harvard, 1981). Although previous studies documented the syndepositional activity of the Ridgeway and the Purbeck Faults during the Jurassic and the Early Cretaceous (Bristow, 1889; Strahan, 1898; House, 1958, 1989; Phillips, 1964; Stoneley, 1982; Lake, 1985; Butler, 1998; Harvey and Stewart, 1998; Smith and Hatton, 1998; Underhill and Paterson, 1998; Underhill and Stoneley, 1998; Underhill, 2002), no clear evidence has been published concerning the possible syndepositional setting of these faults specifically during Purbeck time (Late Jurassic-Early Cretaceous). Underhill (2002) presented a diagram proposing a syndepositional setting of the Purbeck Fault during Purbeck time, however he did not provide clear data (field or seismic data) supporting his proposed interpreted depositional model.

In this study integration of subsurface data (*i.e.* 2-D and 3-D seismic profiles and borehole data) provides documentation for an increase in thickness from north to south through fault blocks in Bournemouth Bay (Figs. 3.7; 3.12 and 3.15). This constitutes clear evidence for a syndepositional setting of the Ridgeway and Purbeck Faults during deposition of Purbeck sediments. Two other east-west well correlation panels (Figs. 3.7; 3.8; 3.13 and 3.14) together with the time thickness map (Fig. 3.15) have identified possibly position of two depocentres, one southeast of the studied area with a northwest-southeast trend orientation and one south with a northeast-southwest trend orientation during Purbeck time.

In addition the absence of Purbeck rocks north of the faults and on the footwall blocks suggest either a non-deposition or deposition and subsequent erosion of the exposed land to the north either long after or penecontemporaneously with the deposition in the hanging-wall blocks. If this happened long after the deposition, and if the Purbeck Limestone Group was deposited, the subsequent erosion happened on the uplifted footwall blocks possibly during the intra Aptian-Albian unconformity (refer to Chapter 2) and prior the deposition of the Gault Formation; if the Purbeck Group were never deposited, areas north to the faults would have been exposed throughout the latest Jurassic and earliest Cretaceous with the deposition of the Purbeck Limestone Group in the hanging-wall blocks, this suggests syn-depositional fault activity that possibly allowed the area north of the faults to be exposed and eroded.

A relay ramp area is thought to be located in the centre part of the studied area and linking Ridgeway and Purbeck Faults (Underhill and Paterson, 1998; Underhill, 2002). The 2-D seismic data examined in this study seems to image this feature. The Purbeck Limestone Group has been identified in the seismic profiles within the relay ramp area although not all elements are imaged (Figs. 3.10; 3.16; 3.18 and 3.19) however it is difficult to identify a possible tilting (Peacock and Sanderson, 1991, 1994) due to over-print of the tectonic inversion (Cenozoic). The Purbeck Limestone Group is absent in footwall areas eastwards of the relay ramp area (Fig. 3.10) and in places south of the Purbeck Fault (Figs. 3.10 and 3.17) and the geological map (British Geological Survey, 2000) shows that the Purbeck Limestone Group is covered by Quaternary deposits in this area. However one exposure described by previous authors (Strahan, 1898; Arkell, 1933, 1947; House, 1989), Holworth House in Ringstead Bay (Fig. 3.1), is interpreted to contain lower Purbeck deposits in shallow environment (Strahan, 1898; Arkell, 1947; Townson, 1975; House, 1993; West, 2013c) and constitute the only field exposure in the relay ramp area. Together with the seismic and well data presented here it is clear that the Ridgeway and Purbeck Faults were active and linked by a relay ramp area during Purbeck time.

## 6. Conclusion

This chapter presents results from the interpretation of seismic profiles of 2-D onshore and offshore seismic profiles and a 3-D block in south Dorset. Two seismic picks, top Purbeck and top Portland were targeted to identify possible thickness variations across the studied area. Integration of borehole data (both offshore and onshore) allowed the creation of a time thickness map and well correlation panels of the Purbeck interval (Purbeck Limestone Group) constrained by the Portland and Purbeck surfaces.

Two east-west extensional faults dipping south, the Purbeck Fault (east part and rooted in the basement) and the Ridgeway Fault (west part and rooted in the Triassic salt) were imaged. These are linked by a relay ramp imaged on a few seismic profiles. Away from the relay ramp the faults evolve into fault zones (respectively Purbeck fault zone and Ridgeway fault zone). The better characterisation of the relay ramp area needs integration with field study and will be presented in Chapter 7.

The identification and interpretation of top Portland and top Purbeck picks on the seismic lines provide data to create two surface maps, Portland surface map and Purbeck surface map. These were used to create a thickness map of the Purbeck interval and identification of thickness variations in the Purbeck Limestone Group. Together with well correlation panels

(one north-south, and two west-east transects) and seismic profiles it can be seen that the deposition seems to preferably occur in the centre part of two sub-basins (greater thickness southwards of Bournemouth Bay following a northeast-southwest trend and eastwards following a northwest-southeast trend) and in the hanging-wall blocks of the Purbeck and Ridgeway Faults rather than in the footwall blocks. The identification of the Purbeck Limestone Group within the relay ramp area shows also that the faults were active and propagating at this time. This indicates a syndepositional nature of the Purbeck and Ridgeway Faults during Purbeck time (Late Jurassic - Early Cretaceous).

The extension of the seismic interpretation to the entire succession (Triassic to Cenozoic) brings new data for the syndepositional nature of the main faults from the Early Jurassic to the Early Cretaceous. The unconformity known regionally as the Albian unconformity is identifiable and erodes deposits from the Gault until the Kimmeridge Clay Formations. The seismic data also images the tectonic inversion highlighted by the reverse movement of the main faults due to north-south compression and linked to the alpine inversion phase (Cenozoic) registered all across Europe.

## Chapter 4

# Facies of the Mupe Member, Purbeck Limestone Group



## 1. Introduction

Many geologists have studied facies of the Purbeck Limestone Group, but most of them have focused on the middle and upper parts of the group, *e.g.* Durlston Bay (Clements, 1993). There have been fewer studies on the details of the lower part of the Mupe Member (Westhead and Mather, 1996) or “the Caps and Dirt Beds”, the “Broken Beds” and the “Cypris Freestone” of earlier authors (Austen, 1852; Arkell, 1933; House, 1969; Clements, 1993; review in Chapter 2). Notable exceptions are West (1975, 1979), Francis (1982, 1983, 1984, 1986) and Bosence (1987). In this chapter a new facies classification is proposed for the lower part of the Mupe Member of the Purbeck Limestone Group of Dorset (Tab. 4.1) and each of the facies are interpreted in terms of their depositional environments (Tab. 4.1). This work is based on examination and logging of successions at 22 localities described in Chapter 6 (all measured sections are given in Appendix 3), preparation of 228 slabbed specimens and thin sections. Classic petrography and microscopy (*i.e.* plain polarised light or PPL and cross-polarised light or XPL) was performed for all the thin sections. In addition to for selected facies the insertion of a gypsum plate with 530 nm retardation from the SE quadrant to identify uniaxial/biaxial crystals and fast/slow axis (the slow axis is NE-SW orientated gypsum plate used in this study). Cathodoluminescence (CL) was also used to identify diagenetic phases. From these analyses 9 facies were established as listed in table 4.1. The depositional environments of the Mupe Member are described in Chapter 6 and the facies distributions across south Dorset are presented in Chapter 7.

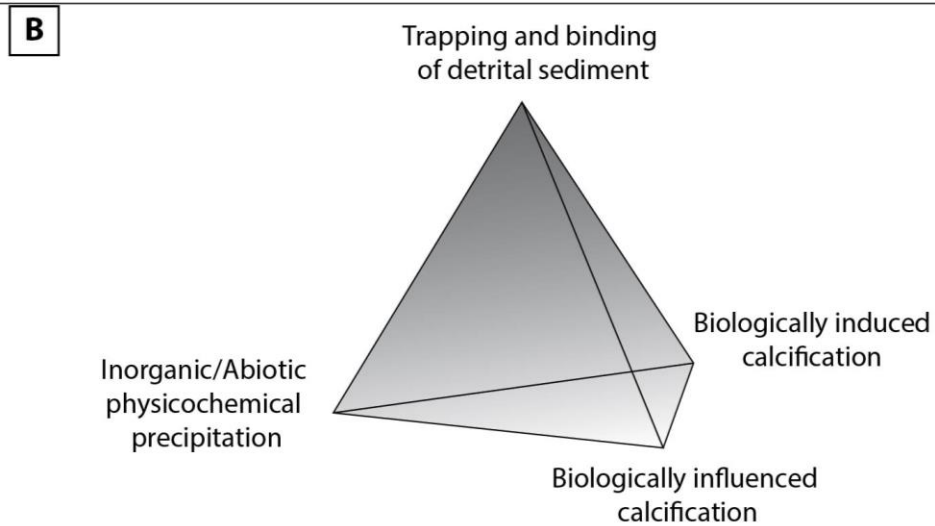
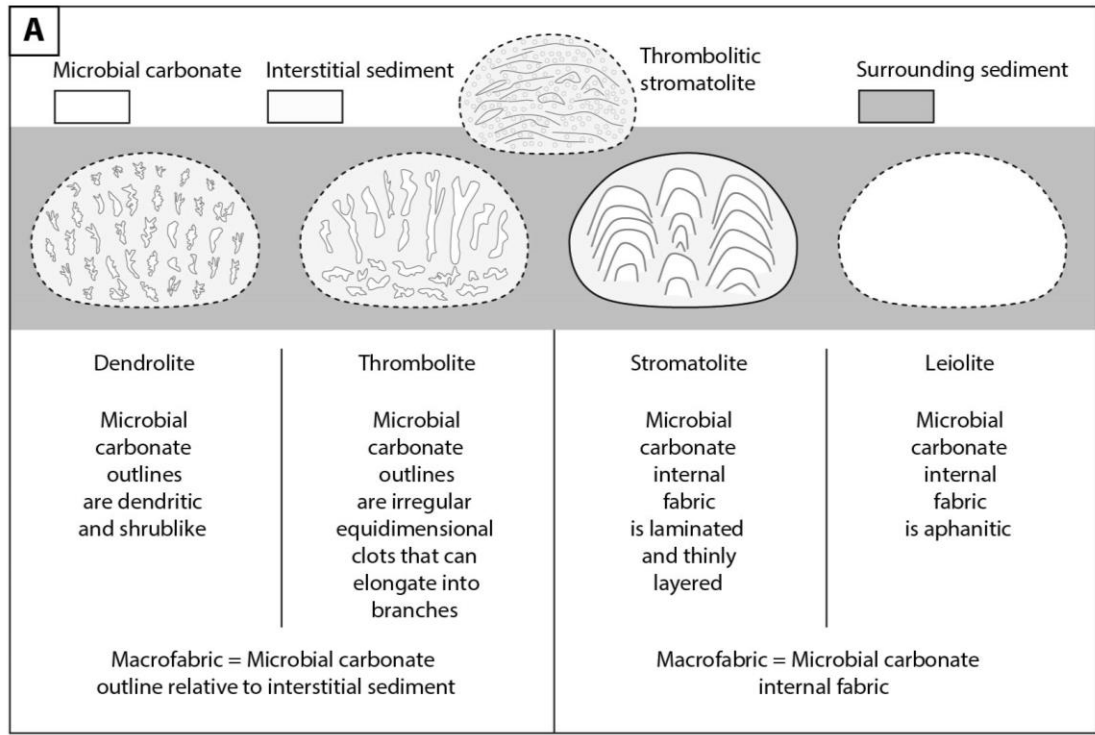
Facies	Subfacies	Texture	Components	Sedimentary structures	Depositional environments	Typical thickness	Bed occurrence	Location occurrence
Microbialite	Thrombolite	Clotted	Peloids, Geopetal, Chalcedony, Gastropods, Microbial filaments	cm scale growth layers	Littoral brackish lacustrine	5 to 50 cm	Skull Cap, Hard Cap and Soft Cap	Everywhere
	Stromatolite	Peloidal packstone-grainstone	Peloids, Ostracods, Microbial filaments	Crinkled laminations	Littoral brackish lacustrine	5 to 10 cm	Hard Cap and Soft Cap	Everywhere
	Burrowed peloidal packstone	Packstone-fine grainstone	Peloids, Chalcedony, Geopetal sediment	Burrows, burrow infill/lining	Littoral brackish lacustrine	2 to 15 cm	Skull Cap, Hard Cap and Soft Cap	Everywhere
Intraclastic peloidal packstone-grainstone		Packstone-grainstone	Peloids, Ostracods, Gastropods, Ooids, Microbial intraclasts	Planar lamination, Structureless	Littoral brackish lacustrine	50 cm to 3 m	Skull Cap, Hard Cap and Soft Cap	Everywhere
Cross-bedded peloidal packstone-grainstone		Packstone-grainstone	Peloids, Ostracods, Gastropods, Bivalves, Ooids, Evaporite pseudomorphs	Waves rippled, Cross-bedded lamination, Herring Bone cross-stratification	Littoral saline lacustrine	1 to 50 cm	Cypris Freestone	Everywhere
Wackestone to fine grainstone		Wackestone, packstone to grainstone	Peloids, Ostracods, Gastropods, Bivalves	Planar lamination	Deep brackish and saline to hypersaline lacustrine	20 to 50 cm	Between Portland Group and Basal Dirt Bed, Lower Skull Cap of Francis (1982) Basal Cast Bed of Arkell (1941)	Portesham Quarry Poxwell Quarry Chalbury Hell's Bottom Swanworth Quarry Fishermen's Ledge Durlston Bay God Nore Lawnshead Quarry Portland Bill
Gypsiferous peloidal packstone		Calcsiltite	Calcite crystals, Micritic matrix		Transition shallow-deep lacustrine (slope)	about 2 cm within a unit of 50 cm	Cypris Freestone	Coombefield Quarry South West Bowers
Calcareous sandstone		Grainstone	Quartz grains, Peloids, Ooids, Ostracods	Cross-bedded lamination	Beach lacustrine	30 to 80 cm	Cypris Freestone	Lulworth area
Conglomerate		Conglomerate	Limestone pebbles, Silicified logs, tree trunks and stumps		Rendzina soil profile	1 to 50 cm	Great Dirt Bed	Everywhere
Carbonaceous marl		Marl		Planar lamination	Immature rendzina soil profile	1 to 10 cm	Basal Dirt Bed and Lower Dirt Bed	Everywhere
Evaporite	Vuggy	Crystalline	Calcite crystals, Evaporite pseudomorphs, Cherts	Planar lamination	Marginal hypersaline lacustrine	10 to 30 cm	Base of Cypris Freestone	From Lulworth area eastwards
	Breccia	Brecciated with a grainstone matrix	Clasts of peloidal packstone-grainstone cross-bedded facies, Evaporite pseudomorphs, Cherts		Marginal hypersaline lacustrine	1 to 5 m thick 2 to 10 m wide	Base of Cypris Freestone (Broken Beds)	From Lulworth area eastwards

**Table 4.1** Facies classification of the lower part of the Mupe Member of the Purbeck Limestone Group and interpretation of depositional environments. Note that the numbering corresponds to the one used in the quantitative analysis for facies succession, presented in Chapter 6.

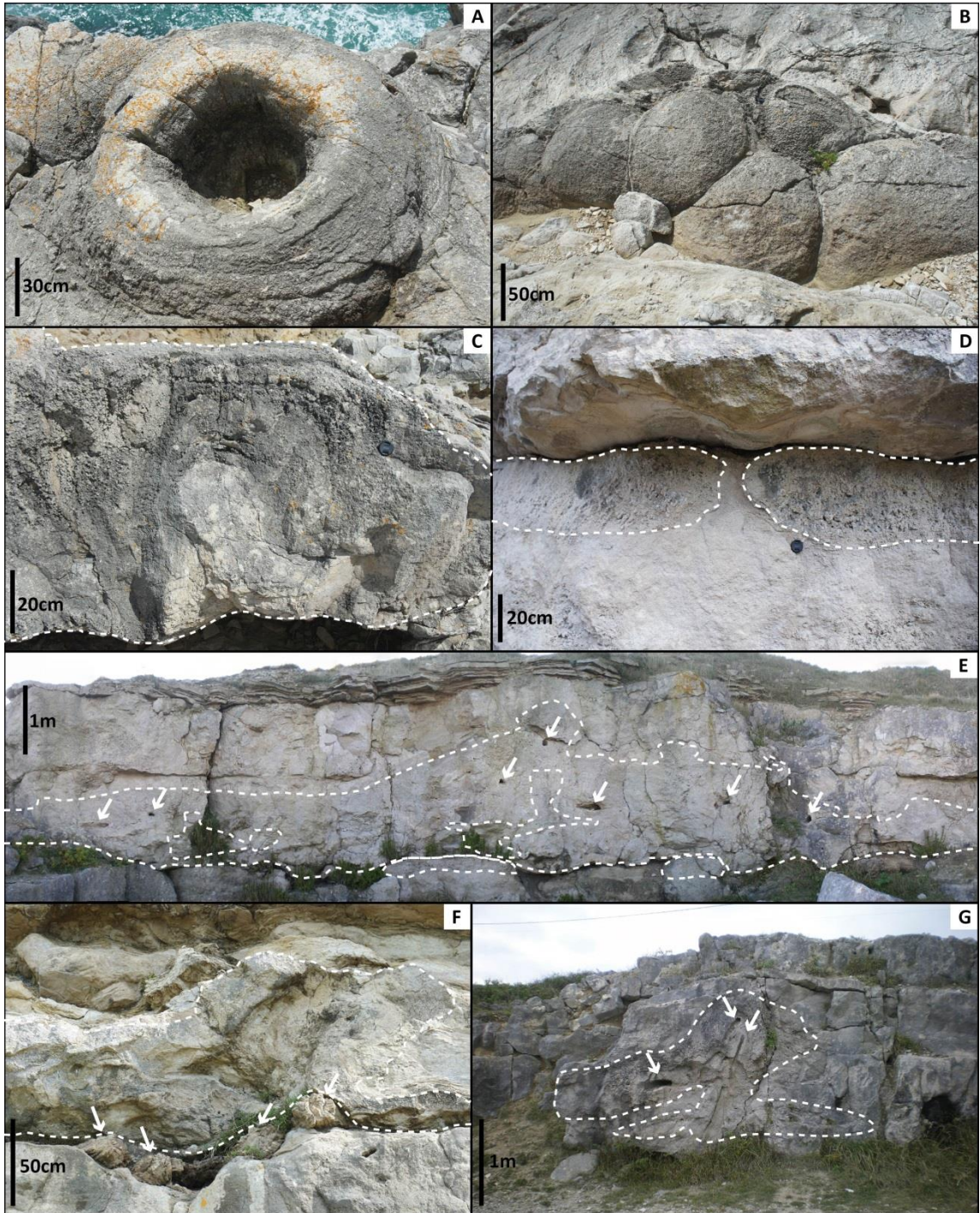
## 2. Microbialite facies

This facies can be encountered within three beds in the lower part of the Mupe Member, Skull Cap, Hard Cap and Soft Cap and sandwiched between three palaeosols, the Basal Dirt Bed, the Lower Dirt Bed and the Great Dirt Bed (refer to Chapter 2 for more details). This facies is present from the Isle of Portland in the west to Fishermen's Ledge in the east although it tends to disappear eastwards, revealed by its absence in Durlston Bay and further east in Portsdown borehole (refer to Chapter 7 for facies distribution). This facies is divided into three sub-facies, thrombolite, stromatolite and burrowed peloidal packstone. Mounded structures constructed by the three sub-facies are abundant in these three beds. At macro-scale mounds are hard limestones containing crinkled laminations (Fig. 4.11), small columns (Fig. 4.8) and/or clotted macrofabric (Figs. 4.3B and 4.6). At the micro-scale laminations, alignment of grains (mainly peloids), micritic threads and micritic tube networks are common in all these sub-facies (Figs. 4.4D, 4.5, 4.6, 4.7 and 4.12). The mounds can vary from a rather simple to more complicated shapes (Fig. 4.2) and their sizes vary between 50 cm and 20 m in width and 10 cm and 3 m in height (refer to Chapter 5 for more descriptions and analysis of shapes and sizes). Mounds commonly have cylindrical holes (Figs. 4.2, 4.3D, 4.13 and 4.15) from 5 to 40 cm in diameter which exhibits on their inner surfaces the imprints of trees and locally the remains of silicified logs, tree branches, tree roots or tree stumps.

These rocks are interpreted as microbialites following the definition of Burne and Moore (1987) as "*organosedimentary deposits that have accreted as a result of a benthic microbial community trapping and binding detrital sediment and/or forming the locus of mineral precipitation*". In addition to this, this thesis follows classifications based on their internal structures and the metabolism involved in their growth (Riding, 1977; Burne and Moore, 1987; Bosence *et al.*, 2015). From the classification based on the internal structure (Fig. 4.1), only two were recognised in this study: stromatolites as "*laminated benthic microbial deposits*" (Kalkowski, 1908; Riding, 1991, 2011a) and thrombolites as "*cryptalgal structures related to stromatolites, but lacking lamination and characterized by a microscopic clotted fabric*" (Aitken, 1967; Riding, 2011a). From the classification based on processes involved in the growth (Fig. 4.1), trapping and binding, abiotic precipitation, biologically induced precipitation and biologically influenced precipitation were possibly identified (Riding 1977; Burne and Moore, 1987; Dupraz *et al.*, 2009; Bosence *et al.*, 2015).



**Figure 4.1** Classification of microbialites. A – Relating to the internal structures (Riding, 2011a). B – Relating to the metabolisms/processes involved in microbial growth (redrawn after Riding, 1977; Bosence *et al.*, 2015).



**Figure 4.2** Mounds as seen in the field. Outlines of the mounds in white dashed lines in all the pictures. A – Mound showing a 50 cm hole with tree bark imprint in the inner part, plan view (Soft Cap, Fossil Forest). B – Six laterally stacked mounds, plan view (Soft Cap, Fossil Forest). C – Cross section of a mound showing the growth layers (Soft Cap, Lulworth Cove). D – Cross section across two mounds (Skull Cap, Tout Quarry, Isle of Portland). E – Cross section of a mound with 10 centimetre wide holes (white arrows) and inter-mound bedding (Hard Cap, God Nore, Isle of Portland). F – Cross section of a mound with silicified roots of ancient trees at the base (white arrows, Hard Cap, east coast of the Isle of Portland). G – Cross section of a mound around tree trunks and branches most probably in living position, the white arrows indicate tree moulds (Hard Cap, Freshwater Bay, Isle of Portland).

## 2.1. Thrombolite sub-facies

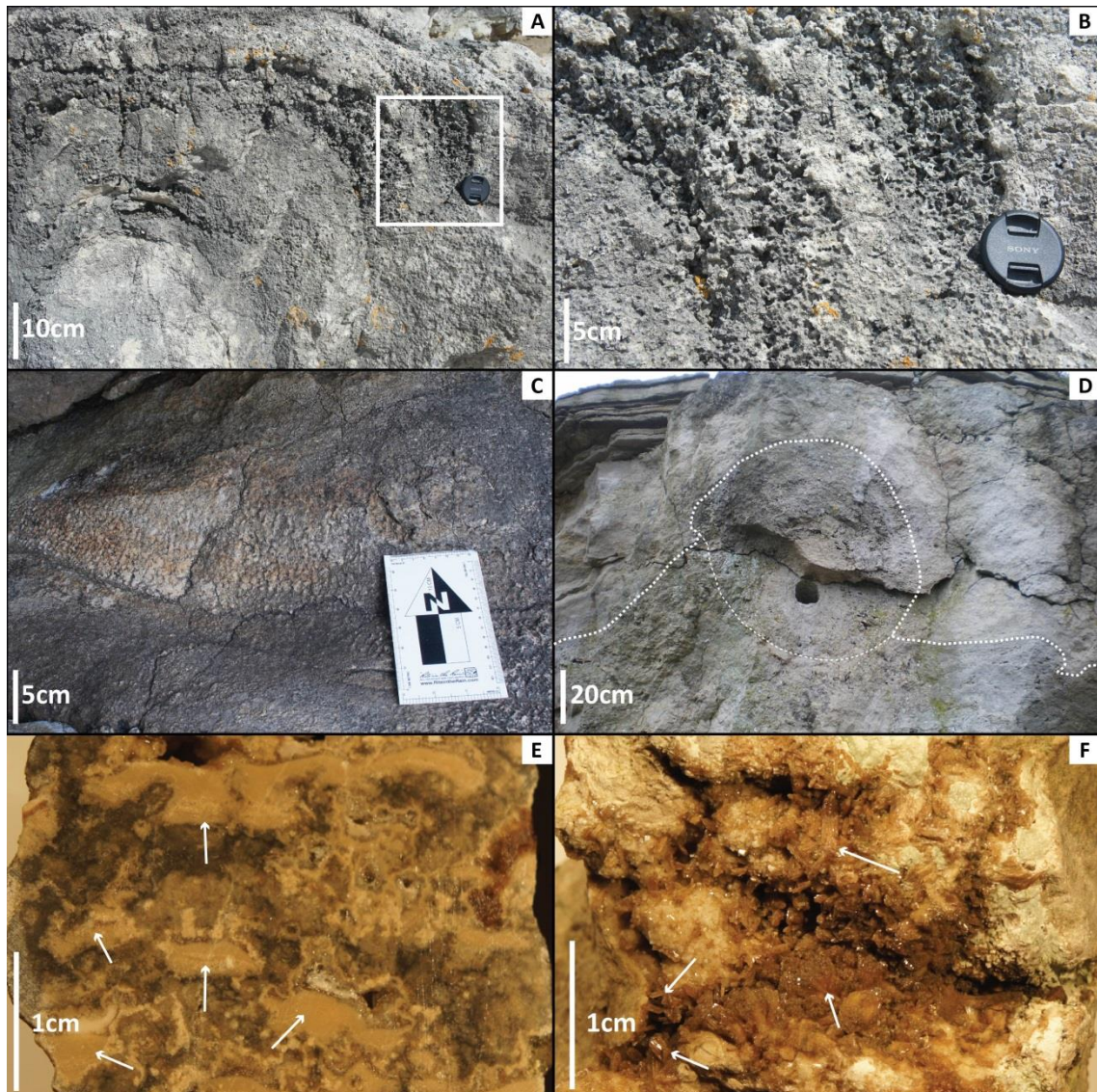
### 2.1.1. Description

This sub-facies is abundant in three beds, the Skull Cap, the Hard Cap and the Soft Cap and its thickness varies between 5 and 50 cm. This sub-facies is always found overgrowing the burrowed peloidal packstone sub-facies (Figs. 4.13A and 4.15) and/or the stromatolite sub-facies (Figs. 4.11A and 4.15). Tree moulds are commonly found associated with this sub-facies (Figs. 4.2, 4.3D and 4.15) and typically has greater thickness above than below the tree moulds (Fig. 4.3D).

At macroscale this sub-facies is characterised by centimetre to decimetre scale growth layers (Fig. 4.3A-B) and is the main components of the mounded structures (Figs. 4.3D and 4.15). The growth layers are made of a clotted macrofabric (Fig. 4.2B) and can contain occasionally millimetre scale columnar structures (Fig. 4.8A-B). In plan view, the external growth layer can exhibit a cerebroid texture (Fig. 4.3C) or just a bumpy surface (Fig. 4.1B). The macro-pores of this sub-facies may be filled with geopetal sediment (Fig. 4.3E). Locally on the Isle of Portland and only in the Hard Cap bed, brown to dark red radiating crystal aggregates are found on the walls of cavities (Fig. 4.3F). These aggregate crystals are between 1 mm and 2 cm long made of about 500  $\mu\text{m}$  flat and between 1 mm and 2 cm tabular to elongated crystals are interpreted to be barite (also found associated with the Burrowed peloidal packstone sub-facies presented in section 2.3 of this chapter). This sub-facies reveals shades of grey, white to pale yellow at the outcrop and pale grey or white when broken.

At microscale the clotted macrofabric (Fig. 4.4C) exhibits mesoclots/lumps (1 to 2 mm) with micritic walled tubes (Figs. 4.4D, 4.5, 4.6 and 4.7) and micritic threads (Figs. 4.4D and 4.5) within a fine-grained, non-luminescent to micritic matrix (Fig. 4.4B). The tubes are radiated towards the external surface of the Thrombolite sub-facies (Figs. 4.7 and 4.8B) but at a smaller-scale they are usually circular in cross-section and can be found in all directions (Figs. 4.6 and 4.7A) or rather elongated and straight (Fig. 4.7C, E, G) in longitudinal sections. The diameters of the tubes are mainly between 30 and 40  $\mu\text{m}$  but vary between 20 and 80  $\mu\text{m}$  and the branching can show 3 different morphologies, dichotomous (Fig. 4.7C), right-angle (Fig. 4.7E) or group of acute angle branching (Fig. 4.7G). The clots are located in the external part of the mounded structures and the internal structure of the clots presents two distinctive layers. The internal layer is made of a finely laminated layer made of micritic laminae (from 50  $\mu\text{m}$  and up to 600  $\mu\text{m}$  thick) non-luminescent under CL and the external layer comprises radial calcite crystals that alternate between dull and bright orange under CL although this layer is

not always present (from 0 and up to 500  $\mu\text{m}$  thick, Fig. 4.7C-D). The external part of this thrombolite sub-facies (*i.e.* the mounds) and in contact with the Intraclastic peloidal packstone-grainstone facies (*i.e.* the inter-mound) is usually made of the small two-layer clots just described (Fig. 4.8C-D).



**Figure 4.3** Macroscale thrombolite sub-facies. A – Clotted texture of a simple mound (Soft Cap, Fossil Forest). B – Zoom in square in A of the clotted texture. C – Cerebroid texture in plan view (Hard Cap, Fossil Forest). D – Mound with the tree mould, note the difference in thickness below the tree mould and above (Hard Cap, God Nore, Isle of Portland). E – Geopetal sediment (arrows) infilling the base of framework pores (SH1, Hard Cap, Sand Hole, Isle of Portland). F – Barite crystal aggregates (arrows) infilling pores (SH1, Hard Cap, Sand Hole, Isle of Portland).

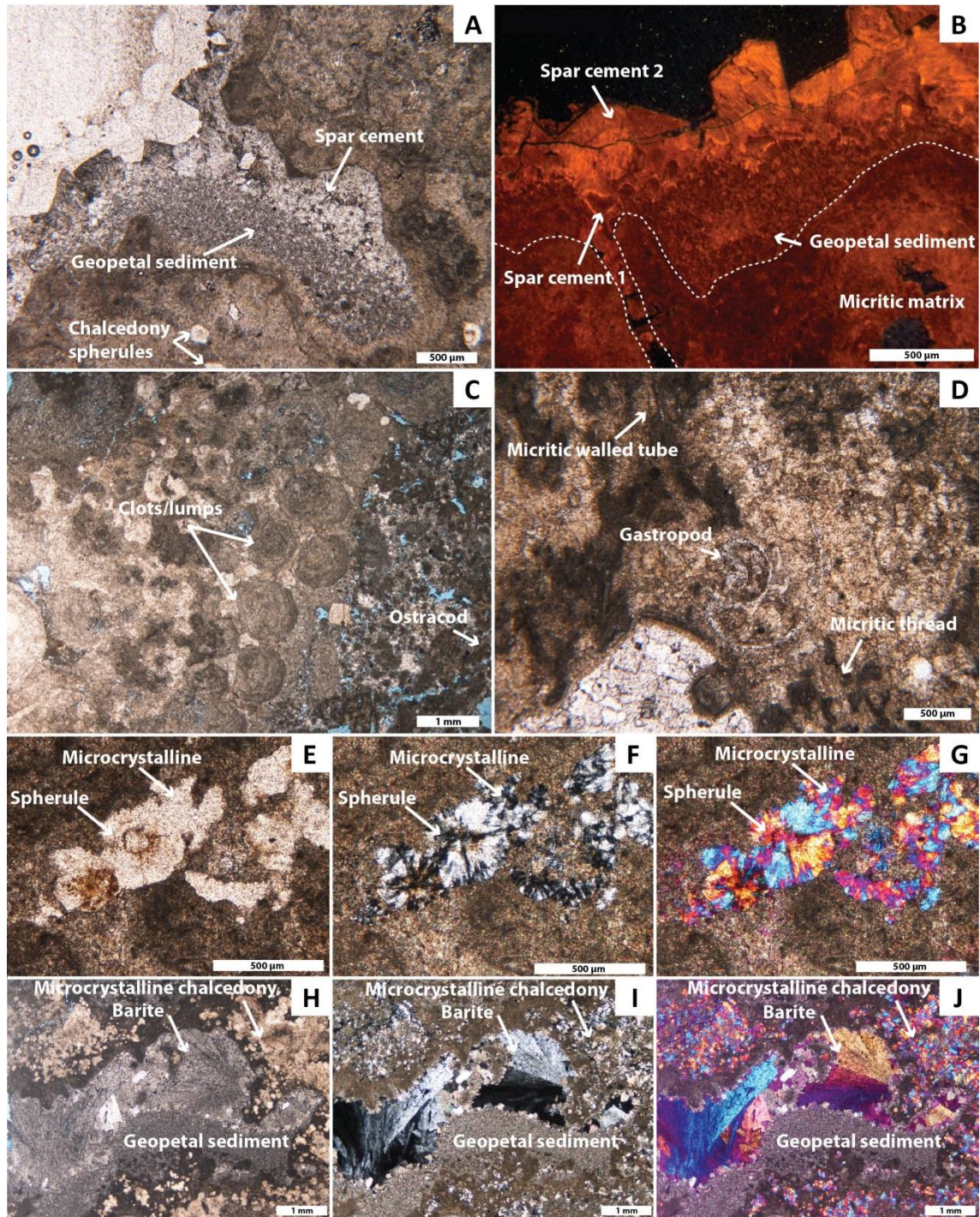
Ostracods (Fig. 4.4C) and molluscs (Fig. 4.4D) are found either in the micritic matrix or the inter-mound facies made of the Intraclastic peloidal packstone-grainstone facies described in section 3.1 of this chapter.

Commonly pale yellow to brown nodular crystals in PPL (Fig. 4.4E) with a first order (grey scale) radial extinction cross in XPL (Fig. 4.4F) interpreted to be chalcedony spherules are found in this sub-facies. When inserting a gypsum plate the NE and SW quadrants of the cross show a second order extinction (blue to green, positive retardation) and the NW and SE quadrants a first order (yellow, negative retardation, Fig. 4.4G). These crystals can be either tiny with a more spherical shape between 50 and 500  $\mu\text{m}$  isolated in the matrix (Fig. 4.4A) or bigger up to 3 mm and with an irregular shape (framboid) and made of several smaller spherules about 2  $\mu\text{m}$  in diameter (Fig. 4.4E-G). The internal structure of the spherules is made of alternation between dark and bright layers (between 10 and 20  $\mu\text{m}$  thick, Fig. 4.4E) both non-luminescent under CL.

Locally on the Isle of Portland and only in the Hard Cap bed, are found crystal aggregates of elongated and colourless to grey to pale yellow in PPL interpreted to be barite (Fig. 4.4H). These crystals can form botryoids and infilling the pore space (Fig. 4.4H). The crystals are between 1 and 2 mm long (Fig. 4.4H) and have a first order rolling extinction in XPL (Fig. 4.4I). When inserting a gypsum plate these crystals show a first order straight extinction of the elongated crystals perpendicular to the slow axis (negative retardation) and a second order straight extinction of the elongated crystals parallel to the slow axis (positive retardation, Fig. 4.4J).

The pore types are intragranular, growth framework and microporosity. The pore space may be filled by a fine geopetal sediment dull orange under CL (when present, Fig. 4.4A-B) and/or a mosaic to blocky spar calcite cement (Fig. 4.4A) organised into two cements under CL (Fig. 4.4B). The first cement is isopachous, thin (50 to 100  $\mu\text{m}$ ), lining pores and fractures and is zoned (non-luminescent, bright and non-luminescent orange, Fig. 4.4B). The second cement is made of bigger calcite crystals (100 to 500  $\mu\text{m}$ ), that tend to occupy the remaining pore space and are zoned dull brown to orange (Fig. 4.4 B).





**Figure 4.4** Microphotographs of the thrombolite sub-facies. A – Geopetal sediment infill of a tubular structure in a mound in PPL (CQ2, Skull Cap, Coombefield Quarry, Isle of Portland). B – CL image showing luminescence of silt sediment and spar blocky cement (CQ2, Skull Cap, Coombefield Quarry, Isle of Portland). C – Clots/lumps at the external border of mounded structure in PPL (BQ8, Hard Cap, Broadcroft Quarry, Isle of Portland), mound on the right and peloidal grainstone (*i.e.* inter-mound) on the left. D – Gastropod in microcrystalline fabric, micritic threads and walled tubes in PPL (GN6, Hard Cap, God Nore, Isle of Portland). E – Chalcedony spherules in micritic fabric in PPL (WLC3, Hard Cap, West Lulworth Cove). F – Same as E in XPL showing the extinction crosses centered in the spherules and the straight extinction in the microcrystalline silica. G – Same as E and F in XPL with gypsum plate showing a positive retardation in the NE and SW quadrants and negative in the NW and SE quadrants. H – Geopetal sediment and boytroid crystals of barite in the framework pores in PPL (SH1, Hard Cap, Sand Hole, Isle of Portland). I – Same as H in XPL showing the rolling first order extinction if the botryoids. J – Same as H and I in XPL with gypsum plate showing a positive retardation of the elongated crystals of barite perpendicular to the slow axis and negative retardation parallel to the slow axis.

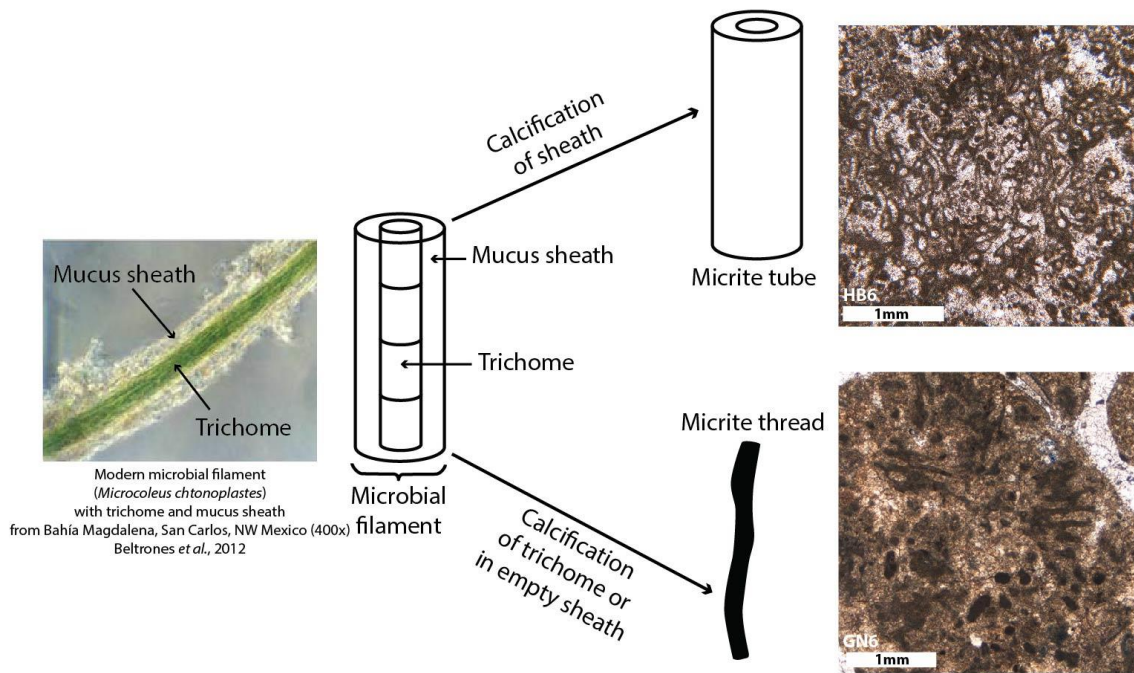
## **2.1.2. Interpretation**

### **2.1.2.1. Clotted macrofabric**

The clotted macrofabric with micritic walled tubes and micritic threads at microscale is interpreted to be the result of microbial activity. Following Burne and Moore (1987) and Riding (1977) a clotted macrofabric in a microbial carbonate is classified as a thrombolite (Fig. 4.1). These thrombolites can develop in a wide range of environments (*i.e.* freshwater, brackish, alkaline water and continental or marine environments) and extreme conditions (such as high temperature or hypersaline conditions) so they are not be critical in the determination of the depositional environment. Thrombolites are very well documented all over the world both in the fossil record (Fisher, 1965; Aitken, 1967; Garrett, 1970; Awramik, 1971, 1982, 1992; Monty, 1973; Walter, 1976; Latham and Riding, 1988; Grotzinger, 1989; Riding, 1991, 2006, 2011*a*, 2011*b*; Leinfelder and Schmid, 2000; Riding and Awramik, 2000; Awramik and Bucheim, 2015) and in modern environments (Logan, 1961; Vasconcelos and McKenzie, 1997; Arp *et al.*, 1998, 1999*a,b*, 2003; Freytet and Verrecchia, 1998, 1999; Wright, 1999; Dupraz *et al.*, 2004; Wright and Wacey, 2005; Dupraz and Visscher, 2005). In the fossil record, thrombolites are found for example in the Green River Formation, USA (Fig. 4.6 C, D; Bradley, 1929; Eardley, 1938; Carozzi, 1962; Eugster and Surdam, 1973; Sandberg, 1975; Surdam and Wray, 1976; Leggitt *et al.*, 2007; Bristow *et al.*, 2012; Buchheim and Awramik, 2013; Sarg *et al.*, 2013). In modern environments lacustrine thrombolites are found for example in the Lake Thetis (Australia, Grey *et al.*, 1990; Reitner *et al.*, 1996; Grey and Planavsky, 2009), the Lake Clifton (Australia, Burne and Moore, 1993; Moore, 1993; Konishi *et al.*, 2001; Luu *et al.*, 2004), the Great Salt Lake (Utah, USA, refer to Chapter 6 for more description) and the Laguna Bacalár (Mexico, refer to Chapter 6 and Appendix 1 for description).

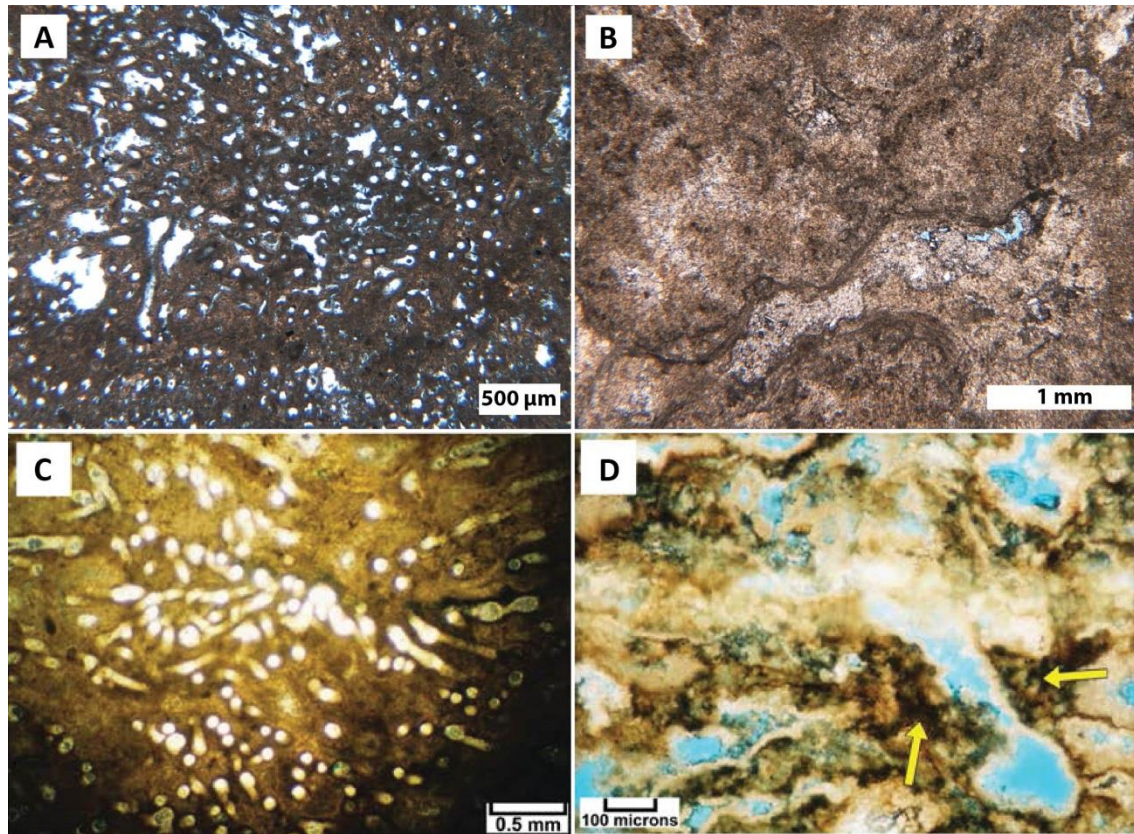
### **2.1.2.2. Micritic walled tubes**

The tubes and threads composing this thrombolite sub-facies are consistent in size and shape with traces left by calcified microbial filaments (Fig. 4.6) as described by Golubić (1976) and Wright and Wright (1985). The micritic tubes being formed by calcification of the mucus sheath of filaments around the trichomes of the microbial filaments (Fig. 4.5). The micritic threads are considered to have formed by a micrite infill in empty threads (Fig. 4.5). In this study the main features encountered are the micrite-walled tubes that together with the clotted macrofabric and the clots/lumps that form the Thrombolite sub-facies in the mounds.



**Figure 4.5** Schematic diagram of microbial filament organisation and calcification types and results (redrawn from Wright and Wright, 1985). Comparison between modern microbial filament on the left of the image and ancient with microphotographs of two samples for the Hard Cap bed on the right.

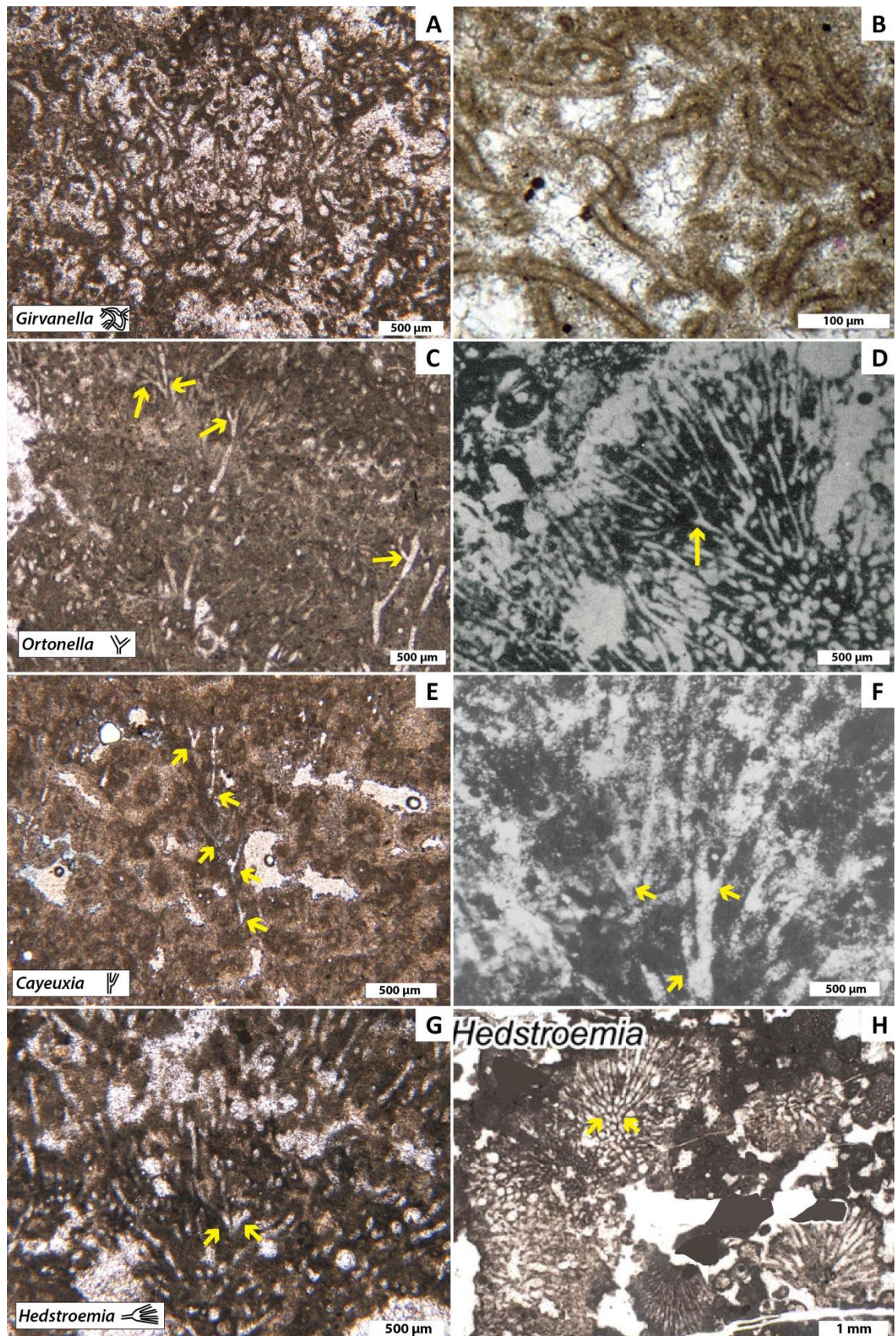
During the growth of the thrombolites, microbial filaments can incorporate gastropods (Fig. 4.4D), peloids (Fig. 4.4C-D) and ostracods. The thrombolite growth direction is also identifiable thanks to the preferential orientation of the microbial filaments at microscale and the orientation of the clotted texture (small columns and clots, Fig. 4.7A, B). Figure 4.3D shows that the thrombolites are thicker above tree moulds than below. This indicates that thrombolites were preferentially growing upwards and towards light. It is also well known and well documented that there are cyanobacteria involved in the early calcification of the microbial filaments (Walcott, 1914; Aitken, 1967; Awramik and Margulis, 1974; Monty and Hardie, 1976; Krumbein *et al.*, 1977; Dupraz *et al.*, 2009). These cyanobacteria are photosynthetic organisms that are phototrophic. The thicker part of the thrombolites being above the tree moulds, shows that the microbial activity was mainly located above the tree moulds and that the microbes were most likely cyanobacteria growing upwards to catch as much light as they could for the photosynthetic process. At a smaller scale the orientation of the small columns and clots perpendicular to the edges of the moulds (Fig. 4.8A, B) with convex-up layering (Figs. 4.3A, D and 4.8A) also implies an upwards growth direction (Gebelein, 1969; Kennard and James, 1986; Janhert and Collins, 2012).



**Figure 4.6** Clotted microfibrils. A – Micritic walled tubes in PPL (SWB2, Skull Cap, South West Bowers, Isle of Portland). B – Clotted microstructure in PPL (WLC3, Hard Cap, West Lulworth Cove). C – Photomicrograph of tubular or filamentous texture from the Green River Formation in PPL (Utah, USA, from Chidsey *et al.*, 2015). D – Photomicrograph of clotted texture from the Green River Formation in PPL (Utah, USA, from Chidsey *et al.*, 2015).

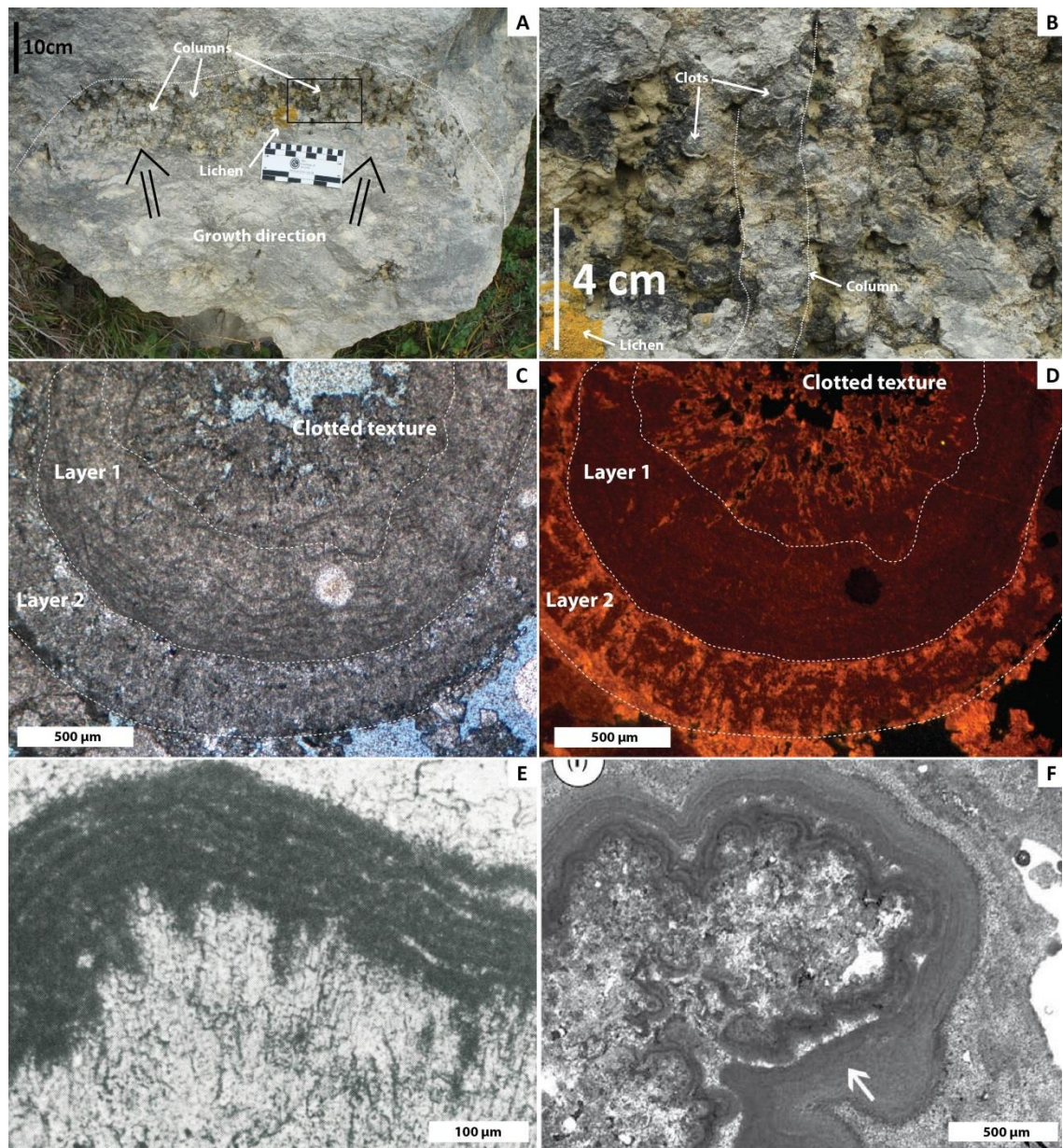
The morphologies, sizes and type of branching of the microbial filaments help to determine possible taxonomy (genus) of the fossil cyanobacteria (Wray, 1977). However this cannot be used as palaeoenvironmental indicators as no clear modern day equivalent can be proven. In this study the classification defined by Wray (1977) was used. The filaments that do not show any preferential orientation, no branching and found in all directions are considered to be *Girvanella* (Fig. 4.7A-B). *Girvanella* is very common in fossil records from the Cambrian to Cretaceous and is found worldwide (Klement and Toomay, 1967; Wray, 1977). The other types of filaments found in this study show some similar characteristics, they have more or less the same size about 30-40 µm in diameter and with an elongated and straight shape. As a consequence branching types will be critical to determine possible genera. Wray (1977) defined dichotomous branching to be representative of *Ortonella* genus (Fig. 4.7C-D); the right-angle branching of a single branch to be representative of *Cayeuxia* genus (Fig. 4.7E-F) and the branches that form groups of acute angles to be representative of *Hedstroemia* genus

(Fig. 4.7G-H). The four different morphologies described in the section above of this sub-facies are thought to correspond to these four genera (Fig. 4.7).



**Figure 4.7** Microbial filaments taxonomy. Typical branching on left bottom of C, E and G are after Wray (1977). A – *Girvanella* from the Skull Cap (HB6, Hell’s Bottom). B – *Girvanella* from the Simla-Blue Ridge Formation (Upper Devonian) of Alberta, Canada (from Scholle and Ulmer-Scholle, 2003). C – *Ortonella* from the Skull Cap (WT1B, Worbarrow Tout). D – *Ortonella* from the Mississippian of England (from Johnson, 1943). E – *Cayeuxia* from the Hard Cap (PQ6, Portesham Quarry). F – *Cayeuxia* from the Kesrouane Limestone (Upper Jurassic) of Jabal Jai, Mount Lebanon, Lebanon (from Basson and Edgell, 1971). G – *Hedstroemia* from the Hard Cap (WT3, Worbarrow Tout). H – *Hedstroemia* from Ordovician deposits of the Tarim Basin, northwest of China (from Liu *et al.*, 2016).

As described in the previous section, the external part of the Thrombolite sub-facies is made of layered clots. The first layer made of micritic laminae (layer 1 in Fig. 4.8C-D) is a stromatolitic layer as observed in ancient and modern environment in the external part of a microbial mound (Fig. 4.8E-F; Wray, 1977, Fig. 78; Della Porta, 2015). The alternation between light and dark layers is the result of the trapping and binding process typical for stromatolite development (Monty, 1976; Riding, 1977, 1991; Pentecost, 1991; and described in section 2.2 of this chapter). The second layer made of radial calcite (layer 2 in Fig. 4.8C-D) may be due to two mechanisms. Microbially induced calcite can explain it as the radial structures can be due to microbial filaments driving precipitation of calcite crystals (Monty, 1976; Cross and Klosterman, 1981; Monty and Mas, 1981; Riding, 1991; Freytet and Verrecchia, 1998). However the radial calcite cement found here does not show any clear evidence of microbial influence (*i.e.* microbial filament moulds nor laminations). This calcite cement is most likely due to physico-chemical (abiotic) precipitation and this is very common in lakes and ephemeral pond environments where it creates a calcite fringe or coating around pretty much everything present in the water (Pedley, 1990; Freytet and Verrecchia, 1998; Gierlowski-Kordesch, 2010; Della Porta, 2015). This kind of calcite cement has already been suggested and described for the Purbeck Limestone Group of Dorset by Perry (1994) (refer to Chapter 2). Perry calls these “freshwater tufas” and demonstrates that to obtain such fringe cement, a protected environment is needed with an overconcentration of carbonate ions in freshwater. It is likely that this mechanism took place at Purbeck time and is the origin of this calcite fringe cement.

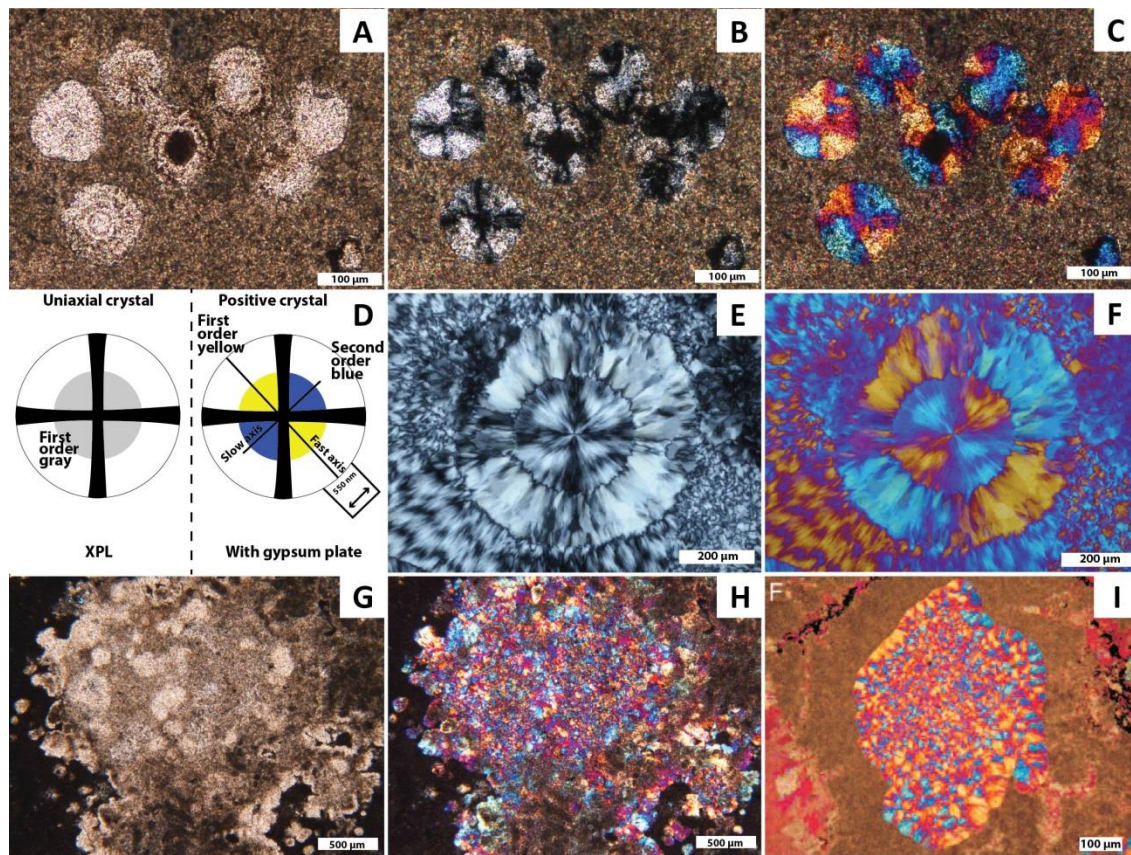


**Figure 4.8** Growth direction and clots. A – Mound showing columns in the external part with a round top surface. Black box locates B (Hard Cap, God Nore, Isle of Portland). B – Detail of columns with clots, note the very external layer of the clots visible at that scale and detailed in C, D (Hard Cap, God Nore, Isle of Portland). C – Details of one clot with layered organisation in PPL. Layer 1 is a laminated layer; Layer 2 is made of radial calcite crystals (HB6, Skull Cap, Hell’s Bottom). D – CL image of C showing luminescence of diagenetic phases. E – *Archaeolithoporella* encrusting laminae in PPL (Permian, Texas, USA Wray, 1977). F – Tight dense micrite laminae overlain by microsparite crusts in PPL (white arrow, Mono Lake, California, USA Della Porta, 2015).

### 2.1.2.3. Chalcedony spherules

The pale yellow to brown radial crystals (Figs. 4.4E and 4.9A) show an extinction cross centered that indicates that they are uniaxial crystals (Figs. 4.9B and D; Gribble and Hall, 1985; Nelson, 2014), an increasing birefringence (blue) on the NE and SW quadrants (according to Michel-Lévy chart) and a decreasing birefringence (yellow) in the SE and NW quadrants (Fig. 4.9C, H). Because the birefringence increases in the quadrants parallel to the slow axis of the gypsum plate these crystals are positive (Fig. 4.9D; Gribble and Hall, 1985; Nelson, 2014). The aspect in PPL (Figs. 4.9A and G) and the cross extinction in XPL (Figs. 4.9B, D and E) show typical features of silica. The birefringence, when the gypsum plate is inserted, shows typical extinction of quartzine crystals or length-slow chalcedony (Fig. 4.9C, E, F). These can be found as spherules (Fig. 4.9A-C) and as microcrystalline (Fig. 4.9G-I). Boggs (2009) demonstrated that chalcedony often develops a spherulitic structure and that it is the main mineral for the formation of cherts. He also described that the brownish colour is due to water inclusions in layers. Because the spherules in this sub-facies are not colourless they are interpreted to result from recrystallisation of the micritic matrix and the dark and bright layers are growth layers maybe with some water inclusions. Folk and Pittman (1971) demonstrated the importance of identifying length-slow chalcedony as evidence of former evaporites and took as an example the quartzine described by West (1964) from the Purbecks in Durlston Bay. West (1973) in a discussion specified that length-slow chalcedony does not always indicate vanished evaporites. He explained that celestite and lutecite are positive evidence of former calcium sulphate evaporites (as West, 1964 and 1975 found in Durlston Bay). In this study length-slow chalcedony replaces micritic texture of the thrombolites and there is no clear evidence of former evaporites (such as evaporite pseudomorphs as found in overlying beds of the Cypris Freestone, see section 10 of this chapter). Bustillo (2010) proposed that the source of silica in lacustrine environments is mainly from redistributed biogenic silica (diatoms and phytoliths) because this is very unstable and easily dissolved. Bustillo (2010) also specified that microbialite carbonates are preferential sites for precipitation of this dissolved silica when the pore fluids become oversaturated with regard to silica. In fact the decomposition of organic matter of the biofilms lowers the pH due to increase in CO<sub>2</sub> content that triggers calcite dissolution and favours silica precipitation (Siever, 1962; Knoll, 1985; Konhauser and Ferris, 1996; Woodruff *et al.*, 1999; Konhauser *et al.*, 2004; Bustillo, 2010). This mechanism is thought to be responsible of the replacement of the micritic thrombolites in chalcedony rather than as a replacement of evaporites, because chalcedony spherules are only found within the thrombolites.



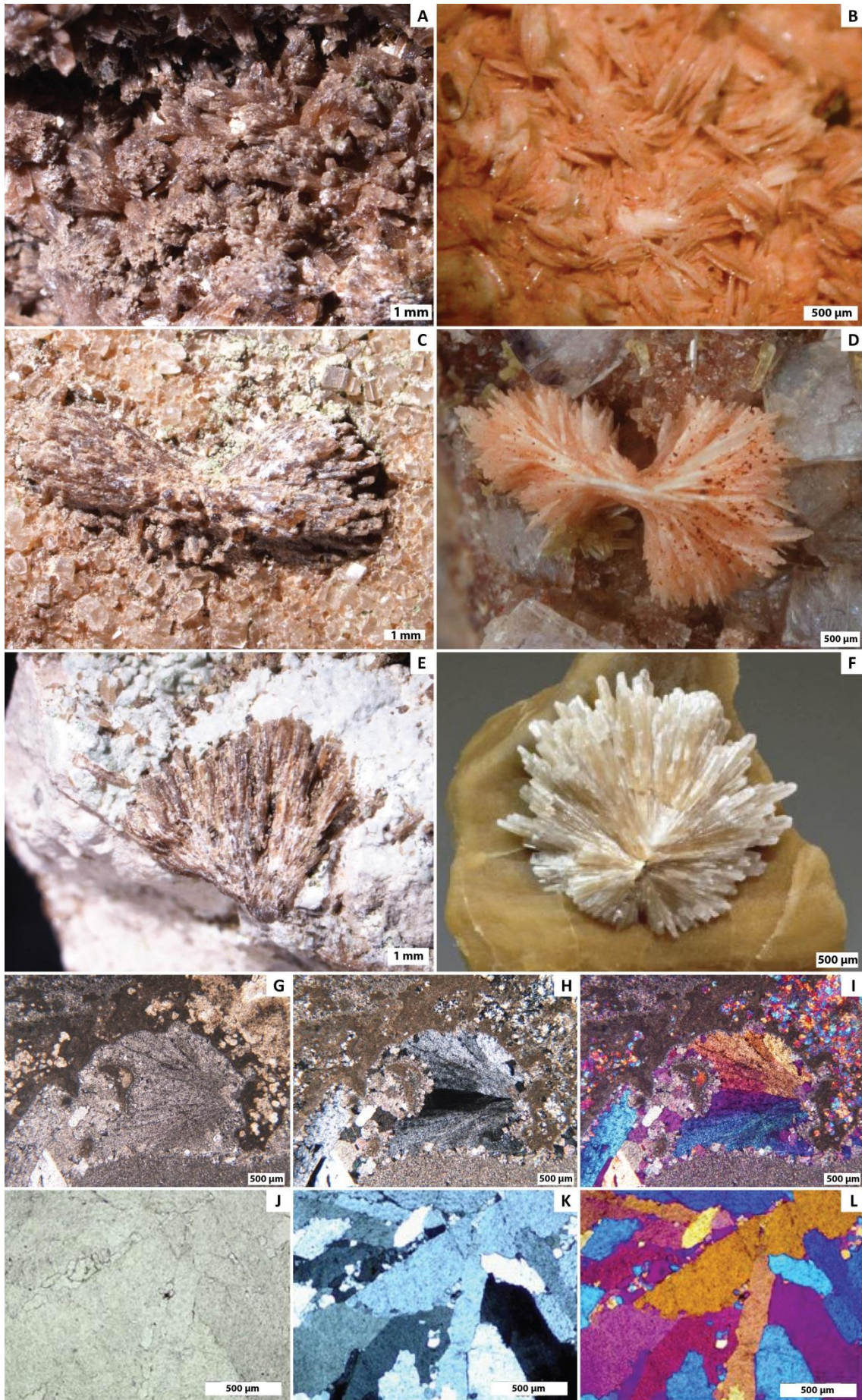


**Figure 4.9** Microphotographs of chalcedony spherules. A – Replacing micrite in thrombolite subsurfaces with a core darker than the rims in PPL (TQ7, Hard Cap, Tout Quarry, Isle of Portland). B – Same as A in XPL showing the extinction crosses of the spherules. C – Same as A and B in XPL with gypsum plate showing a second order extinction (positive retardation) in the NE and SW quadrants and a first order extinction (negative retardation) in the NW and SE quadrants (see text for explanation). D – Expected extinctions for uniaxial crystals in XPL and positive crystals with gypsum plate (redrawn after Nelson, 2014). E – Detail of a spherulite (Kerrouchene, Meknès-Tafilalet Region, Morocco, ©Amir Akhvan). F – Same as E in XPL with gypsum plate showing that length-fast chalcedony spherulite is surrounded by quartzine (length-slow chalcedony) which in turns is surrounded by length-fast chalcedony. G – Quartzine (length-slow chalcedony) aggregate replacing micritic matrix of the thrombolite (TQ7, Hard Cap, Tout Quarry, Isle of Portland). H – Same as G in XPL with gypsum plate showing that the aggregates display a microcrystalline texture rather than nodular. I – Microcrystalline quartz infilling pores in oncolitic limestone in XPL with gypsum plate of the Triassic Cerro Puntundo Formation (San Juan, Argentina, modified after Benavente *et al.*, 2014).

#### 2.1.2.4. Barite crystal aggregates

The crystal aggregates only found on the Isle of Portland that are brown to dark red radiating crystals at macro-scale correspond to the colourless to grey to pale yellow crystals described above at microscale (in PPL). They form elongated crystals (Figs. 4.3F and 4.10) that can form aggregates (Fig. 4.10A-B), twisted crosses (Fig. 4.10C-D) and botryoids (Fig. 4.10E-F). The morphologies and colours resemble barite crystals and aggregates found worldwide (Fig. 4.10). The red to brown colour is thought to be oxidised iron-rich barite. Petrographic analyses confirm this as these crystals are elongated, “dirty” and sometimes feather like in PPL

(Fig. 4.10G) and with rolling first order extinction in XPL due to the botryoidal morphology (Fig. 4.10H). The extinctions, after insertion of a gypsum plate from the SW quadrant, show that the crystals present a second order extinction perpendicular to the slow axis and a first order extinction parallel to the slow axis (Fig. 4.10I) which define negative crystals. Figure 4.10J to L (with gypsum plate inserted from the NE quadrant) show typical barite crystals extinctions that are similar to those found in the Purbeck. The study and comparison of these crystals both at macro- and micro-scale help the identification of oxidised barite crystals in this sub-facies. Barite crystals can be found either as sedimentary deposits (in which case it forms a solid solution series with Celestine; Hanor, 2000) or as a diagenetic feature (Hanor, 2000). In the former case stratiform barites are expected to deposit while in the latter case barite is expected to crystallise in pore space as dispersed cements or spherules (Gribble and Hall, 1985; Hanor, 2000). In the Hard Cap bed on the Isle of Portland, barite crystals and aggregates are found infilling pores and are clearly diagenetic features rather than sedimentary deposits. Breit *et al.* (1990) studied dispersed barite cements of the Morrison Formation (Late Jurassic sandstone deposits) exposed in the Colorado Plateau (Colorado, USA) dispersed over a 250 by 250 km area. They found that barite crystallisation is located on a similar extent as underlying bedded evaporite deposits from the Hermosa Formation (Pennsylvanian) from 2 km below. They found high concentration of sulphate and strontium contents in the barite and suggested that ascending sulphate-rich fluids are at the origin of these barite cements. The fluids would have circulated through the Dolores fault zone in western Colorado and led to the formation of the dispersed barite cements in the sandstones of the Morrison Formation (Breit *et al.*, 1990). In the Purbeck limestones, barite is found as cements however only precipitated in the Hard Cap bed on the Isle of Portland. Open joints are known by locals as “gullies”, “slyvers”, “southers”, “north-easters” or “rangers” depending on the direction, to cross-cut the Isle of Portland and create a complex joint network (Hounsell, 1952; Godden, 2012) however no studies were undertaken to understand the timing of joint formations or their maximum depth extent. Thick evaporite deposits (about 500 m) of the Mercia Mudstone Group are found deeper below the Purbeck Limestone Group (about 1.5 km) in the Wessex Basin (Underhill and Stoneley, 1998). If a similar mechanism as the Morrison Formation of the Colorado Plateau was at the origin of the barite, dispersed cements would be expected in a much broader area and not only in one bed. Further analyses such as strontium isotopes and fluid inclusions are needed to decipher the source of the fluids that led to the precipitation of this barite.



**Figure 4.10** Barite crystals and aggregates. A – Stereo zoom microscope photograph of barite aggregates (Hard Cap, Sand Hole, Isle of Portland). B – Cockscomb barite crystals from a quartz spherule (Calton Hill Quarry, Blackwell-in-the-Peak, Derbyshire, U.K., ©Andy Thompson). C – Barite crystals forming a twisted cross (Hard Cap, Sand Hole, Isle of Portland). D – Barite crystals and mimetite on fluorite (Montmeniers Mines, Beaujeau, Rhône-Alpes, France, ©Chollet Pascal). E – Botryoidal barite (Hard Cap, Sand Hole, Isle of Portland). F – Acicular barite crystals (Warden Point, Isle of Sheppey, Swale, Kent, U.K., ©Bill Dameron). G – Botryoidal barite overgrowing geopetal sediment in framework pores in PPL (TQ7, Hard Cap, Tout Quarry, Isle of Portland). H – Same as G in XPL. I – Same as G and H in XPL with gypsum plate showing the second order extinction of the elongated crystals parallel to the slow axis and first order perpendicular. J – Barite aggregate in PPL (from Józwiak-Niedźwieszka *et al.*, 2015). K – Same as J in XPL. L – Same as J and K in XPL with gypsum plate inserted from the NE quadrant showing second order extinction parallel to the slow axis and first order perpendicular.

The geopetal sediments at the base of the framework pores (Fig. 4.3E) specify the way up which corresponds to the present vertical position. This feature shows that most probably the thrombolite sub-facies has remained in the same position since its deposition.

The rather coarse-grained texture (peloidal packstone-grainstone) of the interdigitated inter-mound facies indicates a high energy and the occurrence of brackish water ostracods (Strahan, 1898; Barker *et al.*, 1975; Anderson, 1985; Horne, 2002) and gastropods (Strahan, 1898; Arkell, 1941; Clements, 1973; Radley, 2002) suggest a brackish water condition (rather than freshwater condition suggested by Perry, 1994) in a shallow marginal lacustrine environment.

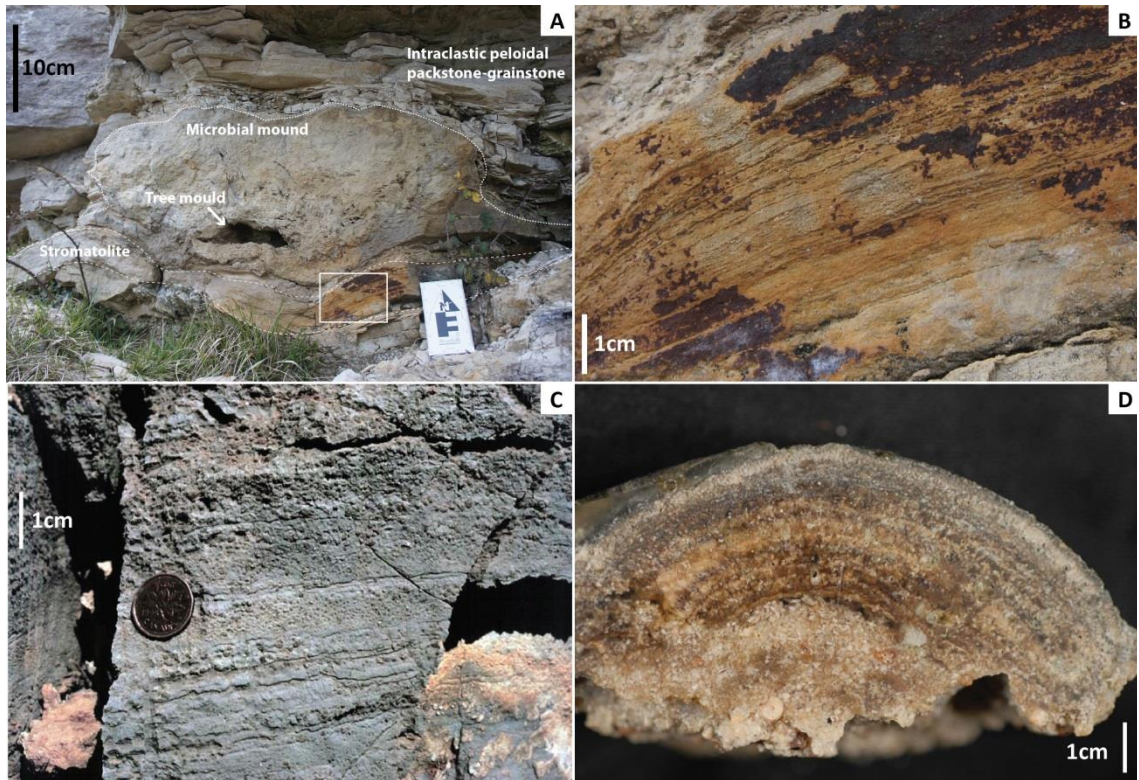
## **2.2. Stromatolites**

### **2.2.1. Description**

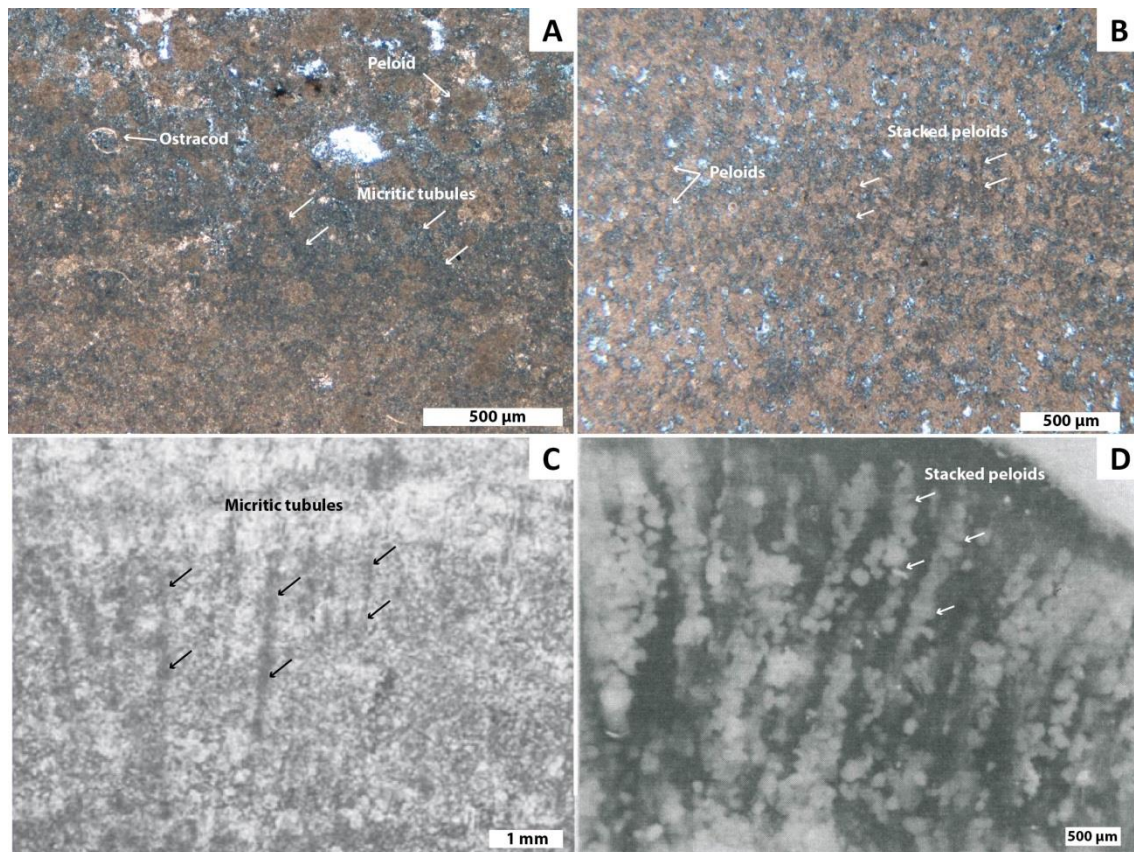
This sub-facies is found very locally and only at the bottom of the Hard Cap bed (Fig. 4.11A) forming lenticular beds of about 5 to 10 cm thick. These lenticular beds are not always present but when they are, they are located below one of the mounds described in the previous section of this chapter. At macroscale this sub-facies exhibits crinkled laminations of about 2 to 5 mm thick (Fig. 4.11B). This sub-facies appears as shades of grey at the outcrop and white to grey when broken.

At the microscale this sub-facies is made of a peloidal packstone to grainstone which presents alignment of vertically stacked peloids (Fig. 4.12A) and vertical micritic tubules (Fig. 4.12B), both normal to the laminations. Horizontal laminations can also be present, about 1 mm thick and highlighted by micritic horizons.

Peloids (Fig. 4.12A, B) and few ostracods (Fig. 4.12A) are found in this sub-facies. The porosity type is intergranular to vuggy (Fig. 4.12A, B).



**Figure 4.11** Stromatolite facies in the field. A – Hard Cap from Portesham Quarry with stromatolitic bed at the bottom. B – Crinkled laminations, close-up view on white box from A. C – Crinkled laminations from the Cararra Formation (Early Cambrian, western USA, from Grotzinger, 2011). D – Crinkled laminations in a domal structure from the Lake Clifton (western Australia, from Phillips, 2009).



**Figure 4.12** Stromatolite microfacies. A – Peloidal packstone with micritic tubules in PPL (SWB4, Hard Cap, South West Bowers, Isle of Portland). B – Peloidal grainstone with vertically stacked peloids in PPL (BQ4, Hard Cap, Broadcroft Quarry, Isle of Portland). C – Ancient stromatolite with micritic tubules from Mavor Formation in PPL (Paleoproterozoic) at Sanikiluaq, Belcher Islands (Qikiqtaaluk Region, Nunavut, Canada, from Hoffmann, 1977). D – Modern stromatolite with stacked peloids from Lee Stocking Island, Bahamas (from Browne *et al.*, 2000).

### 2.2.2. Interpretation

The stromatolite sub-facies found at the base of the Hard Cap bed, either below or surrounded by thrombolite mounds shows that the development of these stromatolites can be either older or contemporaneous with initial thrombolite development. Following the Logan *et al.* (1964) classification these stromatolites can be classified as Spaced Laterally Linked Hemispheroid (LLH-S).

Alignment of vertically stacked peloids and vertical micritic tubules are due to microbial activity and are relicts of erected microbial filaments trapping sediment (Gebelein, 1969; Burne and Moore, 1987; Pentecost, 1991). The micritic horizontal laminae are also relicts of microbial filaments binding grains trapped when the filaments are prostrate (Gebelein, 1969; Burne and Moore, 1987; Pentecost, 1991). Trapping and binding together with induced cementation are the principal mechanisms used by microbes and in particular cyanobacteria

(Awramik and Margulis, 1974) to form layered structures (Monty, 1965, 1976; Gebelein, 1969; Golubić, 1973; Riding, 1977, 1991; Pentecost, 1988, 1991; Riding, 1991, 2011a, 2011b; Dupraz and Visscher, 2005).

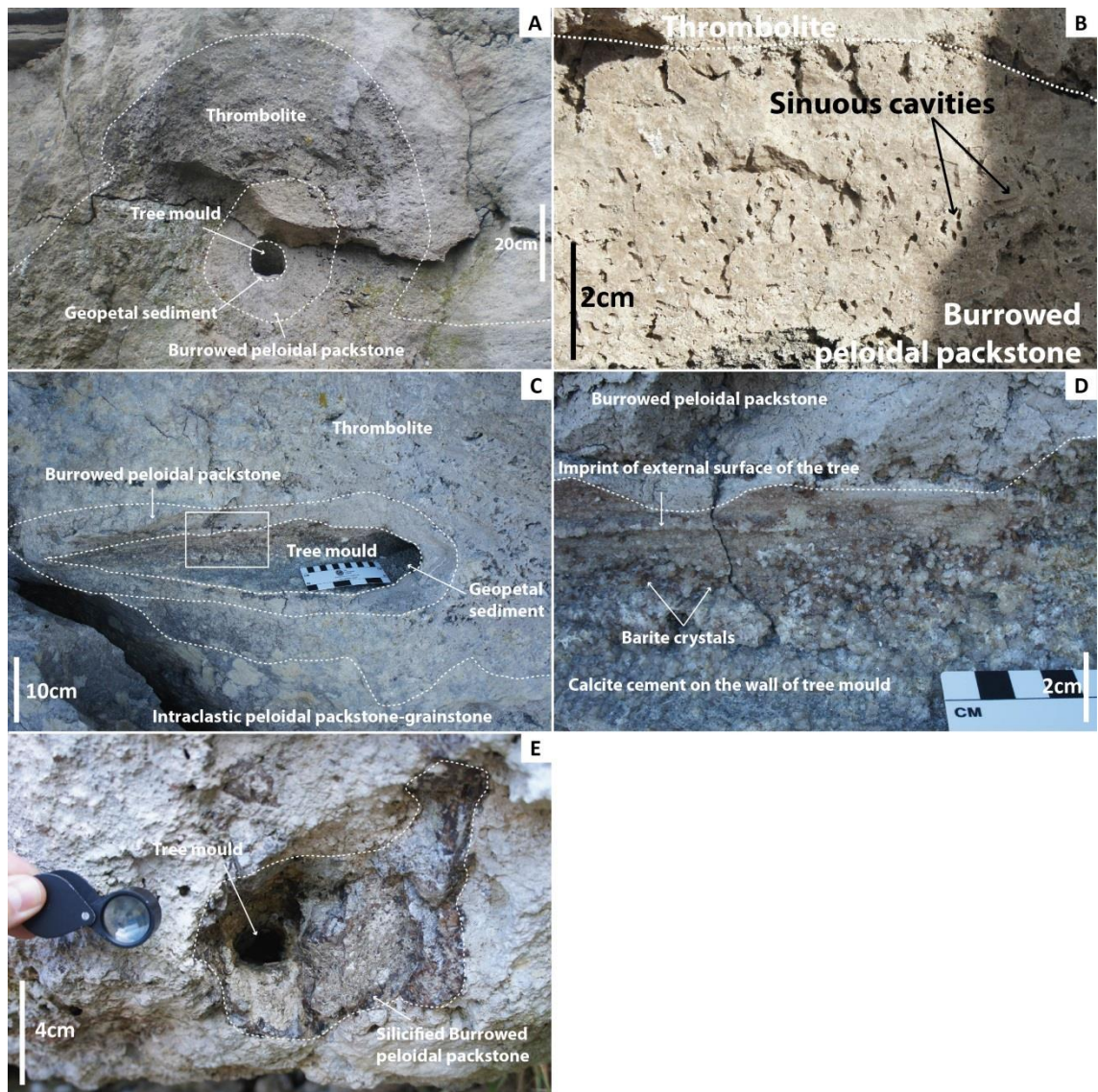
Following the Burne and Moore (1987) and Riding (1991) classifications laminated macrofabrics together with trapping and binding process are typical features of stromatolites. Stromatolites are very well documented all over the world both in the fossil record (Fig. 4.12C; Kalkowsky, 1908; Vologdin, 1962; Hofmann, 1969, 1973, 1977, 2000; Walter, 1976; Grotzinger, 1989; Grotzinger and Knoll, 1999; Awramik *et al.*, 2000) and in modern environments (Fig. 4.12D; Browne *et al.*, 2000, Jahnert and Collins, 2011, 2012; Baskin *et al.*, 2012; Bosak *et al.*, 2013; Della Porta, 2015).

The peloidal micrograinstone with some ostracods indicates that these stromatolites most likely developed into rather quiet marginal lacustrine environment.

### **2.3. Burrowed peloidal packstone sub-facies**

#### **2.3.1. Description**

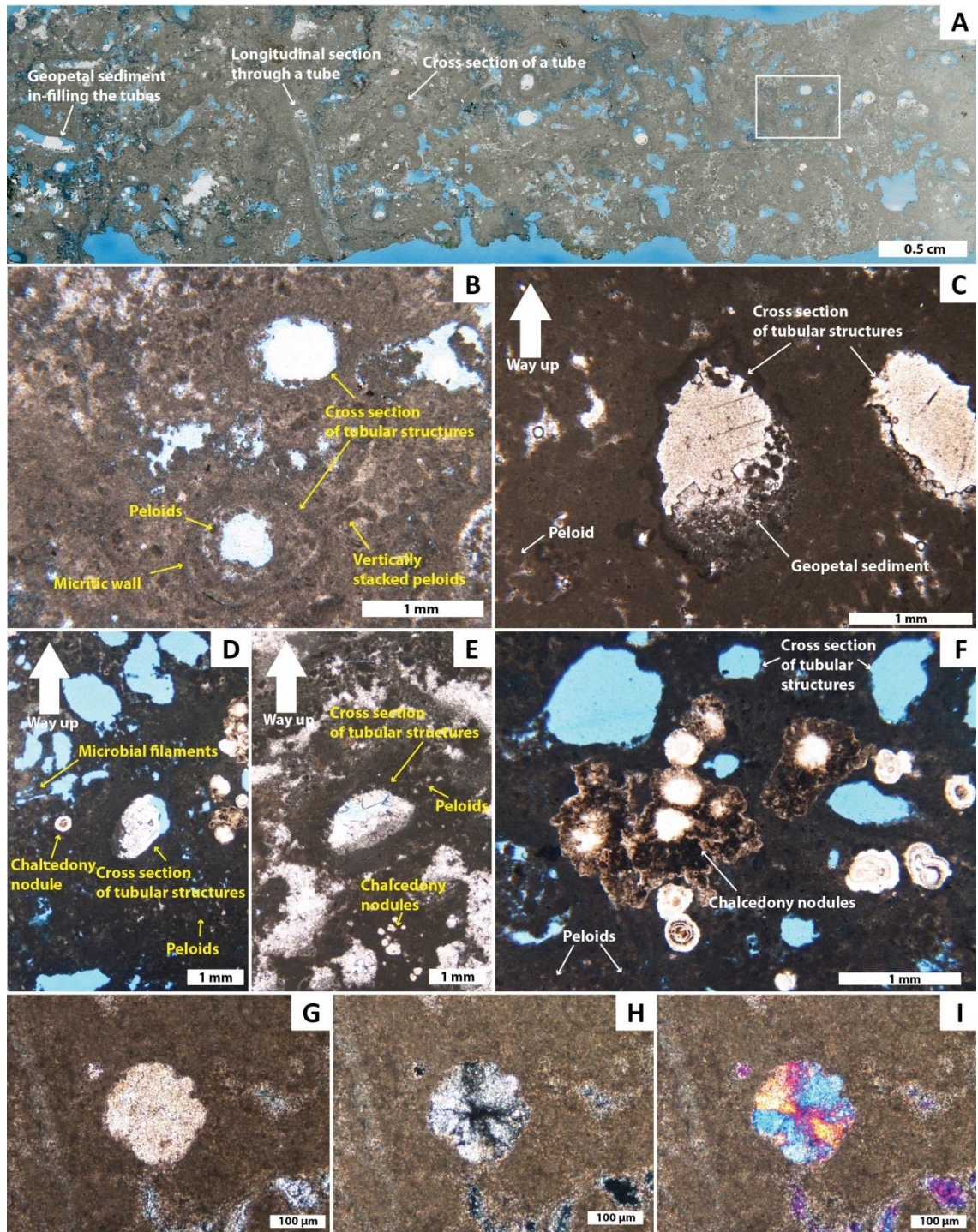
This sub-facies is found only in the Hard Cap and Soft Cap beds and associated with trees. It forms isopachous sub-circular casing or collar around trees and varies in thickness between 2 and 15 cm (Fig. 4.13C). When this sub-facies is found on a plan-view horizontally around fallen trees or vertically around tree stumps (as for the Soft Cap bed) its length varies between 50 cm and 3 m. The inner surface of this casing preserves moulds of the longitudinally ribbed external surface of the trees (Fig. 4.13). These will be referred as tree moulds in this thesis. Within these tree moulds are commonly found geopetal sediments overlain by calcite cements (Fig. 4.13) and only on few locations on the Isle of Portland barite macro-crystals are also found (Fig. 4.13) as described in the previous section. In very rare locations (*i.e.* Chalbury disused quarry, Appendix 3) this sub-facies is silicified along with the adjacent tree wood (Fig. 4.13). It appears with grey to beige colours at outcrop and white to beige when freshly broken. The casing is composed of a complex sinuous and irregular mm-scale tubular network within a fine peloidal packstone texture (Fig. 4.13B). The tubular structures can be orientated radially away from the trees (Fig. 4.13B) or do not show any preferential orientation (sinuous network).



**Figure 4.13** Burrowed peloidal packstone macrofacies. A – Occurrence of the burrowed peloidal packstone sub-facies around tree moulds and overlain by the thrombolite sub-facies (Hard Cap, God Nore, Isle of Portland). B – Burrows as seen in the field around tree moulds (Soft Cap, Fossil Forest, 50°36'58.37"N; 2°14'23.09"W). C – Mound from God Nore with location of Thrombolite and Burrowed peloidal packstone macrofacies. Note the Burrowed peloidal packstone all around the tree mould (Hard Cap, God Nore, Isle of Portland). D – Close-up view on the Burrowed peloidal packstone sub-facies from the box in C. E – Partly silicified Burrowed peloidal packstone sub-facies around a branch mould (Hard Cap, Chalbury).



At the microscale the matrix is made of mudstone to wackestone with some peloids (Fig. 4.14B-F) and non-luminescent under CL as described previously. Chalcedony spherules are commonly found in the micritic matrix (Fig. 4.14D-I) and are similar to the chalcedony found in the Thrombolite sub-facies. They are yellow to brown in PPL with a first order cross extinction in XPL and with second order extinction in the NE and SW quadrants and first order in the NW and SE quadrants in XPL with gypsum plate (Fig. 4.14G-I). The tubular structures commonly show micritic laminated wall between 50 and 200  $\mu\text{m}$  wide (Fig. 4.14A-F) and stacked peloids about 30  $\mu\text{m}$  in diameter (Fig. 4.14B-F). Those tubular structures are sub-circular to oval in cross-section (Fig. 4.14B-F) and vary between 0.5 to 1 mm in diameter. Note that the walls and stacked peloids are not always present (Fig. 4.14C, F). The tubular structures are often filled in with geopetal sediments at the bottom overgrown by sparry calcite cements (Fig. 4.14C-E) that have the same luminescence under CL as described previously. The geopetal sediments show three different orientations: they either lie at the bottom of the tubular structures (Fig. 4.14C), or only on one side with a 90° angle from the present vertical (Fig. 4.14D), or with a 30 to 45° angle from the present vertical (Fig. 4.14E). The tubes are rarely completely filled in and intragranular porosity (tubular moulds) remains. Rarely microbial filaments (10 to 10  $\mu\text{m}$  wide and up to 500  $\mu\text{m}$  long, Fig. 4.14D) and vertically stacked peloids are observed (Fig. 4.14B). The other types of porosity identifiable are intergranular and vuggy (Fig. 4.14).



**Figure 4.14** Burrowed peloidal packstone microfacies in the Hard Cap. A – Thin section scan illustrating the complex network, white box locates B (BQ6, Broadcroft Quarry, Isle of Portland). B – Peloidal packstone with cross sections of tubular structures in PPL (BQ6, Broadcroft Quarry, Isle of Portland). C – Geopetal sediment within a tubular structure, sediment darker at the bottom overgrown by calcite cement in PPL (CQ3, Coombefield Quarry, Isle of Portland). D – Geopetal sediment within a tubular structure with a 90° angle from present day horizontal in PPL (sample from O’Beirne, 2011; E251107, God Nore, Isle of Portland). E – Geopetal sediment within a tubular structure with a 45° angle from present day horizontal in PPL (TQ6A, Tout Quarry, Isle of Portland). F – Chalcedony spherules developing in the micritic matrix in PPL (sample from O’Beirne, 2011; E251107, God Nore, Isle of Portland). G – Detail of a slow-length chalcedony spherule in PPL (PB9, Portland Bill, Isle of Portland). H – Same as G in XPL showing first order cross extinction. I – Same as G and H in XPL with gypsum plate showing second order extinction in NE and SW quadrants and first order in NW and SE quadrants.

### 2.3.2. Interpretation

The tubular structures network is interpreted to be the result of burrows, borings or rhizoliths and which involves organisms. Polychaetes, lamellibranchs, insect larvae, aquatic plant roots or rooting portion of algal thalli can create such a complex network for habitat, shelter or as a support to grow. They can develop into unconsolidated sediments (burrows, rhizoliths) or rocks (borings, rhizoliths). The tubular structures encountered here are not simple straight tubes but are rather very sinuous (Fig. 4.14A) which discard lamellibranch burrows and rhizoliths that are known to create straight walled tubes aligned to each other (Klappa, 1980; Ekdale *et al.*, 1984; Bromley, 1996; Košir, 2004; Hasiotis, 2006; Alonso-Zarza and Wright, 2010; Knaust and Bromley, 2012) and caddisfly larvae cases that are known to create vertical and stratified tubes (Leggitt and Loewen, 2002; Paik, 2004; Dashtgard and Gingras, 2012). Concentric laminations inside the tubes and on pseudo-circular walls with micritic laminations and stacked peloids (Fig.4.14C) show that the organism responsible constructed micritic lined walls, possibly to avoid collapse of the burrow network.

Insect larvae are common in lacustrine sediments and found burrowing soft sediment, and they create tubes by accreting grains they can find close by. The tubes are constructed with micritic laminations that consolidate the wall (Leggitt and Loewen, 2002; Paik, 2004). Such tubes can be partially inside the substrate and partially outside. In ancient (Green River Formation, Eocene, Utah, USA) or modern environments, caddisfly larvae are known to burrow into sediment along lacustrine shores (Dashtgard and Gingras, 2012), and their oldest occurrence is dated from the Triassic (Howell *et al.*, 1998; Grimaldi and Engel, 2005). However caddisfly larvae are unlikely to be at the origin of this sub-facies because the tubes they create form tiers of stacked tubes perpendicular to the tier and more or less parallel with each other (Leggitt and Loewen, 2002) and are usually bigger (between 3 and 5 mm) than those of the Purbecks.

Polychaetes live in soft sediment where they can find shelter and habitat. They are found only in the oxygenated environments (Cohen, 1982; Kraus and Hasiotis, 2006) and the shape on the burrow is commonly related to water depth (Seilacher, 2007; Knaust and Bromley, 2012; Prothero, 2013): random, very tortuous and deep in shallow areas while straight and shallow in deep areas (Dashtgard and Gingras, 2012; Knaust and Bromley, 2012). Polychaetes can either create layered calcitic walls or not to their burrows (Ekdale *et al.*, 1984; Bromley, 1996; Knaust and Bromley, 2012).

Bosence (1987) interpreted these burrows to be very similar to modern-day chironomid larvae burrows. Such larvae like microbe-rich substrates, including calcareous tufas, and create tubes less than 3 mm in diameter in soft substrates (Scott *et al.*, 2009). The tubes are vertical U-shaped and Y-shaped when the substrate is more than 10 mm thick and horizontal when less than 10 mm thick (McLachlan and Cantrell, 1976; Uchman and Álvaro, 2000; Gingras *et al.*, 2007; Scott *et al.*, 2009). The larvae create their tubes gathering debris from the aperture and consolidate them with salivary secretion (Brennan and McLachlan, 1979; Scott *et al.*, 2009). Apart from the size, the burrows found here are rather different than the ones created by modern day chironomid larvae and are not thought to be the organisms that created the burrows of this sub-facies.

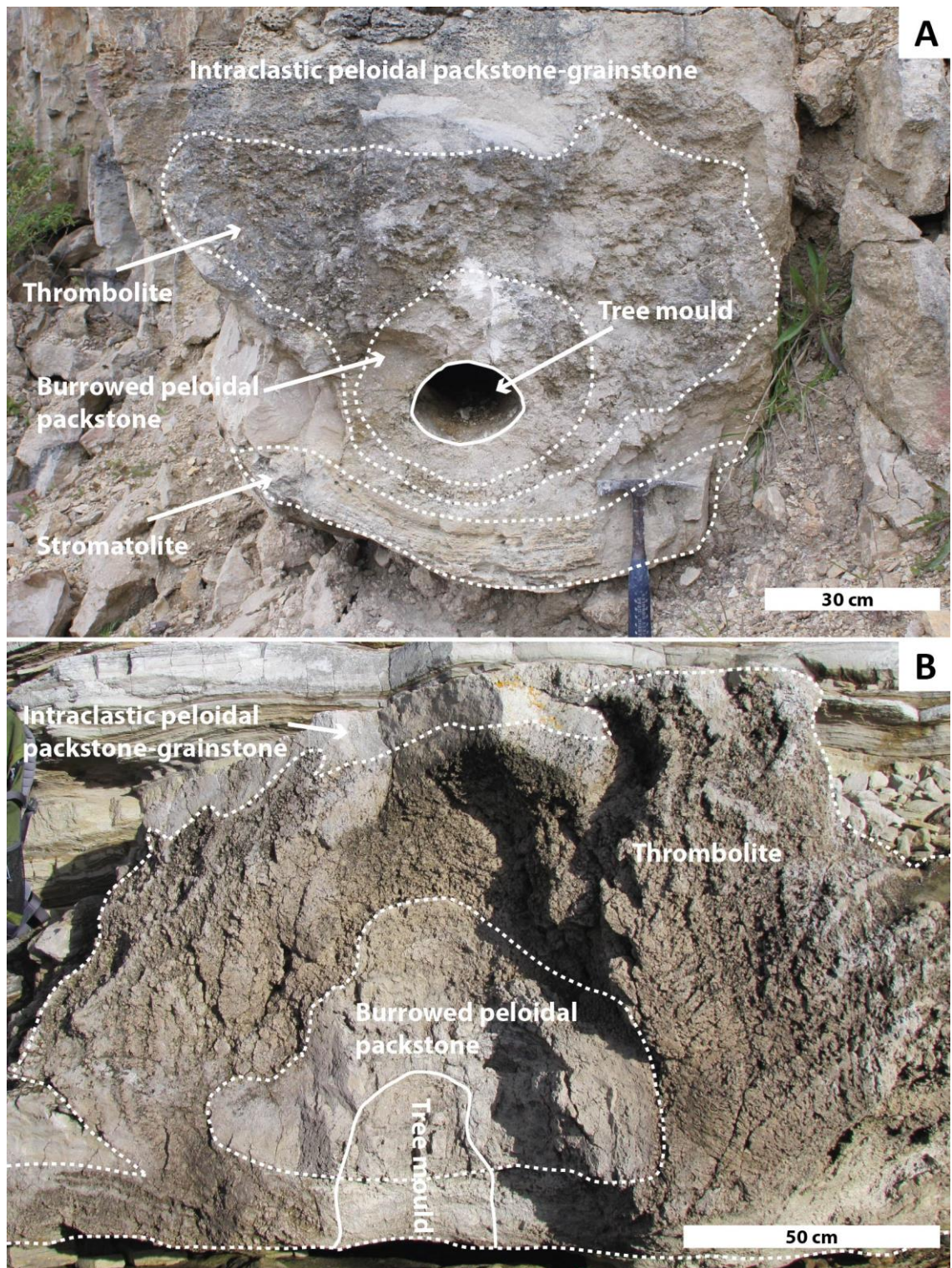
Only based on petrographic analysis and without any preserved body fossils the possible candidates for the originators of these burrows are either polychaetes or insect larvae.

This burrowed peloidal packstone sub-facies is always found prior to the growth of the thrombolite facies (Figs. 4.13A-C and 4.15), either around tree trunks, branches and stumps or at the bottom of the corresponding bed. The peloidal packstone texture indicates a rather low energy, possibly in a protected area. Together all the aspects of this sub-facies indicates a brackish water condition in a shallow marginal lacustrine environment. The fact that it is found surround tree branches, trunks and stumps forming a more or less isopachous casing around them with occasional vertically stacked peloids and microbial filaments suggest a microbial mediation to bind peloidal sediments and preserve the casing around trees in a vertical position. This is confirmed with the identification in some locations of the deposition of the geopetal sediments in the burrows with 90° and 30° to 45° angles (Fig. 4.14C-E). The geopetal sediments found with a 90° angle with the present day horizontal indicates that this facies was originally orientated 90° from its present day orientation. Instead of being in current sub-horizontal position, it was originally in a vertical position around the upright tree trunks, branches or stumps. Concerning the 30° to 45° angle geopetal sediments with the present day horizontal, this can indicate that the trees fell but did not reach the sub-horizontal position, only an angle between 30° and 45°. Later the tree trunks and/branches together with the burrowed peloidal packstone casing fell as indicated by the geopetal sediment deposited at the bottom of some tubes at the present day vertical. This is also documented by Bosence (1987) who identified in a sample from the Isle of Portland two geopetal sediments at right angle in the same facies that he labelled as a "*Burrowed thrombolite*" (refer to Chapter 2). He showed that the first geopetal sediments in the inner part (*i.e.* close to the tree) are at a right angle with the present day horizontal that shows that the trees were sub-vertical during the

deposition. The second geopetal sediments found in the outer part (*i.e.* close to the external border) are concordant with the present day vertical that shows that the trees fell in a sub-horizontal position prior the deposition of the second geopetal sediments. In this study the two orientations of the geopetal sediments were not constrained to a specific location relating to the trees but disseminated everywhere, however they are not observed to overlie each other.

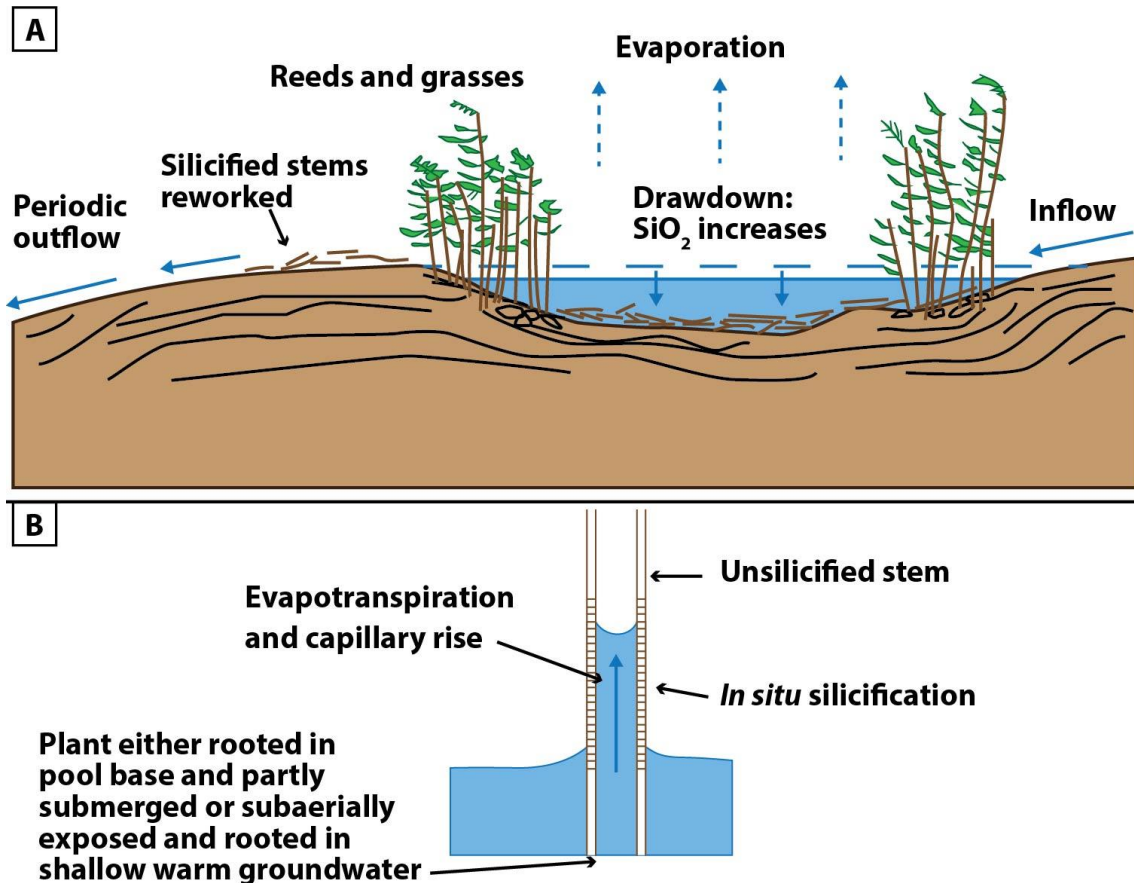
#### **2.4. Formation of the microbial mounds**

The previous sections detailed each sub-facies of the Microbialite facies and showed that they form microbial mounds around tree trunks, branches and/or stumps. These mounds are composed of the Stromatolite sub-facies found locally and always at the base of the mounds (Fig. 4.15A); the Burrowed peloidal packstone sub-facies that forms a more or less isopachous casing around the tree remains (see above, Fig. 4.15); and the Thrombolite sub-facies that forms an anisopachous coating around the Burrowed peloidal packstone sub-facies thicker on the upper part than on the lower part of the tree remains (Fig. 4.15). These mounds are surrounded by the Intraclastic peloidal packstone-grainstone facies detailed in the next section (refer to Chapter 5 for description of mound morphologies and relationship between the microbial mounds and associated facies). Palaeoenvironments with integration of palaeocurrents and water level estimation will be presented in Chapters 5 and 6.



**Figure 4.15** Microbial mounds. A – Developed around a fallen tree or a tree branch (Hard Cap, Broadcroft Quarry, Isle of Portland). B – Developed around a tree stump *in situ* (Soft Cap, Fossil Forest, picture courtesy of Estanislao Kozlowski).

Silicified tree remains can be found in the Hard Cap and Soft Cap and that were rooted in the Lower Dirt Bed and the Great Dirt Bed. Francis (1982, 1983) described and identified the trees to be ancient cypress trees (*Protocupressinoxylon purbeckensis*) illustrated in figure 4.17A (refer to Chapter 2). The process that led to the silicification of wood appears to be very complex and a lot of uncertainties still remain. Leo and Barghoorn (1976) showed that wood acts as an active template for silica precipitation and that silicification might occur through the permineralisation process via infilling and impregnation. Similarly Renaut *et al.* (2002) showed that in small ponds downstream the Ngakoingora Ridge (Turkana Basin, Kenya) reeds are found silicified only on their lower part (Fig. 4.16B). In this setting the silica comes from the hot-spring ridge and feeds ponds where reeds and grasses grow (Fig. 4.16A; Renaut *et al.*, 2002). The reeds and grasses are described as acting as a "magnet" for the silica and due to evapotranspiration and/or capillarity, silica-rich water rises up the stems and silicifies the plants (Fig. 4.16B; Renaut *et al.*, 2002). Only the lower part was silicified due to a lack of capillary forces and the remaining (unsilicified) upper part have either decayed or broken off and fallen into the ponds (and probably later silicified; Renaut *et al.*, 2002). This process was also suggested by Francis (1982) to be responsible for the silicification of the Purbeck trees in the Lower and Great Dirt Beds. She showed that the silicification occurred after drowning of the forests, soon after the death of the trees and before the decay of the wood in an anaerobic environment due to the very good preservation of the wood cells. She identified tree remains that are made of quartzine (length-slow chalcedony) that was most likely originally deposited as amorphous quartz which turned into chalcedony after a long period of time ( $10^7$  to  $10^8$  years according to Siever, 1962). Francis (1982) demonstrated that following Folk and Pittman's (1971) study quartzine indicates evaporative conditions and is an indicator of semi-arid alkaline environments. The source of the silica was most likely biogenic from planktonic organisms (such as diatoms) which are very common in modern day lacustrine environments (Francis, 1982). According to Francis (1982) these dissolved organisms would have formed a molecular silicic acid ( $H_4SiO_4$ ) because it is the only form of soluble silica found in nature (Siever, 1962) and is the only agent able to penetrate fine wood cells (due to its hygroscopic particles). Francis (1982) found only one specimen with length-fast chalcedony in a tree from the Lower Dirt Bed at Chalbury Camp (north of Weymouth) and interpreted this silica type to reflect less alkaline conditions than the length-slow chalcedony.

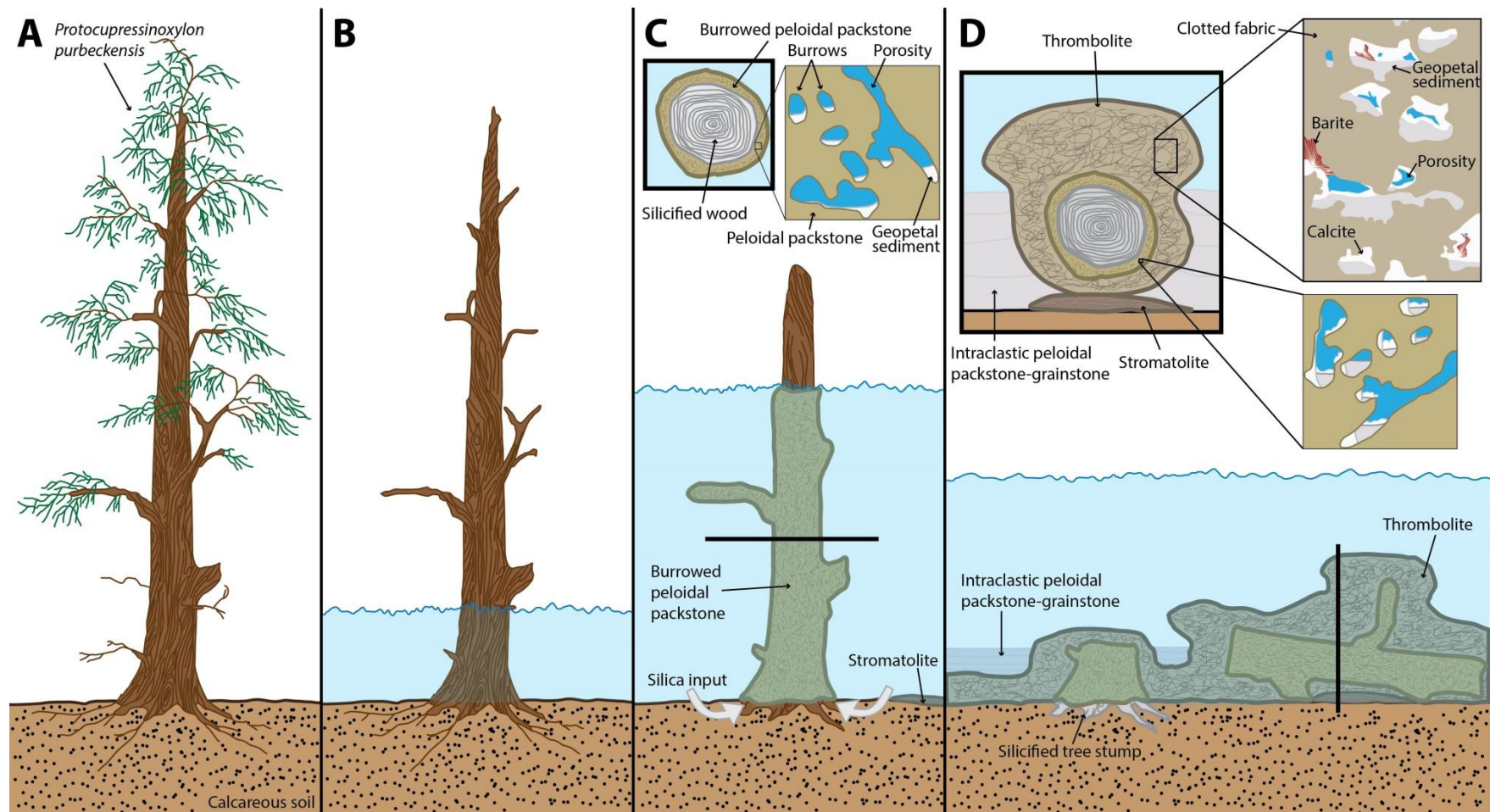


**Figure 4.16** Schematic model for the origin of the silicified plants on the western marginal slope of the Ngakoringora Ridge (Turkana Basin, Kenya, redrawn from Renault *et al.*, 2002). A – Terrace pool showing the inferred distribution of the plants and plant remains. B – Silicification process by evapotranspiration and/or capillarity of a reed stem. Note that the plants can be submerged and rooted in the pool base or exposed and rooted in warm groundwater.

Figure 4.17 illustrates the sequence of possible events for the origin of the formation of the microbial mounds and the silicification of the trees (refer to Chapter 6 for interpretation of palaeoenvironments). The conifer forest was rooted on the Lower and Great Dirt Beds (Fig. 4.17A). Following the transgression of the brackish water lake, the soils were inundated, the trees waterlogged and killed (Fig. 4.17B, also proposed by West, 1975 and Francis, 1982). After the lake level reached a certain height the Burrowed peloidal packstone sub-facies accumulated all around the trees being stabilised by polychaetes or insect larvae burrowing (Fig. 4.17B). Contemporaneously with the deposition of the Burrowed peloidal packstone sub-facies the silicification of the wood occurred before the decay of the wood material (Fig. 4.17B). The silica was most likely of biogenic origin (as interpreted by Francis, 1982) from the dissolution of planktonic organisms that were living in the brackish water lake. This dissolved silica was remobilised as a molecular silicic acid (Siever, 1962; Francis, 1982) and



attracted by the wood material as per the Renaut *et al.* (2002) capillarity model (Fig. 4.17B) to silicify *in situ* trees soon after their death (4.17C). In the meantime geopetal sediments were deposited in the tubular cavities of the Burrowed peloidal packstone sub-facies (Fig. 4.17C) and locally directly on the lake floor the Stromatolite sub-facies (Fig. 4.17C). Francis (1982) measured preferential orientations of the tree holes in the Hard Cap and Soft Cap (refer to Chapter 2) and interpreted northerly blowing winds due to their mainly north-south orientations. Relatively strong winds and/or wind-driven currents could have caused the broken-off upper part of the trees to fall on the lake floor (Fig. 4.17D). Due to the Burrowed peloidal packstone casing around the trees the broken-off portions are thought to be heavier than wood and avoided long distance drifts. These broken-off trees were then deposited not too far from their stumps (Fig. 4.17D). After their deposition the Thrombolite sub-facies accumulated and as the cyanobacteria are photosynthetic organisms, they developed mainly upwards (Fig. 4.17D). This explains the anisopachous morphology of the Thrombolite sub-facies around the trees (Fig. 4.17D). In the meantime a second generation of geopetal sediments were deposited in the cavities of the Thrombolite sub-facies and in the tubes of the Burrowed peloidal packstone sub-facies (Fig. 4.17D). Later during the burial the two calcite spar cements were deposited followed by the barite crystals (Fig. 4.17D). Bosence (1987) proposed a similar interpretation for the formation of the microbial mounds from the Hard Cap bed although he called them “tufas”.



**Figure 4.17** Reconstruction of events at the origin of the formation of the microbial mounds. Not to scale. A – *Protocupressinoxylon purbeckensis* tree (after Francis, 1982). B – Transgression of brackish water lake and death of the trees. Note that the silica input may be from lake or ground waters (as per Renault *et al.*, 2002 model) C – Deposition of the Burrowed peloidal packstone and Stromatolites sub-facies. Black line locates the cross-section on the top. D – *In situ* stump with broken off tree trunk and branch and deposition of Thrombolite sub-facies. Black line locates the cross section on top.

### 3. Intraclastic peloidal packstone-grainstone facies

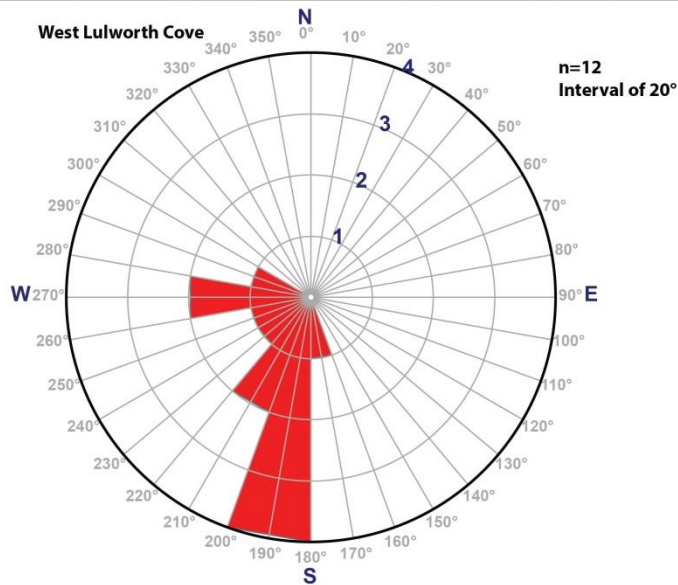
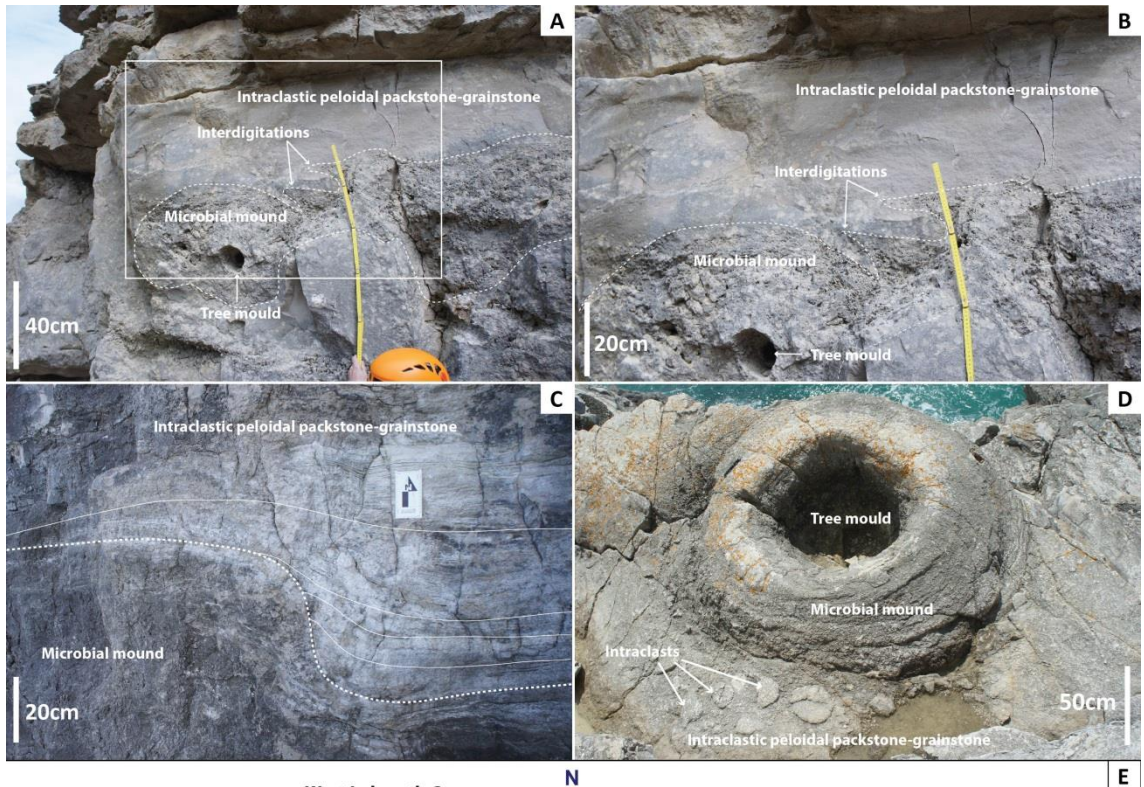
#### 3.1. Description

This facies is found only in the Skull Cap, Hard Cap and Soft Cap beds and throughout the studied area. It is always associated with microbial mounds (described in the previous section) surrounding and interdigitating with them (Fig. 4.18). The thickness of this facies varies very rapidly from 50 cm to up to 3 m because of its infilling of the irregular depositional topography associated with the microbial mounds (Figs. 4.17D and 4.18C; refer to Chapter 5 for further description of this relationship).

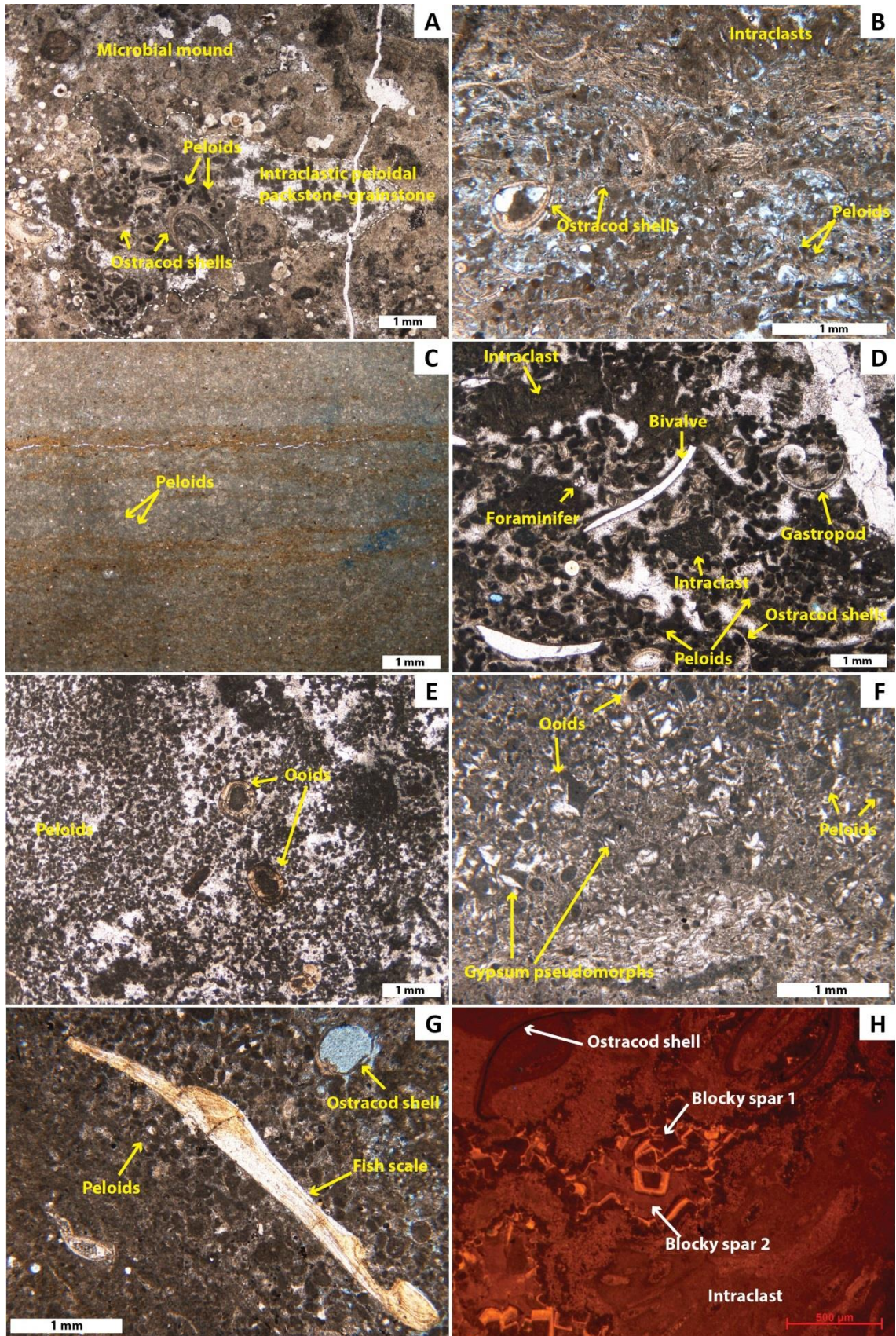
At the macroscale few planar laminations are identified in this sub-facies but commonly there are no sedimentary structures. The texture can be either coarse grainstone (*i.e.* in Freshwater Bay) or fine grainstone sometimes packstone. Sub-rounded intraclasts between 5 mm and 20 cm in diameter are found in the vicinity to the mounds resulting in coarser textured rudstones (Fig. 4.18D). The bases of the beds are scoured when deposited directly above paleosols and in few cases the bed bases are made of coarser material. This facies appears white to beige at the outcrop and when broken. Only at West Lulworth Cove at the top of the Hard Cap some cross-lamination were identified. Twelve orientation measurements were done and revealed one main direction at 190° and two secondary at 210° and 290° (Fig. 4.18E).

At microscale the texture varies between packstones and grainstones sometimes more bioclastic (Fig. 4.19B) sometimes more peloidal (Fig. 4.19C). Peloids are the most abundant grains in this facies. They are micritic, angular to sub-angular (Fig. 4.19), their diameter varies between 50 and 200 µm, they are well sorted (Fig. 4.19), and are non-luminescent under CL (Fig. 4.19H). Ostracod shells together with intraclasts are the second most abundant grains in this facies. They are either found scattered in the matrix or reworked into ostracod-rich horizons (about 0.5 cm thick, Fig. 4.19A-E). The thicknesses of the ostracod shells vary between 100 to 300 µm (Fig. 4.19) and they appear yellow to orange in PPL (Fig. 4.19) and dull to non-luminescent under CL (Fig. 4.19H). Molluscs are also common in this facies with gastropods (Fig. 4.19D) and bivalves (Fig. 4.19D, E) and are also non-luminescent under CL. Gastropod shell diameters vary between 1 and 1.5 mm with micritic envelopes (Fig. 4.19D). Bivalves are rare, usually replaced by calcite with a micritic envelope and are often broken up between 2 and 4 mm long and 200 to 500 µm thick (Fig. 4.19E). Lozenge-shaped grains with a micritic outer surface and filled with spar cement interpreted to be gypsum pseudomorphs (Fig. 4.19F, 4.21), are present only in the Hard and Soft Cap beds. These are mainly from

Lulworth area eastwards and at only two locations in the Isle of Portland: King Barrow Quarries and only in the Soft Cap at God Nore. Coated grains (Figs. 4.19E, F and 4.22) are found only in the Hard Cap at five locations on the Isle of Portland at Coombefield and Broadcroft Quarries; and in Lulworth area at West Lulworth Cove, Mupe Bay and Worbarrow Tout. These coated grains are made of a core surrounded by a calcitic coating and interpreted to be ooids (Fig. 4.19E, F and 4.22). The core is usually made of an angular micritic grain with a clotted structure between 300 and 500  $\mu\text{m}$  in diameter (Figs. 4.19E, F and 4.21). In the Soft Cap at Worbarrow Tout and in the Hard Cap at Mupe Bay the cores of the coated grains are made of the gypsum pseudomorphs with a micritic outer ring coated grains between 100 and 200  $\mu\text{m}$  long (Fig. 4.21E, F). In addition to these types of cores in the Hard Cap at West Lulworth Cove the cores can be made of one or two coated grains between 100 and 200  $\mu\text{m}$  in diameter each. The coating can be made of numerous concentric laminae with radial fabric and micritic laminae of yellow to brown calcite crystals between 30 and 100  $\mu\text{m}$  thick (Figs. 4.19E and 4.22C); or only one or two concentric laminae yellow calcite crystals about 30  $\mu\text{m}$  thick (Figs. 4.19F and 4.22A). Micritic intraclasts are common, with a clotted macrofabric and/or microbial filaments and vary between 100  $\mu\text{m}$  and 2 mm in diameter (Fig. 4.19D, H). Rare rather elongated yellow grain in PPL and with a rolling extinction in XPL, and with internal concentric laminated structures are locally found (Fig. 4.19G). Very rare foraminifers are found in this facies and are made of several small chambers (about 10  $\mu\text{m}$  each chamber) with a micritic envelope and are about 100  $\mu\text{m}$  in diameter (Fig. 4.19D). The porosity types are intergranular to mouldic and both primary and secondary pores are very commonly filled with a mosaic to blocky spar cement with the same zoned luminescence described in the Thrombolite sub-facies (Fig. 4.19H).



**Figure 4.18** Intraclastic peloidal packstone-grainstone macrofacies. A – Interdigitation of a microbial mound and the Intraclastic peloidal packstone-grainstone facies without sedimentary structures, white box locates B, dashed line outlines the microbial mound (Hard Cap, Tout Quarry, Isle of Portland). B – Interdigitation of microbial mound and Intraclastic peloidal packstone-grainstone facies (close-up view from A), dashed line outlines the microbial mound. C – Onlaps of Intraclastic peloidal packstone-grainstone with planar laminations on microbial mound, dashed line outlines microbial mound, plain lines outline planar laminations (Hard Cap, Fossil Forest). E – Orientation and direction measurements of the cross-laminations at West Lulworth Cove with 12 measurements.



**Figure 4.19** Intraclastic peloidal packstone-grainstone microfacies. A – Intraclastic peloidal grainstone within the Microbialite facies with ostracods and peloids in PPL (CQ2, Skull Cap, Coombefield Quarry, Isle of Portland). B – Intraclastic peloidal packstone-grainstone with ostracods, peloids, and intraclasts, note the ostracod rich horizon on top in PPL (PQ3, Skull Cap, Portesham Quarry). C –

Intraclastic peloidal packstone with irregular shapes of peloids and planar laminations in PPL (WT2, Hard Cap, Worbarrow Tout). D – Intraclastic peloidal grainstone with foraminifer, molluscs (gastropods and bivalves), intraclasts, peloids and ostracods in PPL (WT3, Hard Cap, Worbarrow Tout). E – Fine intraclastic peloidal grainstone with coated grains and peloids in PPL (WLC5, Hard Cap, West Lulworth Cove). F – Peloidal packstone with peloids, ooids and gypsum pseudomorphs in calcite (lozenge-shaped) (MB5A, Hard Cap, Mupe Bay). G – Peloidal packstone with a fish scale (yellow laminated grain), ostracods and peloids (PQ7, Soft Cap, Portesham Quarry). H – CL image of a peloidal grainstone with ostracods and microbial intraclasts; showing the luminescence of the micritic grains and the blocky spar cement (CQ1, Skull Cap, Coombefield Quarry, Isle of Portland).

## 3.2. Interpretation

### 3.2.1. Peloids

The term peloid was introduced by McKee and Gutschick in 1969 to describe cryptocrystalline carbonate grains similar to pellets and does not imply a specific origin. Flügel (1982) described peloids as “*well-rounded, non-laminated, structureless micritic particles of various origin*”. Peloids are a very common and important constituent of carbonate deposits and are described by lots of authors in both ancient and modern and in both marine and non-marine settings (Bathurst, 1971; Flügel, 1982; Tucker and Wright, 1990). Origin of peloids is difficult to determine because of their micritic aspect and the lack of structures within the grains. Their origin can be due to several processes: deposition of faecal pellets; reworked micritic clasts; micritisation of grains; or purely chemical nucleation (Bathurst, 1966; Tucker and Wright, 1990). Faecal pellets are produced by organisms (such as shrimps) and the resulted peloids are rather ovoid ellipsoidal and elongated (long axis 1.5 to 3 times their short diameter; Tucker and Wright, 1990) and usually between 40 and 300 µm in diameter (Bathurst, 1971). Peloids from mud clasts are reworked and rounded intraclasts or lithoclasts from pre-existing micritic substrates (mudstone deposits, Tucker and Wright, 1990 or algal remains, Wolf, 1965). The micritisation of grains can be due to micro-organism borings (algal or fungal) on all types of carbonate grains (mollusc shells, ostracod shells, calcareous algae, etc...) leading to the partial (micritic envelope) or complete (peloid) micritisation of the grains (Bathurst, 1966, 1971, 1975; Tucker and Wright, 1990; Scholle and Ulmer-Scholle, 2003). Peloids from chemical nucleation are actually micron-sized cements of very small calcite crystals around a nucleus (Bathurst, 1971; Macintyre, 1985; Tucker and Wright, 1990).

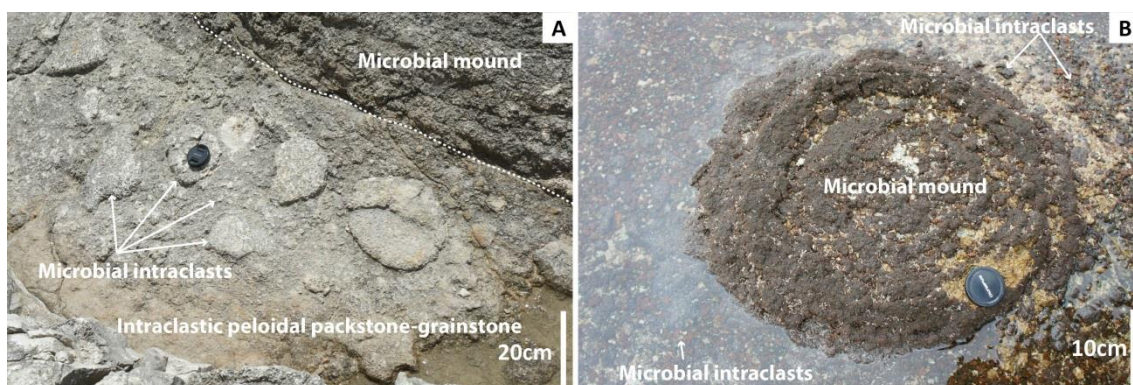
The peloids found in this facies correspond completely to McKee and Gutschick's (1969) definition as they are micritic, structureless, and angular to sub-angular as well as rounded (Fig. 4.19). Their origin can be due to a combination of many of the processes described above, however it is not possible to identify only one. The peloids can be from reworked algal

deposits (the surrounded microbial mounds would be the source), micritised broken-up crustacean and/or mollusc shells (found in great quantity in this facies). Nevertheless the peloids found here are much bigger than those that are usually generated by broken-up shells of ostracods or molluscs; are angular to sub-angular; and the different stages of micritisation of shells from partially to totally micritised were not observed. For these reasons they are thought to be mainly reworked from the surrounded microbial mounds. The micritic structure of these peloids (Fig. 4.19) may be due either to the original matrix they derived from or from the micritisation process (see above). West (1975) in his facies A (refer to Chapter 2) found pelletoids that are defined as “*small rounded allochems of microcrystalline carbonate*” but did not provide possible origins. Brown (1963) described pellets of the same facies from the Lower Purbeck of Dorset as anhydrite replacements because of straight outlines, rectangular re-entrants and calcite spar filling. Such pellets were never found in this study and such an origin appears unlikely.

### **3.2.2. Intraclasts**

The intraclasts are made of a clotted macrofabric (Fig. 4.19D) that indicates that they are microbial intraclasts and therefore derived from the adjacent mounds (Fig. 4.20). This derivation may be due to different processes: storms may break up microbial mounds into intraclasts that are redeposited in the surrounding areas; high energy system (wind-driven currents) that can break up unconsolidated microbial mounds; or via bioerosion (Tucker and Wright, 1990). In this study the intraclasts are rather big (between few millimetres and up to 20 cm) and there is no evidence of bioerosion (both at macro- and micro-scale). High energy system (storms or currents) is most likely to have created those intraclasts. Similar microbial intraclasts are found both in ancient (Green River Formation, Uinta Basin, Utah, USA, Chidsey *et al.*, 2015) and modern day lakes (Laguna Bacalar, Yucatan Peninsula, refer to Appendix 1; Gischler *et al.*, 2008, 2011; Great Salt Lake, Utah, USA; Eardley, 1938; Eby and Chidsey, 2013; Chidsey *et al.*, 2015).





**Figure 4.20** Intraclasts of the Intraclastic peloidal packstone-grainstone facies. A – Centimetre-sized microbial intraclasts next a microbial mound, dashed line outlines the microbial mound (Soft Cap, Fossil Forest). B – Decimetre-scale microbial intraclasts (orange to brown) surrounding a microbial mound (SW of Antelope Island, Great Salt Lake, Utah, USA).

### 3.2.3. Ostracods

The ostracods from the lower part of the Mupe Member of Dorset (Fig. 4.19) are reported to correspond to the lower part of the *Cypridea dunkeri* ostracod subzone (Strahan, 1898; Barker *et al.*, 1975; Kilenyi and Neale, 1978; Anderson, 1967, 1973, 1985; Horne, 1995, 2002). Although lots of studies described ostracods from the lower part of the Purbeck Limestone Group there is no clear identification of the exact stratigraphic level or location of collection of the samples. Modern day non-marine equivalents of ostracod faunas of the Purbeck Limestone Group of Dorset was demonstrated by Horne (2002, refer to Chapter 2) and the Purbeck ostracods are therefore considered as non-marine species. Anderson's (1985) assemblage 1 (refer to Chapter 2) covers the Skull Cap to Broken Beds. This assemblage is made of 4 faunicycles (refer to Chapter 2). Faunicycle 1 is based on ostracods collected in the Wiltshire (Swindon) and in the Buckinghamshire (Aylesbury) and therefore is not really relevant for this study. Although faunicycles 2 to 4 are partly constructed with ostracods collected from Dorset (White Nothe, Poxwell Quarry and Portesham Quarry) as well as from Wiltshire (Swindon), Buckinghamshire (Aylesbury) and Sussex (Henfield), Anderson did not detail the quantity of ostracods collected from each locations, it is then again difficult to interpret and conclude on the palaeoenvironments and palaeosalinities in a particular location such as Dorset. In general the assemblage 1 defined from between the Hard Cap and the Broken Beds contains the rare occurrence of *Cypridea* sp.. The rarity of this C-phase ostracods and the abundance of S-phase ostracod suggest a brackish water condition for the lower part of the Mupe Member (Anderson and Bazley, 1971; Anderson, 1985). Nevertheless Horne (1995) discussed Anderson's (1985) interpretation and interpreted variations between C- and S-phases as a

change from close to open system rather than a change in the salinity. Barker *et al.* (1975) identified ostracods in the Hard Cap bed and in the equivalent of the Great Dirt Bed at Portesham Quarry. They could identify marine, and brackish water (euhaline and oligohaline) ostracod groups (refer to Chapter 2). Because of a mixture of different salinity tolerant species in all the beds Barker *et al.* (1975) interpreted that the water was brackish and that the marine ostracods were most likely reworked. In a related project conducted at RHUL Dharmarajah (2015) attempted to identify ostracods from three locations on the Isle of Portland. However this study was inconclusive due to the difficulty to extract unbroken carapaces (refer to Chapter 2).

#### **3.2.4. Molluscs**

The mollusc gastropods (Fig. 4.19D) from the lower part of the Mupe Member of Dorset are not very well documented in the literature (Arkell, 1941; Clements, 1973; Radley, 2002). However Arkell (1941) remains the only author to provide a detailed study on gastropods from the Purbeck of Dorset. He described in total four gastropod species and only one brackish to hypersaline water tolerant gastropod species was found in the Caps at Ridgeway (refer to Chapter 2). Radley (2002) described mollusc gastropod assemblages from cherty and conglomeratic marls about 4 m above the base of the Purbeck Limestone Group at Portesham Quarry. These assemblages are made of a mixture of freshwater and marine species and that were most likely deposited during periodic mixing of fresh- and marine waters (Radley, 2002). However Radley (2002) interpreted these species to reflect fresh- to brackish water conditions in a closed lake system. In addition Clements (1973) identified marine species in equivalent unit in Poxwell Quarry (refer to Chapter 2). However, these marine species could be reworked from the underlying Portland Group.

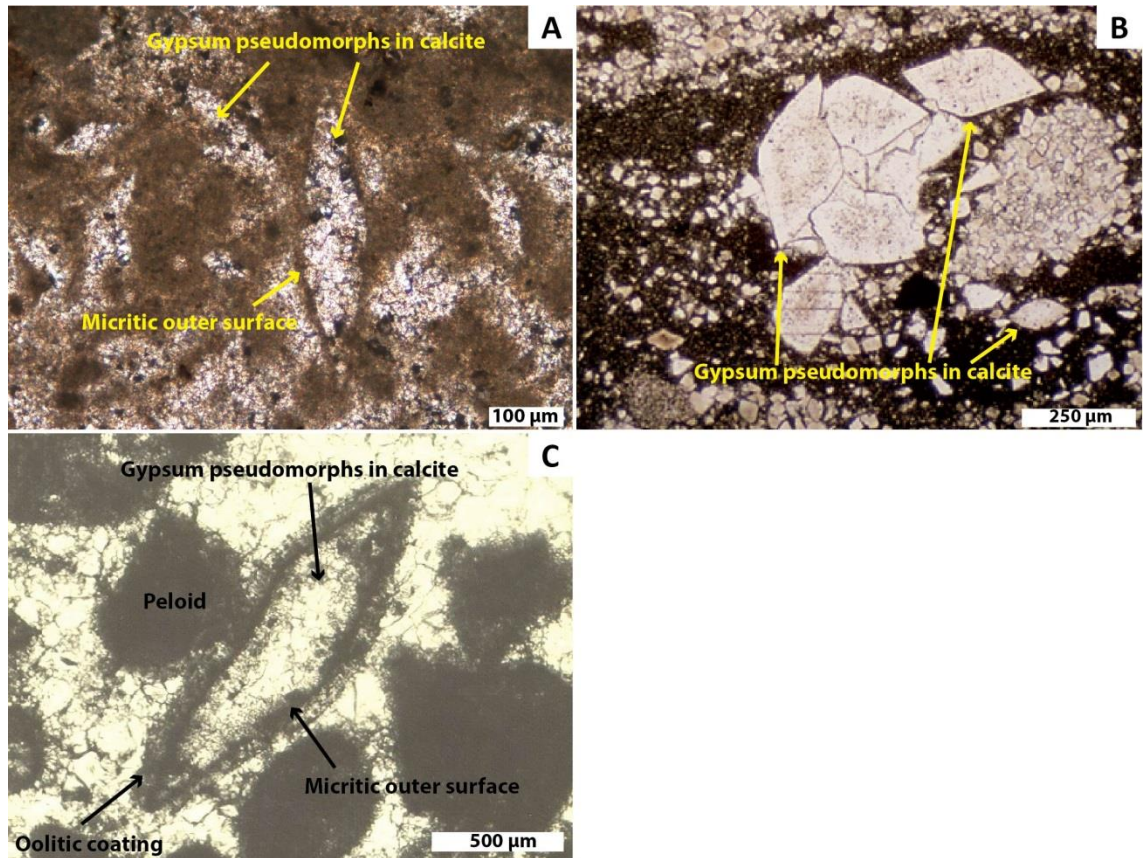
The bivalve molluscs are also very poorly documented in the literature (refer to Chapter 2). West (1975) only cites occurrence of bivalves in his facies A although without any descriptions and Radley (2002) only reports that "*bivalves await documentation*". Strahan (1898) identified freshwater species in the Purbeck Limestone Group but did not indicate in which beds or members they were found. However they were most likely found in higher units (Marly Freshwater Beds onwards) as freshwater bivalves are documented from these beds. The nature and identification of bivalves found in this Intraclastic peloidal packstone-grainstone facies remains unknown.

### 3.2.5. Gypsum pseudomorphs

The micritic lozenge-shaped cavities are interpreted to correspond to pseudomorphs of gypsum crystals (Figs. 4.19F and 4.21), known to be unstable in marine and lower salinity waters and may dissolve away easily soon after their precipitation (Schreiber and Walter, 1992; Scholle and Ulmer-Scholle, 2003; Flügel, 2010). The original gypsum crystals (now replaced by calcite) reflect former hypersaline water conditions (West, 1964, 1975; Schreiber and Walter, 1992; Scholle and Ulmer-Scholle, 2003; Flügel, 2010). An interesting feature of these gypsum pseudomorphs is that they have a micritic rim. This feature has never been published in the literature and it is not clear how these micritic envelopes can form around gypsum crystals or pseudomorphs. A possible origin is that these gypsum crystals were transported and micritised during the transport, however, in such situation the crystals are expected to be rounded while in this facies they are found intact. Another possible origin is that soon after their early replacement by calcite, micro-bores made by endolithic micro-organisms such as algae, cyanobacteria or fungi may be filled with a micritic cement that resulted in the creation of a micritic envelope (as per Bathurst's, 1966 definition). The latter situation is thought to be more likely to form these micritic envelopes given the complete lozenge shapes of the gypsum pseudomorphs.

West (1975) described and detailed similar occasional lenticular replaced gypsum crystals in his facies B in the Cap beds of Dorset (Fig. 4.21C, refer to Chapter 2). He showed similarities of shapes and sizes of the Purbeck lenticular gypsum of Dorset with the modern day Persian Gulf hypersaline lagoons (documented by Shearman, 1966 and Butler, 1969) where lenticular gypsum crystals precipitate in the intertidal zone. West (1975) interpreted the gypsum to precipitate in the intertidal to supratidal zones of tidal flats and during a long regressive phase.

As described earlier, these gypsum pseudomorphs are mainly found in the eastern part of the studied area (from Lulworth eastwards) and are rare on the Isle of Portland. This shows that conditions were more hypersaline to the east and less hypersaline (*i.e.* more brackish?) to the west. The two locations in the Isle of Portland (King Barrow Quarries and God Nore) where gypsum pseudomorphs are might reflect a change in the environment to a more protected or closed area very locally.



**Figure 4.21** Gypsum pseudomorphs of the Intraclastic peloidal packstone-grainstone facies. A – Details of gypsum pseudomorphs, note the outer micritic surface in PPL (SQ9B, Soft Cap, Swanworth Quarry). B – Gypsum pseudomorphs in calcite from the Arroyo Peñasco Group of the Espiritu Santo Formation (Mississippian, Tournaisian), New Mexico in PPL (from Scholle and Ulmer-Scholle, 2003). C – Calcite pseudomorph after syngenetic gypsum lens in PPL (sample from the Soft Cap at Dungy Head, from West, 1964). Note the oolitic coating around the micritic outer surface.

### 3.2.6. Ooids

The coated grains (Fig. 4.19E, F) identified in this facies are made of a nucleus (*i.e.* the core) and a cortex (*i.e.* the coating) that are specific to ooids (Lyell, 1855; Flügel, 1978; Strasser, 1986; Tucker and Wright, 1990). Ooids can be found in marine and non-marine environments. The mineralogy of marine ooids can be predicted according to the mineralogy of the seas through time (Sandberg, 1983; Tucker and Wright, 1990). However the mineralogy of non-marine ooids is more complex and depends on water chemistry, hydrodynamics, palaeoclimate, etc... (Strasser, 1986; Tucker and Wright, 1990). Popp and Wilkinson (1983) suggested that non-marine ooid cortices are in aragonite when formed in hypersaline lakes (also documented by Khale, 1974; Sandberg, 1975 and Halley, 1977) and in calcite when formed in low-salinity lakes (also documented by Wilkinson *et al.*, 1980; Geno and Chafetz,

1982; Richter, 1983; Tucker and Wright, 1990). The cortical microfabric can also indicate depositional processes such as hydrodynamics (Richter, 1983; Tucker and Wright, 1990). Although all types of cortical composition and organisation can be found in all kind of environments, tangential fabrics are commonly found in marine environments while radial fabrics are commonly found in non-marine environments and random fabrics are formed in many depositional settings (Davies *et al.*, 1978; Tucker and Wright, 1990). In addition, ooids with tangential microstructures are typically found in high energy settings and radial microstructures are typically found in low energy settings (Loreau and Purser, 1973; Davies *et al.*, 1978; Richter, 1983; Tucker and Wright, 1990). Rusnak (1960a) and Land *et al.* (1979) specified that tangential cortices are usually formed due to very slow precipitation in strong agitation; radial cortices due to slow precipitation in quiet waters; and micritic cortices due to rapid precipitation in quiet and agitated waters. The hydrodynamic effects on cortical microstructures is documented in ancient deposits (Richter, 1983) in the Cambrian Warrior Formation of Pennsylvania (Heller *et al.*, 1980), in the Devonian of northern Spain (Reijers and Ten Have, 1983), in the Cambrian of Newfoundland (Chow and James, 1987), in the Purbeckian of Switzerland and France (Strasser, 1986); and in modern day in the Great Salt Lake, Utah, USA (Medwedeff and Wilkinson, 1983).

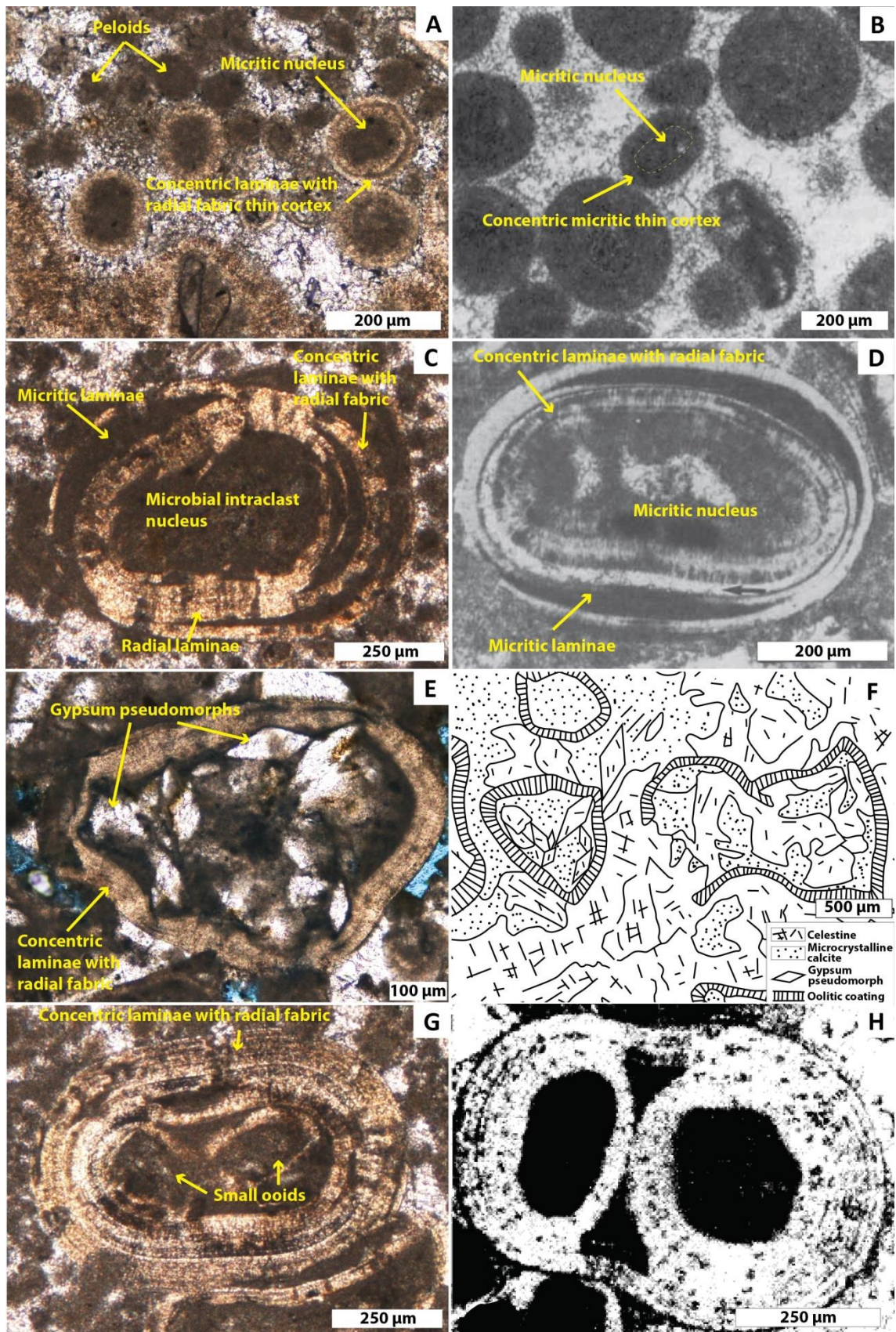
The microfabric of the cortex of the Purbeck ooids is made of radial calcite that suggests a preservation of the original calcitic structure (according to Sorby, 1879 and Walter, 1976). According to Popp and Wilkinson's (1983) proposal (above), the calcitic cortices of the Purbeck ooids might indicate that they were formed in fresh- to brackish water lakes. The ooids deposited in the Cap beds of the Mupe Member are made of two types of cortex microstructures (Fig. 4.22). The first type of cortex is made of one or two concentric laminae considered to be calcite (Fig. 4.22A, E) and was identified in all the locations where ooids were deposited. They are the only type to be found at Coombefield and Broadcroft Quarries (Isle of Portland). This type of ooid cortex is very similar to type 1 ooids defined by Strasser (1986) for the Purbeck of Jura (Fig. 4.22B). Strasser (1986) defined this type of ooids as superficial ooids and interpreted their thin laminae to have formed in quiet-water energy (also documented by Bathurst, 1967). He suggested that these type 1 ooids were deposited in low-energy lagoonal settings associated with cyanobacteria development because of the micritic aspect of the cortices. The second type of cortex found in this study is made of a mixture of two microstructures with radial and micritic with concentric and irregular laminae of calcite (Fig. 4.22C) and was identified at West Lulworth Cove and Worbarrow Tout. The second type of ooid cortex is similar to the Strasser's (1986) type 6 (Fig. 4.22D) who interpreted this

mixture of microstructures to reflect rapid changes in water energy (also documented by Reijers and Ten Have, 1983; Poncet, 1984). Strasser (1986) deduced that the radial microstructure reflects rather quiet waters where the calcite crystals have time to develop on the surface of the nucleus. The radial fabric reflects abrasion during transport (Strasser, 1986). The micritic microstructure is interpreted by Strasser (1986) to indicate very rapid precipitation of calcite crystals due to abrasion during bedload transport dragging of the grains (Strasser, 1986). He interpreted these type 6 ooids to have formed in different environments and that they characterised abrupt changes in depositional environments (Strasser, 1986).

The nuclei of the ooids found in the Mupe Member of the Purbeck Limestone Group are of three types, described here in order of abundance. The most common type of nucleus is characterised by sub-angular micritic grains with clotted structures (Fig. 4.22A, C) and is found in all the locations where ooids were formed. They are interpreted to be microbial intraclasts (refer to section 3.2.2.) that derive from the surrounding microbial mounds. The second most common type of nucleus is the lozenge-shaped micrite coated grains interpreted as gypsum pseudomorphs in the previous section (Fig. 4.22E) and is found only in the Hard Cap at Mupe Bay and West Lulworth Cove and in the Soft Cap at Worbarrow Tout. This type of nucleus is thought to be reworked from a nearby *in-situ* source. The gypsum pseudomorphs appear to be wrapped by oolitic coating and never replace it (Fig. 4.22E) which would be expected if the gypsum crystals grew after the cortex. This shows that this type is similar to the first type in that the nucleus is reworked. These ooids were described by West (1964) as "*oolitically coated spherules with calcite pseudomorphs after gypsum lenses*" (Fig. 4.22F). These ooids were interpreted by West (1975) to have formed around gypsum in a shallow lagoon on the edge of a tidal flat after the precipitation of the gypsum in the sediment and still formed in waters saturated or supersaturated for gypsum. The less common type of nucleus is made of smaller ooids that show only one or two laminae in their cortex (Fig. 4.22G) and was only found in the Hard Cap at West Lulworth Cove. These form grapestones which were coated with an oolitic coating soon after their formation. This type of ooid is defined by Carozzi (1964) as compound reworked ooids with two or more nuclei (Fig. 4.22H); by Tucker and Wright (1990) as botryoidal lumps; and by Scholle and Ulmer-Scholle (2003) as composite ooids. They can be produced in agitated oolite shoals as well as protected environments (Tucker and Wright, 1990).

All the ooids found in this facies are interpreted to be originally in calcite with radial and micritic microfabrics. These ooids are thought to have formed in lacustrine settings contemporaneously with the microbial mound developments when microbial intraclasts are

found as nucleus, or transported from a close source when gypsum pseudomorphs, ooids or grapestones are found as nucleus. This helps to discount a possible reworked origin from the underlying Portland Group where complex ooids with a thicker cortex than those found in this facies are found in great quantity. Their cortical structures are rather similar to that of Purbeck (calcitic mineralogy both radial and tangential fabrics) but their nuclei are made of broken up mollusc shells (bivalves and gastropods) and quartz grains. The Purbeck ooids may also reflect the nature of the environment, such as hydrodynamics and/or the chemistry of the water body. The presence of radial together with micritic microstructures makes it difficult to determine a unique depositional environment for their formation. However the micritic fabric may reflect a high hydrodynamics while radial fabric may reflect a low hydrodynamics and the alternation between one and the other fabrics (*i.e.* random) can reflect abrupt changes in the hydrodynamics (as suggested by Strasser, 1986).



**Figure 4.22** Ooids of the Intraclastic peloidal packstone-grainstone facies. A – Peloidal grainstone with superficial ooids in PPL (BQ10, Soft Cap, Broadcroft Quarry, Isle of Portland). B – Micritic well rounded ooids with micritic nucleus and fine concentric laminae with radial fabric cortex in PPL (type 1 ooid, modified after Strasser, 1986). C – Mixed ooid showing concentric laminae with radial fabric and



micritic irregular laminae of the cortex around a microbial intraclasts nucleus in PPL (WLC5, Hard Cap, West Lulworth Cove). D – Mixed ooid with concentric laminae with radial fabric and micritic irregular laminae around a recrystallised nucleus in PPL (type 6 ooid, modified after Strasser, 1986). E – Gypsum pseudomorphs in nucleus of ooid with thin concentric laminae with radial fabric cortex in PPL (WT5B, Hard Cap, Worbarrow Tout). F – Sketch of thin section from the Caps at Worbarrow Tout with “oolitically coated spherules with calcite pseudomorphs after gypsum” (West, 1964) and celestite replacement of the micritic matrix (sample L.P. 148, redrawn after West, 1964). Note the radial microstructure of the cortices. G – Ooid made of grapestone as nucleus with two small ooids with one concentric laminae with radial fabric, and numerous concentric laminae with radial fabric cortex (WLC5, Hard Cap, West Lulworth Cove). H – Compound ooid with two nuclei from the Triassic lake deposits of Virginia, USA (from Carozzi, 1964).

### **3.2.7. Fish scales**

The yellow grains are interpreted to be phosphatic fish scales that are either well preserved (Fig. 4.19G) or, most commonly, found as fragments. Fish in the Mupe Member were previously identified and described by Griffith and Patterson (1963) as *Ichthyokentema purbeckensis*. They were later identified by West (1975) and Francis (1982) in the Skull and Hard Cap beds (refer to Chapter 2).

### **3.2.8. Foraminifers**

Foraminifers in the Mupe Member of the Purbeck Limestone Group of Dorset have surprisingly never been studied in the literature. Most of authors note the occurrence of foraminifers but no attempt was ever done in their recognition. For example West (1975) defined his facies A as “Limestones with Foraminifera” but did not describe nor identify what kinds of foraminifera are encountered (refer to Chapter 2). The very rare foraminifers found in this facies were therefore not identified. Because very few foraminifers were found there is a possibility that they were either windblown transported from a nearby marine environment or reworked from the underlying Portland Group.

### **3.2.9. Palaeocurrents**

The cross-laminations provide information on palaeocurrent directions and are very common in coastal environments. Tucker (2003) proposed that at least 30 measurements are necessary to be reliable to give a good interpretation of palaeocurrents. The cross-lamination orientation measurements performed in this facies were only 12 (Fig. 4.18E) and the measurements show a southerly prevalent palaeocurrent direction, which is consistent with

palaeocurrents interpreted by Francis (1982) on fallen tree and branch orientations (refer to Chapter 2). This aspect will be discussed further in Chapters 6 and 7.

### 3.2.10. Summary

The packstone to grainstone texture indicates moderate to high energy environment that is also supported with the occurrence of ooids. The presence of brackish water ostracods, gastropods and bivalves and the interdigitation with microbial mounds support an interpretation of brackish water conditions west of the Lulworth area. Furthermore the presence of gypsum pseudomorphs (even though transported) east of Lulworth area indicates a possible change in the water condition to hypersaline eastwards. The environmental setting of the Mupe Member is discussed further in Chapters 6 and 7. Overall the depositional environment was a brackish to hypersaline shallow marginal lacustrine system.

## 4. Cross-bedded peloidal packstone-grainstone facies

### 4.1. Description

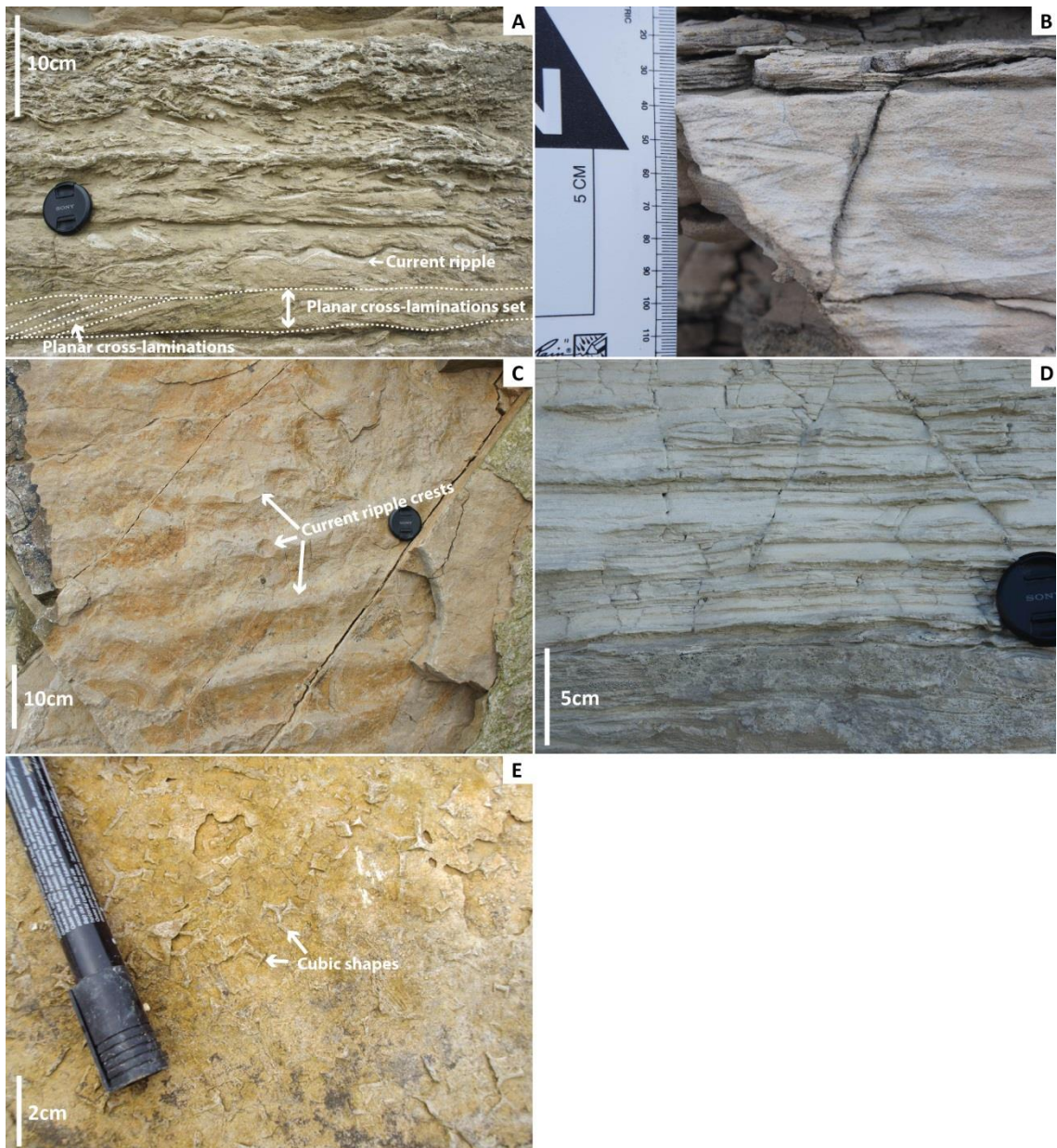
This facies is unique to and is the main lithology of the Cypris Freestone unit (refer to Chapter 2) and is present throughout the studied area from the Isle of Portland to Durlston Bay and north of Weymouth (*i.e.* Portesham Quarry) varying in thickness from 1 to 50 cm (Fig. 4.23) in beds that can be either massive or laminated (Fig. 4.23). The laminations are planar cross-laminations and organised in sets (Fig. 4.23A) which measure between 1 and 6 cm in thickness. The base of the Cypris Freestone unit can be found locally broken up into centimetre to decimetre scale blocks to create the Evaporite breccia sub-facies of the Broken Beds described in section 10.2 of this chapter.

At the macroscale this facies exhibits cross-bedded stratification, cross-lamination, wave ripple, herring bone stratification (Fig. 4.23B) and sometimes planar lamination (Fig. 4.23D). The texture varies between coarse and fine peloidal packstone to grainstone (Fig. 4.23B). On the surfaces of most of the beds mudcracks and cubic shapes between 1 and 2 cm long may be found and are interpreted to be halite pseudomorphs (Fig. 4.23E). This facies appears beige at the outcrop and when broken. Measurements of cross-bedding stratification were performed in selected locations at Portesham Quarry, the Isle of Portland (South West Bowers and God Nore) and at Fossil Forest and reveal different palaeocurrent directions (Fig. 4.24D). At Portesham only 2 measurements were possible (Fig. 4.24A) giving a 270° direction. On the Isle

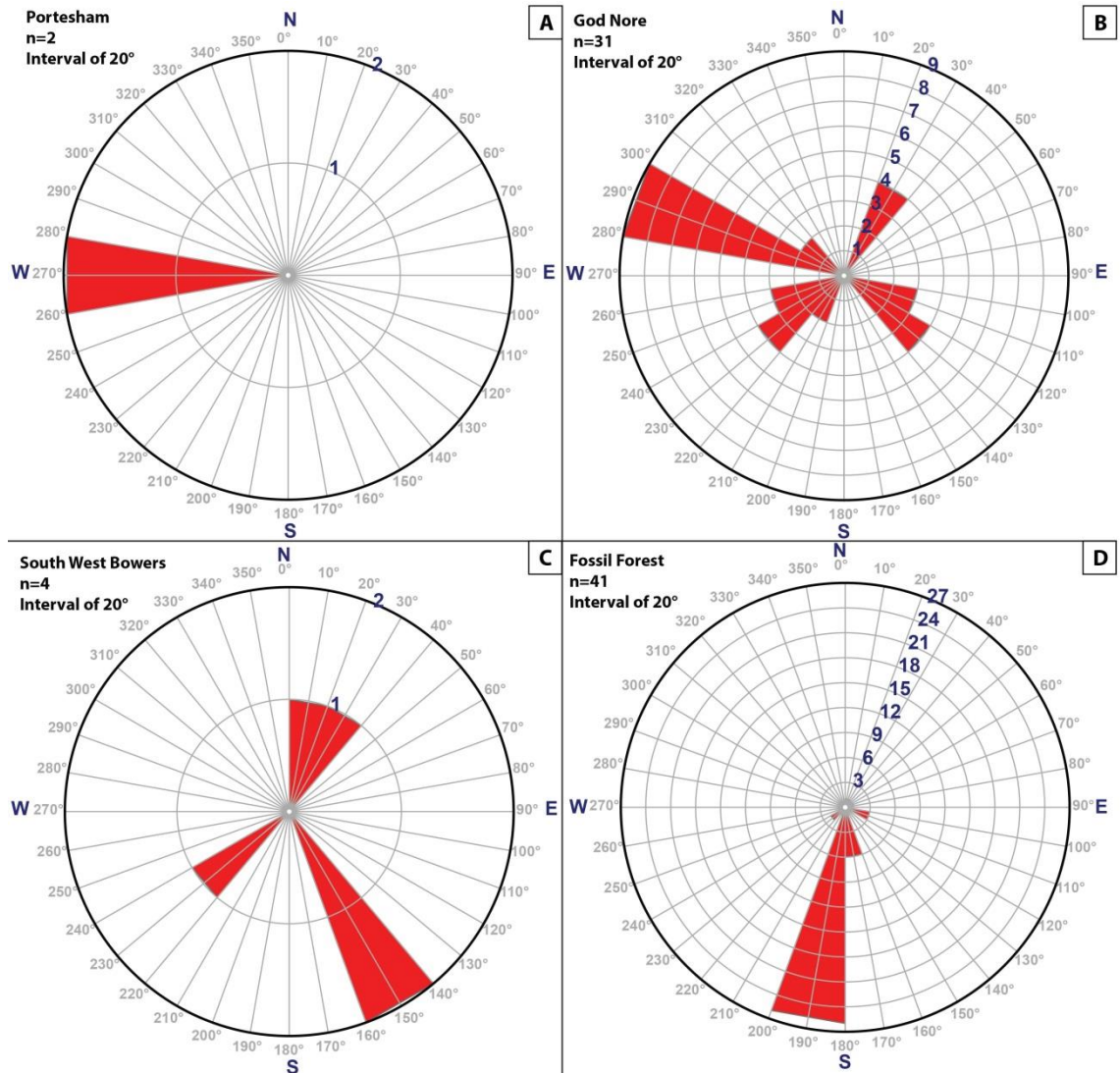
of Portland in South West Bowers (NE of the island) the main directions are 20°; 230° and 150° (Fig. 4.24C) and in God Nore (SW of the island) mainly N290 and with three secondary directions 30°; 130° and 230° (Fig. 4.24B). At South West Bowers location only 4 measurements were possible (Fig. 4.24C; far from the 30 necessary to assess palaeocurrent directions more precisely, following Tucker, 2003). At God Nore, 31 measurements were taken (Fig. 4.24B) revealing a polymodal palaeocurrent pattern which reflect shoreline or shoreface environment where wave and storm processes are common (Tucker, 2003). At Fossil Forest 41 measurements revealing a unique direction at 190° (Fig. 4.24D), this indicates a main current directed into the half graben basin (refer to Chapter 6 and 7).

At the microscale the texture varies as at macroscale between a packstone to a grainstone with some wackestone horizons (Fig.4.25). The most abundant grains are micritic peloids, between 50 and 500 µm in diameter, usually poorly sorted. They are three types depending on internal structures, sizes and shapes: between 200 and 500 µm and sub-rounded with a rather clotted internal structure; between 50 and 200 µm sub-rounded and elongated with a micritic internal structure; and around 50 µm and sub-circular with a micritic internal structure (Fig. 4.25). In addition, some peloids show an internal clotted structure (Fig. 4.25A-B). The second more abundant grains after the peloids in this facies are ostracods (Fig. 4.25A-B). These are very thin, yellow and between 100 and 500 µm long and 20-30 µm thick. The ostracods are most commonly intact but sparse fragments of about 20-50 µm can be found (Fig. 4.25A-B). Only in three locations (West Lulworth Cove, Mupe Bay and Worbarrow Tout) similar ooids as found in the Intraclastic peloidal packstone-grainstone facies are present in this facies in a great quantity. The nuclei are about 50 µm in diameter and the calcitic cortices are between 10 and 50 µm thick (Figs. 4.25A-D and 4.26). As with the ooids of the previous facies the nuclei are made of peloids, microbial intraclasts or grapestones and the cortices are made of concentric laminae with radial fabric and micritic laminae to form superficial and mixed ooids (Figs. 4.25C-D and 4.26A-D). Some of the ooids are broken up (in half usually) and a new generation of calcite crystals developed around these broken up ooids (Figs. 4.25B and 4.26E). Molluscs are common in this facies (gastropods and bivalves) commonly with a micritic envelope (Fig. 4.25A-B). Micritic intraclasts with either a clotted microfabric or a peloidal packstone-grainstone texture are commonly found, sub-angular to sub-rounded and between 50 µm and 1.5 mm in diameter (Figs. 4.25A-B and 4.27). Some angular clear crystals of detrital quartz are identifiable about 50-100 µm (Fig. 4.25) and with a first order straight extinction in XPL. Rare foraminifers are present with a conical shape of about 500 µm long and 200 µm wide and made of several chambers of about 50 µm in diameter (Fig. 4.25D). The pore types in this

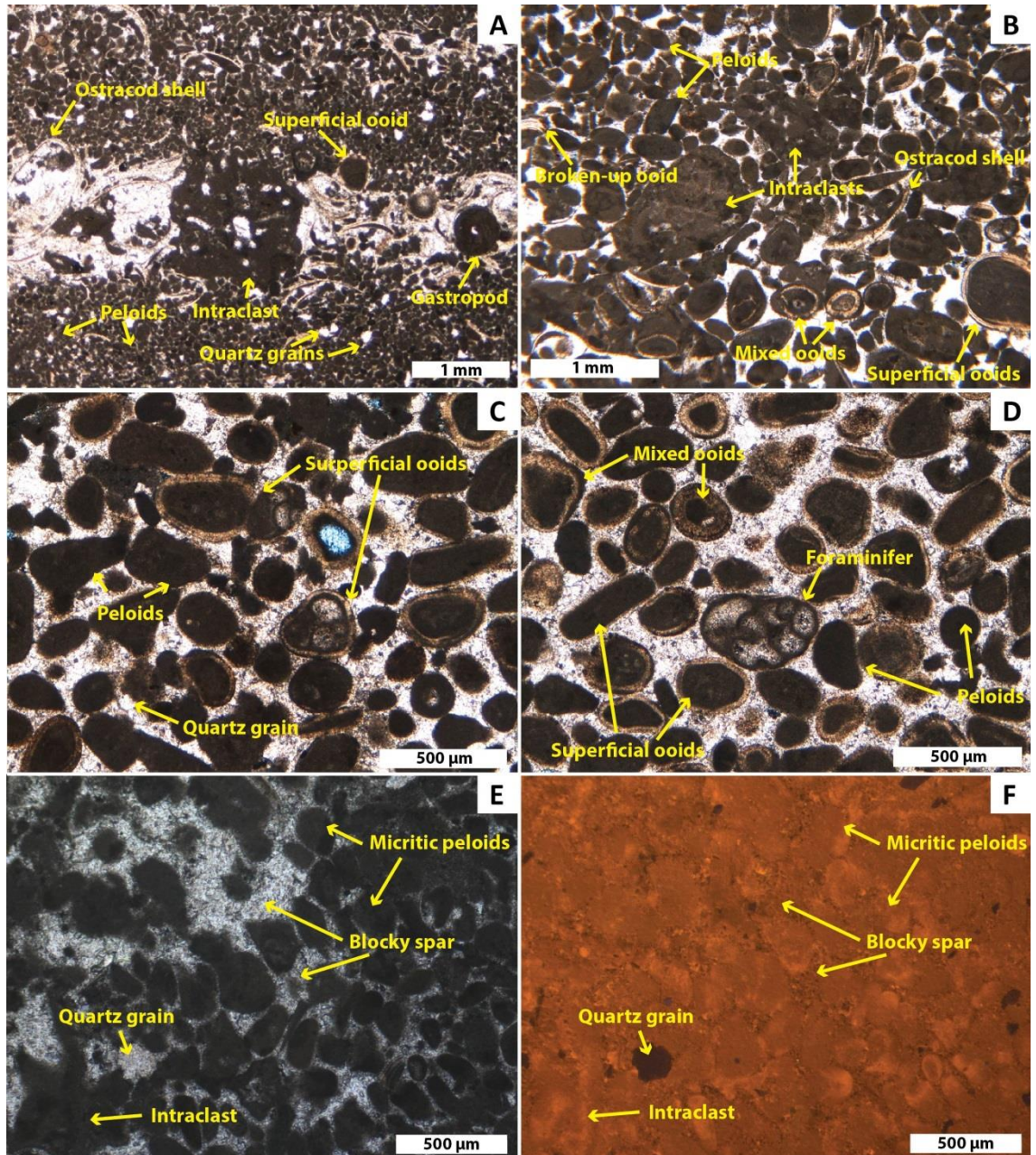
facies are intergranular and intragranular to mouldic and are commonly filled only with the second kind of blocky spar cement described in the previous facies (blocky spar 2, dull orange to brown, Fig. 4.25F).



**Figure 4.23** Cross-bedded peloidal packstone-grainstone facies in the field. A – Planar cross-lamination and wave ripple (cross-section, Pondfield Cove). B – Herring-bone cross-stratification (cross-section, Fossil Forest). C – Current ripple on plan view (Pondfield Cove). D – Planar laminations (cross-section, South West Bowers, Isle of Portland). E – Halite pseudomorphs in plan view on surface of bed (Broadcoft Quarry, Isle of Portland).



**Figure 4.24** Orientation and direction measurements of the cross-laminations of the Cross-bedded peloidal packstone-grainstone facies. A – Portesham Quarry with 2 measurements. B – God Nore with 31 measurements. C – South West Bowers with 4 measurements. D – Fossil Forest with 41 measurements.



**Figure 4.25** Cross-bedded peloidal packstone-grainstone microfacies. A – Peloidal grainstone with peloids, ostracods, microbial intraclasts, superficial ooids, quartz grains and gastropods (WLC8, West Lulworth Cove). B – Peloidal grainstone with peloids, ooids, ostracods and microbial intraclasts (WT13, Worbarrow Tout). C – Peloidal grainstone with peloids, quartz grains and superficial ooids with microbial intraclasts and grapestone nuclei (WT12, Worbarrow Tout). D – Peloidal grainstone with peloids, ooids and foraminifers (WT12, Worbarrow Tout). E – Peloidal grainstone showing the blocky spar cement in PPL (WT14, Worbarrow Tout). F – CL image of E showing dull luminescence of the micritic peloids, weak luminescence of the blocky spar cement and the non-luminescence of quartz grains (WT14, Worbarrow Tout).

## **4.2. Interpretation**

### **4.2.1. Peloids**

The peloids found in this facies are generally considerably bigger (between 50 and 500  $\mu\text{m}$ ) than the peloids found in the Intraclastic peloidal packstone-grainstone facies (between 50 and 200  $\mu\text{m}$ ). Brown (1964) described peloids of the Cypris Freestone of the Lower Purbeck of Dorset to be rod-shaped, showing opaque inclusions (described by Illing, 1954 on modern faecal pellets) in their internal structure and with some remaining organic matter. These indications together with the evidence of increasing fauna in this unit helped Brown (1964) to interpret these as faecal pellets. West (1975) also described faecal pellets together with pelletoids, following the same definition presented in the previous facies. In this study the elongated sub-rounded peloids (between 50 and 200  $\mu\text{m}$ ) are thought to be faecal pellets as per Bathurst's (1971) definition (internal structure and size) and as previously proposed by Brown (1964). However there are two other types of peloids from numerous possible origins. The biggest peloids (between 200 and 500  $\mu\text{m}$ ) that exhibit an internal clotted structure are thought to be reworked and rounded clasts from the microbial mounds deposited in the underlying beds as these are more sub-rounded than the faecal pellets (also described in the previous sections). The smallest peloids (around 50  $\mu\text{m}$  in diameter) can be either inorganic precipitates, micritised shell fragments of molluscs (bivalves and gastropods) or crustaceans (ostracods) or mud clasts.

### **4.2.2. Ostracods**

Ostracods are very abundant in this facies however due to the hardness of the limestone their extraction is very difficult and their identification based only on thin section views is impossible (pers. comm., David Horne, May 2015). The Cypris Freestone beds where this facies was deposited have been interpreted to contain ostracods from the *Cypridea dunkeri* subzone (Strahan, 1898; Barker *et al.*, 1975; Kilenyi and Neale, 1978; Anderson, 1967, 1973, 1985; Horne, 1995, 2002). As explained in the previous facies the ostracods of the Mupe Member are considered as non-marine species by comparison with modern-day equivalent species (Horne, 2002). Strahan (1898) following interpretation of Forbes (1850) identified three species in his "Lower Purbeck Beds" (Cypris Freestone beds in this study) and were considered as freshwater species (refer to Chapter 2). Later Anderson (1985) defined ostracod assemblages and faunicycles (refer to Chapter 2) and determined that the faunicycles of the Cypris Freestone

are mainly made of S-phase ostracod species that are thought to live in saline to hypersaline waters. Barker *et al.* (1975) identified three other saline (euhaline) species in equivalent beds of the Broken Beds at Portesham Quarry (refer to Chapter 2).

### 4.2.3. Ooids

The ooids are very abundant in this facies and because the concentric laminae with radial calcitic fabric structures of the cortex are visible, as for the previous facies with ooids, they are thought to have preserved the original calcitic mineralogy (Sorby, 1879; Walter, 1976). Most of the ooids found in this facies (Fig. 4.26) are very similar to the superficial (Fig. 4.22A) and mixed ooids (Fig. 4.22C) of the previous facies but a new morphology appears with broken-up ooids acting as nuclei (see below).

Superficial ooids have nuclei that may be peloids, microbial intraclasts and/or grapestones with cortices of one or two laminae of concentric laminae with radial calcite fabric (Fig. 4.26A). This type of ooids are also very common in the hypersaline Great Salt Lake (Utah, USA; Mathew, 1930).

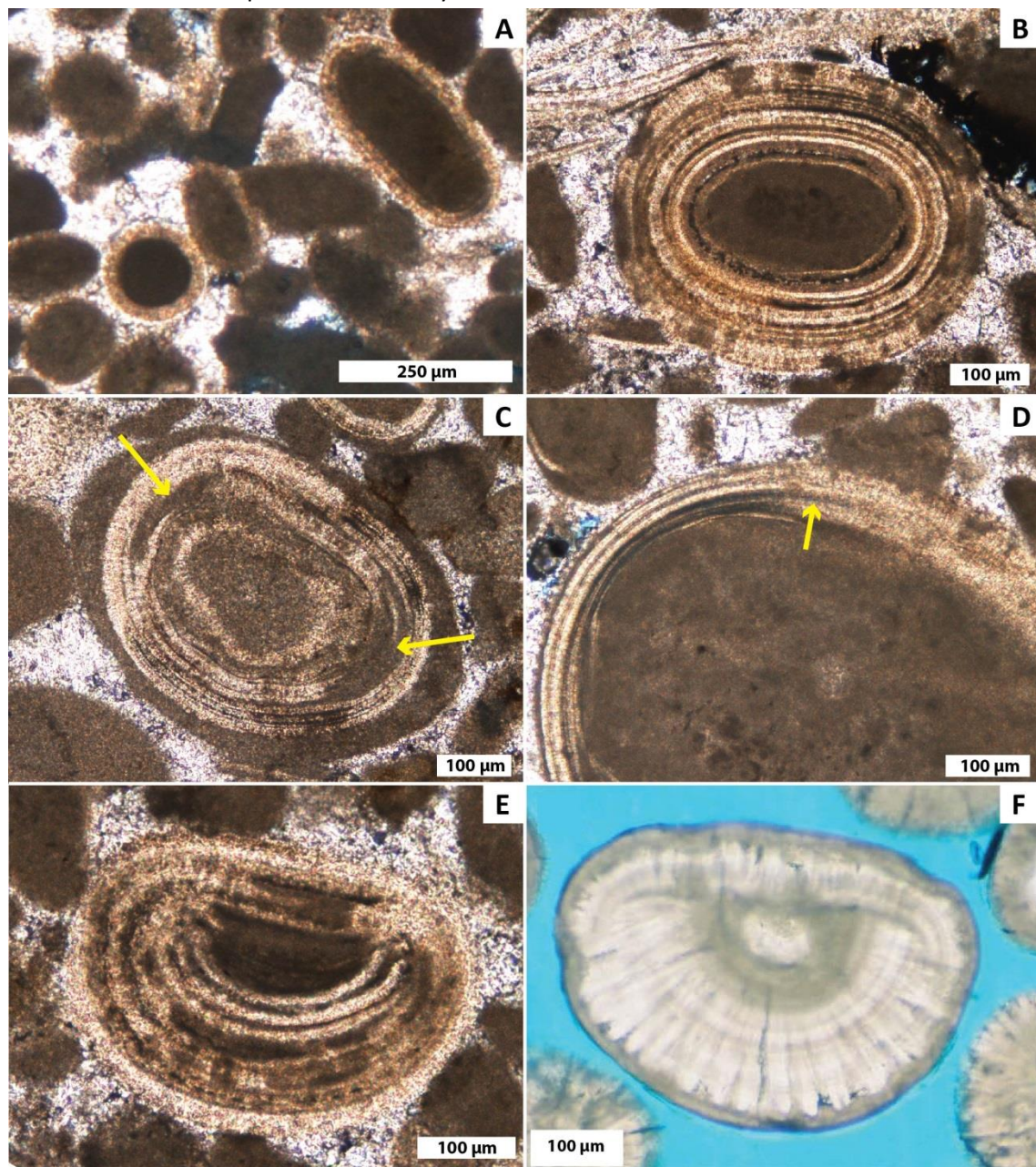
Mixed ooids have nuclei usually made of only peloids and rarely grapestones with concentric with radial fabric and micritic irregular laminae cortices (Fig. 4.26B-C). One difference with the mixed ooids of the previous facies is that cortices of these mixed ooids are thicker and may be patchily more micritised (Fig. 4.26B-C). According to Strasser (1986), this might suggest longer reworking time and/or transport of the ooids on the lake floor. This type of ooids is also very common in the Great Salt Lake (Utah, USA; Chidsey *et al.*, 2015).

Ooids with nuclei made of broken-up ooids that are then recoated are only found in this facies (Fig. 4.26E). These types of ooids were described for the first time by Berg (1944) who defined them as hiatusooids. Flügel (1982) described them as broken or abraded ooids formed by the mechanical break-up in agitated waters in hypersaline environments. Carozzi (1961) when studying the ooids of the hypersaline Great Salt Lake (Utah, USA) redefined these types of ooids as regenerated ooids. They were also found in ancient environments in the lagoonal Keuper deposits of Poland (Labeci and Radwanski, 1967), Neocomian deposits of Yugoslavia (Radoičić, 1960) and shallow marine Miocene deposits of Italy (Roda, 1965); and in modern day environments such as the Great Salt Lake (Fig. 4.26F; Eby and Chidsey, 2013; Chidsey *et al.*, 2015 and refer to Chapter 6).

A few ooids present in this facies and only found in Worbarrow Tout show a lateral change in the cortex microstructure from finely radial to coarsely radial within the same



laminae (Fig. 4.26D). This feature is not documented in the literature and an explanation of this may be a replacement of the original fine concentric laminae to a coarser fabric, as ghosts of concentric laminae persist a short way into the coarser radial calcite fabric.

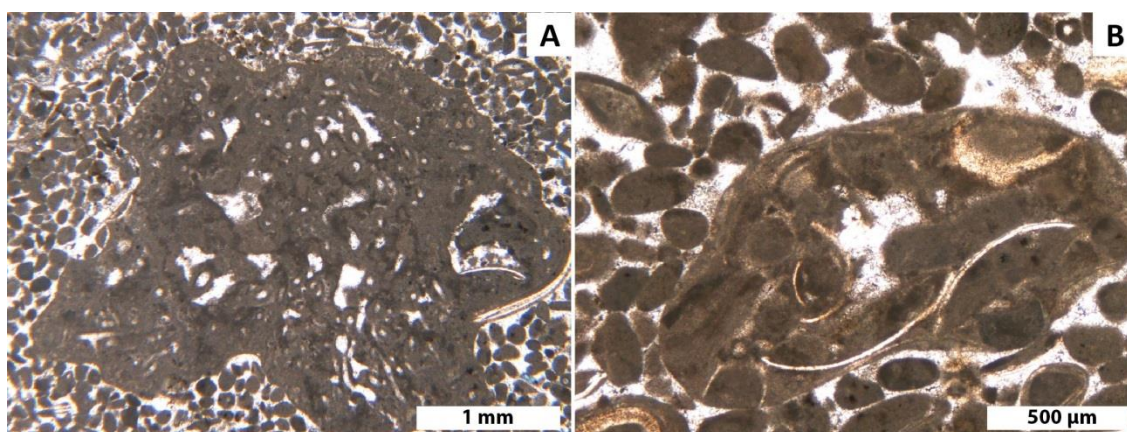


**Figure 4.26** Ooids of the Cross-bedded peloidal packstone-grainstone facies. A – Superficial ooids with peloids (WT10, Wrodarrow Tout). B – Mixed ooid with micritic nucleus and concentric calcitic laminae with radial fabric cortex. Note the micritisation mainly in the outer part (WLC8, West Lulworth Cove). C – Mixed ooid with micritic nucleus and concentric laminae with radial fabric and micritic irregular laminae. Note the micritisation on the extremities (arrows) and of the last laminae (WT13, Worbarrow Tout). D – Strange ooid with microbial intraclasts as nucleus and the replacement of the cortex from finely radial to coarsely radial concentric laminae. Arrow shows the concentric laminae recognisable in the coarse radial fabric (WT13, Worbarrow Tout). E – Regenerated ooid with a mixed microstructure cortex concentric laminae with radial fabric (WLC8, West Lulworth Cove). F – Regenerated ooid with radial fabric from the Great Salt Lake, Utah, USA (from Chidsey *et al.*, 2015).

#### 4.2.4. Intraclasts

The intraclasts with a clotted microfabric (Fig. 4.27A) as with the intraclasts of the previous facies (see previous section) are interpreted to originate from reworked material from microbial mounds of either underlying beds (Skull, Hard or Soft Cap beds) or adjacent accumulated microbial mounds.

The intraclasts with a peloidal packstone-grainstone texture (Fig. 4.27B) are most likely reworked material from underlying beds within the Cypris Freestone unit.



**Figure 4.27** Intraclasts of the Cross-bedded peloidal packstone-grainstone facies. A – Microbial intraclast in a peloidal grainstone (WT14, Worbarrow Tout). B – Peloidal packstone with ostracod shells and ooids intraclast within a peloidal grainstone with ooids (WT13, Worbarrow Tout).

#### 4.2.5. Molluscs

Gastropods present in this facies were observed only in thin section, are neomorphosed in a calcite spar, some filled with micrite (Fig. 4.25A), and have not been identified. From the Cypris Freestone Strahan (1898) described three fresh- to brackish water tolerant gastropod species; Arkell (1941) recorded two freshwater tolerant gastropod species; Clements (1973) described two other brackish water tolerant gastropod species; and more recently Radley (2002) described another brackish water tolerant species (refer to Chapter 2). Despite different findings from different authors the overall conclusion is that the low diversity of gastropod species indicates brackish to hypersaline conditions within an estuarine or lacustrine environment closed system (Radley, 2002).

Similarly, the bivalves are neomorphosed in a mosaic or drusy calcite spar in well lithified limestones and have not been identified in this study. Strahan (1898) described only one freshwater tolerant species and Radley (2002) one marine tolerant species (refer to Chapter 2). As for the interpretation from the gastropod species, the low diversity of bivalve species indicates brackish to hypersaline conditions in a closed system (Radley, 2002). However the

environmental interpretation remains unclear due to the occurrence of marine species together with brackish and freshwater species that suggests a mixing of molluscan material (Radley, 2002).

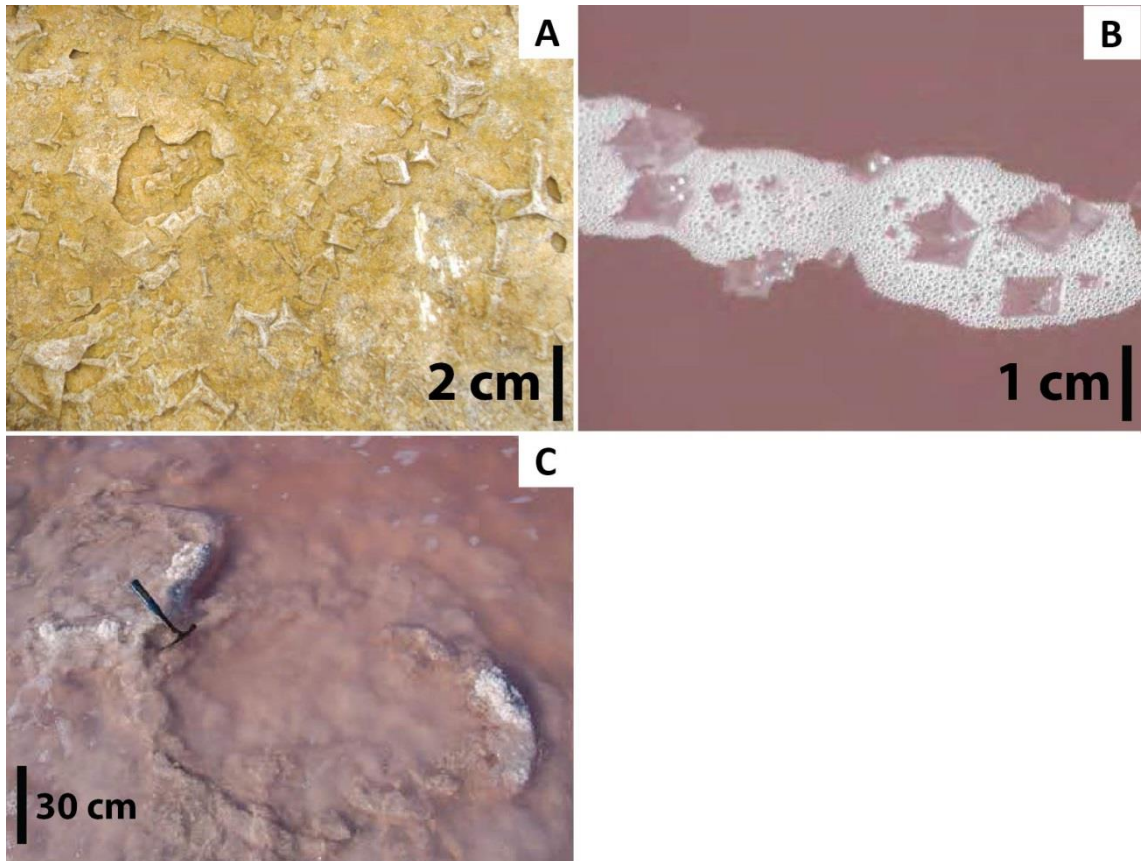
#### **4.2.6. Foraminifers**

As explained for the previous facies, occurrence of foraminifers in the Mupe Member (and the Purbeck Limestone Group in general) is cited by most authors but no identification was ever published. This is also valid for the Cypris Freestone unit where this facies was deposited.

#### **4.2.7. Halite pseudomorphs**

Cubic shaped moulds are commonly found on the base surfaces of the bedding planes (Figs. 4.23E and 4.28A) and are commonly used as way-up structures (Collinson and Thompson, 1987). These moulds are filled with the surrounding sediments (*i.e.* the Cross-bedded peloidal packstone-grainstone) indicating a very rapid dissolution after deposition. These are often referred to hopper crystal cast of halite cubes and are typical of evaporitic environments (Handford, 1991). Most of the published studies documenting halite deposition/crystallisation are for shallow marine environments but the same deposition/crystallisation processes can be applied to non-marine environments (Eugster and Hardie, 1978; Talbot and Allen, 1996). Processes of halite precipitation are due to intense evaporation of the water body leading to subaqueous growth of halite crystals at the water-air interface and/or directly on the lake floor (Arthurton, 1973; Lowestein and Hardie, 1985; Collinson and Thompson, 1987; Handford, 1991). Halite pseudomorphs result from influx of slightly fresher waters into the lake that dissolve the halite crystals and create moulds on the lake floor (Collinson and Thompson, 1987). These moulds are then quickly filled with the surrounded sediments allowing their preservation (Collinson and Thompson, 1987).

Hopper crystals of halite cubes are documented in modern day hypersaline Great Salt Lake (Baskin, 2014; Chidsey *et al.*, 2015). In the northern part of the Great Salt Lake (Gunnison Bay) halite hoppers are forming at the surface of the hypersaline water (Fig. 4.28B) before sinking to the lake floor when too heavy as per Handford's (1991) model. These can be deposited on the surface of the oolitic sediment or encrusting microbial mounds (Fig. 4.28C; Chidsey *et al.*, 2015).



**Figure 4.28** Hoppers of halite of the Cross-bedded peloidal packstone-grainstone facies. A – Hoppers of halite pseudomorphs on a surface of a bed (Broadcroft Quarry, Isle of Portland). B – Hoppers of halite (possibly forming a raft) nucleated at the water surface in the northern part of the Great Salt Lake (Utah, USA). Note in both pictures (B and C) the pinkish colour of the water due to sulphate reducing microbes. (from Baskin, 2014). C – Halite encrusting circular dead microbial mounds in the Great Salt Lake, Utah, USA (from Chidsey *et al.*, 2015).

The hoppers of halite pseudomorphs found in this facies are thought to have precipitated on the surface of hypersaline water before sinking and being deposited or to have grown from the lake floor (as per Handford's, 1991, model). After a change in the water chemistry they may be dissolved away and filled with the surrounding sediment that preserved their moulds on the base of the bed surfaces (as per Collinson and Thompson, 1987, concept).

#### 4.2.8. Quartz grains

The quartz grains are often present throughout the area although in small quantities that indicates some siliciclastic input to the system from time to time possibly from a freshwater input from the west or exposed footwall areas (refer to Chapter 6 for discussion).

#### 4.2.9. Palaeocurrents

As described in the previous facies cross-lamination and current ripples provide information on palaeocurrent directions (Tucker, 2003) and are very common in coastal environments (Tucker and Wright, 1990). In this facies the measurements done at Portesham cannot be really used as reliable palaeocurrent determination as only two directions were recorded (as per Tucker, 2003; see in previous section). However at Fossil Forest and South West Bowers enough measurements were recorded (see above) to indicate a prevalent southerly current direction in the Lulworth area (Fig. 4.24D), easterly direction in the Portesham area (Fig. 4.24A) and rather variable directions (although easterly directions appear to prevail, Fig. 4.24B-C) over the Isle of Portland area. Few authors have studied palaeocurrent directions within the Purbeck strata. Allen *et al.* (1998) determined palaeo-wind directions inferred from global simulations for the western Tethyan region and input into General Circulation Models (usually used in modern weather forecasts) for early Purbeck time. They showed that the prevailing winds were westerly during summers and easterly during winters. They also specified that there was an overall northeasterly wind direction during the whole Purbeck time that is in accordance with Francis (1982) works on fallen trees from the Cap beds (refer Chapter 2) . This will be detailed and discussed further in Chapters 6 and 7.

Herring bone cross-stratifications are usually found in the tidally influenced zone in marine environments (Tucker and Wright, 1990), and to create such sedimentary structures in a lakes is only possible in certain conditions. They can occur in big lakes with a water body big enough to be influenced by gravitational forces (the moon and the sun) as in the Lake Superior (about 82.103 km<sup>2</sup>), Lake Erie (about 25.744 km<sup>2</sup>) or Lake Michigan (about 58.000 km<sup>2</sup>) in the Great Lakes region in northern America (Mortimer and Fee, 1976; Kennish, 1986; Mann and Lazier, 1991; Mortimer, 2004; Trebitz, 2006). Alternatively they can be wind-driven as documented by Rusnak (1960b) for a hypersaline lake Laguna Merida (about 1.230 km<sup>2</sup>) in Texas (USA), Ainsworth *et al.* (2012) in the Lake Eyre (9.500 km<sup>2</sup>) in Australia and by Illing *et al.* (1965) in the Dohat Faishakh lagoon (about 10 km<sup>2</sup>) in the Persian Gulf. They can also be due to seiche event where two waves of opposite direction are combined to create a unique and bigger wave (Sager *et al.*, 1985; Mortimer, 2004). The Wessex Basin being about 45.000 km<sup>2</sup> (refer to Chapter 2) tides or seiche events would be expected to create such herring bone stratification. However the Portland-Wight sub-basin is much smaller, about 12.000 km<sup>2</sup> (refer to Chapter 2) having a similar area to Lake Eyre (see above) where wind-driven currents

control the formation of herring bone stratification. This will be discussed further in Chapters 6 and 7.

#### **4.2.10. Summary**

The packstone to grainstone texture indicates a moderate to high energy environment supported by the sediment structures and the presence of intraclasts, ooids (in particular the broken-up and regenerated ooids) and grapestones. The presence of brackish to hypersaline ostracods indicates together with the occurrence of evaporite pseudomorphs, that hypersaline waters occurred at times. The association of all these features reveals a variably brackish to hypersaline shallow marginal lacustrine environment with a siliciclastic pulse from time to time. This lake was subject to winds of variable orientation based on the palaeocurrents and the herring-bone cross-stratifications.

## **5. Wackestone to fine grainstone facies**

### **5.1. Description**

This facies is mainly present in the lowermost beds of the Mupe Member of the Purbeck Limestone Group, labelled by Francis (1982) and West (2015) as the Transition Bed. This facies erosionally overlies the Portland Group and is overlain by the Basal Dirt Bed paleosol (refer to Chapter 2 for lithostratigraphy; Fig. 4.29A). This facies is only found north of Weymouth at Portesham and Poxwell Quarries, to the east at Swanworth Quarry, Fishermen's Ledge and Durlston Head and southwest of the Isle of Portland at God Nore, Lawnsheds Quarry and Portland Bill.

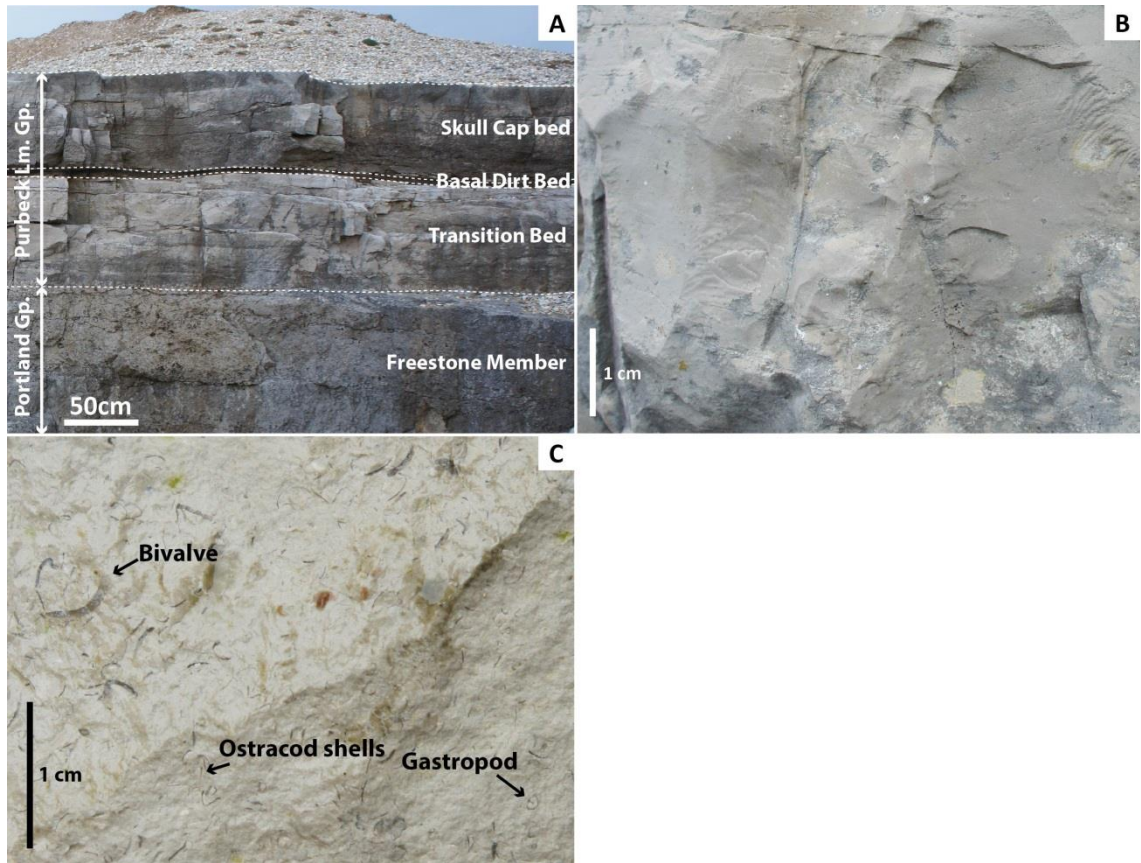
At the macro-scale this facies is massive, organised in beds of 20 to 50 cm thick commonly with planar laminations (Fig. 4.29A). This fine grained-facies contains molluscs (bivalves and gastropods) and few ostracods (Fig. 4.29B). It weathers to shades of grey to white at the outcrop and also when broken.

At the micro-scale three fine-grained textures characterise this facies; fine peloidal grainstone (Fig. 4.30B), peloidal packstone and wackestone (Fig. 4.30B). Rounded to well-rounded micritic peloids are very common in this facies. They are relatively sorted with diameters varying from 10-20  $\mu\text{m}$  to 50-100  $\mu\text{m}$ . Ostracods are abundant can be broken up or intact and between 300  $\mu\text{m}$  and 1 mm long. Gastropod shells were only found at Portland Bill on the Isle of Portland and replaced by calcite (Fig. 4.31C). These were found with both a flat helix and more elongated helicoidal shapes. Bivalves with two different shell microstructures

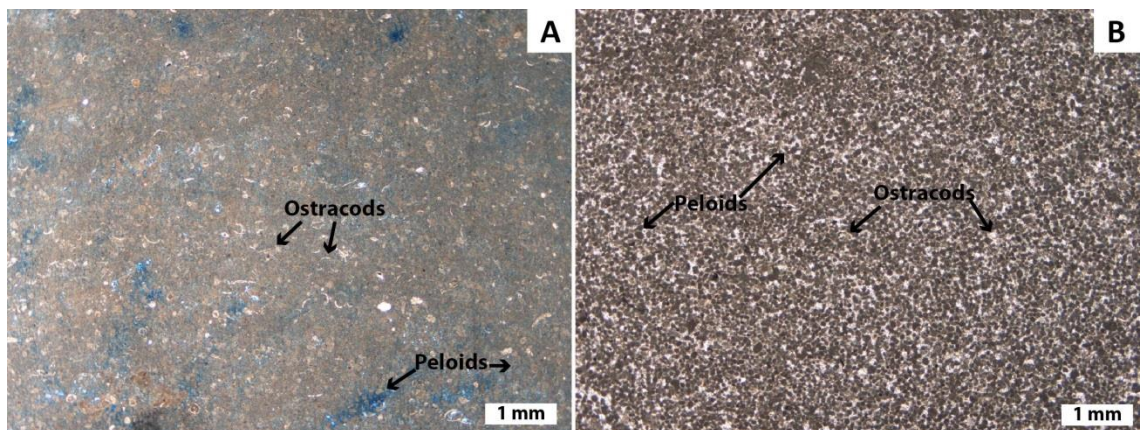
are found locally, yellow to beige fibrous and prismatic calcite (Fig. 4.31B) and sparite of calcite within a micritic envelope (Fig. 4.31A). The yellow to beige bivalve shells (whole or broken-up) are about 1 mm wide and 1 cm long with a fibrous calcite and a rolling extinction (Fig. 4.31B). Locally these bivalve shells can be silicified with small spherules replacing the fibrous shell (Fig. 4.31B). The bivalves with both prismatic and fibrous shells were only found at God Nore and Portland Bill. They are broken-up about 800  $\mu\text{m}$  long and 400  $\mu\text{m}$  wide and made of brown prismatic calcite crystals of about 150  $\mu\text{m}$  long and 10-20  $\mu\text{m}$  wide (Fig. 4.31B).

Only at Broadcroft Quarry, God Nore and Portland Bill on the Isle of Portland are found ooids. The ooids are of two types: mixed and heavily micritised ooids (Figs. 4.31 and 4.32) between 100 and 700  $\mu\text{m}$  in diameter with bioclast fragments or quartz grains as nucleus; or superficial ooids (Fig. 4.31) about 50  $\mu\text{m}$  in diameter with peloids as nucleus.

All the clasts described below are found very rarely and some cases only one occurrence was seen. Foraminifera were found only at Portland Bill and are about 200  $\mu\text{m}$  wide and 300  $\mu\text{m}$  long (Fig. 4.31G). At God Nore and Broadcroft Quarry rounded microporous clasts were found, and occasionally some with a tubular internal microstructure of between 1 and 2 mm in diameter. Some clasts have concentric laminae preserved interpreted to be *Solenopora* fragments (Figs. 4.31E and 4.33). Only at Portland Bill were found more or less squared-sided brown calcitic clasts about 1 mm long and wide with a rugose aspect and showing birefringence in XPL interpreted to be echinoderm plates (Fig. 4.31F). Intraclasts of oolitic and peloidal grainstone were found at Broadcroft Quarry and Portland Bill. They are between 500  $\mu\text{m}$  and 1 mm in diameter coated with an oolitic coating (Fig. 4.31D). Only at God Nore was found a rectangular clast with cells in its internal structure interpreted as bryozoan fragment (Fig. 4.31G). This clast is about 1.5 mm long and 500  $\mu\text{m}$  wide and the cells are more or less circular about 100  $\mu\text{m}$  in diameter (Fig. 4.31G).

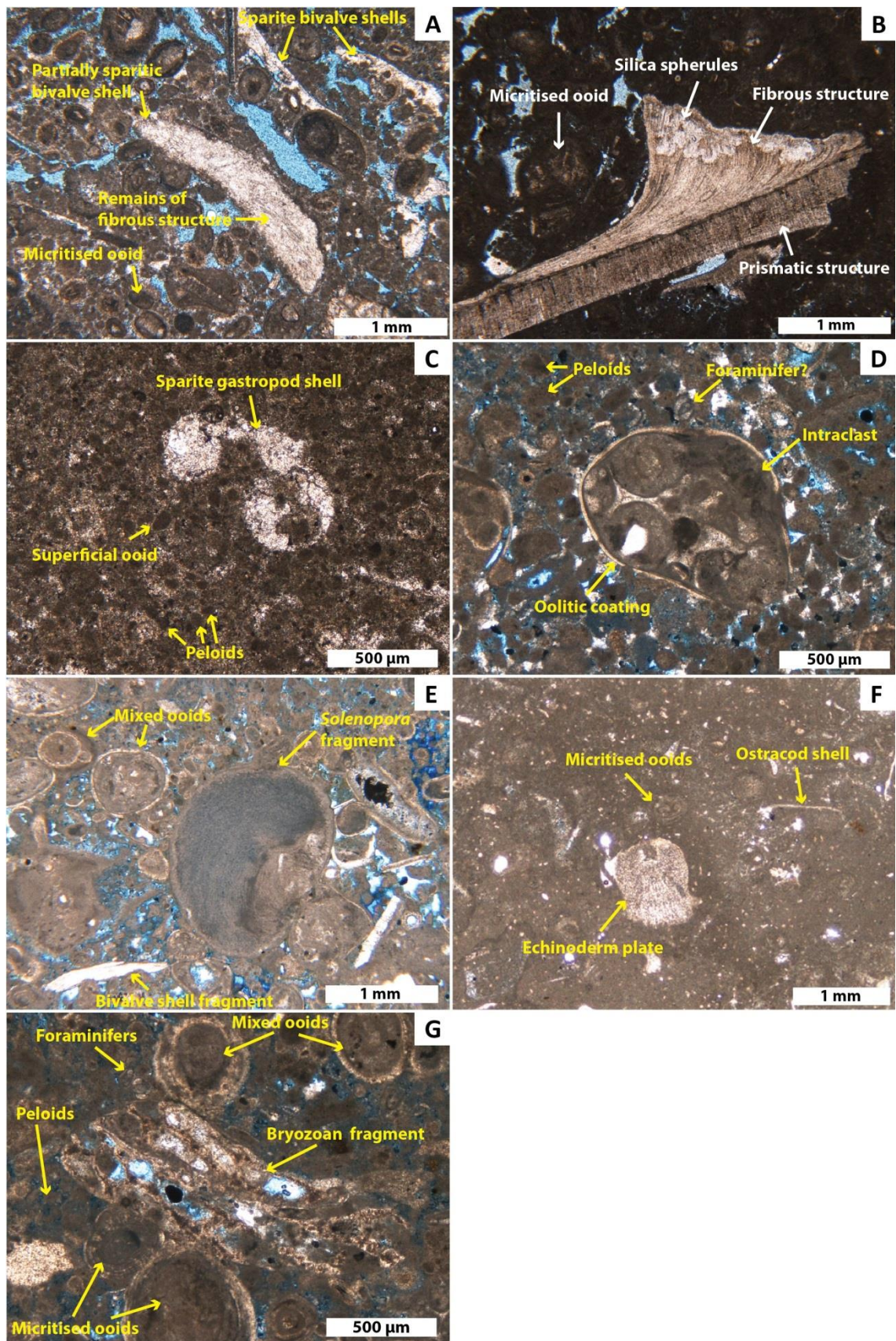


**Figure 4.29** Wackestone to fine grainstone facies in the field. A – Transition between Portland Group and Purbeck Limestone Group (Portland Bill, Isle of Portland). B – Close-up view on wackestone to fine grainstone macrofacies laminated (God Nore, Isle of Portland). C – Close-up view of wackestone to fine grainstone facies with ostracods and molluscs (Pondfield Cove).



**Figure 4.30** Wackestone to fine grainstone microfacies. A – Wackestone with peloids and ostracods (GN2, God Nore, Isle of Portland). B – Fine peloidal packstone with peloids and ostracods (PB2, Portland Bill, Isle of Portland).





**Figure 4.31** Clasts and fossils of the Wackestone to fine grainstone facies. A – Sparite and fibrous bivalve shells and micritised ooids in a fine peloidal grainstone (BQ1, Broadcroft Quarry, Isle of Portland). B – Bivalve shell showing both fibrous and prismatic structures and micritised ooids in a peloidal packstone (PB1, Portland Bill, Isle of Portland). C – Sparite gastropod shell, peloids and

superficial ooids in a fine peloidal grainstone (PB3, Portland Bill, Isle of Portland). D – Intraclast of oolitic grainstone with an oolitic coating, peloids and foraminifer in a fine peloidal grainstone (GN3, God Nore, Isle of Portland). E – *Solenopora* fragment, mixed ooids and fibrous bivalve shell fragments in a fine peloidal grainstone (GN3, God Nore, Isle of Portland). F – Echinoderm plate (with straight extinction in XPL), micritised ooids and ostracod shell fragments (PB1, Portland Bill, Isle of Portland). G – Bryozoan fragment, foraminifers, peloids and mixed and micritised ooids in a fine peloidal grainstone (GN3, God Nore, Isle of Portland).

## **5.2. Interpretation**

### **5.2.1. Peloids**

The peloids found in this facies are significantly smaller than those found in previous facies (Intraclastic and Cross-bedded peloidal packstone-grainstones). Due to their small size and their homogenous micritic microstructure no clear origin can be drawn, however some origins can be discarded. As described earlier, faecal pellets are rather elongated and usually between 40 and 300 µm in diameter. The peloids found in this facies are rather spherical and much smaller than faecal pellets; as a consequence they are unlikely to be faecal pellets. Similarly they are too large to be micritised ostracod shell fragments. This origin can also be discarded. Other possible origins are micritised mollusc shell fragments, micritised microbial intraclasts, reworked mud clasts and/or reworked faecal pellets. Mollusc shells (bivalves and gastropods) are locally very abundant and can be easily broken-off micritised and reworked (similar origins were interpreted by Samankassou *et al.* 2005, for peloids from the Cinder Bed upwards). Microbial intraclasts are found in a few locations and can be derived from contemporaneously deposited microbial sediments laterally. There are no records in the literature of underlying mud deposits or from a source nearby; they are unlikely to be at the origin of the peloids. The most probable sources of the peloids found in this facies are micritised mollusc fragments, microbial deposits derived from a syn-depositional source and/or reworked faecal pellets.

### **5.2.2. Ostracods**

The ostracods present here are difficult to identify for the same reasons presented earlier and no studies specifically refer to this unit. Anderson's (1985) first faunicycle (Quanton faunicycle) might correspond stratigraphically to the beds where this facies is found however this faunicycle is only based on ostracods found in the Buckinghamshire (Aylesbury) and Wiltshire (Swindon). As this unit is locally developed in south Dorset it is unwise to make a long distance correlation to these occurrences.

### 5.2.3. Molluscs

The molluscs are locally found with different characteristics, replaced by calcite gastropods (Fig. 4.31C), thick and long bivalve shells with fibrous calcite crystals often partially replaced by silica (Fig. 4.31B), bivalve shell fragments with prismatic calcite (Fig. 4.31B) and thick bivalve shells replaced by sparite of calcite (Fig. 4.31A).

The gastropod shells were only found at Portland Bill where they are rather abundant and because they are replaced by sparite of calcite they are thought to be originally aragonitic. Arkell (1941) and Clements (1973) described four species in these transition beds (refer to Chapter 2). Only one of them has a flat helix shape *Valvata helicoides*, while the three others have a helicoidal elongated shape and belong to two genera *Hydrobia* and *Loriolina*. Clements (1973) determined that these species were brackish water tolerant in a relatively open system (refer to Chapter 2). Because gastropod shells are found intact, they are thought to be deposited *in-situ* in early Purbeck time.

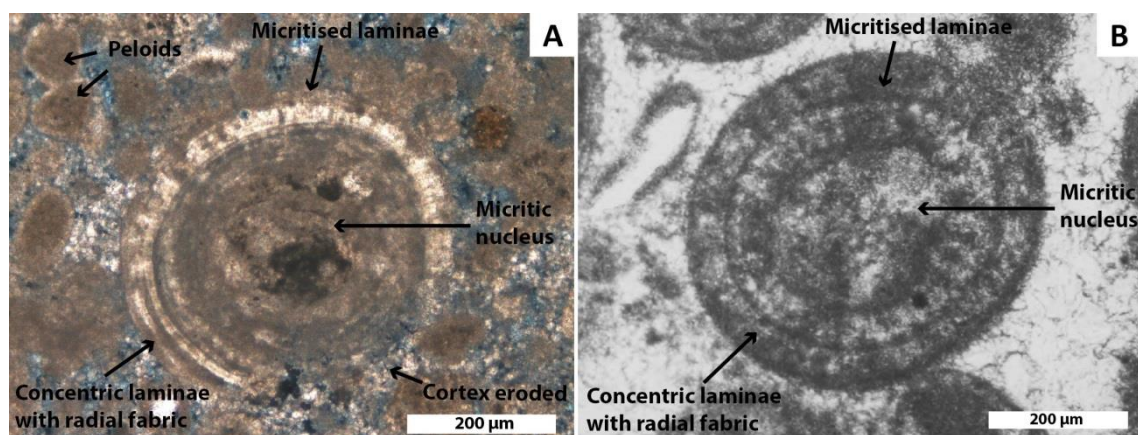
The three types of bivalve shells can possibly be three different species. In the Purbeck Limestone Group only one species of bivalve was identified from these beds by Strahan (1898) as freshwater *Cyrena media* that forms thick aragonitic shells (refer to Chapter 2). Similar aragonitic bivalve shells were identified by Townson (1971) in the underlying oolitic bed (Roach Bed) of the Portland Group. These belong to the Trigoniid, Pleuromyoid and Cardiid genera and are known to be found in marine settings (Townson, 1971). The intact (sometimes with both valves preserved) shells are thought to be deposited *in-situ* and to be *Cyrena media* bivalves. However, concerning the fragments of bivalves found replaced by calcite with a micritic envelop, these are thought to either be fragmented *Cyrena media* or reworked and redeposited bivalve shells from the underlying Roach Bed. The other types of bivalve shells are bigger and preserved their original calcitic microstructures as suggested by the fibrous and prismatic calcite crystals. Such thick and long bivalve shells have never been recorded in the Purbecks but similar shells have been identified in the underlying Roach Bed of the Portland Group. These were identified as marine species and to belong to the Pectinid, *Isognomenida*, *Limida* and *ostreids* genera and are very abundant in the Roach Bed (Arkell, 1947; Townson, 1971, 1975). These are found in this facies as variable sized fragments indicating a possible transport and redeposition. For these reason these types of bivalve shells are thought to be reworked and redeposited from the underlying marine deposits of the Roach Bed.

#### 5.2.4. Ooids

The ooids are only found at three locations in the Transition Bed on the Isle of Portland and are of two types; either superficial ooids usually with a peloid as nucleus or mixed ooids and heavily micritised.

The calcitic superficial ooids do not show any micritisation of their cortices and are preserved with their original concentric laminae with calcitic fabric microstructure. These are similar to the superficial ooids found in previous facies. The radial fabric of the concentric laminae may indicate quiet waters (Bathurst, 1967; Strasser, 1986). The nuclei are micritic peloids and do not show any internal structures. They are thought to be mainly sourced from the surrounding peloids. For these reasons these superficial ooids are thought to have formed *in-situ* in a rather quiet-water energy system consistent with the depositional textures.

The mixed ooids (Fig. 4.32) have their cortices and nuclei heavily micritised (more so than the ooids described in previous facies). Few of them show one or two concentric laminae with radial calcitic fabric on the external part that tend to classify them as superficial ooids with reworked ooids as nucleus (Fig. 4.31D). According to Strasser (1986) micritic microstructure indicates strong-energy and transport of the ooids on the lake floor while Rusnak (1960a) and Land *et al.* (1979) interpret the micritic microstructure to be due to rapid precipitation (in either quiet or agitated waters). However the ooids of this facies are very similar to those found in the underlying oolitic bed (Roach bed) of the Portland Group (Fig. 4.32B). The micritisation of the ooids is usually not complete as some of the original microstructures of the nucleus are observable.

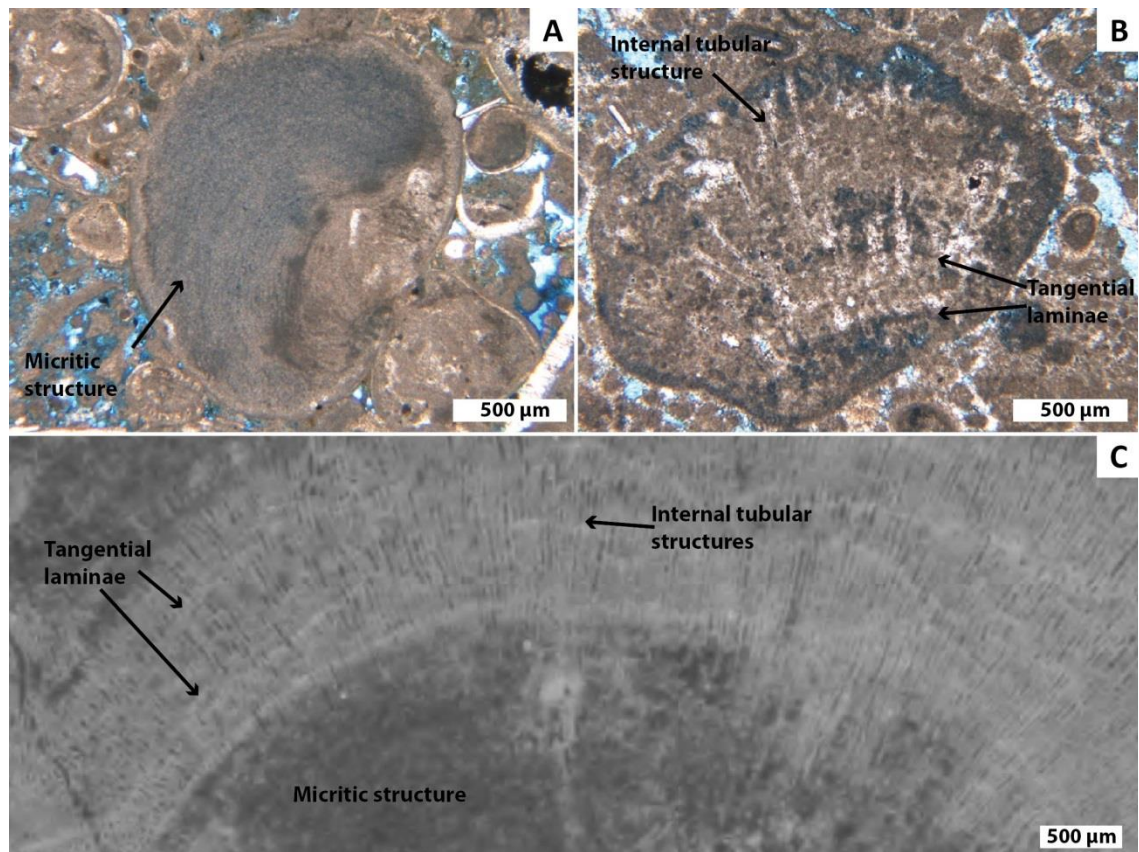


**Figure 4.32** Mixed ooids of the Wackestone to fine grainstone facies. A – Typical mixed ooid with concentric laminae with radial fabric and micritic laminae of the cortex and a micritic nucleus. Note the eroded cortex on the right bottom possibly showing erosion during transport (GN3, God Nore, Isle of Portland). B – Typical ooid of the Freestone Member of the Portland Group from the Central Area of Dorset with similar microstructures (from Townson, 1971).

Townson (1971) described ooids from the Portland Group to be 500 µm in diameter on average with concentric laminae or completely micritised (due to algal boring) cortices around quartz grains or skeletal fragments. For these reasons they are thought to be reworked from the underlying Roach Bed. These ooids were used as nuclei that were occasionally coated with a superficial oolitic coating of one or two laminae. In such case they have to be considered as superficial ooids deposited *in-situ* and most likely in a quiet-water energy system as the superficial ooids described above.

#### **5.2.5. *Solenopora* fragments**

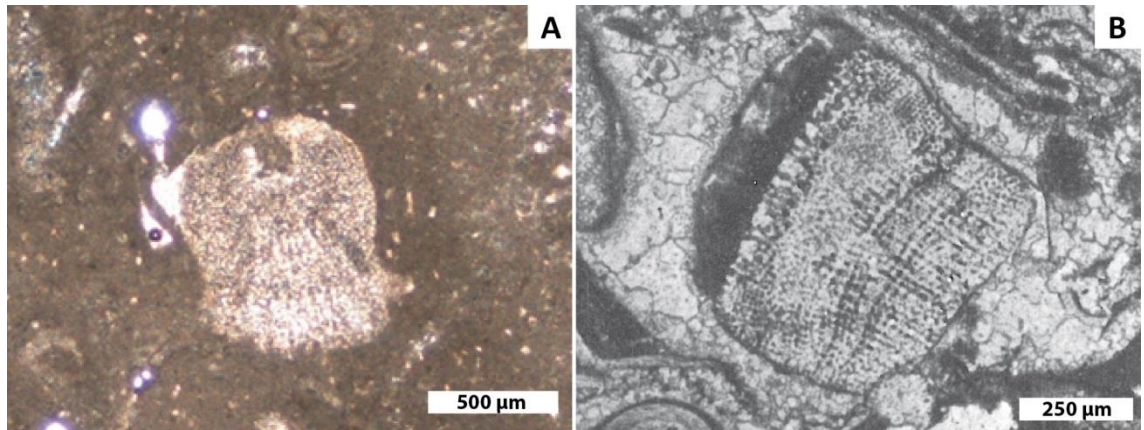
These clasts are rare and only two were found, one at Broadcroft Quarry and one at God Nore on the Isle of Portland. They both show a microporous internal microstructure with radial cells organised in tangential zones between 500 µm and 1 mm thick. These are very similar to *Solenopora* red algae (Fig. 4.33) abundant and that form reefs in the underlying Freestone Member of the Portland Group on the Isle of Portland (Townson, 1971, 1975). Due to the rarity and roundness of these clasts in this facies, they are thought to have been reworked and redeposited from the underlying Freestone Member.



**Figure 4.33** *Solenopora?* of the Wackestone to fine grainstone facies. A – *Solenopora?* clast with micritic and microporous structure that corresponds to the micritic structure of C (GN3, God Nore, Isle of Portland). B – *Solenopora?* clast with tubular structure organised in tangential laminae that corresponds to the upper part in C (BQ1, Broadcroft Quarry, Isle of Portland). C – Banded *Solenopora?* from the Freestone Beds of the Portland Group showing both micritic and tubular structures organised in laminae (modified after Townson, 1971).

### 5.2.6. Echinoderm plates

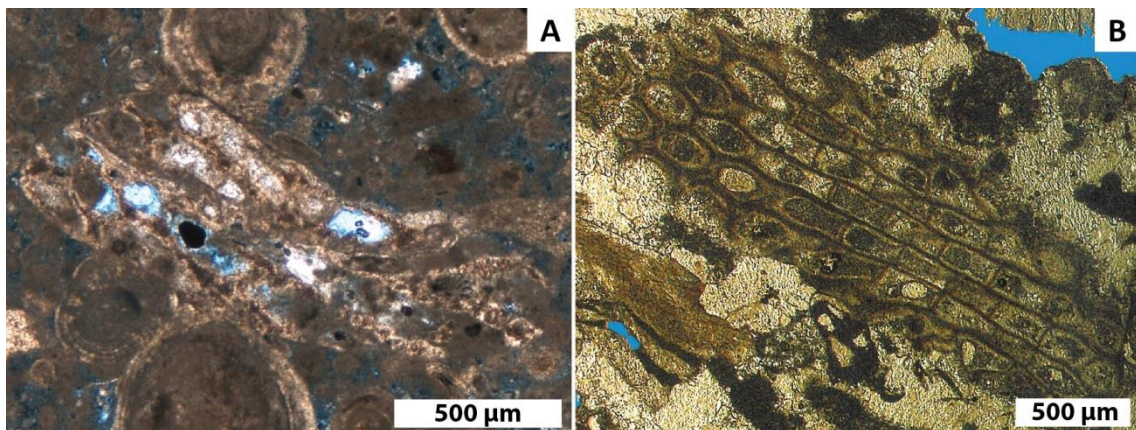
These clasts are also rare and were only identified at Portland Bill. Their rather squared shape together with their rugose internal microstructure and their straight extinction in XPL are specific of echinoderm plate fragments (Fig. 4.34). No echinoderms were described from the Purbeck Limestone Group but echinoids and asterozoan-derived (*Hemicidoroidea* and *Echinoidea*) are found in the underlying Freestone Member of the Portland Group (Townson, 1971). Due to their rarity and their roundness, they are thought to reworked and redeposited from the underlying Freestone Member.



**Figure 4.34** Echinoderm plates of the Wackestone to fine grainstone facies. A – Fragment of echinoderm plate with rugose microstructure in a wackestone (PB1, Portland Bill, Isle of Portland). B – Echinodermal plate from the Bethel Formation, Chester Series, Upper Mississippian, Hardin County, Kentucky, USA (from Horowitz and Potter, 1971).

### 5.2.7. Bryozoan fragment

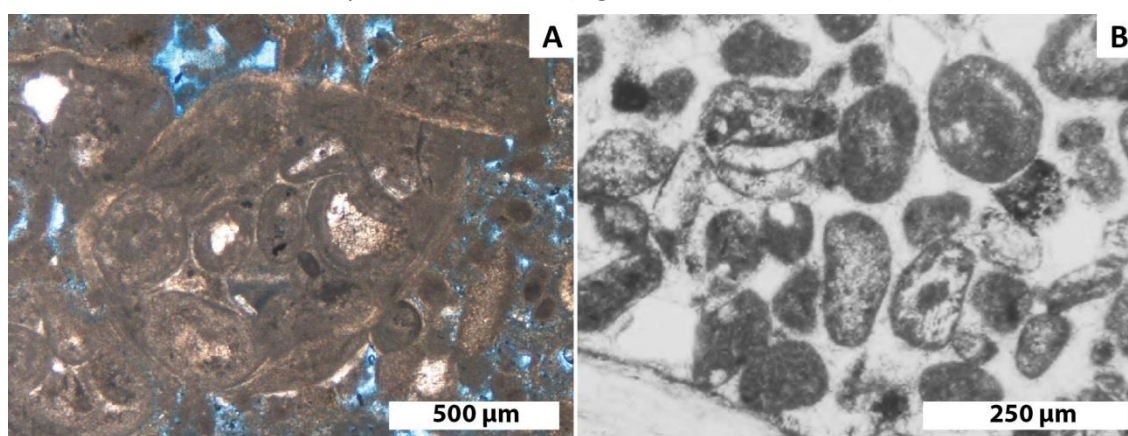
These clasts are again rare and few were found at Broadcroft Quarry and God Nore on the Isle of Portland. They show circular and elongated cells with micritic walls that are specific to bryozoan (Fig. 4.35). Bryozoans have never been recorded from the Purbeck Limestone Group but are common in the underlying Freestone Member of the Portland Group (Townson, 1971). These were identified as *Diastoporida* (order *Cyclostomata*) by Townson (1971). Due to their rarity and their broken-up aspect, they are thought to reworked and redeposited from the underlying Freestone Member.



**Figure 4.35** Bryozoan fragment of the Wackestone to fine grainstone facies. A – In a fine peloidal packstone, close-up view from figure 4.31G (GN3, God Nore, Isle of Portland). B – Bryozoan clast from the Jandaíra Formation of the Potiguar Basin from Mossoró Quarry, Brasil, Turonian to Campanian (from Dias-Brito and Tibana, 2015).

### 5.2.8. Intraclasts

The intraclasts found in this facies are again rare and only found at God Nore on the Isle of Portland. These are of two types either made of fine peloidal grainstone or oolitic grainstone (Fig. 4.36) and some of them are oolitic coated with a simple or two laminae of tangential calcite (Fig. 4.31D). The intraclasts with a fine peloidal grainstone texture are thought to be reworked and redeposited from an underlying or lateral bed of the Transition Bed of the Purbeck Limestone Group. While the intraclasts with the oolitic grainstone texture are thought to be reworked and redeposited from the underlying Roach Bed of the Portland Group where the beds are characterised by a similar texture (Fig. 4.37B; Townson, 1971).



**Figure 4.36** Intraclasts of the Wackestone to fine grainstone facies. A – Four oolitic grainstone intraclasts with a superficial oolitic coating in a fine peloidal grainstone (GN3, God Nore, Isle of Portland). B – Typical oolitic grainstone from the Lower Freestone Beds of the Portland Group from the east of the Isle of Purbeck that shows similar texture with the intraclasts found in this study (from Townson, 1971).

### 5.2.9. Summary

The rather fine grained textures of the sediments (wackestone to fine grainstone) with planar laminations indicate a low energy system suggesting a protected shallow or a deep environment. This low energy system is confirmed with the superficial ooids and the superficial oolitic coatings on some of the clasts. The brackish water tolerant ostracods and mollusc gastropods indicate a change in the environment from marine of the underlying oolitic Portland Group to the non-marine of the Purbeck Limestone Group. This was also suggested by West (2015). The low diversity of ostracods and gastropods indicate a rather closed system as suggested by Radley (2002). Occurrences of reworked marine fossils and clasts (red algae, oolitic intraclasts, micritised ooids and bryozoans) from the underlying Freestone Member of the Portland Group indicate that the Portland Group was exposed and eroded prior the



deposition of this Transition Bed (refer to Chapters 6 and 7). Altogether these clasts plus the texture indicate brackish water condition in a deep setting in a rather closed lacustrine system.

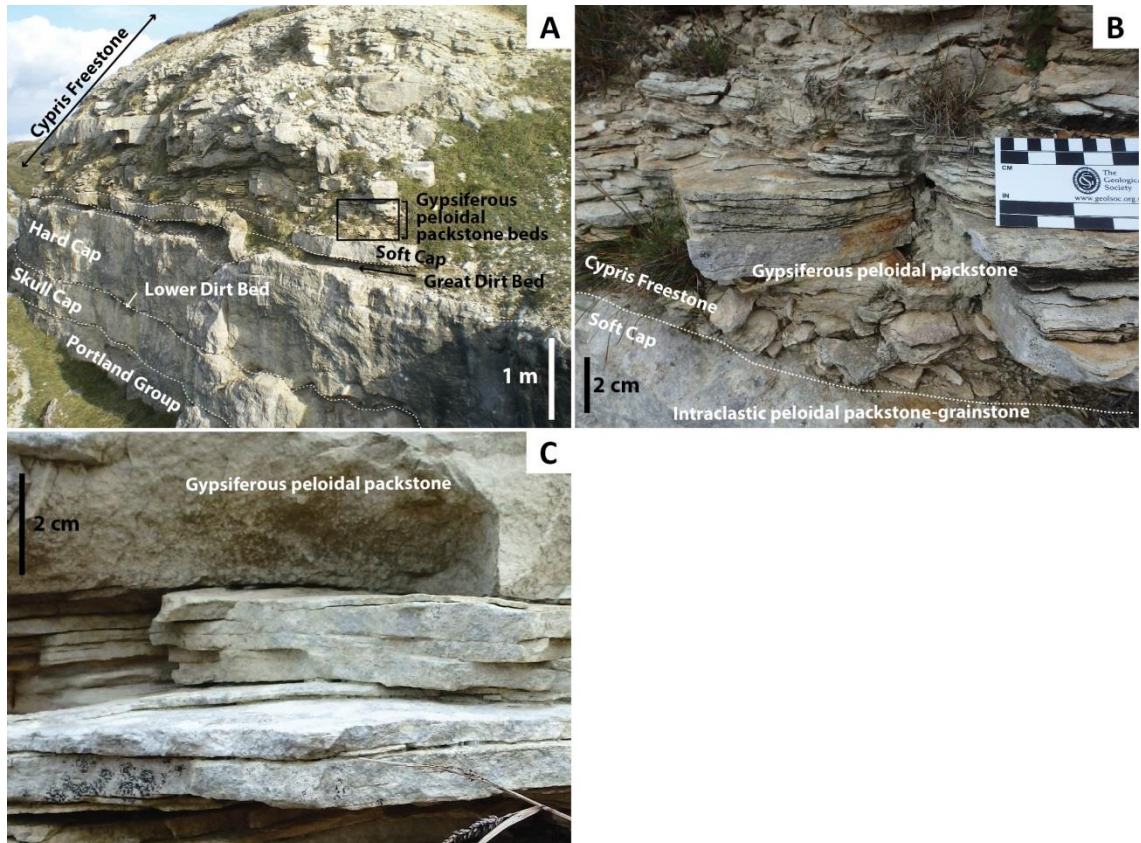
## 6. Gypsiferous peloidal packstone facies

### 6.1. Description

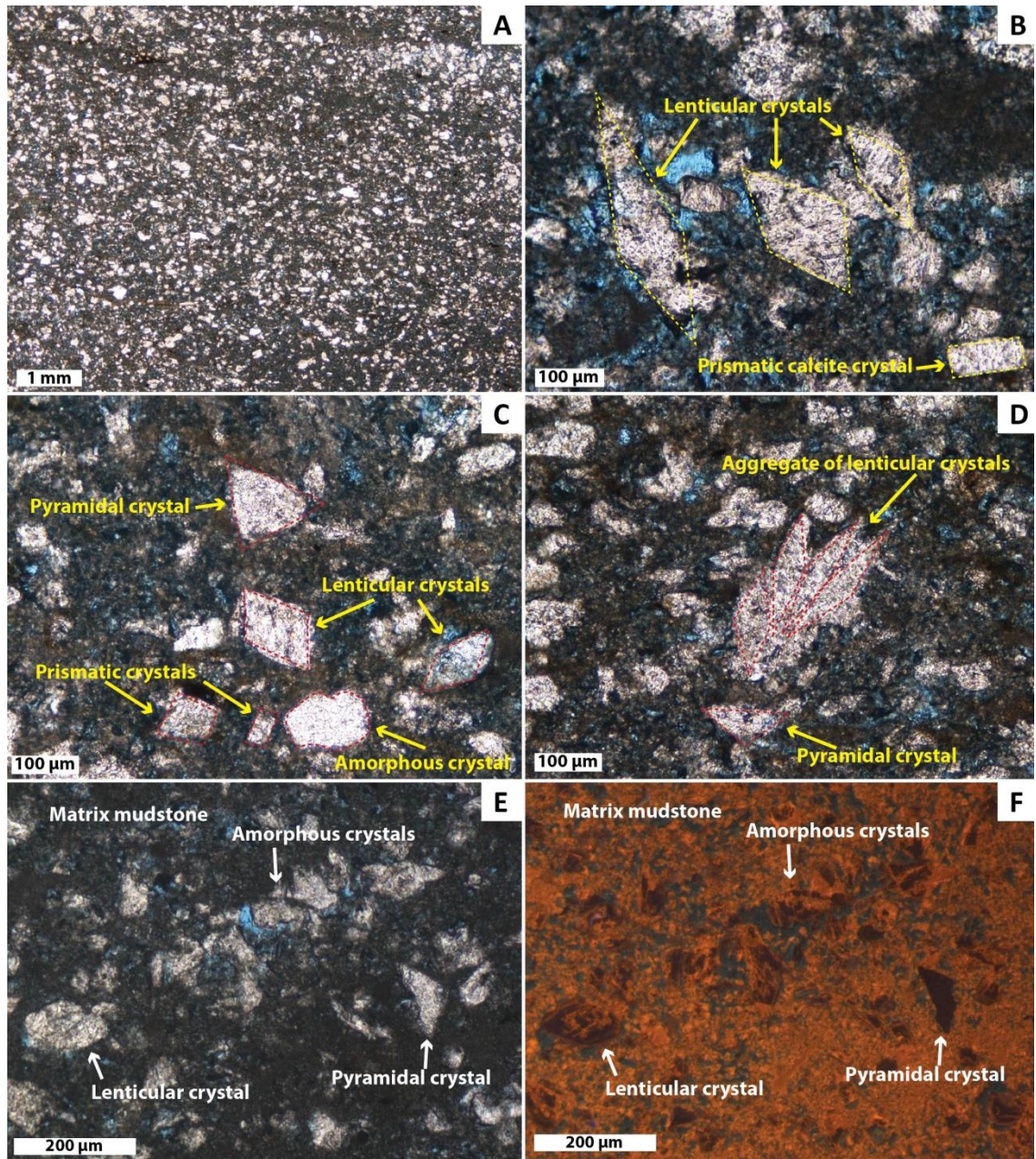
This facies is only found at the base of the Cypris Freestone unit (just above the Soft Cap bed, Fig. 4.37) and consists of beds of about 1 to 2 cm thick within a unit of about 50 cm thick (Fig. 4.37). This facies was only found on the Isle of Portland at Tout Quarry, Coombefield Quarry and South West Bowers. The absence elsewhere of this thin unit may be due to a non-deposition or erosion or it does not crop out.

At the macroscale the unit comprises fine-grained limestones that have planar laminations (Fig. 4.37). It weathers to shades of grey to white at the outcrop and similar tones are seen when broken.

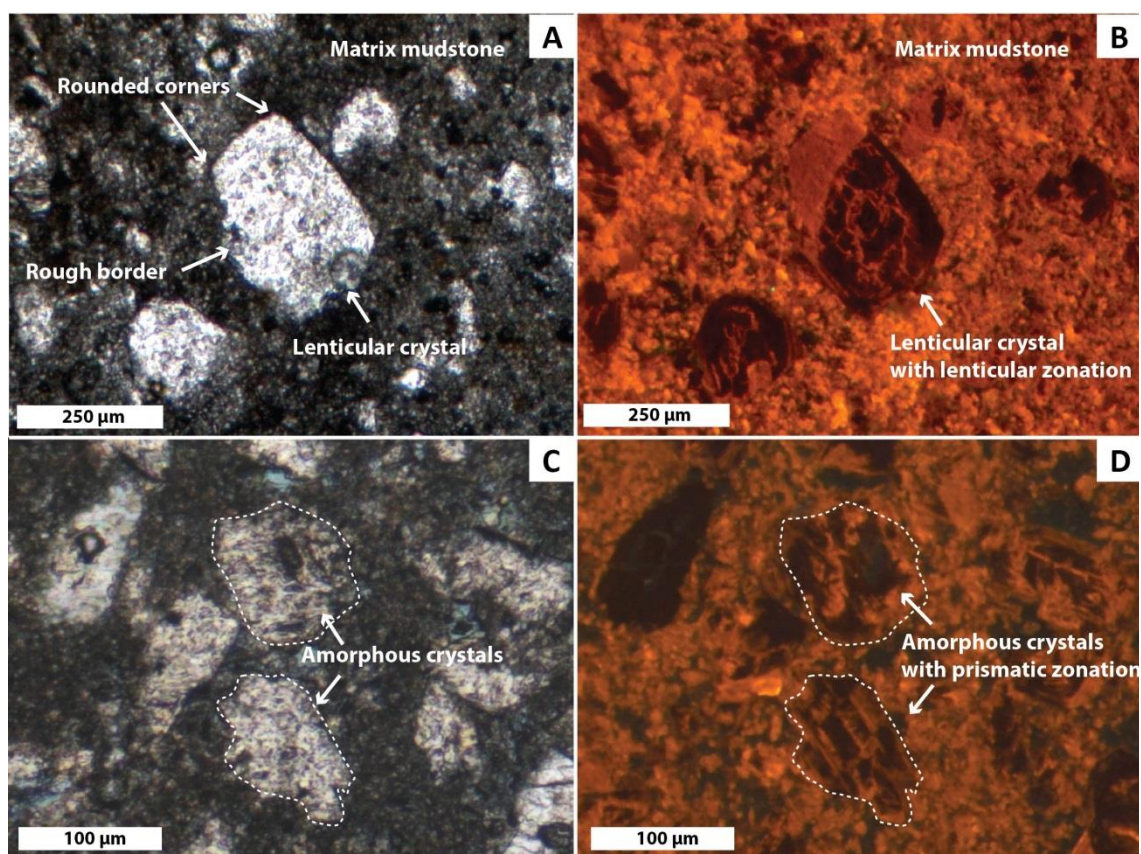
At the microscale this facies comprises poorly sorted calcite crystals that are sub-angular to rounded (Fig. 4.38, 4.39) and their morphologies are prismatic, lenticular (*i.e.* lozenge-shaped), pyramidal and amorphous (Fig. 4.38). Most of the crystals are monocrystals although some are found made of two or three calcite crystals (Fig. 4.38D). Under CL they are non-luminescent with rectangular (Fig. 4.39C-D) or lenticular (Fig. 4.39A-B) zonations and microfractures (Fig. 4.39) of orange laminae. These crystals are of silt and sand size (according to Wentworth's, 1922, classification) between 20 and 300  $\mu\text{m}$  in diameter with predominantly coarse silt size crystals (about 60% of the crystal diameters are between 30 and 60  $\mu\text{m}$ , Figs. 4.38 and 4.39) within a micritic matrix (Figs. 4.38 and 4.39). Under CL the matrix reveals a dull luminescence orange (Figs. 4.38F and 4.39).



**Figure 4.37** Gypsiferous peloidal packstone macrofacies. A – Location of the laminated beds just above the Soft Cap bed and at the base of the Cypris Freestone unit. Black box locates B and C (South West Bowers Quarry, Isle of Portland). B – Laminated beds (South West Bowers Quarry, Isle of Portland). C – Beds with planar laminations (South West Bowers Quarry, Isle of Portland).



**Figure 4.38** Gypsiferous peloidal packstone microfacies. A – Prismatic calcite crystals and gypsum pseudomorphs within a mudstone matrix (CQ10, Coombefield Quarry, Isle of Portland). B – Details of gypsum pseudomorphs (highlighted with dashed lines) and prismatic calcite crystals within a mudstone matrix (TQ11, Tout Quarry, Isle of Portland). C – Prismatic, amorphous, pyramidal and lenticular calcite crystals within a mudstone matrix in PPL (TQ11, Tout Quarry, Isle of Portland). D – Aggregate of lenticular calcite crystals and pyramidal calcite crystal within a mudstone matrix (TQ11, Tout Quarry, Isle of Portland). E and F – Bright white amorphous, lenticular and pyramidal calcite crystals within a mudstone matrix in PPL and dull calcite crystals with microfractures in orange under CL (SWB7, South West Bowers, Isle of Portland). Note the lenticular orange laminae in the calcite crystal.



**Figure 4.39** PPL and CL microphotographs of the calcite crystals. A and B – Lenticular calcite crystal showing a lenticular orange zonation in the center of the crystal under CL (CQ10, Coombefield Quarry, Isle of Portland). C and D – Amorphous calcite crystals showing a prismatic orange zonation in the crystals under CL (SWB7, South West Bowers, Isle of Portland).

## 6.2. Interpretation

The silt size calcite crystals found here in great quantity are poorly sorted and embedded in a micritic matrix that was neomorphosed to microsparite as revealed under CL (Figs. 4.38F and 4.39).

As described above the lenticular crystals have the morphology of gypsum crystals and are interpreted as gypsum pseudomorphs replaced by calcite. In this facies the calcite crystals preserve the original internal structure of the former gypsum crystals due to the lozenge-shaped growth lines as revealed under CL (Fig. 4.39B). However, these crystals appear to be broken up and/or abraded as the original lozenge shape of the gypsum crystals is often destroyed (Figs. 4.38 and 4.39). In addition, the corners of the crystals are often slightly rounded (Fig. 4.39A) and the borders are rough (Fig. 4.39A). These can be due to two processes, either a transport of gypsum crystals in hypersaline waters; or *in situ* displacive gypsum crystal growth in soft sediments locally incorporating micrite. In both cases, the gypsum crystals are thought to be later replaced during the early diagenesis during shallow

burial. The rough borders and smooth corners can be due to erosion of the original gypsum crystals during transport or partial dissolution of the crystals during the early diagenesis and the replacement with calcite.

The pyramidal crystals are also interpreted as broken-up gypsum pseudomorphs as they show same aspect in PPL and same kind of luminescence in CL. This also supports the suggestion for the reworked origin of these gypsum pseudomorphs, as these pyramidal shapes would have formed during the transport.

The prismatic shaped calcite crystals could be considered to have a different origin. Quine and Bosence (1991) described disarticulated prismatic crystal Inoceramid bivalve shells from Late Cretaceous of Normandy that had been eroded and redeposited. However such bivalves are not present in the underlying Purbeck beds or Portland Group. Bivalves such as Pectinid, *Isognomenida*, *Limida*, Ostreid, Triigonid, Pleuromyoid and Cardiid (Townson, 1971) are abundant in the underlying Freestone Beds of the Portland Group; however, several points argue against these as a possible source. First, most of these bivalves have fibrous calcitic shells and only a few have prismatic shells (Townson, 1971). This source is unlikely as a great amount of prismatic bivalve shells would have been needed to create such facies. Secondly, the Portland Group is too far stratigraphically from the beds made of this facies (about 4-5 m above, refer to Chapter 6) and no syndepositional faults have been identified nearby that could permit these bivalve shells to be reworked to a higher level in the stratigraphy. These crystals could also be reworked anhydrite pseudomorphs following the same process proposed for the gypsum pseudomorphs. Similarly as the gypsum pseudomorphs the calcite crystals preserved the original internal structure of the crystals as revealed by the rectangular orange laminae under CL (Fig. 4.39D). For the same reason as has been given for the gypsum pseudomorphs, anhydrite pseudomorphs might derive from penecontemporaneous deposits. However, the origin of the prismatic crystals is unlikely to be from anhydrite crystals as these are rarely found as primary crystals and are known to replace gypsum by dehydration in subsurface environments (Murray, 1964; West, 1964). Another argument against this origin is the luminescence under CL. These prismatic crystals have the same non-luminescence with orange zonation as the gypsum (Fig. 4.39). For these reasons these prismatic crystals are thought to be reworked, eroded and/or abraded and redeposited gypsum crystals.

Similar facies was described by Sanz *et al.* (1994) in the lacustrine Miocene Intermediate Unit deposits of the Madrid Basin exposed in Spain. They described a facies made of broken-up and eroded (physically and chemically) gypsum crystals within a mudstone matrix (Sanz *et al.*, 1994). Although the sizes of the crystals appear to be greater than the crystals found in the

Gypsiferous peloidal packstone facies of this study, morphologies are very similar. The gypsum crystals found in the Madrid Basin have tabular hemipyramidal, lenticular, prismatic and rounded shapes, abraded and/or broken and between 60  $\mu\text{m}$  and 1 cm (Sanz *et al.*, 1994). They interpreted this facies to have formed due to reworked and redeposited gypsum crystals and they defined it as detrital gypsum (Sanz *et al.*, 1994). This detrital gypsum is found in three different types of beds, infilling scour-based beds of 15 cm thick and 1 m wide; in beds with parallel laminations and low-angle cross-laminations in units of 20 to 170 cm thick and hundreds of meters wide and organised in beds of 2 mm to 5 cm thick; or in beds with trough and planar cross-stratification of 10 to 20 cm thick sometimes with an erosive base (Sanz *et al.*, 1994). According to this description the second type is similar to the Gypsiferous peloidal packstone beds in this study. They proposed two different models for the formation of these detrital gypsum beds with parallel laminations and low-angle cross-laminations; at the inner mudflat-lake margin transition or on the lake margins in both cases of a saline lake (Sanz *et al.*, 1994). In the former model the detrital gypsum beds are found after the deposition of gypsum-rich mudstones where gypsum monocrystals are found displacive in the sediment (Sanz *et al.*, 1994). Each detrital gypsum bed would have formed due to several and episodic terrestrial flows or sheetfloods (episodic heavy rains typical of arid to semi-arid climate, Hardie *et al.*, 1978; Handford, 1982; Chen *et al.*, 1991) of the saline mudflat that reworked and redeposited the gypsum (Sanz *et al.*, 1994). In the latter model the detrital gypsum would have been formed after reworking of *in-situ* selenitic gypsum beds by waves on the lake beaches (Sanz *et al.*, 1994). This model is supported by the occurrence of ripples, low-angle cross-laminations and parting lineation that are specific of beach environments (Elliot, 1986; Sanz *et al.*, 1994).

In this study only parallel laminations were identified at macro-scale within beds of 1 to 2 cm thick on units of about 50 cm thick. Because these crystals are found in a micritic matrix and the beds show planar laminations, and there are no records of *in-situ* selenitic deposits in the area of the Isle of Portland (only recorded at Durlston Bay, see below), the first model proposed by Sanz *et al.* (1994) could be applied to the Gypsiferous peloidal packstone found in this study. The only difference with this model is the non-occurrence of the gypsum-rich beds deposited prior the detrital gypsum beds in the Madrid Basin (Sanz *et al.*, 1994). This can be explained by the erosion of the entire gypsum-rich beds with all the gypsum crystals reworked and redeposited in the mudflat. As a consequence this facies is thought to have been deposited in a protected mudflat of a saline lake with episodic floods eroding gypsum-rich beds, reworking and redepositing almost *in-situ* the gypsum crystals.

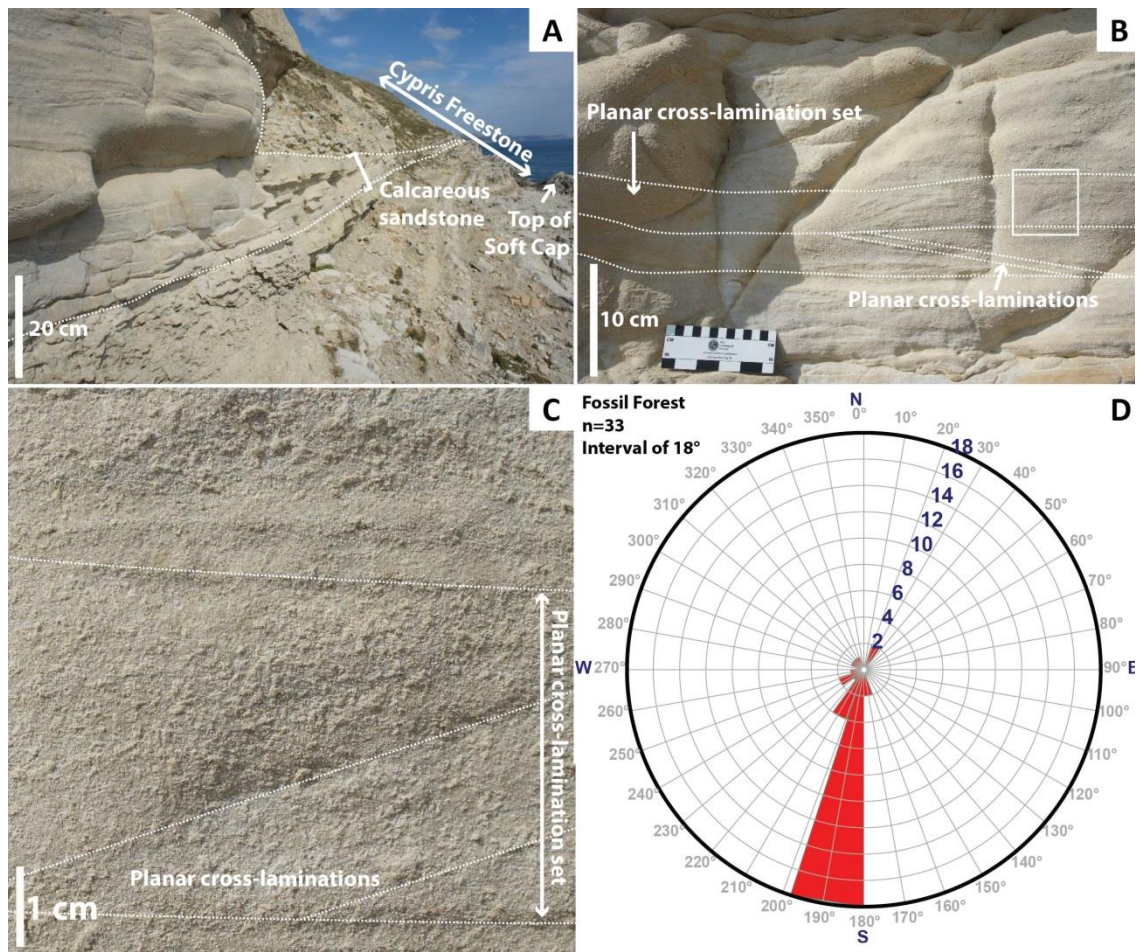
## 7. Calcareous sandstone facies

### 7.1. Description

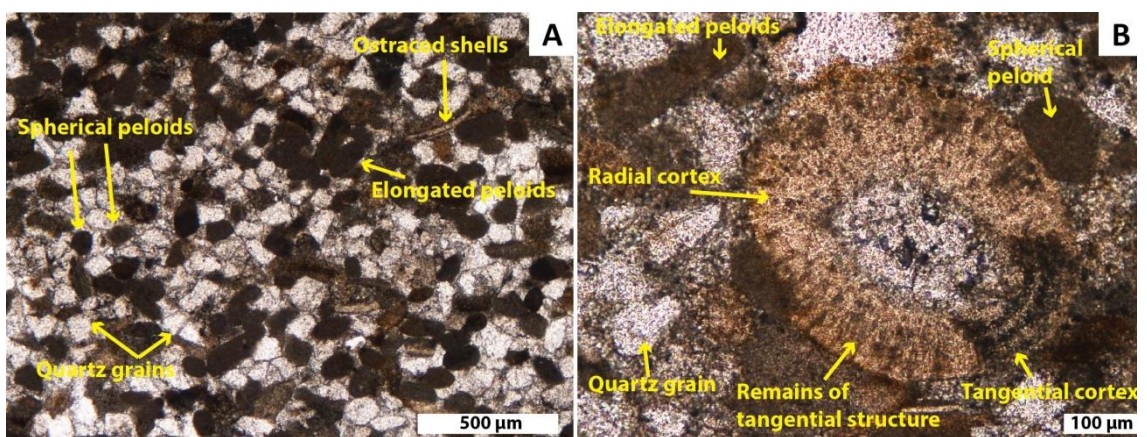
This facies is found within beds in the Cypris Freestone unit ranging between 30 and 80 cm thick (Fig. 4.40A). These beds disappear laterally to the west as they are present only in West Lulworth Cove, Fossil Forest, Mupe Bay and Worbarrow Tout locations. Their absence can be explained because of non-deposition or lack of outcrop.

At the macroscale this facies exhibits planar cross-laminations organised in sets ranging between 1 and 6 cm in thickness (Fig. 4.40B-C). This facies has a yellow to beige colour both at the outcrop and when broken. 33 measurements of orientation of cross-laminations were done at Fossil Forest where this bed is particularly well exposed and they reveal one main direction at 190° (Fig. 4.40D).

At the microscale this facies is characterised by more than 50% of angular, well sorted silt and sand size (Wentworth, 1922) of transparent crystals ranging in size from 20 and 400 µm (with about 70% of grains between 60 and 150 µm, predominantly very fine sand size, Fig. 4.41). Those crystals have a straight extinction and first order colours (shades of grey) in XPL and are surrounded by equigranular microspar cement (Fig. 4.41). Sub-angular to rounded micritic peloids are the second most abundant grains in this facies (Fig. 4.41). They show elongated and spherical shapes and measure between 100 and 200 µm long and 50 to 100 µm wide (Fig. 4.41A). Few ostracod shell fragments are also present between 100 and 500 µm long (Fig. 4.41A). Only one mixed ooid was found (Fig. 4.41B) with a crystalline nucleus and brownish radial coating (Fig. 4.41B).



**Figure 4.40** Calcareous sandstone facies. A – Location of calcareous sandstone facies in the field within Cypris Freestone unit (Fossil Forest). B – Herring-bone cross-stratifications in this bed. White square locates C (Fossil Forest). C – Calcareous sandstone facies in details with abundant quartz grains (Fossil Forest). D – Orientation and direction measurements of the cross-laminations at Fossil Forest with 33 measurements.



**Figure 4.41** Calcareous sandstone microfacies. A – Quartz grains, elongated and spherical peloids, ostracod shells and calcite cement (WLC9, West Lulworth Cove). B – Close-up view of the ooid with change of the fabric in the same laminae from finely to coarsely radial calcite crystals, elongated and spherical peloids and quartz grains (WLC9, West Lulworth Cove).



## 7.2. Interpretation

The transparent crystals with a first order extinction are identified as quartz grains. The abundance of angular quartz grains (more than 50% compared to the next most abundant calcitic grain, peloids) suggests this facies was deposited not too far from a clastic supply into the system. This facies is found only in the relay ramp area as identified on seismic sections through the region (*i.e.* Lulworth Cove, refers to Chapter 3 and 7). The cross-bedded laminations, the sand size of the quartz grains together with the broken up ostracods indicate a high energy marginal lacustrine environment.

The peloids are rather bigger than in previous facies and show a preferential elongated shape (Fig. 4.41A) that suggests they may be faecal pellets (according to Bathurst, 1971 and Flügel, 1982).

The ostracods are not as abundant as in previous facies and are mainly found as fragments in this facies. The beds where this facies is found belong to the Cypris Freestone beds that were described previously to be within the *Cypridea dunkeri* subzone (Strahan, 1898; Barker *et al.*, 1975; Kilenyi and Neale, 1978; Anderson, 1967, 1973, 1985; Horne, 1995, 2002). Similar interpretation as for the Cross-bedded peloidal packstone-grainstone facies may be applied for the ostracods found in this facies. They are non-marine species (Horne, 2002) and are saline to hypersaline waters tolerant species (refer to Chapter 2) as they are mainly S-phase species found in the Cypris Freestone beds (Anderson, 1985).

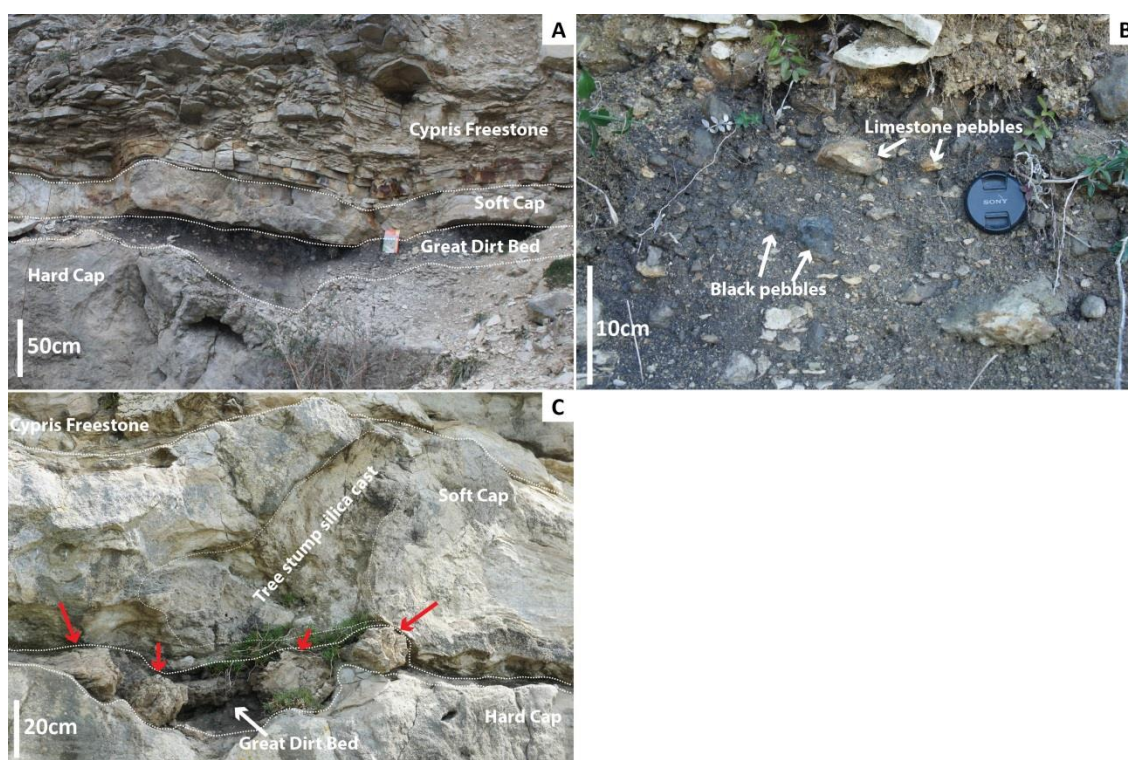
The mixed ooid found in this facies shows a crystalline nucleus that is thought to be microsparite of calcite (Fig. 4.41B). The change of crystal microstructures along the same laminae in the cortex suggests replacement of the fine into coarse radial fabric of the cortex (Fig. 4.41B). This is supported with the remains of fine fabric within the coarse radial fabric (Fig. 4.41B).

Measurement of orientation and direction of cross-laminations help to interpret palaeocurrent directions (as for the Intraclastic peloidal packstone-grainstone facies). The measurements in this facies show a main direction at N190 that reflects a northerly direction of palaeocurrents. This is concordant with the palaeocurrent directions interpreted from previous facies at West Lulworth Cove (refer to Chapters 6 and 7) and the consistency of the palaeocurrents suggests a possible fluvial system running down the slope of the relay ramp and bringing siliciclastic material from the adjacent footwall block into the lacustrine system.

## 8. Conglomerate facies

### 8.1. Description

This facies is exclusively found in the Great Dirt Bed (ranging between 1 and 50 cm, Fig. 4.42) throughout the studied area. The base and the top of this bed are irregular (Fig. 4.42A, C) and more pronounced at the base than at the top of the Great Dirt Bed. The bed has a carbonaceous marl (brown to black) matrix containing approximately 60-70% of angular white limestone pebbles ranging between 100  $\mu\text{m}$  and 25 cm (Fig. 4.42B) and angular black limestone pebbles ranging between 100  $\mu\text{m}$  and 15 cm (Fig. 4.42B). These pebbles present similar lithologies to those in the underlying Hard Cap bed (peloidal packstone-grainstone and microbialites). In addition fossil plant remains ranging between 1 and 5 cm, silicified logs about 15 cm long and 10 cm wide (Fig. 4.42C) and *in situ* silicified tree trunks with roots ranging between 10 and 50 cm in diameter (Fig. 4.42C) are commonly found in the Great Dirt Bed.



**Figure 4.42** Conglomerate macrofacies. A – Location of the Great Dirt Bed with conglomerate facies (Penn’s Weare, Isle of Portland). B – Conglomerate facies with black pebbles and limestone pebbles (South West Bowers, Isle of Portland). C – Silicified tree roots remains (red arrows) within the Great Dirt Bed and stump silica cast just above and in the Soft Cap (West Cliff, Isle of Portland).

## 8.2. Interpretation

The irregular base indicates an erosion phase of the underlying beds (*i.e.* the Hard Cap) prior to the deposition of this facies. The abundance of fossil plant remains and especially tree trunks found in live position with their roots in growth position are the most diagnostic features for the identification of this unit as a paleosol (Retallack, 1981, 2001; Francis, 1982, 1986). The carbonaceous matrix is due to the calcareous underlying beds degraded into carbonaceous marl during pedogenesis. This palaeosol was studied in detail by Francis (1983, 1984, 1986) as well as the fossil trees found rooted into it (refer to Chapter 2). She interpreted this paleosol to be a well-developed carbonaceous A/C rendzina soil profile and to have formed under semi-arid climate of Mediterranean type (refer to Chapter 2). Rendzina soil profiles observed in modern day environments are determined by the nature of the parent rocks rather than the climate (Francis, 1986). These are also found on Mediterranean limestones (Townsend, 1973), on Chalk in England (Townsend, 1973) or on coral limestones in the Seychelles (Lionnet, 1952).

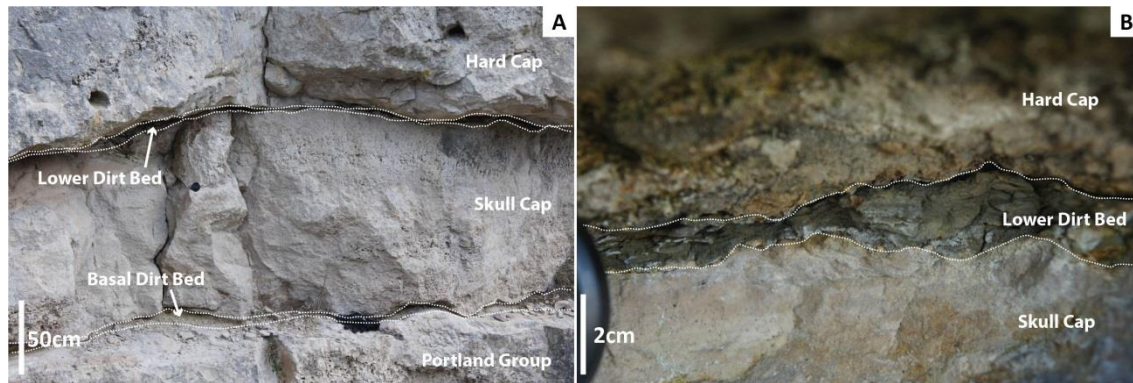
The black and white pebbles were also studied in detail by Francis (1982, 1983, 1986) and she described them as being made of the same lithologies and textures as the underlying Hard Cap bed (refer to Chapter 2). For this reason she interpreted these pebbles to have formed during the pedogenesis (refer to Chapter 2). In addition she noticed that the black colour is due to the presence of organic matter and that calcretes are often associated with black pebbles which are taken to be evidence for sub-aerial exposures (refer to Chapter 2). Similar pebbles can be observed in the rock record such as from the Purbeckian of Jura (Cotillon, 1960; Bläsi, 1980; Strasser and Davaud, 1983) as well as in modern day environment at Isla Mujeres, Quitana Roo, Mexico (Ward *et al.*, 1970; Francis, 1986).

## 9. Carbonaceous marl facies

### 9.1. Description

This facies is found only in Basal Dirt Bed (located between the Transition Bed and the Skull Cap bed) and the Lower Dirt Bed (located between the Skull Cap and the Hard Cap beds, Fig. 4.43A). These beds are present throughout the studied area with similar thicknesses ranging between 1 and 10 cm (Fig. 4.43) with an irregular base, although less pronounced than the Great Dirt Bed (Fig. 4.43). These brown to black carbonaceous marls exhibit dark planar to

undulated laminations (Fig. 4.43). Silicified logs, *in situ* silicified tree trunks and white limestone pebbles were found by Francis (1986).



**Figure 4.43** Carbonaceous marl macrofacies. A – Location of the Lower Dirt Bed and Basal Dirt Bed where the carbonaceous marl facies can be found (Tout Quarry, Isle of Portland). B – Close-up view on the Lower Dirt Bed, black and brown laminations can be seen (South West Bowers, Isle of Portland).

## 9.2. Interpretation

As with the Conglomerate facies, the Carbonaceous marl facies was studied in great detail by Francis (1982, 1986). Francis (1986) interpreted this facies to be a paleosol, however this interpretation was less straightforward than for the Great Dirt Bed (refer to Chapter 2). Francis (1986) also described tree stumps rooted in the Lower Dirt Bed but never observed these in the Basal Dirt Bed to confirm a palaeosol origin. The absence of large pebbles indicates that the underlying beds were not totally lithified before the pedogenesis (Francis, 1986). The high content of carbonate and the calcareous parent rocks show that these paleosols were immature probably compacted and eroded rendzina soil profiles (refer to Chapter 2).

## 10. Evaporite facies

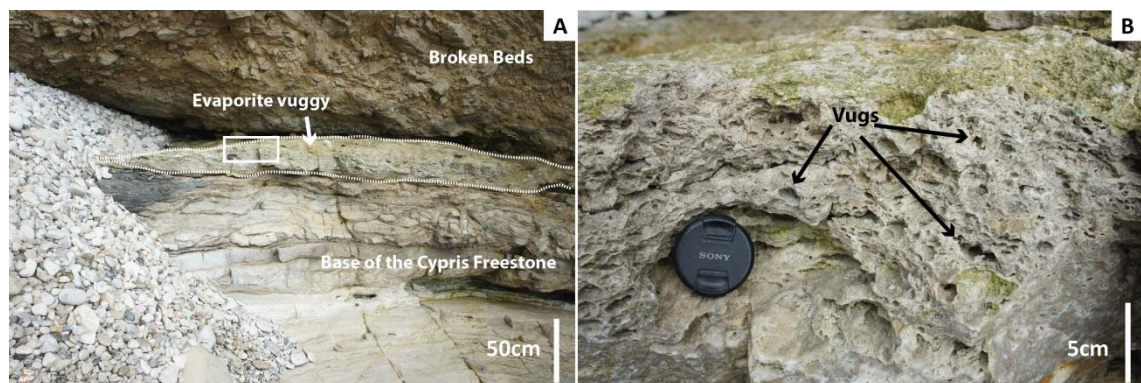
This facies is subdivided into two sub-facies, vuggy and breccia. The former is mainly present directly on top of the Soft Cap and at the bottom of the Cypris Freestone unit (Figs. 4.44A and 4.47A) from Lulworth area eastwards (refer to Chapter 6 for discussion) and is equivalent to the thick anhydrite deposits described by West (1975) in Portsdown well near Portsmouth further east (refer to Chapter 3). The latter lies directly above the Evaporite vuggy sub-facies when present at the bottom of the Cypris Freestone unit (Figs. 4.44A and 4.47A). These two sub-facies are closely related to each other as the Evaporite breccia sub-facies is present only when the Evaporite vuggy sub-facies is also present.

## 10.1. Vuggy sub-facies

### 10.1.1. Description

This sub-facies is found in beds ranging between 10 and 30 cm thick overlying the Soft Cap. At macroscale this sub-facies appears crystalline with irregular planar laminations and mm to cm unfilled vugs (Figs. 4.44B and 4.45C). Chert spherules ranging between 5 and 10 cm are often found in this sub-facies (Figs. 4.45A, B and 4.46E, F) and the beds can be locally, entirely silicified. This sub-facies appears white, yellow to beige at the outcrop and white to beige when broken.

At microscale the texture is crystalline with rare microcrystalline dark laminae (Fig. 4.45C). The crystals are calcite crystals ranging between 40  $\mu\text{m}$  and 1 mm with different morphologies (Fig. 4.45). The small crystals (40-100  $\mu\text{m}$ ) form an anhedral mosaic cement (Fig. 4.46) and are bright orange, and sometimes zoned, under CL (Fig. 4.46). The large crystals (100  $\mu\text{m}$ -1 mm) have prismatic shapes more or less elongated with triangular extremities and have a first order straight extinction in XPL (Fig. 4.45B) and are non-luminescent under CL (Fig. 4.45E-F) interpreted as quartz crystals. At Durlston Head only, crystals occur that have a euhedral elongated shape between 100  $\mu\text{m}$  and 2 mm long and 30 and 200  $\mu\text{m}$  wide (Figs. 4.45E and 4.46A-D) and a first order colours in XPL and non-luminescent under CL (Fig. 4.46A-D) interpreted as Celestine crystals. Vugs are also abundant ranging between 200  $\mu\text{m}$  and 2mm and as observed at macroscale are unfilled (Fig. 4.46A-D). The only clasts found in this sub-facies are very rare and are intraclasts either with a peloidal packstone-grainstone or a clotted microfabric (Fig. 4.45E).



**Figure 4.44** Evaporite vuggy macrofacies. A – Location of the evaporitic beds below the Broken Beds, white box locates B (Worbarrow Tout). B – Close-up view on A, note the vugs up to 1cm in diameter (Worbarrow Tout).

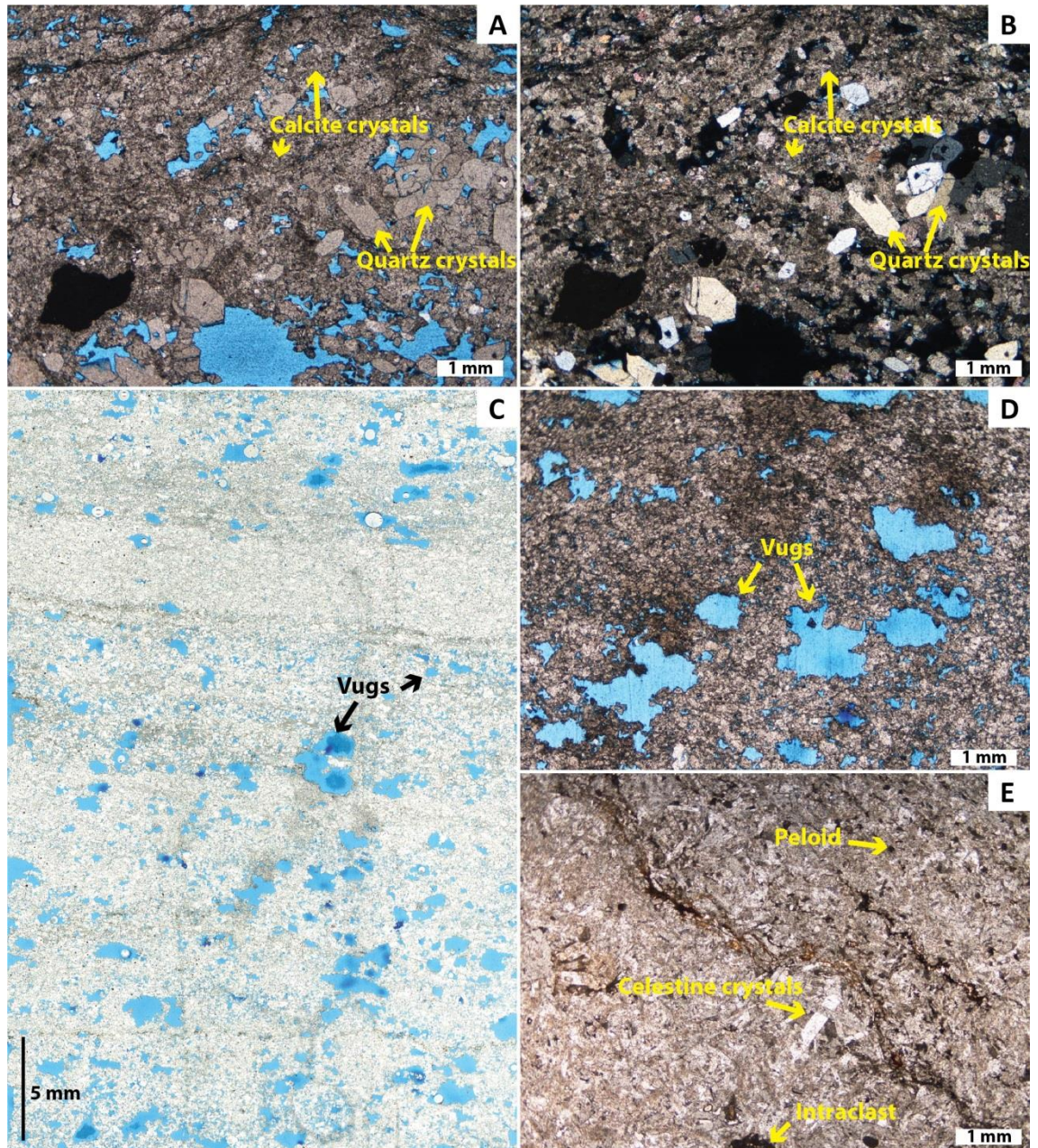
### 10.1.2. Interpretation

The small calcite crystals composing the mosaic cement are most likely a diagenetic calcite formed after neomorphism of a precursor.

The large prismatic calcite crystals are likely to be prismatic anhydrite crystal pseudomorphs replaced by calcite as suggested by West (1964, 1975). West (1964) presented evidence for a secondary calcite in replacements of anhydrite as chert spherules after anhydrite, a “net-texture” (anhedral crystalline cement) and ghosts of anhydrite crystals are commonly found.

The large prismatic crystals with a first order extinction (Figs. 4.45A-B and 4.46E-F) are euhedral quartz crystals replacing either gypsum or anhydrite (West, 1964) which are commonly found associated with or replacing evaporites (Hanor, 2000, 2004).

The vugs found at macro- and micro-scale in this sub-facies are likely to be dissolution vugs commonly occurring in evaporitic deposits from dissolution of anhydrite or gypsum spherules (Warren, 2006). Such dissolution vugs are formed in brackish water lakes where the more freshwater circulate into the evaporitic sediments and dissolve away gypsum or anhydrite crystals leading to the creation of vugs and sometimes pipes (Lowenstein and Hardie, 1985; Warren, 2006).

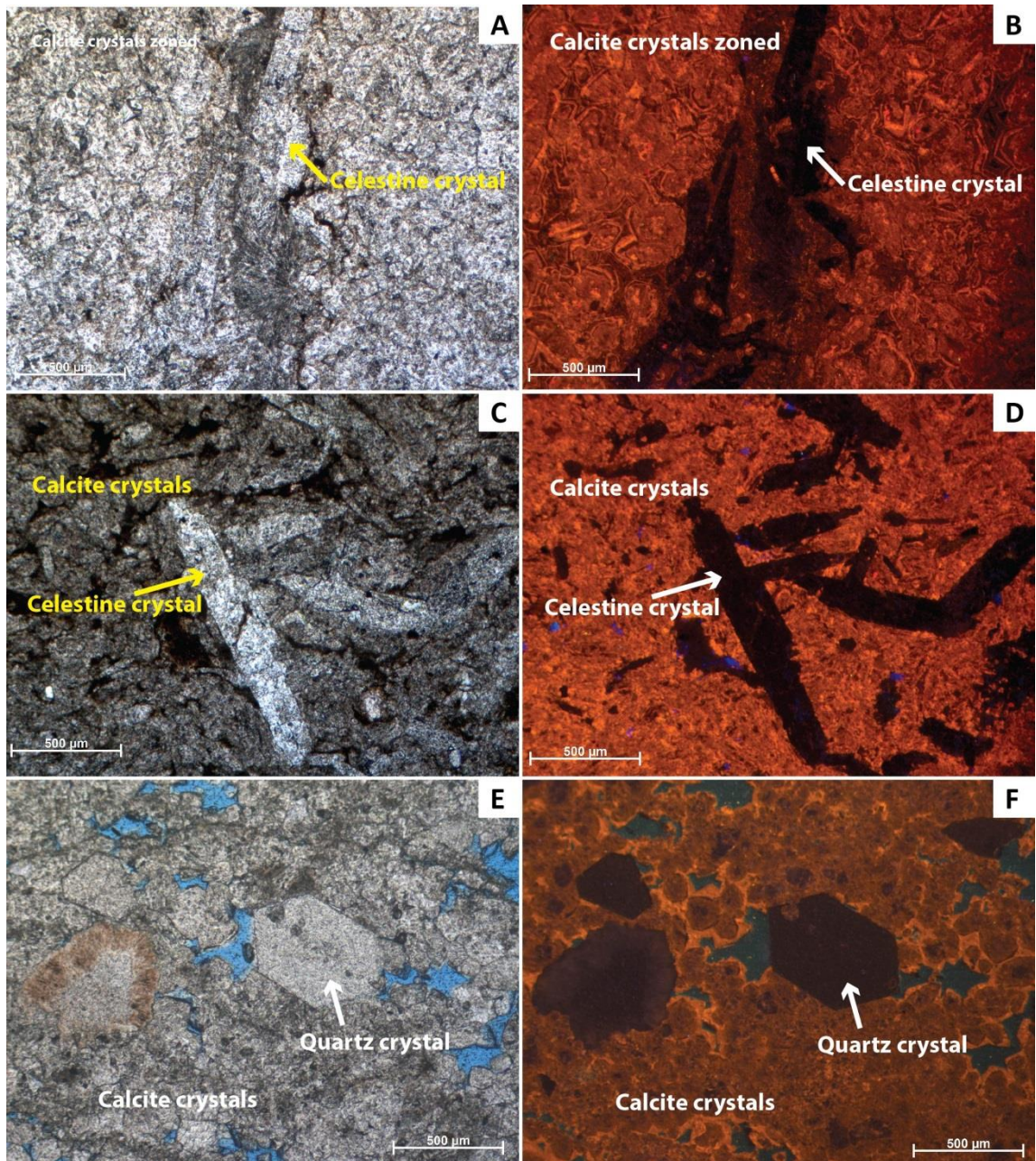


**Figure 4.45** Evaporite vuggy microfacies. A and B – Quartz crystals (between 500  $\mu\text{m}$  and 1 mm and first order colour with straight extinction in XPL) and calcite crystals (WT8). C – Thin section scan (partial) with 1-2 mm vugs in a crystalline texture (MB11). D – mm vugs in a crystalline (calcite) texture (MB11). E – Celestine crystals with few microbial intraclasts and peloids (DH1).

The crystals found mainly at Durlston Head were also found and described by West (1960) as celestine crystals. Celestine ( $\text{SrSO}_4$ ) is a common but minor diagenetic mineral in modern and ancient shallow marine (Wood and Shaw, 1976; Olausson, 1981; Boyce *et al.*, 1990; Scholle *et al.*, 1990) and lacustrine environments (Murdock and Web, 1940; West, 1960; Andrew and Collins, 1991) and is known to form massive ore bodies (De Brodtkorb, 1989; Scholle *et al.*, 1990; Taberner *et al.*, 2002; Hanor, 2004; García-Veigas *et al.*, 2015). Celestine crystals precipitate following the reaction between hypersaline strontium-rich waters and gypsum and/or anhydrite crystal deposits (Hanor, 2000). Celestine is known to be precipitated following two main mechanisms: a syngenetic mechanism with precipitation of primary crystals from evaporated seawater (Müller and Puchelt, 1961; Müller 1962; De Brodtkorb *et al.*, 1982) or an epigenetic mechanism with replacement of a carbonate or evaporitic precursor (Carlson, 1987; Scholle *et al.*, 1990; Hanor, 2000, 2004; García-Veigas *et al.*, 2015). In the case of the Purbeck Limestone Group, the celestine-bearing beds are sandwiched between lacustrine deposits (underlain by the Soft Cap and overlain by the Cypris Freestone) detailed in previous sections of this chapter, so a marine seawater rich in strontium origin is unlikely to have reacted with evaporites and most probably there were Sr-bearing lacustrine waters (as suggested by West, 1960). West (1960) argued for a syngenetic origin of the celestine crystals due to the common euhedral crystal shape, the distribution of the celestine crystals only in few beds between 10 and 30 cm thick in the basal Purbeck and the lenticular aspect of these celestine beds. Moreover the absence of evidence for replacement from an evaporitic precursor (ghosts of gypsum or anhydrite) and the large area of occurrence of celestine (at least until Mountfield Mine in Sussex, West, 1964) confirm the syngenetic origin proposed by West (1960). However, strontium isotope analyses are needed to distinguish between an origin from hypersaline fluids or an epigenetic origin (Hanor, 2004).

The planar laminations might indicate a low-energy environment also highlighted by the microcrystalline laminae. The evaporite pseudomorphs and vugs suggest hypersaline water conditions most probably in a lacustrine environment.



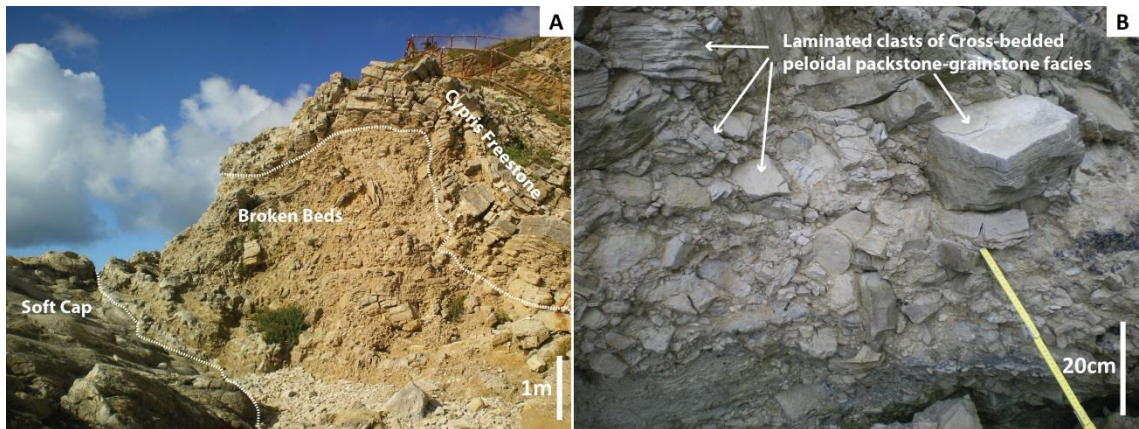


**Figure 4.46** CL images of Evaporite vuggy sub-facies. A – Crystalline microfabrics made of calcite and celestine crystals (DH6). B – CL image of A showing the zoned calcite crystals and non-luminescent celestine crystals (DH6). C – Crystalline microfabrics made of calcite and celestine crystals (DH5). D – CL image of C showing the non-zoned calcite crystals and non-luminescent celestine crystals (DH6). E - Crystalline microfabrics made of anhedral calcite and euhedral quartz crystals (WT8). F – CL image of E showing zoned calcite crystals and non-luminescent euhedral quartz crystals (DH6).

## 10.2. Breccia sub-facies

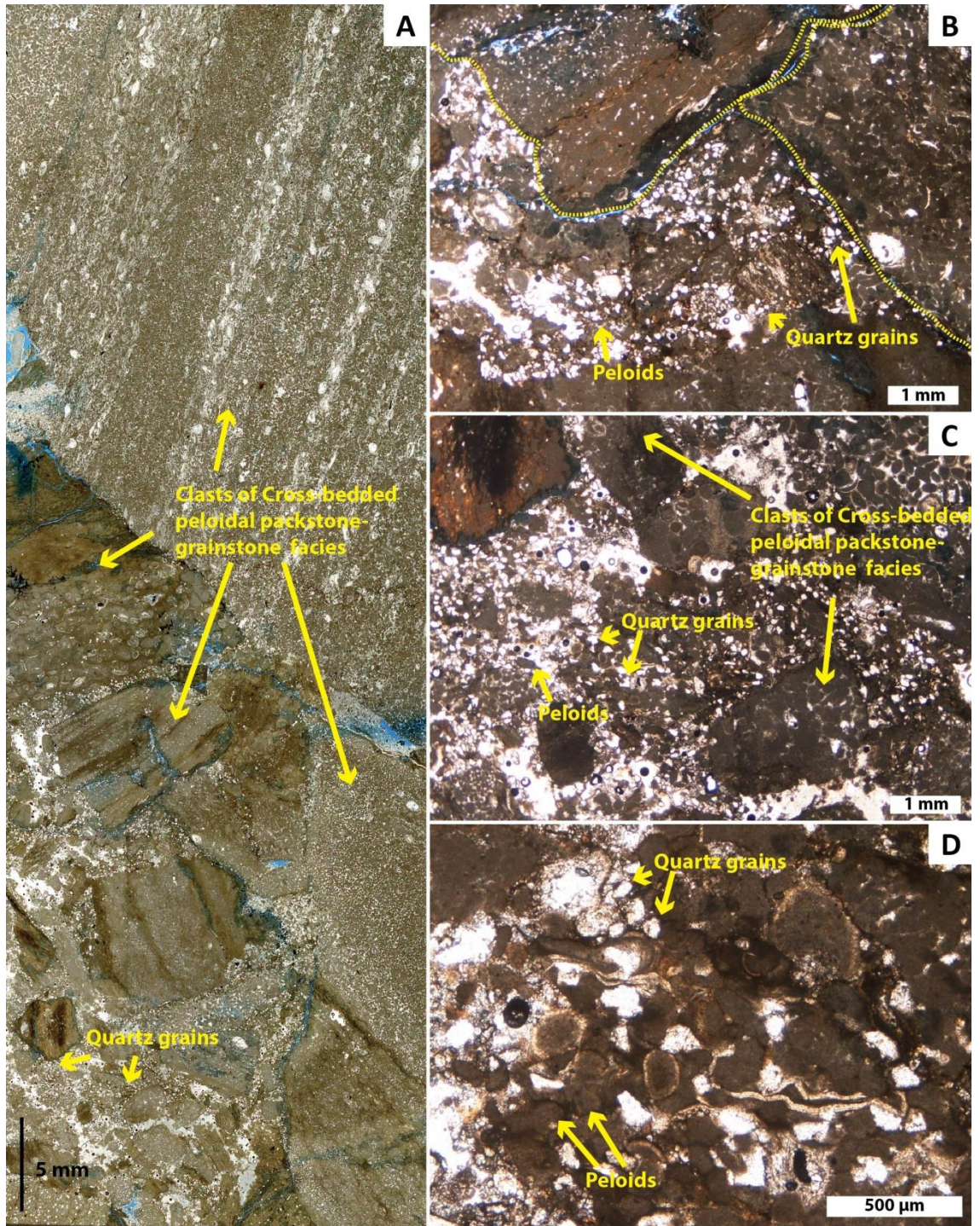
### 10.2.1. Description

This sub-facies is mainly present from the Lulworth area eastwards and is locally known as the Broken Beds. This sub-facies is a massive unit and its thickness ranges between 1 and 5 m while its lateral extent at outcrop is between 2 and 10 m. This sub-facies is composed of large angular clasts of very coarse sand to boulder size some of which are interlocking shapes (Figs. 4.47B and 4.48A; Wentworth, 1922). The clasts are made of the laminated beds from the base of Cypris Freestone unit (described in section 4 of this chapter, Fig. 4.47B). This sub-facies exhibits a wide range of colours due to the range of clasts but it is yellow, white to beige both at the outcrops and when broken.



**Figure 4.47** Evaporite breccia sub-facies. A – Location of the Broken Beds unit with the brecciated facies (Fossil Forest). B – Close-up view on the Broken Beds made of pluricentimetric blocks (West side of Lulworth Cove).

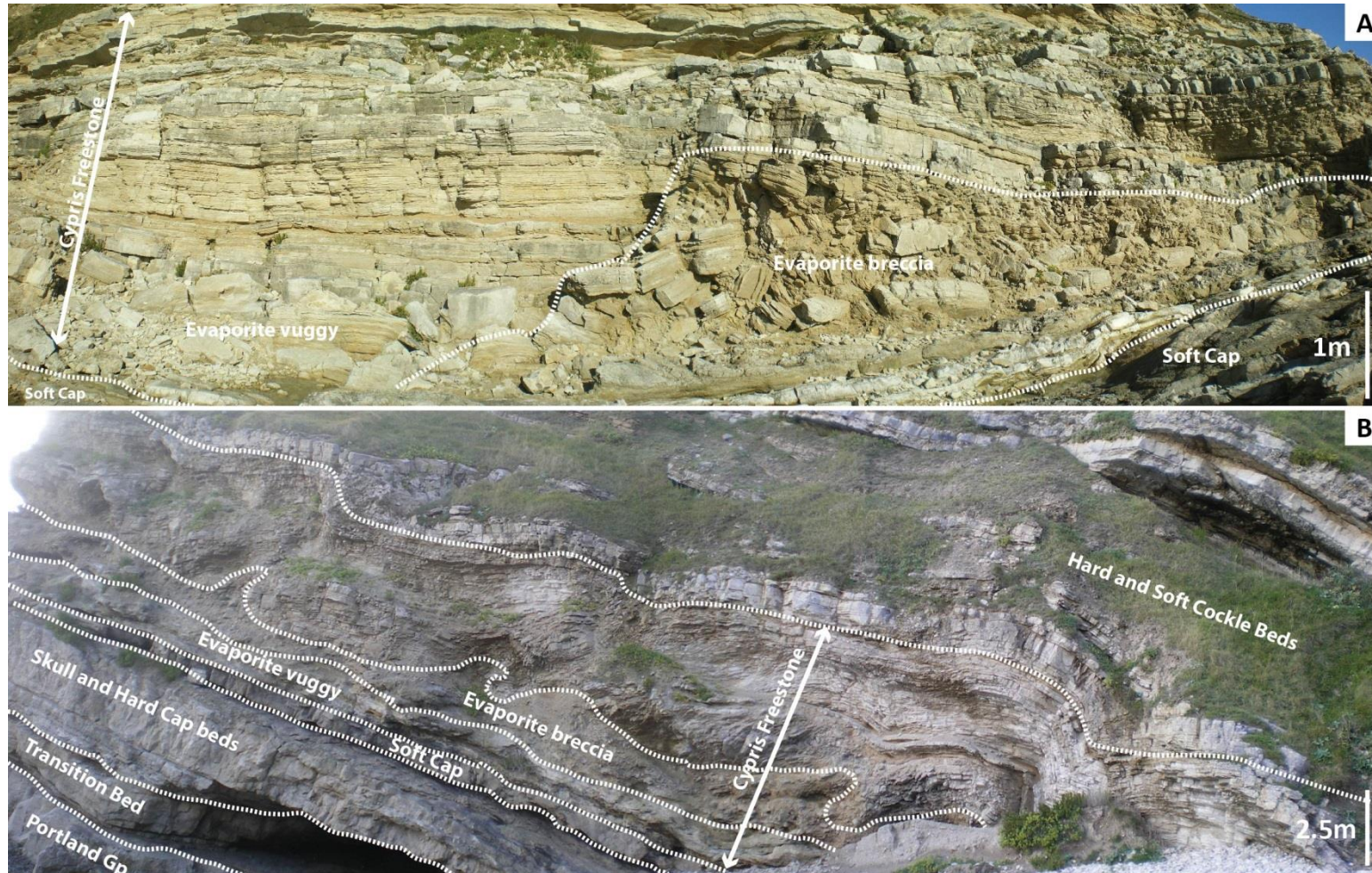
At microscale the layered large clasts are made of the Cross-bedded peloidal packstone-grainstone facies microfabric (detailed in section 4 of this chapter, Fig. 4.48). These large clasts are contained within a matrix of peloidal grainstone with some quartz grains (Fig. 4.48). The peloids are rounded, micritic and range between 10 and 200  $\mu\text{m}$ , fine silt to fine sand size. The quartz grains are angular, present a first order colour in XPL and of silt size, between 4 and 10  $\mu\text{m}$ .



**Figure 4.48** Evaporite breccia microfacies. A – Thin section scan showing large clasts of Cross-bedded peloidal packstone-grainstone facies (WLC7, West Lulworth Cove). B – Close-up view on A, the matrix is composed of quartz grains and peloids (WLC7, West Lulworth Cove). C – Close-up view on A, smaller blocks can be identified within a matrix made of quartz grains and peloids. D – Close-up view on C detailing the matrix (WLC7, West Lulworth Cove).

### 10.2.2. Interpretation

A lot of debate and discussion (reviewed in Chapter 2) over the origin of this facies has taken place since its first description (Fisher, 1856). This breccia occurs locally at the bottom of the Cypris Freestone unit (Figs 4.47A and 4.49A) and in the vicinity of the Purbeck extensional Faults. The base of the Cypris Freestone unit is characterised by the Evaporite vuggy sub-facies beds (described in the previous section) that could have been partially dissolved after their deposition by circulation of freshwater, resulting in a collapse breccia (Figs. 4.47A and 4.49A). These units (undisturbed Cypris Freestone and collapse breccias) could have been modified by later tectonic events (possibly during the Cenozoic Alpine inversion) as suggested by the folded structures observable in Mupe Rocks Cove (Fig. 4.49B) orientated northwards so towards the faults. The remaining evaporites could have acted as a *décollement* surface. West (1960; 1964; 1975) and D'el-Rey Silva (2001) interpreted this breccia to be the result of a combination of both tectonic and diagenetic events. They proposed that the dissolution of part of the Evaporite vuggy sub-facies beds (described in the previous section) resulted in a collapse breccia that was reworked by later tectonic movements later on. All the arguments presented in this study confirm West's (1960; 1964; 1975) and D'el-Rey Silva's (2001) interpretations. Similar structures were identified in the Madison Limestone of the Bighorn Basin in Wyoming and Montana, USA (Sonnenfeld, 1996).



**Figure 4.49** Large scale field view of the Evaporite breccia sub-facies. A – Laterally and abruptly facies change from *in situ* Cypris Freestone beds on the left to the Evaporite breccia sub-facies on the right (Fossil Forest). B – Folded structures orientated northwards (towards the faults) suggesting tectonic movement post-deposition with the Evaporite breccia sub-facies at the base of the folds (Mupe Bay).

## 11. Summary

This chapter provides the description and palaeoenvironmental interpretations of nine facies identified in the Mupe Member of the Purbeck Limestone Group of south Dorset. The Microbialite facies composed of the Stromatolite, Thrombolite and Burrowed peloidal packstone sub-facies is closely associated with the Intraclastic peloidal packstone-grainstone facies and are exclusively found in the Skull, Hard and Soft Cap beds in the lower part of the Mupe Member. These facies are interpreted to represent shallow water deposits formed on the margins of a brackish water lake. These Cap beds are interbedded with the Carbonaceous marl and Conglomerate facies of the Basal, Lower and Great Dirt Bed paleosols, that were interpreted by Francis (1982, 1983, 1984, 1986) to be Rendzina paleosols developed under semi-arid climate Mediterranean type with cycadophytes and, sometimes rooted, ancient conifers (*Protocupressinoxylon purbeckensis*). The Cross-bedded peloidal packstone-grainstone facies constitutes the main facies of the Cypris Freestone beds and is interbedded with the Gypsiferous peloidal packstone and Calcareous sandstone facies. Together these facies were formed in a hypersaline shallow lacustrine margin environment. The Evaporite facies was subdivided into Vuggy and Breccia sub-facies and is locally found at the base of the Cypris Freestone beds. These facies were interpreted to represent shallow water deposits on a margin of a hypersaline lake. The Wackestone to fine grainstone facies is exclusive to the Transition Bed locally deposited at the bottom of the Mupe Member and was interpreted to represent deeper water deposits in a brackish water lake.

Facies transition analyses have been undertaken to better understand the relationships between the facies presented in Chapter 6. Subsequently this analysis is used to define a sequence stratigraphy and to create facies models for the Mupe Member presented in Chapter 6. Finally, these facies together with the tectonic settings (refer to Chapter 3) are used to create tectono-sedimentary models for the lower part of the Mupe Member presented in Chapter 7.

## Chapter 5

Microbial mounds;

Occurrence, size, shape,  
and relation to inter-mound  
facies

## 1. Introduction

The previous chapter presented the facies of the lower part of the Mupe Member and their interpretation. This chapter will focus on two important facies and their relationships; the Microbialite facies (composed of stromatolite, thrombolite and burrowed peloidal packstone sub-facies) and the Intraclastic peloidal packstone-grainstone facies. As described in the previous chapter the Microbialite facies is the main facies constructing the mounds (*i.e.* microbial mounds). These mounds are surrounded by an inter-mound facies, the Intraclastic peloidal packstone-grainstone facies.

Lidar (Light Detection and Ranging) scans were undertaken to image 2-D mound morphologies and sizes of the Skull and Hard Cap in seven quarries on the Isle of Portland (Fig. 5.1 and Tab. 5.1): King Barrow Quarries, Bower Quarry, South West Bowers, Coombefield Quarry, Freshwater Bay, God Nore and Sand Holes. These locations were chosen for their quality of outcrop, easy accessibility and to ensure good coverage of a range of spatial variations (from north to south and east to west) of mound shapes, sizes and distribution. Over the Isle of Portland the uppermost layer of mounds in the Soft Cap bed is poorly exposed and exhibits mounds only locally (refer to Chapter 6). As a consequence the Skull and Hard Cap beds were the main targets of the surveys while one survey of the top surface of the Soft Cap was undertaken in King Barrow Quarries.

The integration of qualitative field geology is essential to characterise more precisely mound shapes and sizes and relationships between mound and inter-mound facies both in 2-D and 3-D. The appraisal of the 3-D is only possible locally when the surfaces of the mounds are exposed. This is case at Portland Bill (Isle of Portland) where some mounds of the Skull Cap are exposed in 3-D; on the east side of Lulworth Cove where three mounds of the Hard Cap are exposed in 3-D; and at Fossil Forest, King Barrow Quarries (Isle of Portland) and Mutton Cove (Isle of Portland) where lots of mounds of the Soft Cap are exposed in 3-D.

Scan names	Coordinates (Lat.; Long.)	Number of scan positions	Original number of points	Number of points interpreted	Length	Maximum height
King Barrow Quarries	50°33'22.42"N; 2°26'10.00"W	2	9,450,520	9,450,520	30 m	5.5 m
Bowers Quarry	50°32'46.78"N; 2°26'44.78"W	6	25,672,756	6,338,663	415 m	9 m
South West Bowers	50°32'40.06"N; 2°27'10.56"W	5	26,153,732	7,746,377	200 m	6 m
Coombefield Quarry	50°31'58.25"N; 2°26'33.65"W	5	26,043,156	4,269,999	255 m	8.5 m
Freshwater Bay	50°31'51.24"N; 2°26'14.83"W	4	29,330,748	14,024,845	75 m	6 m
God Nore	50°31'31.41"N; 2°26'22.51"W	7	36,305,813	20,277,046	230 m	7.5 m
Sand Holes	50°31'22.42"N; 2°26'34.58"W	5	32,486,206	7,534,676	150 m	7 m

**Table 5.1** Locations and characteristics of lidar point clouds from north to south.



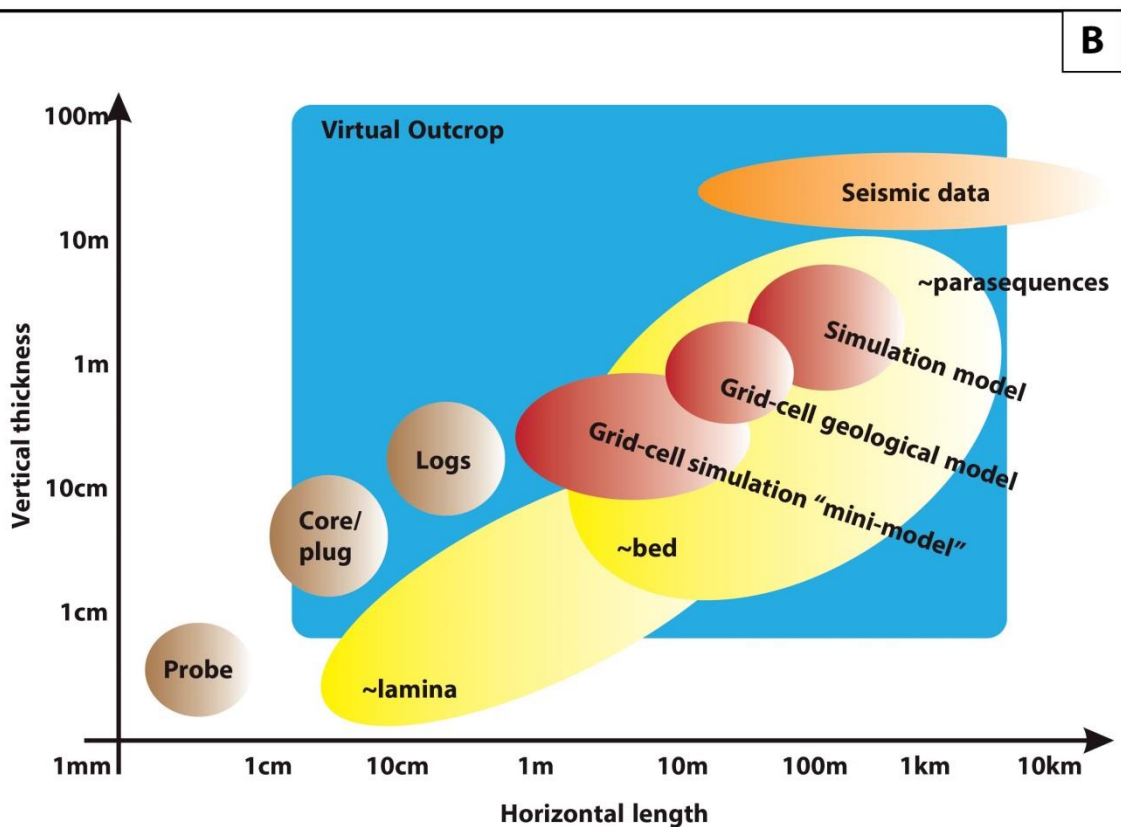
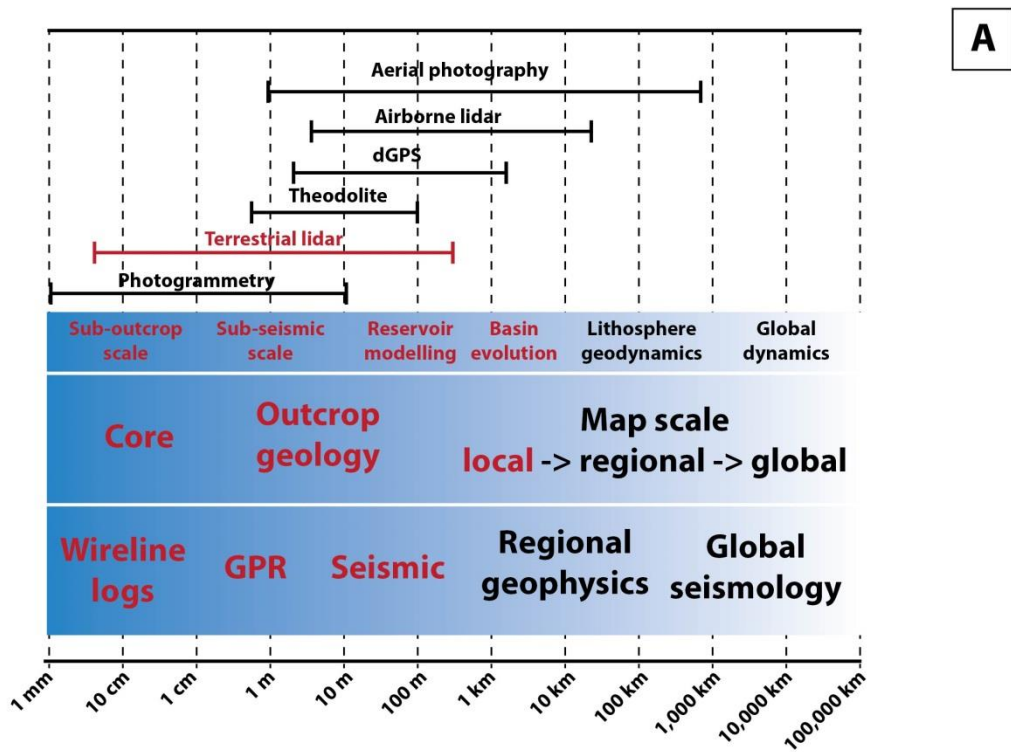


**Figure 5.1** Location map of the lidar surveys acquired on the Isle of Portland (south Dorset). Map © 2016 GoogleEarth.

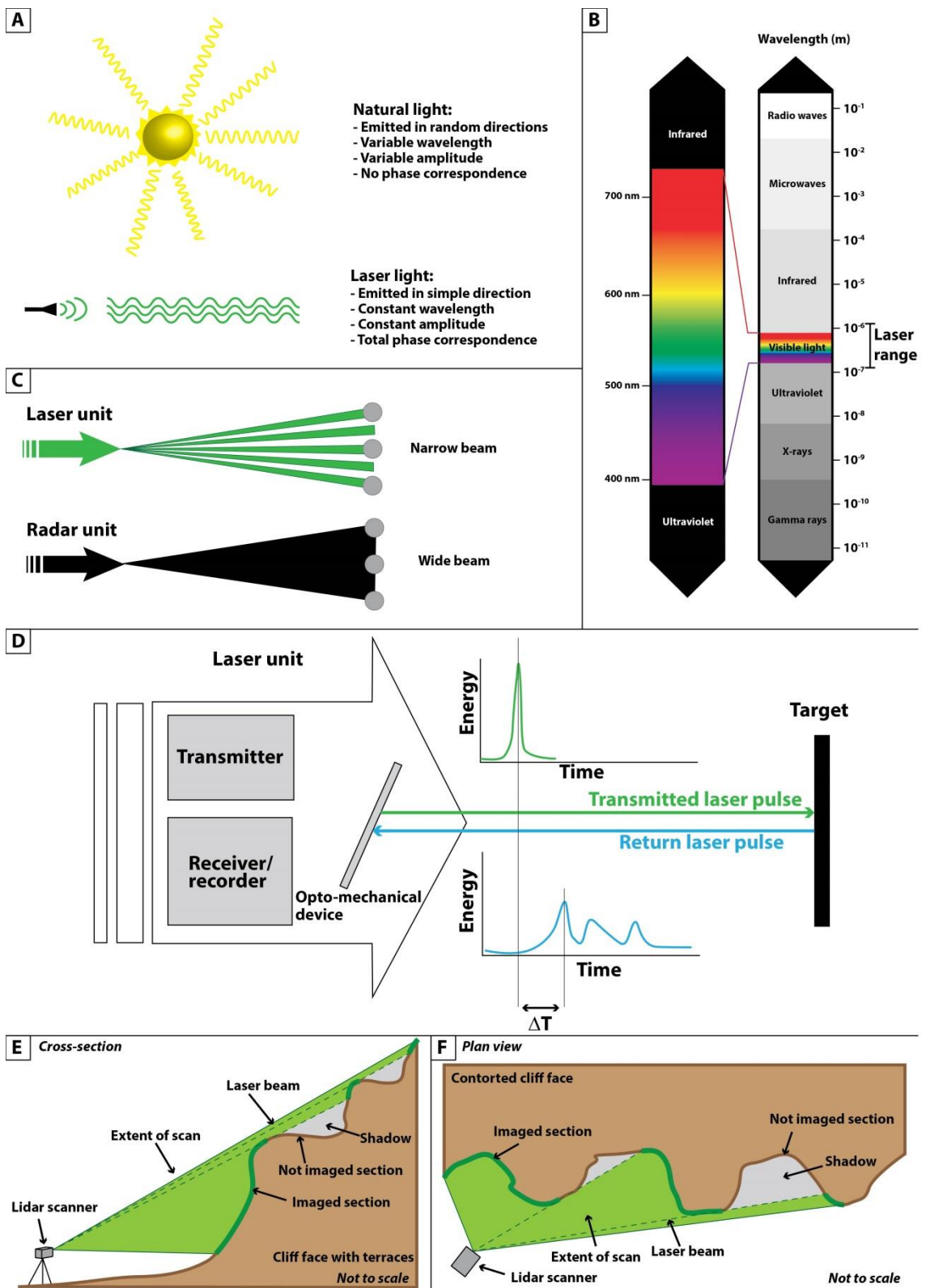
## 2. Methodology

### 2.1. Light detection and ranging (lidar) principle

A wide range of imaging techniques can be used to digitise outcrops depending on the scales of geological objects under study (Fig. 5.2). Figure 5.2 highlights the importance of terrestrial lidar (Light Detection And Ranging) system as it allows imaging of geological objects from sub-outcrop to reservoir model scales (Hodgetts, 2013). The lidar system is a remote sensing technique and has become very popular over the last few years in petroleum geoscience in the modelling of reservoir analogues (Hodgetts, 2013). This system is a relatively quick method to acquire 3-D data in the field and can be coupled with traditional techniques such as sedimentary logs or geological mapping (Hodgetts, 2013). In addition the technique can also be coupled to a wide range of digital data (multispectral and hyperspectral imagery or ground penetrating radar) and different attributes of the rocks and the rock surfaces can be imaged (intensity, colour, dip, azimuth, co-linearity, co-planarity, etc... Hodgetts, 2013). The principle of lidar is simple and based on reflectivity (scattered light) of laser (Light Amplification by the Stimulated Emission of Radiation) beams off rock surfaces (Heritage and Large, 2009). Laser beams are emitted from a transmitter and recorded on an adjacent receiver/recorder (Fig. 5.3; Heritage and Large, 2009). As photons travel at constant velocity (speed of light), the scanner records the time difference ( $\Delta T$ ) between emission and reception of the laser beams and calculates the distance of the target from the equation  $d = ct/2$  (where  $d$  = distance;  $c$  = speed of light; and  $t = \Delta T$ ; Fig. 5.3). The advantage of using laser light is that, unlike natural light (*i.e.* sunlight), laser beams are emitted in a unique direction with a narrow divergence beam enabling measurements of small scale objects (Fig. 5.3). With such laser beams the energy frequency and wavelength are stable and coherent giving relatively accurate data (Heritage and Large, 2009). The emitted laser beams are backscattered and modified by rock surfaces dependant on the distance and rock properties (Heritage and Large, 2009). One of the main issues though is, that because the beam is unidirectional, shadows are frequent due to uneven surfaces and appear in the point cloud (Heritage and Large, 2009). The best solution to avoid those shadows is to realise numerous surveys with different positions along the outcrops/rock surfaces to obtain continuous point clouds. If shadows happen laterally (*i.e.* horizontally), the position of the scanner needs to be shifted all along the outcrop to cover the maximum scanned area. However if shadows happen vertically, airborne lidar are essential to avoid this problem (Heritage and Large, 2009). In this study relatively flat vertical quarry faces were surveyed therefore the scanner only needed to be moved laterally along the outcrops.



**Figure 5.2** Comparison of size of geological objects, processes and imaging technologies. A – Technologies easily applicable to research projects. Note in red the application of terrestrial lidar and the typical size of geological features relevant to this study (redrawn after Hodgetts, 2013). B – Typical size of sedimentary structures and usual measurement techniques and reservoir models (redrawn after Enge *et al.*, 2007).



**Figure 5.3** Main characteristics of laser light (modified after Heritage and Large, 2009). A – Comparison of natural and laser lights. B – Electromagnetic spectrum and respective wavelength. Note the laser range extent from low frequencies of infrared to high frequencies of ultraviolet and including visible light wavelengths. C – Comparison of laser beam and radar beam. Note that with laser the beam is narrower and allow imaging of smaller objects than with the wider radar beam imaging bigger objects. D – Principle of lidar scanner (see text for explanation). E and F – Illustration of the shadow issue vertically (E) and horizontally (F).

## 2.2. Point clouds

### 2.2.1. Acquisition with Leica ScanStation C10

In this study the targets consist of vertical quarry faces between about 1 and 9 m high either without or with very few quarrying terraces. As a consequence terrestrial lidar was used as vertical shadows were not an important issue. The seven surveys were done in collaboration with Professor Ken McCaffrey and Doctor Vishal Bandugula from Durham University with a Leica ScanStation C10 (Fig. 5.4) over a week in July 2013. This scanner model contains a green pulsed laser with a wavelength of 532 nm that allows scanning from a distance between 0 and 300 m away from rock faces (best resolution between 0 and 50 m away) of up to 50,000 points/sec with a maximum horizontal and vertical resolution down to less than a millimetre. This scanner procures a field-of-view of 270° vertically and 360° horizontally and was mounted on top of a tripod to ensure its stability. Each scan position was recorded using a GPS into WGS 84 UTM Zone 30N coordinate system with less than 1 cm error. This accuracy was achieved because of the close location of the Portland Bill ground control station (Royal Air Force base, 50°30'56.24"N; 2°27'31.25"W).

During scans, high resolution images were taken by an in-built camera (1920x1920, 4 megapixels) and registered full 360° (horizontal) x 270° (vertical) hexagonal photographs. In each location several scans were necessary to avoid the shadow issue described above. The exact number dependant on the length of outcrops and sinuosity of rock faces in order to obtain one single point cloud for each location, exact geo-localisation between each scan position was essential. Local triangulation of the scanner was performed for each scan position by scanning in first instance three reflectors placed around the outcrop (Fig. 5.4). This triangulation allows the scanner to know where it is located in space compared to the last scanning position. This is essential in order to combine the different point clouds recorded at each position into one single point cloud. When the scanner was moved, ideally the triangulation had to be done with the reflectors at the exact same position. However commonly one or two reflectors were not reachable by the scanner due to topography. In such situation one or two reflectors needed to be moved, trying to keep at least one target at the exact same location as for the previous scan in order to increase the accuracy of the triangulation. Following the triangulation two types of scans were performed for each scan position. A low resolution scan covering 360° horizontally and a high resolution scan covering the actual rock face to be later interpreted in great detail.

Subsequently the point clouds were post-processed by Ken McCaffrey and Vishal Bandugula at Durham University. They assembled the different geo-referenced point clouds acquired at each scan position to create one single file for each location. In addition they textured the point clouds by assigning each point to the corresponding RGB colour value determined from the photographs. Ultimately they created projects with RiscanPro software (© 2005 RIEGL LMS GmbH) that was used for the cleaning and interpretation of the data by the author at RHUL (see below).

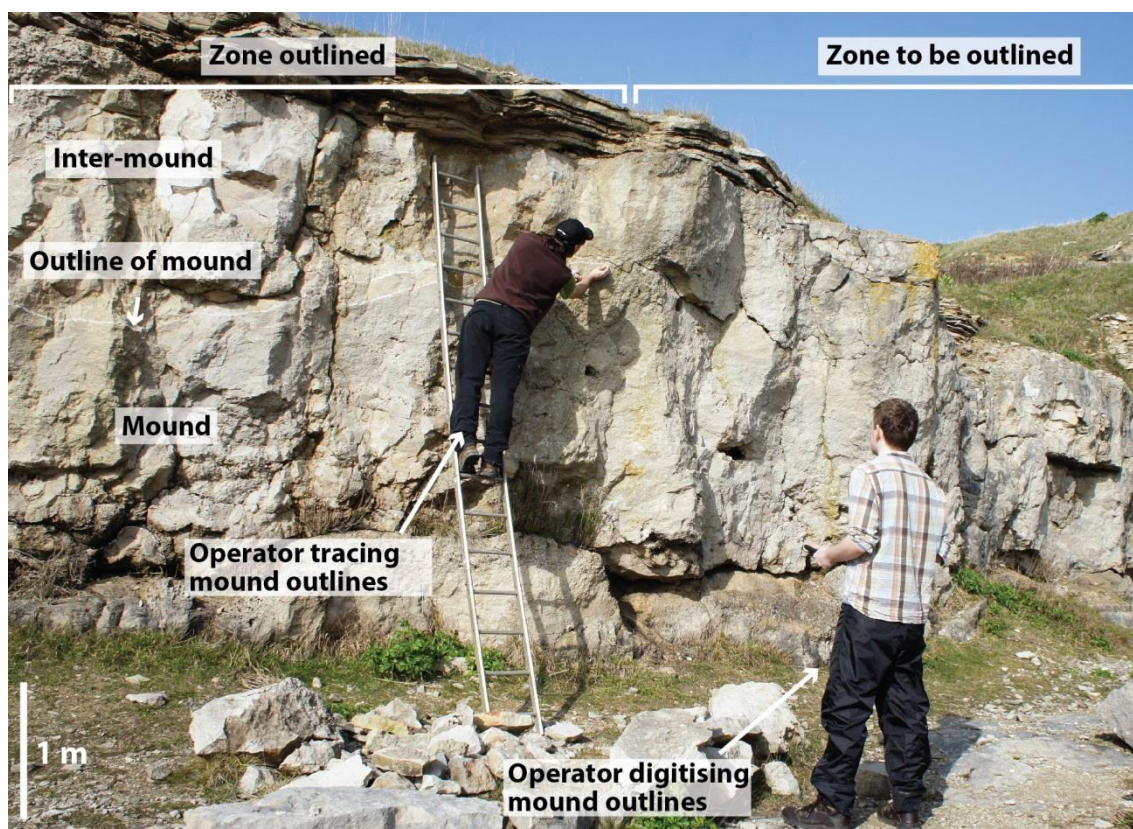


**Figure 5.4** Lidar scanner characteristics. A – Details of the Leica ScanStation C10. B – Detail of one reflector used for the triangulation. C – Example of triangulation at Freshwater Bay.

### 2.2.2. Workflow for interpretation

In order to interpret the point clouds to obtain areas of the inter-mound facies as well as perimeters, areas, heights and widths of 2-D cross-sectional views of 3-D mounds, a rather complex and long workflow had to be followed.

Although the laser scanning and pictures taken by the in-built camera were of high resolution, the texturing of the point clouds did not allow the tracing of the subtle boundaries between mounds and inter-mound facies. As a consequence the first step consisted in tracing the outline of the mounds with chalk in the field on the quarry faces (Fig. 5.5). The mound outline in 2-D was continued until the outline was closed. As a consequence two mounds very close to each other most likely connected in 3-D were considered as 2 unique mounds. The digitation of these outlines on high resolution pictures (taken by Kevin D'Souza) was done with the help of Adam Creaser (Master by research at RHUL at that time) who digitised the outlines with a tablet in the field (Fig. 5.5).



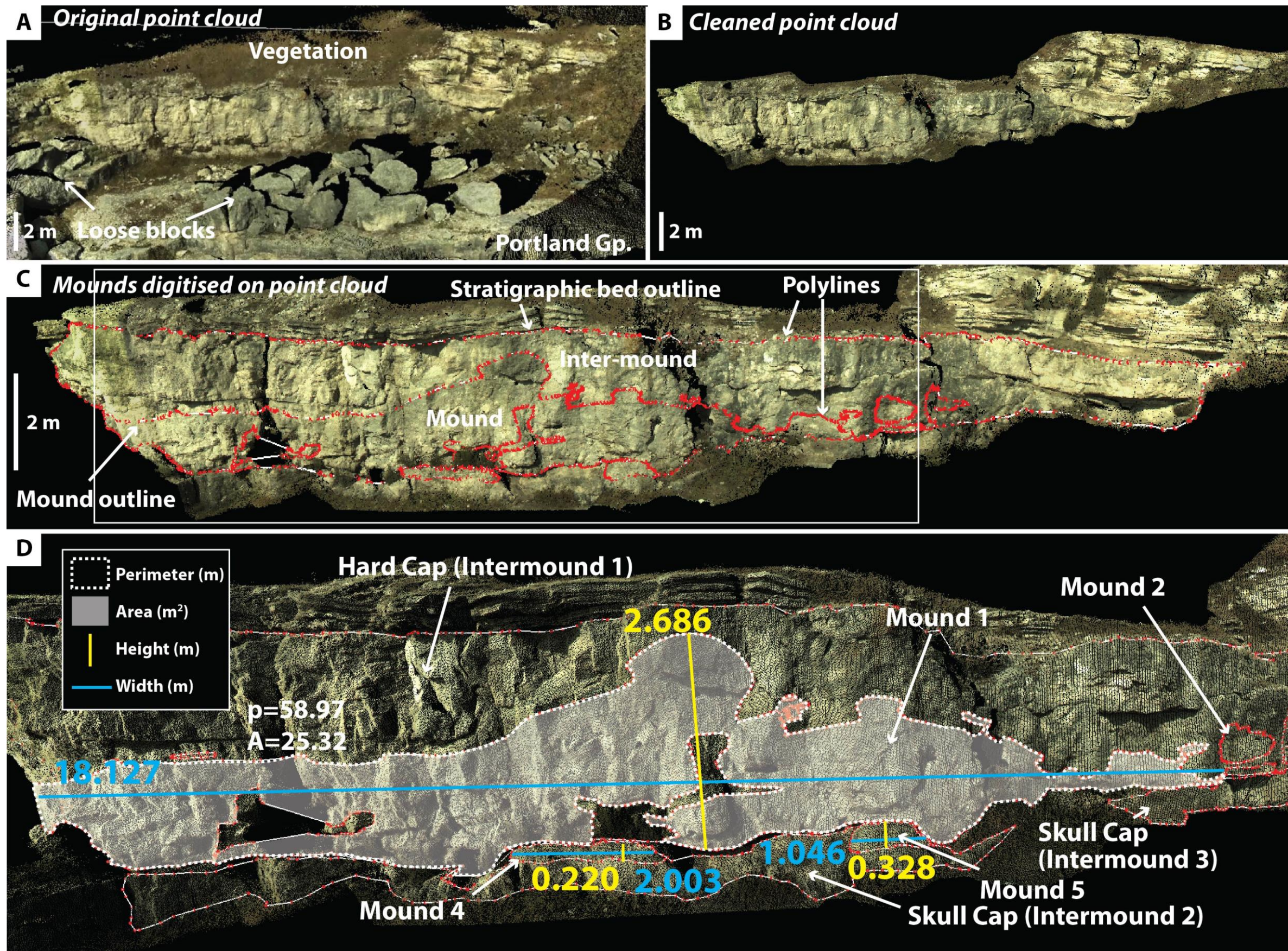
**Figure 5.5** Tracing out white chalk lines to indicate boundary between mound and inter-mound facies at God Nore.

The second step consisted in the cleaning of the point clouds prior to interpretation (Fig. 5.6A-B). The cleaning was done manually by deleting all the unnecessary points in RiscanPro (*i.e.* neighbouring rock faces, vegetation, loose rocks/blocks, underlying Portland Group and overlying beds). This resulted in a size reduction of the files that were then easier and quicker to interpret (less glitches or fixed images due to heavy files).

The third step was the longest step and consisted in the manual digitisation of polylines on the point clouds in RiSCAN. These polylines were drawn as per chalk outlines of mounds recorded in the field. This resulted in the digitisation of mound–inter-mound surfaces and adjacent beds (*i.e.* Skull Cap or Hard Cap; Fig. 5.6C).

The fourth step consisted in the geometrical measurements of mounds, inter-mounds and stratigraphic beds (Fig. 5.6D). Perimeters, heights and widths were measured from RiscanPro and recorded for each mound (refer to Appendix 2.1). While perimeters were directly recorded from the length of the polylines drawn in RiscanPro, widths and heights needed to be measured manually for each mound. These measurements were done according to the maximum width and maximum height that a unique mound has and disregarding its shape. This is illustrated in figure 5.6D where the blue line that depicts the maximum width, disregards the internal variations (the inter-mound facies within the mound) and the irregularities on the top surface of the mound (and identically for the yellow line that depicts the height). However RiscanPro does not allow calculation of areas. To obtain areas the exportation of the polylines onto .dxf files (autocad type) was necessary to be subsequently imported into GoCAD software (© 2013 Paradigm). With this software the calculation of areas were done after conversion of the polylines into three dimensional surfaces (also known as meshing). The determination of inter-mound areas was calculated by deduction of mound areas from the stratigraphic bed areas (Fig. 5.6C).





**Figure 5.6** Workflow applied to interpret lidar point clouds. A – Raw data showing the high definition point cloud (God Nore). B – Same view as B after removing unnecessary imaged objects such as vegetation, loose blocks and the Portland Group beds. C – Interpreted lidar point cloud with outlines of mounds and stratigraphic beds. Note that the white box locates D and that the inter-mound was calculated by deducting mound areas to stratigraphic bed areas (God Nore). D – Example of measurement performed on mounds, here from God Nore (refer to Appendix 2.1 for full list of values). p: perimeter, A: area.

### 2.3. Additional combined techniques

As previously explained, lidar point clouds can be coupled with other techniques to better characterise mound and inter-mound facies. In this study two other techniques were also tested to see if they could improve imaging of these complex 3-D structures: hyperspectral imaging and ground penetrated radar (GPR) surveys.

Hyperspectral imaging is based on mineral reflectance spectra and allows automatic image mapping of areas of different mineralogies of an outcrop and in 3-D when coupled to lidar surveys (Kurz *et al.*, 2012). The main aim of such scanning in this study was to see if this technique could differentiate automatically microbial mound (supposedly made of relatively pure calcite) and inter-mound facies (possibly containing “impurities” such as clay or quartz grain contents). Laboratory scans were done by Tobias Kurz and John Howell from Bergen University on five selected samples (refer to Appendix 2.2). The main outcome of this test was that although there were slight differences in the reflectance between the two facies this was not different enough to be visible when scanning at outcrop. Although this method looked promising, the outcome indicated that it would not work on these Purbeck rocks and this survey was not undertaken for this project.

Ground penetrated radar (GPR) is a method providing images of the shallow subsurface geological features (Bristow and Jol, 2003). GPR is based on propagation of electromagnetic waves in the shallow subsurface responding to changes in the electromagnetic properties of the underground layers (Baker *et al.*, 2007). This system is based on the relative permittivity contrast between layers and is measured in travel time units (*i.e.* time for the waves to travel down to an interface and to back up to the surface, Baker *et al.*, 2007). The relative permittivity is the ability of a material to store and then release electromagnetic energy when a field is applied (Baker *et al.*, 2007). In this study one test scan was done in South West Bowers disused quarry in collaboration with Julien Moreau and Trine Hansen from University of Copenhagen (Appendix 2.3). This location was chosen for its easy access with the survey machine, the location of an exposed portion of the top surface of the Hard Cap and because a sedimentary log and lidar data had been acquired there. Although the image from this test was considered to be good (refer to Appendix 2.3), to undertake an extensive survey it would have been necessary to the surface of the bed to be bare of any shaly deposits (*i.e.* modern soils or paleosols). Because such conditions are met in very few locations along the studied area and many of the interquarry sections are covered in dense shrub, it was decided to not proceed further with GPR.

### 3. Microbial mound shapes and sizes and inter-mound facies relationships

This section details the main results from the lidar point cloud interpretation and documents the mound and inter-mound characteristics and their inter-relationships.

#### 3.1. Microbial mounds

Microbial mounds are constructed by Microbialite facies composed of the Stromatolite, Thrombolite and Burrowed peloidal packstone sub-facies (refer to Chapter 4). The mounds are found in the Skull, Hard and Soft Cap beds and overlie paleosols. These mounds developed around tree branches and trunks in the Hard Cap, tree stumps and fallen trees in the Soft Cap but appear not to be related to any wood remains in the Skull Cap. As explained previously lidar surveys were mainly undertaken on the Isle of Portland that offers very good quality of outcrop along 2-D freshly exposed quarry faces. However mainly the Hard and Skull Cap were surveyed in detail cross-sectional views as the Soft Cap bed is poorly exposed over Portland and only its top surface was surveyed in King Barrow Quarries. The pseudo 3-D characterisation of the mounds was only possible in selected places, in the Hard Cap at Lulworth Cove and Portland Bill and the Soft Cap at King Barrow Quarries, Mutton Cove and Fossil Forest. Table 5.2 summarises the main size characteristics of the 2-D mounds and inter-mound areas for each location as obtained from lidar scanning of the Skull and Hard Cap on the Isle of Portland.

Locations	Number of mounds imaged		Mean height (m) ( $\sigma$ )		Mean width (m) ( $\sigma$ )		Mean area (m <sup>2</sup> ) ( $\sigma$ )		Mean perimeter (m) ( $\sigma$ )	
	Skull Cap	Hard Cap	Skull Cap	Hard Cap	Skull Cap	Hard Cap	Skull Cap	Hard Cap	Skull Cap	Hard Cap
King Barrow Quarries	9	13	0.29 (0.12)	0.69 (0.56)	1.42 (1.16)	2.50 (2.56)	0.21 (0.16)	1.73 (3.45)	2.49 (1.53)	6.94 (7.59)
Bowers Quarry	NI	71	NI	1.06 (0.70)	NI	2.52 (1.67)	NI	1.86 (1.98)	NI	7.55 (5.36)
South West Bowers	14	47	0.45 (0.16)	0.96 (0.57)	1.78 (0.63)	2.30 (1.79)	0.52 (0.23)	1.47 (1.80)	4.39 (1.74)	7.11 (6.20)
Coombeheld Quarry	16	51	0.48 (0.15)	0.98 (0.66)	3.34 (1.95)	1.86 (1.50)	1.55 (1.13)	1.28 (1.85)	8.09 (4.40)	6.86 (7.20)
Freshwater Bay	NI	15	NI	0.85 (0.72)	NI	2.36 (2.03)	NI	1.88 (3.43)	NI	8.05 (8.22)
God Nore	17	37	0.46 (0.27)	0.64 (0.55)	3.07 (1.55)	1.67 (2.87)	1.09 (1.13)	1.31 (4.16)	7.67 (4.82)	5.51 (9.60)
Sand Holes	2	33	0.28 (0.06)	0.91 (0.55)	1.05 (0.35)	2.13 (1.69)	0.18 (0.04)	1.34 (1.77)	2.77 (1.18)	7.06 (5.91)
Totals	58	267	0.43 (0.20)	0.92 (0.65)	2.51 (1.65)	2.18 (1.97)	0.94 (0.99)	1.54 (2.49)	6.15 (4.20)	7.00 (6.87)

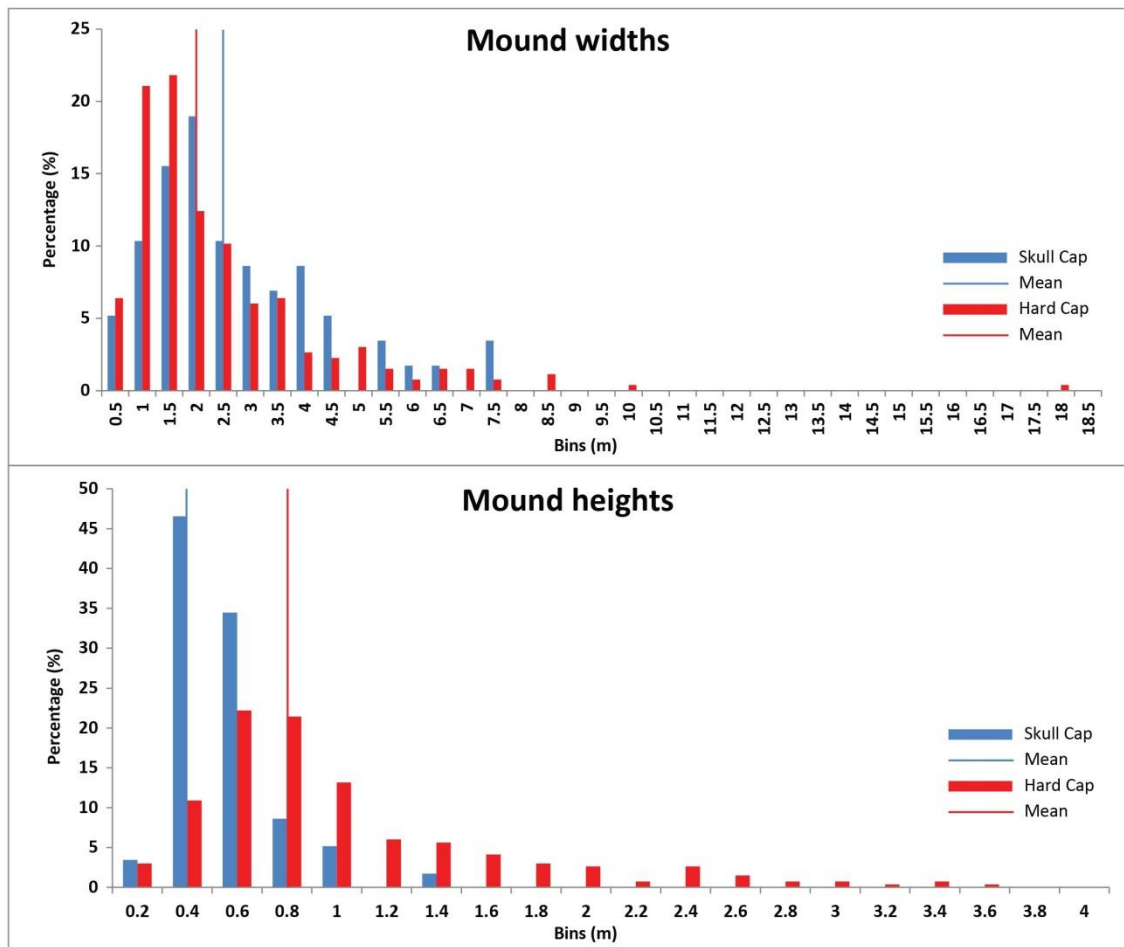
**Table 5.2** Mean size of Skull and Hard Cap mounds measured from the lidar point clouds over the Isle of Portland (from north to south). NI: not imaged;  $\sigma$ : standard deviation. Refer to text for further explanations.

### 3.1.1. Size

The maximum widths and heights for each mound were measured in RiscanPro, recorded and listed in tables (refer to Appendix 2.1). These helped to characterise their shape and to illustrate predominant morphologies (refer to next section). Figure 5.7 shows the distribution of widths and heights of all the mounds measured.

In the Skull Cap the mounds vary between about 9 cm and 7.5 m in width and about 5 cm and 1.3 m in height (Fig. 5.7; Appendix 2.1). However they commonly exhibit widths between 0.5 and 5 m and heights between 40 and 60 cm (Fig. 5.7). This shows that the mounds in the Skull Cap tend to be rather flat and elongated (see next section for morphological characterisation).

In the Hard Cap the mounds vary between about 11 cm and 18 m in width and about 7 cm and 3.5 m in height (Fig. 5.7; Appendix 2.1). However they commonly exhibit widths between 1.5 and 4 m and height between 40 cm and 1 m (Fig. 5.7). This shows that the mounds in the Hard Cap tend to be taller and narrower than in the Skull Cap (refer to next section for morphological characterisation).



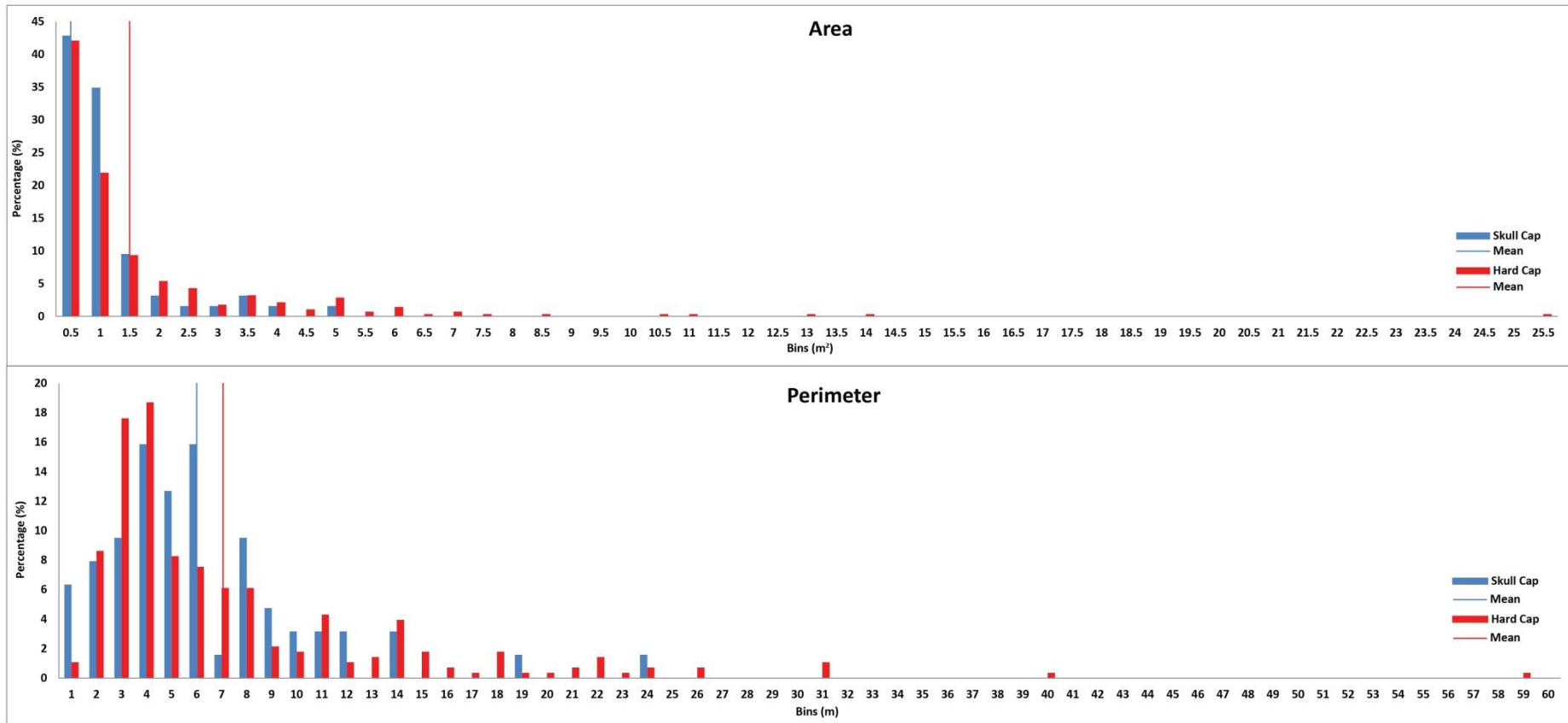
**Figure 5.7** Width and height measurements of all the mounds (refer to Appendix 2.1 for list per locations). Note that the mean values from table 5.2 are illustrated with the plain lines.

Measurement of perimeters and calculation of areas are shown in figure 5.8 (and detailed for each location in Appendix 2.1).

In the Skull Cap cross-sectional areas of mounds vary between about 40 cm<sup>2</sup> and 5 m<sup>2</sup> and perimeters between about 25 cm and 23.5 m (Fig. 5.8 and Appendix 2.1). However they are commonly between 50 dm<sup>2</sup> and 1 m<sup>2</sup> in area and with perimeters between 4 and 6 m (Fig. 5.8).

In the Hard Cap areas of mounds vary between about 3 dm<sup>2</sup> and 25 m<sup>2</sup> and perimeters between about 8 cm and 60 m (Fig. 5.8 and Appendix 2.1). However the areas are commonly between 50 dm<sup>2</sup> and 1 m<sup>2</sup> and perimeters between 3 and 4 m (Fig. 5.8).

Most of the mounds from both units are between 0.5 and 7.5 m in width, 0.2 and 1 m in height, and 50 dm<sup>2</sup> and 5 m<sup>2</sup> in area and 0.5 and 14 m in perimeter (Figs. 5.7, 5.8). This suggests first that the mounds appear to be rather similar in both Skull and Hard Cap; and second that small mounds are abundant in both bed units whilst big mounds are only found in the Hard Cap (Figs. 5.7 and 5.8).

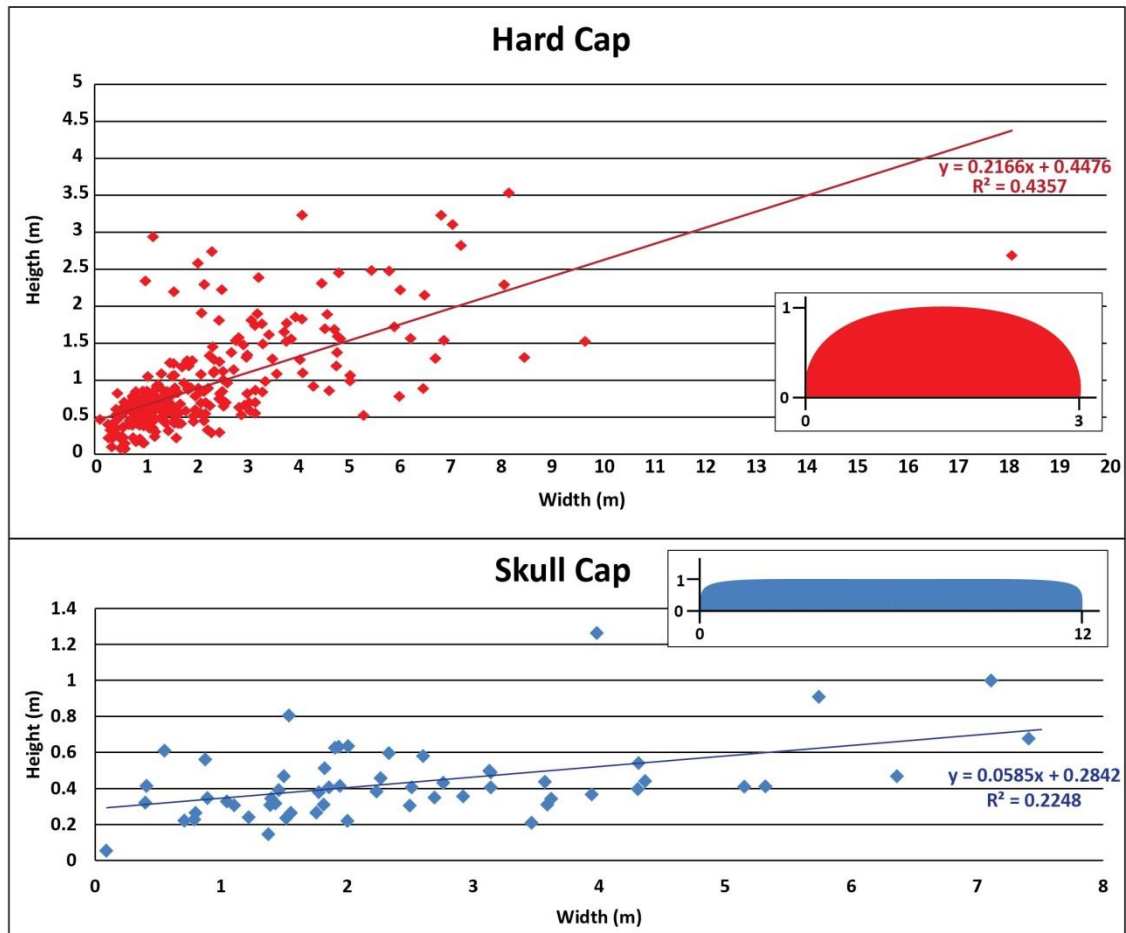


**Figure 5.8** Distribution of areas and perimeters of all the mounds. Note that the mean values from table 5.2 are illustrated with the same plain lines.

### 3.1.2. Morphologies

The characterisation of 2-D mound morphologies was done through field observations and interpretation of the measurements introduced in the previous section. The aspect ratio is used to determine preferential elongation of the height or width and the roundness parameter is used to characterise simple and complex or irregular shapes in 2-D (Merkus, 2009). The sizes of the mounds were also classified according to the orientations of the quarry faces, however no preferential alignment of the mounds was found in 2-D (refer to Appendix 2.1).

The first parameter used was the aspect ratio which allows comparison of the major and minor axes of a shape to decipher a possible elongation in 2-D. In this study this parameter is used to illustrate the relationship between heights and widths of the mounds for the Skull and the Hard Cap by plotting heights against widths (Fig. 5.9). In the Skull Cap mound heights and widths are correlated with a 1:12 ratio meaning that an increase in height will be accompanied with a 12 times larger increase in width (Fig. 5.9). This indicates a rather simple tabular shape (wider than taller) which is also illustrated in figure 5.7. In addition this relationship shows that when the size of the mounds increases, the shape appears to remain tabular (Fig. 5.9). This shows that the mounds were expanding laterally (rather than vertically) and suggests that their growth was controlled by relatively shallow water depths of the lake. In the Hard Cap the relationship between height and width is more complex than for the Skull Cap. There is a similar simple relationship for small mounds (values up to about 1.5 in height and 3 m in width; Fig. 5.9) where heights and widths appear to be proportional following an approximate 1:3 ratio. This shows that in the Hard Cap the mounds have a domal or bun shape when they are small (Fig. 5.9). However for mounds bigger than 3 m wide and 1.5 m high, they do not appear to follow this ratio anymore as shown with the scattered data points (Fig. 5.9) and these larger mounds are interpreted to have more complex and irregular morphologies. Because the mounds in the Hard Cap do not show tabular shapes and have rather domal shapes together with greater heights, they are interpreted to have grown in slightly deeper water depth than the mounds of the Skull Cap (see above) but still in shallow lake margin settings. This aspect of mound growth is discussed further in section 3.3.2. of this chapter and in Chapter 6 where compared with modern analogues.



**Figure 5.9** Relationship between mound heights and widths. Note that the very big mound of about 18 m wide (from God Nore shown in Figs. 5.6, 5.7 and 5.8) is not shown in this figure to help to see relationship for smaller values.

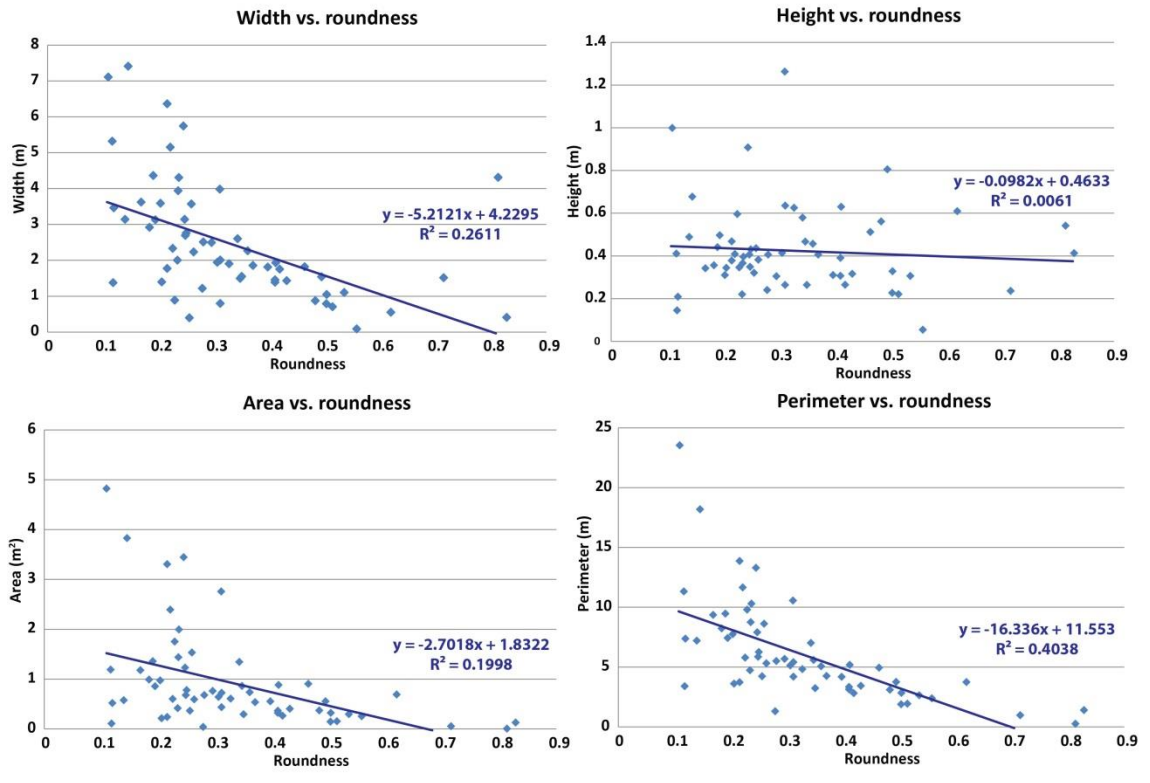
The second parameter used was the roundness to better characterise the complexity of the cross-sectional morphologies of the mounds. The roundness is defined as a ratio between areas and perimeters, and is expressed on a scale between 0 and 1 with 1 being a circular shape (Merkus, 2009). Numerous definitions exist (Merkus, 2009) and in this study the following equation was used:  $\text{Roundness} = 4\pi A/P^2$ ; where A = projected area and P = perimeter (Figs. 5.10 and 5.11; refer to Appendix 2.1 for full value lists). The four measurements recorded previously (*i.e.* widths, heights, perimeters and areas) were plotted against the roundness values (Fig. 5.10). The mounds in both units of the Caps have similar trends of widths, areas and perimeters when plotted against the roundness values. The roundness decreases as the size increases while the heights appear to be more scattered (Fig. 5.10). The Skull Cap mounds are poorly rounded as most of them show roundness values between 0 and 0.5 (Fig. 5.10). This is in accordance with the tabular shapes identified when plotting heights against widths (Fig. 5.9). They also present a gradient from small sizes with slightly better roundness (close to 1) gradually increasing for bigger sizes with poorer roundness values (close to 0; Fig. 5.10). This



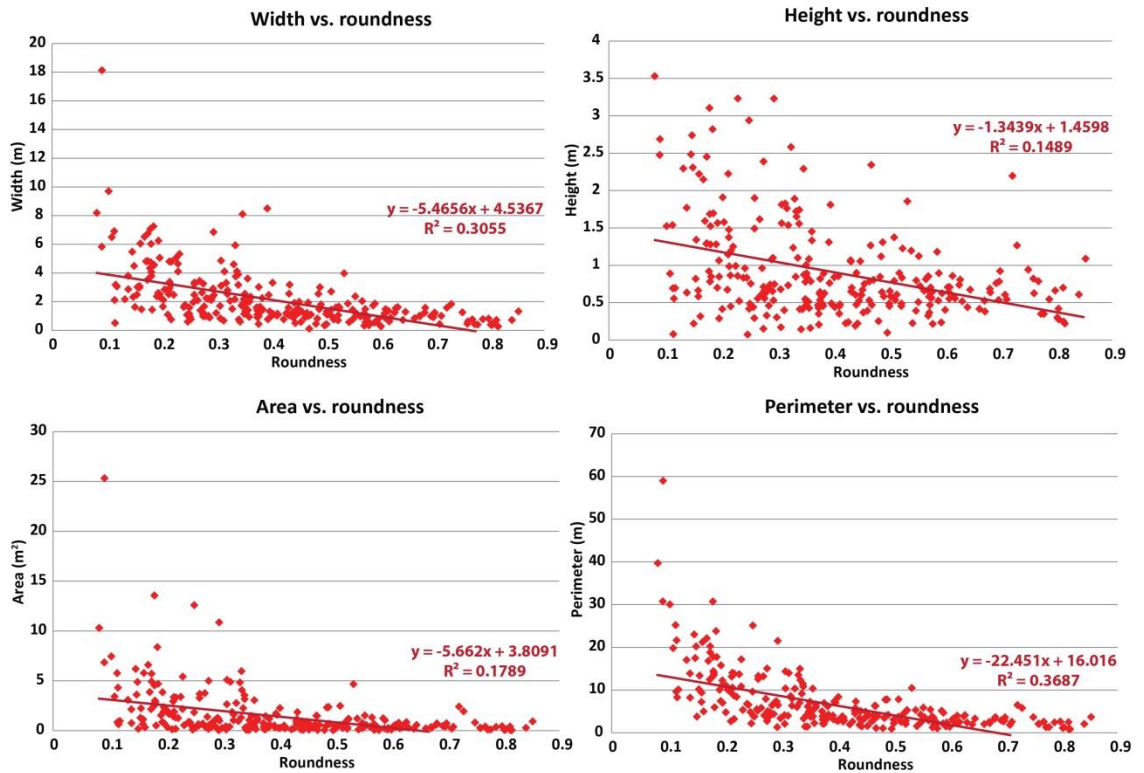
is also in accordance with the fact that mounds in the Skull Cap tend to grow laterally (see above). When height is plotted against roundness the points appear to be more scattered and this indicates that the shapes of the mounds are not influenced by heights. Note that most of the height values are between 20 and 60 cm and appear randomly distributed between 0.1 and 0.5 roundness values (Fig. 5.10). For the Hard Cap, mound morphologies are more diverse from well to poorly rounded. Most of the small mounds (less than 2 m in width, 2.5 m<sup>2</sup> in area and 10 m perimeter) show roundness values spread out between 0.3 and 0.9 (Fig. 5.10). This indicates that small mounds are preferentially well to moderately rounded while bigger mounds are poorly rounded (Fig. 5.10). As with the Skull Cap when height is plotted against roundness, the points are much scattered (Fig. 5.10). However in the Hard Cap shallow mounds (less than 1 m in height) appear to be spread between 0.1 and 0.9 roundness while taller mounds (more than 1 m) are mainly found between 0.1 and 0.3 (Fig. 5.10). This shows that for shallow mounds the height does not seem to control the morphology as appears to be the case for mounds in the Skull Cap. However for tall mounds the spread of height measurements might reflect an increasing complexity in mound shape. Overall these measurements suggest that the shape complexity of the mounds increases with mound size.

In addition the perimeters were plotting against the root squares of the areas (as per equation presented above with a roundness of 1:  $P=2\sqrt{\pi}*\sqrt{A}$ , Fig.5.11). Each point was colour coded, according to the class of roundness value it belongs to, to illustrate evolution of the shape complexity with the size (Fig. 5.11). To help interpretation, the values of a circle (perfect circular shape) were also plotted (Fig. 5.11). For both bed units these plots show that the overall complexity of the mound shapes increase with size as illustrated with the well-rounded mounds (roundness of 0.8-0.9) close to the circle values and the poorly rounded mounds (roundness of 0.1-0.2) further from the circle values (Fig. 5.11). In the Skull Cap the shapes of the mounds appear to become gradually and slowly less rounded as their sizes increase (Fig. 5.11). Taking into account the width and height trends (Fig. 5.9) this is interpreted to highlight (as previously proposed, see above) that the lateral development of the mounds in the Skull Cap was maintained through different mound sizes and that this tabular shape may have been constrained by mound growth in shallow waters. In the Hard Cap, another interesting aspect is illustrated as for each class of roundness (Fig. 5.11) the perimeters and root squares of the areas appear to be correlated (each colour coded class in figure 5.11 follows an approximate straight line). This is interpreted to show that mounds started to develop with a given shape and that they did not modify this original shape when they keep growing but only modified their size.

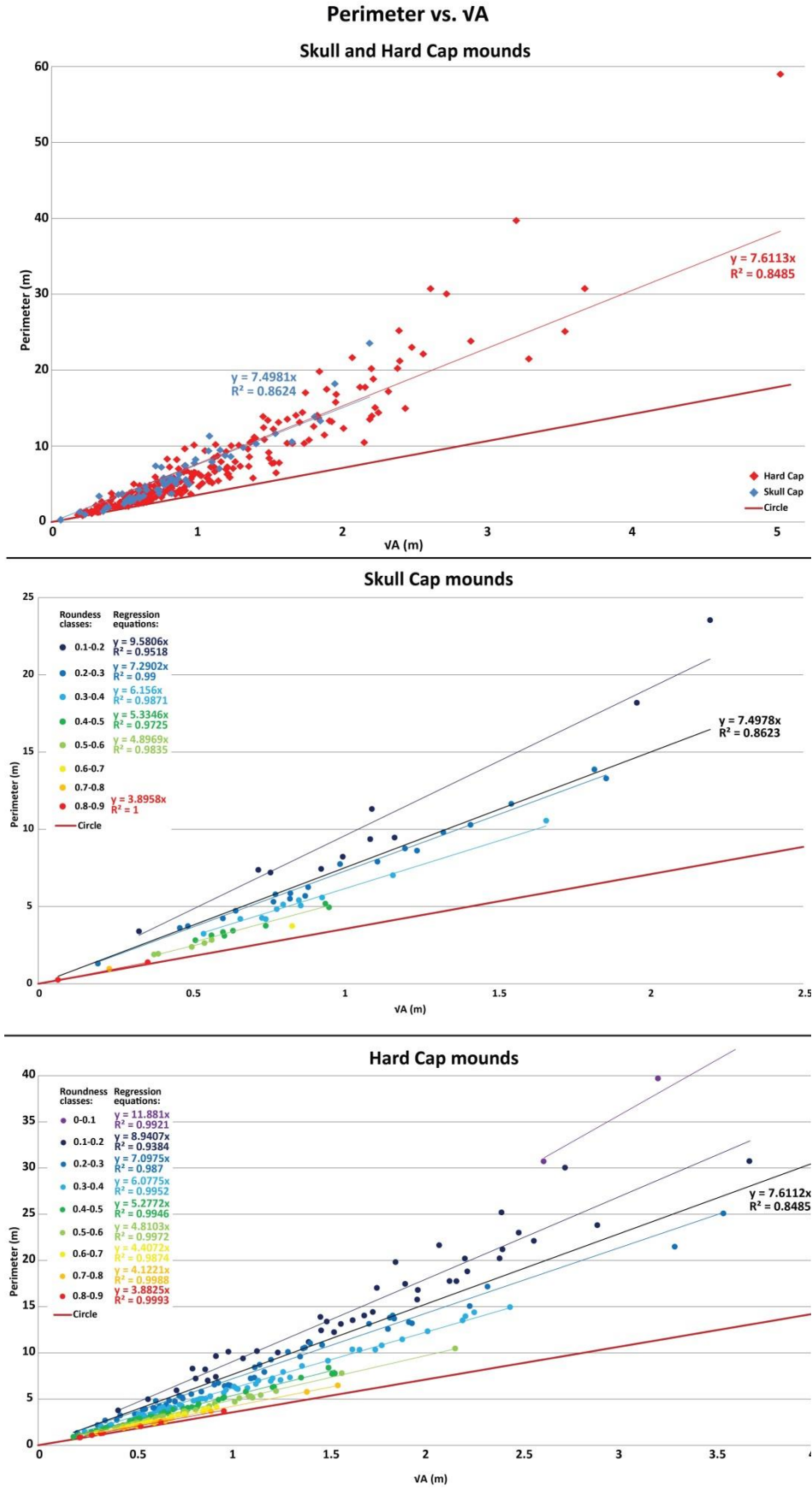
### Skull Cap mounds



### Hard Cap mounds



**Figure 5.10** Roundness parameter plots for the Skull Cap (top) and Hard Cap (bottom) mounds. Note the correlation lines are located to the bottom of the graphs showing the better roundness for smaller values.



**Figure 5.11** Relationships between perimeters and areas and roundness for both Skull and Hard Cap mounds (top), Skull Cap mounds only (middle) and Hard Cap mounds only (bottom).

### **3.2. Inter-mound facies**

The inter-mound facies is found in the Skull, Hard and Soft Cap beds and is described in Chapter 4 to be made exclusively of the Intraclastic peloidal packstone-grainstone facies. Due to the biotas (ostracods, gastropods and bivalves), the generally clean and coarse-grained texture mainly made of peloids, and microbial intraclasts derived from the microbial mounds and its very close association with the microbial mounds this facies was interpreted to be deposited in marginal inter-mound areas (shallow waters) of a brackish water lake (refer to Chapter 4). Only few planar laminations were identified in this facies. The lack of sedimentary structures is interpreted to be due to the fact that this facies was deposited between the mounds that were creating turbulent palaeocurrents. Evidences of increasing energy levels compared to the underlying beds (*i.e.* the paleosols) are in the formation of scours and erosional bases of the Skull, Hard and Soft Cap beds.

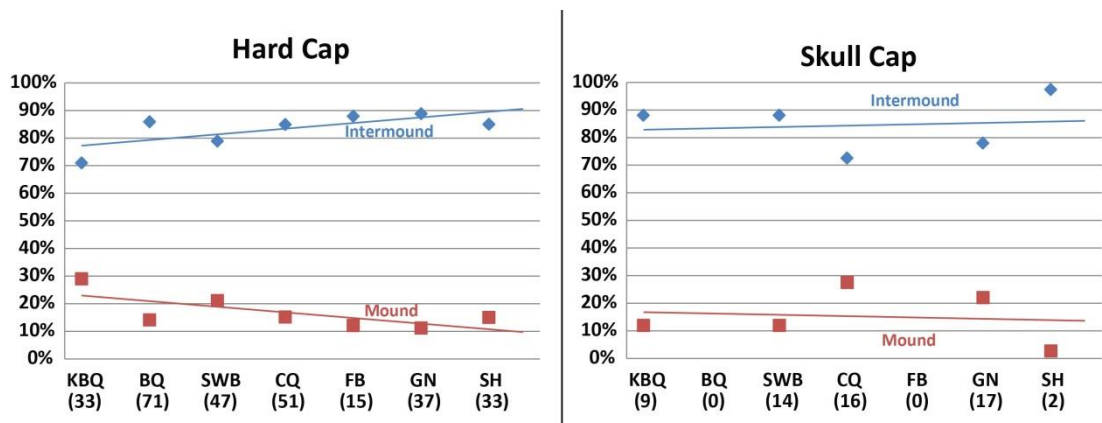
### **3.3. Relationship between mound and inter-mound facies**

#### **3.3.1. Mounds vs. inter-mounds coverage**

The cross-sectional surface areas of the inter-mound facies were recorded from the lidar point clouds by subtracting mound areas to the bed areas for scanned panels of the quarry face (Fig. 5.12; refer to Appendix 2.1 for exact values).

For the Hard Cap the mounds occupy about 30% of surveyed surfaces to the north of Portland and 15% in the south of the surface areas while the respectively remaining 70% and 85% are occupied by the inter-mound facies as illustrated with the regression lines (Fig. 5.12). This illustrates that the distribution of these proportions of mound and inter-mound facies over the Isle of Portland tends to decrease from the north (KBQ, King Barrow Quarries) to the south (SH, Sand Holes) (Fig. 5.12).

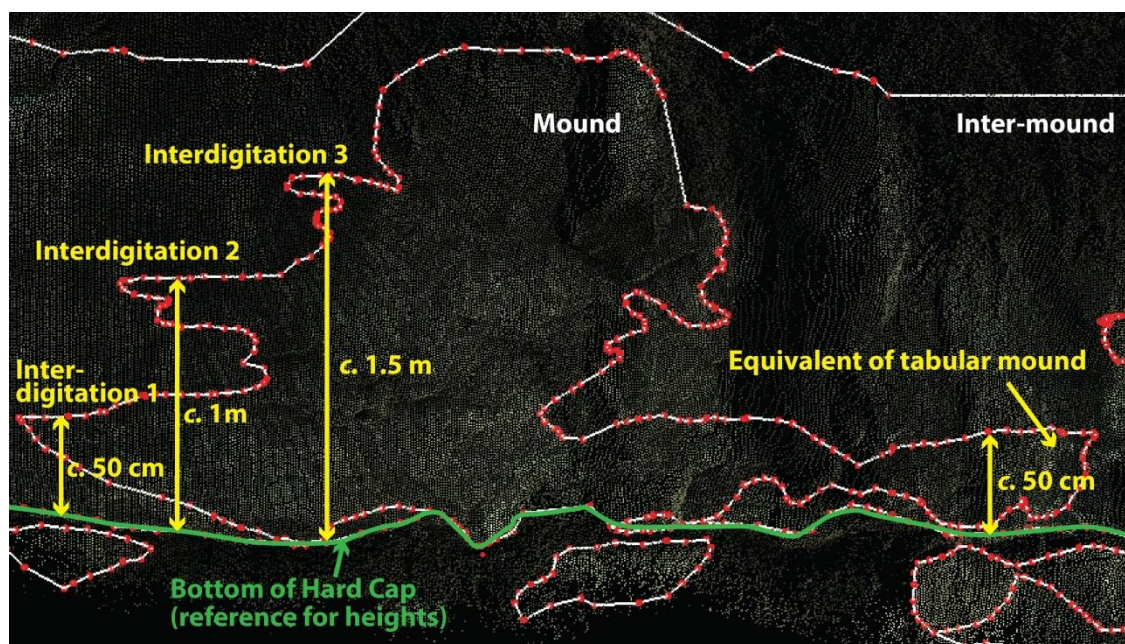
For the Skull Cap the mounds occupy about 15-20% of the surface areas while the remaining 75-80% is occupied by the inter-mound facies everywhere. This illustrates that the distribution of these proportions of mounds and inter-mounds over the Isle of Portland is relatively similar from the north (KBQ, King Barrow Quarries) to the south (SH, Sand Holes) (Fig. 5.12).



**Figure 5.12** Proportions of mound and inter-mound facies over the Isle of Portland from the north (left) to the south (right). Note the numbers in brackets correspond to the number of mounds identified at each location.

### 3.3.2. Relationships between mound and inter-mound sediments

As described in the previous sections the mounds have an overall tabular shape in the Skull Cap and a more domal shape in the Hard Cap (refer to section 3.1.2). However at a more detailed scale very commonly the mounds of the Hard Cap show the development of wings or extensions into the surrounding inter-mound sediments (Fig. 5.13). The result is an interdigitation of the mound and inter-mound facies and onlaps of these facies onto the mounds (Fig. 5.13, also described in Chapter 4, section 3 and figure 4.18). The study of all the mounds of the Hard Cap shows that when mounds form a tabular shape their top surface is on average always around 50 cm from the bottom of the bed (as illustrated in figure 5.13 with one mound, refer to Appendix 2.1); and when mounds form a more complex shape, they show 3 main sets of interdigitations that are on average around 50 cm, 1 m and 1.50 m from the bottom of the bed (as illustrated in figure 5.13 with one mound, refer to Appendix 2.1). As these interdigitations are very common on the mounds throughout the Isle of Portland they may be used to indicate palaeo-lake level fluctuations (Trevor Burchette, pers. comm., March 2016). If they were formed on selected mounds throughout the Isle of Portland, they would show local water depth variations.

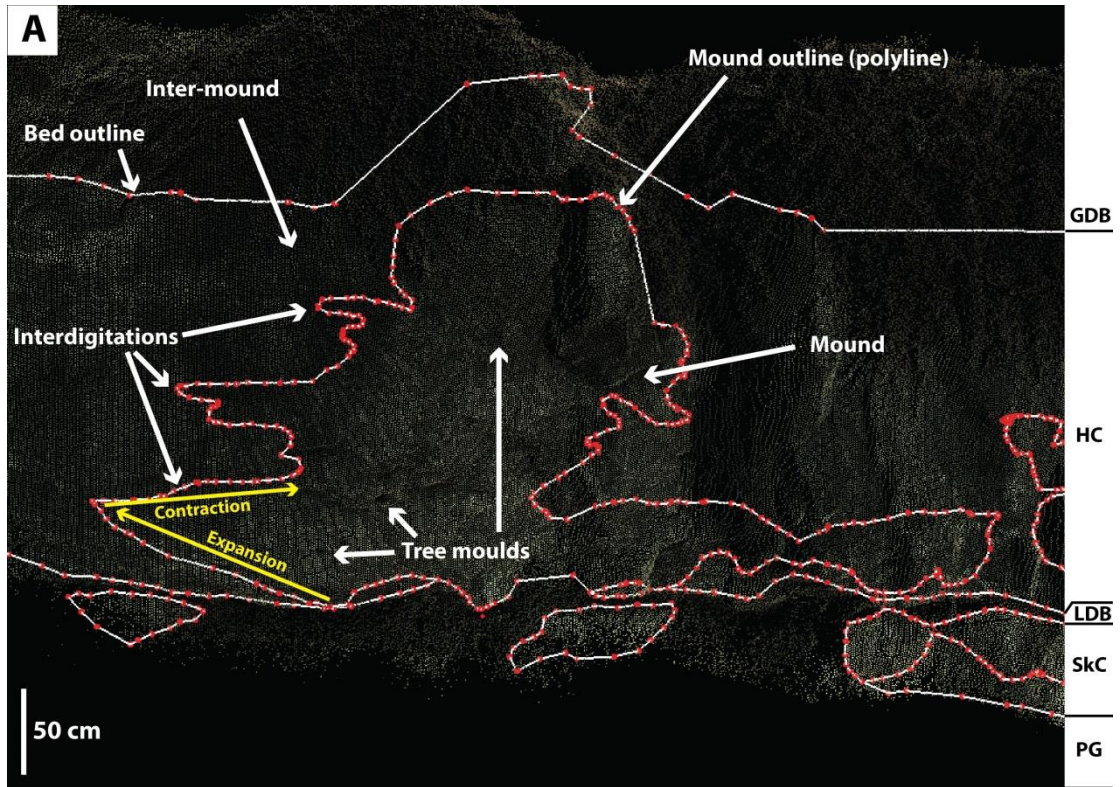


**Figure 5.13** Example of heights of top surfaces of tabular mound (right) and interdigitations of complex mound (left). Note that the top surface of the tabular mound on the right corresponds to the top surface of the first interdigitation of the complex shaped mound on the left. *c.* stands for *circa*.

These interdigitations can be due to different processes that involve sedimentation rate and microbial growth rate both influenced by external controls (such as lake level fluctuations, tectonic or climate). If the sedimentation rate was higher than the mound growth rate, the sediment would cover the mounds killing the microbial community and stopping its development. If the microbial growth rate was higher than the sedimentation rate, the mounds would keep growing until they fill the accommodation space and constitute the main (maybe the only) deposit. If the growth rate was similar to the sedimentation rate, this would neither allow the mound to expand or to contract laterally but to aggrade vertically.

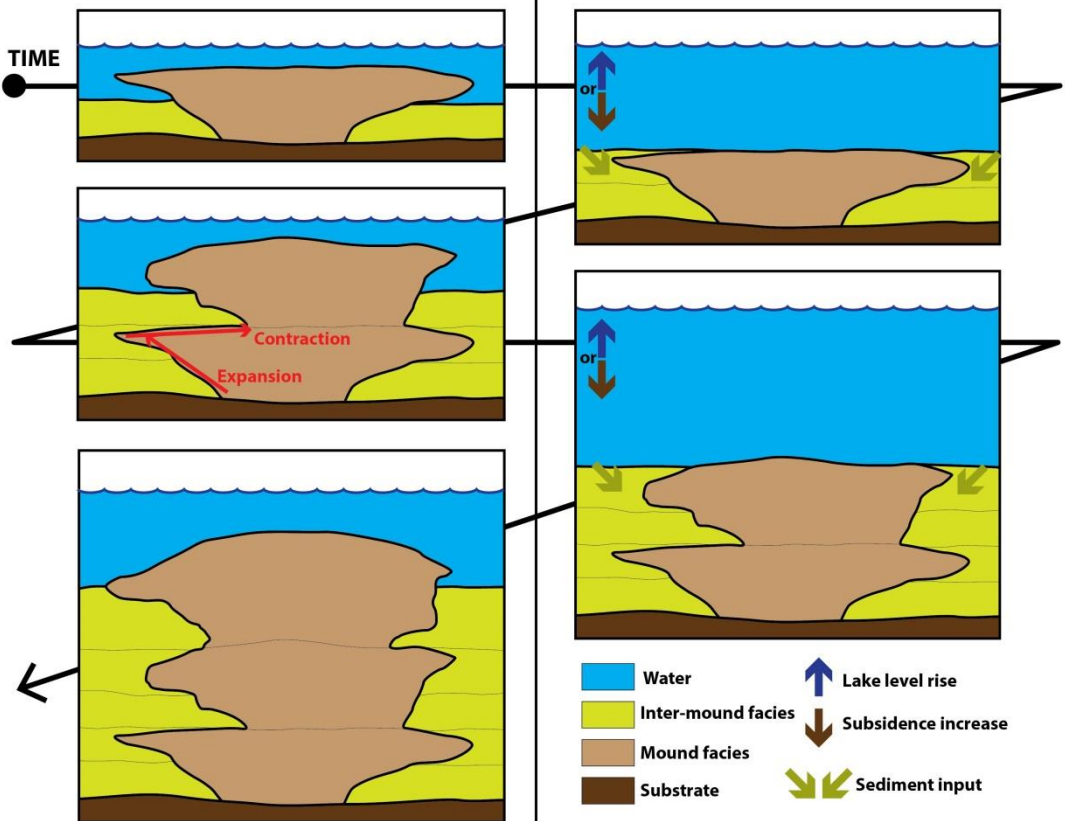
In the example shown in figure 5.14 the mound shows expansions before contractions with a repetition of this pattern three times until the mound was completely covered with sediment or it reached the lake surface and stopped growing. In the Hard Cap this phenomenon is common as lots of mounds developed these interdigitations (refer to Appendix 2.1). In addition if there was one main current direction the interdigitations would expect to be situated always in the same direction when viewed in 3-D. However no preferential direction of orientations in 3-D of the interdigitations is recorded. This indicates that there was no current, or that it was too slow, or that it was not unidirectional. In the Purbeck mounds, these lateral expansions/contractions are interpreted to reflect the balance between growth rate and sedimentation rate. In such a situation the mounds were partially

covered with sediment possibly during pulses of increased sedimentation and expanding laterally when sedimentation rates were reduced. Because shape of mounds and surrounding sediments remain similar these pulses of sediment input were most likely accompanied with constant lake level rise or subsidence increase or a combination of both. In addition because the mounds developed laterally and created the interdigitations with moderate to high energy sediments that show that they were most likely growing in shallow waters (as for the mounds of the Skull Cap). If they were growing in deep water they would be expected to develop more vertically to try to reach light and warmer waters.



**B** Slightly greater growth rate than sedimentation rate  
=> Mounds develop laterally in shallow waters

Lake level rise or subsidence increase  
=> More important sediment input partially covering mounds



**Figure 5.14** Relationships between mound and inter-mound facies. A – Lidar point clouds interpreted showing interdigitations at South West Bowers. Note the stratigraphy on the right. PG: Portland Group, SkC: Skull Cap, LDB: Lower Dirt Bed, HC: Hard Cap, GDB: Great Dirt Bed. Note that this is the same mound as in figure 5.13. B – Cartoons depicting possible growth steps of one mound.



### 3.3.3. Distribution of microbial mounds

Integration of outcrop studies and mapping along the studied area together with lidar interpretation over the Isle of Portland help to understand mound distribution. This was done for two scales, at regional scale to identify proximal and distal areas and at a more local scale to identify external factors influencing the microbial growth and mound distribution. In addition when no field evidence was identified on the mound distribution numerical modelling (3-D forward modelling) was used to propose possible external controls. The numerical modelling was undertaken by Kozłowski (*in prep.*) in a joint PhD project where different scenarios were modelled to attempt to constrain the distributions presented in this chapter.

#### 3.3.3.1. Regional scale

At a regional scale (throughout the studied area in south Dorset) microbial mounds show lateral changes as well as vertical changes depending on the bed they are found in. As presented before, microbial mounds are found in three beds, the Skull, Hard and Soft Cap beds in the lower part of the Mupe Member.

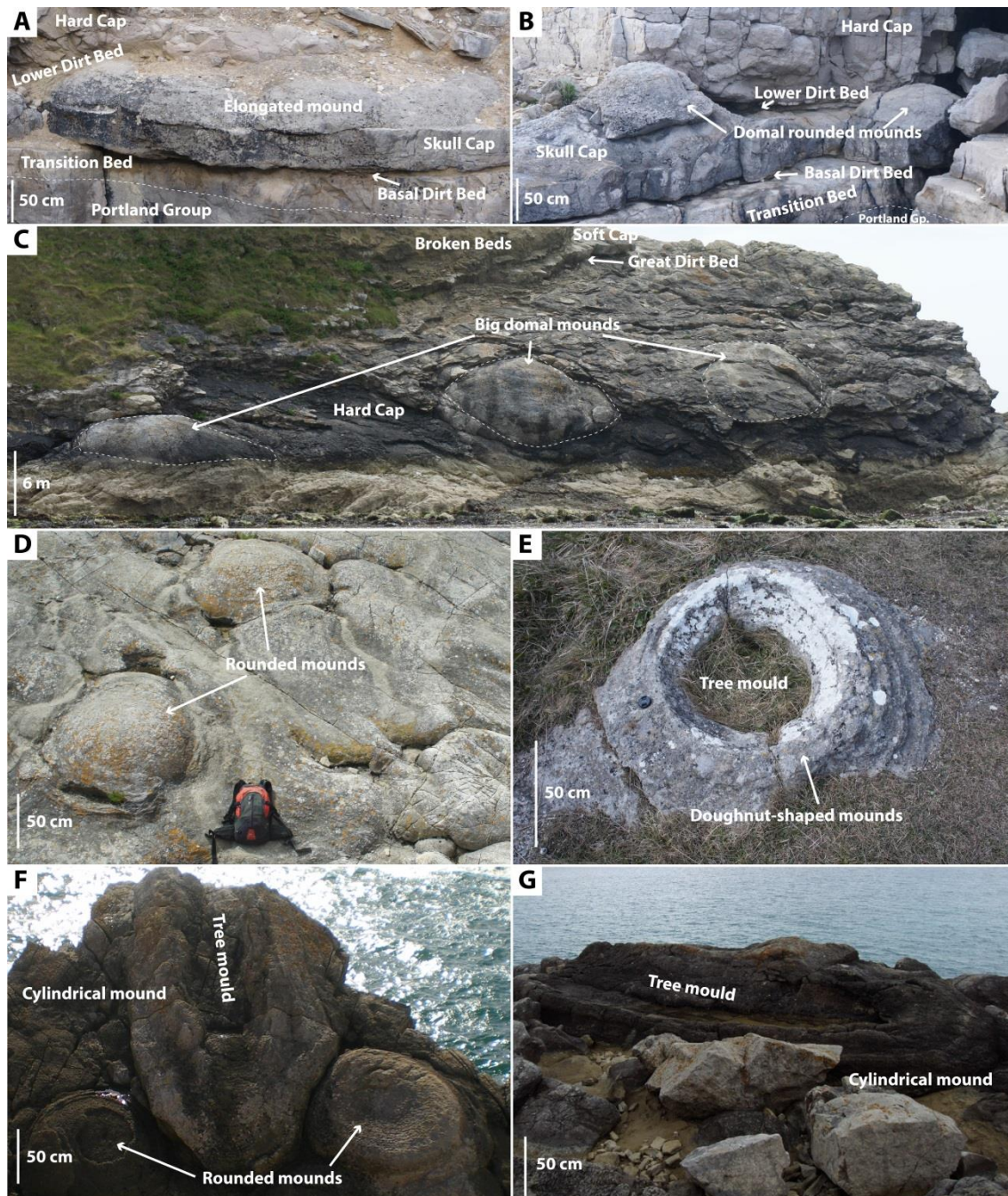
In the Skull Cap, mounds were never found associated with tree remains and have a tabular positive relief between 20 and 60 cm high (see section 3.1.1. of this chapter). Synoptic reliefs are commonly determined using onlaps on the sides of the mounds, domed and/or when buried by flat-topped beds with a different sediment (Hofmann, 1973; Hoffman, 1974). In the Skull Cap no onlaps were seen but mounds have tabular shapes (elongated or rounded) that may indicate a maximum synoptic relief of about 60 cm. The top surfaces of mounds of the Skull Cap are only exposed at Portland Bill on the Isle of Portland that allows the characterisation of the shapes and sizes in 3-D. There, mounds show rounded and elongated tabular shapes (Fig. 5.15A-B), however elongated tabular mounds are not very well exposed and only pseudo 3-D is seen (Fig. 5.15A). The rounded tabular mounds are about 50 cm in diameter and the elongated tabular are about 5 m long (Fig. 5.15A-B). This shows that although with the lidar scans mainly elongated shape are imaged, a few smaller rounded mounds are also present. Mounds in the Skull Cap are found all along the studied area and are rather morphologically similar apart from in Swanworth Quarry where they appear to change laterally to stromatolitic deposits (refer to Chapters 6 and 7 and Appendix 3).

In the Hard Cap, mounds are commonly found associated with tree remains that left sub-vertical to sub-horizontal moulds about 20 cm in diameter either empty or filled with silicified

tree trunks or branches (refer to Chapter 4). These mounds are bigger (between 20 cm and 3 m) than in the Skull Cap (refer to section 3.1.1. of this chapter) and formed domal positive relief on the lake floor as suggested with the interdigitations (refer to previous section). These domes together with onlaps, locally observed (refer to Chapter 4, Fig. 4.18C), indicate synoptic reliefs from 20 to 60 cm. The top surfaces of three mounds of the Hard Cap are exposed on the eastern side of Lulworth Cove (Fig. 5.15C). There the mounds are domal and rounded and about 6.50 m in diameter. This is in accordance with the lidar interpretation and measurements from the point clouds that show big and tall rounded shapes and widths of up to 6.5 m are common. Mounds in the Hard Cap are found throughout the studied area with the exceptions of Mupe Bay, Worbarrow Tout and Swanworth Quarry where they appear to change laterally for stromatolitic deposits (refer to Chapters 6 and 7 and Appendix 3). The tree holes in these mounds were studied in detail by Francis (1982) where she measured diameters and orientations (refer to Chapter 2). She determined that tree moulds are on average 10 cm in diameter and between 20 cm and 2 m long with an average dip of 5° to the south (refer to Chapter 2). However she interpreted this southerly direction to be mainly measured from branches that have 40° angle with the trunks in modern conifers and that cannot be used for interpretation of palaeowind directions but rather only a north-south orientation of the tree trunks (refer to Chapter 2).

In the Soft Cap, mounds are also commonly associated with tree remains that left circular moulds or sub-horizontal elongated moulds (*i.e.* cylindrical) about 50 cm in diameter empty that corresponds to either *in-situ* tree stumps (circular) or fallen trees (sub-horizontal) (refer to Chapter 4). In addition when there is no association with tree remains, mounds have a domal shape (Fig. 5.15D). These mounds have similar heights as the Skull Cap mounds between 20 and 60 cm positive relief with domal shapes. This indicates that a maximum synoptic relief of about 60 cm. The top surfaces of mounds of the Soft Cap are exposed at Fossil Forest, and Mutton Cove and King Barrow Quarries on the Isle of Portland (Fig. 5.15D-G). The doughnut-shaped and rounded mounds have similar sizes and are around 1 m in diameter (Fig. 5.15E) while the cylindrical mounds are found between 2 and 3 m long (Fig. 5.15F-G). Mounds in the Soft Cap are only present eastwards of the Isle of Portland-Lulworth zone with the best exposure at Fossil Forest (refer to Chapters 6 and 7 and Appendix 3). As for the mounds of the Hard Cap Francis (1982) studied in details the tree moulds of the Soft Cap mounds (refer to Chapter 2). She determined that the moulds in the mounds are in average around 46 cm in diameter and when elongated moulds are between 7 and 54 cm long when exposed (refer to

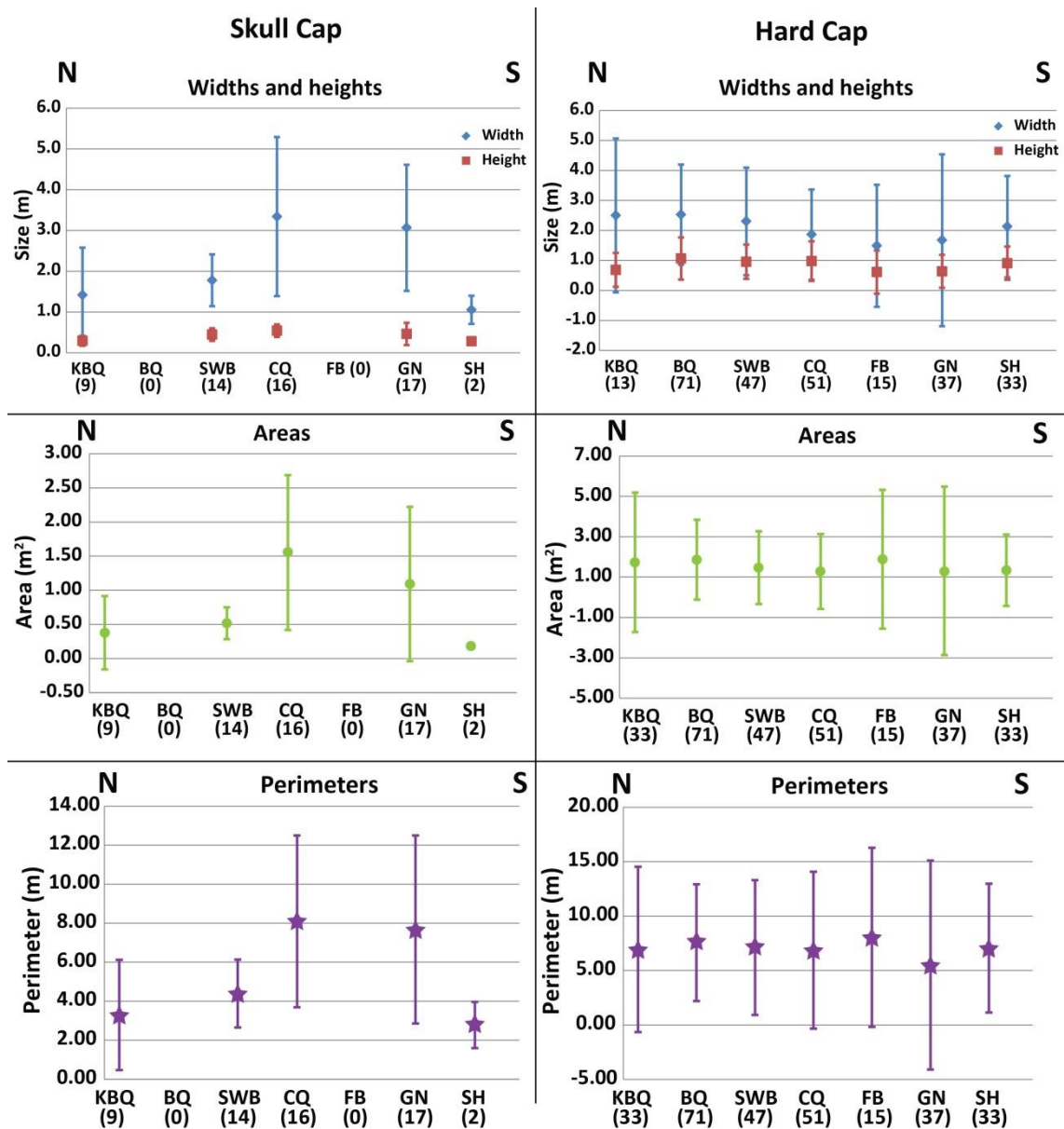
Chapter 2). She interpreted that the elongations were due to logs and preferentially orientated in a north-south direction that indicated a northerly blowing wind direction (refer to Chapter 2).



**Figure 5.15** Views of mounds in 3-D in the field. A – Elongated tabular mound from the Skull Cap at Portland Bill (Isle of Portland). B – Rounded tabular mound from the Skull Cap at Portland Bill (Isle of Portland). C – Big rounded domal mounds from the Hard Cap on the eastern side of Lulworth Cove. D – Domal rounded mounds from the Soft Cap at Fossil Forest. E – Doughnut-shaped mound with tree trunk mould from the Soft Cap at King Barrow Quarries (Isle of Portland). F – One cylindrical and two domal mounds from the Soft Cap at Fossil Forest. G – Cylindrical mound from the Soft Cap at Fossil Forest (photo courtesy of Sila Pla-Pueyo).

### 3.3.3.2. Local scale

At a local scale over the Isle of Portland, figure 5.10 showed that the shapes of the mounds of the Skull Cap are flatter than in the Hard Cap (tabular against domal). Figure 5.11 showed that the sizes of the mounds in the Skull Cap are smaller than in the Hard Cap with Skull Cap mounds rather similar to the small mounds of the Hard Cap. As explained above at a regional scale, field studies show that the mounds from the Skull and Hard Cap beds at a local scale also differ in their association with tree remains (trunks, branches or stumps). At a local scale and at outcrop no tree remains were ever found associated with the tabular mounds of the Skull Cap while numerous sub-horizontal tree moulds (dip angles average about 20° and generally less than 5°) were identified in the mounds of the Hard Cap on the Isle of Portland (refer to previous section and Chapter 2 as this feature was also noticed by Francis, 1982). Figure 5.16 shows the distribution of the average size (widths and heights), areas and perimeters of the mounds from the north to the south of the Isle of Portland. The mounds in the Skull Cap appear to be slightly bigger in the south than in the north (Fig. 5.16) while in the Hard Cap they appear to be rather similar over Portland. However as all the data are within the standard deviations of the size measurements, no clear conclusions on possible size variations and trends can be drawn. Outside of the Isle of Portland, although mounds were identified all along the studied area (see above), mounds similar to those characterised on the Isle of Portland are mainly found in Lulworth area (refer to Chapter 6 and Appendix 3). Mounds are interpreted to have developed overall in shallow waters (see above and refer to Chapters 4 and 6) with the tabular shaped-mounds of the Skull Cap in the shallowest part of the margins; and the domal shaped-mounds of the Hard Cap in slightly deeper water of the margins. Consequently microbial mounds are preferentially developed either on the margins or on palaeohighs on the floor of a brackish water lake (refer to Chapters 4 and 6). This is a very common feature in modern day environments (refer to Chapter 6) such as Laguna Bacalar (Mexico) where flat-topped thrombolite mounds are only found on the margins of this freshwater lake growing from the shore and around mangrove trees in a shallow waters away from the shoreline (refer to Chapter 6 and Appendix 1). Similarly in the Great Salt Lake (Utah, USA) flat circular mounds that form rings are only found on the shallowest part of the margins of this hypersaline lake and change laterally in deeper waters to domal structures (refer to Chapter 6). In the Great Salt Lake, mounds develop on top of pebbles and sedimentary structures such as current ripples or dunes (refer to Chapter 6).

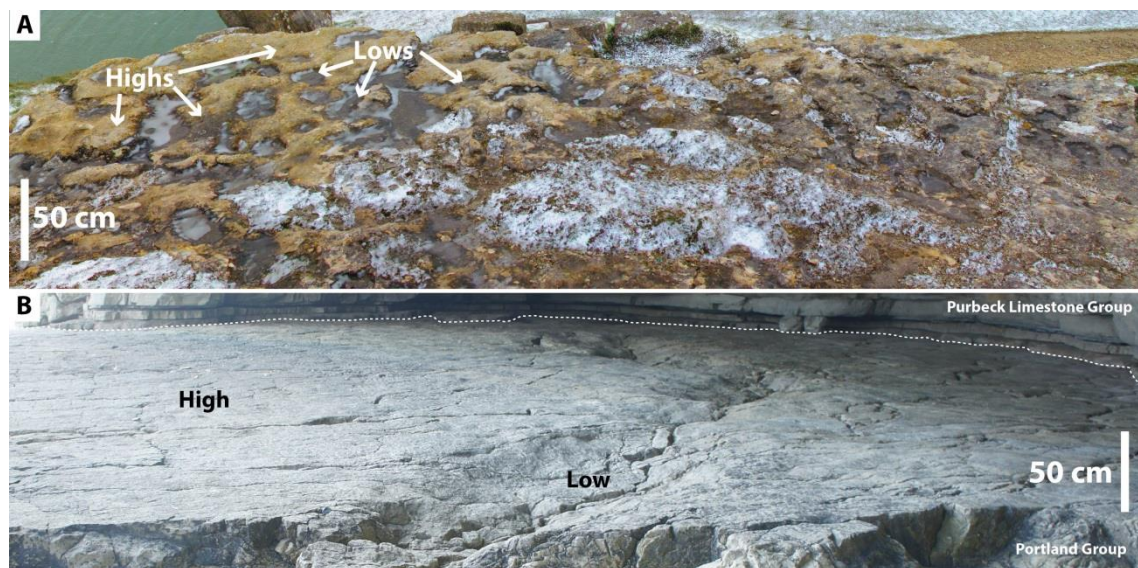


**Figure 5.16** Mound sizes (widths and heights), areas and perimeters distributions over the Isle of Portland from the north to the south. KBQ: King Barrow Quarries, BQ: Bowers Quarry, SWB: South West Bowers, CQ: Coombefield Quarry, FB: Freshwater Bay, GN: God Nore, SH: Sand Holes. Note that the numbers in brackets correspond to the number of mounds and the plain lines are the error bars.

### 3.3.3.3. Controls on mound morphologies

Controls on microbial growth can be inferred from the shape of the mounds, the type of microbialites and from the type of substrate used by the microbial community to grow. This is well documented in the literature from modern (such as Laguna Bacalar or Great Salt Lake, described in Chapter 6) and in ancient (such as the Green River Formation) environments (more modern and ancient analogues are described in Chapter 6). In Laguna Bacalar (Mexico) thrombolite mounds use the shorelines (possibly previously indurated) and mangrove trees as

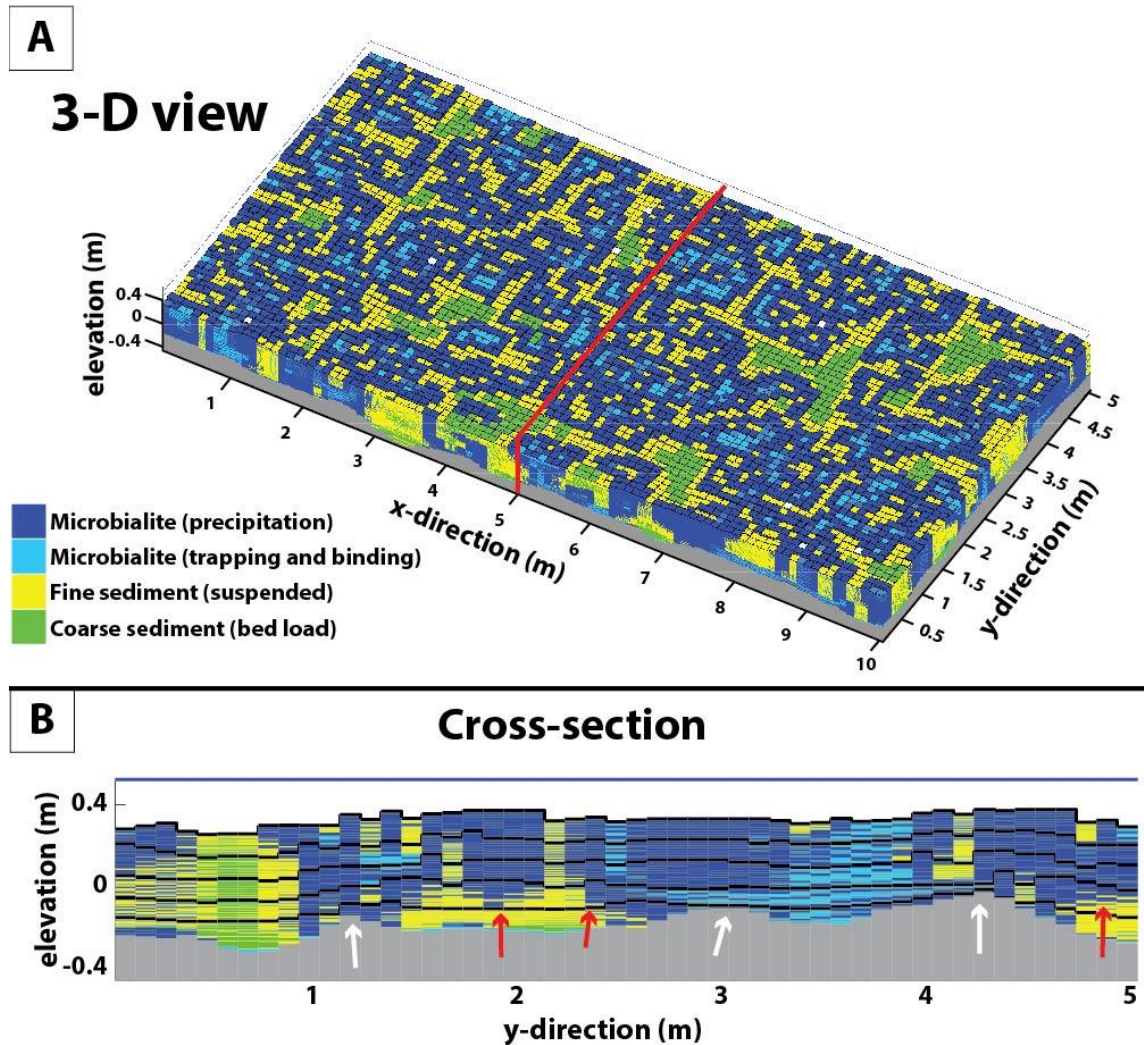
substrates (refer to Chapter 6 and Appendix 1). In the Great Salt Lake (Utah, USA) thrombolite mounds grow from indurated mud pebbles and positive sedimentary structures (current ripples and dunes) that formed in the littoral zone (refer to Chapter 6). In ancient environments Chidsey *et al.* (2015) showed that branching stromatolites used as a substrate indurated silt and mud in the Green River Formation (Eocene) exposed in Utah (USA). Such hard substrates were never identified at the base of the mounds in the Skull Cap from fieldwork (no trees, no pebbles or sedimentary structures were identified). In this bed the mounds appear to develop either above a paleosol (the Basal Dirt Bed) or directly on the micro-karstic top surface of the Portland Formation (Fig. 5.17).



**Figure 5.17** Irregularities on the top surface of the Portland Group. A – Erosional surface showing small frequency and short amplitude irregularities (South West Bowers Quarry, Isle of Portland, photo courtesy of Estanislao Kozlowski). Note that the white substance is snow and that lows are highlighted with the ice that formed inside. B – Exposure surface showing greater frequency and amplitude irregularities on the upper surface of the Portland Group (Mupe Bay).

Based on fieldwork and lidar interpretation mounds appear to grow in both lows and highs created on the palaeotopography although the original point of mound growth can never be ascertained in 2-D exposures. To assess the external controls involved in the growth and the distribution of the mounds, 3-D forward numerical modelling was used (Fig. 5.18). Kozlowski (*in prep.*) specified that at the small scale microbial growth, shape and the relationship with the inter-mound facies are controlled by a balance between microbial growth rate and the sedimentation rate (as also stated with fieldwork studies, see above). The main outcome of importance for this study is that it allows the determination of the controls of the palaeotopography on the distribution of the type of mounds found in the Skull Cap. Figure 5.18 shows one possible model in 3-D and a 2-D cross-section of the current level of work by

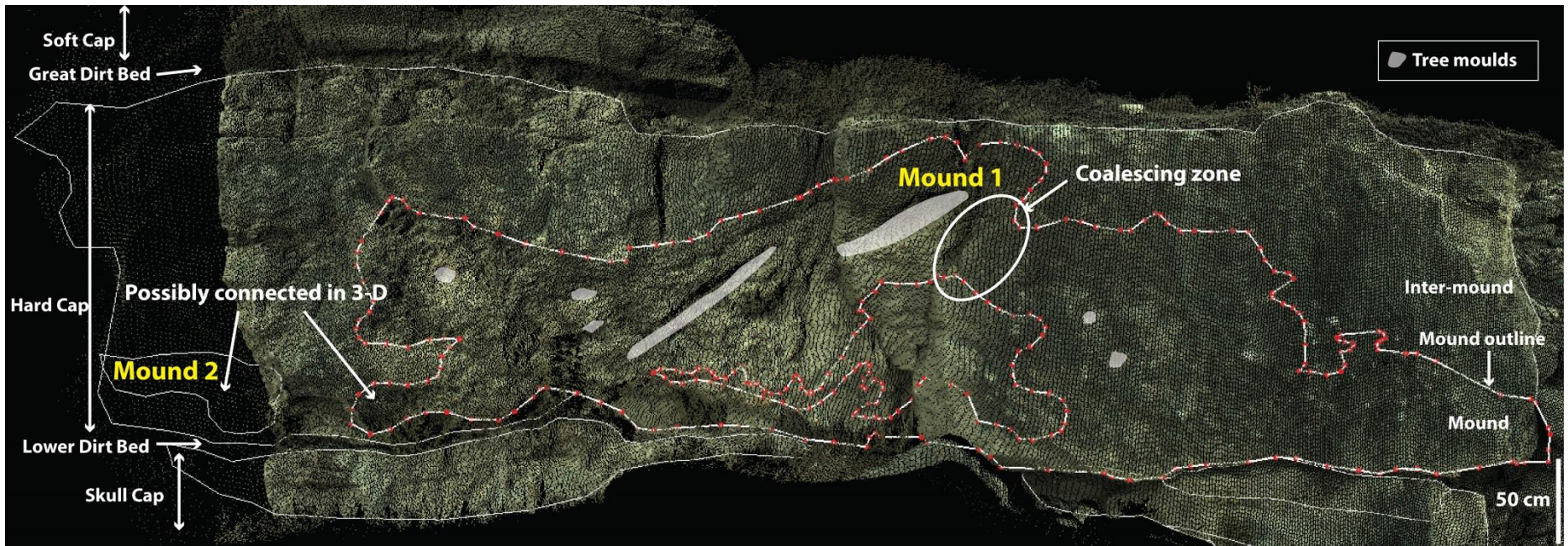
Kozłowski (*in prep.*). This model shows that the mounds preferentially start to develop on highs present on the palaeotopography and with time develop laterally over lows and the inter-mound facies. Depending on where the cross-section (or cliff faces) is taken the point of origination can either be imaged or not. As a conclusion for the mounds of the Skull Cap, their distribution could be controlled by the micro-karst that formed on the top surface of the underlying Portland Group; or the irregularities of the top surface of the Basal Dirt Bed paleosol.



**Figure 5.18** Small-scale 3-D forward numerical model from Kozłowski (*in prep.*). This model represents 50 years of accumulation (one iteration per year) following these characteristics: vertical growth of 0.01 m/yr; lateral growth of 0.05 m/yr; maximum rate of deposition of 4 cm/yr; a repose angle for the coarse sediment of 10°; a maximum erosion rate for the coarse sediment of 1 cm/yr; lake level rise with a period of 300,000 years and an amplitude of 5 m. The initial topography (in grey) is based on the amplitude and frequency of the surface of the Portland Group as recorded in the field (as in figure 5.17). Note that the fine and coarse sediments represent the Intraclastic peloidal packstone-grainstone facies. A – 3-D block model with the red plain line that locates the cross-section in B. B – 2-D cross-section following red line in A that shows that mounds preferentially start to grow on highs (white arrows) and develop both vertically and laterally over lows (red arrows) over time.

In the Hard Cap, most of the mounds are found around tree remains (branches, trunks or stumps; refer to Chapter 4) in sub-horizontal position (dip angles average around 20°). This is interpreted to indicate that the main control on the mound distribution in the Hard Cap is the occurrence of tree remains. However in several occasions mounds do not appear to be associated with tree remains in 2-D (as mound 2 in Fig. 5.19). This can be explained due to the same process described for the mounds of the Skull Cap and their actual distribution in 3-D (Fig. 5.18). The mounds of the Hard Cap used tree remains as substrates in addition to palaeotopographic highs due to irregularities on the top surface of the Lower Dirt Bed paleosol. When a mound does not appear to be associated with trees, it was probably located somewhere near tree remains but with the mainly 2-D views (*i.e.* cliff faces) it may appear that a mound is isolated from trees within the inter-mound facies (as for mound 2 in Fig. 5.19). In such situation only part of the mound is seen while its actual extent in 3-D is much greater than the limited 2-D extent seen at outcrop. In addition the development around sub-vertical tree remains justifies the difference in size between the mounds of the Skull and Hard Cap. In the Hard Cap the mounds used the sub-horizontal trees as substrates for the growth that were most likely creating overhangs above the lake floor. These overhangs would allow mounds to reach greater heights and widths than in the Skull Cap where the mounds remained tabular. Another important characteristic only identified in the Hard Cap is the lateral coalescence of mounds (as in mound 1 in Fig. 5.19). Very commonly mounds appear to form “bridges” in 2-D that appears to result from the lateral coalescence of two interdigitations, accompanied with significant increase of the lateral extent over the inter-mound facies (Fig. 5.19). These “bridges” can be of two origins when the 3-D is considered; it could be two neighbouring mounds that created interdigitations (as previously described) and coalesced when extended laterally; or it could be the interdigitations of a same mound that extended separately and re-joined.





**Figure 5.19** Lateral extent of mounds in the Hard Cap illustrated from the interpretation of the lidar point clouds at King Barrow Quarries. The stratigraphy is notified on the left. Note that shape of mound 1 appears to be controlled by the position of the trees that also controls the possibility of coalescence.

## 4. Conclusion

Interpretation of lidar point clouds coupled with qualitative outcrop studies enabled the definition of two main shapes of microbial mounds; short tabular and wide in the Skull Cap and a mixture of short tabular and domal shapes and tall and wide complex shapes in the Hard Cap. In addition measurements (widths, heights, surface areas and perimeters) illustrated that the mounds of the Skull Cap are generally smaller than of the Hard Cap. Although the Hard Cap mounds exhibit a wide range of sizes, the small mounds have similar sizes than the mounds of the Skull Cap. This is interpreted to indicate shallow waters for the Skull Cap mounds as the tabular mounds tend to extend laterally (constrained with the water depth) rather than vertically as is seen in the Hard Cap mounds. In addition maximum synoptic reliefs of the mounds appear to be similar in the three units (up to 60 cm) and down to 20 cm in the Hard Cap.

The identification and characterisation of interdigitations of mounds with the inter-mound facies helped to determine the complex relationships between mound growth and sedimentation rate. In addition the lake level was most likely fluctuating due to pulses either due to a lake level rise, increasing subsidence or a combination of both. In most of the big mounds a maximum of 3 interdigitations were identified more or less at the same distance from the base of the bed (differences may be due to the uneven erosional surface of the underlying paleosols). This shows that 3 palaeo-lake fluctuations occurred more or less simultaneously over the area of the Isle of Portland.

The integration of 3-D forward modelling together with outcrop studies helped to determine possible controls of the mound distribution and on microbial growth. Numerical modelling showed that mounds are preferentially growing above highs on the palaeotopography and developed laterally. In addition the greater thickness of the mounds of the Hard Cap is due to the position of sub-vertical tree remains that provided substrates for the microbial growth. Outcrop studies and numerical modelling also show that mounds can coalesce in 3-D and that this increases their lateral extent (*i.e.* connectivity) and that mounds that appear laterally close to each other are most likely connected in 3-D.

These features (vertical growth around tree remains and coalescence between mounds) have important implications in the interpretation of the connectivity of the mounds in 3-D. In Chapter 4 the Thrombolite sub-facies (*i.e.* main facies of the mounds) was described to be highly porous providing a potential good hydrocarbon reservoir although surrounded by a poorly porous facies (the Intraclastic peloidal packstone-grainstone facies). The integration of

outcrop studies and numerical forward modelling helps to predict mound distribution and connectivity in 3-D which can be valuable information in the production process in a petroleum system.

## Chapter 6

Palaeoenvironments of the  
Mupe Member: logs, facies  
associations and facies models

## 1. Introduction

This chapter and accompanying Appendix 3 present graphic logs through the Mupe Member and four facies associations, comprising the facies defined in Chapter 4. Graphic logs are also used to identify facies transitions and thickness variations, both spatially (laterally) and stratigraphically (vertically). This chapter also presents a sequence stratigraphic analysis of the Mupe Member. The integration of all these investigations together with the analyses of shape and size of the microbial mounds (refer to Chapter 5) enables the definition of two facies models; an earlier brackish water lake and later hypersaline water lake as the depositional environments for the Mupe Member.

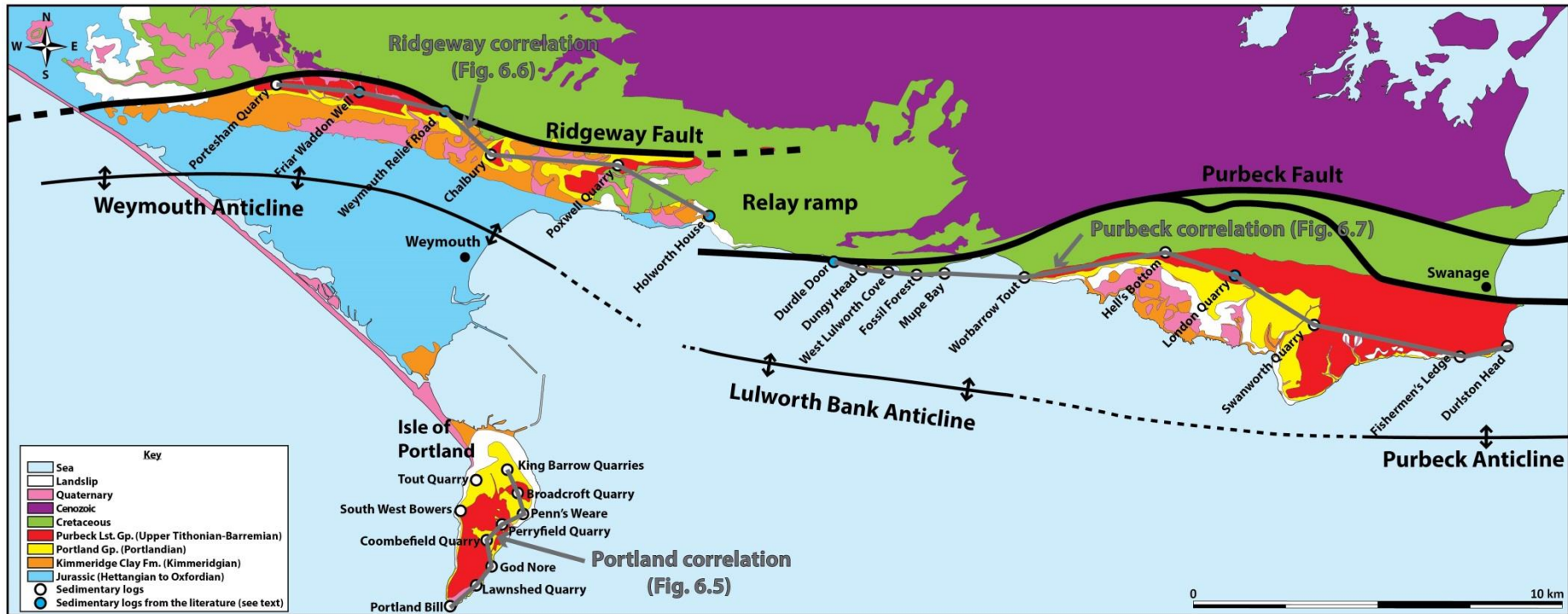
## 2. Sedimentary logs

Purbeck exposures in south of England are described in Chapter 2, and because this study focuses on the Mupe Member in south Dorset, 22 locations were chosen to cover the greatest area possible and to document the controls on the facies distribution (refer to Chapters 3 and 7 for more details). These sedimentary logs are located in three critical regions and well exposed (Tab.6.1; Fig. 6.1), to the west and close to the Ridgeway Fault; to the east and close to the Purbeck Fault; and to the south on the southern limb of the Weymouth Anticline (*i.e.* the Isle of Portland). These logs were recorded from the uppermost bed of the Portland Group to the lowermost bed of the Hard Cockle Beds (Fig. 6.2, Appendix 3).

The sedimentary log thicknesses depend on stratigraphic thickness and also on outcrop quality and accessibility and vary between about 1.80 m (Chalbury) and 24.5 m (Mupe Bay). In each location samples were collected in each bed (when possible) and were used to define and classify facies presented in Chapter 4. Table 6.1 presents main characteristics of all the sedimentary logs and the logs are presented in Appendix 3.

Sedimentary logs	Coordinates Latitude; Longitude	Thickness recorded	Number of samples (Name of samples)	Beds present
Broadcroft Quarry	50°32'53.74"N; 2°25'35.07"W	9.60 m	16 (BQ)	TB; BDB; SkC, LDB, HC, GDB, SoC, CF; HCB
Chalbury	50°39'9.54"N; 2°26'6.58"W	1.80 m	3 (C)	TB [...] SkC; LDB; HC
Coombefield Quarry	50°31'58.25"N; 2°26'33.65"W	9.65 m	14 (CQ)	BDB; SkC; LDB; HC; GDB; SoC; CF
Dungy Head	50°37'8.92"N; 2°15'43.10"W	3.50 m	Not sampled	BDB; SkC; LDB; HC; GDB; BB
Durlston Head	50°35'43.58"N; 1°59'3.73"W	8 m	6 (DH)	BDB; SkC; LDB; HC; GDB; BB; CF
Fishermen's Ledge	50°35'27.11"N; 1°59'7.26"W	12.10 m	15 (FL)	TB; BDB or LDB; SkC and/or HC; BB; CF
Fossil Forest	50°36'58.37"N; 2°14'23.09"W	22.60 m	4 (FF)	TB; BDB; SkC; LDB; HC; GDB; SoC; BB; CF; HCB
God Nore	50°31'31.41"N; 2°26'22.51"W	12.50 m	11 (GN)	TB; BDB; SkC; LDB; HC; GDB; SoC; CF; HCB
Hell's Bottom	50°37'11.60"N; 2°6'54.88"W	3.80 m	6 (HB)	TB; BDB; SkC
King Barrow Quarries	50°33'22.42"N; 2°26'10.00"W	7.80 m	12 (KB)	BDB; SkC; LDB; HC; GDB; SoC; BB; CF
Lanwshed Quarry	50°31'13.32"N; 2°26'41.79"W	2.95 m	7 (LQ)	TB; BDB; SkC; LDB; HC
Mupe Bay	50°36'58.37"N; 2°13'42.20"W	24.50 m	23 (MB)	BDB; SkC; LDB; HC; GDB; SoC; BB; CF; HCB
Penn's Weare	50°32'27.46"N; 2°25'35.31"W	6.95 m	17 (PW)	BDB; SkC; LDB; HC; GDB; SoC; CF
Perryfield Quarry	50°32'20.56"N; 2°26'6.30"W	10.10 m	15 (PEQ)	TB; SkC; LDB; HC; GDB; CF; HCB
Portesham Quarry	50°40'18.03"N; 2°33'8.62"W	7.20 m	16 (PQ)	TB; BDB; SkC; LDB; HC; GDB; CF
Portland Bill	50°30'53.20"N; 2°27'31.43"W	2.60 m	12 (PB)	TB; BDB; SkC; LDB; HC
Poxwell Quarry	50°39'3.84"N; 2°21'52.12"W	2.40 m	6 (POQ)	TB; SkC; LDB; HC
South West Bowers	50°32'40.06"N; 2°27'10.56"W	9 m	9 (SWB)	DBD; SkC; LDB; HC; GDB; SoC; BB; CF
Swanworth Quarry	50°36'18.15"N; 2°2'29.13"W	2.90 m	11 (SQ)	TB; BDB; SkC; LDB; HC; GDB; CF
Tout Quarry	50°33'11.57"N; 2°26'36.83"W	7.10 m	14 (TQ)	BDB; SkC; LDB; HC; GDB; SoC; CF
West Lulworth Cove	50°37'1.27"N; 2°14'55.18"W	18.90 m	13 (WLC)	SkC; LDB; HC; GDB; SoC; BB; CF; HCB
Worbarrow Tout	50°36'55.95"N; 2°11'11.70"W	21.10 m	18 (WT)	SkC; LDB; HC; GDB; BB; CF; HCB

**Table 6.1** Main characteristics of sedimentary logs undertaken for this study. TB: Transition Bed; BDB: Basal Dirt Bed; SkC: Skull Cap; LDB: Lower Dirt Bed; HC: Hard Cap; GDB: Great Dirt Bed; SoC: Soft Cap; BB: Broken Beds; CF: Cypris Freestone; HCB: Hard Cockle Bed. Note that at Chalbury the beds between the Transition Bed and the Skull Cap were not exposed (refer to Appendix 3).



**Figure 6.1** Simplified geological map of south Dorset with locations of sedimentary logs measured in this study (white disks) and presented in Appendix 3. Note outcrops of Purbeck Limestone Group shown in red. Grey lines illustrate the correlation panels of sedimentary logs presented in this chapter in figures 6.5, 6.6 and 6.7.

### 3. Facies succession and bed transition

#### 3.1. Qualitative description

The generalised log presented in figure 6.2 is for the Mupe Member of south Dorset and gives the characteristic facies of each bed. The facies succession and bed transitions are described below in stratigraphic order. The Transition Bed is located at the base of the Purbeck Limestone Group and is only made of the Wackestone to fine grainstone facies with an erosional surface at the base (Fig. 6.2). This erosional surface marks the contact between Portland Group and Purbeck Limestone Group. The Basal Dirt Bed is an immature rendzina paleosol made of Carbonaceous marl facies with an erosional surface at its base (Fig. 6.2). The Skull Cap bed comprises the Thrombolite sub-facies and the Intraclastic peloidal packstone-grainstone facies (Fig. 6.2). The base of the Skull Cap is made of tabular microbial mounds and the transition with the underlying Basal Dirt Bed is planar (Fig. 6.2). The middle part of the Skull Cap is usually made only of the Intraclastic peloidal packstone-grainstone facies overlain by tabular microbial mounds (Fig. 6.2, refer to Chapter 5). The Lower Dirt Bed is an immature rendzina paleosol made of the Carbonaceous marl facies with an erosional surface at the base (Fig. 6.2). The Hard Cap bed comprises the Microbialite facies (Stromatolite, Burrowed peloidal packstone and Thrombolite sub-facies interdigitated with the Intraclastic peloidal packstone-grainstone facies and the transition with the underlying Lower Dirt Bed is planar (Fig. 6.2). This bed comprises *in-situ* microbial mounds (refer to Chapter 5) mostly developed around tree trunks and branches in places interdigitated with the Intraclastic peloidal packstone-grainstone facies in its lower part (Fig. 6.2). The transition between the lower and upper part of this bed is marked by a finer packstone texture which can onlap onto the sides of large microbial mounds. The Great Dirt Bed is a rendzina paleosol made of the Conglomerate facies with an erosional surface at the base (Fig. 6.2). The Soft Cap bed comprises the Microbialite facies and the Intraclastic peloidal packstone-grainstone facies with a planar surface at the base (Fig. 6.2). In this bed the microbial mounds developed around fallen trees and *in-situ* tree stumps with a domed or doughnut shape interdigitated with the Intraclastic peloidal packstone-grainstone facies (refer to Chapter 5). The overlying Cypris Freestone beds comprise mainly the Cross-bedded peloidal packstone grainstone facies with intercalations of Gypsiferous peloidal packstone and Calcareous sandstone facies beds (Fig. 6.2, Appendix 3). The basal surface is planar, overlying the Soft Cap. The Cypris Freestone beds are overlain by the Hard Cackle Beds, the top of the Mupe Member being located within the Cypris Freestone beds (Appendix 3). In some locations the base of the Cypris Freestone is made of the Broken Beds that comprise the



Evaporite (Breccia and Vuggy sub-facies) facies with a planar surface at the base (Fig. 6.2, refer to Appendix 3). The lower part of these beds are made of the Evaporite vuggy sub-facies, covering the microbial mounds of the underlying Soft Cap bed, and overlain by the Evaporite breccia sub-facies (Tab. 2.2, refer to Appendix 3). The lateral correlation and distribution of these facies is described in section 5.

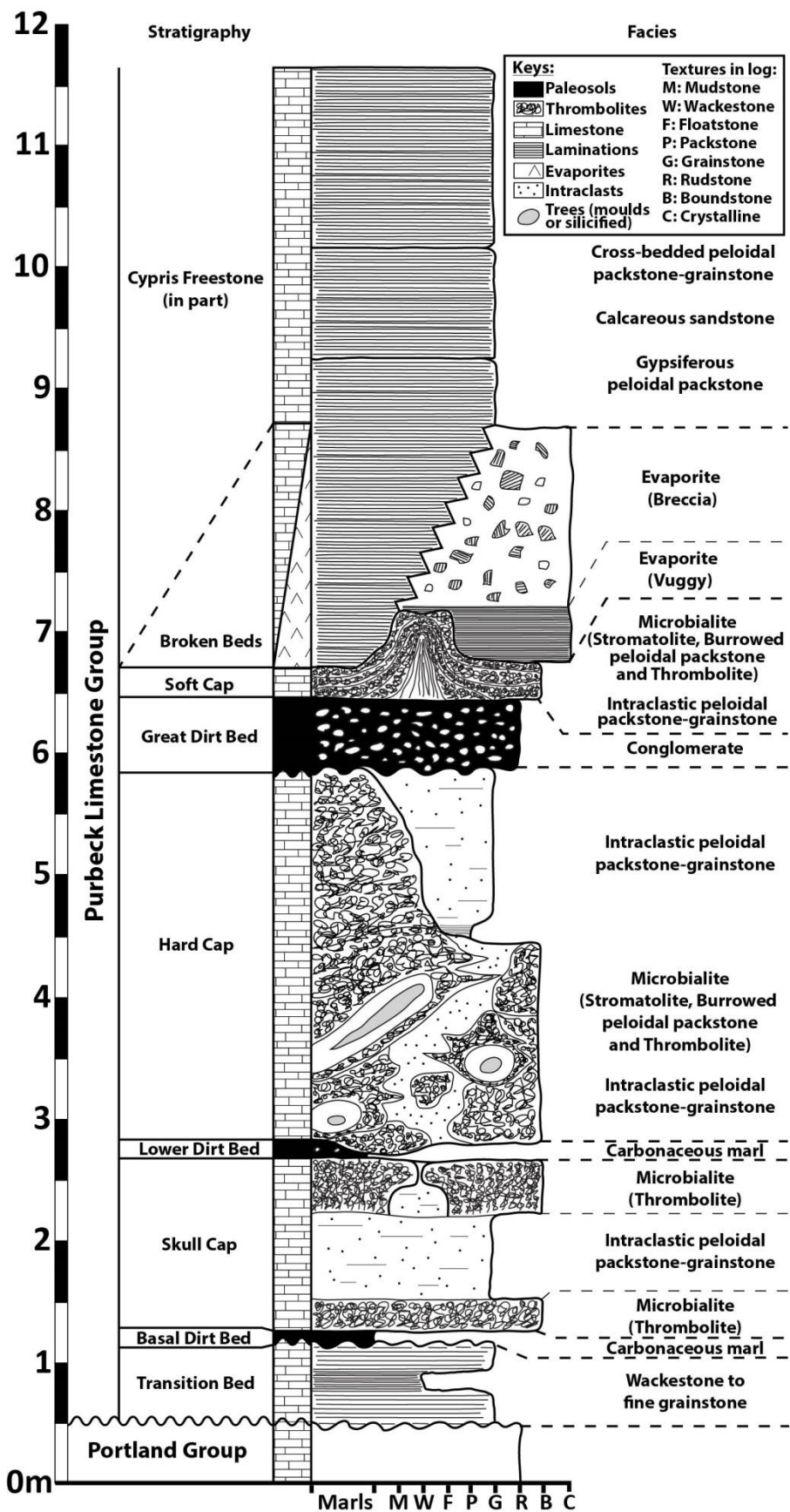


Figure 6.2 Idealised log for the Mupe Member of the study area drawn with average thickness of each bed (refer to Annexe 3 to consult the 22 sedimentary logs used to create this idealised log).

### 3.2. Quantitative analysis

A facies succession analysis as presented in Walker (1979) was used in this study to understand the relationships between facies and to aid in the interpretation of depositional environments. This analysis involves counting each transition between each facies from the recorded logs and this is listed in a matrix (Appendix 3). The result of this facies succession analysis is a facies relationship diagram (Fig. 6.3) that illustrates which transitions of facies are more likely to occur, if facies transitions are not random, according to the difference of probability values (Walker, 1979).

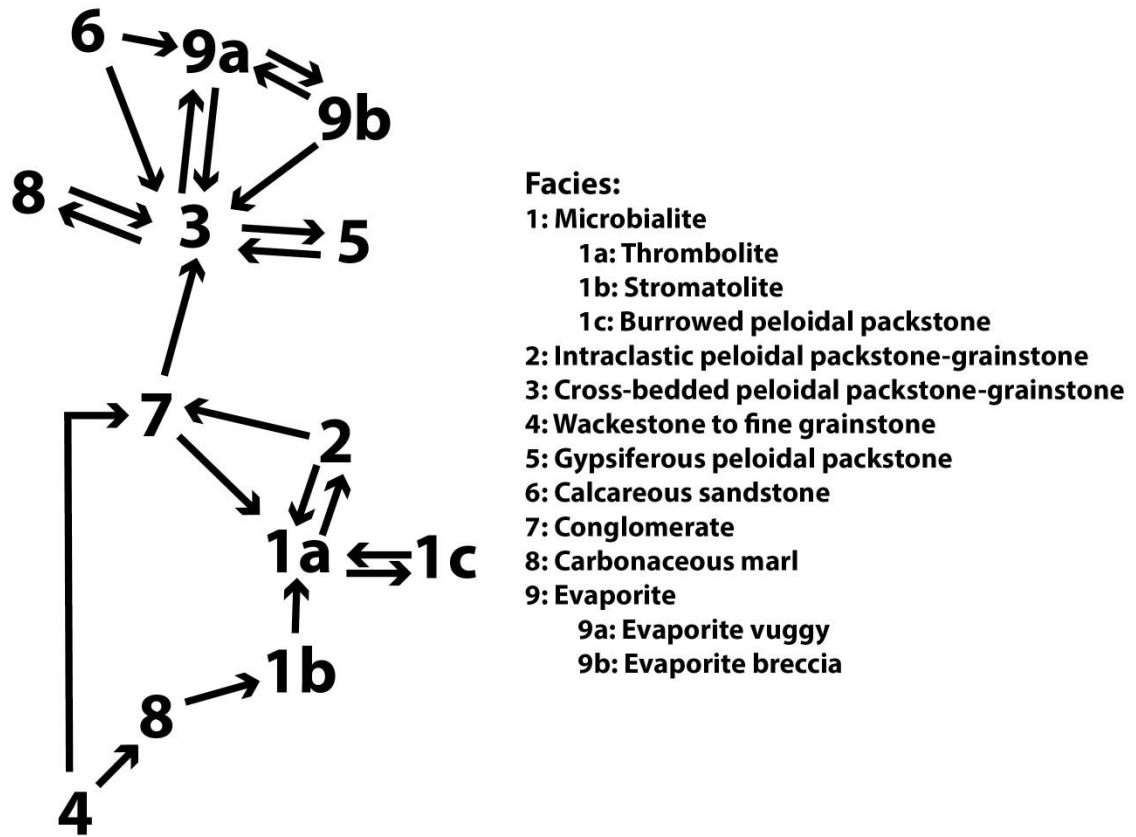
The facies relationship diagram presented in figure 6.3 together with description and interpretation of facies presented in Chapter 4 helps in the definition of five facies associations characterising two main depositional environments (defined and detailed in sections 4 and 5 of this chapter). From the bottom to the top of the lower half of the facies relationship diagram (Fig. 6.3), the Wackestone to fine grainstone facies (facies 4) is always found prior the deposition of the Conglomerate and Carbonaceous marls facies (respectively facies 7 and 8). This is also identified in the sedimentary logs, the Wackestone to fine grainstone facies (facies 4) is mainly found in the Transition Bed at the base of the Mupe Member and overlain by a paleosol (either Conglomerate or Carbonaceous marl facies). The Carbonaceous marl (facies 8) occurs prior the deposition of the Stromatolite sub-facies (facies 1b). The Conglomerate facies (facies 7) is found either prior to the deposition of the Thrombolite sub-facies (facies 1a) or after the deposition of the Intraclastic peloidal packstone-grainstone facies (facies 2). The Thrombolite sub-facies (facies 1a) is found either after the deposition of the Stromatolite sub-facies (facies 1b) and/or interbedded with the Burrowed peloidal packstone sub-facies (facies 1c) and/or interbedded with the Intraclastic peloidal packstone-grainstone sub-facies (facies 2). All of these indicate a succession of strata where microbial mounds (facies 1a, b and c) occur interbedded with the Intraclastic peloidal packstone-grainstone facies (facies 2) and are intercalated between either paleosols, usually overlying the Carbonaceous marl facies and capped by the Conglomerate facies (Fig. 6.3). The Conglomerate facies is found prior to the deposition of the Thrombolite facies which itself is interbedded with the Intraclastic peloidal packstone-grainstone facies and prior the deposition of the Conglomerate facies. This indicates a repetition of succession with this group of strata (Fig. 6.3). This diagram shows that facies transitions are more likely between the Thrombolite and the Burrowed peloidal packstone sub-facies and Intraclastic peloidal packstone grainstone facies (Fig.6.3). The Stromatolite sub-facies is less common and found at the bottom of the succession, if present (Fig.6.3).

Concerning the upper half of the facies relationship diagram (Fig.6.3), the most commonly occurring facies is the Cross-bedded peloidal packstone-grainstone facies (facies 3) as all the other facies transition into this one. As described in Chapter 4, this facies is the most abundant facies of the Cypris Freestone beds (also documented by West, 1975; Anderson, 1985; Horne, 2002). The Carbonaceous marl facies (facies 8), the Gypsiferous peloidal packstone facies (facies 5) and the Evaporite vuggy sub-facies (facies 9a) are all interbedded with the Cross-bedded peloidal packstone-grainstone facies (facies 3). The Evaporite breccia sub-facies (facies 9b) occurs either prior the deposition of the Cross-bedded peloidal packstone-grainstone facies (facies 3) or interbedded with the Evaporite vuggy sub-facies (facies 9a). This indicates a non-random succession with the Evaporite vuggy sub-facies at the bottom, overlain by the Evaporite breccia sub-facies and capped by the Cross-bedded peloidal packstone-grainstone facies on top (Fig. 6.3). The Calcareous sandstone facies (facies 6) is found prior the deposition of the Cross-bedded peloidal packstone-grainstone facies or the Evaporite vuggy facies. This indicates that this facies is rather uncommon and less likely to be deposited than the other facies which is confirmed by the recorded sedimentary logs (Fig. 6.3 and refer to Annexe 3 for more details).

The link between the lower and upper halves (Fig. 6.3) is made via the Conglomerate facies (facies 7, paleosol). This facies is found prior the deposition of the Cross-bedded peloidal packstone-grainstone facies (facies 3) and after the deposition of the Wackestone to fine grainstone facies (facies 4) or the Intraclastic peloidal packstone-grainstone facies (facies 2).

This facies relationship diagram (Fig. 6.3) illustrates the commonest facies successions observed in the field and reported in the sedimentary logs and helps to predict which facies are most likely to occur after a given facies (Fig. 6.3; refer to Annexe 3 for more details). In the lower part of the diagram the thrombolites appear to form: after the deposition of stromatolites above a carbonaceous marl paleosol; directly on top of a conglomeratic paleosol without prior deposition of stromatolites; or exclusively inter-related with the Burrowed peloidal packstone sub-facies (Fig. 6.3). This suggests that the thrombolites need an indurated substrate to grow, the pebbles of the conglomeratic paleosol, the Stromatolite sub-facies and/or the Burrowed peloidal packstone sub-facies were used as solid substratum for the Thrombolite sub-facies to develop, as does overgrowth around trees.

In the upper part of the diagram the Cross-bedded peloidal packstone grainstone facies appears to be the most abundant facies and the Calcareous sandstone, Gypsiferous peloidal packstone and Evaporites facies are inter-bedded within it.



**Figure 6.3** Facies relationship diagram for the Mupe Member in south Dorset illustrating facies successions more common than would be expected if the facies transitions were random.

#### 4. Facies associations

Five facies associations are defined on basis of the interpretations of their facies (refer to Chapter 4), the facies transition analysis and their occurrence in the field. These facies associations are: Deep lacustrine, Emergent, Mounded marginal lacustrine, Hypersaline lacustrine and Bedded marginal lacustrine. Table 6.2 presents the main characteristics of each facies association arranged from stratigraphically oldest at base to youngest at top.

Facies associations	Facies	Depositional environments	Thicknesses recorded	Bed occurrence	Location occurrence
<b>Bedded Marginal Lacustrine</b>	- Cross-bedded peloidal packstone-grainstone - Calcareous sandstone	Marginal hypersaline lacustrine	4.50 to 10 m	Cypris Freestone	Throughout study area
<b>Hypersaline Lacustrine</b>	- Evaporite - Gypsiferous peloidal packstone	Marginal hypersaline lacustrine	3.20 to 8.70 m	Broken Beds (Base of Cypris Freestone)	Dungy Head West Lulworth Cove Fossil Forest Mupe Bay Worbarrow Tout Fishermen's Ledge Durlston Head
<b>Mounded Marginal Lacustrine</b>	- Intraclastic peloidal packstone-grainstone - Microbialite	Marginal brackish lacustrine	1 cm to 5.90 m	Soft Cap Hard Cap Skull Cap	Throughout study area
<b>Emergent</b>	- Carbonaceous marl - Conglomerate	Semi-arid climate Mediterranean type	0 to 60 cm	Cypris Freestone Great Dirt Bed Lower Dirt Bed Basal Dirt Bed	Throughout study area
<b>Deep Lacustrine</b>	- Wackestone to fine grainstone	Deep brackish lacustrine	1 cm to 1.20 m	Transition Bed	Portesham Quarry Poxwell Quarry Chalbury Hell's Bottom Swanworth Quarry Fishermen's Ledge Durlston Head God Nore Lawnshed Quarry Portland Bill

**Table 6.2** Main characteristics of facies associations in stratigraphic order from base to top. The colours used are those that identify the facies associations throughout the figures in the thesis.

#### 4.1. Deep lacustrine

The Deep lacustrine facies association comprises just one, rather distinct, facies, the Wackestone to fine grainstone facies. This facies association is found at the base of the Mupe Member in the Transition Bed (West, 2013a) and its occurrence is shown in table 6.2. The thickness of this facies association varies between 1 cm and 1.20 m with an average thickness of 60 cm (Tab. 6.2). The Wackestone to fine-grainstone facies is made of peloids and ostracods and no sedimentary structures such as wave induced features are preserved apart from some planar laminations locally (refer to Chapter 4 for complete description). Because of the fine-grained texture and the absence of sedimentary structures, this facies association is interpreted to be deposited in a deep lake setting, below wave base between meters and tens of meters water depth and in what is interpreted as a brackish water lacustrine environment on basis of the biotas. The local erosion of the shallow marine Portland limestones results in the presence of intraclasts and also marine bioclasts (bivalves, gastropods and echinoids) reworked into this facies. This hypothesis is supported by the observation that the top surface of the Portland Group throughout the studied area is very irregular and eroded (refer to sections 3 and 5 of this chapter).

## 4.2. Emergent

The Emergent facies association comprises the Carbonaceous marl and the Conglomerate facies. This facies association is found in the three paleosols; Basal Dirt Bed, Lower Dirt Bed and Great Dirt Bed (Tab. 6.2) and as described and interpreted in Chapter 4. The thickness of this facies association varies between 1 and 60 cm with an average thickness of about 15 cm (Tab. 6.2). The paleosols and their contents were documented by Francis (1983, 1984, 1986) as reviewed in Chapters 2 and 4. Francis (1986) demonstrated that these paleosols have a Rendzina profile (mature with profiles A/C for the Great Dirt Bed and immature for the Basal and Lower Dirt Beds). The paleosols contain rooted and fallen/drifted ancient conifers (*Protocupressinoxylon purbeckensis*, Francis, 1983) together with cycadophytes (Fitton, 1827; Buckland and De la Bèche, 1836). The type of soil and the occurrence of conifers and cycads were used as evidence by Francis (1986) to interpret these paleosols to have formed under a semi-arid Mediterranean type climate.

## 4.3. Mounded marginal lacustrine

The Mounded marginal lacustrine facies association comprises the Microbialite and the Intraclastic peloidal packstone-grainstone facies. This facies association is found in all the locations studied, in the Skull Cap, Hard Cap and Soft Cap beds (Tab. 6.2) and the thickness varies between 1 cm and 5.90 m with an average thickness of 3.50 m (Tab. 6.2). The coarse-grained texture of the facies (refer to Chapter 4) indicates a rather high energy environment following Dunham's (1962) concepts and classification and consequently a marginal depositional environment interpretation. This is supported by its association with paleosols (Fig. 6.3) and the presence of tabular and mounded low synoptic relief microbial mounds which are interpreted to have grown to lake level in a shallow margin (refer to Chapter 5). The presence of non-marine brackish water ostracods (refer to Chapter 2, according to Anderson, 1985) and gastropods (refer to Chapter 2, according to Clements, 1973 and Radley, 2002) suggests that this facies association represents a brackish water lacustrine (*i.e.* non-marine) environment. This is confirmed by stable isotope (carbon and oxygen) geochemistry analyses, showing signatures of brackish water open lacustrine system (refer to Chapters 2 and 4, Dharmarajah, 2015). The Microbialite facies on their own are not thought to be diagnostic of specific environments (discussed in section 7 of this chapter). The combination of all these

features indicates that this facies association was deposited along the margins of a shallow brackish water lake that flooded over coniferous vegetated shorelines.

#### **4.4. Hypersaline lacustrine**

The Hypersaline lacustrine facies association comprises the Evaporite facies and the Gypsiferous peloidal packstone (Tab. 6.2) and is found at Dungy Head, West Lulworth Cove, Fossil Forest, Mupe Bay, Worbarrow Tout, Fishermen's Ledge and Durlston Head (Tab. 6.2). This facies association is located in and adjacent to the Breccia sub-facies in the Broken Beds at the base of the Cypris Freestone (Tab. 6.2) and its thickness varies between 3.20 and 8.70 m with an average thickness of 2.75 m (Tab. 6.1). The presence of sulphate evaporite crystal pseudomorphs (anhydrite and gypsum) infilled with sediments reflects hypersaline conditions. Because the underlying (Mounded marginal lacustrine) and overlying (Bedded marginal lacustrine) facies associations reflect lacustrine environments; this facies association was most likely deposited in a hypersaline lacustrine system. The important change between the previous facies association and this one is detailed later in sections 5 and 6 of this chapter.

#### **4.5. Bedded marginal lacustrine**

The Bedded marginal lacustrine facies association is composed of the Cross-bedded peloidal packstone-grainstone and Calcareous sandstone facies (Tab. 6.2). This facies association is unique to the Cypris Freestone and is found at all the locations studied. Its true thickness could be measured only at five locations where the Hard Cockle Beds was completely exposed (Tabs. 6.1, 6.2, Appendix 3) and varies between 4.5 and 10 m with an average thickness of 6 m (Tab. 6.2). The occurrence of non-marine biotas such as hypersaline tolerant S-phase ostracods (Anderson, 1985; Horne, 2002), brackish to hypersaline tolerant mollusc gastropods living in a closed system (Clements, 1973) and halite pseudomorphs indicate non-marine hypersaline conditions. This coarse-grained facies with high energy sedimentary structures such as cross-lamination, cross-stratification and herring-bone cross-stratification indicate a shallow marginal environment. Altogether these features suggest a marginal shallow hypersaline lacustrine (*i.e.* non-marine) environment.

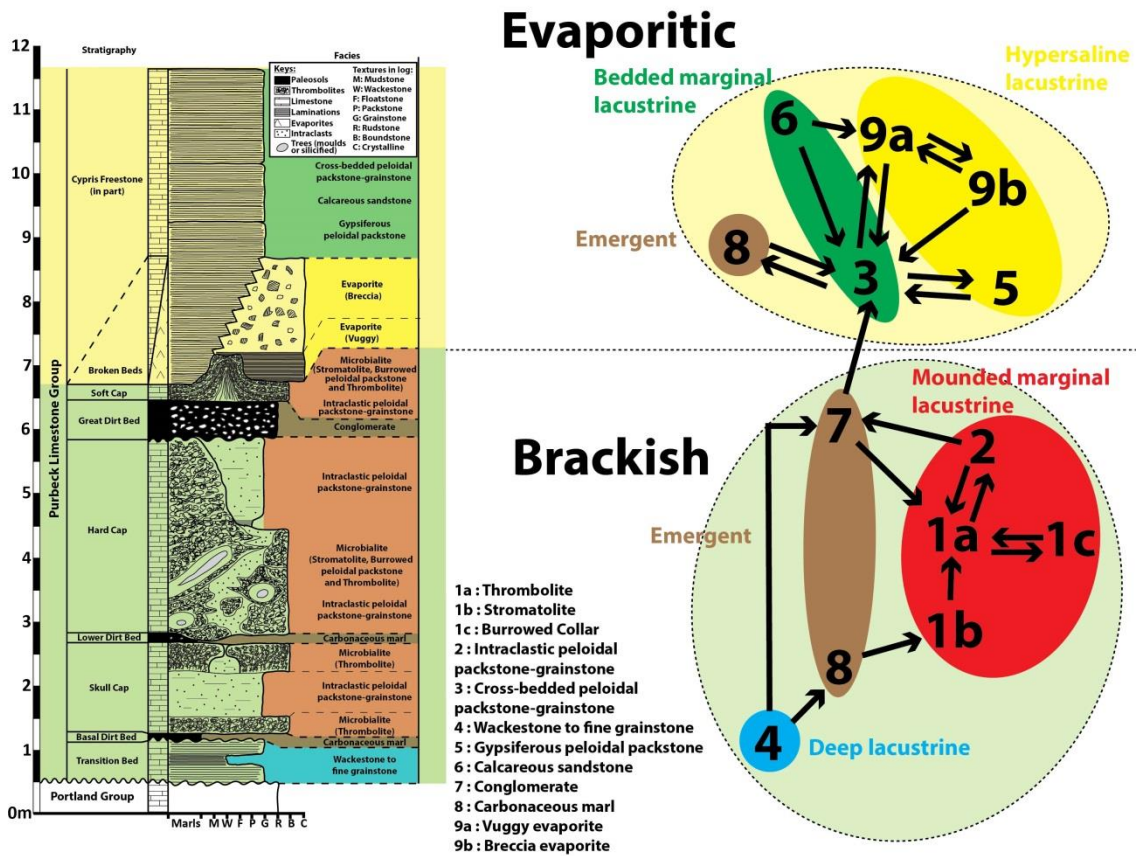


#### 4.6. Facies association successions

The insertion of these five facies associations into the vertical facies transition diagram (Fig. 6.3) allows the identification of successions and vertical relationships between the facies associations (Fig. 6.4). The Deep lacustrine facies association is found at the bottom of the succession and is overlain by the Emergent facies association. Figure 6.4 shows that the latter is closely related to the Mounded marginal lacustrine facies association as it is mainly found in between paleosols (Fig. 6.4). The Emergent facies association is more likely to be overlain by the Bedded marginal lacustrine facies association as indicated in the centre of figure 6.4. The Hypersaline and Emergent (partially) facies associations are interbedded with the Bedded marginal lacustrine facies association (Fig. 6.4). In addition this facies relationship diagram enables the identification of two main depositional environments, brackish water condition at the bottom and evaporitic condition at the top and that are expected to be separated by a paleosol and a flooding surface (Fig. 6.4). The transition between the brackish and the hypersaline water environments is found between the Soft Cap and the Cypris Freestone (Fig. 6.4).

Interpretations of depositional environments of the Mupe Member were proposed by previous authors (refer to Chapter 2). The most important contributors remain West (1975), Francis (1982) and Bosence (1987). West (1975) compared the lack of fossil remains and especially the occurrence of stromatolites in the Skull, Hard and Soft Cap beds of the Purbeck limestones to be very similar to those found in the Persian Gulf hypersaline lagoons. This interpretation was supported by the semi-arid climate Mediterranean type interpreted by Francis (1982, 1983, 1984, 1986) from her study on the paleosols and ancient conifers (refer to Chapter 2). This interpretation was questioned by Bosence (1987) who proposed that the palaeosalinities for the microbialite Cap beds were rather freshwater (refer to Chapter 2). He based his interpretation on occurrence of brackish water bivalves and ostracods, cheironomid larvae burrows (typical in modern day fresh water tufas), trace fossils, ancient conifers, early cements and absence of evaporites (refer to Chapter 2). The data presented in this study do not support the interpretations of West (1975) and Francis (1982, 1983, 1984, 1986) and partially validate Bosence (1987) proposal. In this study it is demonstrated that the microbialites and associated peloidal packstones-grainstones and their close relationship with paleosols bring evidence for marginal lacustrine environment (refer to Chapter 4 and 5) but not on palaeosalinities. However the geochemistry on stable isotopes (carbon and oxygen show typical values of fresh to brackish water conditions (refer to section 7.2 of this chapter).

This together with the brackish water faunas (molluscs and ostracods, refer to Chapters 2 and 4) and the general absence of evaporite pseudomorphs and charophytes indicate marginal lacustrine brackish water conditions for the lower part of the Mupe Member.



**Figure 6.4** Facies relationship diagram with facies association and depositional environments together with the generalised log. Note that the environmental change is found between the Soft Cap and the Cypris Freestone.

## 5. Sedimentary log correlations

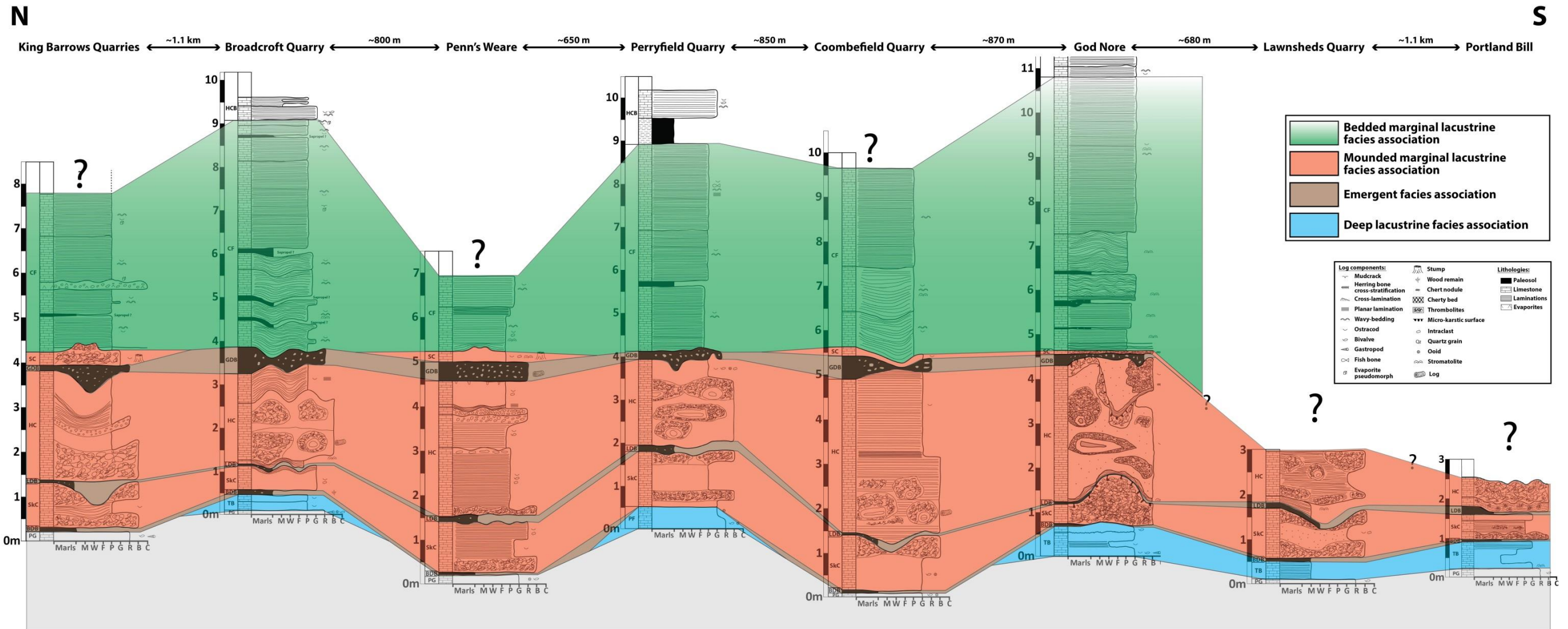
Three sedimentary log correlation panels, named Isle of Portland (Fig. 6.5), Ridgeway (Fig. 6.6) and Purbeck (Fig. 6.7) correlations, were created in order to illustrate the lateral thickness variation of the facies associations. These correlation panels are flattened at the base of the Bedded marginal lacustrine facies association (*i.e.* Cypris Freestone beds) to illustrate thickness variations in the underlying Cap beds and Dirt Beds. If a facies association was only partially exposed, the flattening was done at the top of the nearest previous fully exposed facies association (Figs. 6.5, 6.6, 6.7). Some of the correlation panels include sedimentary logs from the literature for sections no longer accessible and from borehole data. This integration of logs from the literature was possible because the facies described by previous authors can be adapted to those defined in this study and because each bed corresponds to a unique facies

association throughout the studied area. As a consequence the stratigraphic interpretations (*i.e.* beds recognition) of previous authors were used to correlate their sections with those proposed in this study. These correlation panels were used to create the south Dorset fence diagram presented in figure 6.8.

### **5.1. Isle of Portland correlation**

This north-south correlation panel (Fig. 6.5) is located in the southern limb of the Weymouth Anticline on the east coast of the Isle of Portland, and is far from the faults in the northern part of the area (Fig. 6.1). This panel is made of sedimentary logs recorded from north to south in King Barrow Quarries, Broadcroft Quarry, Penn's Weare, Perryfield Quarry, Coombefield Quarry, God Nore, Lawnsheds Quarry and Portland Bill (Fig. 6.5). In this correlation panel the Hypersaline lacustrine facies association was not identified (Fig. 6.5) providing evidence for more open lacustrine waters in their area. Purbeck exposures in Lawnsheds Quarry and Portland Bill are near the present day soil and are cut into by Quaternary beach deposits so it is not certain if the top of the Mounded marginal lacustrine facies association was reached or not (Fig. 6.5). The Deep lacustrine facies association is present only in Broadcroft Quarry to the north and in God Nore, Lawnsheds Quarry and Portland Bill to the south (Fig. 6.5). This may be explained as either a lateral facies transition or a deposition and subsequent erosion of this bed. In the former case, this might represent the transition between shallower areas to the north and the west and deeper areas to the south and to the east of the Isle of Portland (refer to Chapter 7). In the latter case, differential erosion of this bed may have occurred prior to, or part of the development of the overlying paleosol (Basal Dirt Bed) as reworked clasts (mainly from Portland Group, refer to Chapter 4) are common in this facies and that the base and top bed contacts are erosional. The Mounded marginal lacustrine facies association is present everywhere over the Isle of Portland with a thickness between 3.50 and 5.50 m, however no significant thickness variations are identifiable (Fig. 6.5).

An important feature for the facies distribution of this correlation panel is that individual beds such as the Skull Cap, Lower Dirt Bed, Hard Cap, Great Dirt Bed and Cypris Freestone can be traced over the Isle of Portland and are laterally extensive at this scale (Fig. 6.5). These are opposed to the Transition Bed, Basal Dirt Bed and Soft Cap that appear to be more irregularly present and less laterally extensive (Fig. 6.5).



**Figure 6.5** North to south Isle of Portland correlation panel of sedimentary logs. Note that logs are spaced evenly for presentation. In the stratigraphic column (on the left of each log) are the names of the beds where PG: Portland Group; TB: Transition Bed; BDB: Basal Dirt Bed; SkC: Skull Cap; LDB: Lower Dirt Bed; HC: Hard Cap; GDB: Great Dirt Bed; SC: Soft Cap and CF: Cypris Freestone. The texture at the bottom of each log correspond to Dunham (1962) classification with M: Mudstone, W: Wackestone, F: Floatstone, P: Packstone, G: Grainstone, R: Rudstone, B: Boundstone and C: Crystalline. Location of the panel in figure 6.1.

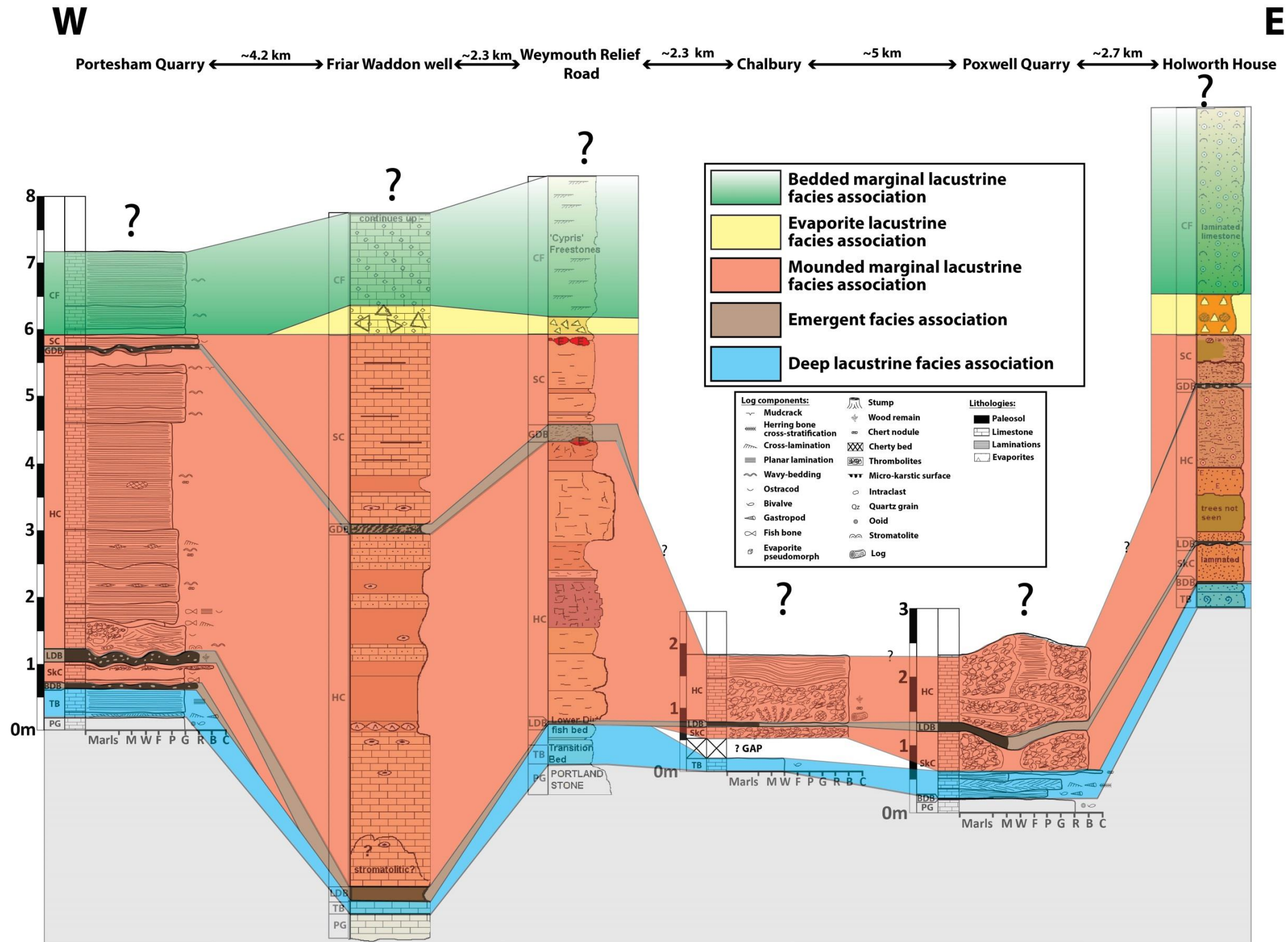
## 5.2. Ridgeway correlation

This panel (Fig. 6.6) is located on the northern limb of the Weymouth Anticline, into the north-west of the studied area, south of the Ridgeway Fault and with an east-west trend (Fig. 6.1). This correlation panel is made of sedimentary logs recorded in Portesham Quarry, Chalbury and Poxwell Quarry (Fig. 6.6). In addition published sedimentary logs from Holworth House (50°38'1.00"N; 2°20'16.94"W) from West (1975), Friar Waddon well (50°40'14.85"N; 2°29'35.44"W) from West *et al.* (2013), Weymouth relief road (50°39'54.88"N; 2°27'41.94"W) from West *et al.* (2013) are included. This correlation panel shows that the four facies associations are present in the six locations, apart from the Hypersaline lacustrine facies association which is absent from Portesham Quarry (Fig. 6.6). Purbeck exposures in Chalbury and Poxwell Quarry are limited in extent and it is not certain if the top of the Mounded marginal facies association was reached or not (Fig. 6.6).

The Deep lacustrine facies association (Transition Bed of West, 2013a) is between 25 and 50 cm thick, is present at the six locations and does not show significant thickness variation along this transect (Fig. 6.6).

The Mounded marginal lacustrine facies association is present at the six locations although microbial mounds are less abundant compared with the Isle of Portland. Here (just south of the Ridgeway Fault, Fig. 6.6) deposits reflect more freshwater conditions as evidenced by freshwater gastropods, ostracods and charophytes in a chert (West, 1961; Barker *et al.*, 1975). Friar Waddon well log presents the greatest thickness (about 8.5 m) for the Mounded marginal facies association followed by Portesham Quarry (about 5.5 m) and Weymouth Relief Road (about 6.5 m) logs; whilst the Holworth House section is slightly thinner (about 3.70 m). Portesham Quarry, Friar Waddon and Weymouth Relief sections are located in the central part of the Ridgeway Fault (Figs. 6.1 and 6.6) and have greater thickness of the Mounded marginal facies association compared to locations near the tips of the fault (*i.e.* Holworth House). This evidence supports the interpretation of fault activity during the deposition of the Mounded marginal lacustrine facies association. Moreover the occurrence of more freshwater conditions (West, 1961; Barker *et al.*, 1975) provides evidence for a fluvial input to this area (refer to Chapter 7).

As for the previous correlation panel an important feature for the facies distribution is that all the beds (apart from the Skull Cap and the Basal Dirt Bed in Friar Waddon well and Weymouth Relief Road) can be traced throughout this panel (Fig. 6.6).



**Figure 6.6** Ridgeway correlation of sedimentary logs both recorded and from the literature; Friar Waddon well (West *et al.*, 2013), Weymouth Relief Road (West *et al.*, 2013) and Holworth House (West, 1975). Correlation between the logs recorded in this study and the ones from the literature was done using interpretation from authors. In the stratigraphic column (on the left of each log) are the names of the beds where PG: Portland Group; TB: Transition Bed; BDB: Basal Dirt Bed; SkC: Skull Cap; LDB: Lower Dirt Bed; HC: Hard Cap; GDB: Great Dirt Bed; SC: Soft Cap and CF: Cypris Freestone. The texture at the bottom of each log correspond to Dunham (1962) classification with M: Mudstone, W: Wackestone, F: Floatstone, P: Packstone, G: Grainstone, R: Rudstone, B: Boundstone and C: Crystalline. Location of the panel in figure 6.1.

### 5.3. Purbeck correlation

This panel (Fig. 6.7) is located also in the northern limb of the Weymouth Anticline comprising coastal sections, to the east of the studied area, south of the Purbeck Fault and with an east-west trend (Fig. 6.1). This correlation panel is made of sedimentary logs recorded in Dungy Head, West Lulworth Cove, Fossil Forest, Mupe Bay, Worbarrow Tout, Hell's Bottom, Swanworth Quarry, Fishermen's Ledge and Durlston Head (Fig. 6.7). In addition London Door Quarry (50°36'44.68"N; 50°36'44.68"N) and Durdle Door sedimentary logs from West (1975) were also included. Purbeck exposures are limited at Dungy Head and London Door Quarry as the top of the Hypersaline lacustrine facies association is no longer exposed (Fig. 6.7). Similarly in Hell's Bottom the top of the Mounded marginal lacustrine facies association was not exposed (Fig. 6.7).

The Deep lacustrine facies association is present in Fossil Forest, although it is very thin (about 10 cm thick) and eastwards in Hell's Bottom, London Quarry, Swanworth Quarry, Fishermen's Ledge and Durlston (Fig. 6.7). This facies association is rather thin and relatively constant between 20 and 50 cm at these locations (Fig. 6.7). The contained clasts were partially eroded from the underlying Portland Group as shown by the occurrence of bivalves, gastropods, echinoid plates, ooids, and other marine fossils typical the Portland Group (refer to Chapter 4).

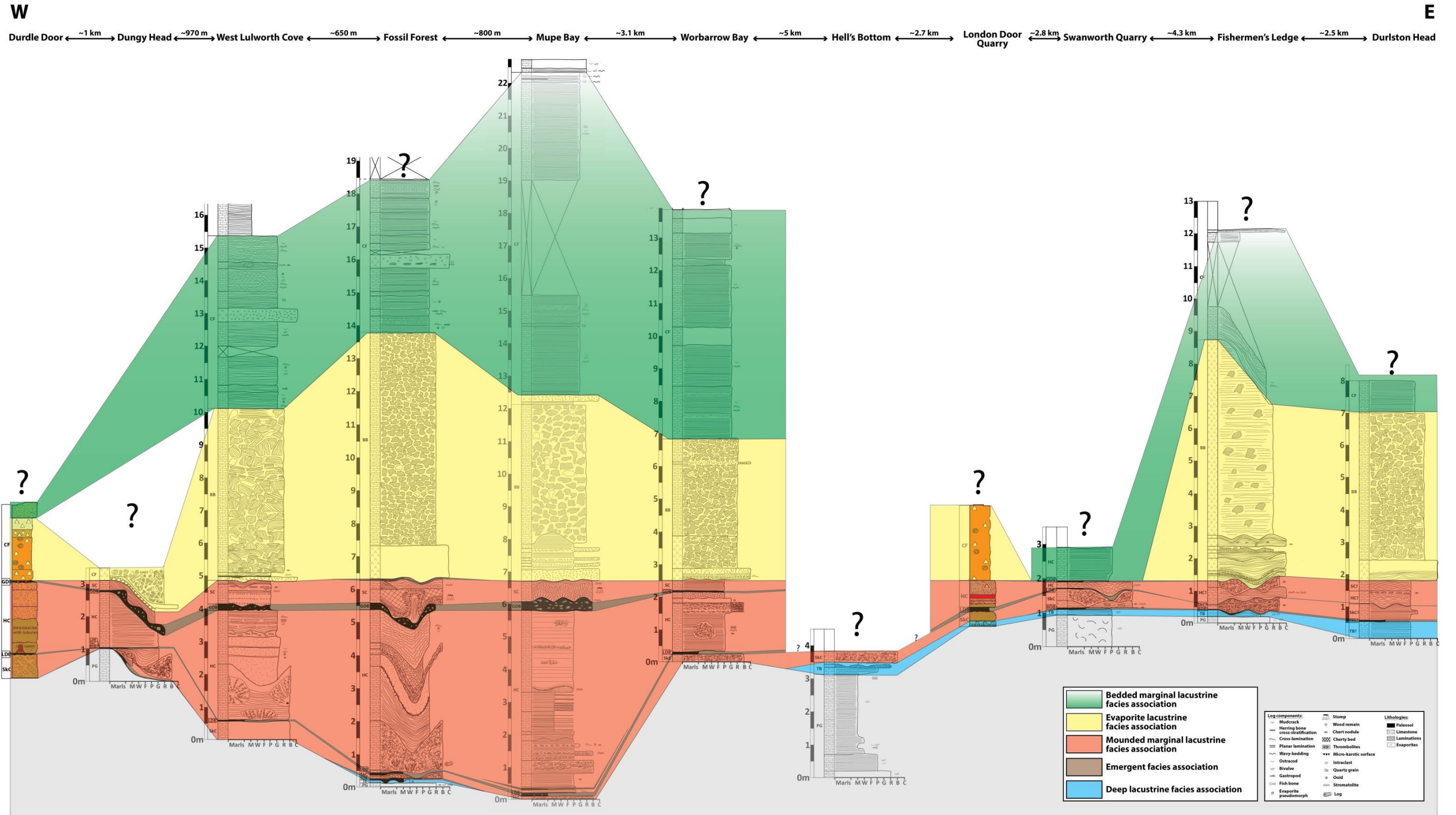
The Mounded marginal lacustrine facies association is present everywhere and is between about 2 and 6.75 m to the west of this panel and between about 80 cm and 1.25 m to the east (Fig. 6.7). The thickest areas are located in the hanging-wall block of the Purbeck Fault and close to the fault (Fig. 6.1) and indicate greater accommodation during deposition (Fig. 6.7). From London Door Quarry eastwards (Figs. 6.1 and 6.7), the measured sections are recorded progressively further away from Purbeck Fault (Figs. 6.1 and 6.7) and have a much thinner Mounded marginal lacustrine facies association. This can be explained with two scenarios: 1) less fault-related subsidence leading to less accommodation space and resulting in much thinner shallow lacustrine deposits; or 2) deeper water would imply thinning out of shallow facies accompanied with loss of both mound developments and paleosols. The Skull Cap at Dungy Head presents a feature that was never found anywhere else in the studied area. This bed together with the Basal Dirt Bed paleosol are observed to onlap on the top of the Portland Group and to be capped by the Lower Dirt Bed paleosol (Fig. 6.7). This is interpreted to show the position of a portion of a palaeoshoreline. However the Skull Cap was deposited laterally as indicated by its occurrence to the west at Durdle Door and to the east at Lulworth Cove that

implies that this feature is very localised (Fig. 6.7). This palaeohigh might locate the position of an island or a peninsula of eroded Portland limestones (refer to Chapter 7).

The Hypersaline lacustrine facies association is present in all the locations except Hell's Bottom (due to exposures limitation) and Swanworth Quarry (Fig 6.7). Although deposited at Dungy Head and London Door Quarry, the top of the Hypersaline lacustrine facies association was not accessible in the field (Fig. 6.7). Where deposited, the thickness is more or less similar, but varying between 4.50 and 6.50 m, except at Durdle Door where the thickness is about 2 m. This thickness variation is similar to that of the Mounded marginal lacustrine facies association for these locations. As argued above, this is thought to be controlled by syn-tectonic setting associated movement of the Purbeck Fault in this area (Lulworth Cove to Worbarrow Bay, Fig. 6.7). Because this facies association is thinner at Durdle Door than the other eastwards locations, it is thought that the subsidence was greater in the central part of the Purbeck Fault compared to the fault tips (Fig. 6.7).

As for the previous panels, similar conclusion can be drawn in the extent of the facies associations throughout the eastern part of the studied area (Fig. 6.7). Most of individual beds can be traced along the panel apart from the Transition Bed and the Soft Cap (Fig. 6.7).

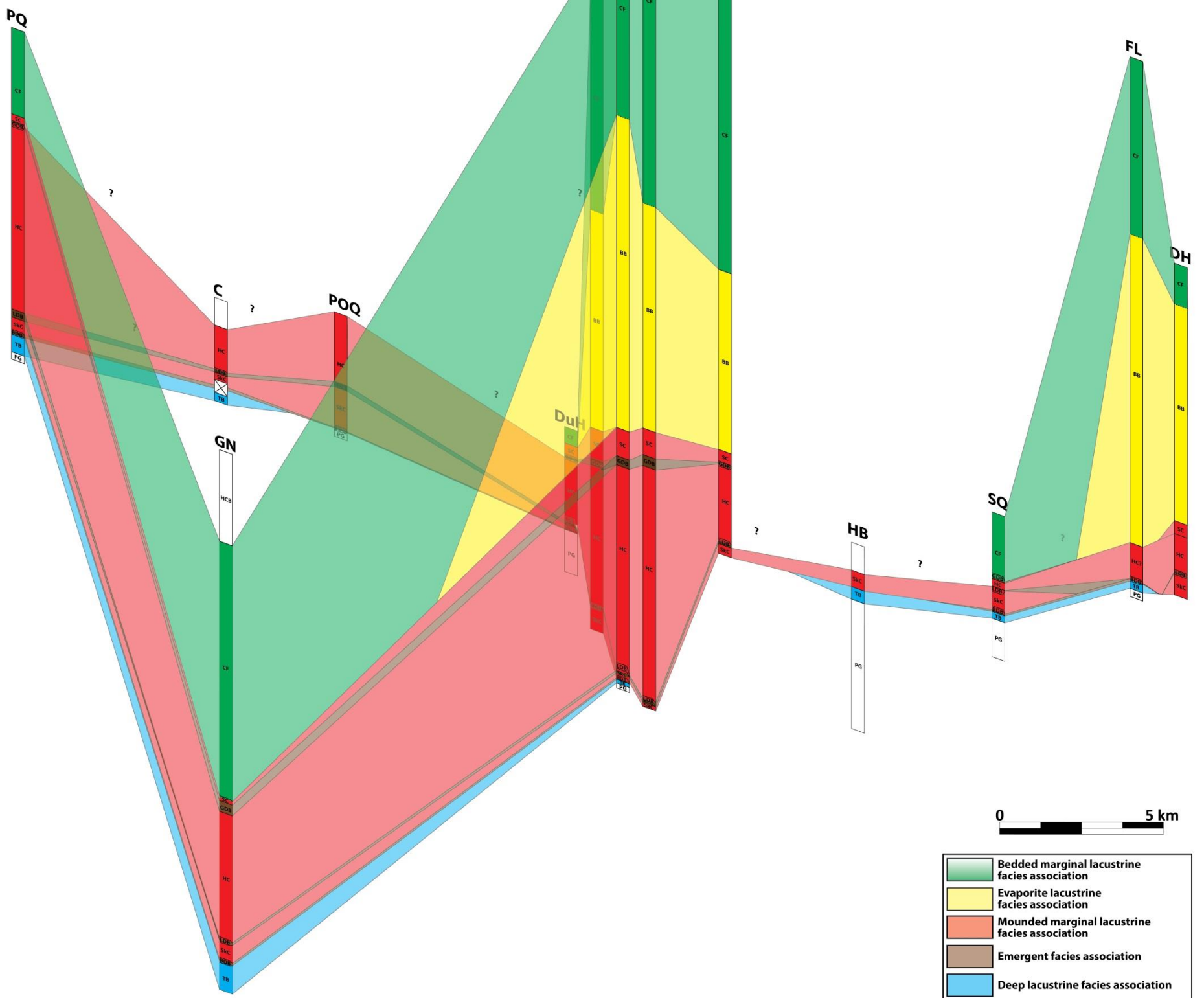
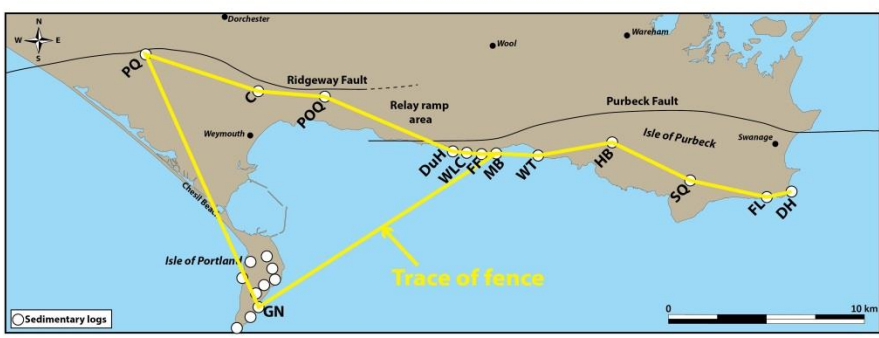




**Figure 6.7** Purbeck correlation of sedimentary logs both recorded and from the literature. Durdle Door and London Door Quarry logs are from West (2015). Correlation between the logs recorded in this study and the ones from the literature was done using interpretation from authors. In the stratigraphic column (on the left of each log) are the names of the beds where PG: Portland Group; TB: Transition Bed; BDB: Basal Dirt Bed; SkC: Skull Cap; LDB: Lower Dirt Bed; HC: Hard Cap; GDB: Great Dirt Bed; SC: Soft Cap, BB: Broken Beds and CF: Cypris Freestone. The texture at the bottom of each log correspond to Dunham (1962) classification with M: Mudstone, W: Wackestone, F: Floatstone, P: Packstone, G: Grainstone, R: Rudstone, B: Boundstone and C: Crystalline. Location of the panel in figure 6.1.

#### 5.4. Summary

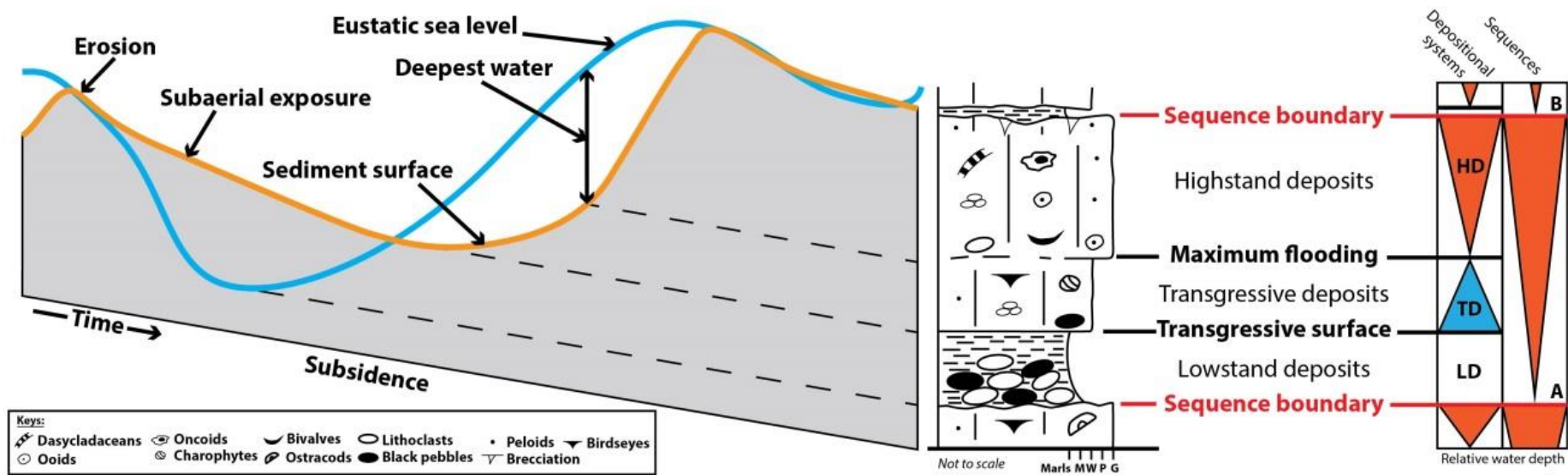
The three correlation panels of sedimentary logs show that the beds and facies associations can be traced throughout the studied area. This is also depicted in figure 6.8 where a fence diagram over the studied area shows similar thickness variations. The Deep lacustrine and Emergent facies associations show more or less consistent thicknesses when exposed, both between 10 and 50 cm. Concerning the Mounded marginal lacustrine facies association, its thickness varies depending on the bed considered. In the Skull Cap this facies association is thicker over the Isle of Portland (around 1 m thick), in the Soft Cap around Lulworth area (around 1 m thick) and in the Hard Cap to the north and close to the faults (around 5-6 m thick). To the west the Mounded marginal lacustrine facies association makes up the section due to the absence of the Hypersaline lacustrine facies association in the Isle of Portland (refer to Chapter 7). However to the north-west both Mounded marginal lacustrine and Hypersaline lacustrine facies associations were deposited, although the Hypersaline lacustrine facies association is very thin (less than 50cm) between Friar Waddon well and Holworth House (Figs. 6.6 and 6.8). In the centre part of the studied area (east side of the Purbeck correlation) there is a similar thickness of the Mounded marginal and Hypersaline lacustrine facies associations (Figs. 6.5 and 6.8). To the east the Mounded marginal lacustrine facies association thins and the Hypersaline lacustrine facies association thickens and this represents a more basinward direction (Figs. 6.7 and 6.8). This facies change is interpreted to reflect more brackish water conditions in the margins of the basin to the west and more hypersaline water conditions towards the centre of the basin to the east. This suggests two different lacustrine systems, an open system also shown by stable isotope measurements done in the inter-mound facies on the Isle of Portland (refer to Chapter 4 and section 7.2 of this chapter) to the west and a closed system to the east. This spatial change may be due to a geographical barrier as illustrated by a high on the lake floor due to fault-controlled offset separating naturally the lake into two sub-basins in the Great Salt Lake (Utah, USA); or it could be due to an isolation of two or more hydrologically different lakes as Rottneest Island lakes (Western Australia) illustrates. This will be detailed in Chapter 7 with integration of all the data presented in this project.



**Figure 6.8** Fence diagram of the facies associations throughout the studied area. Note that on the Isle of Portland God Nore log summarises all the logs of the island. C: Chalbury, DuH: Dungy Head, DH: Durlston Head, FL: Fishermen's Ledge, FF: Fossil Forest, GN: God Nore, HB: Hell's Bottom, MB: Mup Bay, PQ: Portesham Quarry, POQ: Poxwell Quarry, SQ: Swanworth Quarry, WLC: West Lulworth Cove, WB: Worbarrow Bay. In the stratigraphic columns are the names of the beds where PG: Portland Group; TB: Transition Bed; BDB: Basal Dirt Bed; SKC: Skull Cap; LDB: Lower Dirt Bed; HC: Hard Cap; GDB: Great Dirt Bed; SC: Soft Cap, BB: Broken Beds and CF: Cypris Freestone.

## 6. Sequence stratigraphy of the Mupe Member

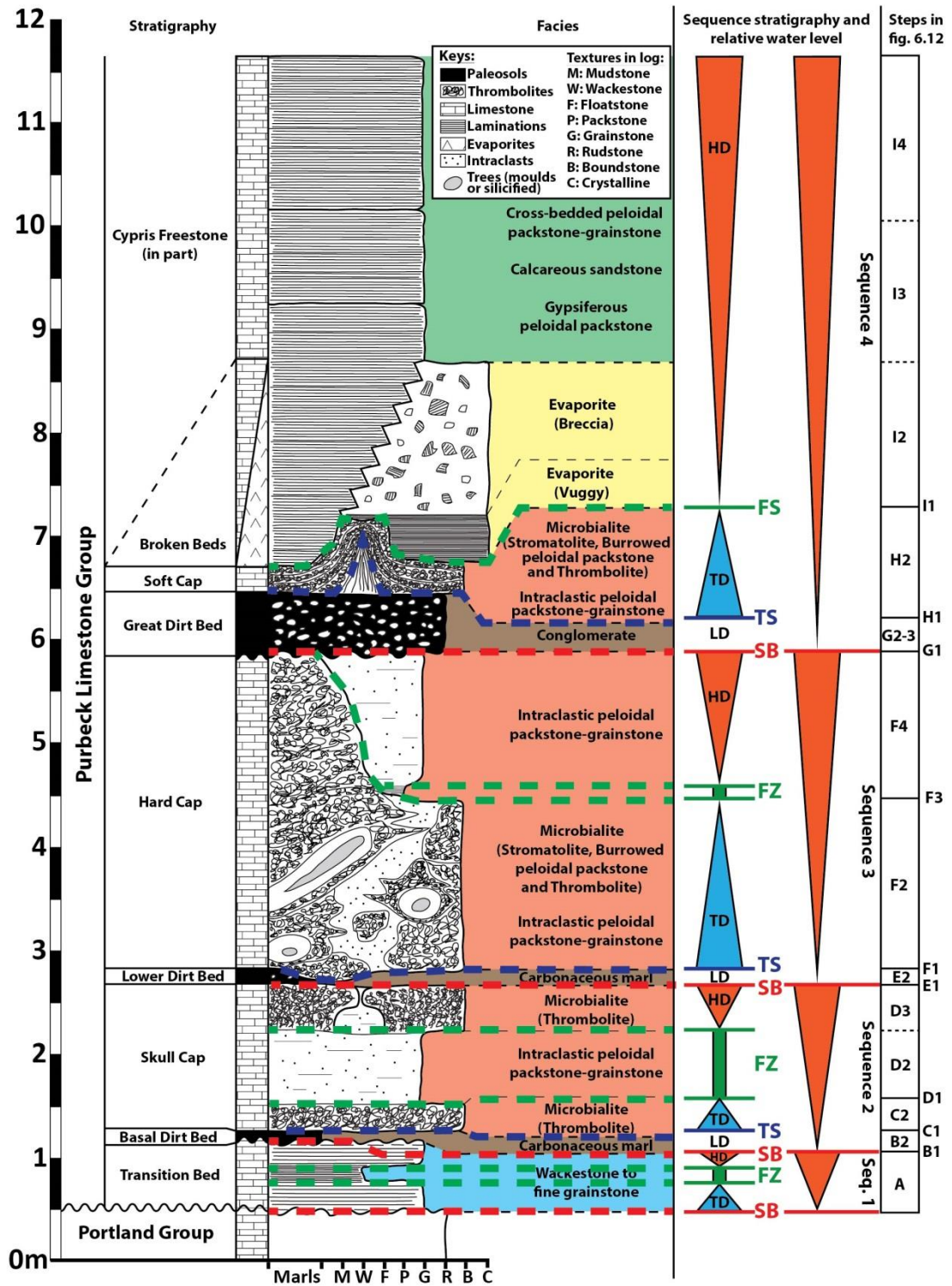
A sequence was defined by Sloss *et al.* (1949) as a stratigraphic unit (later redefined as genetically related strata by Mitchum, 1977) bounded by subaerial unconformities. This definition was later retaken by Posamentier (1988), Galloway (1989), Catuneanu (2006) and Miall (2010). Sequences may be subdivided into systems tracts that group strata deposited during a similar shoreline shift due to rise and fall of water (sea or lake) levels (Brown and Fisher, 1977; Catuneanu, 2006). As demonstrated by Catuneanu (2006), sequences and systems tracts are independent of scale (time, thickness or lateral extent). This important point makes the sequence stratigraphic analysis applicable in this study. Strasser (1994) presented high-resolution sequence stratigraphy and interpretation of sea-level change for peritidal deposits (Fig. 6.9). These deposits are from the Tidalites-de-Vouglans and Goldberg Formations deposited during late Tithonian and early Berriasian and exposed in the French Jura Mountains. These deposits are time-equivalents to the Purbeck Limestone Group of south of England but were deposited in different depositional settings. The model for how depositional sequences and system tracts may be controlled by sea-level change as presented by Strasser (1994) is used in this study to interpret depositional sequences of the Mupe Member deposits (Fig. 6.10). Strasser (1994) defined depositional systems that compose sequences (bounded by unconformities) where each depositional system corresponds to a systems tract (Fig. 6.9; after Vail *et al.*, 1984; Vail, 1987; Sarg, 1988). Strasser's (1994) depositional sequences illustrate shallowing-upward trends indicated by progressive change from deeper to shallower facies (Fig. 6.9). Another important point, that is relevant to this study, is the interpretation of the paleosols as lowstand deposits bounded by subaerial unconformities at their base and by transgressive surfaces at their tops (Fig. 6.9; Strasser, 1994). The rise of sea-level results in the deposition of deepening-upward deposits due to increasing of accommodation space as the shoreline moves landwards (Fig. 6.9; Strasser, 1994). These transgressive deposits are top-bounded by a maximum flooding surface that corresponds to the maximum water depth in the sequence (Fig. 6.9; Strasser, 1994). Note that if a unique flooding surface is not clearly identifiable, Strasser *et al.* (1999) defined maximum-flooding zones. This flooding results in the deposition of highstand deposits that either prograde or aggrade towards the centre of the basin due to a decreasing rate of rise of sea-level (Fig. 6.9; Strasser, 1994). These highstand deposits are terminated by a subsequent sea-level fall and creation of a new subaerial exposure surface that defines the top sequence boundary (Fig. 6.9; Strasser, 1994).



**Figure 6.9** Hypothetical model to illustrate how depositional systems can be related to cyclic changes in water depth. Peritidal deposits of Tidalites-de-Vouglans and Goldberg Formations (Upper Tithonian-Lower Berriasian) from French Jura Mountains (modified after Strasser, 1994 and Strasser *et al.*, 1999). HD: Highstand Deposits; LD: Lowstand Deposits; TD: Transgressive Deposits.

The Skull Cap and Hard Cap and the intervening Dirt Beds of the Purbeck limestones are interpreted using this model. In the Purbeck limestones, sequence boundaries correspond to subaerial exposure surfaces on top of previous deposits and are characterised by irregular erosion surfaces interpreted to result from drop of the lake level (Fig. 6.10). The overlying lowstand deposits correspond to soil development in the Emergent facies association with reworked limestone and black pebbles from the underlying beds, *in-situ* or fallen tree trunks and cycadophytes (refer to Chapter 4). The top of the lowstand deposits is marked by a transgressive surface followed by transgressive deposits topped by a flooding zone when the system reaches its maximum water depth (Fig. 6.10). The flooding zone is interpreted to correspond to the maximum depth but where a flooding surface cannot be determined precisely. This flooding zone is commonly a finer-grained (packstone) than the underlying transgressive and overlying highstand deposits that indicate a reduction of the carbonate production interpreted to represent slightly deeper and/or calmer water. The transgressive deposits are characterised by deepening-upwards trends in the Microbialite facies interdigitated with the Intraclastic peloidal packstone-grainstone facies (Fig. 6.10). The overlying highstand deposits are characterised by shallowing-upward trends capped by irregular erosional surface indicating the top sequence boundary and defines the top of these two depositional sequences (Fig. 6.10). These highstand deposits are characterised either by the Wackestone to fine grainstone facies in the Deep lacustrine facies association (Transition Bed, blue area in figure 6.10); or the Intraclastic peloidal packstone-grainstone facies in the Mounded marginal lacustrine facies association (red areas in figure 6.6); or the Cross-bedded peloidal packstone-grainstone facies in the Bedded marginal lacustrine facies association (green area in figure 6.10); or the Evaporite facies in the Hypersaline lacustrine facies association (yellow area in figure 6.10).

Figure 6.10 presents an idealised sedimentary log with the most representative and best expression of facies for each bed. This results in the identification and definition of four, meter-scale lacustrine cycles that are deepening-upward and then shallowing-upward, and depositional systems in the Mupe Member (refer to Appendix 3). These cycles are bounded by subaerial exposure surfaces prior development of paleosols that can therefore be named sequences (Fig. 6.10). Sequences 2 and 3 are symmetrical while sequences 1 and 4 appear to be asymmetric (Fig. 6.10).



**Figure 6.10** Idealised log with interpretation of depositional cycles. Red triangles are for shallowing-upward trends and blue triangles are for deepening-upward trends. The coloured areas in the facies column correspond to the facies association and are the same as in table 6.2. SB: Sequence Boundary; FS: Flooding Surface; FZ: Flooding zone; HD: Highstand Deposits; LD: Lowstand Deposits; TD: Transgressive Deposits; TS: Transgressive Surface. Numbering in the right column corresponds to detailed steps in figure 6.12.

The first depositional sequence corresponds to the Transition Bed and is bounded by two subaerial surfaces (Fig. 6.10). The bottom subaerial surface corresponds to the exposed and eroded top of the Portland Group and the top subaerial exposure corresponds to the top of the Transition Bed when it was exposed and eroded (Fig. 6.12). In this sequence the sequence boundary and transgressive surface are expressed with only one surface. This surface is overlain by transgressive deposits characterised by fine grainstone facies of the Deep lacustrine facies association that can locally contain reworked material from the Portland Group (refer to Chapter 4). This transgressive system is bounded on top by flooding zone due to a rise in lake level to its maximum depth in this sequence, characterised by finer-grained facies such as wackestones of the Deep lacustrine facies association (Fig. 6.10). This flooding surface zone is overlain by highstand deposits composed of fine grainstone facies of the Deep lacustrine facies association (Fig. 6.10). The overall fine-grained texture indicates a rather low energy environment and the lowest in the entire depositional system of the Mupe Member.

The second depositional sequence corresponds to the Basal Dirt Bed and the Skull Cap bed and is bounded by two subaerial exposure surfaces (Fig. 6.12). The underlying surface corresponds to the eroded surface of the previous sequence (*i.e.* the top of the Transition Bed) and the top subaerial surface corresponds to the upper part of the Skull Cap bed when it was exposed and eroded (Figs. 6.10 and 6.12). The Basal Dirt Bed is interpreted as a lowstand deposit represented by Carbonaceous marl facies. This paleosol is bounded by a transgressive surface due to a rising lake level. This resulted in the deposition of the first part of the Skull Cap bed as transgressive deposits made of tabular thrombolitic microbial mounds and capped by a flooding zone (*sensu* Strasser *et al.*, 1999). This flooding zone is composed of the Intraclastic peloidal packstone-grainstone facies that indicates that the carbonate production and/or the energy in the system remained the same as the underlying bed but without the microbial mounds. This flooding zone is capped by highstand deposits made of more tabular thrombolitic microbial mounds indicating shallowing-upwards and subsequent subaerial exposure of the overlying erosion surface and sequence boundary (Fig. 6.10). In this sequence, only shallow facies were deposited indicating that the water depth remained shallow during the transgression and illustrating a catch-up phase (Catuneanu, 2006) prior a second forced regression resulting from a drop of the lake level, the exposure and erosion of the tabular microbial mounds (Fig. 6.12).

The third depositional sequence corresponds to the Lower Dirt Bed and the Hard Cap bed and is bounded by two subaerial surfaces (Fig. 6.10). The bottom subaerial surface corresponds to the eroded surface on top of the previous sequence exposures (*i.e.* the top of



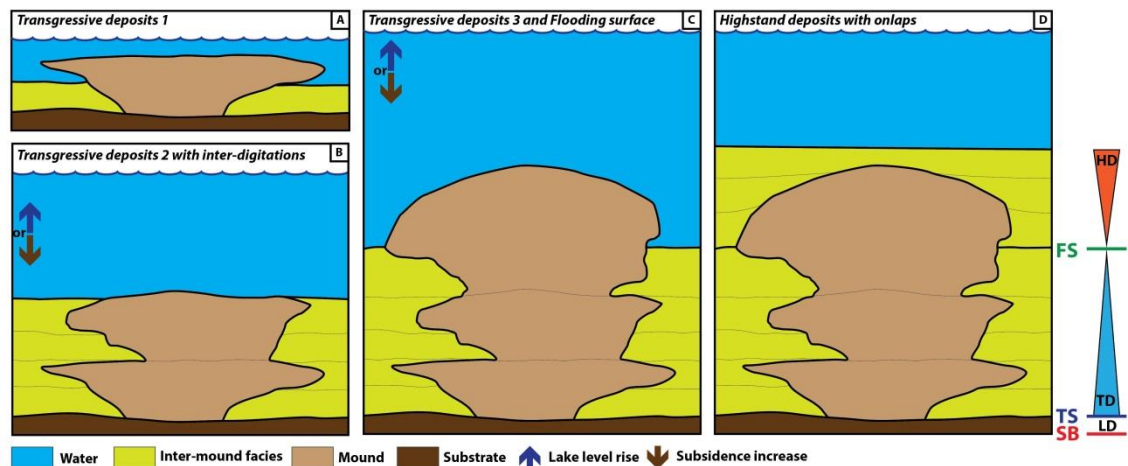
the Skull Cap bed; Figs. 6.10 and 6.12). The top subaerial surface corresponds to where the Hard Cap bed was exposed and eroded (Figs. 6.10 and 6.12). The Lower Dirt Bed is interpreted as a lowstand depositional system represented by Carbonaceous marl facies bounded on top by a transgressive surface (Figs. 6.10 and 6.12). This transgressive surface is overlain by transgressive deposits characterised by the Microbialite facies interdigitated with the Intraclastic peloidal packstone-grainstone facies (Fig. 6.10). These microbialite deposits are locally stromatolitic but more often they are large and with complex shaped thrombolitic mounds deposited around tree trunks and branches (refer to Chapter 5 for description of mound sizes and shapes). This transgressive system is bounded on top by a flooding zone due to a rise in lake level to its maximum depth in this sequence. This flooding surface is overlain by what are interpreted as highstand deposits characterised by the Intraclastic peloidal packstone-grainstone facies and bounded by a subaerial surface due to a drop in the lake level and a forced regression (Figs. 6.10 and 6.12). The finer-grained texture (packstone) at the bottom of the highstand deposits (Fig. 6.10) indicates a reduction of the carbonate production interpreted to represent slightly deeper and/or calmer water. Note that these highstand deposits are commonly overlapping on the large domed microbial mounds (Fig. 6.12 and refer to Chapter 4 Fig. 4.18 and Chapter 5, Fig. 5.14) that indicates that the microbial growth stopped. There is no clear indication of why mound growth stopped but this could have been caused due to change in environmental factors such as water chemistry, energy, water depth or a combination of two or more (see below for further discussion). Termination of mound growth is also suggested by the absence of inter-digitation of the highstand deposits (refer to Chapter 5, Fig. 5.18). These are very common in the transgressive deposits prior to the finer grained packstones of the flooding zone.

The fourth depositional sequence corresponds to the Great Dirt Bed, the Soft Cap and the Cypris Freestone beds and is bounded at the bottom by a subaerial exposure surface that corresponds to the eroded surface of the previous sequence (*i.e.* the surface of the Hard Cap bed; Fig. 6.10). As for the previous sequences, the paleosol is interpreted as a lowstand deposit represented in this sequence by Conglomerate facies in the Emergent facies association (Fig. 6.10). These lowstand deposits are bounded on top by a transgressive surface due to a rise in lake level accompanied by an increase of the carbonate production. The overlying transgressive deposits are characterised by tabular and domed microbial mounds that developed around *in situ* tree stumps and fallen trees (Fig. 6.10; refer to Chapter 5 for description of mound sizes and shapes). These transgressive deposits are bounded on top by a flooding surface (Fig. 6.10) associated with a break in the deposition as in the overlying

deposits neither mound nor inter-mound facies were deposited (Fig. 6.12). The overlying highstand deposits correspond to the lower part of the Cypris Freestone characterised by the Cross-bedded peloidal packstone-grainstone and/or the Evaporite facies (Fig. 6.10). As in the previous sequence a change in environmental factors occurred that led to a break-down of microbial growth due to either a rise in the lake level or a change in water chemistry or a combination of both (see below for more explanation). However in this sequence the hypersalinity suggested with the deposition of halite and gypsum pseudomorphs might indicate predominantly a change in water chemistry possibly associated with a change in water energy and water depth. Because the beds in this highstand deposits (*i.e.* the Cypris Freestone) do not change significantly in terms of facies and thicknesses these deposits are thought to be deposited with a rather constant subsidence and/or rise of lake level keeping the accommodation space rather constant.

In section 4 of this chapter are presented the sedimentary log correlations along the studied area and that shows that the facies associations are more or less consistent and can be correlated at least over that distance. West (1975) demonstrated similar correlations and showed that deposits can be correlated at a regional-scale. This implies that the sequence stratigraphy proposed here can also be traced regionally indicating that one lake or system of interconnected lakes was present.

Environmental factors controlling the microbial growth are of particular interest for this study. The sequence stratigraphy defined above shows that microbial mounds are preferably growing as transgressive (deepening-upward) or highstand (shallowing-upward) deposits (Fig. 6.10). In few locations in the Hard Cap (such as God Nore on the Isle of Portland), domed microbial mounds are present in the highstand deposits but do not present the typical inter-digitation of the microbialite with the Intraclastic peloidal packstone-grainstone facies in the underlying transgressive system. This is interpreted as evidence for a reduction of microbial growth penecontemporaneous of the highstand deposits (Fig. 6.11). The packstone interval at the base of the highstand deposits onlapping these domed mounds supports quieter water deposition which appears to be coinciding with the termination of microbial growth (Fig. 6.11).



**Figure 6.11** Cartoons depicting the transgressive and highstand deposits. A and B are redrawn from figure 5.14 where the mounds inter-digitate with the inter-mound facies. C – Last step of the transgressive deposits followed by the flooding surface with the termination of mound growth. D – Highstand deposits where the inter-mound facies onlaps on the dead mounds. SB: Sequence Boundary, TS: Transgressive Surface, FS: Flooding surface, LD: Lowstand Deposits, TD: Transgressive Deposits, HD: Highstand Deposits.

At the top of the preserved highstand deposits the microbial growth is stopped due to a drop of the lake level that resulted in the emergence of the microbial mounds that would have killed the microbial community.

When deposited in a transgressive system the termination of the microbial growth is interpreted from a flooding due to a rise of the lake level. However this flooding surface can reflect several processes all resulting in the break-down of microbialite growth due to the death of the microbial community. Pentecost (1991) and Merz-Preiß (2000) showed that supersaturation with respect to calcium carbonate in the waters (as in Laguna Bacalar, refer to Appendix 1) is essential for the microbial calcification to occur (also demonstrated by Dupraz *et al.*, 2009). According to this, a change in the saturation with respect to the calcium carbonate of the water will result either a slow-down or a termination in microbial growth. Alternatively if the sedimentation rate is greater than the growth rate of the microbial community, the microbialite will be killed because it will be covered with sediments. Della Porta (2015) added that microbial developments are also influenced by hydrodynamic energy, the stability of the substrate, water depth (calcification of cyanobacteria is driven in part by photosynthesis) and/or the sediment supply. In the Purbeck outcrops the Intraclastic peloidal packstone-grainstone facies of the inter-mound areas is similar below and above the flooding surfaces. This indicates that the hydrodynamic energy was relatively similar before and after the flooding and therefore was probably not the mechanism responsible for the death of the microbialites. Similarly, the substrate the microbial community was using was the previous

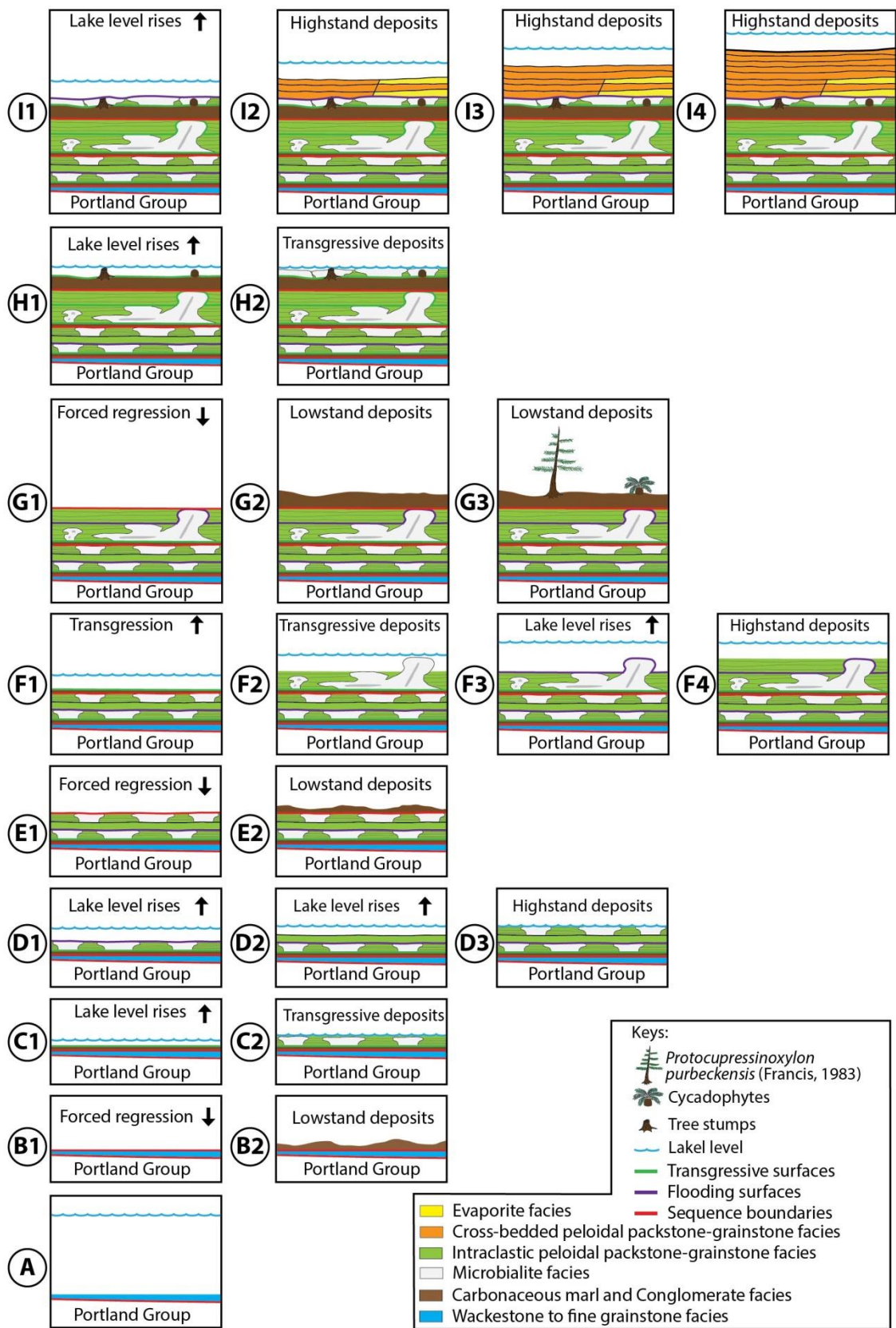
generation of microbial community and this did not change from the transgressive to the highstand deposits. The mound facies are the same in both units. Consequently the main processes thought to be responsible for the termination of microbial growth are a change in the water chemistry or of water depth or a combination of both. As microbialites occur in a range of salinities (refer to section 7), a modification of the salinity is not thought to be responsible in the death of a microbial community. However a change in the water chemistry through a modification of the saturation in calcium carbonates and/or of the pH appears to be the main process for the preservation of microbialites (Dupraz and Visscher, 2005). The lack of dissolved carbonate may not necessarily kill the microbial community but the calcification of the microbial filaments and their preservation may no longer be possible (Dupraz and Visscher, 2005). This mechanism potentially occurred in the Skull, Hard and Soft Cap beds with two different consequences to sediment accumulation. In the Skull and Hard Cap beds the Intraclastic peloidal packstone-grainstone facies covers the microbial mounds and remains the same below and above the flooding zones. This suggests a slight decrease of the saturation in respect to calcium carbonate of the waters that resulted in the termination of the microbial filament calcification but did not influence other carbonate factories (biotas, intraclasts and peloids). In the Soft Cap the facies surrounding the microbial mounds changes from the Intraclastic peloidal packstone-grainstone to the Evaporite or Cross-bedded peloidal packstone-grainstone facies (both hypersaline indicators) that covers the mounds (Figs. 6.10, 6.12). This indicates a modification in both the saturation in respect to calcium carbonate that terminated the microbial growth and the salinity of the waters that resulted in the covering of the mounds with evaporites.

Another possible process that has an impact on microbial growth can be the eutrophication of the lake waters. Hallock and Schlager (1986) demonstrated that an excess of nutrients into reef systems causes a decrease of carbonate production and the death of the reef community. This can be due to an overfeeding stress, increasing competition for space, crystal poisoning, bioerosion and/or reduction of light penetration (Hallock and Schlager, 1986). Anoxia is often associated with such increase of nutrient contents in waters (Hallock and Schlager, 1986). In such systems the carbonate production would decrease or stop due to a lack of oxygen necessary for carbonate producers to proliferate. Although based on marine environments, Hallock and Schlager (1986) study shows that the overall carbonate production of a system decreases when quantity of nutrients increase. Similarly Smith *et al.* (1999) showed that eutrophication in lacustrine systems is accompanied by algal bloom (cyanobacteria) due to an enrichment of nutrients. Algal blooms in lakes have also negative

effect such as decrease of the clarity of the water, death of other animals or plants, increase of pH and decrease of oxygen content (Smith *et al.*, 1999). In this case eutrophication appears to favour microbial growth as possible competitors (*i.e.* other carbonate producers) are removed. The application of these general rules to this study would involve a radical change of the nature and the components of the sediments as the carbonate producers (such as ostracods and molluscs) would not be able to grow in nutrient-rich, higher pH and oxygen-poor waters. However in the Skull, Hard and Soft Cap beds, the inter-mound facies remains similar if found deposited contemporaneously with or after the death of the microbial mounds, as similar organisms (ostracods and molluscs) are found in rather similar quantities. As a consequence the possible eutrophication of lake waters is not thought to be responsible for the death of the microbial community in this study.

A change in the water depth involves a decreasing carbonate production due to diminution of temperature, light (impacting on the photosynthesis) and energy, and results in the deposition of fine-grained carbonate sediments (Bathurst, 1975). This mechanism potentially caused the death of the microbial community in the Hard Cap bed as in this bed the mounds are covered and overlapped by a muddier interval (Fig. 6.10, 6.12). The increased depth might cause a diminution of the light penetration that resulted in a slow-down or a termination of the photosynthesis followed by the death of the microbial community. This death could be due to a lack of light that stopped the photosynthesis and killed the microbial community; or caused a decrease in the growth rate that became lower than the sedimentation rate and resulted in the covering of the mounds with sediments.

In conclusion the process responsible for the termination of microbial growth of the microbial mounds in the Skull, Hard and Soft Cap beds is thought to be a modification in the saturation in respect to calcium carbonate of the waters. This process was most likely accompanied with an increase of lake level in the Hard Cap as the overlying beds are overlapping on the mounds; and with an increase of salinity for the Soft Cap mounds as they are covered with hypersaline deposits (the Evaporite or Cross-bedded peloidal packstone-grainstone facies). Following termination of mound growth in the Skull and Hard Cap beds lake level fall resulted in erosion of the tops of the mounds at the sequence boundaries.



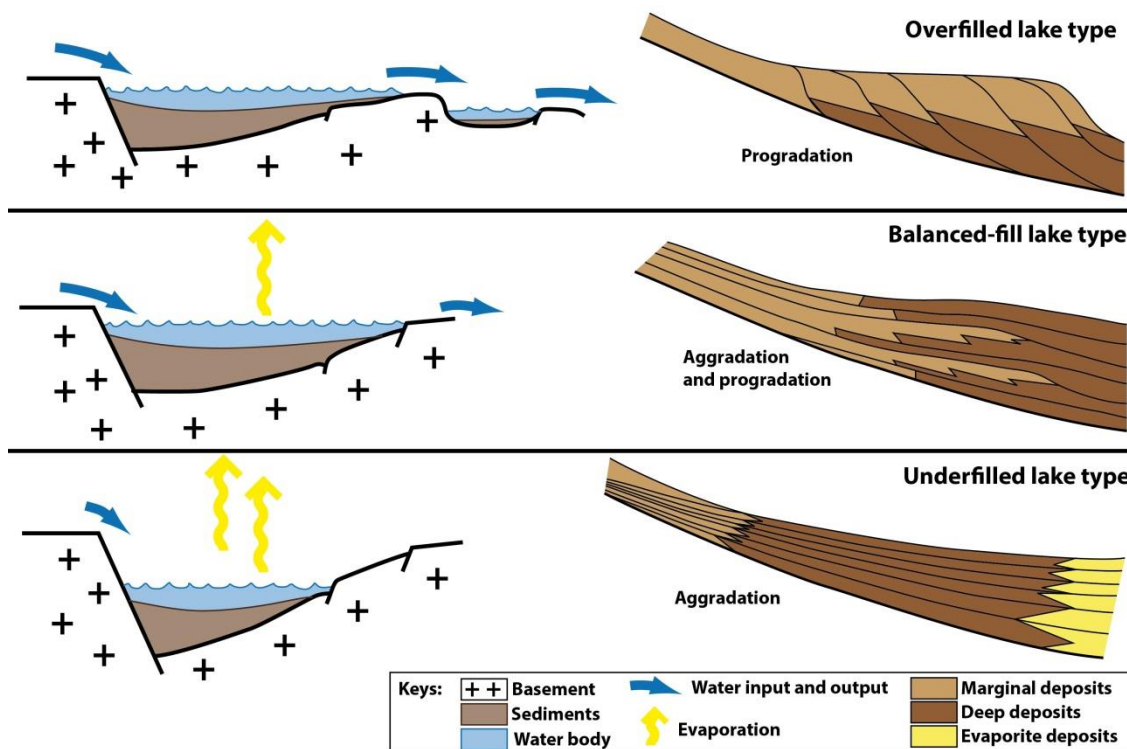
**Figure 6.12** Generalised depositional reconstruction and lake level fluctuations. Numbering corresponds to depositional systems and surfaces in figure 6.10.

## 7. Facies models

This section presents the integration of all the work presented in this chapter and comparisons with eight analogues (ancient and modern) to propose two facies models for the Mupe Member. Two main depositional environments were identified above; a brackish water lake in the lowermost part of the Mupe Member and a hypersaline water lake in the uppermost part (Fig. 6.4). The generalised log (Fig. 6.10) illustrates this vertical facies succession. The sequence stratigraphy (Fig. 6.10) and depositional reconstruction (Fig. 6.12) show the sequence of events leading to the accumulation of the succession.

The lower part of the Mupe Member was an open lacustrine system with through-flowing freshwater with a fluvial and/or groundwater input as suggested by the sustained brackish water conditions until the flooding surface in depositional sequence 4 overlying the Soft Cap bed (Fig. 6.10). Microbial mounds are identified in this lower part of the Mupe Member and described in Chapter 4 (sedimentology), in Chapter 5 (shape and size) and in section 4 of this chapter (depositional settings). The upper part of the Mupe Member was a more restricted lacustrine system as indicated by the sustained indicators of hypersaline water conditions after the flooding surface in depositional sequence 4 (Fig. 6.10). Comparison with theoretical models of lake depositional systems (Figs. 6.13, 6.14), modern (Figs. 6.15 to 6.20) and ancient (Figs. 6.21) analogues helps to interpret facies distribution in the Mupe Member. Ultimately the original field data and all these comparisons have been used to build facies models for the Mupe Member (Figs. 6.23, 6.24).

Bohacs *et al.* (2000) defined three lake types based on the water flow through a lacustrine system: overfilled, when the water input exceeds the evaporation rates and these are characterised by fluvio-lacustrine facies associations; balanced-fill, when water input and evaporation reach an equilibrium characterised by fluctuating-profundal facies associations; and underfilled lakes, when evaporation exceeds water input and these are characterised by evaporite facies associations (Fig. 6.13). Each of these lake types is characterised by a specific stacking pattern: maximum progradation with poorly defined parasequences or sequences (Van Wagoner, 1995) for overfilled lakes (Fig. 6.13); progradation and aggradation with well-defined parasequences or sequences for balanced-fill lakes (Fig. 6.13); and maximum aggradation with either poorly- or well-defined parasequences or sequences for underfilled lakes (Fig. 6.13; Bohacs *et al.*, 2000).



**Figure 6.13** Characteristics of lake types (redrawn after Bohacs *et al.*, 2000). On the left are the relationships between water input and evaporation. On the right are the expected corresponding stacking patterns.

Figures 6.14 shows general lithology trends proposed by Bohacs *et al.* (2000) for balanced-fill (Fig. 6.14A) and underfilled (Fig. 6.14B) lake types based on observed modern lakes and depending on margin slopes (low-relief margins to the left and high-relief margins to the right).

In balanced-fill lake types (Fig. 6.14A) the system reaches an equilibrium between (fresh)water input (via river systems or groundwater), accommodation and evaporation (Bohacs *et al.*, 2000). Lake shores are relatively stable through time and climatic controls on water level fluctuation are common (Bohacs *et al.*, 2000). In their model the deposition is organised into cycles usually with progradation of clastic sediments and aggradation of “chemical” sediments (such as carbonates; Bohacs *et al.*, 2000). Highstand deposits are characterised by carbonates (or clastics) in relatively open or through-flowing systems where microbially mediated deposits are common (Bohacs *et al.*, 2000). Lowstand deposits are restricted to basinal areas in shallow lakes due to rapid lake level changes according to Bohacs *et al.* (2000). These are characterised by carbonate (or clastic) deposits with aggradational parasequences or sequences (Van Wagoner, 1995) showing evidence of desiccation (Bohacs *et al.*, 2000). Talbot and Allen (1996) had already described this type of lake as an open lake characterised by a relative stability of the shorelines. In such open lakes smaller-scale



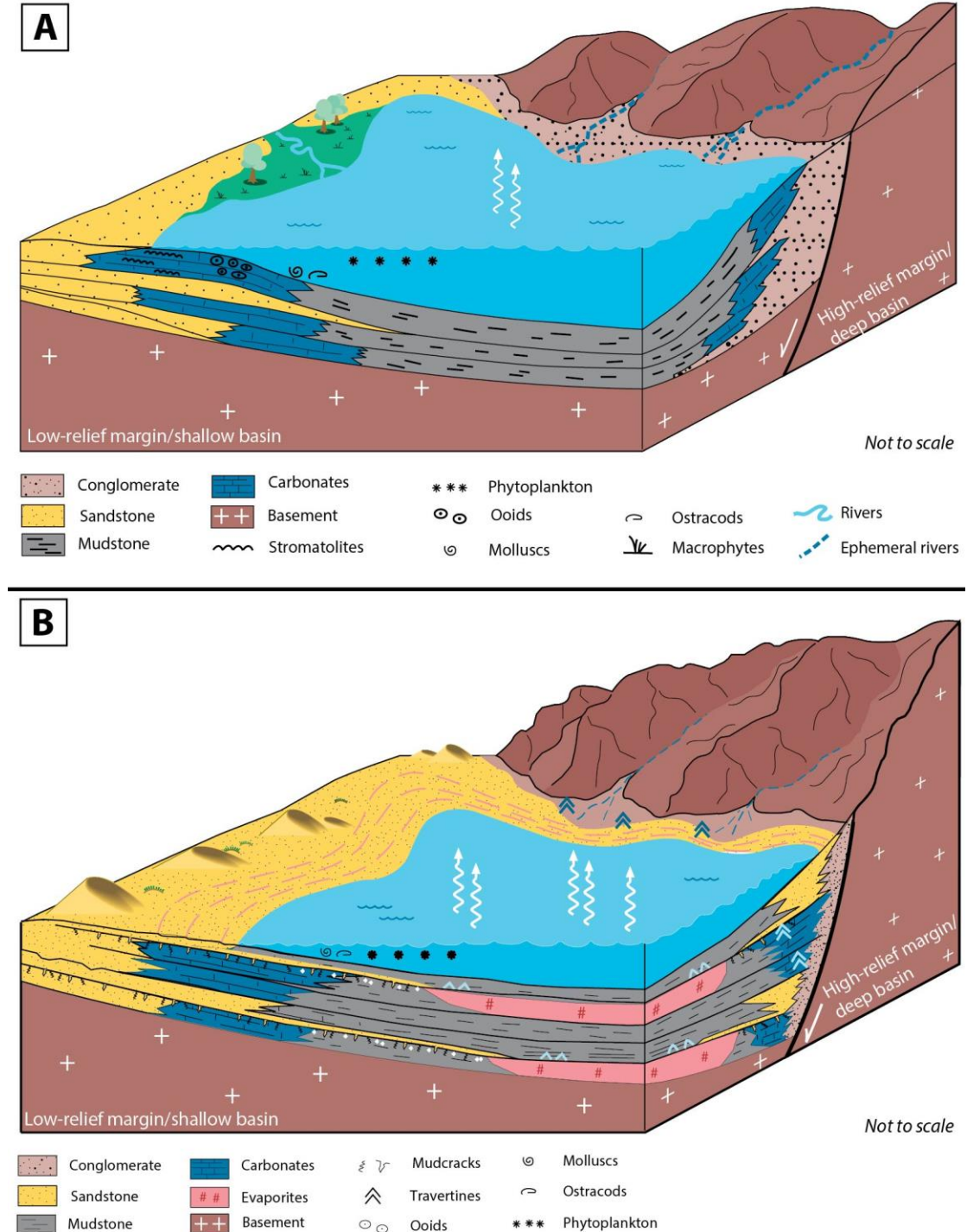
sequences commonly reflect expansion-contraction of lake margins while larger-scale sequences reflect hydrological fluctuations of the entire lacustrine system (Talbot and Allen, 1996).

In underfilled lake types (Fig. 6.14B), highstand deposition is characterised by a general stability of lake shores (*i.e.* perennial lakes) and low accommodation. Coarse-grained facies (clastic and carbonates) are usually deposited in shallow areas and fine-grained facies (clastic) in deep areas (Fig. 6.14B; Bohacs *et al.*, 2000). Gypsum, halite or anhydrite can deposit in both shallow and deep areas due to evaporation and very low freshwater (fluvial) input under arid climatic conditions (Fig. 6.43B, Bohacs *et al.*, 2000). In strong evaporative settings, thickening of evaporitic deposits basinward is common (Bohacs *et al.*, 2000). Highstand deposits are rather thick and normally made of one or two parasequences (*sensu* Van Wagoner, 1995 according to Bohacs *et al.*, 2000). Lowstand deposition is characterised by instability of the lake shores (*i.e.* ephemeral lakes) due to strong cyclicity between wetter and dryer periods (Bohacs *et al.*, 2000). These lowstand deposits are usually covered by basinal deposits marking a major and rapid flooding of the shallow lake (Bohacs *et al.*, 2000). Talbot and Allen (1996) had already described this type of lake as a closed lake characterised by unstable shorelines. In such closed lakes transgressive-regressive cycles are common due to frequent rise and fall of the lake level (Talbot and Allen, 1996).

The implications for the Mupe Member when applying Bohacs' *et al.* (2000) models (Figs. 6.13, 6.14) concern the facies and their distribution. The main differences of both models are that in the Purbeck limestones, although clastic deposits are interpreted to be to the east (see below), there are little clastic deposits (few sandstone but no conglomerate deposits) and little direct evidence of freshwater input via river systems. However these models are comparable to the Mupe Member for most of the other features described above. Particularly relevant to the Purbeck limestones is the distribution of coarse-grained carbonate deposits with development of stromatolites in the shallowest part of the lake (*i.e.* the margins) and fine-grained abiotic facies in the deepest part of the lake (*i.e.* basinal areas). Vegetated soils are more likely to form in low-relief margins rather than high-relief margins as depicted by Bohacs *et al.* (2000) (Fig. 6.14).

In the lower part of the Mupe Member, characterised by brackish water conditions, the absence of evaporites and conglomerate-size facies (despite the presence of the extensional faults nearby); together with the abundance of sand-size carbonate facies, microbial buildups and paleosols with conifer forests suggest a low-relief lake margins profile of a balanced-fill or open lake.

In the upper part of the Mupe Member, characterised by hypersaline conditions, the abundance of sand-size carbonate facies with evaporite pseudomorphs; together with the absence of microbial build-ups and paleosols suggest a low-relief lake margins profile of an underfilled or closed lake.



**Figure 6.14** Lake type models (redrawn after Bohacs *et al.*, 2000). A – Balanced-fill lake type model. Note facies distribution with fine-grained facies (mudstone in grey) in deep areas and carbonates with stromatolites (in dark blue) on the margins. This figure represents low-relief margins to the left and high-relief margins to the right. B – Underfilled lake type model. Note facies distribution with fine-grained facies (mudstone) and evaporites in the deep area and carbonates and sandstones on the margins. This figure represents low-relief margins to the left and high-relief margins to the right.

## **7.1. Analogues**

### **7.1.1. Introduction**

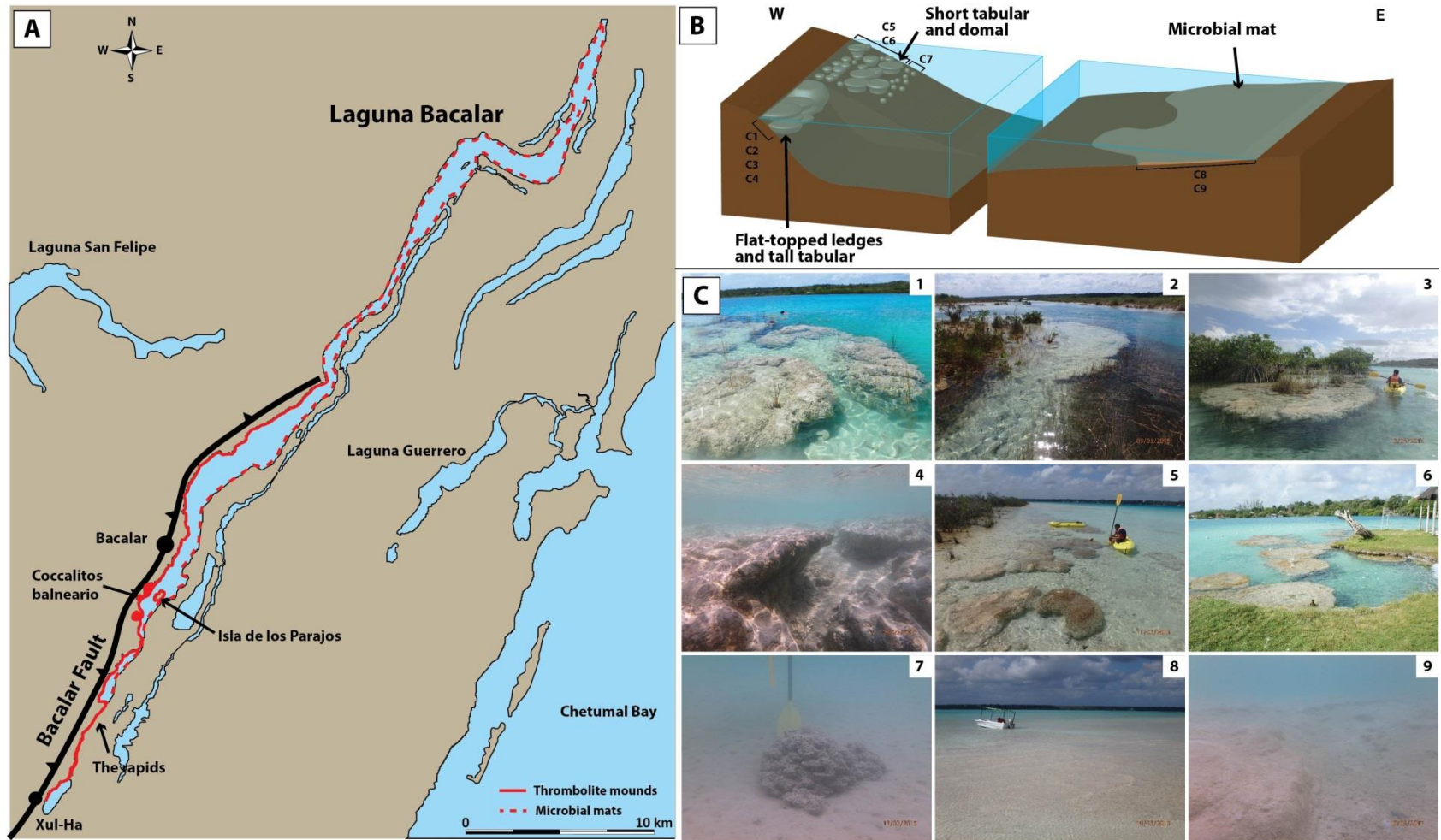
This section describes and compares possible analogues for the lower part of the Mupe Member. Because of the occurrence of thrombolite mounds associated with soils and developed around trees and their inter-digitation with shallow lacustrine peloidal packstone-grainstones, only shallow water modern and ancient lakes are described here. In this section lake size, climate, hydrology, facies and facies distribution of six modern day lakes (freshwater, brackish and hypersaline) and one ancient brackish water lacustrine are described. Two of them were visited during this study, the hypersaline Great Salt Lake in Utah (USA) in October 2013 and the freshwater Laguna Bacalar in the Yucatan Peninsula (Mexico) in March 2015. The others described are based on literature with the hypersaline marine lagoon of Hamelin Pool (Shark Bay), hypersaline lakes of Rottneest Island, hypersaline Lake Thetis, the brackish water Lake Clifton and the freshwater Lake Richmond all being located on the western coast of Australia. The ancient brackish water lacustrine system is the Green River Formation of the Piceance Basin exposed in Utah (USA) is also presented as a possible analogue.

### **7.1.2. Laguna Bacalar, Mexico**

Laguna Bacalar (Quintana Roo, Mexico) is a groundwater-fed freshwater lake about 50 km long, 1-2 km wide and 20 m deep maximum under tropical climate (Gischler *et al.*, 2008; 2011). On the shores, thrombolite mounds occur with a wide range of shape and sizes (refer to Appendix 1 for description). A trip of one week in March 2015 to Laguna Bacalar was undertaken to study the mounds and their inter-mound sediments as a possible analogue for the Purbeck mounds. This trip enabled observation and recording of thrombolite mounds, coarse-grained facies (grainstones with mollusc shells, Fig. 6.15) deposited in the shallow margins of the lake and inter-mound coarse-grained facies both in between mounds and on top of tabular mounds (Fig. 6.15C1, flat-topped ledges of Gischler *et al.*, 2008). These thrombolite mounds were mainly observed on the southern part of the lake (south of Bacalar town) and are absent on the northern half (Gischler *et al.*, 2008). However Gischler *et al.* (2011) described microbial mats to develop on all the northern and eastern margins of the lake. They also showed that thrombolite mounds and microbial mats distribution is controlled by the carbonate concentration of the water. In fact to the south, where thrombolite mounds are developing a high carbonate concentration was recorded, while to the north, where

thrombolite mounds disappear and microbial mats develop, a much lower carbonate concentration was recorded (Gischler *et al.*, 2011 and Appendix 1). In deeper areas finer carbonate sediments made of silt and mud sized carbonate sediment occurs but no mounds are recorded from sonar data (as reported by Gischler *et al.*, 2008). The microbialites of Laguna Bacalar were described as thrombolites because of “*inhomogeneous internal structure*” that comprise finely laminated and upward radiating filament areas (Gischler *et al.*, 2011). Both areas are composed of calcified moulds of *Homeothrix* filaments, the difference between the laminated and radiating areas is in the diameter of these filaments (greater in the latter, Gischler *et al.*, 2008, 2011). In both microstructures molluscs, ostracods and diatoms are incorporated and on the external surface are usually found mussels attached in the microbial mat (as observed during our visit and as reported by Gischler *et al.*, 2008, 2011).

This lake is located in the equatorial zone and with freshwater conditions supplied by groundwater through-flow, however the carbonate factories and microbial mound sizes, morphologies and internal microstructures are similar to those in the lower part of the Mupe Member. The main features comparable with the interpreted environments of the Purbeck limestones are the depositional system (fully carbonate) with thrombolite mounds only in the shallowest part of the lake and associated with peloidal grainstone facies with ostracods and molluscs (Fig. 6.15). The internal microstructure of the thrombolites is similar to that of the Purbeck as both have heads of upward radiating filament moulds incorporating the surrounding sediments and fossils. These thrombolites exhibit several sizes and morphologies, microbial mats, small tabular mounds, flat-topped ledges and large mounds (up to 2 m high, Fig. 6.11 and Appendix 1). The mounds develop along the shores and grow towards the lake basin and are commonly found growing around roots of mangrove trees. The microbialites show very rapid growth rates of up to 1 cm/year as measured during the March trip (refer to Appendix 1 for description). In basinal areas (*i.e.* deep part of the lake) peloidal fine-grained carbonates are deposited (Gischler *et al.*, 2008, 2011).

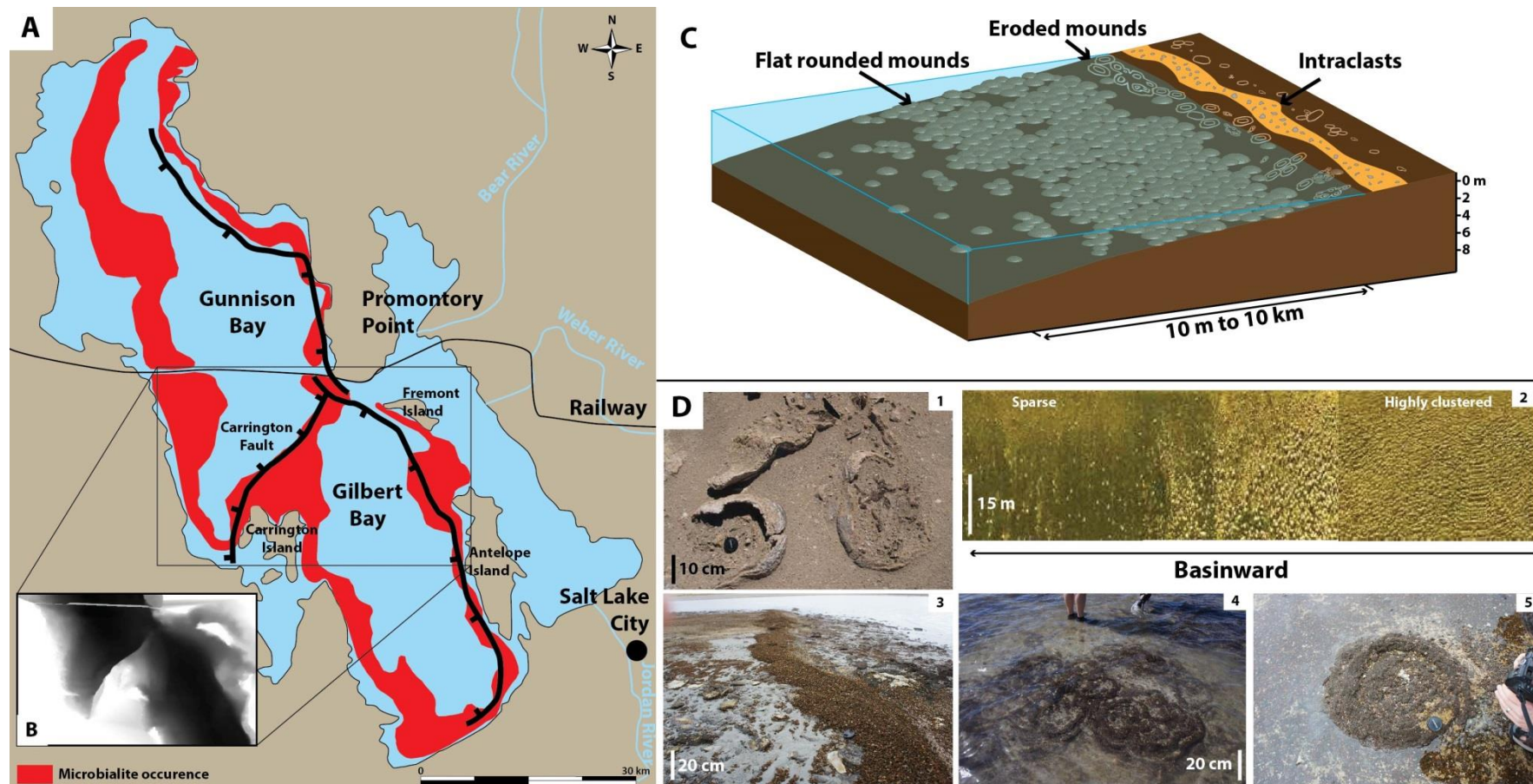


**Figure 6.15** Laguna Bacalar, Yucatan Peninsula, Mexico. A – Map of the lake with microbialite occurrence in red (after Gischler *et al.*, 2008, 2011). B – Facies model with an east-west section showing microbial mound distribution. C – Field images illustrating microbial mounds and distribution; C1-3 – Flat-topped ledge mounds, south of The Rapids; C4 – Flat-topped ledge mounds underwater, south of The Rapids; C5 – Short tabular mounds, west of Isla de los Parajos; C6 – Tall tabular mounds, Cocalitos balneario; C7 – Domed mounds in deep areas underwater, south of the Rapids; C8 – Shallow microbial mats, west shores; C9 – Deeper lacustrine microbial mats.

### 7.1.3. Great Salt Lake, Utah, USA

The Great Salt Lake (Utah, USA) is a hypersaline lake divided into Gunnison Bay (240-260 ppt) and Gilbert Bay (120-140 ppt) (Chidsey *et al.*, 2015) (Fig. 6.16A). The lake was visited in September 2013 where flat circular microbial mounds that form rings were observed on the margins of Antelope Island in Gilbert Bay. This lake is 10 m maximum deep with microbial mounds on the margins that develop on top of crusts composed of lithified oolites and muds (Chidsey *et al.*, 2015). The internal microstructure of the microbialites varies from leolites to thrombolites (Della Porta, 2015) and comprises abundant calcitic spherulites linked with acicular cements and/or microbial filaments (Chidsey *et al.*, 2015). These microbialites can incorporate peloids, detrital grains, ooids or even bird feathers and the external part is usually encrusted with tubes of brine fly larvae (Post, 1977; Chidsey *et al.*, 2015; Della Porta, 2015). The surrounding sediment is made of grainstones with peloids (including faecal pellets), detrital grains, ooids and microbial intraclasts (Della Porta, 2015). The 2013 visit also allowed the identification of ooidal carbonate sands and carbonate muds forming wave ripples around thrombolitic mounds in the southern part of the lake (Gilbert Bay). Locally the microbial mounds can be surrounded by microbial intraclasts forming low-relief linear dunes (Fig. 6.16; also described by Chidsey *et al.*, 2015). Deeper in the lake the amount of microbial mounds decreases considerably as water depth increases (Chidsey *et al.*, 2015) while their size increases (*pers. comm.* Robert Baskin, September 2013). In the deepest part of the lake fine-grained sediments such as muds and fine carbonate sands are deposited and microbial mounds are absent (Baskin, 2014). In Gunnison Bay there is a higher salinity (240 to 260 ppt) than Gilbert Bay that results in a pink coloration of the water due to *Dunaliella salina* bacteria creating  $\beta$ -caroten in hypersaline waters (Post, 1977), identifiable from the satellite images. The northern half of the lake has been closed by a railroad causeway built between 1953 and 1959 creating a closed hypersaline system with freshwater input via four major river systems located in the southern part (Fig. 6.16; Chidsey *et al.*, 2015). In this northern part, microbialites are present but because of the extreme salinity (close to the salt-saturation point, Chidsey *et al.*, 2015), they are dead and lithified. These microbialites are covered by hypersaline ooids and microbial intraclasts. Additionally, halite hopper crystals are crystallising on the surface water, sinking when too heavy to float and are deposited on the lake floor as cm-thick salt deposits in deep waters (Fig. 6.16; Baskin, 2014 and refer to Chapter 4 for description). Consequently halite crystals can be found encrusted in the dead microbialites (Fig. 6.16B ; Chidsey *et al.*, 2015).

As for previous examples, the Great Salt Lake differs in water chemistry from that interpreted for the lower part of the Mupe Member of the Purbeck limestones. However this lake is similar to that of the upper part (refer to section 4 and Fig. 6.4) as both bays are hypersaline and Gunnison Bay is close to the halite saturation point. Similar features are lake margins with microbial thrombolitic mounds that show similar morphologies (such as the flat circular mounds in figure 6.16D5 similar to mounds of the Soft Cap, refer to Chapter 5) and microstructures. Both examples have mounds that are surrounded by coarse-grained carbonate facies in the shallowest part of the lake and by fine-grained deposits in the deepest part. In the Great Salt Lake microbial mounds tend to increase their size with the depth before disappearing completely beyond 4 m of water depth (Fig. 6.16D2). The ooids found in the Great Salt Lake are partially similar to those of the Purbeck. They differ in the microstructure of the cortex as in the Great Salt Lake the ooids show radial calcite crystals while in the Purbeck they have mixed cortices but tend to show more tangential microstructure (refer to Chapter 4). However one type of ooids is similar in both lakes, the regenerated ooids where the nucleus consist of a broken ooid (refer to Chapter 4). Microbialites are nowadays dead due to the extremely high salinity in Gunnison Bay and covered with evaporitic deposits (halite crusts). A similar process might be responsible for the locally death of the Soft Cap microbial mounds of the Mupe Member. In fact from Durdle Door eastwards (refer to section 4.6 of this chapter) rounded mounds are covered with evaporites (gypsum and anhydrite). The restriction of this part of the lake might have induced higher salinity that killed the microbial community and stopped the thrombolite development.



**Figure 6.16** Great Salt Lake, Utah, USA. A – Map of the lake with microbial occurrence in red and location of extensional faults. B – Digital elevation model of the lake bathymetry showing fault-controlled offset due to the Carrington Fault (white is shallow and black is deep). Note that microbial mounds at this location are located in the shallow part. C – Facies model showing mound morphologies and their distribution, data compiled from Baskin (2014) and Chidsey *et al.* (2015). D – Field and sonar images illustrating microbial mounds and distribution; D1 – Eroded and dead flat rounded mounds on the lake shore (image from Chidsey *et al.*, 2015); D2 – Side-scan (CHIRP) sonar image showing distribution of mounds. Note the increasing sparse mounds distributed basinward (image compiled from Baskin, 2014); D3 – Low-relief linear dunes formed of reworked microbial intraclasts; D4-5 – Circular domed mounds in shallow margins.

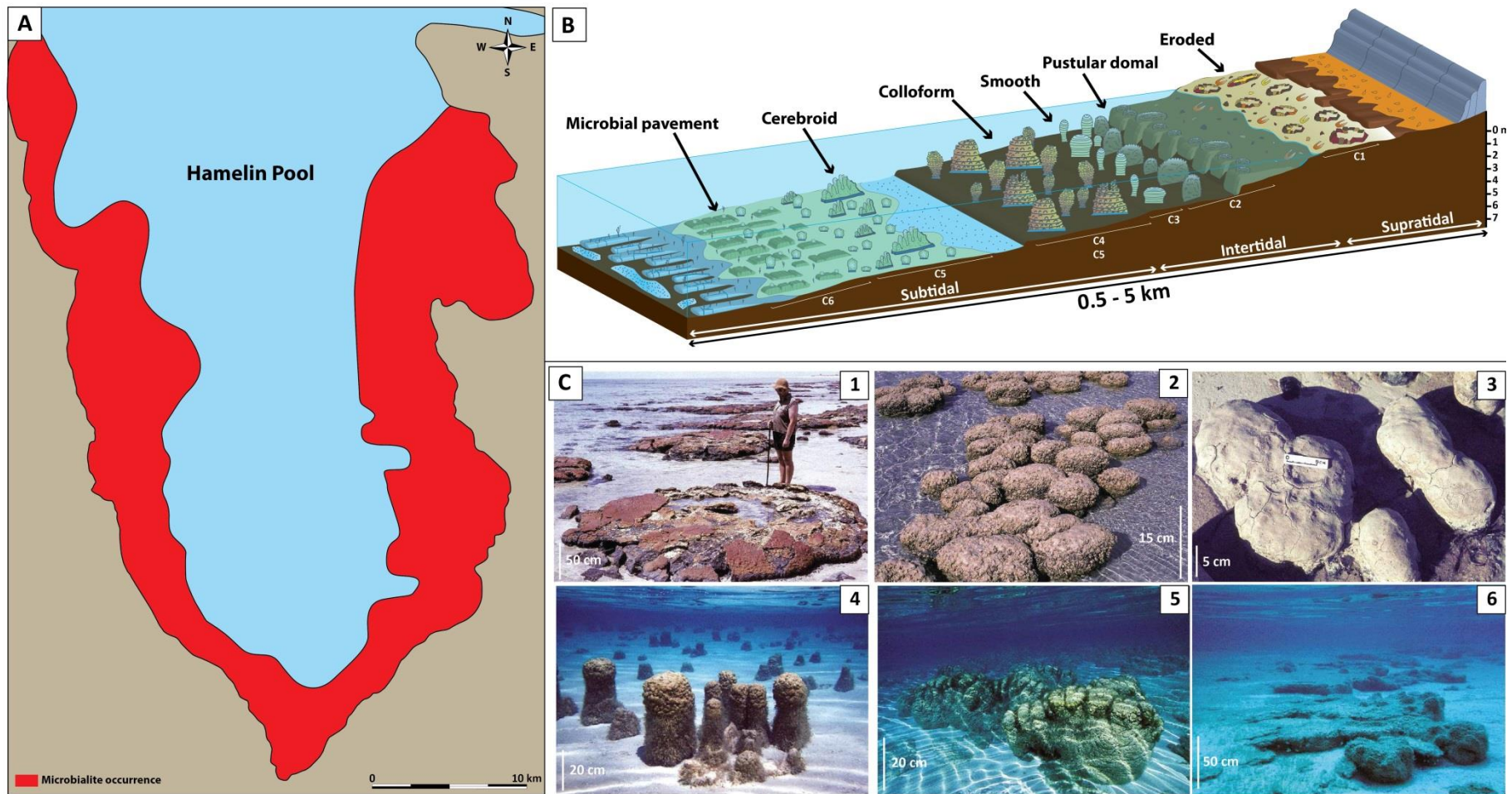


#### 7.1.4. Hamelin Pool, Shark Bay, Australia

Hamelin Pool (Shark Bay, western Australia) is a restricted hypersaline (about 56-70 ppt; Jahnert and Collins, 2012) marine embayment partially disconnected from the sea to the north by a seagrass bank (Fig. 6.17; Jahnert and Collins, 2011). This embayment is 10 m deep maximum with supratidal, intertidal, subtidal and embayment plain zones (Fig. 6.17B ; Logan *et al.*, 1974; Jahnert and Collins, 2011, 2012). Microbial development occurs in the shallow areas down to 6 m depth (in the intertidal and subtidal zones; Fig. 6.17) and surrounded by bioclastic sand and mud or ooidal sand (Jahnert and Collins, 2012). Microbial mounds are found under five distinct morphologies related to water depth: pustular domes, smooth, colloform, cerebroid and microbial pavement (Fig. 6.17; Jahnert and Collins, 2011, 2012). Their internal microstructures vary depending on water depth and environmental conditions (Jahnert and Collins, 2012). Clotted fabrics that consist of coccoid cyanobacteria are found in the pustular domes; laminated stromatolites due to trapping and binding of peloids and bioclasts are found in the smooth and colloform mounds; non-laminated fabrics that result from micritisation and coalescence of peloids are found in the cerebroid mounds; and lithified bioclastic grainstone are found in the microbial pavement (Jahnert and Collins, 2012). In the supratidal zone, dead rounded microbial mounds are found (Fig. 6.17B-C, spherical eroded mounds of Jahnert and Collins, 2011, 2012), and flat-topped mounds in the intertidal zone (Fig. 6.17B-C, smooth pustular forms of Jahnert and Collins, 2011, 2012). In the subtidal zone the mounds tend to be columnar, more massive until about 6 m water depth where only microbial pavements are found (Fig. 6.17B-C, Jahnert and Collins, 2011, 2012). In the deepest areas (beyond 6-7 m water depth and in the embayment plain; Fig. 6.17) fine-grained facies (bivalve shells with muds) are deposited.

As with the previous examples, the water chemistry is rather different from that interpreted for the Mupe Member of the Purbeck limestones. However microbial mound morphologies and associated carbonate facies show some similarities. In this example mounds are restricted to water depth of 2 to 6 m (intertidal to subtidal zones) and the morphologies tend to flatten and shorten basinwards (pustular coalescent to pavement, Fig. 6.17B). The laminated microfabrics of the smooth and colloform mounds are very similar to the stromatolites of the Purbeck and the clotted fabrics of the pustular domes are very similar to those of the thrombolites of the Purbeck limestones at thin section scale. The facies surrounding microbial mounds are coarse-grained, as in the Skull, Hard and Soft Cap beds of

the Purbeck limestones; whilst in the embayment plain muds with bivalve shells occur, as in the Transition Bed of the Purbeck limestones (refer to Chapter 4 for description).

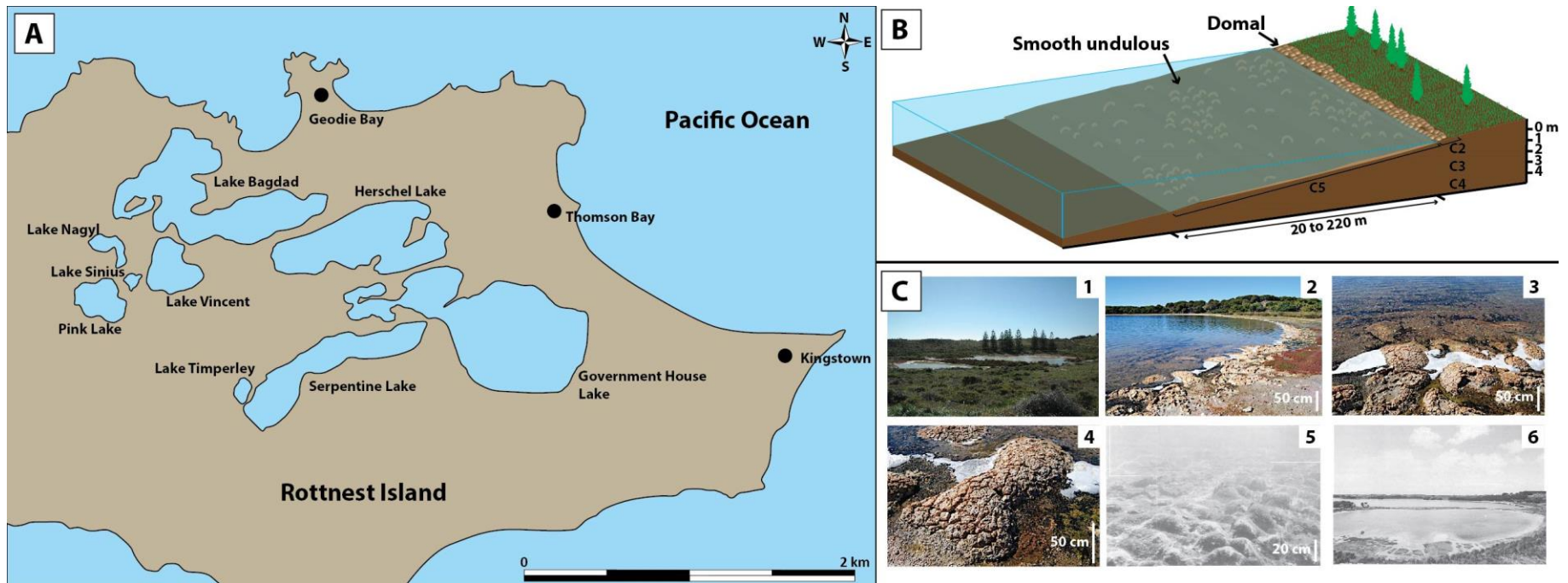


**Figure 6.17** Hamelin Pool, Shark Bay, Australia. A – Map of the lagoon with microbialite occurrence in red. B – Facies model showing mound morphologies and distribution (from Jahnert and Collins, 2011). C – Field images illustrating microbial mounds and distribution (from Playford *et al.*, 2013); C1 – Eroded and dead mounds on the shores; C2 – Pustular domed mounds; C3 – Smooth mounds; C4 – Columnar colloform mounds; C5 – Cerebroid mounds; C6 – Microbial pavement.

#### 7.1.5. Rottnest Island, Australia

Rottnest Island (western Australia) is a 10.5 km long and 4.5 km wide island in the southern Pacific Ocean (Fig. 6.18). On this island microbial deposits occur in 10 shallow (between 250 m and 1 km long, 100 to 750 m wide and down to 8.5 m deep) permanent hypersaline lakes (minimum of 68 ppt in Lake Timperley and exceeding 200 ppt in bigger lakes; Playford and Leech, 1977; Playford, 1988; John *et al.*, 2009). This island is characterised by a Mediterranean type climate (wet winters and extremely dry summers) with growth of cypress trees (*Callitri preissii*, Fig. 6.18; Pen and Green, 1983; Playford, 1988). In these lakes, microbial mounds are developed in association with gypsum and lime mud (Hassell and Kneebone, 1960) and occur in the shallowest areas between 20 cm and 3 m depth (Fig. 6.18B). The mounds are 5 to 10 cm high with a maximum of 20 cm with nodular, branching columns and smooth undulous morphologies (Playford, 1988) and can develop around water-logged tree branches (Playford, 1988). Few information are available in the literature relating to their microstructures but they were described by John *et al.* (2009) as being made of coccoid cyanobacteria forming gel-like mats.

All the lakes on Rottnest Island are hypersaline so the water chemistry differs to that inferred for the lower part of the Mupe Member of the Purbeck limestones but are similar to that for the upper part. However the lakes of Rottnest Island present some other similar features to that of the lower part of the Mupe Member. The Mediterranean climate type with cypress trees growing on the shores of the lakes can be compared to the lower part of the Mupe Member. Microbial mounds are relatively small (up to 20 cm thick), restricted to the shallowest areas down to 3 m depth and even found growing on logs. These comparisons were also made by Francis (1983) when she studied the Purbeck soils and trees (refer to Chapter 2).

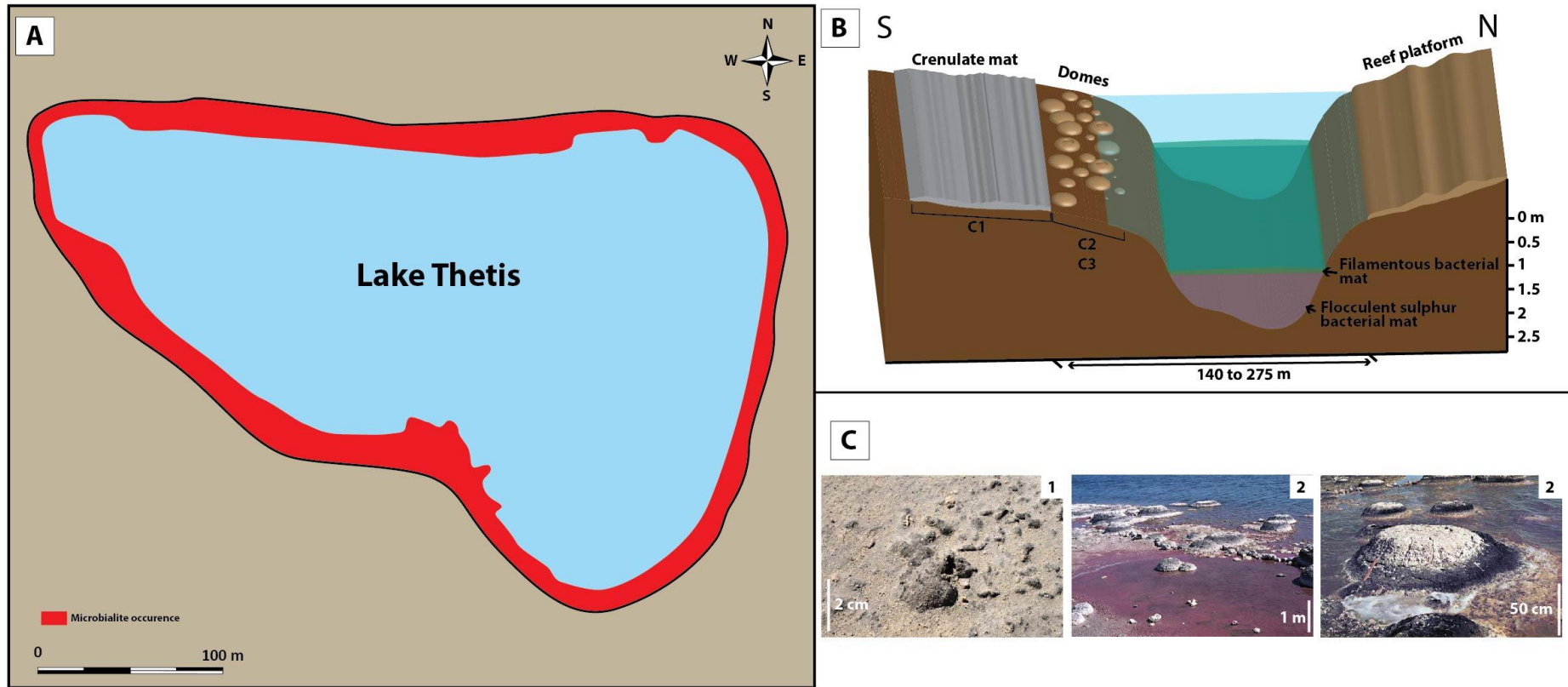


**Figure 6.18** Rottnest Island, western Australia. A – Map of the island showing distribution of lakes. B – Facies model showing typical mound morphologies and distribution (data compiled from Playford, 1988). C – Field images illustrating microbial mound morphologies and distribution; C1 – Ephemeral hypersaline ponds illustrating landscape with *Callitri preissii* cypress trees in the background (image from virtualtourist.com); C2 – Eroded and dead domed stromatolites on the shores (image from © MMIX Paul R. Weaver); C3-4 – Domed stromatolites of shallow lake margins (image from © MMIX Paul R. Weaver). C5 – Domed stromatolites (smooth undulous) in deep lake margins (image from Playford, 1988); C6 – View from small brackish water Timperley Lake to big hypersaline Serpentine Lake (image from Playford, 1988).

#### 7.1.6. Lake Thetis, Australia

Lake Thetis (Cervantes, western Australia) is a hypersaline lake with salinities varying between 39 and 53 ppt and under a Mediterranean type climate (Grey *et al.*, 1990). This lake is about 450 m long and 300 m wide with a maximum depth of 2.25 m (Grey and Planavsky, 2009; Fig. 6.19). In this lake (Fig. 6.19), microbialites are domed and crenulated along the southern coast (the leeward shore) and “*platy*” in the northern coast (the windward shore). Mounds are 5 to 10 cm thick (Reitner *et al.*, 1996) and surrounded by a carbonate mud containing shell fragments (Grey *et al.*, 1990). In the deepest part of the lake a flocculent sulphur bacterial mat is found overlain by a filamentous bacterial mat (Fig. 6.19B; Grey *et al.*, 1990). The crenulate mat is characterised by filamentous and coccoid bacteria layers intercalated with calcareous mud, the crenulate aspect is due to frequent desiccation of the microbial mat (Grey *et al.*, 1990). The domed mounds show two internal microfabrics, the inner part made of thrombolitic fabric and the outer part made of laminated stromatolites with columnar elements (Grey *et al.*, 1990). The columnar structures are only found in quiet areas of the lake (*i.e.* to the south) and are between 5 and 10 cm long and 1 to 5 cm in diameter (Grey *et al.*, 1990). The stromatolitic layer is made of fibrous fan-like to botryoidal aragonite lithifying microbial filament sheaths (Reitner *et al.*, 1996). The lithified stromatolite platform is characterised by a crust between 1 and 5 cm thick that consists of an undulated surface and a fenestral inner part (Grey *et al.*, 1990).

This lake shows mainly differences with the Purbeck limestones such as the water chemistry, the size extension of the lake and the muddy sediments surrounding microbialites. However this lake presents microbial mounds on the shores only. An interesting feature in this lake is that the morphology of the mounds is controlled by the water energy that is wind-driven. In the wind-protected shore domed mounds occur while in the wind-exposed shore mounds are more like a crust (Fig. 6.19). The internal structures of the domed mounds composed of thrombolite core rimmed by stromatolitic columns is very similar to the laminated external part of the Purbeck thrombolites that locally show small columns (refer to Chapter 4).



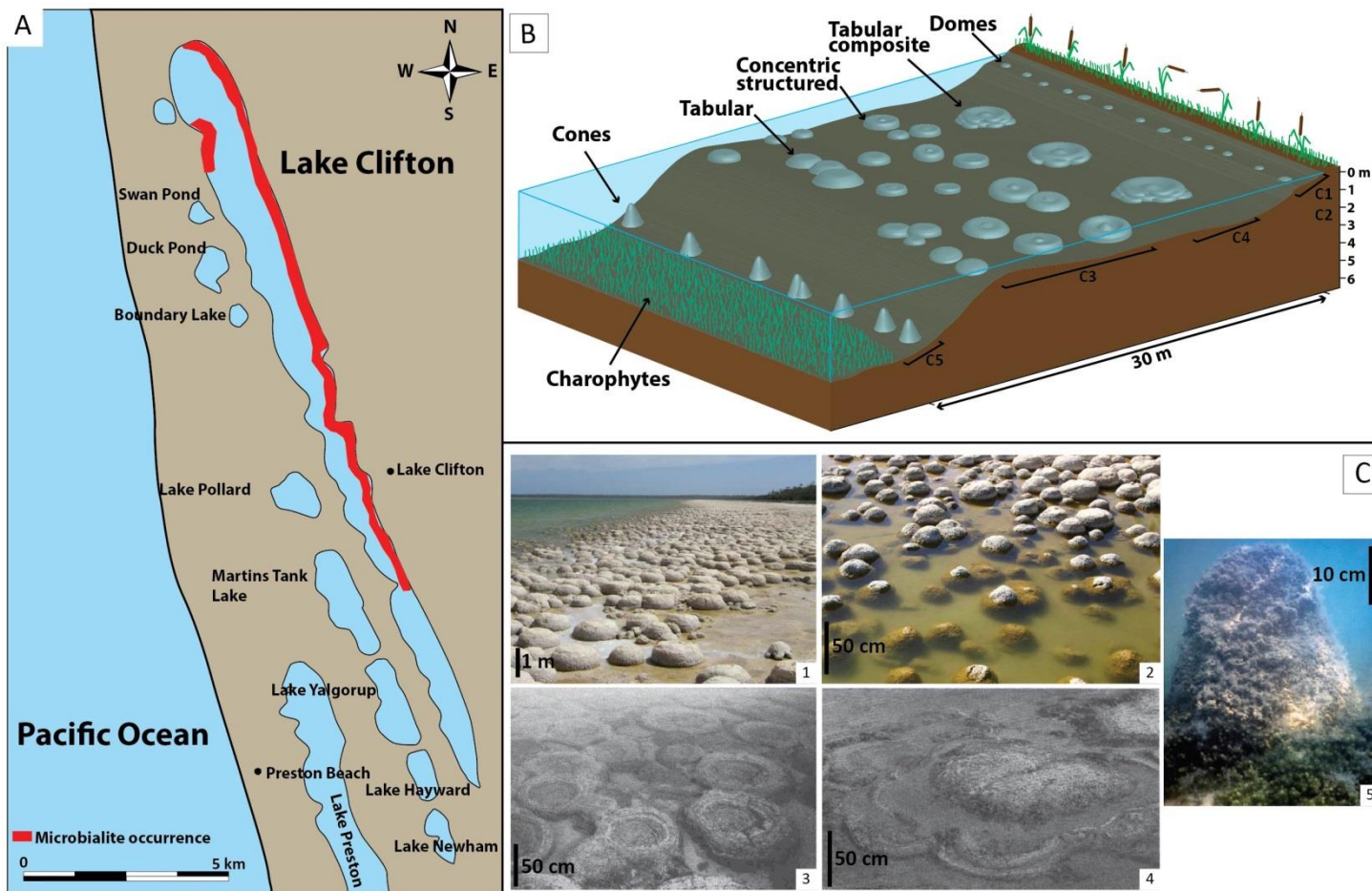
**Figure 6.19** Lake Thetis, Cervantes, western Australia. A – Map of the lake with microbialite occurrence in red. B – Facies model showing microbial mound morphologies and their distribution (data compiled from Grey *et al.*, 1990 and Grey and Planavsky, 2009). C – Field images illustrating microbial mound morphologies (images from Grey and Planavsky, 2009); C1 – Crenulate mat on the south shore; C2-3 – Domed tabular mounds on shallow south shore. Note the purplish colour of the water due to sulphate reducing bacterial mats.

### 7.1.7. Lake Clifton, Australia

Lake Clifton (Rockingham, western Australia) is a brackish water lake with salinities varying between 15 and 32 ppt and under a Mediterranean type climate (Moore, 1993). This lake is 21.5 km long and 1.5 km wide maximum with a maximum depth of 3.5 m (Burne and Moore, 1993; Moore and Burne, 1994; Luu *et al.*, 2004). Luu *et al.* (2004) noticed that the salinity increased between 1985 and 2005 from 15 to 34 ppt due to a decrease of rainfall caused by climate change. In this lake, microbialites are found mainly on the eastern shore forming a “reef”. Those mounds develop in an area about 30 m wide from the shore and down to 3 m depth (Moore and Burne, 1994; Fig. 6.20). The main morphologies of the microbial mounds are conical, domed, discoidal and tabular, can be up to 1.3 m high. These mounds are surrounded by a carbonate mud containing ostracods, gastropods, peloids, charophytes and microbialite intraclasts (Moore and Burne, 1994; Fig. 6.20). The internal microstructure of the microbial mounds is made of clots classifying them as thrombolite mounds (Moore, 1993; Burne *et al.*, 1994). These have an external stromatolitic part (2 to 5 mm thick) made of radiating microbial filaments diatoms and gastropods (Moore, 1993; Burne *et al.*, 1994).

This lake is most similar to the lower part of the Mupe Member of the Purbeck limestones as it is a brackish water lake with microbial mounds growing on its shallow shores under a Mediterranean type climate. The only difference here consists in the muddy sediment deposited around the mounds and in the deep part of the lake that indicate rather low energy while in the Purbeck, microbial mounds are always associated with coarse-grained sediments that is interpreted to document high energy. However the morphologies of the thrombolitic mounds are very similar to that of Purbeck and Burne and Moore (1993) have already compared these with the Soft Cap mounds from Dorset. These thrombolites also exhibit similar internal microfabric to those of Purbeck with the clotted inner part and the stromatolitic outer part. As with the previously described western Australian lakes the development of mounds is controlled by the water energy (wind-driven) as microbial mounds are mainly found on the windward shore.



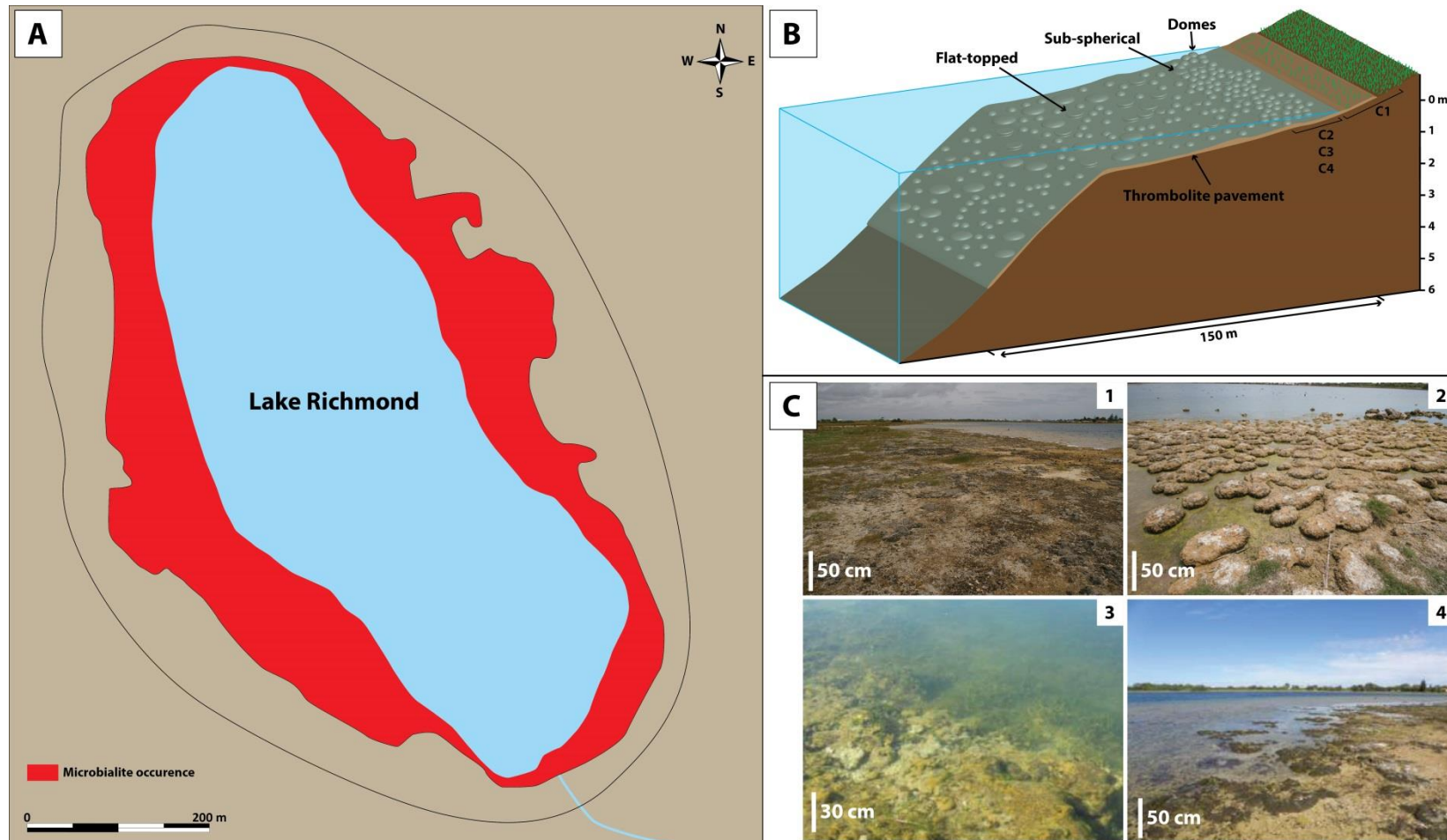


**Figure 6.20** Lake Clifton, western Australia. A – Map of the lake with microbialite occurrence in red. B – Facies model showing microbial mound morphologies and distribution (redrawn after Burne and Moore, 1993). C – Field images illustrating microbial mound morphologies; C1 – Domed thrombolites on shallow margins exposed in summer (image from McNamara, 2012); C2 – Close-up view of domed thrombolite mounds (image from McNamara, 2009); C3 – Concentric structured mounds in intermediate depth (image from Burne and Moore, 1993); C4 – Tabular composite mounds (image from Burne and Moore, 1993); C5 – Conical shape mounds in deeper area of lake (image from Burne *et al.*, 1994).

### 7.1.8. Lake Richmond, Australia

Lake Richmond (Rockingham, western Australia) is a freshwater lake (salinities varying between 0.14 and 0.56 ppt) under a Mediterranean type climate (Kenneally *et al.*, 1987; Ecoscape, 2009) that is 1 km long and 600 m wide with a maximum depth of 15 m (Fig. 6.21; Kenneally *et al.*, 1987; Ecoscape, 2009). Ecoscape (2009) noticed that before the installation of drains in the 1960s the salinity was about 2 to 3.5 ppt (slightly brackish) and that has since dropped to 0.3-0.4 ppt. In this lake, microbialites are located in a 150 m band on the shallowest part (down to 4 m depth) with the best development on the windward side (*i.e.* eastern side) of the lake (Ecoscape, 2009; Guerreiro *et al.*, 2015; Fig. 6.21). Microbialites developed as a thrombolitic pavement occur in most of the lake and this is overlain by mounded structures forming gentle domes, sub-spherical, discoidal and flat-topped structures (Guerreiro *et al.*, 2015). Guerreiro *et al.* (2015) also described the internal microfabrics of these mounds as thrombolitic and coarse laminoid. The clots of the thrombolites are formed by calcified bacterial sheaths and associated with radial microcrystalline aragonite aggregates and peloids (Guerreiro *et al.*, 2015).

This lake differs again in water chemistry compared to the Purbeck limestones although before the 1960s, brackish waters were dominant. However this freshwater lake presents similar mound morphologies and internal thrombolitic microfabrics but differ in sizes compared to the Purbeck thrombolites. As with the previously described western Australian lakes there is a control of water energy (wind-driven) as mounds are growing preferentially on the windward shores.



**Figure 6.21** Lake Richmond, Rockingham, western Australia. A – Map of the lake with microbialite occurrence in red and maximum extent of water level with the black line. B – Facies model showing microbial mound morphologies and distribution (data compiled from Kenneally *et al.*, 1987; Ecoscape, 2009 and Guerreiro *et al.*, 2015). C – Field images illustrating microbial mound morphologies; C1 – Thrombolite pavement on the shores (image from © 2015 Nabipon); C2 – Flat-topped thrombolites (image © Perdita Phillips); C3 – Gentle domed thrombolites in shallow margins (image from Vogwill, 2012); C4 – Sub-spherical to discoidal mounds in temporary exposed margins (image from Vogwill, 2012).

### 7.1.9. Green River Formation (Piceance Basin) from Utah, USA

Possibly the best analogue from the fossil record for the Purbeck carbonates comes from the Piceance Basin of the Green River Formation (Eocene, Fig. 6.22; Sarg *et al.*, 2013). In this shallow lake (Moncure and Surdam, 1980; Cole, 1985) microbial development (stromatolites and thrombolites) occurred on the margins (littoral to lower sublittoral zones) and associated with coarse-grained facies (oolitic-peloidal-quartz packstones and grainstones; Fig. 6.22C; Sarg *et al.*, 2013). Microbial mound developments appear to have occurred in rather wet climate and rising lake level (Tanavsuu-Milkeviciene *et al.*, 2012). In addition Tanavsuu-Milkeviciene and Sarg (2012) interpreted this lake to be a balanced-fill lake with fluctuating salinities although the Sarg *et al.* (2013) study suggests rather saline waters. Mound morphologies change from small domes in the upper sublittoral zone, to flatter laterally linked hemispheroids in the lower sublittoral zone (Fig. 6.22B-C; Sarg *et al.*, 2013). In the basal areas fine-grained facies including laminated oil shales that occur below the thermocline (Fig. 6.22B; Sarg *et al.*, 2013; Feng *et al.*, 2014). These deposits are organised in deepening-upward sequences due to lake level rises with initial deposition of lake marginal facies that serve as substrate for microbial mounds that are capped by deeper water mudstone (Fig. 6.22B; Sarg *et al.*, 2013). The microbialites show four main internal microstructures, stromatolitic agglutinated, stromatolitic agglutinated dendritic, stromatolitic fine-grained, and thrombolitic microfabrics (Sarg *et al.*, 2013). The stromatolite agglutinated microfabrics are made of irregular coarse-grained (peloids, quartz grains and intraclasts) laminae (Sarg *et al.*, 2013). The stromatolite agglutinated dendritic are composed of alternation of coarse-grained (as for the previous fabric) and dendritic laminae (Sarg *et al.*, 2013). The fine-grained stromatolites are composed of laterally extensive laminae (from meters to tens of meters) and were interpreted to have formed in deeper water where the microbial community expand laterally to catch light (Sarg *et al.*, 2013). The thrombolites are characterised by clotted structure with a micritic matrix incorporating ooids, peloids and quartz grains (Sarg *et al.*, 2013).

Analogies with Purbeck limestones are the balanced-fill lake type, the microbial mound morphologies and sizes which are similar to those of the Purbeck and in both cases form domed mounds. Another similar feature here is the distribution of the mounds in littoral and sublittoral zones (*i.e.* on shallow margins). However this lake differs in salinities and climate from that of the Purbeck. The microfabrics of the fine-grained stromatolites (as deep expression of microbial growth) and the thrombolites (as marginal) are also very similar to those of the Purbeck

limestones. Although the deposits are organised in deepening-upward cycles the environmental interpretation of the deposits are similar to those of the Purbeck limestones. Sarg *et al.* (2013) defined the shallowest facies to be made of packstone-grainstone; the intermediate water depth facies to be made of bindstone to boundstone (microbialites) that are organised from the agglutinated stromatolites as the shallowest, passing to thrombolites as intermediate and the fine-grained stromatolites as the deepest; and the carbonate mudstone as the deepest facies.



### 7.1.10. Summary

The description of these analogues shows that the water chemistry and the climate do not appear to have any influence on microbial mound shapes as similar mounds are found in a range of environments under different climates: in freshwater lakes with a tropical climate such as at Laguna Bacalar (Mexico) and Mediterranean at Lake Richmond (Australia); in brackish water lakes with Mediterranean climate as Lake Clifton (Australia); in hypersaline lakes with continental climate as Great Salt Lake (USA); and in hypersaline marine water with Mediterranean climate such as at Shark Bay (Australia). However the lake depth seems to be a limiting factor to microbial growth as none of these microbial mounds are found beyond 3 to 4 m water depth in the examples above (albeit taken from those with shallow water mounds). Despite the variations in water chemistries and climates, all these examples above present similar facies and sedimentology to the Mupe Member and are used to understand facies distribution in the models presented below. In all the examples described above, on the margins are deposited peloidal to oolitic grainstones with ostracod carapaces and mollusc shells (gastropods and bivalves) associated with microbial mounds, while in the deepest part mudstones are deposited (sometimes with ostracods and mollusc shells). Microbial mound internal microstructures and morphologies are also very similar when compared to that of the Mupe Member. The microstructures described in these possible analogues do not appear to be important in the type of microfabrics as filamentous and coccoid cyanobacteria are found in both thrombolitic and stromatolitic fabrics. However the water depth appears to play an important role as coarse stromatolitic and thrombolitic fabrics are preferentially found in the shallowest areas while fine-grained stromatolitic fabric are found in the deepest areas. Similarly the morphologies seem to follow a continuum from very thin and tabular mounds in the shallowest part passing through domes in intermediate-deeper water depth to flat and thin pavement areas in the deepest parts of the lakes (apart from Great Salt Lake where the mound size keeps increasing before they disappear suddenly).

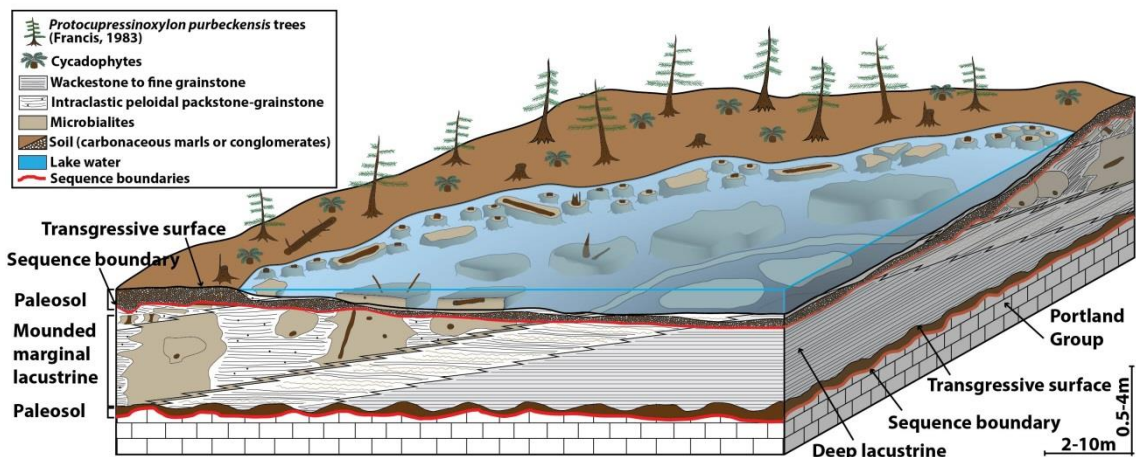
An important conclusion that can be drawn after describing all these analogues is that in ancient systems thrombolite mounds on their own will only be critical in the recognition of marginal versus basinal areas but will not give too much information in terms of palaeosalinities or palaeoclimate (as they are found in all sorts of depositional settings and climates in modern day environments). However the careful study of sediments associated with microbial mounds as well as the underlying and overlying beds will be more critical in the assessment of palaeosalinities and palaeoclimate. Concerning the associated sediments, the

fossils and their salinity tolerance (such as ostracods, molluscs or plant remains) and clasts (such as ooid types and presence/absence of evaporite pseudomorphs), coupled with geochemistry analyses (stable isotopes of carbon and oxygen) will bring more valuable information on the palaeosalinities. Concerning the underlying and overlying beds the types of sediments deposited will bring valuable information on both the palaeosalinities and palaeoclimate. If paleosols were deposited, the type of paleosol can indicate what type of climate was prevailing. If sediments were deposited, the nature of the components as explained above will bring information on palaeosalinity variations through time.

## 7.2. Facies models for the Mupe Member

Integration of the features illustrated with ancient and modern analogues in the previous section together with facies interpretations of Chapter 4 and the sequence stratigraphy of section 6 of this chapter has been used to create two facies models for the earlier brackish and later hypersaline water lake margins of the Mupe Member (Figs. 6.23 and 6.25).

The lower part of the Mupe Member is interpreted to be brackish water, open lake system of Talbot and Allen (1996) or balanced-fill lake type of Bohacs *et al.* (2000) based on their facies, biotas (Chapter 4) and stable isotope analyses (Chapter 2). Figure 6.23 illustrates the proposed depositional setting of an idealised depositional sequence on a low-relief prograding margin of this lake system based on the integration of work in this thesis and general facies models from ancient and modern settings.



**Figure 6.23** Facies model for prograding brackish water open lake margin for the lower part of the Mupe Member. Note that 1.5 sequences are illustrated in this model.

This facies model comprises the Deep lacustrine and Mounded marginal lacustrine facies associations as one complete depositional sequence between two sub-paleosol erosion



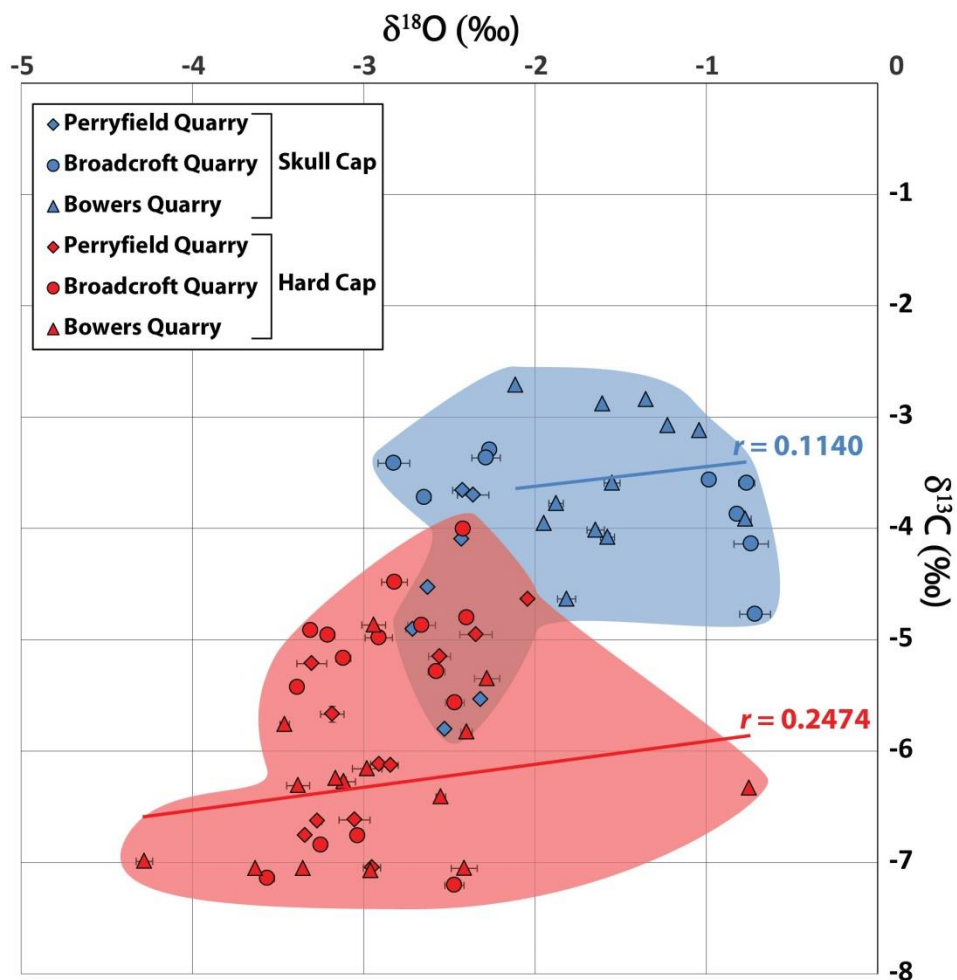
surfaces overlain by the transgressive deposits of a second sequence. The paleosols were deposited after a drop in lake level and erosion of underlying deposits (Fig. 6.12). The erosional surface (sequence boundary) cuts into either the Portland Group (for the Basal Dirt Bed) or the previous sequence (for the Lower and Great Dirt Beds, Figs. 6.10 and 6.23). After a rise of the lake level indicated by the transgressive surfaces on top of the paleosols, the transgressive deposits were deposited. On the emergent lake margins the paleosols supported vegetation of ancient cypress trees and cycadophytes. In the littoral zone and shallowest parts of the lake small tabular microbial mounds occurred either around tree stumps, or associated with trees, and surrounded by inter-mound coarse-grained facies (Intraclastic peloidal packstone-grainstone). Where the accommodation space is greater in slightly deeper waters the mounds are higher, more irregularly shaped, thicker and developed around tree trunks and branches (as suggested by the domed mounds found in intermediate depth in modern day environments). These are surrounded by an inter-mound coarse-grained facies with mound-derived intraclasts. Deeper into the lake in the sub-littoral zone microbial activity formed mats alternating with horizons of coarse-grained facies as suggested by the rather flat and thin pavements found in the deepest part of the margins in modern day environments (refer to Chapter 5 for description of size and shapes of mounds versus water depth). These deeper water mats did not develop into tabular or complex mounds due to either a lack of light and/or a lack of or excess of sediments (Dupraz *et al.*, 2009), or a lack of dissolved carbonate (Dupraz *et al.*, 2009) or due to a subsidence rate too high that resulted in the drowning of the mounds (as suggested by Jahnert and Collins, 2012), or a combination of all these external parameters. In the deepest part of the lake, in the profundal zone, the fine-grained facies of the Deep lacustrine facies association occurs with no associated microbial build-ups. As suggested by studying modern day environments (see previous section) and general lacustrine facies models (Figs. 6.13 and 6.14), the Purbeck brackish water lake of this study was most likely with low-relief margins and with microbial development constrained in the littoral zone (*sensu* Platt and Wright, 1991).

Depositional environments of the Cap beds and Dirt Beds have been debated since Arkell (1947) who was the very first one to propose freshwater environment because of the trees and the interpretation of tufa deposits. Later West (1975) proposed a lagoonal environment with hypersaline waters with algal limestones based on inferred palaeosalinities from biotas and comparison with Persian Gulf salinities (refer to Chapter 2). This idea was proposed earlier by Brown's (1963, 1964) work on the algal limestones and later supported by Francis's (1982, 1982, 1984, 1986) work on the Dirt Beds (*i.e.* the paleosols). Brown (1963, 1964) detailed the

types of algae associated with the algal deposits in hypersaline environments (refer to Chapter 2). Francis (1982, 1983, 1984, 1986) demonstrated that the paleosols were rendzina profiles at different stages of maturity that supported conifer and cycadophyte forests that developed under semi-arid climate Mediterranean type (refer to Chapter 2). According to Francis (1982) the hypersalinity of the waters is concordant with this type of climate and with the rapid death and preservation of the trees when drowned. It was only with Bosence's (1987) work on facies of the Cap beds and Dirt Beds and Perry's (1994) work on the tufa deposits that the freshwater origin was reconsidered. Bosence (1987) demonstrated that stromatolites are a minor component of the "algal limestones" of previous workers and therefore have to be referred to as thrombolites originating in freshwater environments (refer to Chapter 2). Perry (1994) supported this idea and interpreted freshwater calcitic cements coating phytoclasts that brings more evidence for freshwater origin of the environment (refer to Chapter 2). Radley's (2002) work on mollusc assemblages showed that due to the low diversity of gastropod species and the mixing of low-salinities and marine species the environment was most likely a closed brackish water system periodically hypersaline (refer to Chapter 2).

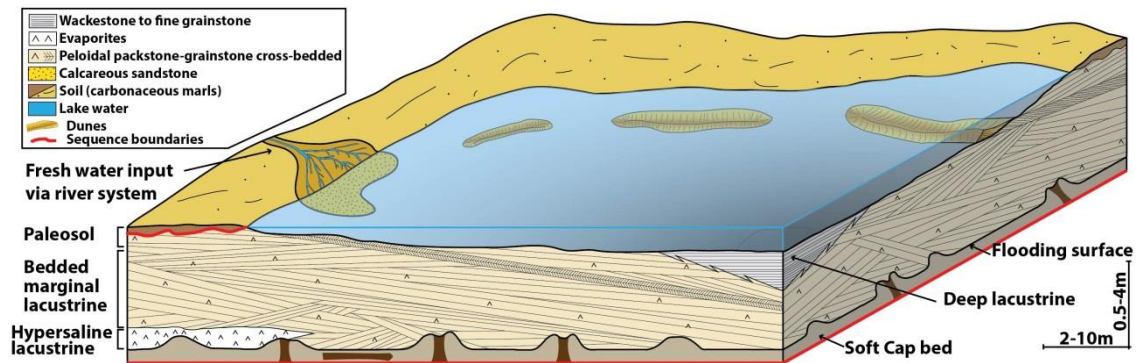
Biotic assemblages (ostracods and molluscs) identified by previous workers (such as Arkell, 1941; Clements, 1973; Anderson, 1985; Horne, 1995, 2002; reviewed in Chapter 2) indicate fresh to brackish water tolerant species. This is possibly supported by the stable isotope (carbon and oxygen) data acquired during this project (Fig. 6.24) on bulk rock samples in the Intraclastic peloidal packstone-grainstone facies. These were sampled in the Skull and Hard Cap beds at three locations on the Isle of Portland, Perryfield, Broadcroft and Bowers Quarries (refer to Chapter 2). The  $\delta^{13}\text{C}$  data vary between -4.63 and -0.72 ‰ (with a precision of 0.03 ‰) and the  $\delta^{18}\text{O}$  data between -2.71 and 7.20 ‰ (with a precision of 0.12 ‰; Fig. 6.24). As the stable isotope analyses achieved during this project were performed on bulk rock samples, this means that the signatures measured do not directly reflect palaeosalinities but a mixture of palaeosalinities, diagenetic modifications and/or vital effects. As a consequence further investigations and more detailed analyses are needed to fully characterise the palaeosalinities of the lake waters. However general trends can be drawn as these data fall in the general trends for lake waters defined by Leng and Marshall (2004) that showed that the carbon and oxygen isotopic signatures of freshwater lakes are slightly negative while in saline lakes they are slightly positive. In this study carbon and oxygen isotopic signatures are slightly negative that indicates a deposition in fresher lakes rather than more saline. The data from the Hard Cap suggests more negative values than in the Skull Cap that may suggest a slight

freshening in the Hard Cap than in the Skull Cap (Dharmarajah, 2015). In addition Talbot (1990) stated that the co-variance between carbon and oxygen data is more common in closed lakes than in open lakes. He proposed that closed lakes show typical regression coefficients ( $r$ ) greater than 0.8 and that open lakes show smaller values. In this study the regression coefficients are about  $r=0.11$  for the Skull Cap (Fig. 6.24A) and  $r=0.24$  for the Hard Cap (Fig. 6.24A) suggesting rather open lake systems. Taken together with the petrographic evidence of a general absence of evaporites and charophytes these data all indicate brackish water conditions in an open lacustrine system (refer to Chapter 2). This invalidates West's (1975) and Francis' (1982, 1983, 1984, 1986) hypersaline lagoon, Perry's (1994) freshwater origin and of Radley's (2002) closed system; and validates Bosence's (1987) interpretation of brackish water lacustrine system. Moreover the recognition of microbialite deposits around trees provides detail in support of Bosence's (1987) and Perry's (1994) interpretation of tufa deposits as complex thrombolite mounds.



**Figure 6.24** Plot diagram of the  $\delta^{18}\text{O}$  vs.  $\delta^{13}\text{C}$  stable isotope data of the Intraclastic peloidal packstone-grainstone facies.

The upper part of the Mupe Member is considered to have been deposited in a more closed lacustrine system of Talbot and Allen (1996) or underfilled lake type of Bohacs *et al.* (2000) as indicated by the evaporites and the biota. Figure 6.25 illustrates the depositional setting of low-relief margin of this hypersaline water, closed-lake based on facies interpretations in Chapter 4 and comparison with modern day analogues.



**Figure 6.25** Facies model for regressive hypersaline water lake margin for the upper part of the Mupe Member. Note that the upper paleosol is only locally developed compared with the previous model for the lower part of the Mupe Member.

The main analogue for this depositional setting is taken as the northern arm (Gunnison Bay) of the Great Salt Lake (Utah, USA). This facies model indicates the depositional sequence of the Cypris Freestone beds (as described in section 6 of this chapter) with all the facies preserved in a prograding lake margin. This facies model comprises the Hypersaline lacustrine and Bedded marginal lacustrine facies associations as highstand deposits and the Emergent facies association as lowstand deposits conformably overlying the previous deposits in a normal regression. As the paleosols are interpreted as lowstand deposits, they accumulated on the eroded surface (SB) on the previous sequence. Note that these paleosols are rare throughout the studied area (refer to section 5 of this chapter). In the littoral to sub-littoral zones of the lake, cross-bedded, coarse-grained facies accumulated in rather high energy conditions as indicated by the ripples and cross-laminations, the peloidal grainstones and the presence of well sorted intraclasts and ooids (refer to Chapter 4). These are organised in dunes and ripples aligned with the coast as suggested by the palaeocurrent measurements (refer to Chapter 4). The presence of evaporite crystals (calcite or sediment pseudomorphs after gypsum, anhydrite and halite) in this peloidal packstone-grainstone indicates arid climatic conditions and hypersaline waters. The presence of halite pseudomorphs in calcite only on the top surfaces of the beds suggests more arid conditions and desiccation towards to the top of the beds (Talbot and Allen, 1996). Possible temporary and local freshwater input via river systems provided occasional clastic material from the land and led to the deposition of a

quartz rich facies (the Calcareous sandstone facies). Rather more localised and closed areas within this lake provided the conditions for the formation of true evaporite facies. In the deepest part (*i.e.* profundal zone) of the lake the deposition of fine-grained facies (Deep lacustrine facies association) occurs as in the previous facies model. The absence of microbial activity can be explained by two possible processes: either a rise in lake level (*i.e.* flooding) that stopped microbial growth due to a higher sedimentation rate (sediment input became greater than the growth rate); or a change in the chemistry of the water due to geographical barriers that reduced flows, increased salinities and resulted in the death of the microbial community. In the first case this is interpreted from the observations that microbialites are never found beyond 4 m of water depth in modern day environments. The second case is interpreted from Dupraz *et al.* (2009) work that proposed that a lack of dissolved carbonates associated with either a lack or excess of sediments are deleterious for microbial health and growth. However the peloidal packstones-grainstones facies described in this study (refer to Chapter 4) are also typical of marginal areas. As a consequence an increase in salinity as indicated by the appearance of evaporite pseudomorphs is the more likely cause for the death of the microbialites. Contrarily to the previous facies model (Fig. 6.23), the hypersaline model (Fig. 6.25) is concordant with most of the previous interpretations of depositional environment and especially West's (1975) hypersaline conditions. Radley's (2002) interpretation of closed lacustrine system is also concordant with data presented in this study and the hypersaline facies model of figure 6.25.

## 8. Conclusion

The definition of five facies associations grouping facies defined in Chapter 4 allowed the interpretation of two main depositional environments and facies models: brackish water lake facies model and hypersaline water lake facies model. This change in depositional environment occurs up-section in the stratigraphy as well as spatially and will be detailed in Chapter 7. Integration of new stable isotope data previously acquired for the lower part of the Mupe Member helps to invalidate most of the previous studies and shows a brackish lacustrine open system during the deposition of the Skull and Hard Cap beds. Facies analysis and sequence stratigraphy helps to identify 4 sequences during the deposition of the Mupe Member bounded by sub-aerial exposure surfaces on the tops of the Portland Group, Transition Bed, Skull Cap and Hard Cap.

The correlation panels indicate a change from brackish water lake to the west to hypersaline to the east possibly due to a high in the palaeotopography. This was previously interpreted and described by West (1975) and Francis (1982) and will be used and discussed in Chapter 7 to build tectono-sedimentary models of the Mupe Member.

The comparison of the facies models created in this study with modern day environments helps to reach an understanding of the facies distribution and to draw some general conclusions. As is the case in marine environments, coarse-grained facies are deposited in the shallowest areas above wave base on the margins of lakes but in this lacustrine setting these are closely associated with microbialites. Fine-grained facies are deposited in more protected areas or in the deepest parts of the lakes. Microbialites are found only on the margins and their shapes and sizes are dependent on water depth while the salinity does not appear to be a limiting factor in modern day environments for mound shapes and internal fabrics (from freshwater to hypersaline; including hypersaline marine waters). An important control though appears to be the carbonate concentration in the waters that has to be high enough for the microbial communities to calcify (as observed in Laguna Bacalar by Gischler *et al.*, 2011, 2012; refer to Appendix 1).

The stratigraphical (vertical) change in depositional environments from open (brackish waters) lake system to closed (hypersaline waters) lake system may be due to different external factors. A modification in the climate, subsidence rate, fault activity, hydrology or a combination of all those parameters could be responsible for such a change in depositional environments. This is illustrated and discussed in Chapter 7 where the integration of all the data acquired during this project is used to establish tectono-sedimentary models for the Skull, Hard and Soft Cap beds of the lower part of the Mupe Member.

## Chapter 7

# Tectono-sedimentary models for the Mupe Member

## 1. Introduction

This chapter presents the integration of work on seismo-stratigraphy and sedimentology undertaken during this study to propose three new tectono-sedimentary models for the Mupe Member. The sub-surface data analysis and interpretation provides the syn-sedimentary setting of the Purbeck and Ridgeway Faults as well as the traces of the faults and their maximum lateral extent (Chapter 3). The definition of 9 facies (Chapter 4) and their interpretation in terms of depositional environments and facies models (Chapters 4 and 6) provide the depositional settings of the Mupe Member deposits with the interpretation of the marginal and basinal areas. This is supported with the facies association distribution and the correlation panels of sedimentary logs that show that all the beds and facies associations are traceable along the studied area with a greater thickness of deposits close to faults in hanging-wall depocentres (Chapter 6). The morphological characterisation of the microbial mounds that are summarised and integrated together with the facies distribution in the two facies models (Chapters 5 and 6) helps to constrain the depositional settings. All these have resulted in the revision of palaeogeographies proposed by previous authors (West, 1975; Francis, 1982; Underhill, 2002) and are here integrated with the tectonic setting to propose three new tectono-sedimentary models for the Skull, Hard and Soft Cap beds. Despite the fact that although the study area is well exposed and has a considerable amount of subsurface data the contouring of the facies and thicknesses could not produce one solution. As a result of integration of published models for extensional faults in rift basins and for lacustrine facies has enabled the construction of two scenarios: 1) influenced by the relay ramp; and 2) with two, partially isolated, E-W hanging-wall depocenters.

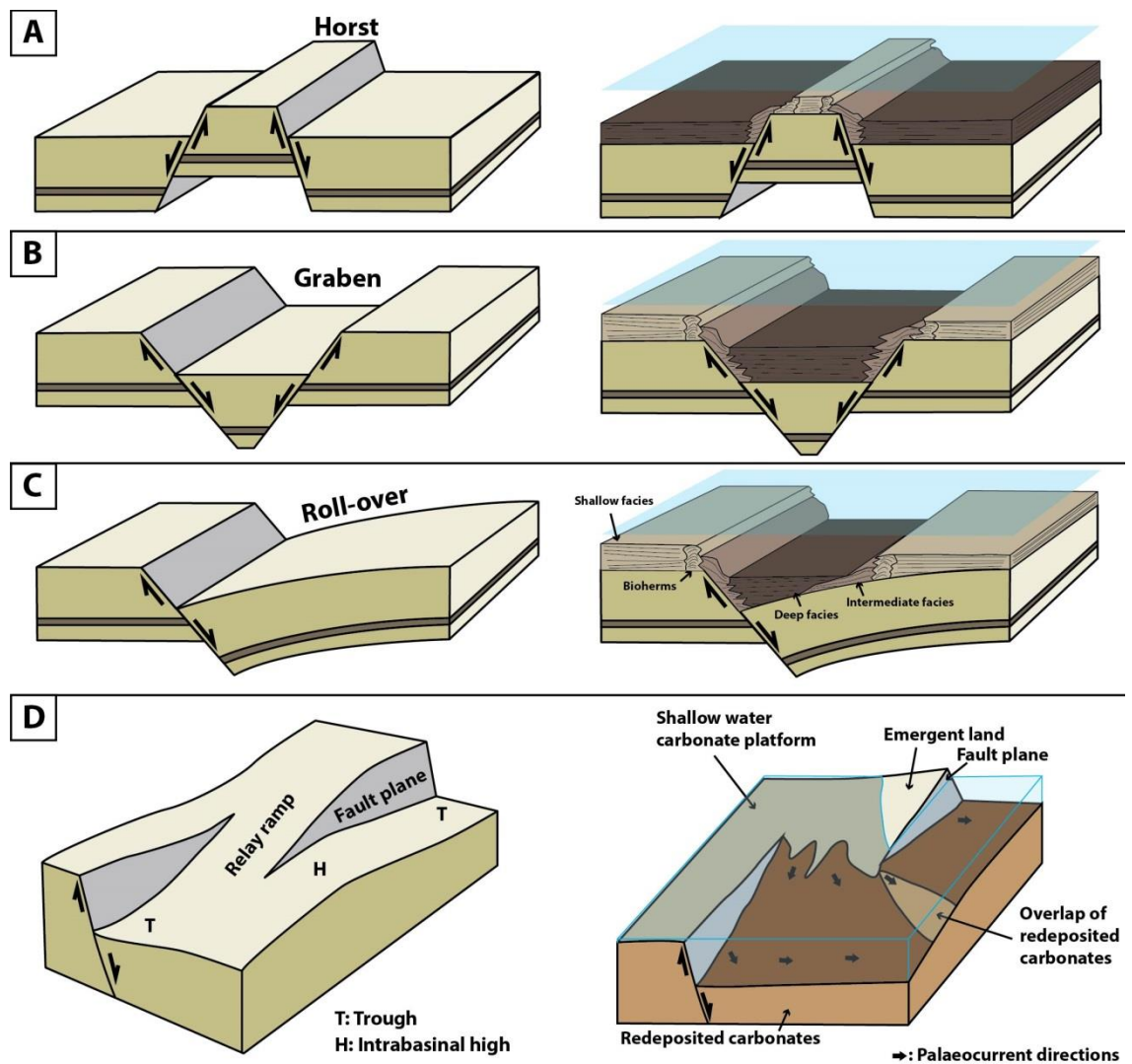
## 2. Controls on non-marine carbonate sedimentation

Facies distribution in lacustrine environments is mainly controlled by tectonics and climate that influence the hydrology, sediment input and temperature changes (Wright, 1990; Platt and Wright, 1991; Gierlowski-Kordesch, 2010).

Generalised published models provide main depositional trends influenced by tectonics that can be applied to marine and non-marine (lacustrine) settings. In extensional rift systems normal faulting can create symmetric grabens and/or horsts if the basin is bounded by two antithetic normal faults (Fig. 7.1A-B); or asymmetric grabens, also called half-grabens, if the basin is only bounded by one normal fault (Fig. 7.1C; Fossen, 2010). In these rift basin systems,

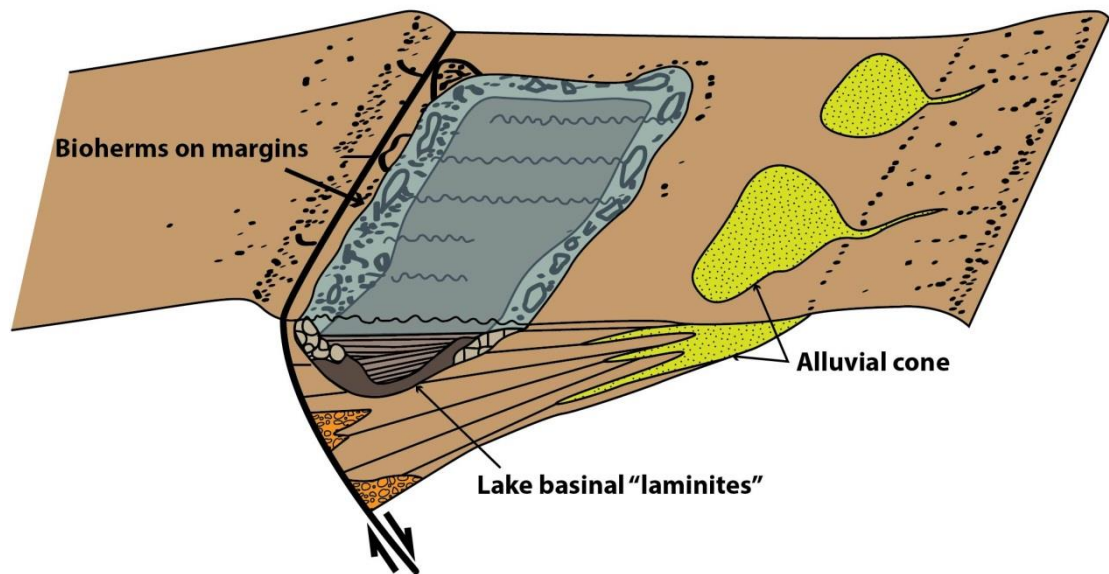


carbonate facies will be distributed parallel to the faults when the basin is bordered by one single normal fault (Fig. 7.1A-C); and both parallel and perpendicular or oblique to the faults where faults are linked by a relay ramp system or transfer zone (Fig. 7.1D; Cross and Bosence, 2008; Wilson *et al.*, 2000). In a horst system shallow or emergent areas will be expected on top of the horst (*i.e.* on the footwall block, Fig. 7.1A). In a graben system shallow areas will be located adjacent to the fault scarps on the footwall blocks with deep facies in hanging-wall depocentres (Fig. 7.1B). In half-graben systems roll-over anticlines are commonly created due to the asymmetry (Fossen, 2010) and shallow areas will be located on the fault scarp on the footwall blocks and on top of the roll-over anticline (Fig. 7.1C). In relay ramp system or transfer zone shallow areas are aligned with the relay ramp area in the hanging-wall depocentre in addition to the sites previously mentioned (Fig. 7.1D).



**Figure 7.1** General tectono-sedimentary models in rift settings. A – Horst system model on the left (redrawn after Fossen, 2010) and general depositional trends on the right from Dorobek (2008). B – Graben system model on the left (redrawn after Fossen, 2010) and general depositional trends on the right from Dorobek (2008). C – Half-graben or roll-over system on the left (redrawn after Fossen, 2010) and general depositional trends on the right from Dorobek (2008). D – Relay ramp system (redrawn after Gawthorpe and Hurst, 1993) and simplified block diagram of the Tonasa Formation during the Oligocene in central Pangkajene, northern Barru in Indonesia on the right (redrawn after Wilson *et al.*, 2000).

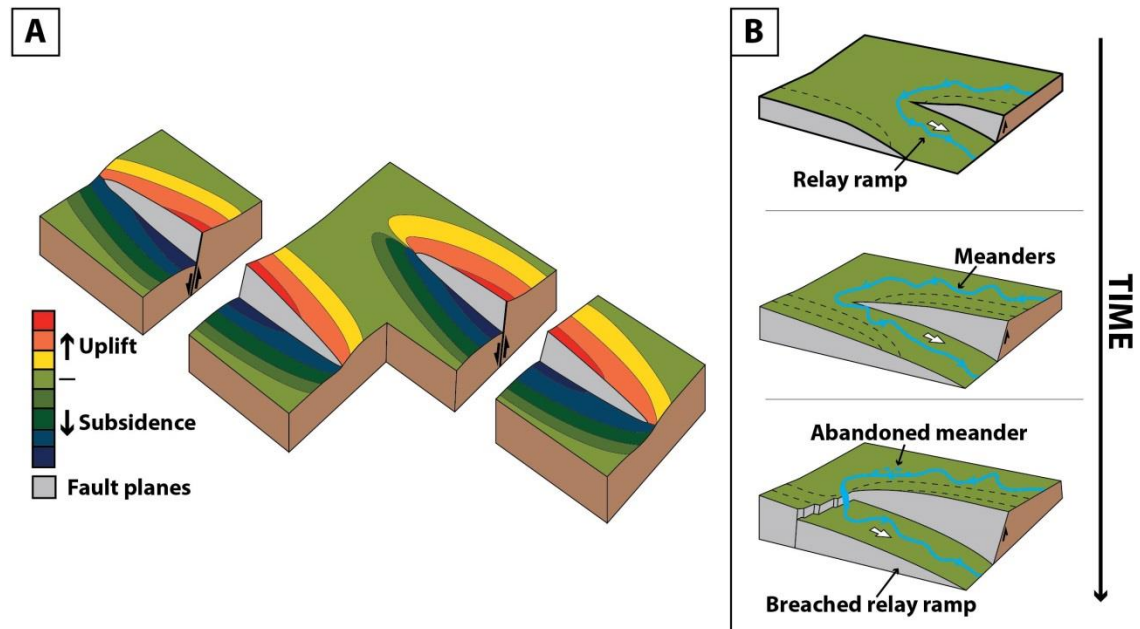
Platt and Wright (1991) proposed a tectono-sedimentary model for lacustrine carbonate facies distribution in a half-graben system (Fig. 7.2). Although this model shows facies distribution in 3-D, it is only based on 2-D vertical succession (the third dimension was inferred from this 2-D vertical succession). As a consequence this model has a very limited predictive value of facies distribution in the three dimensions. They showed that lakes are likely to form on hanging-wall areas parallel to the fault trace with a depocentre close to the fault (Fig. 7.2). They also showed that shallow-water bioherm deposition would occur on the margins of the lakes with deep facies such as laminites in the centre part of the lake in basinal areas (Fig. 7.2).



**Figure 7.2** Lacustrine carbonate facies in a half-graben system (redrawn from Platt and Wright, 1991). Note that the colours of the facies are the same as in figure 7.1.

Another important aspect for this study is in the preferential accumulation sites and tectonic controls on facies distribution in rift systems that are very well documented in the literature. Anders and Schlische (1994) and Gawthorpe *et al.* (1994) demonstrated that in extensional systems, the accommodation space is the greatest in the centre part of the hanging-wall blocks of normal faults and decreases gradually towards the tips (Fig. 7.3A). Cowie and Scholz (1992) and Kim and Sanderson (2005) additionally demonstrated that there is a linear relationship between the maximum vertical displacement (that can be approximated to accommodation space) and the length of the fault. An average ratio can be determined where the length equals 100 times the maximum vertical displacement of a fault (Kim and Sanderson, 2005). All these mean that for example for 5 m thick deposits deposited close to a fault, the length of the fault needs to be at least 500 m long.

Trudgill (2002) and Athmer and Luthi (2011) demonstrated that preferential drainage in a relay ramp system occurs through the relay ramp area and the fault scarps; and subsequent deposition occurs respectively downstream on the relay ramp and on the hanging-wall blocks of the faults (Fig. 7.3B).



**Figure 7.3** Relay ramp depositional zones and main drainage routes. A – Schematic normal faults illustrating the accommodation space created during the formation of relay ramp area (redrawn after Gawthorpe *et al.*, 1994). B – Schematic evolution of a relay ramp area with preferential drainage route (redrawn after Athmer and Luthi, 2011 and Trudgill, 2002).

Surprisingly little has been published on the preferential sites for accumulation of carbonate in lacustrine extensional basins. Gawthorpe and Hurst (1993) showed that in marine settings relay ramp zones are preferential input of clastic sediments into hanging-wall depocentres and that carbonate platforms can develop in shallow ramp sites but only if the clastic input is very low. Cross and Bosence (2008) added that the initial low-relief topography favours carbonate platform development that becomes steeper and might form an intrabasinal high with time. Wilson *et al.* (2000) demonstrated that carbonate deposition in this type of system is mainly the result of shallow water carbonates redeposited as illustrated in figure 7.1D. They found that in the Oligocene deposits of the Tonasa Formation of Indonesia a carbonate platform developed on the footwall with redeposited carbonate facies in the hanging-wall depocentres and reworked through a relay ramp area (Fig. 7.1D). Most importantly for this study they showed that there was a main depositional area that developed oblique to the relay ramp mainly and located on top of a palaeohigh on the seafloor (called “overlap” in figure 7.1D).

### 3. Tectono-sedimentary models of the Mupe Member

This section describes three tectono-sedimentary models for each of the Skull, Hard and Soft Cap beds (Figs. 7.4, 7.5, 7.7 and 7.8). As a consequence of the uneven distribution of logged sections, and despite the extent of the outcrops and the subsurface data some key areas have missing data. Therefore two different scenarios are presented for each of these three units. The contouring of the data points lead to palaeogeographies that can be interpreted as in scenario 1 where two sub-basins/lakes are separated by a lake floor high (Figs. 7.4 and 7.5) or as in scenario 2 where one elongated and narrow lake basin formed (Figs. 7.7 and 7.8). In addition, as the Deep lacustrine facies association was never observed to be deposited laterally to the Mounded marginal lacustrine facies association, two versions for each model are illustrated, with and without the Deep lacustrine facies association deposited. Because of the resolution of the seismic data (the entire Purbeck Limestone Group is contained within two reflectors; refer to Chapter 3) the traces of the Ridgeway and Purbeck Faults are kept the same in both sets of models. In the models the dots locate the position of the sedimentary logs and the colours (dots and polygons) correspond to the facies associations defined in Chapter 6. In all the models, exposed land is interpreted to be located north of the faults (Figs. 7.4, 7.5, 7.7 and 7.8) due to the absence (non-deposition or deposition and subsequent erosion) in both sub-surface data and field exposures of the Purbeck Limestone Group (refer to Chapter 3). Consequently, the traces of faults are considered to locate the palaeoshorelines (Figs. 7.4, 7.5, 7.7 and 7.8). However there are more uncertainties to the south as only limited data are available in this area.

#### 3.1. Scenario 1

##### 3.1.1. Models

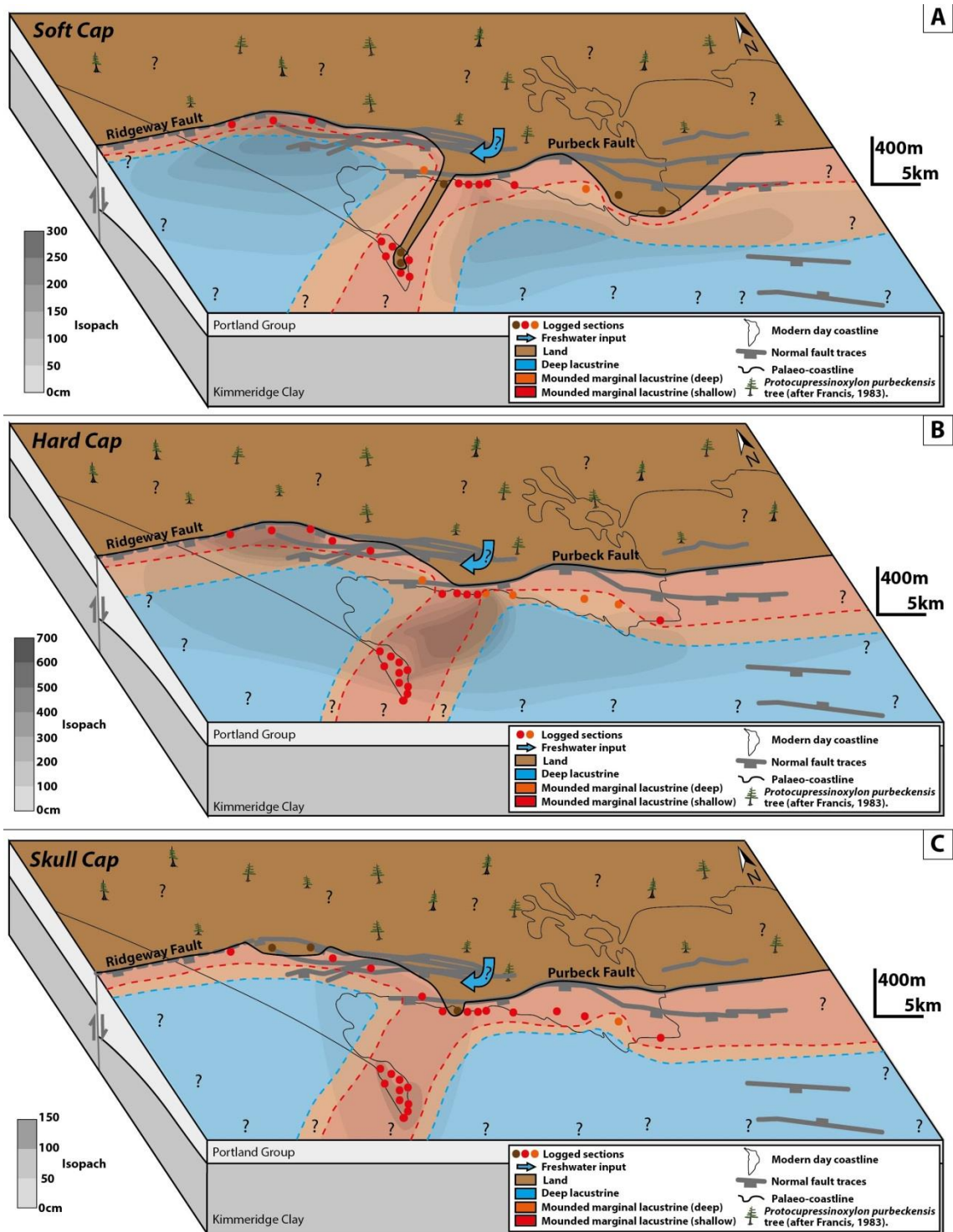
This first scenario is driven by the possible influence of the relay ramp area identified in the sub-surface data (refer to Chapter 3) and by previous authors (refer to Chapter 2). In addition this scenario follows the general depositional model in relay ramp setting as presented in the previous section (Fig. 1C; Wilson *et al.*, 2000; Fossen, 2010).

In this scenario shallower areas (*i.e.* the margins in red in figures 7.4 and 7.5) are located on the hanging-wall blocks and along the faults and following a NE-SW facies trend in the centre part of the studied area connecting the Lulworth region, located on the fault scarp, to the Isle of Portland exposures, located over the dip slope (Figs. 7.4 and 7.5). Consequently

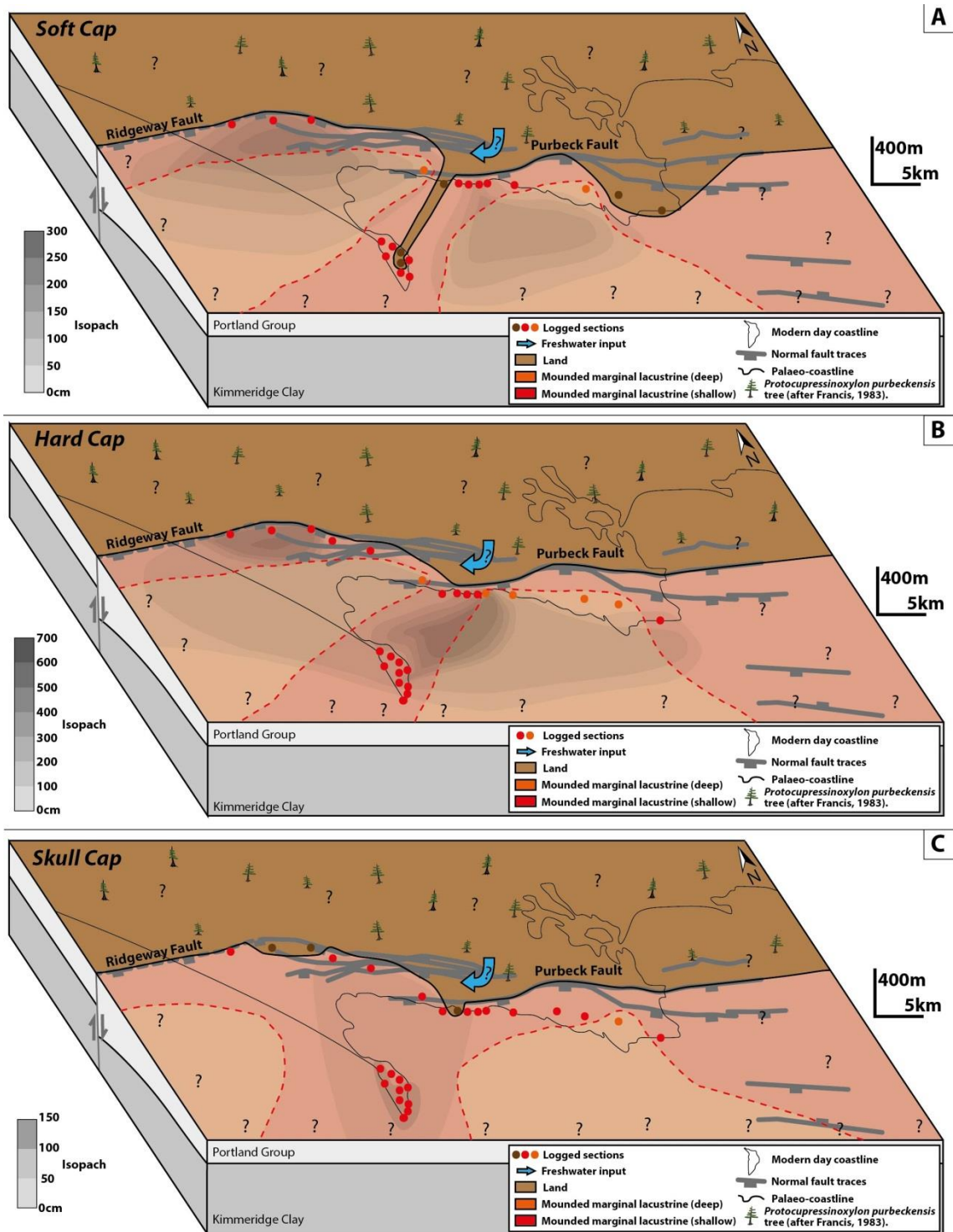
deeper areas (in blue and/or orange in figures 7.4 and 7.5) were most likely located to the east and to the west of this NE-SW facies trend (Figs. 7.4 and 7.5).

The three models for the Skull, Hard and Soft Cap beds do not show significant changes through time in the facies distribution with this NE-SW trend located at the same position (Figs. 7.4 and 7.5). This facies trend appears to be located in the centre part of the area and aligned with the relay ramp area (Figs. 7.4 and 7.5; refer to Chapter 3). The main emergent areas are seen at the Ridgeway relief road cutting, Friar Waddon well and Dungy Head at the time of the deposition of the Skull Cap (Figs. 7.4C and 7.5C); and at Broadcroft Quarry, Perryfield Quarry and Holworth House at the time of the deposition of the Soft Cap (Figs. 7.4A and Fig. 7.5A) where lacustrine facies are absent. These areas are interpreted to locate emergent areas with soils.

The main changes between the three models for of the Cap beds are in the locations of the interpreted depocentres. At the time of the Skull Cap deposition, thicknesses do not exceed 1.50 m and one depocentre is interpreted to be located following the NE-SW facies trend with the thickest deposits over the Isle of Portland (Figs. 7.4C and 7.5C). At the time of the Hard Cap deposition thicknesses do not exceed 7 m and with or without the Deep lacustrine facies association, two depocentres are interpreted (Figs. 7.4B and 7.5B); one located on the hanging-wall block in the centre of the Ridgeway Fault; and one that coincides with the NE-SW facies trend. To the east of the studied area less than 2 m of strata was deposited (Figs. 7.4B and 7.5B). Similarly, at the time of the Soft Cap an important feature is the emergent area between Lulworth and the Isle of Portland that might separate a basin to the west from a basin to the east (Figs. 7.4A and 7.5A). Therefore two depocentres are also interpreted at that time; one in the hanging-block of the Ridgeway Fault; and one east of the NE-SW facies trend in the central part of the studied area (Figs. 7.4A and 7.5A).



**Figure 7.4** Tectono-sedimentary models of the Mupe Member following scenario 1 with the Deep lacustrine facies association. A – At the time of the Soft Cap bed deposition. B – At the time of the Hard Cap bed deposition. C – At the time of the Skull Cap bed deposition. Note that the western part of the Ridgeway Fault trace in dashed line was not imaged with seismic data and is after Harvey and Stewart (1998). Note that the red areas correspond to the shallow microbial mounds (tabular and small, refer to Chapter 5) and the orange areas correspond to the deeper expression of the microbial mounds (the big and complex shaped mounds and stromatolites, refer to Chapter 5).



**Figure 7.5** Tectono-sedimentary models of the Mupe Member following scenario 1 without the Deep lacustrine facies association. A – At the time of the Soft Cap bed deposition. B – At the time of the Hard Cap bed deposition. C – At the time of the Skull Cap bed deposition. Note that the western part of the Ridgeway Fault trace in dashed line was not imaged with seismic data and is after Harvey and Stewart (1998). Note that the red areas correspond to the shallow microbial mounds (tabular and small, refer to Chapter 5) and the orange areas correspond to the deeper expression of the microbial mounds (the big and complex shaped mounds and stromatolites, refer to Chapter 5).



### 3.1.2. Validity of the scenario 1 models

The facies trends interpreted in the three models proposed in this study show that the shallowest areas are on (1) the hanging-wall blocks of the faults; and (2) aligned with the relay ramp area with a NE-SW trend. Due to their vicinity and relationship with tectonic features (fault traces and relay ramp area) these facies trends suggest a tectonic control on the facies distribution.

The application of these general principles presented in the previous section helps in the interpretation of the possible controls on the facies distribution of the Skull, Hard and Soft Cap beds. Facies are only found in the hanging-wall depocentres that indicate a non-deposition or a deposition and subsequent erosion on the footwall blocks (refer to Chapter 3). This suggests that the lower part of the Mupe Member most probably deposited in graben or half-graben system (as per description in the previous section). Due to the limitation of the sub-surface data coverage publically available, no information is available south of the Isle of Portland. Consequently in this study the half-graben system will be considered as the most appropriate tectonic model. In such condition the application of Platt and Wright's (1991) model for lacustrine environments in half-graben setting appears to be the most relevant for this study (as per figure 7.2). However other authors interpreted one long (Butler, 1998) or two or three shorter (Lake, 1985; Harvey and Stewart, 1998; Underhill and Stoneley, 1998) north-dipping faults south of the Isle of Portland (refer to figure 2.2 in Chapter 2). If such faults were formed and were active at the time of the deposition of the Skull, Hard and Soft Cap beds, a graben system was more likely to occur than half-graben.

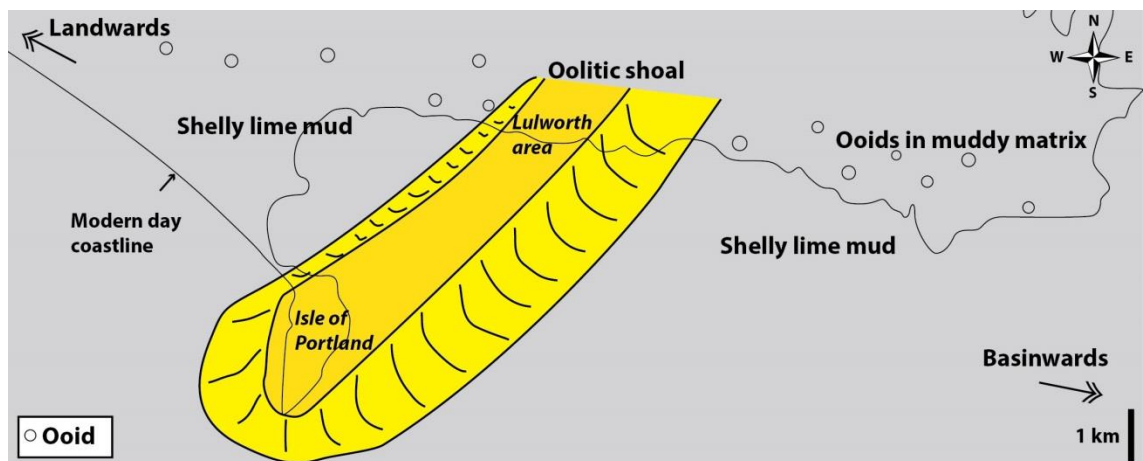
The location of the depocentre in the centre part of the Ridgeway Fault (to the west) and absence of strata on the footwall blocks, suggests that there was a tectonic control during the deposition (Figs. 7.4 and 7.5). Moreover the maximum thickness recorded in these depocentres is around 5 m in the Hard Cap and 2.50 m in the Soft Cap (refer to Chapter 6) which means that the fault was respectively at least 500 m and 250 m long. The seismic interpretation and published works resulted in the recognition of the Ridgeway Fault over at least 40 km, which is compatible with this result. Concerning the northern part of the depocentre located near the NE-SW facies trend (around Lulworth area, Figs. 7.4 and 7.5), its location and the rapid thickness changes (refer to Chapter 6) suggest that there was also a tectonic control on the deposition. The maximum thickness recorded is about 5.50 m in the Hard Cap and 1.50 m in the Soft Cap meaning that the fault was respectively at least about 550 m and 150 m long. The seismic interpretation helps to identify the Purbeck Fault over at least

40 km, however this depocentre appears to be located only on the western tip of the fault. This suggests that only a short portion of the Purbeck Fault was active during the deposition of the Hard Cap. As defined above, the maximum thickness recorded suggests that the fault was about 550 m long minimum. However the sedimentary logs where the thickest Hard Cap is recorded are West Lulworth Cove ( $\pm 3.50$  m), Fossil Forest ( $\pm 5$  m) and Mupe Bay ( $\pm 5.50$  m) with consequent thinning at Dungy Head ( $\pm 1.70$  m) to the west and Worbarrow Tout ( $\pm 2$  m) to the east (refer to Chapter 6). These locations are spread over about 5.5 km that suggest that the portion of the Purbeck fault active at the time of the Hard Cap deposition was centred more or less in Lulworth Cove and extended over this same length.

The preferential deposition in the hanging-wall blocks of the faults was also suggested by Underhill (2002). However his depositional model is driven by application of general models of relay ramp systems to the facies of the Mupe Member limestones defined by West (1975) (refer to Chapter 2). In his model, Underhill (2002) proposed the deposition of conglomeratic fans in the vicinity of the faults and resulting from the erosion of the exposed Portland Group. However such a facies has never been found either by previous authors (Strahan, 1898; Arkell, 1933, 1947; West, 1975; Francis, 1982, 1983, 1984, 1986) or in this study (field observations coupled with subsurface data analysis). Two possible reasons can explain the absence of this facies in Dorset; (1) as defined by Davison and Underhill (2012) the conglomeratic supply probably never reached the volume needed to deposit such coarse-grained alluvial fans in the hanging-wall blocks; or (2) the deposition of the eroded materials from the footwalls was routed away from the hanging-wall blocks possibly through relay ramp (Peacock and Sanderson, 1991); or (3) the faults did not break through to the surface and created a fault scarp necessary to create fans; or (4) if the eroded land was mainly limestone then most erosion would have been by dissolution rather than physical processes. If the two latter cases occurred, it will be impossible to find such facies as the supposed deposition area would have been eroded after the formation of the Weymouth Anticline (submarine outcrop of Oxford Clay in Weymouth Bay; refer to Chapter 3).

Concerning the depocentres that coincide with shallow areas following a NE-SW facies trend in the Skull and Hard Cap beds, they appear to be aligned with the relay ramp area (Figs. 7.4 and 7.5). The relay ramp could have been the main water input via rivers into the lake (according to general models previously described, Fig. 7.3B). The running waters were presumably enriched in calcium carbonate through erosion and dissolution of exposed older carbonate deposits (such as the Portland limestones) and transported to the lake. This resulted in a saturation in respect of the calcium carbonate of the lake waters which is necessary for

the calcification of the microbial filaments to occur (as discussed in Chapter 6). Townson (1971) described and detailed facies and palaeoenvironment reconstructions of the underlying Portland Group and specifically the location of a NE-SW trend, or swell, in the central part of the area (Fig. 7.6). Townson (1971) showed that this swell had already formed during the deposition of the uppermost beds of the underlying Kimmeridge Clay Formation and that it persisted through to the uppermost beds of the Portland Group (the Freestone Beds). He showed that in the uppermost part of the Freestone Beds an oolitic shoal was deposited with a NE-SW trend that connected coastal outcrops at Lulworth area between Durdle Door and Mupe Bay with those of the west side of the Isle of Portland and that it was surrounded by carbonate mudstone to wackestone in deeper areas (Fig. 7.6). He showed that the shelly lime muds to the west of the oolitic shoal were deposited in a lagoon with the land located further to west; and to the east in deeper areas in a basinward direction (Fig. 7.6). However and although syn-rift tectonic settings are very well documented from the Permian to the mid-Cretaceous (refer to Chapter 2), Townson (1971) did not take into account possible tectonic controls on the facies distribution and on the position of the swell. Nevertheless, this NE-SW oolitic shoal might have created a high with respect to areas accumulating lime mud and this high might have been inherited through to the NE-SW trend in the Skull, Hard and Soft Cap beds.



**Figure 7.6** Palaeoenvironmental reconstruction of the uppermost part of the Freestone Beds of the Portland Group (redrawn after Townson, 1971). The oolitic shoal in the centre part with a NE-SW trend is surrounded by shelly lime mud (the Top Grey Micrite).

Another implication of the interpretation of this high on the palaeotopography is in the possible isolation of two sub-basins with different hydrologies. In Chapter 4 gypsum pseudomorphs are found in the Intraclastic peloidal packstone-grainstone facies in the Hard Cap sections eastwards from West Lulworth Cove and in the nucleus of ooids in the Soft Cap at

Mupe Bay and Worbarrow Tout; whereas evaporites are absent from sections to the west. The position of such high in the Hard Cap and the emergent land in the Soft Cap west of Lulworth (Figs. 7.4A-B and 7.5A-B) may have acted as a barrier to fluid flow and mixing. Following this scenario, the principal water input into the lake was most likely via the relay ramp area (Figs. 7.4 and 7.5). Such a situation would involve a more brackish condition to the west and more saline or hypersaline condition to the east consistent with the field data on the occurrence of evaporites. Similar depositional settings are observed in the Great Salt Lake (Utah, USA) where an extensional fault crosscuts the lake from Hat Island to Promontory Point and separates a north basin from a south basin (refer to Chapter 6; Baskin, 2014). Most of the freshwater input (95%) is into the south basin via four river systems, creating local variation of water conditions in the south and in the north due to variability in freshwater input, physical barrier, evaporation, currents and wind (Hahl and Langford, 1964; Baskin, 2014).

This facies trend or “swell” was previously described by other authors such as West (1975) and Francis (1982) and was considered to be present through Purbeck time (refer to Chapter 2). These studies focused on the palaeoenvironmental reconstructions of the Mupe Member deposits through comparisons with modern day environments such as the Persian Gulf or Shark Bay (Australia; refer to Chapter 2) and did not take into account the tectonic setting of the study area. Although both authors interpreted hypersaline waters throughout the area, they considered that this “swell” in the central part of the area might define western and eastern sub-basins that could explain the slight difference of salinity from west to east (refer to Chapter 2). If the extensional faults and the relay ramp area were taken into consideration (see above) then this provided a possible explanation for the NE-SW facies belts of West (1975). Underhill (2002) did take into account the tectonic settings and in addition to the preferential sediment accumulation in hanging-wall blocks, he demonstrated that sediment supply could have occurred through the relay ramp (refer to Chapter 2).

## **3.2. Scenario 2**

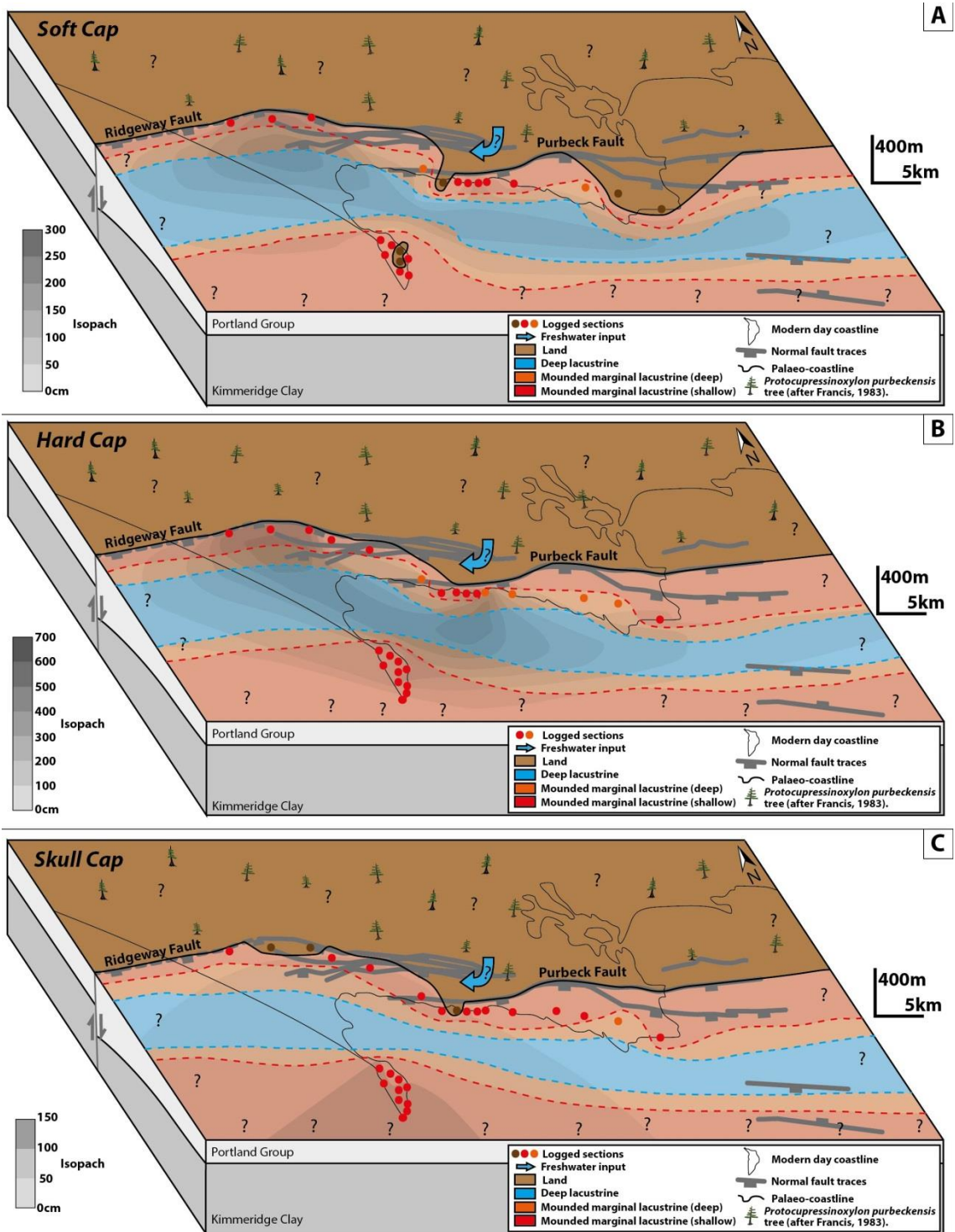
### **3.2.1. Models**

This second scenario is driven by the possible influence of normal fault features and geometries as imaged on the sub-surface data (refer to Chapter 3) that are also very common in half-grabens in rift systems (Fossen, 2010).

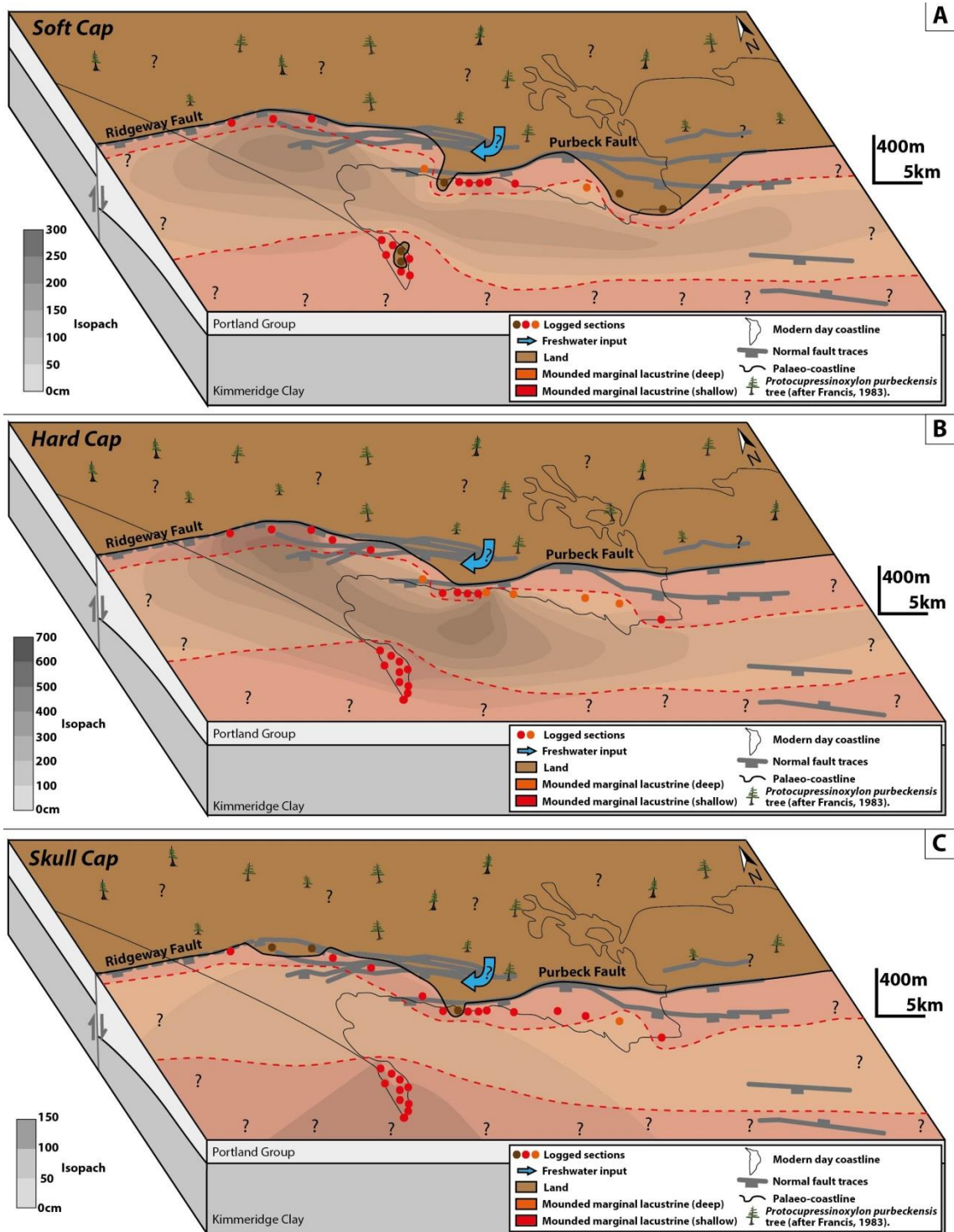
In this scenario the same data points are contoured into two shallower areas (*i.e.* the margins in red in figures 7.7 and 7.8). These shallow areas are interpreted to show an E-W

trend, located along the faults to the north and in a potential shallow area to the south that correspond to the dip slope of the hanging-wall block. Consequently deeper areas (in blue and/or orange in figures 7.7 and 7.8) are located in the central part of the study area with the same E-W trend as the margins. Therefore with this scenario the lake appears to be rather elongated E-W and parallel to the shoreline and the relay ramp has insignificant topography (Figs. 7.7 and 7.8).

With this scenario the facies trends appear to be similar in the three Cap beds apart from the same exposed areas described in the previous models and the interpreted isopachytes (see above). The isopachs can also be contoured to match the E-W facies trends. At the time of the Skull Cap deposition only one depocentre is interpreted to be located to the south area around Portland (Figs. 7.7C and 7.8C). At the time of the Hard Cap deposition the isopachs are interpreted to have E-W facies trends, however, two main depocentres appear to be located at the same position as per previous scenarios (Figs. 7.7B and 7.8B): one on the hanging-wall block of the Ridgeway Fault and one in the central part of the area near the Purbeck Fault with a NE-SW trend (Figs. 7.7B and 7.8B). At the time of the Soft Cap deposition only one main depocentre can be contoured which is centered on the hanging-wall block and in the centre area of the Ridgeway Fault (Figs. 7.7A and 7.8A).



**Figure 7.7** Tectono-sedimentary models of the Mupe Member following scenario 2 with the Deep lacustrine facies association. A – At the time of the Soft Cap bed deposition. B – At the time of the Hard Cap bed deposition. C – At the time of the Skull Cap bed deposition. Note that the western part of the Ridgeway Fault trace in dashed line was not imaged with seismic data and is after Harvey and Stewart (1998). Note that the red areas correspond to the shallow microbial mounds (tabular and small, refer to Chapter 5) and the orange areas correspond to the deeper expression of the microbial mounds (the big and complex shaped mounds and stromatolites, refer to Chapter 5).



**Figure 7.8** Tectono-sedimentary models of the Mupe Member following scenario 2 without the Deep lacustrine facies association. A – At the time of the Soft Cap bed deposition. B – At the time of the Hard Cap bed deposition. C – At the time of the Skull Cap bed deposition. Note that the western part of the Ridgeway Fault trace in dashed line was not imaged with seismic data and is after Harvey and Stewart (1998). Note that the red areas correspond to the shallow microbial mounds (tabular and small, refer to Chapter 5) and the orange areas correspond to the deeper expression of the microbial mounds (the big and complex shaped mounds and stromatolites, refer to Chapter 5).

### 3.2.2. Validity of the scenario 2 models

The facies trends interpreted in this second scenario for the Skull, Hard and Soft Cap beds show two E-W trends to the north along the faults and to the south crossing the Isle of Portland (Figs. 7.7 and 7.8). The depocentres were re-contoured with this scenario for the facies distribution but remain more or less similar and at similar position to those shown for the previous models with the exception of the Skull Cap (Figs. 7.7 and 7.8). In this second scenario the Skull Cap depocentre appears to be to the south of the area rather than with a NE-SW direction in the central part (Figs. 7.7C and 7.8C).

The application of the general models for deposition in rift systems presented above help to support the second scenario models. First of all in this study the horst model is not thought to have occurred as the Ridgeway and the Purbeck Faults are both south-dipping and no faults were imaged south of the Isle of Portland (refer to Chapter 3). According to this scenario the half-graben system is the most appropriate tectonic model as it is not possible to know if there is a fault south of the Isle of Portland as for the previous scenario. This half-graben system was previously proposed by Underhill and Paterson (1998).

During the deposition of the Skull Cap bed, the one depocentre is further to the south compared to the previous models (Figs. 7.7C and 7.8C). This can be interpreted due to a tectonic control following the half-graben system model or with no fault-related control. In the case of a half-graben system control the activity of the normal fault south of the Isle of Portland identified by previous authors is critical as the roll-over anticline with the greatest accommodation space may have been located on the hanging-wall block of this fault. In the case of no fault-related controls, the facies trends and the depocentre location show that the deposition occurred on a margin of a gently southerly sloping basin floor (with local and lateral variation of facies) with the depocentre located in a southern basinward direction.

During the deposition of the Hard and Soft Cap beds, the E-W facies trends and the depocentres are relatively similar showing a preferential accumulation overall in the central part (Figs. 7.7A-B and 7.8A-B). Two slightly more important sites for the accumulation appear to be located in the hanging-wall block of the Ridgeway Fault to the west and in the central part of the studied area between the Isle of Portland and Lulworth area (Figs. 7.7A-B and 7.8A-B). With this scenario, if a fault to the south of the Isle of Portland exists and was active then a graben can be thought to control the facies trends. If the fault does not exist then a half-graben system is more likely. In the case of a graben system, the shallow margins were located to the north and to the south on the fault scarps separated by a deeper area in between (as



per facies trends in figures 7.7A-B and 7.8A-B). Following this model, the graben will control the shape and size of the lake. However in such a model, the deposition is more likely to occur on top of the footwall of the faults (as per general models in figure 7.1B).

These scenario models appear to be closer to the Platt and Wright (1991) general model for lacustrine carbonate deposition in graben system (Fig. 7.2) where the size and shape of the lake is controlled by the size of the roll-over anticline. However in the Hard Cap the depocentre with a NE-SW trend in the central part of the area indicates that the relay ramp was most likely developing at the same time. The relay ramp would be the main route for water input as suggested by the shallow and thick deposits (as per previous scenario).

## 4. Summary and conclusion

The two scenarios presented in this chapter show slightly different interpretations of the same data on facies distribution and thickness variations. However the first scenario with a NE-SW facies trend in the central part of the area is thought to better illustrate the depositional and tectonic settings at the time of the deposition of the Skull, Hard and Soft Cap beds. The integration of field data, facies distribution and depositional settings (as defined in previous Chapters) appears to be better constrained with the first scenario. The lateral correlation of facies trends and the location of the depocentres suggest tectonic controls on the hydrology, water flow and deposition. In addition this scenario is constrained with the possible palaeotopography inherited from the palaeogeographies of the uppermost part of the Freestone Beds of the Portland Group. This scenario is also comparable to previous palaeogeographies for the Mupe Member (West, 1975 and Francis, 1982) even if these differ in depositional settings with the models proposed in this study.

According to these models the Hard and Soft Cap facies distributions are similar and different from that of the Skull Cap. The southern location of the interpreted depocentre in the Skull Cap suggests that there were no tectonic controls on the facies distribution at the time of the deposition of this bed. This suggests a rather gently south-dipping margin with very minor variations in thickness. With respect to the Hard and Soft Cap beds, the facies distribution and location of the depocentres indicate clear tectonic controls. However as no deep facies were recorded in the field, the occurrence of the Deep lacustrine facies association can only be inferred from the facies models and its occurrence in the lowest part of the Mupe Member (refer to Chapter 6).

Tectonics are also thought to control the deposition at a larger scale where the relay ramp influenced the sediment routes and preferential accumulation at the more local scale that overall occurred on top of a roll-over anticline within the half-graben system. The thicknesses of the Hard Cap in the hanging-wall depocentres near the Ridgeway and Purbeck Faults possibly supplies information of fault activity. The Ridgeway Fault was most likely the main fault active during the deposition of the Hard Cap while a shorter section (about 5.5 km long and centered in Lulworth area) of the Purbeck Fault was active at that time.

Concerning the controls on the deposition of the whole Mupe Member (in particular for the Cypris Freestone beds and including the Broken Beds) an important variation of facies is observed from west to east. To the west the facies and biotas reflect a more brackish water lake while they reflect a more hypersaline water lake to the east (refer to Chapter 6). This suggests that either the NE-SW facies trend persisted through from the Cypris Freestone beds; or that it controlled the creation of a lake floor high separating two sub-lakes with different hydrology as per Hard and Soft Cap beds deposition. As proposed above for the Skull, Hard and Soft Cap beds the relay ramp might have provided a freshwater input into the system, that was running and eroded exposed carbonate rocks of underlying beds. This water input coming from the land would have promoted carbonate sediment production in the shallow waters of the relay ramp that would then have built up the interpreted NE-SW high (refer to Chapter 6).

# Chapter 8

## Synthesis and conclusions

## 1. Introduction

This thesis describes and discusses, from basin- to local-scale, the origin of the lacustrine carbonates of the Mupe Member of the Purbeck Limestone Group that are extensively exposed along the south Dorset coast. As a conclusion this chapter aims to answer the research questions posed in the introduction (Chapter 1) and to summarise the main findings that have been presented in each chapter. This highlights the new findings of this study and the importance of studying lacustrine carbonate analogues, such as the Mupe Member deposits, to reduce uncertainty in petroleum exploration and development.

## 2. Syn-rift setting of the Wessex Basin

Published tectonic models for non-marine carbonates in extensional basins setting, unlike their marine counterparts, are few and limited in their predictive value. General models for sediment accumulation within an extensional terrain propose that stratigraphic thicknesses are expected to be greater in hanging-wall depocentres, strata thicken through the basin towards the faults and also towards the central part of the fault traces (Withjack *et al.*, 2002; Dorobek, 2008; Fossen, 2010). Although these models, in the main, are based either on fieldwork or on borehole data correlations, they are very generalised and do not contain enough details particularly concerning facies distribution in such extensional basins. The widely cited Platt and Wright (1991) model for half-graben system, as presented in figure 7.2 in Chapter 7, documents the expected location of lake formation to be in the hanging-wall blocks and near the fault with the footwall block exposed, and with thickness of lacustrine deposits increasing towards the fault. In addition these authors documented at the regional-scale, the facies distribution in these hanging-wall lakes, with laminites deposited in basinal areas and bioherms deposited in marginal areas. Although this model shows lake locations, it remains too generalised to decipher possible controls on facies distribution at the local-scale and in particular which facies are expected to be deposited and their relationships. Similarly Bohacs *et al.* (2000) models for underfilled and balanced-fill lake types, as presented in figure 6.14 in Chapter 6, illustrate a comparable scenario with lakes forming preferably in the hanging-wall blocks of extensional faults while the footwall area is exposed. They also documented that thickness of lacustrine deposits increases towards the faults and commonly show greater dips than on lakes without tectonic controls. In addition they illustrated the facies distribution at the same regional-scale as Platt and Wright (1991) with carbonates on the marginal areas and

mudstones in the basinal areas. However, as for previous models presented, very few details were brought on the different types of carbonates possibly deposited on the margins (only stromatolites expected in the shallowest parts and ooids in slightly deeper areas) and it appears that, according to these models, carbonates are not deposited in deeper areas.

The seismic interpretation, undertaken in this study in Chapter 3, integrates 2-D and 3-D seismic profiles, from onshore and offshore, calibrated with borehole data and nearby coastal outcrop geology. Correlations of borehole data integrated to the seismic interpretation have enabled the production of a time thickness map for the Purbeck Limestone Group. This shows that the Ridgeway and Purbeck Faults were active during the deposition of the Purbeck Limestone Group as the thicknesses of the three units (anhydrite, limestone and claystone), very well documented onshore, are greater in hanging-wall depocentres and towards the faults. Within these hanging-wall depocentres, the facies distribution appears to be controlled by the lateral propagation of the syn-sedimentary extensional faults and the development of a relay ramp.

Although the syn-rift setting of the Wessex Basin is very well documented from the Permian through to the mid-Cretaceous, nothing has previously been published for the time of the deposition of the Purbeck Limestone Group. The seismic interpretation undertaken in this study shows that during the deposition of the non-marine carbonates of the Mupe Member the Wessex Basin was in an active extensional setting. Consequently this study brings a new analogue for lacustrine deposition in extensional setting and emphasises the importance of the integration of seismic interpretation with borehole data correlations and field geology to better constrain and characterise tectonic setting of depositional successions.

### **3. Non-marine carbonates of the Mupe Member**

The intensive fieldwork undertaken during this project resulted in the production of 22 sedimentary logs: 3 located to the west near the Ridgeway Fault; 9 located to the east near the Purbeck Fault; and 10 located to the south over the Isle of Portland and far from the faults. The systematic sampling and thin section analysis of most beds enabled the definition of 9 facies grouped into 5 facies associations: the Deep lacustrine facies association composed of the Wackestone to fine grainstone facies; the Emergent facies association composed of the Conglomerate and Carbonaceous marl facies; the Mounded marginal lacustrine facies association composed of the Microbialite facies (sub-divided into the Thrombolite, Stromatolite and Burrowed peloidal packstone sub-facies) and the Intraclastic peloidal

packstone-grainstone facies; and the Hypersaline lacustrine facies association composed of the Cross-bedded peloidal packstone-grainstone, the Gypsiferous peloidal packstone, the Calcareous sandstone and the Evaporite facies (sub-divided into Vuggy and Breccia sub-facies). The integration of this facies classification with facies transition analysis, field observations and comparison with modern analogues results in the interpretation of 2 depositional environments and 2 facies models for the Mupe Member: an earlier brackish water lake and a later hypersaline water lake. In addition this illustrates a separation between a western area where more brackish waters existed and an eastern area that was more hypersaline, possibly due to a high in the palaeotopography aligned with the relay ramp area.

This study indicates that the palaeoenvironments were initially brackish water lacustrine as opposed to the hypersaline lagoons as interpreted by West (1975, 1979) and by Francis (1982). In addition the 2 new facies models depicting the two depositional environments proposed in this study help to understand that the hypersaline conditions interpreted by West (1975) only appeared in the second half of the Mupe Member (from the Soft Cap upwards) and were mainly located to the east of the studied area (Lulworth eastwards).

In a broader context, this study provides more detail to the generalised facies models for lacustrine carbonates defined by Platt and Wright (1991) and Bohacs *et al.* (2000) giving new perspectives on the importance of tectonic setting, on facies distribution at small-scale on shallow lacustrine margins, and in particular on microbial mound distribution.

#### 4. Microbial mounds

A main focus of this project was on the morphologies, sizes and distribution of microbial mounds deposited in the Skull, Hard and Soft Cap beds in association with the inter-mound facies (the Intraclastic peloidal packstone-grainstone facies). The detailed study and interpretation of the lidar surveys over the Isle of Portland, with integration of fieldwork, resulted in the definition of two main mound types; tabular to domal. These latter mounds are also taller and more complex and can be developed around tree remains such as *in-situ* stumps, fallen trees and/or branches. In the Skull Cap bed, mounds are rather small, up to 50 cm high and 1 m wide in 2-D with a tabular shape and are not associated with tree remains. In the Hard Cap bed, mounds exhibit a wide range of complex morphologies and sizes with tabular to domal mounds up to 50 cm high and 1 m wide; and tall mounds between 20 cm and 3 m high with sub-circular plan views up to about 6.50 m in diameter with complex shapes in 2 and 3-D. These mounds are very often associated with *in-situ* and transported tree trunks and

branches. In the Soft Cap bed the mounds are similar to those of the Skull Cap bed with the difference that they tend to be more domal shape and to develop around *in-situ* tree stumps and fallen trees that gives them an overall doughnut shape in 3-D.

The study of the relationships between microbial mounds and inter-mound facies shows that when the mounds are tall with a complex shape, they developed interdigitations with the inter-mound facies. In total 3 interdigitations are identified in these mounds that are thought to form positive relief on the lake floor topography. These interdigitations are identified at about 50 cm, 1 m and 1.50 m from the base of the Hard Cap bed, that most likely reflect palaeo-lake level fluctuations.

Geometrical characterisation of mound morphologies with shape and roundness parameters indicates that the mounds tend to be tabular to domal when small and evolving to more complex shapes with size; and that these differences are due to external physical controls such as sediment input, lake water level fluctuations and calcium carbonate saturation of the waters. Such morphological characterisation of microbial mounds using geometrical techniques (also called morphometrics) is surprisingly not commonly used in the literature as Hofmann's (1976 and 1994) microbialite morphometric studies are the only available in the literature. As a consequence this study shows the importance of the geometrical characterisation of microbial mound morphologies and sizes in 2-D and 3-D (wherever possible). This can lead to interpretation of physical external controls on microbial growth and microbial mound shapes and sizes such as described above with water level fluctuations, sediment input, water chemistry and climate effect, and their inter-relationships.

## 5. Lacustrine sequences in the Mupe Member

The analysis of the sedimentary logs and upward facies transitions enables the identification of four meter-scale lacustrine cycles, that are deepening upward and then shallowing-upward after a flooding surface, during the deposition of the Mupe Member. These correspond to the Transition Bed, Skull Cap, Hard Cap, Soft Cap and Cypris Freestone beds. These cycles are bounded by sub-aerial exposure surfaces corresponding to the tops of the Portland Group, Transition Bed, Skull Cap and Hard Cap beds and can therefore be labelled as sequence. These sequences are composed from bottom to top of lowstand deposits made of paleosols with rooted trees; a transgressive surface; transgressive deposits made of microbial mounds and inter-mound facies; a flooding surface or zone exclusively made of the inter-mound facies; and highstand deposits made of microbial mound and/or inter-mound facies or

the Evaporite facies and/or the Cross-bedded peloidal packstone-grainstone facies. Most importantly for this study is that microbial mounds appear to develop preferentially as transgressive deposits as lake margins expanded.

In addition the sequence stratigraphic analysis proposed here helps to understand external controls on microbial growth and shows that the termination of growth was most likely due to a change in the calcium carbonate saturation of the lake waters when microbial mounds grow in a transgressive deposit system; and due to lake level fall consequently associated with exposure and erosion of microbial mounds that grew within lake highstands.

This study is the first to identify depositional sequences and a sequence stratigraphic model for the Mupe Member of the Purbeck Limestone Group and shows that in lacustrine settings, carbonate deposition is highly variable with changes that can happen very rapidly through time and space. This is illustrated with the Deep lacustrine facies association of the Transition Bed that is bounded by two sub-aerial surfaces and paleosols; and with the termination of microbial growth due to rise of lake level and modification of water chemistry.

In addition the transgressive microbial deposits in a deepening-upward trend is in accordance with published generalised models for lacustrine carbonates (Bohacs *et al.*, 2000, 2003; Hanneman and Wideman, 2010; Tänavsuu-Milkeviciene *et al.*, 2012; Sarg *et al.*, 2013). Particularly this study shows that lake type evolved from an earlier balanced-fill to a later underfilled model of Bohacs *et al.* (2000) where carbonate deposition is more likely to occur in these lake types. Bohacs *et al.* (2000) also specified that lacustrine carbonates are usually formed through vertical aggradation with flooding surfaces marked by distinct lithologic changes. Overall the sequence stratigraphic analysis proposed here helps to better understand the controls on the accumulation of lacustrine carbonates such as lake level fluctuations, subsidence, water chemistry, climate or sediment input (Platt and Wright, 1991; Gierlowski-Kordesch, 2010; detailed below).



## 6. Controls on facies distribution

Controls on lacustrine carbonates distribution are numerous and strongly inter-related, and can affect carbonate deposition at several scales. Platt and Wright (1991) and Gierlowski-Kordesch (2010) summarised these controls and defined three main factors that control lacustrine carbonate deposition, hydrology, sediment input and temperature changes that are themselves impacted by tectonics and climate. Below these aspects are discussed at two scales.

### 6.1. Basin-scale

In this study, the Mounded marginal lacustrine facies were deposited in the shallowest parts of the lake in a half-graben basin in the hanging-wall depocentres and on the hanging-wall dip slope over the Isle of Portland. The Deep lacustrine facies were deposited in the deepest parts of the lake possibly in the central area of the half-graben basins. The Hypersaline lacustrine facies were predominantly deposited eastwards of Lulworth area, away from the lake margins and towards the basin centre. The Bedded marginal lacustrine facies were deposited across the study area. Because the focus of this study was on the microbial mounds and associated facies, 3 tectono-sedimentary models for the Skull, Hard and Soft Cap beds are proposed according to 2 possible scenarios. However scenario 1 with the development of a NE-SW facies trend aligned with the relay ramp is preferred because it better integrates all the data acquired (seismic interpretation, fieldwork, facies distribution and inherited structures from the underlying Portland Group).

At the basin scale the deposition at Hard and Soft Cap times appear to be tectonically controlled: 1) by the lateral propagation of the extensional faults as illustrated with the locations of the depocentres in the hanging-wall blocks very close to the Ridgeway and Purbeck Fault traces; and 2) by the development of the relay ramp as illustrated with the NE-SW facies trend aligned with the relay ramp area. In this system and at this scale, microbial mounds are found in the shallowest parts of the lake where their growth was most likely controlled by lake level fluctuations and calcium carbonate saturation of the waters. These were controlled either by tectonics that resulted in an increase of subsidence and accommodation space; or by the climate with which an increasing precipitation rate resulting in a rise of lake level and increase of accommodation space (see also below); or a combination of both. Contrarily, during the deposition of the Skull Cap bed no main depocentres or facies

trends were recorded. This indicates that the deposition was most likely occurring in gently south-dipping margins and it appears that at that time tectonics was not controlling lake level fluctuations but rather that the climate was an important influence on the water chemistry and sediment input.

This study is in accordance with the published models for extensional non-marine basins that show that tectonics control the distribution, nature and thickness of deposits in hanging-wall depocentres (Platt and Wright, 1991). Following these models, lakes are expected to form in the hanging-wall depocentres and with thicknesses of deposits expected to be greater close to and in the central part the fault traces (Platt and Wright, 1991). This is documented to be the case in the Purbecks but, in addition shows the important 3-D effect of a fault relay ramp and how specific facies occur in different parts of this basin. Platt and Wright's (1991) models are mainly illustrating deposition in 2-D which limit their predictive value. This study shows the importance of integrating different techniques in 3-D in order to characterise basin-scale controls on lacustrine carbonate deposition and to increase the predictive value of such models.

## **6.2. Small-scale**

At a smaller-scale the detailed study of the microbial mounds shows that they grew on the shallowest areas either around tree remains or when not associated with trees, they tend to prefer highs in palaeotopography inherited from the underlying irregular sub-aerial exposure surfaces and paleosols. In addition the integration of the sequence stratigraphic analysis, characterisation of mound morphologies and sizes and comparison with modern analogues help to define the main controls on the microbial mound growth. The tabular shapes of the mounds indicate that the microbial communities could not continue with upward growth due to water level limitations and consequently developed laterally. Domal mounds can locally be found together with tabular mounds and this suggests that most likely mounds start to form as domal shapes and, if unconstrained continue to grow with this morphology, but they may modify their shape to tabular if constrained by lake level. The three interdigitations of the tall and complex shaped mounds with inter-mound sediments indicate control of morphology by palaeo-lake levels. In addition the expansion and contraction of the wings of these complex shaped mounds suggest that the microbial growth was mainly controlled by sediment input rather than water level fluctuations. However the occurrence of

trees and the water chemistry can have additional important roles in the microbial growth and resulted morphologies.

Concerning the occurrence of trees, in the Hard Cap bed, mounds are clearly associated with tree trunks and branches, *in-situ* or transported, that, together with deeper lake waters enabled the microbial community to grow higher than in the Skull and Soft Cap beds; and that resulted in the tall and complex shapes that are stratigraphically thicker units. In the Soft Cap bed, mounds are associated with *in-situ* tree stumps and large fallen trees but did not grow as in the Hard Cap bed and remained short, domal and tabular probably due to shallower lake waters than in the Hard Cap bed. Alternatively, in the Skull Cap bed, mounds were never identified associated with tree remains and with short and tabular shapes. This indicates that the morphology of these mounds was controlled by water level and in shallow water lake margins, rather than due to occurrence of tree remains. In addition, in this bed, mounds were preferentially growing from highs before growing over lows inherited from the erosional surface of the Portland Group (as imaged with the integration of 3-D forward modelling). These show that the occurrence of trees together with lake level fluctuations and sediment input lead to different morphologies.

Concerning the water chemistry and in transgressive depositional systems, the inter-mound sediments are either covering pre-existing mounds and/or onlapping onto domal mounds. This suggests that the mounds stopped growing before being covered with sediments. This termination of growth can be due to a decrease of the saturation in regards to calcium carbonate of the waters that reduced the calcification of microbial filaments; or to an increase of sediment input into the lake; or a combination of both processes.

This study provides a valuable new case study of fossil microbial mounds that developed on the shallow margins of a brackish water lake and the importance of integrating a morphological characterisation of the mounds. This integration resulted in a characterisation of the external controls on the microbial growth and mound distribution such as the importance of palaeo-lake level fluctuations, water chemistry (in particular the calcium carbonate saturation), sediment input into the lake and topography of the lake floor (including occurrence of tree remains); and provided relevant information for palaeoenvironmental reconstructions. In addition the preliminary integration of 3-D forward modelling illustrates the importance of numerical modelling to further characterise these controls (Kozłowski, *in prep.*). This study also emphasises the high variability of non-marine carbonate deposition as illustrated with the rapid modifications in the facies distribution in a syn-rift setting through time and space.

## 7. Potential petroleum system

Preliminary characterisation of the pore system using classic petrographic analyses coupled with fieldwork and lidar surveys at outcrop scale helped to propose potential reservoir and seal units.

The main units that are potential reservoirs are the microbial mounds and inter-mound facies of the Skull Cap, Hard Cap, Soft Cap beds and the coarse-grained facies of the Cypris Freestone. The potential seal units or units that might be barriers to flow would be the fine-grained facies of the Transition Bed, the paleosols of the Basal Dirt Bed, Lower Dirt Bed and Great Dirt Bed and the evaporites of the Broken Beds.

The microbial mounds of the Cap beds show a very high macro-porosity inherited from the thrombolitic texture together with the tree moulds that create mm- to dm-scale cavities. This high porosity is also confirmed at micro-scale with high framework, intergranular and micro-porosity types characterising the Microbialite facies. As a consequence the microbial mounds are thought to be the best reservoir units in this potential petroleum system. However these highly porous mounds are surrounded by the inter-mound facies that does not appear to be porous at outcrop scale despite the coarse-grained texture. This low porosity is confirmed at micro-scale where the Intraclastic peloidal packstone-grainstone facies shows a rather low porosity with two main types intergranular and mouldic porosity types and both primary and secondary pores largely filled with mosaic to blocky calcite cements in samples obtained from outcrops.

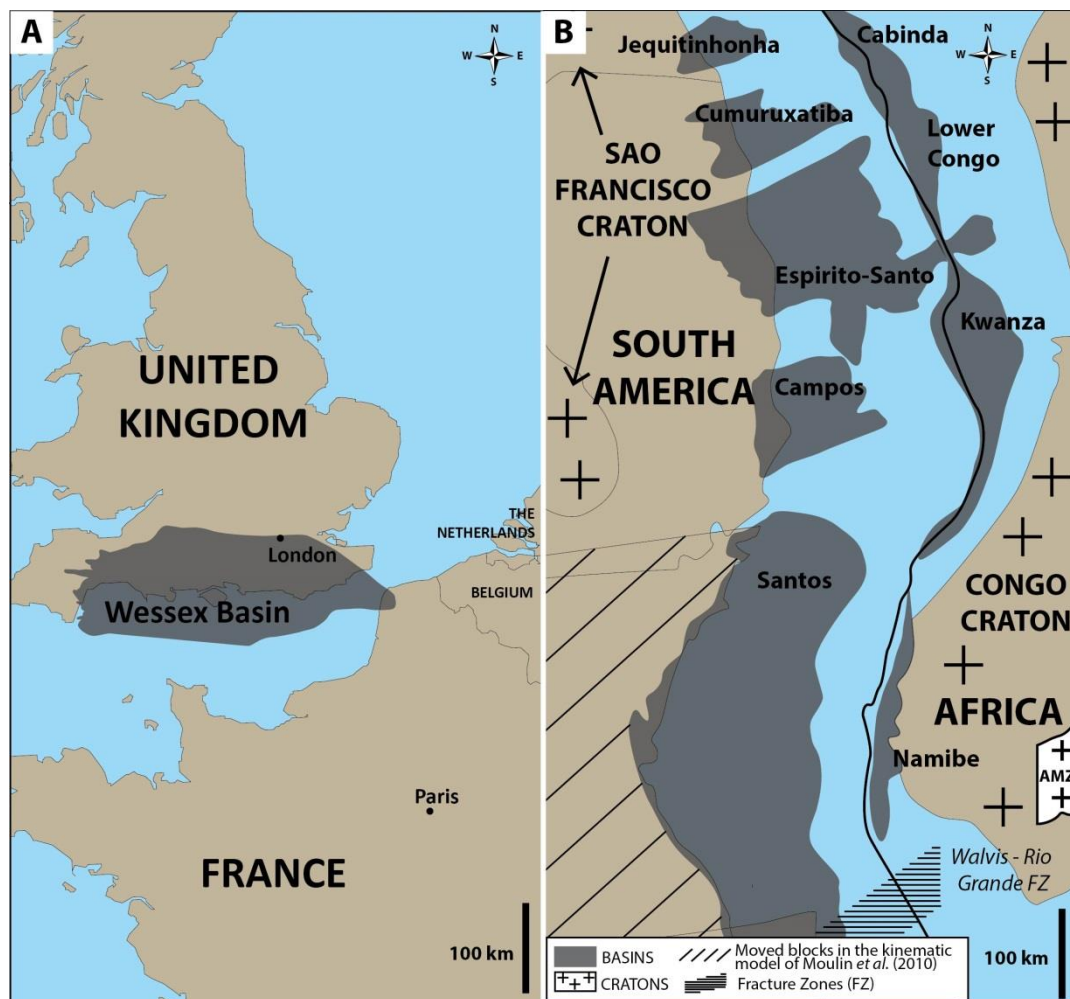
The Cap beds where microbial mounds are found are bounded by sub-aerial surfaces and deposition of low to impermeable paleosols. Moreover at outcrop and in 2-D view, the highly porous microbial mounds appear to be isolated within the less porous inter-mound facies. This illustrates the high lateral heterogeneity of such potential reservoir units and in such situation this petroleum system will be very risky to produce as the uncertainty will be very high. This uncertainty will be due to the non-predictive value of fieldwork-based study and numerous vertical wells would be needed to reach as many mounds as possible. However this study documents that these highly porous microbial mounds appear to be found in three extensive units at least in an area about 50 km long (from the Isle of Portland to Swanage) and 15-20 km wide (from Portesham to the Isle of Portland). This illustrates that although the reservoir units show a high lateral heterogeneity, this potential petroleum system appears to be layered and extensive. In such situation, horizontal wells along each of these reservoir units might be the

best solution to reduce the uncertainty and consequent risk in the production of this potential petroleum system.

To reduce this uncertainty and improve the predictive value of this study, a multi-scale approach and the integration of stratigraphic 3-D numerical forward modelling is needed. This study was realised as part of a wider project that involves another PhD (Kozłowski, *in prep.*). In this inter-related study the third dimension was considered in order to test multiple scenarios of fault activity and carbonate production. This will help to predict the facies distribution at the regional scale and the mound distribution and the controls on microbial growth at a more local scale. This project shows the importance of inter-related multi-scale approach type of study to 1) enhance the predictive value of purely field-based studies or purely numerical modelling studies; and 2) reduce the uncertainty and the effective cost in the production of similar petroleum systems such as the South Atlantic reservoirs as described in the introduction of this thesis.

## 8. Analogue of South Atlantic reservoirs

The Purbeck Limestone Group is considered as a possible analogue for the South Atlantic basins as they share a number of similarities. The lacustrine deposits in the southeast Atlantic basins evolve from freshwater, brackish to alkaline lake waters with development of microbial build-ups on fault blocks in a syn-rift setting (Chaboureau *et al.*, 2013; Saller, 2015; Saller *et al.*, 2016). Similarly in the Wessex Basin (southern England), the Purbeck limestones are interpreted to be deposited in brackish, saline and freshwater lakes. In this thesis it is shown that microbial mounds occurred in brackish water conditions overlain by sulphate evaporites (gypsum and anhydrite). The Atlantic margins are organised in several extensional basins (Campos offshore Brazil, and Namibe and Kwanza offshore Africa for example, Fig. 8.1) that are elongated and about 200-300 km long (Fig. 8.1). Similarly the Wessex Basin is about 400 km long, made of three extensional sub-basins (Fig. 8.1); the Portland-Wight, Pewsey and Weald and each of these is about 200 km long and rather elongate (refer to Chapter 2).



**Figure 8.1** Size comparison between the Wessex Basin (A) and South Atlantic basins (B, redrawn after Chaboureau *et al.*, 2013).

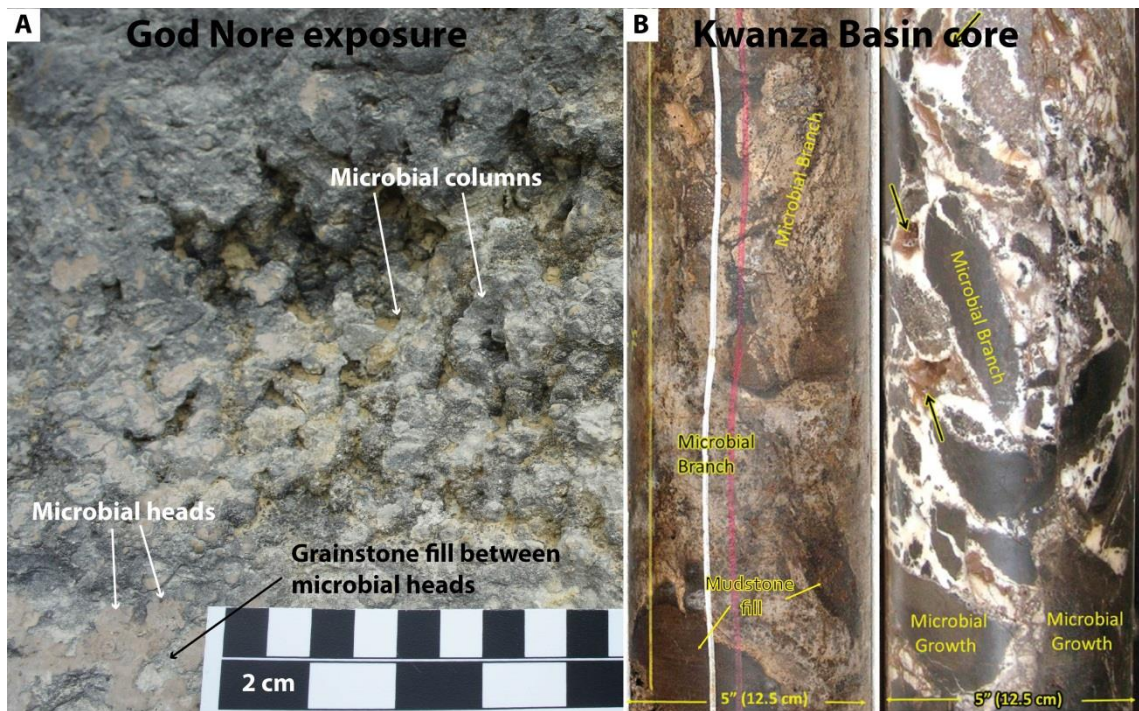
The syn-rift phase of the Brazilian and West African margin basins is dated as Early Cretaceous (Mid-Hauterivian to Early Aptian, Fig. 8.2, Beglinger *et al.*, 2012) and as Late Jurassic-Early Cretaceous for the Wessex Basin (Fig. 8.2). Syn-rift deposits in both cases occurred in basins created on the hanging-wall blocks of extensional faults along the margins of these basins (Norvick and Schaller, 1998; Calassou and Moretti, 2003; Dickson *et al.*, 2003; Beglinger *et al.*, 2012). Although deposition occurred in both cases in lacustrine environments, in the southeast Atlantic basins the water lake hydrology evolved from fresh to brackish to saline (Fig. 8.2); while in the Wessex Basin the water lake evolved from brackish to saline to freshwater (Fig. 8.2).

		Brazilian basins		Wessex Basin		West African basins	
Eras, Sub-eras, periods		Main lithologies	Basin evolution	Main lithologies	Basin evolution	Main lithologies	Basin evolution
Cenozoic	Neogene	NOT PRESENT					
		Marine clastic sedimentation Shallow to deep	Post-rift	Marine (clastics and carbonates)	Alpine inversion	Marine clastic sedimentation Shallow to deep	Post-rift (drift-marginal sag)
	GAP						
	Mesozoic	Late Cretaceous	Shallow-marine (ramp carbonates)	Syn-rift	Deep-marine (carbonates)	Post-rift	Shallow-marine (ramp carbonates)
Continental (clastics)							
Early Cretaceous		Lacustrine	Saline Brackish Fresh	Lacustrine	Fresh Saline Brackish	Fluv. Ma. Restr. Mar. Lacustrine Brackish Fresh	
Basalt		Pre-rift	Lacustrine	Syn-rift	Lacustrine Fluvial Alluvial	Pre-rift	
Jurassic				Shallow-marine (carbonates)			
				Deep-marine			

**Figure 8.2** Comparison of basin evolutions between Brazilian margin basins (modified after Moreira *et al.*, 2007), the Wessex Basin of southern England (modified after Underhill, 1998) and West African margin basins (modified after Beglinger *et al.*, 2012). Note that red areas highlight intervals of this study and their counterparts in the South Atlantic.

Concerning facies at the macroscale little has been published on the South Atlantic lacustrine deposits. However the microbial build-ups found in the Kwanza Basin are similar to the microbial mounds found in the Purbeck Limestone Group of the Wessex Basin (Fig. 8.3). The microbialites of the Kwanza Basin are made of clotted to laminated branches (Fig. 8.3), very similar to the microbial heads and columns found in the external part of the microbial mounds in the Wessex Basin (Fig. 8.3). The main differences between West African and southern England deposits lie in the associated facies and the mineralogies. In the Kwanza Basin microbialites are made of original silica (Cazier *et al.*, 2014) possibly precipitated from

silicifying coccoid cyanobacteria (*Pleurocapsa*) as found in the modern-day Lake Magadi (Kenya) (Saller *et al.*, 2016); while in the Wessex Basin they are preserved as their original calcite. Concerning facies associated with microbialites, mudstone carbonates fill the framework porosity in the Kwanza Basin deposits (Fig. 8.3B); in the Wessex Basin peloidal packstones to grainstones are deposited around the microbial mounds and in the framework porosity (Fig. 1.3A).

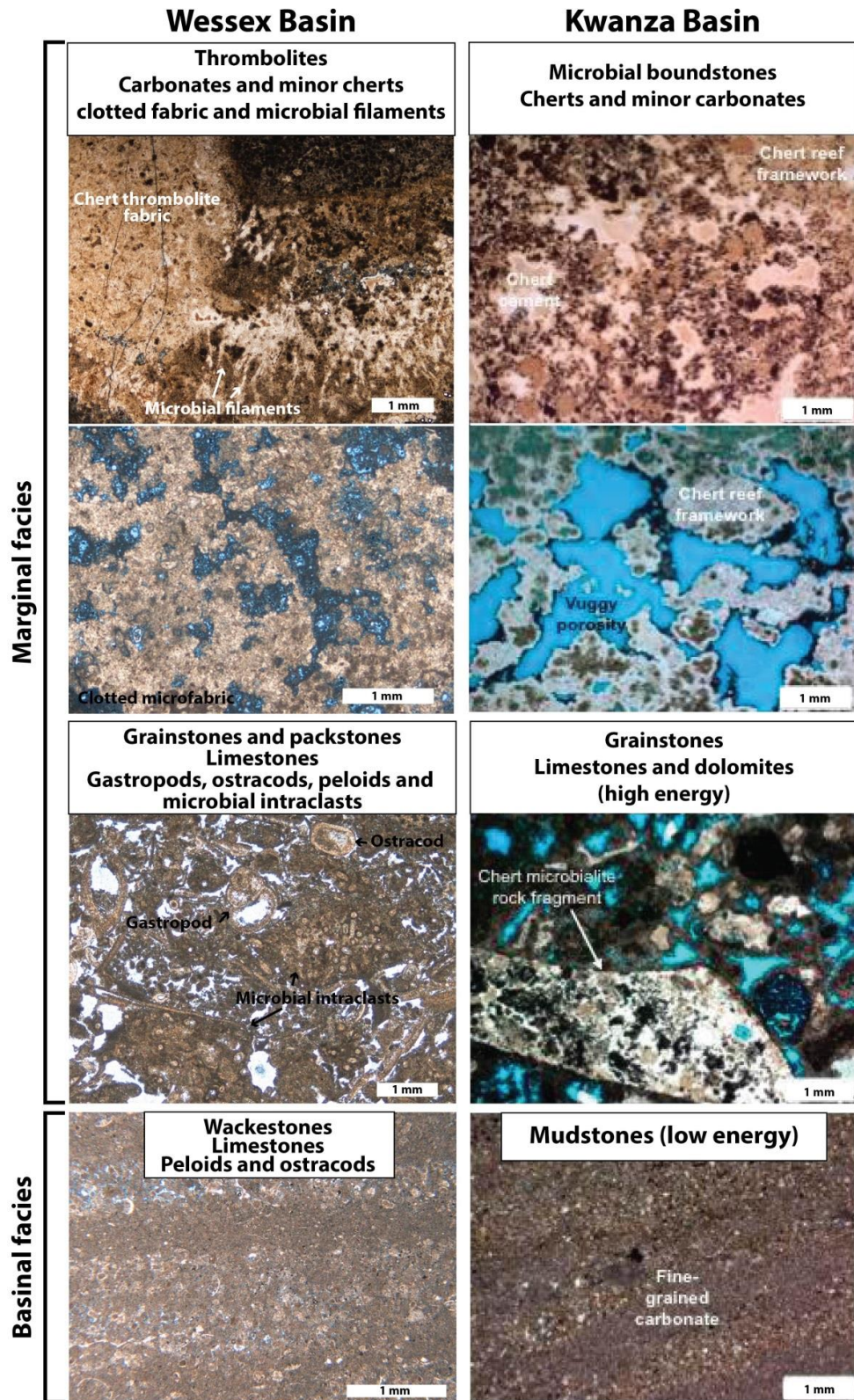


**Figure 8.3** Macrofacies comparison between a microbial mound from the Purbeck Limestone Group of the Wessex Basin (A, from the Isle of Portland) and the South Atlantic microbialites (B, Kwanza Basin well, from Saller *et al.*, 2016).

At a microscale many of the facies have similar textures but they differ in their mineralogies. In the Wessex Basin all the facies are preserved in their original calcite apart from chert nodules that are found replacing thrombolites (Fig. 8.4). In the Kwanza Basin the main mineralogy associated with the microbial mounds is original silica (together with shrubby calcite travertines, spherulites and stevensite) and stable isotope analysis (C and O) suggests the deposition occurred in fresh to moderately saline (alkaline) lake waters (Saller, 2015; Saller *et al.*, 2016). These Kwanza microbial mounds are surrounded by packstones, grainstones or mudstones, however, these are commonly highly altered to dolomite (Cazier *et al.*, 2014; Saller *et al.*, 2016). The coarse-grained facies (grainstones) of the Kwanza Basin are interpreted as high-energy deposits (Cazier *et al.*, 2014) as in the case with the Wessex Basin and thus reflect marginal lacustrine facies. Similarly, the fine-grained facies (mudstones) of the Kwanza Basin



are interpreted as low-energy deposits (Cazier *et al.*, 2014) as for the wackestones to fine grainstones found in the Wessex Basin and thus reflect basinal deposits.



**Figure 8.4** Microfacies comparison between the lacustrine Purbeck Limestone Group of the Wessex Basin on the left and the lacustrine facies of the Kwanza Basin on the right (modified after Cazier *et al.*, 2014).

In conclusion the basins located on the south Atlantic eastern margins appear to be more similar to the Purbeck limestones rather than the western margins. The differences between the south Atlantic and the Wessex Basins are the hydrology evolution of the lakes; the mineralogies (dolomite, calcite and silica in the south Atlantic and only calcite in the Wessex Basin); and the associated facies to the microbialites that are mudstones in the Kwanza basin and grainstones to packstone in the Wessex Basin. However both basins present similarities with the basin sizes about 300-400 km across; the basin evolution as the deposition occurred in lacustrine and syn-rift evolution of the basins; the occurrence of microbialites (thrombolites); and the facies distribution (coarse-grained in shallow areas and fine-grained in deeper areas).

# Reference list

- Ager, D.V. & Wallace, P. 1966. The environmental history of the Boulonnais, France. *Proceedings of the Geologists' Association*, **77**, 385-417.
- Ainsworth, R.B., Hasiotis, S.T., Amos, K.J., Krapf, C.B.E., Payenberg, T.H.D., Sandstrom, M.L., Vakarelov, B.K. & Lang, S.C. 2012. Tidal signatures in an intracratonic playa lake. *Geology*, **40**, 607-610.
- Aitken, J.D. 1967. Classification and environmental significance of cryptalgal limestones and dolomites, with illustrations from the Cambrian and Ordovician of southwestern Alberta. *Journal of Sedimentary Research*, **37**, 1163-1178.
- Allen, P., Alvin, K.L., Andrews, J.E., Batten, D.J., Charlton, W.A., Cleevely, R.J., Ensom, P.C., Evans, S.E., Francis, J.E. & Hailwood, E.A. 1998. Purbeck–Wealden (early Cretaceous) climates. *Proceedings of the Geologists' Association*, **109**, 197-236.
- Allen, P. & Wimbledon, W. 1991. Correlation of NW European Purbeck-Wealden (nonmarine Lower Cretaceous) as seen from the English type-areas. *Cretaceous Research*, **12**, 511-526.
- Alonso-Zarza, A.M. & Wright, V.P. 2010. Palustrine Carbonates. In: Alonso-Zarza, A.M. & Tanner, L.H. (eds.) *Developments in Sedimentology*. Elsevier, 103-131.
- Anders, M.H.S., R. W. 1994. Overlapping faults, intrabasin highs, and the growth of normal faults. *Journal of Geology*, **102**, 165-180.
- Anderson, E.J. 2004. Facies patterns that define orbitally forced third-, fourth-, and fifth-order sequences of sixth-order cycles and their relationship to ostracod faunicycles: the Purbeckian (Berriasian) of Dorset, England. In: D'Argenio, B., Fischer, A.G., Premoli Silva, I., Weissert, H. & Ferreri, V. (eds.) *Cyclostratigraphy – an Essay of Approaches and Case Histories*, SEPM Spec. Publ. **81**, 243-258.
- Anderson, F.W. 1967. Ostracods from the Weald clay of England. *Bulletin of the geological Survey of Great Britain*, **27**, 237-269.
- Anderson, F.W. 1973. The Jurassic-Cretaceous transition: the non-marine ostracod faunas. In: Casey, R. & Rawson, P.F. (eds.) *The Boreal Lower Cretaceous*, Geological Survey of Great Britain, 101-110.
- Anderson, F.W. 1985. Ostracod faunas in the Purbeck and Wealden of England. *Journal of Micropalaeontology*, **4**, 1-67.
- Anderson, F.W. & Bazley, R.A.B. 1971. The Purbeck Beds of the Weald (England). Institute of Geological Sciences, London, 174 pp.
- Andrews, P.R.A. & Collins, R.K. 1991. Celestine in Canada. *Can. Inst. Mining Metall. Bull.*, **84**, 36-39.
- Andrews, W.R. & Jukes-Browne, A.J. 1894. The Purbeck beds of the Vale of Wardour. *Quarterly Journal of the Geological Society*, **50**, 44-71.
- Anon. 1975. Colloque sur la limite Jurassique-Crétacé. *Mémoires de Bureau de Recherches Géologiques et Minières*, **86**, 379-393.
- Arkell, W.J. 1933. The Jurassic system in Great Britain. Oxford University press, Oxford, 681 pp.
- Arkell, W.J. 1936. The tectonics of the Purbeck and Ridgeway faults in Dorset. *Geological Magazine*, **LXXIII**, 97-118.
- Arkell, W.J. 1938. Three tectonic problems of the Lulworth district: studies on the middle limb of the Purbeck fold. *Quarterly Journal of the Geological Society*, **94**, 1-60.

- Arkell, W.J. 1941. The gastropods of the Purbeck Beds. *Quaternary Journal of the Geological Society*, **97** (1-4), 79-128.
- Arkell, W.J. 1947. The Geology of the Country Around Weymouth, Swanage, Corfe & Lulworth. H.M. Stationery Office.
- Arp, G., Hofmann, J. & Reitner, J. 1998. Microbial fabric formation in spring mounds ("microbialites") of alkaline salt lakes in the Badain Jaran sand sea, PR China. *Palaios*, **13**, 581-592.
- Arp, G. & Mennerich, C. 2008. Ostracod assemblages, palaeoenvironment and cyclicity of Purbeck-type sediments of the Mnder Formation (Lower Cretaceous, Hils Syncline, N-Germany). *Palaeogeography, Palaeoclimatology, Palaeoecology*, **264**, 230-249.
- Arp, G., Reimer, A. & Reitner, J. 1999. Calcification in cyanobacterial biofilms of alkaline salt lakes. *European Journal of Phycology*, **34**, 393-403.
- Arp, G., Reimer, A. & Reitner, J. 2003. Microbialite formation in seawater of increased alkalinity, Satonda Crater Lake, Indonesia. *Journal of Sedimentary Research*, **73**, 105-127.
- Arp, G., Thiel, V., Reimer, A., Michaelis, W. & Reitner, J. 1999. Biofilm exopolymers control microbialite formation at thermal springs discharging into the alkaline Pyramid Lake, Nevada, USA. *Sedimentary Geology*, **126**, 159-176.
- Arthurton, R.S. 1973. Experimentally produced halite compared with Triassic layered halite-rock from Cheshire, England. *Sedimentology*, **20**, 145-160.
- Athmer, W. & Luthi, S.M. 2011. The effect of relay ramps on sediment routes and deposition: A review. *Sedimentary Geology*, **242**, 1-17.
- Austen, J.H. 1852. A guide to the geology of the Isle of Purbeck, and the south-west coast of Hampshire. W. Ship. 20 pp.
- Awramik, S.M. 1971. Precambrian columnar stromatolite diversity: reflection of metazoan appearance. *Science*, **174**, 825-827.
- Awramik, S.M. 1982. The pre-Phanerozoic fossil record. In: Holland, H.D. & Schidlowski, M. (eds.) *Mineral Deposits and the Evolution of the Biosphere*. Springer, 67-81.
- Awramik, S.M. 1992. The history and significance of stromatolites. In: Schidlowski, M., Golubic, S., Kimberley, M.M., McKirdy, D.M. & Trudinger, P.A. (eds.) *Early Organic Evolution: Implications for mineral and energy resources*. Springer-Verlag, 435-449.
- Awramik, S.M. & Buchheim, H.P. 2015. Giant stromatolites of the Eocene Green River Formation (Colorado, USA). *Geology*, **43**, 691-694.
- Awramik, S.M., Corsetti, F.A. & Shapiro, R. 2000. Stromatolites and the pre-Phanerozoic to Cambrian history of the area south east of Death Valley. *Bulletin of the San Bernardino County Museum*, **47**, 65-74.
- Awramik, S.M. & Margulis, L. 1974. Definition of stromatolite. In: Walter, E. (ed.) *Stromatolite Newsletter*, **2**, 5.
- Baker, G.S., Jordan, T.E. & Pardy, J. 2007. An introduction to ground penetrating radar (GPR). *Geological Society of America Special Papers*, **432**, 1-18.
- Barker, D., Brown, C.E., Bugg, S.C. & Costin, J. 1975. Ostracods, land plants, and charales from the basal Purbeck beds of Portesham Quarry, Dorset. *Palaeontology*, **18**, 419-436.

- Barton, C., Woods, M., Bristow, C., Newell, A., Westhead, R., Evans, D., Kirby, G. & Warrington, G. 2011. Geology of south Dorset and south-east Devon and its World Heritage Coast: Special Memoir for 1: 50 000 geological sheets 328 Dorchester, 341/342 West Fleet and Weymouth and 342/343 Swanage, and parts of sheets 326/340 Sidmouth, 327 Bridport, 329 Bournemouth and 339 Newton Abbot. British Geological Survey, Keyworth, Nottingham, 161 pp.
- Baskin, R.L. 2014. Occurrence and spatial distribution of microbial bioherms in Great Salt Lake, Utah. PhD, University of Utah, 204 pp.
- Baskin, R.L., Wright, V.P., Driscoll, N., Kent, G. & Hepner, G. 2012. Microbialite bioherms in Great Salt Lake, Utah: Influence of active tectonics and anthropogenic effects. *AAPG Hepberg Conference "Microbial Carbonate Reservoir Characterisation"*. AAPG, Houston, Texas, USA.
- Basson, P.W. & Edgell, H.S. 1971. Calcareous algae from the Jurassic and Cretaceous of Lebanon. *Micropaleontology*, **17**, 411-433.
- Bathurst, R.G.C. 1966. Boring algae, micrite envelopes and lithification of molluscan biosparites. *Geological Journal*, **5**, 15-32.
- Bathurst, R.G.C. 1967. Oölitic films on low energy carbonate sand grains, Bimini Lagoon, Bahamas. *Marine Geology*, **5**, 89-109.
- Bathurst, R.G.C. 1971. Carbonate sediments and their diagenesis. First edition ed. Elsevier, Amsterdam. 620 pp.
- Bathurst, R.G.C. 1975. Carbonate sediments and their diagenesis. Second edition ed. Elsevier, Amsterdam, 620 pp.
- Batten, D.J. 2002. Palaeoenvironmental setting of the Purbeck limestone group of Dorset, Southern England. *Special Papers in Palaeontology*, **68**, 13-20.
- Beglinger, S.E., Doust, H. & Cloetingh, S. 2012. Relating petroleum system and play development to basin evolution: West African South Atlantic basins. *Marine and Petroleum Geology*, **30**, 1-25.
- Benavente, C.A., D'ANGELO, J.A., Crespo, E.M. & Mancuso, A.C. 2014. Chemometric approach to Charophyte preservation (Triassic Cerro Puntudo Formation, Argentina): paleolimnologic implications. *Palaios*, **29**, 449-459.
- Berg, G. 1944. Vergleichende Petrographie oolithischer Eisenerze. Reichsamt für Bodenforschung, Berlin, 128 pp.
- BGS. 2000. *West Fleet and Weymouth* 1:50,000 series England and Wales Sheet 341 and part of sheet 342.
- Bläsi, H. 1980. Die Ablagerungsverhältnisse im "Portlandien" des schweizerischen und französischen Juras. PhD unpublished thesis, University of Bern, 151 pp.
- Blundell, D.J. 2002. Cenozoic inversion and uplift of southern Britain. *Geological Society, London, Special Publications*, **196**, 85-101.
- Boggs, S. 2009. Petrology of sedimentary rocks. Second Edition ed. Cambridge University Press, New York, USA, 600 pp.
- Bohacs, K.M., Carroll, A.R. & Neal, J.E. 2003. Lessons from large systems - thresholds, nonlinearity, and strange attractors. In: Chan, M.A. & Archer, A.W. (eds.) *Extreme depositional environments: mega end members in geologic time*, GSA, **370**, 75-90.

- Bohacs, K.M., Carroll, A.R., Neal, J.E. & Mankiewicz, P.J. 2000. Lake-basin type, source potential, and hydrocarbon character: an integrated-sequence-stratigraphic-geochemical framework. *In: Gierlowski-Kordesch, E.H. & Kelts, K.R. (eds.) Lake basin through space and time. AAPG*, **46**, 3-34.
- Bosak, T., Knoll, A.H. & Petroff, A.P. 2013. The meaning of stromatolites. *Annual Review of Earth and Planetary Sciences*, **41**, 21-44.
- Bosence, D.W.J. 1987. Portland and Purbeck Formations of the Isle of Portland. *In: Riding, R. (ed.) 4th Symposium on Fossil Algae, Excursions Guide, Cardiff*.
- Bosence, D.W.J., Gibbons, K., Le Heron, D.P., Morgan, W.A., Pritchard, T. & Vining, B.A. 2015. Microbial carbonates in space and time: introduction. *Geological Society, London, Special Publications*, **418**, 1-15.
- Bousquet, P. 1967. Contribution a l'étude stratigraphique et micropaléontologique du Jurassique et du Crétace de l'île d'Oléron (Charente-Maritime). Doctorat de 3ème cycle, Faculté des sciences de l'Université de Paris (Université Pierre et Marie Curie), 175 pp.
- Boyce, A.J., Fallick, A.E., Hamilton, P.J. & Elorza, J. 1990. Diagenesis of celestite in quartz geodes from the Basque-Cantabric Basin, Northern Spain: Evidence from sulphur and strontium isotopes. *Chemical Geology*, **84**, 354-356.
- Bradley, W.H. 1929. Algae reefs and oolites on the Green River Formation. *US Geological Survey, Reston, VA, Shorter Contributions to General Geology*, **1928**, 203-223.
- Breit, G.N., Goldhaber, M.B., Shawe, D.R. & Simmons, E.C. 1990. Authigenic barite as an indicator of fluid movement through sandstones within the Colorado Plateau. *Journal of Sedimentary Research*, **60**, 884-896.
- Brennan, A. & McLachlan, A.J. 1979. Tubes and tube-building in a lotic chironomid (Diptera) community. *Hydrobiologia*, **67**, 173-178.
- Bristow, C.S. & Jol, H.M. 2003. An introduction to ground penetrating radar (GPR) in sediments. *Geological Society, London, Special Publications*, **211**, 1-7.
- Bristow, H. 1857. Comparative vertical sections of the Purbeck strata of Dorsetshire. *Geol. Surv. Vert. Sections*, **22**.
- Bristow, H., Reid, C. & Strahan, A. 1889. *The Geology of the Isle of Wight*, 349 pp.
- Bristow, T.F., Kennedy, M.J., Morrison, K.D. & Mrofka, D.D. 2012. The influence of authigenic clay formation on the mineralogy and stable isotopic record of lacustrine carbonates. *Geochimica et Cosmochimica Acta*, **90**, 64-82.
- Bromley, R.G. 1996. Trace fossils, biology, taphonomy and applications. Second Edition ed. Springer-Science and Business Media, B. V., 361 pp.
- Brown Jr., L.F. & Fisher, W.L. 1977. Seismic-stratigraphic interpretation of depositional systems: examples from Brazilian rift and pull-apart basins. *Seismic Stratigraphy—Applications to Hydrocarbon Exploration: American Association of Petroleum Geologists, Memoir*, **26**, 213-248.
- Brown, P.R. 1961. Petrology of the Lower and Middle Purbeck beds of Dorset. PhD, University of Liverpool, 205 pp.
- Brown, P.R. 1963. Algal limestones and associated sediments in the basal Purbeck of Dorset. *Geological Magazine*, **100**, 565-573.

- Brown, P.R. 1964. Petrography and origin of some Upper Jurassic beds from Dorset, England. *Journal of Sedimentary Research*, **34**.
- Browne, K.M., Golubić, S. & Seong-Joo, L. 2000. Shallow marine microbial carbonate deposits. In: Riding, R.E. & Awramik, S.M. (eds.) *Microbial sediments*. Springer-Verlag, 233-249.
- Buchanan, J.G. 1998. The exploration history and controls on hydrocarbon prospectivity in the Wessex basins, southern England, UK. *Geological Society, London, Special Publications*, **133**, 19-37.
- Buchheim, H.B. & Awramik, S.M. 2013. Microbialites of the Eocene Green River Formation as analogs to the South Atlantic pre-salt carbonate hydrocarbon reservoirs. *Microbial Carbonates in Space and Time: Implications for Global Exploration and Production. (Abstract)*, 64-65.
- Buckland, W. & De La Beche, H.T. 1835. On the Geology of the Neighbourhood of Weymouth and the adjacent Parts of the Coast of Dorset. *Transactions of the Geological Society of London*, 1-46.
- Burne, R.V. & Moore, L.S. 1987. Microbialites: organosedimentary deposits of benthic microbial communities. *Palaios*, **2**, 241-254.
- Burne, R.V. & Moore, L.S. 1993. Microatoll microbialites of Lake Clifton, Western Australia: Morphological analogues of *Cryptozoön proliferum* Hall, the first formally-named stromatolite. *Facies*, **29**, 149-168.
- Bustillo, M.A. 2010. Silicification of continental carbonates. *Developments in Sedimentology*, **62**, 153-178.
- Butler, G.P. 1969. Modern evaporite deposition and geochemistry of coexisting brines, the sabkha, Trucial Coast, Arabian Gulf. *Journal of Sedimentary Petrology*, **39**, 70-89.
- Butler, M. 1998. The geological history of the southern Wessex Basin — a review of new information from oil exploration. *Geological Society, London, Special Publications*, **133**, 67-86.
- Butler, M. & Pullan, C.P. 1990. Tertiary structures and hydrocarbon entrapment in the Weald Basin of southern England. *Geological Society, London, Special Publications*, **55**, 371-391.
- Calassou, S. & Moretti, I. 2003. Sedimentary flattening and multi-extensional deformation along the West African margin. *Marine and Petroleum Geology*, **20**, 71-82.
- Calkin, J.B. 1968. Ancient Purbeck: an account of the geology of the Isle of Purbeck and its early inhabitants. The Friary Press, Dorchester, 61 pp.
- Carlson, E.H. 1987. Celestite replacements of evaporites in the Salina Group. *Sedimentary Geology*, **54**, 93-112.
- Carozzi, A.V. 1961. Distorted oolites and pseudoolites. *Journal of Sedimentary Petrology*, **31**.
- Carozzi, A.V. 1962. Observations on algal biostromes in the Great Salt Lake, Utah. *The Journal of Geology*, **70**, 246-252.
- Carozzi, A.V. 1964. Complex ooids from Triassic lake deposit, Virginia. *American Journal of Science*, **262** (2), 231-241.
- Casey, R. 1955. The pelecypod family Corbiculidae in the Mesozoic of Europe and the Near East. *Journal of the Washington Academy of Sciences*, **45**, 366-372.



- Casey, R. 1962. The Ammonites of the Spilsby Sandstone and the Jurassic-Cretaceous Boundary. *Proc. geol. Soc. Lond*, 95-100.
- Casey, R. 1963. The dawn of the Cretaceous period in Britain. *Bulletin of the South-East Union of Scientific Societies*, 1-15.
- Catuneanu, O. 2006. Principles of sequence stratigraphy. Elsevier, Amsterdam, The Netherlands, 387 pp.
- Cazier, E.C., Bargas, C., Buambua, L., Cardoso, S., Ferreira, H., Inman, K., Lopes, A., Nicholson, T., Olson, C. & Saller, A. 2014. Petroleum Geology of Cameia Field, Deepwater Pre-Salt Kwanza Basin, Angola, West Africa. *AAPG International Conference and Exhibition*. AAPG, Istanbul, Turkey.
- Chaboureau, A.-C., Guillocheau, F., Robin, C., Rohais, S., Moulin, M. & Aslanian, D. 2013. Paleogeographic evolution of the central segment of the South Atlantic during Early Cretaceous times: Paleotopographic and geodynamic implications. *Tectonophysics*, **604**, 191-223.
- Chadwick, R.A. 1985. *Upper Jurassic to Cretaceous sedimentation and subsidence*. Atlas of Onshore Sedimentary Basins in England and Wales: Post-Carboniferous Tectonics and Stratigraphy **49-52**.
- Chadwick, R.A. 1986. Extension tectonics in the Wessex Basin, southern England. *Journal of the Geological Society*, **143**, 465-488.
- Chadwick, R.A. 1993. Aspects of basin inversion in southern Britain. *Journal of the Geological Society*, **150**, 311-322.
- Channell, J.E.T. 1995. Late Jurassic-Early Cretaceous time scales and oceanic magnetic anomaly block models. *SEPM Special Publications*, Geochronology Time Scales and Global Stratigraphic Correlation, 51-63.
- Chen, X.Y., Bowler, J.M. & Magee, J.W. 1991. Aeolian landscapes in central Australia: gypsiferous and quartz dune environments from Lake Amadeus. *Sedimentology*, **38**, 519-538.
- Chidsey, T.C., Vanden Berg, M.D. & Eby, D.E. 2015. Petrography and characterization of microbial carbonates and associated facies from modern Great Salt Lake and Uinta Basin's Eocene Green River Formation in Utah, USA. *Geological Society, London, Special Publications*, **418**.
- Chow, N. & James, N.P. 1987. Facies-specific, calcitic and bimineralic ooids from Middle and Upper Cambrian platform carbonates, western Newfoundland, Canada. *Journal of Sedimentary Petrology*, **57**, 907-921.
- Cleevely, R.J. & Morris, N.J. 1988. Taxonomy and ecology of Cretaceous Cassiopidae (Mesogastropoda). British Museum (Natural History), 58 pp.
- Clements, R.G. 1969. Annotated cumulative section of the Purbeck Beds between Peveril Point and the Zig-Zag Path, Durlston Bay. *International Field Symposium on the British Jurassic: Excursion*, A1-A77.
- Clements, R.G. 1973. A study of certain non-marine Gastropoda from the Purbeck Beds of England. PhD, University of Hull, 601 pp.
- Clements, R.G. 1993. Type-section of the Purbeck Limestone Group, Durlston Bay, Swanage, Dorset. *Proceedings of the Dorset Natural History and Archaeological Society*, 181-206.

- Cohen, A.S. 1982. Ecological and paleoecological aspects of the rift lakes of East Africa. PhD, University of California, Davis, 314 pp.
- Cole, R.D. 1985. Depositional environments of oil shale in the Green River Formation, Douglas Creek Arch, Colorado and Utah.
- Colin, J.-P., El Albani, A., Fursich, F.T., Martin-Closas, C., Mazin, J.-M. & Billon-Bruyat, J.-P. 2004. Le gisement «Purbeckien» de vertébrés de Cherves-de-Cognac, Charente (SW France): nouvelles données biostratigraphiques. *Comptes Rendus Palevol*, **3**, 9-16.
- Collinson, J.D. & Thompson, D.B. 1989. Sedimentary structures. Second Edition. Chapman & Hall, London, 207 pp.
- Colter, V. & Havard, D. 1981. The Wytch Farm Oil Field, Dorset. In: Illing, L.V. & Hobson, G.D. (eds.) *Petroleum Geology of the Continental Shelf of North-West Europe*. Heyden London, London, 494-503.
- Colter, V.S. & Harvard, D.J. 1981. The Wytch farm oil field, Dorset. In: Illing, L.V. & Hobson, G.D. (eds.) *Petroleum Geology of the Continental Shelf of Northwest Europe*. Institute of Petroleum Geology, London, 494-503.
- Cope, J.C.W., Duff, K. L., Parsons, C. F., Torrens, H. S., Wimbleton, W. A., Wright, J. K. 1980. A Correlation of Jurassic rocks in the British Isles: part two: Middle and Upper Jurassic. Blackwell Scientific Publications, 109 pp.
- Cope, J.C.W. 2012. Geology of the Dorset coast. Geologists' Association, London, 232 pp.
- Cope, J.C.W. & Clements, R.G. 1969. The Purbeck Beds. In: Torrens, H.S. (ed.) *International Field Symposium on the British Jurassic. Excursion No. 1 Guide for Dorset and south Somerset*, University of Keele, A57-A64.
- Cosgrove, M. & Hearn, E. 1966. Structures in the Upper Purbeck Beds at Peveril Point, Swanage, Dorset. *Geological Magazine*, **103**, 498-507.
- Cotillon, P. 1960. Caractère pétrographique et genèse des galets noirs observés dans une coupe des 'Calcaires blancs' de Provence (Jurassique supérieur-Crétacé inférieur). *C. R. Soc. Géol. France*, **1960**, 170-171.
- Couper, R. 1957. British Mesozoic microspores and pollen grains. A systematic and stratigraphic study. *Palaeontographica Abteilung B*, 75-179.
- Cowie, P.A. & Scholz, C.H. 1992. Displacement-length scaling relationship for faults: data synthesis and discussion. *Journal of Structural Geology*, **14**, 1149-1156.
- Crosby, A. & Fletcher, B.N. 1988. Wealden and Purbeck beds strata exposed in cliff sections, surface exposures and underground workings in the Hastings-Dungeness district : with an account of the sea-bed geology east of Dungeness. British Geological Survey.
- Cross, N.E. & Bosence, D.W.J. 2008. Tectono-sedimentary models for rift-basin carbonate systems. *SEPM, Special Publication, Controls on Carbonate Platform and Reef Development*, **89**, 83-105.
- Cross, T.A. & Klosterman, M.J. 1981. Primary submarine cements and neomorphic spar in a stromatolitic-bound phylloid algal bioherm, Laborcita Formation (Wolfcampian), Sacramento Mountains, New Mexico, USA. In: Monty, C. (ed.) *Phanerozoic stromatolites*. Springer-Verlag, 60-73.
- Curtis, L.F., Courtney, F.M. & Trudgill, S.T. 1976. Soils in the British Isles. Longman, New York and London, 364 pp.

- Damon, R. 1860. Handbook to the Geology of Weymouth and the Island of Portland: With Notes on the Natural History of the Coast and Neighbourhood. Stanford, 200 pp.
- Darton, D., Dingwall, R.G. & McCann, D. 1981. Geological and geophysical investigations in Lyme Bay. Institute of Geological sciences, Natural environment research council Report 011884105X.
- Dashtgard, S.E. & Gingras, M.K. 2012. Marine invertebrate neoichnology. *In: Knaust, D. & Bromley, R.G. (eds.) Trace Fossils as Indicators of Sedimentary Environments*. Elsevier, Amsterdam, *Developments in Sedimentology*, **64**, 273-295.
- Davies, G.M. 1935. The Dorset coast: a geological guide. Murby & co, London, 126 pp.
- Davies, P.J., Bubela, B. & Ferguson, J. 1978. The formation of ooids. *Sedimentology*, **25**, 703-730.
- Davison, I. & Underhill, J.R. 2012. Tectonics and sedimentation : implications for petroleum systems. *In: Gao, D. (ed.) Tectonics and sedimentation: Implications for petroleum systems*. American Association of Petroleum Geologists, Tulsa, OK.
- De Brodtkorb, M.K. 1989. Celestite: worldwide classical ore fields. Van Nostrand Reinhold, New York, USA, 332 pp.
- De Brodtkorb, M.K., Ramos, V., Barbieri, M. & Ametrano, S. 1982. The evaporitic celestite-barite deposits of Neuquen, Argentina. *Mineralium Deposita*, **17**, 423-436.
- De La Beche, H.T. 1830. Sections & views, illustrative of geological phaenomena. Treuttel & Würtz, 71 pp.
- Deconinck, J.-F., Baudin, F. & Tribouvillard, N. 2000. The Purbeckian facies of the Boulonnais: a tsunami deposit hypothesis (Jurassic–Cretaceous boundary, northern France). *Comptes Rendus de l'Académie des Sciences - Series IIA - Earth and Planetary Science*, **330**, 527-532.
- Della Porta, G. 2015. Carbonate build-ups in lacustrine, hydrothermal and fluvial settings: comparing depositional geometry, fabric types and geochemical signature. *Geological Society, London, Special Publications*, **418**, 17-68.
- D'El-Rey Silva, L.J.H. 2001. Structures in jurassic rocks of the Wessex Basin, Southern England-I: field example of deformed crustal wedges. *Revista Brasileira de Geociencias*, **31**, 67-74.
- Dharmarajah, V. 2015. Sequences and layering in lacustrine carbonates; Purbeck Limestone, Wessex Basin. MSc, Royal Holloway University of London, 86 pp.
- Dias-Brito, D. & Tibana, P. 2015. Calcários do Cretáceo do Brasil: um atlas. UNESP-IGCE-UNESPetro.
- Dickson, W.G., Danforth, A. & Odegard, M. 2003. Gravity signatures of sediment systems: predicting reservoir distribution in Angolan and Brazilian basins. *In: Arthur, T.J., MacGregor, D.S. & Cameron, N.R. (eds.) Petroleum geology of Africa: new themes and developing technologies*. Geological Society of London, *Special Publication*, **207**, 241-256.
- Dorobek, S.L. 2008. Tectonic and Depositional Controls on Syn-Rift Carbonate Platform Sedimentation. *Controls on Carbonate Platform and Reef Development*. SEPM Society for Sedimentary Geology, **89**, 57-81.
- Dunham, R.J. 1962. Classification of carbonate rocks according to depositional textures.

- Dunham, R.J. 1969. Early vadose silt in Townsend mound (reef), New Mexico. *New Mexico Soc. Econ. Paleont. Min. Spec. Publ.*, **14**, 139-182.
- Dunning, G.C. 1949. The Purbeck Marble industry in the Roman period. *Archaeological newsletter*, **1**, 14-15.
- Dupraz, C., Reid, R.P., Braissant, O., Decho, A.W., Norman, R.S. & Visscher, P.T. 2009. Processes of carbonate precipitation in modern microbial mats. *Earth-Science Reviews*, **96**, 141-162.
- Dupraz, C. & Visscher, P.T. 2005. Microbial lithification in marine stromatolites and hypersaline mats. *Trends in microbiology*, **13**, 429-438.
- Dupraz, C., Visscher, P.T., Baumgartner, L.K. & Reid, R.P. 2004. Microbe–mineral interactions: early carbonate precipitation in a hypersaline lake (Eleuthera Island, Bahamas). *Sedimentology*, **51**, 745-765.
- Playford, P.E., Cockbain, A.E., Berry, A.P., Haines, P.W. & Brooke, B. 2013. The geology of Shark Bay, East Perth, 281 pp.
- Playford, P.E. & Leech, R.E.J. 1977. Geology and hydrology of Rottnest Island. Western Australia Geological Survey. 89 pp.
- Eardley, A.J. 1938. Sediments of Great Salt Lake, Utah. *AAPG Bulletin*, **22**, 1305-1411.
- Eby, D.E. & Chidsey, T.C. 2013. Great Salt Lake, Utah: a modern analog. In: AAPG-RMS, E.E.C. (ed.). Utah Geological Survey and Eby Petrography & Consulting, Inc., Salt Lake City, Utah, USA. Course Notes.
- Ecoscope. 2009. Lake Richmond management plan 2008. Ecoscope (Australia) Pty Ltd. 181 pp.
- Edgar, M. & Hinde, A. 1999. The stone workers of Purbeck. *Rural History*, **10**, 75-90.
- Edmunds, F.H. 1938. Physiography of the Mere district: Purbeck and Portland beds of the Wardour Vale. *Proceedings of the Geologists' Association*, **49**, 188-191.
- Ekdale, A.A., Bromley, R.G. & Pemberton, S.G. 1984. Ichnology - The use of trace fossils in sedimentology and stratigraphy. *SEPM*, **15**, 316 pp.
- Elliott, T. 1986. Siliciclastic shorelines. In: Reading, H.G. (ed.) *Sedimentary environments and facies*. Blackwell, Oxford, 155-188.
- El-Shahat, A. & West, I.M. 1983. Early and late lithification of aragonitic bivalve beds in the Purbeck Formation (Upper Jurassic-Lower Cretaceous) of southern England. *Sedimentary Geology*, **35**, 15-41.
- Elstner, F. & Mutterlose, J. 1996. The Lower Cretaceous (Berriasian and Valanginian) in NW Germany. *Cretaceous Research*, **17**, 119-133.
- Englefield, S.H. 1816. A Description of the Principal Picturesque Beauties, Antiquities, and Geological Phenomena, of the Isle of Wight. William Bulmer and Company Cleveland-Row, 238 pp.
- Ensom, P. 1985. An annotated section of the Purbeck limestone Formation at Worbarrow Tout, Dorset. *Proceedings of the Dorset Natural History and Archaeological Society*, **106**, 87-91.
- Ensom, P. 2002. The Purbeck Limestone Group of Dorset, southern England: a guide to lithostratigraphic terms. *Special Papers in Palaeontology*, **68**, 7-12.

- Ensom, P., Clements, R., Feist-Burkhardt, S., Milner, A., Chitolie, J., Jeffery, P. & Jones, C. 2009. The age and identity of an ichthyosaur reputedly from the Purbeck Limestone Group, Lower Cretaceous, Dorset, southern England. *Cretaceous Research*, **30**, 699-709.
- Eugster, H.P. & Hardie, L.A. 1978. Saline lakes. In: Lerman, A. (ed.) *Lakes: chemistry, geology, physics*. Springer, Berlin, 238-293.
- Eugster, H.P. & Surdam, R.C. 1973. Depositional environment of the Green River Formation of Wyoming: a preliminary report. *Geological Society of America Bulletin*, **84**, 1115-1120.
- Evans, S.E. & Searle, B. 2002. Lepidosaurian reptiles from the Purbeck Limestone Group of Dorset, southern England. In: Milner, A.R. & Batten, D.J. (eds.) *Life and environments in Purbeck times*. The Palaeontological Association, Special Papers in Palaeontology, **68**, 145-160.
- Feng, J., Sarg, J.F., Tanavsuu-Milkeviciene, K. & Suriamin, H. 2014. Climate History, lake evolution, and prediction of organic richness, Green River Formation, Piceance Basin, Colorado. In: AAPG (ed.) *AAPG 2013 Annual Convention and Exhibition*. AAPG, Pittsburgh, Pennsylvania.
- Fischer, A.G. 1965. Fossils, early life, and atmospheric history. *Proceedings of the National Academy of Sciences*, **53**, 1205-1215.
- Fisher, O. 1856. On the Purbeck strata of Dorsetshire. *Transactions of the Cambridge Philosophical Society*, **9**, 555-581.
- Fitton, W.H. 1827. Observations on some of the Strata between the Chalk and the Oxford Oolite, in the South-east of England. *Transactions of the Geological Society of London*, (2), 103-388.
- Fitton, W.H. 1835. Notice on the junction of the Portland and Purbeck strata on the coast of Dorsetshire. *Proceedings of Geological Society*, **2**, 185-187.
- Fitton, W.H. 1836. IV.—Observations on some of the Strata between the Chalk and the Oxford Oolite, in the South-east of England. *Transactions of the Geological Society of London*, 103-389.
- Fleckner, S. 2014. Sea\_oor bathymetry analysis of the Weymouth Anticline and circular structures of Weymouth Bay. MSc, Royal Holloway University of London, 84 pp.
- Flügel, E. 1978. Mikrofazielle Untersuchungsmethoden von Kalken. Springer-Verlag, 454 pp.
- Flügel, E. 1982. Microfacies analysis of limestones. Springer-Verlag, 633 pp.
- Flügel, E. 2010. Microfacies of carbonate rocks: analysis, interpretation and application. Second Edition ed. Springer, 984 pp.
- Folk, R.L. & Pittman, J.S. 1971. Length-slow chalcedony: a new testament for vanished evaporites. *Journal of Sedimentary Research*, **41**, 1045-1058.
- Forbes, E. 1850. On the succession of strata and distribution of organic remains in the Dorsetshire Purbecks. *Reports of the 20th meeting of the British Association for the Advancement of Science in Edinburgh*. British Association for the Advancement of Science, 79-81.
- Fossen, H. 2010. Structural geology. Cambridge University Press, New York, USA, 524 pp.
- Francis, J.E. 1982. The Fossil Forest of the basal Purbeck Formation (Upper Jurassic) of Dorset, southern England. Palaeobotanical and palaeoenvironmental investigations. PhD, University of Southampton, 317 pp.

- Francis, J.E. 1983. The dominant conifer of the Jurassic Purbeck formation, England. *Palaeontology*, **26**, 277-294.
- Francis, J.E. 1984. The seasonal environment of the purbeck (upper jurrasic) fossil forests. *Palaeogeography, Palaeoclimatology, Palaeoecology*, **48**, 285-307.
- Francis, J.E. 1986. The calcareous paleosols of the basal Purbeck Formation (Upper Jurassic), southern England. *Paleosols*. Blackwell Oxford, 112-138.
- Freytet, P. & Verrecchia, E.P. 1998. Freshwater organisms that build stromatolites: a synopsis of biocrystallization by prokaryotic and eukaryotic algae. *Sedimentology*, **45**, 535-563.
- Freytet, P. & Verrecchia, E.P. 1999. Calcitic radial palisadic fabric in freshwater stromatolites: diagenetic and recrystallized feature or physicochemical sinter crust? *Sedimentary Geology*, **126**, 97-102.
- Friedman, G.M., Amiel, A.J., Braun, M. & Miller, D.S. 1973. Generation of carbonate particles and laminites in algal mats--example from sea-marginal hypersaline pool, Gulf of Aqaba, Red Sea. *AAPG Bulletin*, **57**, 541-557.
- Fürsich, F.T., Palmer, T.J. & Goodyear, K.L. 1994. Growth and disintegration of bivalve dominated patch reefs in the Upper Jurassic of southern England. *Palaeontology*, **37**, 131-171.
- Galbrun, B., Rasplus, L. & Le Hégarat, G. 1986. Données nouvelles sur le stratotype du Berriasien: corrélations entre magnétostratigraphie et biostratigraphie. *Bulletin de la Société Géologique de France*, **8**, 575-584.
- Galloway, W.E. 1989. Genetic stratigraphic sequences in basin analysis I: architecture and genesis of flooding-surface bounded depositional units. *AAPG Bulletin*, **73**, 125-142.
- García-Veigas, J., Rosell, L., Cendón, D.I., Gibert, L., Martín, J.M., Torres-Ruiz, J. & Ortí, F. 2015. Large celestine orebodies formed by early-diagenetic replacement of gypsified stromatolites (Upper Miocene, Montevive–Escúzar deposit, Granada Basin, Spain). *Ore Geology Reviews*, **64**, 187-199.
- Garden, I.R. 1987. The Provenance of Upper Jurassic and Lower Cretaceous Coarse-grained Detritus in Southern Britain and Normandy. University of Southampton.
- Garden, I.R. 1991. Changes in the provenance of pebbly detritus in southern Britain and northern France associated with basin rifting. *Geological Society, London, Special Publications*, **57**, 273-289.
- Garrett, P. 1970. Phanerozoic stromatolites: non-competitive ecologic restriction by grazing and burrowing animals. *Science*, **169**, 171-173.
- Gawthorpe, R.L., Fraser, A.J. & Collier, R.E.L. 1994. Sequence stratigraphy in active extensional basins: implications for the interpretation of ancient basin-fills. *Marine and Petroleum Geology*, **11**, 642-658.
- Gawthorpe, R.L. & Hurst, J.M. 1993. Transfer zones in extensional basins: their structural style and influence on drainage development and stratigraphy. *Journal of the Geological Society*, **150**, 1137-1152.
- Gebelein, C.D. 1969. Distribution, morphology, and accretion rate of recent subtidal algal stromatolites, Bermuda. *Journal of Sedimentary Research*, **39**, 49-69.
- Geno, K.R. & Chafetz, H.S. 1982. Petrology of Quaternary fluvial low-magnesian calcite coated grains from central Texas. *Journal of Sedimentary Petrology*, **52**, 833-842.

- Gibbs, A.D. 1984. Structural evolution of extensional basin margins. *Journal of the Geological Society*, **141**, 609-620.
- Gierlowski-Kordesch, E.H. 2010. Lacustrine Carbonates. In: Alonso-Zarza, A.M. & Tanner, L.H. (eds.) *Carbonates in continental settings. Facies, environments and processes*. Elsevier, 1-101.
- Gingras, M.K., Lalond, S.V., Amskold, L. & Konhauser, K.O. 2007. Wintering chironomids mine oxygen. *Palaios*, **22**, 433-438.
- Gischler, E., Gibson, M.A. & Oschmann, W. 2008. Giant Holocene Freshwater Microbialites, Laguna Bacalar, Quintana Roo, Mexico. *Sedimentology*, **55**, 1293-1309.
- Gischler, E., Golubić, S., Gibson, M.A., Oschmann, W. & Hudson, J.H. 2011. Microbial mats and microbialites in the freshwater Laguna Bacalar, Yucatan Peninsula, Mexico. In: Reitner, J., Quéric, N.-V. & Arp, G. (eds.) *Advances in Stromatolite Geobiology*. Springer-Verlag, 187-205.
- Godden, M. 2012. Portland's Quarries and its Stone. 26 pp.
- Golubić, S. 1973. The relationship between blue-green algae and carbonate deposits. In: Carr, N.G. & Whitton, B.A. (eds.) *The biology of blue-green algae*. Blackwell, 434-472.
- Grabowski, J. 2011. Magnetostratigraphy of the Jurassic/Cretaceous boundary interval in the Western Tethys and its correlations with other regions: a review. *Volumina Jurassica*, **9**, 105-128.
- Gradstein, F.M., Ogg, J.G. & Smith, A.G. 2004. A geologic time scale 2004. Cambridge University Press, 589 pp.
- Gramann, F., Heunisch, C., Klassen, H., Kockel, F., Dulce, G., Harms, F.-J., Katschorek, T., Mönnig, E., Schudack, M. & Schudack, U. 1997. Das Niedersächsische Oberjura-Becken--Ergebnisse interdisziplinärer Zusammenarbeit. *Zeitschrift der deutschen geologischen Gesellschaft*, **148**, 165-236.
- Gray, W. 1861. On the geology of the Isle of Portland. *Proceedings of the Geologists' Association*, **1**, 128-147.
- Grey, K., Moore, L.S., Burne, R.V., Pierson, B.K. & Bauld, J. 1990. Lake Thetis, Western Australia and example of Saline Lake Sedimentation dominated by Benthic Microbial Processes. *Marine and Freshwater Research*, **41**, 275-300.
- Grey, K. & Planavsky, N.J. 2009. Microbialites of Lake Thetis, Cervantes, Western Australia: A Field Guide. Record 2009/11 ed. Geological Survey of Western Australia, 21 pp.
- Gribble, C.D. & Hall, A.J. 1985. A Practical Guide to Optical Mineralogy. George Allen & Unwin, London, UK, 249 pp.
- Griffith, J. & Patterson, C. 1963. The structure and relationships of the Jurassic fish Ichthyokentema purbeckensis. *Bulletin of the British Museum (Natural History)*, **8**, 3-43.
- Grimaldi, D. & Engel, M.S. 2005. Evolution of the Insects. Cambridge University Press, New York, USA, 735 pp.
- Grotzinger, J.P. 1989. Facies and evolution of Precambrian carbonate depositional systems: emergence of the modern platform archetype. In: Crevello, P.D., Wilson, J.L., Sarg, J.F. & Read, J.F. (eds.) *Controls on Carbonate Platform and Basin Development*. SEPM, SEPM Special Publications, **44**, 79-106.

- Grotzinger, J.P. 2011. Atlas of stromatolite morphologies and texture. California Institute of Technology, Division of Geological and Planetary Sciences, Pasadena, California, 91108, 146 pp.
- Grotzinger, J.P. & Knoll, A.H. 1999. Stromatolites in Precambrian carbonates: evolutionary mileposts or environmental dipsticks? *Annual Review of Earth and Planetary Sciences*, **27**, 313-358.
- Grover, G.J. & Read, J.F. 1978. Fenestral and associated vadose diagenetic fabrics of tidal flat carbonates, Middle Ordovician New Market Limestone, southwestern Virginia. *Journal of Sedimentary Research*, **48**, 453-473.
- Guerreiro, J.C., Collins, L.B., Parellada, A.L. & Vogwill, R.I. 2015. Environmental Controls, Growth History and Fabrics of Lake Richmond Microbialites, Western Australia. *International Conference & Exhibition*, Melbourne, Australia.
- Hahl, D.C. & Langford, R.H. 1964. Dissolved-mineral inflow to Great Salt Lake and characteristics of the salt lake brine - Part II, technical report, 40 pp.
- Halley, R.B. 1977. Ooid fabric and fracture in the Great Salt Lake and the geologic record. *Journal of Sedimentary Research*, **47**, 1099-1120.
- Hallock, P. and Schlager W. 1986. Nutrient excess and the demise of coral reefs and carbonate platforms. *Palaios*, **1**, 389-398.
- Hamblin, R.J.O., Crosby, A., Balson, P.S., Jones, S.M., Chadwick, R.A., Penn, I.E. & Arthur, M.J. 1992. The geology of the English Channel. British Geological Survey, United Kingdom Offshore Regional Report. HMSO, London, 106 pp.
- Handford, C.R. 1982. Sedimentology and evaporite genesis in a Holocene continental-sabkha playa basin—Bristol Dry Lake, California. *Sedimentology*, **29**, 239-253.
- Handford, C.R. 1991. Marginal Marine Halite: Sabkhas and Salinas. In: Melvin, J.L. (ed.) *Evaporites, petroleum and mineral resources*. Elsevier, Developments in Sedimentology, **50**, 1-66.
- Hanneman, D.L. & Wideman, C.J. 2010. Continental sequence stratigraphy and continental carbonates. In: Alonso-Zarza, A.M. & Tanner, L.H. (eds.) *Carbonates in continental settings, Facies, environments and processes*. Elsevier, Developments in Sedimentology, **62**, 215-273.
- Hanor, J.S. 2000. Barite–celestine geochemistry and environments of formation. *Reviews in Mineralogy and Geochemistry*, **40**, 193-275.
- Hanor, J.S. 2004. A model for the origin of large carbonate-and evaporite-hosted celestine (SrSO<sub>4</sub>) deposits. *Journal of Sedimentary Research*, **74**, 168-175.
- Hardy, T. 1897. The well-beloved: a sketch of a temperament. Macmillan, London.
- Harvey, M.J. & Stewart, S.A. 1998. Influence of salt on the structural evolution of the Channel Basin. In: Underhill, J.R. (ed.) *The development, evolution and petroleum geology of the Wessex Basin*. Geological Society, London, Special Publications, **133**, 241-266.
- Hasiotis, S.T. 2006. Continental trace fossils, 132 pp.
- Hassell, C. & Kneebone, E. 1960. The geology of Rottneest Island. Unpublished Thesis, University of Western Australia.



- Hawkes, P.W., Fraser, A.J. & Einchcomb, C.C.G. 1998. The tectono-stratigraphic development and exploration history of the Weald and Wessex basins, southern England, UK. *In: Underhill, J.R. (ed.) The development, evolution and petroleum geology of the Wessex Basin*. Geological Society, London, Special Publications, **133**, 39-66.
- Heller, P.L., Komar, P.D. & Pevear, D.R. 1980. Transport processes in ooid genesis. *Journal of Sedimentary Research*, **50**, 943-951.
- Hinde, P. 1980. The Development of the Wytch Farm Oilfield. Institution of Gas Engineers.
- Hodgetts, D. 2013. Laser scanning and digital outcrop geology in the petroleum industry: a review. *Marine and Petroleum Geology*, **46**, 335-354.
- Hoffman, P. 1974. Shallow and Deepwater Stromatolites in Lower Proterozoic Platform--to--Basin Facies Change, Great Slave Lake, Canada. *AAPG Bulletin*, **58**, 856-867.
- Hofmann, H.J. 1969. Attributes of stromatolites. *Geological Survey Canada Paper*, **69-39**, 58.
- Hofmann, H.J. 1973. Stromatolites: characteristics and utility. *Earth-Science Reviews*, **9**, 339-373.
- Hofmann, H.J. 1976. Stromatoid morphometrics. *In: Walter, E. (ed.) Stromatolites*. Elsevier, Developments in Sedimentology, **20**, 45-54.
- Hofmann, H.J. 1977. On Aphebian stromatolites and Riphean stromatolite stratigraphy. *Precambrian Research*, **5**, 175-205.
- Hofmann, H.J. 1994. Quantitative stromatoliteology. *Journal of Paleontology*, **68**, 704-709.
- Hofmann, H.J. 2000. Archean stromatolites as microbial archives. *In: Riding, R.E. & Awramik, S.M. (eds.) Microbial sediments*. Springer, Berlin, 315-327.
- Hollingworth, S.E. 1938. The Purbeck broken beds. *Geological Magazine*, **75**, 330-332.
- Hopson, P., Wilkinson, I. & Woods, M. 2008. *A stratigraphical framework for the Lower Cretaceous of England*. British Geological Survey Report **0852726236**.
- Horne, D.J. 1995. A revised ostracod biostratigraphy for the Purbeck-Wealden of England. *Cretaceous Research*, **16**, 639-663.
- Horne, D.J. 2002. Ostracod biostratigraphy and palaeoecology of the Purbeck Limestone Group in southern England. *Special Papers in Palaeontology*, **68**, 53-70.
- Horowitz, A.S. & Potter, P.E. 1971. Introductory petrography of fossils. Springer-Verlag.
- Hounsell, S.S.B. 1952. Portland and its Stone. *Maine and Quarry Engineering Magazine*.
- House, M.R. 1958. The Dorset coast from Poole to the Chesil Beach, 21 pp.
- House, M.R. 1969. The Dorset coast from Poole to the Chesil Beach. 2nd Edition. Geologists' Association, 32 pp.
- House, M.R. 1989. Geology of the Dorset Coast, First edition, 169 pp.
- House, M.R. 1993. Geology of the Dorset coast, Second edition, 164 pp.
- Howell, H.V., Doyen, J.T. & Purcell, A.H. 1998. Introduction to insect biology and diversity. Second Edition ed. Oxford University Press, Oxford, UK, 320 pp.
- Howitt, F. 1964. Stratigraphy and structure of the Purbeck inliers of Sussex (England). *Quarterly Journal of the Geological Society*, **120**, 77-113.
- Hoyer, P. 1965. Fazies, Paläogeographie und Tektonik des Malm im Deister,-Osterwald und Süntel. *Beihefte zum Geologischen Jahrbuch Hannover*, **61**, 1-249.

- Hunt, C.O. 1985. Miospores from the Portland Stone Formation and lower part of the Purbeck Group ( Upper Jurassic/Lower Cretaceous) from Dorset, England. *Pollen et Spores*, **27**, 416-451.
- Hunt, C.O. 2004. Palynostratigraphy of the classic Portland and Purbeck sequences of Dorset, southern England, and the correlation of Jurassic-Cretaceous boundary beds in the Tethyan and Boreal realms. *Geological Society, London, Special Publications*, **230**, 175-186.
- Illing, L.V. 1954. Bahaman calcareous sands. *AAPG Bulletin*, **38**, 1-95.
- Illing, L.V., Wells, A.J. & Taylor, J.C.M. 1965. Penecontemporary dolomite in the Persian Gulf. *SEPM Special Publications*, **13**, 89-111.
- Irion, G. & Müller, G. 1968. Mineralogy, petrology and chemical composition of some calcareous tufa from the Schwäbische Alb, Germany. In: Muller, G. & Friedman, G.M. (eds.) *Recent developments in carbonate sedimentology in Central Europe*. Springer, 157-171.
- Jahnert, R.J. & Collins, L.B. 2011. Significance of subtidal microbial deposits in Shark Bay, Australia. *Marine Geology*, **286**, 106-111.
- Jahnert, R.J. & Collins, L.B. 2012. Characteristics, distribution and morphogenesis of subtidal microbial systems in Shark Bay, Australia. *Marine Geology*, **303–306**, 115-136.
- John, J., Hay, M. & Paton, J. 2009. Cyanobacteria in benthic microbial communities in coastal salt lakes in Western Australia. *Algological Studies*, **130**, 125-135.
- Johnson, J.H. 1943. Geologic importance of calcareous algae with annotated bibliography. Colorado School of Mines, Golden, Colorado, 102 pp.
- Jones, T.R. 1883. On some Fossil Entomostraca from the Purbeck Formation at Boulogne. *Proceedings of the Geologists' Association*, **8**, 54-59.
- Jóźwiak-Niedźwiedzka, D., Gibas, K., Brandt, A.M., Glinicki, M.A., Dąbrowski, M. & Denis, P. 2015. Mineral composition of heavy aggregates for nuclear shielding concrete in relation to alkali-silica reaction. *Procedia Engineering*, **108**, 162-169.
- Kahle, C.F. 1974. Ooids from Great Salt Lake, Utah, as an analogue for the genesis and diagenesis of ooids in marine limestones. *Journal of Sedimentary Research*, **44**, 30-39.
- Kalkowsky, E. 1908. Oolith und Stromatolith im norddeutschen Buntsandstein. *Zeitschrift der deutschen geologischen Gesellschaft*, **60**, 68-125.
- Kelly, S.R.A. 1983. Boreal influence on English Ryazanian bivalves. *Zitteliana*, **10**, 285-292.
- Kelly, S.R.A. 1988. *Laevitrigonia cineris* sp. nov., a bivalve from near the Jurassic-Cretaceous boundary in the Durlston Formation (Purbeck Limestone Group) of Dorset. *Proceedings of the Dorset Natural History and Archaeological Society*, **109**, 113-116.
- Kennard, J.M. & James, N.P. 1986. Thrombolites and stromatolites: two distinct types of microbial structures. *Palaios*, **1**, 492-503.
- Kenneally, K.F., Dell, J., Hussey, B.J.M. & Johnson, D.P. 1987. A Survey of Lake Richmond, Western Australia. *The naturalists News*.
- Kennish, M.J. 1986. Ecology of Estuaries, Volume I: Physical and Chemical Aspects. CRC Press, Inc., Boca Raton FL.
- Kilenyi, T. & Neale, J.W. 1978. The Purbeck/Wealden. In: Bate, R. & Robinson, E. (eds.) *A stratigraphical index of British Ostracoda*, Geology Journal Special Issue, **8**, 299-324.

- Kim, Y.-S. & Sanderson, D.J. 2005. The relationship between displacement and length of faults: a review. *Earth-Science Reviews*, **68**, 317-334.
- Kirkaldy, J.F. 1937. The overstep of the Sandgate Beds in the Eastern Weald. *Quarterly Journal of the Geological Society*, **93**, 94-126.
- Klappa, C.F. 1980. Rhizoliths in terrestrial carbonates: classification, recognition, genesis and significance. *Sedimentology*, **27**, 613-629.
- Klement, K.W. & Toomey, D.F. 1967. Role of the blue-green alga *Girvanella* in skeletal grain destruction and lime-mud formation in the lower Ordovician of West Texas. *Journal of Sedimentary Petrology*, **37**, 1045-1051.
- Knaust, D. & Bromley, R.G. 2012. Trace fossils as indicators of sedimentary environments. Elsevier, 924 pp.
- Knoll, A.H. 1985. Exceptional preservation of photosynthetic organisms in silicified carbonates and silicified peats. *Philosophical Transactions of the Royal Society of London B: Biological Sciences*, **311**, 111-122.
- Koch, C.L. & Dunker, W.B.R.H. 1837. Beiträge zur Kenntniss des norddeutschen Oolithgebildes und dessen Versteinerungen. *Oehme und Mülle, Braunschweig*, **4**, 1-64.
- Konhauser, K.O. & Ferris, F.G. 1996. Diversity of iron and silica precipitation by microbial mats in hydrothermal waters, Iceland: Implications for Precambrian iron formations. *Geology*, **24**, 323-326.
- Konhauser, K.O., Jones, B., Phoenix, V.R., Ferris, G. & Renaut, R.W. 2004. The microbial role in hot spring silicification. *AMBIO: A Journal of the Human Environment*, **33**, 552-558.
- Konishi, Y., Prince, J. & Knott, B. 2001. The fauna of thrombolitic microbialites, Lake Clifton, western Australia. *Hydrobiologia*, **457**, 39-47.
- Košir, A. 2004. Microcodium revisited: root calcification products of terrestrial plants on carbonate-rich substrates. *Journal of Sedimentary Research*, **74**, 845-857.
- Kozłowski, E.N. In prep. Multi-scale forward modelling of microbial lacustrine carbonate. PhD, Royal Holloway University of London.
- Kraus, M.J. & Hasiotis, S.T. 2006. Significance of different modes of rhizolith preservation to interpreting paleoenvironmental and paleohydrologic settings: examples from Paleogene paleosols, Bighorn Basin, Wyoming, USA. *Journal of Sedimentary Research*, **76**, 633-646.
- Krumbein, W.E., Cohen, Y. & Shilo, M. 1977. Solar lake (Sinai). 4. Stromatolitic cyanobacterial mats. *Limnology and Oceanography*, **22**, 635-656.
- Kurz, T.H., Dewit, J., Buckley, S.J., Thurmond, J.B., Hunt, D.W. & Swennen, R. 2012. Hyperspectral image analysis of different carbonate lithologies (limestone, karst and hydrothermal dolomites): the Pozalagua Quarry case study (Cantabria, North-west Spain). *Sedimentology*, **59**, 623-645.
- Labeci, J. & Radwanski, A. 1967. Broken ooids in lagoonal Keuper deposits of the western margin of the Holy Cross Mountains. *Académie Polonaise des Sciences, Bulletin Série des sciences géologiques et géographiques*, **15**, 93-99.
- Lake, S.D. 1985. The structure and evolution of the Wessex Basin. PhD, University of Durham, 390 pp.
- Lake, S.D. & Karner, G.D. 1987. The structure and evolution of the Wessex Basin, southern England: an example of inversion tectonics. *Tectonophysics*, **137**, 347-378.

- Land, L.S., Behrens, E.W. & Frishman, S.A. 1979. The ooids of Baffin Bay, Texas. *Journal of Sedimentary Research*, **49**, 1269-1277.
- Lantz, J. 1958. Etude palynologique de quelques échantillons mésozoïques du Dorset (Grande-Bretagne). *Revue de l'Institut Français du Pétrole*, **13**, 917-943.
- Larsen, P.-H. 1988. Relay structures in a Lower Permian basement-involved extension system, East Greenland. *Journal of Structural Geology*, **10**, 3-8.
- Latham, A. & Riding, R.E. 1988. Thrombolites formed by calcified cyanobacteria in the Lie de Vin Series, Morocco. *Int. Assoc. Sediment. 9th Eur. Region Meet. Abstr., Leuven, Belgium*, 127-128.
- Leggitt, V.L., Biaggi, R.E. & Buchheim, H.B. 2007. Palaeoenvironments associated with caddisfly-dominated microbial-carbonate mounds from the Tipton Shale Member of the Green River Formation: Eocene Lake Gosiute. *Sedimentology*, **54**, 661-699.
- Leggitt, V.L. & Loewen, M.A. 2002. Eocene Green River Formation "Oocardium tufa" reinterpreted as complex arrays of calcified caddisfly (Insecta: Trichoptera) larval cases. *Sedimentary Geology*, **148**, 139-146.
- Leinfelder, R.R. & Schmid, D.U. 2000. Mesozoic reefal thrombolites and other microbolites. In: Riding, R.E. & Awramik, S.M. (eds.) *Microbial Sediments*. Springer-Verlag, Heidelberg, 289-294.
- Leng, M.J. & Marshall, J.D. 2004. Palaeoclimate interpretation of stable isotope data from lake sediment archives. *Quaternary Science Reviews*, **23**, 811-831.
- Leo, R.F. & Barghoorn, E.S. 1976. Silicification of wood. *Botanical Museum Leaflets, Harvard University*, **25**, 1-47.
- Lionnet, J.F.G. 1952. Rendzina soils of coastal flats of the Seychelles. *Journal of Soil Science*, **3**, 172-181.
- Liu, L., Wu, Y., Hongxia, J. & Riding, R.E. 2016. Calcified rivulariaceans from the Ordovician of the Tarim Basin, Northwest China, Phanerozoic lagoonal examples, and possible controlling factors. *Palaeogeography, Palaeoclimatology, Palaeoecology*, **448**, 371-381.
- Logan, B.W. 1961. Cryptozoon and associate stromatolites from the Recent, Shark bay, Western Australia. *The Journal of Geology*, **69**, 517-533.
- Logan, B.W., Hoffman, P. & Gebelein, C.D. 1974. Algal mats, cryptalgal fabrics, and structures, Hamelin Pool, Western Australia. In: Logan, B.W., Read, J.F. & Hagan, G.M. (eds.) *Evolution and diagenesis of Quaternary carbonate sequences, Shark Bay, Western Australia*, AAPG Memoir, **22**, 140-194.
- Logan, B.W., Rezak, R. & Ginsburg, R.N. 1964. Classification and environmental significance of algal stromatolites. *The Journal of Geology*, **72**, 68-83.
- Longman, M.W. 1980. Carbonate diagenetic textures from nearsurface diagenetic environments. *AAPG Bulletin*, **64**, 461-487.
- Loreau, J.-P. & Purser, B.H. 1973. Distribution and ultrastructure of Holocene ooids in the Persian Gulf. In: Purser, B.H. (ed.) *The Persian Gulf*. Springer-Verlag, 279-328.
- Lowenstein, T.K. & Hardie, L.A. 1985. Criteria for the recognition of salt-pan evaporites. *Sedimentology*, **32**, 627-644.
- Luu, R., Mitchell, D. & Blyth, J. 2004. Thrombolite (stromatolite-like microbialite) community of a coastal brackish lake (Lake Clifton), *Interim recovery plan*, **35**, 21 pp.

- Lyell, C. 1855. A manual of elementary geology. John Murray, 40 pp.
- Macintyre, I.G. 1985. Submarine cements—the peloidal question. *In*: Schneidermann, N. & Harris, P.M. (eds.) *Carbonate cements*. Society of Economic Paleontologists and Mineralogists, Tulsa, Oklahoma, Special Publication, **36**, 109-116.
- Mann, K.H. & Lazier, J.R.N. 1991. Dynamics of marine ecosystem. *Blakwell Science*.
- Mansy, J.L., Manby, G.M., Averbuch, O., Everaerts, M., Bergerat, F., Van Vliet-Lanoe, B., Lamarche, J. & Vandycke, S. 2003. Dynamics and inversion of the Mesozoic Basin of the Weald–Boulonnais area: role of basement reactivation. *Tectonophysics*, **373**, 161-179.
- Mathews, A.A.L. 1930. Origin and Growth of the Great Salt Lake Oölites. *The Journal of Geology*, **38**, 633-642.
- McKee, E.D. & Gutschick, R.C. 1969. History of the Redwall Limestone of northern Arizona, 726 pp.
- McLachlan, A.J. & Cantrell, M.A. 1976. Sediment development and its influence on the distribution and tube structure of *Chironomus plumosus* L. (*Chironomidae*, *Diptera*) in a new impoundment. *Freshwater Biology*, **6**, 437-443.
- McMahon, N.A. & Turner, J. 1998. The documentation of a latest Jurassic-earliest Cretaceous uplift throughout southern England and adjacent offshore areas. *In*: Underhill, J.R. (ed.) *The development, evolution and petroleum geology of the Wessex Basin*. Geological Society, London, Special Publications, **133**, 215-240.
- McNamara, K. 2009. Stromatolites. Western Australian Museum, 88 pp.
- McNamara, K. 2012. Western Australia's modern stromatolites/microbialites/thrombolites. *Symposium on research and conservation: south west Western Australia's microbialites*, Kensington, Western Australia.
- Medwedeff, D.A. & Wilkinson, B.H. 1983. Cortical fabrics in calcite and aragonite ooids. *In*: Peryt, T.M. (ed.) *Coated Grains*. Springer-Verlag, 109-115.
- Merkus, H.G. 2009. Particle size measurements: fundamentals, practice, quality. Springer Science & Business Media, **17**.
- Miall, A. 2010. The geology of stratigraphic sequences. Springer, 532 pp.
- Milner, A.C. 2002. Theropod dinosaurs of the Purbeck Limestone Group, southern England. *In*: Milner, A.C. & Batten, D.J. (eds.) *Life and environments in Purbeck times*, Special Papers in Palaeontology, **68**, 191-201.
- Mitchum Jr, R. 1977. Seismic Stratigraphy and Global Changes of Sea Level: Part 11. Glossary of Terms used in Seismic Stratigraphy: Section 2. Application of Seismic Reflection Configuration to Stratigraphic Interpretation.
- Moncure, G. & Surdam, R.C. 1980. Depositional environment of the Green River Formation in the vicinity of the Douglas Creek Arch, Colorado and Utah. *Rocky Mountain Geology*, **19**, 9-24.
- Monty, C.L.V. 1965. Geological and environmental significance of Cyanophyta. PhD, Princeton University.
- Monty, C.L.V. 1973. Precambrian background and Phanerozoic history of stromatolitic communities, an overview. *Ann. Soc. Geol. Belg*, **96**, 585-624.

- Monty, C.L.V. 1976. The Origin and Development of Cryptalgal Fabrics. *In*: Walter, M.R. (ed.) *Stromatolites*. Elsevier, Amsterdam, Developments in Sedimentology, **20**, 193-249.
- Monty, C.L.V. & Hardie, L.A. 1976. The geological significance of the freshwater blue-green algal calcareous marsh. *Developments in Sedimentology*, **20**, 447-477.
- Monty, C.L.V. & Mas, J.R. 1981. Lower Cretaceous (Wealdian) blue-green algal deposits of the province of Valencia, eastern Spain. *In*: Monty, C.L.V. (ed.) *Phanerozoic stromatolites*. Kluwer Academic Publishers, Dordrecht, 3-29.
- Moore, L.S. 1993. The modern microbialites of Lake Clifton, south-western Australia. PhD, University of Western Australia, 266 pp.
- Moore, L.S. & Burne, R.V. 1994. The modern thrombolites of Lake Clifton, western Australia. *In*: Bertrand-Safati, J. & Monty, C. (eds.) *Phanerozoic stromatolites II*. Springer, 3-29.
- Moreira, J.L.P., Madeira, C.V., Gil, J.A. & Machado, M.P. 2007. Bacia de Santos. *Boletim de Geociencias da Petrobras, Rio de Janeiro*, **15**, 531-549.
- Morter, A.A. 1978. Weald Clay Mollusca. *In*: Worsam, B.C. (ed.) *The stratigraphy of the Weald Clay*. Rep. Inst. geol. Sci., **78**, 19-23.
- Morter, A.A. 1984. Purbeck-Wealden Beds Mollusca and their relationship to ostracod biostratigraphy, stratigraphical correlation and palaeoecology in the Weald and adjacent areas. *Proceedings of the Geologists' Association*, **95**, 217-234.
- Mortimer, C.H. 2004. Lake Michigan in motion: Responses of an inland sea to weather, earth-spin, and human activities. University of Wisconsin Press, Madison, Wisconsin, USA, 304 pp.
- Mortimer, C.H. & Fee, E.J. 1976. Free surface oscillations and tides of Lakes Michigan and Superior. *Philosophical Transactions of the Royal Society of London*, **281**, 1-61.
- Moulin, M., Aslanian, D. & Unternehr, P. 2010. A new starting point for the South and Equatorial Atlantic Ocean. *Earth-Science Reviews*, **98**, 1-37.
- Müller, G. 1962. Zur Geochemie des Strontiums in Ozeanen Evaporiten unter besonderer Berücksichtigung der sedimentären Coelestinlagerstätten von Hemmelte-West (Süd-Oldenburg). *Geologie, Supplement* **35**.
- Müller, G. & Puchelt, H. 1961. Die Bildung von Cölestin (SrSO<sub>4</sub>) aus Meerwasser. *Naturwissenschaften*, **48**, 301-302.
- Multer, H.G. & Hoffmeister, J.E. 1968. Subaerial laminated crusts of the Florida Keys. *Geological Society of America Bulletin*, **79**, 183-192.
- Murdoch, J. & Webb, R.W. 1940. Notes on some minerals from southern California. *American Mineralogist*, **25**, 549-555.
- Murray, R.C. 1964. Origin and diagenesis of gypsum and anhydrite. *Journal of Sedimentary Research*, **34**, 512-523.
- Needham, J.E. 2011. Forests of the dinosaurs, Wiltshire's Jurassic Finale. Hobnob Press, 222 pp.
- Nelson, S. 2014. Interference Phenomena, Compensation, and Optic Sign. [http://www.tulane.edu/~sanelson/eens211/interference\\_of\\_light.htm](http://www.tulane.edu/~sanelson/eens211/interference_of_light.htm).
- Neumann, A.C. 1985. Reef response to sea level rise: keep-up, catch-up or give-up. *Fifth International Coral Reef Congress, Tahiti*, 105-110.
- Newell, A.J. 2000. Fault activity and sedimentation in a marine rift basin (Upper Jurassic, Wessex Basin, UK). *Journal of the Geological Society*, **157**, 83-92.

- Norman, D.B. & Barrett, P.M. 2002. Ornithischian dinosaurs from the Lower Cretaceous (Berriasian) of England. *In: Milner, A.R. & Batten, D.J. (eds.) Life and environments in Purbeck times*. The Palaeontological Association, Special Papers in Palaeontology, **68**, 161-190.
- Norris, G. 1969. Miospores from the Purbeck Beds and marine Upper Jurassic of southern England. *Palaeontology*, **12**, 574-620.
- Norris, G. 1970. Palynology of the Jurassic-cretaceous boundary in southern England. *Geoscience and Man*, **1**, 57-65.
- Norvick, M.S. & Schaller, H. 1998. The post-rift paleogeographic evolution of the South Atlantic basins of Brazil and west Africa and the influence of hinterland uplift on drainage and sedimentary depocenters. *AAPG international conference/exhibition*. AAPG, Rio de Janeiro, Brazil, 36-37.
- O'Beirne, E. 2011. Pore systems in Mesozoic microbialites: An analogue study from the Purbeck Formation, Dorset, southern England. MSc, Royal Holloway University of London, 64 pp.
- Oertli, H.J. 1964. The Venice System for the classification of marine waters according to salinity. *Pubblicazioni della Stazione Zoologica di Napoli*, **33 (supplement)**, 611.
- Olaussen, S. 1981. Formation of celestite in the Wenlock, Oslo region Norway-evidence for evaporitic depositional environments. *Journal of Sedimentary Research*, **51**.
- Paik, I.S. 2005. The oldest record of microbial-caddisfly bioherms from the Early Cretaceous Jinju Formation, Korea: occurrence and palaeoenvironmental implications. *Palaeogeography, Palaeoclimatology, Palaeoecology*, **218**, 301-315.
- Peacock, D.C.P. & Sanderson, D.J. 1991. Displacements, segment linkage and relay ramps in normal fault zones. *Journal of Structural Geology*, **13**, 721-733.
- Peacock, D.C.P. & Sanderson, D.J. 1994. Geometry and development of relay ramps in normal fault systems. *AAPG Bulletin*, **78**, 147-165.
- Pedley, H.M. 1990. Classification and environmental models of cool freshwater tufas. *Sedimentary Geology*, **68**, 143-154.
- Pen, L. & Green, J. 1983. Botanical exploration and vegetational changes on Rottnest Island. *Journal of the Royal Society of Western Australia*.
- Pentecost, A. 1988. Growth and calcification of the cyanobacterium *Homoeothrix* crustacea. *Microbiology*, **134**, 2665-2671.
- Pentecost, A. 1991. Calcification processes in algae and cyanobacteria. *In: Riding, R.E. (ed.) Calcareous algae and stromatolites*. Springer-Verlag, 3-20.
- Perry, C.T. 1994. Freshwater tufa stromatolites in the basal Purbeck Formation (Upper Jurassic), Isle of Portland, Dorset. *Geological Journal*, **29**, 119-135.
- Philippe, M. & Bamford, M.K. 2008. A key to morphogenera used for Mesozoic conifer-like woods. *Review of Palaeobotany and Palynology*, **148**, 184-207.
- Philippe, M., Billon-Bruyat, J.P., Garcia-Ramos, J.C., Bocat, L., Gomez, B. & Piñuela, L. 2010. New occurrences of the wood *Protocupressinoxylon purbeckensis* Francis: implications for terrestrial biomes in southwestern Europe at the Jurassic/Cretaceous boundary. *Palaeontology*, **53**, 201-214.
- Phillips, P. 2013. Clotted Life and Brittle Waters. *Landscapes: the Journal of the International Centre for Landscape and Language*, **3**, 1-20.

- Phillips, W.J. 1964. The structures in the Jurassic and Cretaceous rocks on the Dorset coast between White Nothe and Mupe Bay. *Proceedings of the Geologists' Association*, **75**, 373-405.
- Platt, N.H. & Wright, V.P. 1991. Lacustrine carbonates: facies models, facies distributions and hydrocarbon aspects. *In: Anadón, P., Cabrera, L. & Kelts, K. (eds.) Lacustrine facies analysis*, Special publication association of sedimentologists, **13**, 57 - 74.
- Playford, P.E. 1988. Guidebook to the geology of Rottneest Island. Geological Society of Australia, WA Division and the Geological Survey of Western Australia, 75 pp.
- Poncet, J. 1984. Microfabric and origin of Cambrian carbonate ooids—examples from the Cambrian oolite of Carteret (Northeastern Armorican Massif, France). *Sedimentary Geology*, **39**, 273-280.
- Popp, B.N. & Wilkinson, B.H. 1983. Holocene lacustrine ooids from Pyramid Lake, Nevada. *In: Peryt, T.M. (ed.) Coated grains*. Springer-Verlag, Berlin, 142-153.
- Posamentier, H. 1988. Eustatic controls on clastic deposition II—sequence and systems tract models.
- Post, F.J. 1977. The microbial ecology of the Great Salt Lake. *Microbial Ecology*, **3**, 143-165.
- Prothero, D.R. 2013. Bringing fossils to life: An introduction to paleobiology. Third Edition ed. Columbia University Press, 672 pp.
- Pugh, M.E. 1968. Algae from the Lower Purbeck limestones of Dorset. *Proceedings of the Geologists' Association*, **79**, 513-523.
- Quine, M. & Bosence, D. 1991. Stratal geometries, facies and sea-floor erosion in Upper Cretaceous Chalk, Normandy, France. *Sedimentology*, **38**, 1113-1152.
- Radley, J.D. 2002. Distribution and palaeoenvironmental significance of molluscs in the Late Jurassic-Early Cretaceous Purbeck Formation of Dorset, southern England: a review. *In: Milner, A.R. & Batten, D.J. (eds.) Life and environments in Purbeck times*. The Palaeontological Association, Special Papers in Palaeontology, **68**, 41-52.
- Radoičić, R. 1960. Microfaciès du Crétacé et du Paléogène des Dinarides externes de Yougoslavie. *Paléont. Dinarides Yougoslaves, Crna Gora*, 172 pp.
- Ramsay, J.G. & Huber, M.I. 1987. The techniques of modern structural geology. Academic Pr., **2** (2), London, 307 pp.
- Reijers, T.J.A. & Ten Have, A.H.M. 1983. Ooid zonation as indication for environmental conditions in a Givetian-Frasnian carbonate shelf-slope transition. *In: Peryt, T.M. (ed.) Coated Grains*. Springer-Verlag, 188-198.
- Reitner, J., Paul, J., Arp, G. & Hause-Reitner, D. 1996. *Lake Thetis domal microbialites - a complex framework of calcified biofilms and organomicrites (Cervantes, Western Australia)*. *Göttiger Arb. Geol. Paläont*, **Sb2**, 85-89.
- Renaut, R.W., Morley, C.K. & Jones, B. 2002. Fossil hot-spring travertine in the Turkana Basin, northern Kenya: structure, facies, and genesis. *In: Renaut, R.W. & Ashley, G.M. (eds.) Sedimentation in continental rifts*. SEPM, Special publication, **73**, 123-141.
- Retallack, G. 1981. Comment and Reply on "Reinterpretation of the depositional environment of the Yellowstone fossil forests". *Geology*, **9**, 52-53.
- Retallack, G.J. 2001. Soils of the past: an introduction to paleopedology. Second Edition ed. Blackwell, 404 pp.



- Richter, D.K. 1983. Calcareous ooids: a synopsis. *In: Peryt, T.M. (ed.) Coated grains*. Springer-Verlag, 71-99.
- Riding, R. 1977. Skeletal stromatolites. *In: Flügel, E. (ed.) Fossil Algae*. Springer-Verlag, 57-60.
- Riding, R. 1991. Calcareous algae and stromatolites. Springer-Verlag, 571 pp.
- Riding, R. 2006. Microbial carbonate abundance compared with fluctuations in metazoan diversity over geological time. *Sedimentary Geology*, **185**, 229-238.
- Riding, R. 2011a. Microbialites, stromatolites, and thrombolites. *In: Reitner, J. & Thiel, V. (eds.) Encyclopedia of Geobiology*. Springer, Heidelberg, Encyclopedia of Earth Science Series, 635-654.
- Riding, R. 2011b. The nature of stromatolites: 3,500 million years of history and a century of research. *In: Reitner, J., Quéric, N.-V. & Arp, G. (eds.) Advances in Stromatolite Geobiology*. Springer, Lecture Notes in Earth Sciences, **131**, 29-74.
- Riding, R. & Awramik, S.M. 2000. Microbial sediments. Springer, 331 pp.
- Riding, R. & Wright, V.P. 1981. Paleosols and tidal-flat/lagoon sequences on a Carboniferous carbonate shelf: sedimentary associations of triple disconformities. *Journal of Sedimentary Petrology*, **51**, 1323-1339.
- Roda, C. 1965. Livelli e struttura grumosa e livelli ad ooliti rotte e rigenerate nel calcare miocenico del M. Alpi (Potenza). *Geol. Romania*, **4**, 181-220.
- Rusnak, G.A. 1960a. Sediments of Laguna Madre, Texas. *In: Shepard, F.P., Phleger, F.B. & Van Andel, T.H. (eds.) Recent sediments: Northwest Gulf of Mexico*. AAPG, Tulsa, 153-196.
- Rusnak, G.A. 1960b. Some observations of recent oolites. *Journal of Sedimentary Research*, **30**, 471-480.
- Sager, P.E., Richman, S., Harris, H.J. & Fewless, G. 1985. Preliminary observations on the seiche-induced flux of carbon, nitrogen and phosphorus in a Great Lakes coastal marsh. *In: Prince, H.H. & D'Itri, F.M. (eds.) Coastal Wetlands*. Lewis Publishers, Chelsea, Michigan, USA, 59-65.
- Salisbury, S.W. 2002. Crocodilians from the Lower Cretaceous (Berriasian) Purbeck Limestone Group of Dorset, southern England. *In: Milner, A.R. & Batten, D.J. (eds.) Life and environments in Purbeck times*. The Palaeontological Association, Special Papers in Palaeontology, **68**, 121-144.
- Saller, A. 2015. Pre-salt lacustrine sedimentation in the deepwater Kwanza Basin, Angola. *15th Bathurst Meeting*, University of Edinburgh, U.K., Abstract book.
- Saller, A., Rushton, S., Buambua, L., Inman, K., McNeil, R. & Dickson, J.T. 2016. Presalt stratigraphy and depositional systems in the Kwanza Basin, offshore Angola. *AAPG Bulletin*, **100**, 1135-1164.
- Samankassou, E., Tresch, J. & Strasser, A. 2005. Origin of peloids in Early Cretaceous deposits, Dorset, South England. *Facies*, **51**, 264-274.
- Sandberg, P.A. 1975. New interpretations of Great Salt Lake ooids and of ancient non-skeletal carbonate mineralogy. *Sedimentology*, **22**, 497-537.
- Sandberg, P.A. 1983. An oscillating trend in Phanerozoic non-skeletal carbonate mineralogy. *Nature*, **305**, 19-22.

- Sanz, M.E., Rodríguez-Aranda, J.P., Calvo, J.P. & Ordóñez, S. 1994. Tertiary detrital gypsum in the Madrid Basin, Spain: criteria for interpreting detrital gypsum in continental evaporitic sequences. *Sedimentology and Geochemistry of Modern and Ancient Saline Lakes, SEPM Special publication*, **50**, 217-228.
- Sarg, J. 1988. Carbonate sequence stratigraphy. In: Wilgus, C.K., Hastings, B.S., Kendall, C.G.S.C., Posamentier, H.W., Ross, C.A. & Van Wagoner, J.C. (eds.) *Sea Level Changes — An Integrated Approach, Special Publication*. SEPM, **42**, 155-181.
- Sarg, J., Suriamin, Tānavsuu-Milkeviciene, K. & Humphrey, J.D. 2013. Lithofacies, stable isotopic composition, and stratigraphic evolution of microbial and associated carbonates, Green River Formation (Eocene), Piceance Basin, Colorado. *AAPG Bulletin*, **97**, 1937-1966.
- Schlische, R.W. 1991. Half-graben filling models: Implications for the evolution of continental extensional basins. *Basin Research*, **3**, 123-141.
- Schnyder, J., Deconinck, J.-F., Baudin, F., Colombié, C., Du Chêne, R.J., Gardin, S., Galbrun, B. & De Rafélis, M. 2012. Purbeck beds (Late Jurassic) in the Phare de Chassiron section (Île d'Oléron, NW Aquitaine Basin, France): Refined age-assignment and long-term depositional sequences. *Geobios*, **45**, 485-499.
- Scholle, P.A., Stemmerik, L. & Harpoth, O. 1990. Origin of major karst-associated celestite mineralization in Karstryggen, central East Greenland. *Journal of Sedimentary Petrology*, **60**, 397-410.
- Scholle, P.A. & Ulmer-Scholle, D.S. 2003. A Color Guide to the Petrography of Carbonate Rocks: Grains, Textures, Porosity, Diagenesis, AAPG Memoir 77. AAPG, Tulsa, Oklahoma, USA, 459 pp.
- Schönfeld, M. 1979. Stratigraphische, fazielle, paläogeographische und tektonische Untersuchungen im Oberen Malm des Deisters, Osterwaldes und Süntels (NW-Deutschland). *Clausthaler Geologische Abhandlungen*, **35**, 1-270.
- Schreiber, B.C. & Walker, D. 1992. Halite pseudomorphs after gypsum: a suggested mechanism. *Journal of Sedimentary Research*, **62**.
- Schudack, U. 1994. Revision, Dokumentation und Stratigraphie der Ostracoden des nordwestdeutschen Oberjura und Unter-Berriasium. *Berliner Geowissenschaftliche Abhandlungen, Reihe E, Paläobiologie*, **11**, 1-193.
- Scott, J.J., Renaut, R.W., Buatois, L.A. & Owen, R.B. 2009. Biogenic structures in exhumed surfaces around saline lakes: an example from Lake Bogoria, Kenya Rift Valley. *Palaeogeography, Palaeoclimatology, Palaeoecology*, **272**, 176-198.
- Seilacher, A. 2007. Trace fossil analysis. Springer, Heildeberg, 226 pp.
- Sellwood, B.W. & Wilson, R.C.L. 1990. Field Guide No.7: Jurassic sedimentary environments of the Wessex Basin. BSRG. Cambridge.
- Shearman, D.J. 1966. Origin of marine evaporites by diagenesis. *Trans. Inst. Min. Metall*, **75**, 208-215.
- Shigwedha, P. 2014. Syn-rift setting of Jurassic rocks within the Wessex Basin (Bournemouth Bay, southern England). MSc, Royal Holloway University of London, 114 pp.
- Siever, R. 1962. Silica solubility, 0-200°C, and the diagenesis of siliceous sediments. *The Journal of Geology*, **70**, 127-150.

- Sladen, C.P. & Batten, D.J. 1984. Source-area environments of Late Jurassic and Early Cretaceous sediments in southeast England. *Proceedings of the Geologists' Association*, **95**, 149-163.
- Sloss, L.L., Krumbein, W.E. & Dapples, E.C. 1949. Integrated facies analysis. *Sedimentary facies in geologic history: conference at meeting of the Geological Society of America held in New York, New York, November 11, 1948*, Geological Society of America Memoir, **39**, 91-124.
- Smith, C. & Hatton, I.R. 1998. Inversion tectonics in the Lyme Bay-West Dorset area of the Wessex Basin, UK. In: Underhill, J.R. (ed.) *The Development, evolution and petroleum geology of the Wessex Basin*. Geological Society, London, London, Geological Society Special Publications, **133**, 267-282.
- Smith, V.H., Tilman, G.D. and Nekola, J.C. 1999. Eutrophication: impacts of excess nutrient inputs on freshwater, marine, and terrestrial ecosystems. *Environmental pollution*, **100**, 179-196.
- Soil Survey Staff. 1975. Soil Taxonomy: A basic system of soil classification for making and interpreting soil surveys. US Department of Agriculture, Soil Conservation Service.
- Sonnenfeld, M.D. 1996. Sequence evolution and hierarchy within the lower Mississippian Madison Limestone of Wyoming. In: Longamn, M.W. & Sonnenfeld, M.D. (eds.) *Paleozoic systems of the Rocky Mountain region*. Rocky Mountain Section (SEPM), Tulsa, Oklahoma, 1-28.
- Sorby, H.C. 1879. The structure and origin of limestones. *Proc. Geol. Soc. London*, **35**, 56-95.
- Sowerby, J.d.C. 1836. Appendix A, Descriptive notes respecting the shells figured in plates 11–23. In: Fitton, W.H. (ed.) *Observations on Some of the Strata Between the Chalk and the Oxford Oolite in the South– East of England* Transactions Geological Society London, **2**, 103-390.
- Spath, L.F. 1931. On the contemporaneity of certain ammonite beds in England and France. *Geological Magazine*, **68**, 182-186.
- Stoneley, R. 1982. The structural development of the Wessex Basin. *Journal of the Geological Society*, **139**, 543-554.
- Stoneley, R. & Selley, R.C. 1986. A field guide to the Petroleum Geology of the Wessex Basin, London.
- Strahan, A. 1898. The Geology of the Isle of Purbeck and Weymouth, 278 pp.
- Strasser, A. 1984. Black-pebble occurrence and genesis in Holocene carbonate sediments (Florida Keys, Bahamas, and Tunisia). *Journal of Sedimentary Petrology*, **54**, 1097-1109.
- Strasser, A. 1986. Ooids in Purbeck limestones (lowermost Cretaceous) of the Swiss and French Jura. *Sedimentology*, **33**, 711-727.
- Strasser, A. 1988. Shallowing-upward sequences in Purbeckian peritidal carbonates (lowermost Cretaceous, Swiss and French Jura Mountains). *Sedimentology*, **35**, 369-383.
- Strasser, A. 1994. Milankovitch Cyclicity and High-Resolution Sequence Stratigraphy in Lagoonal–Peritidal Carbonates (Upper Tithonian–Lower Berriasian, French Jura Mountains). In: de Boer, P.L. & Smith, D.G. (eds.) *Orbital Forcing and Cyclic Sequences*. Blackwell Publishing Ltd., 285-301.

- Strasser, A. & Davaud, E. 1983. Black pebbles of the Purbeckian (Swiss and French Jura): lithology, geochemistry and origin. *Ecolgae Geologicae Helvetiae*, **76**, 551-580.
- Strasser, A., Pittet, B., Hillgärtner, H. & Pasquier, J.-B. 1999. Depositional sequences in shallow carbonate-dominated sedimentary systems: concepts for a high-resolution analysis. *Sedimentary Geology*, **128**, 201-221.
- Surdam, R.C. & Wray, J.L. 1976. Lacustrine Stromatolites, Eocene Green River Formation, Wyoming. In: Walter, E. (ed.) *Stromatolites*. Elsevier, Amsterdam, Developments in Sedimentology, **20**, 535-541.
- Sylvester-Bradley, P.C. 1940. The Purbeck Beds of Swindon. *Proceedings of the Geologists' Association*, **51**, 349-372.
- Taberner, C., Marshall, J.D., Hendry, J.P., Pierre, C. & Thirlwall, M.F. 2002. Celestite formation, bacterial sulphate reduction and carbonate cementation of Eocene reefs and basinal sediments (Igalada, NE Spain). *Sedimentology*, **49**, 171-190.
- Talbot, M.R. 1990. A review of the palaeohydrological interpretation of carbon and oxygen isotopic ratios in primary lacustrine carbonates. *Chemical Geology: Isotope Geoscience Section*, **80**, 261-279.
- Talbot, M.R. & Allen, P.A. 1996. Lakes. In: Reading, H.G. (ed.) *Sedimentary Environments: Processes, Facies and Stratigraphy* Blackwell Publishing, Oxford, 83-124.
- Tänavsuu-Milkeviciene, K. & Sarg, J.F. 2012. Evolution of an organic-rich lake basin - stratigraphy, climate and tectonics: Piceance Creek basin, Eocene Green River Formation. *Sedimentology*, **59**, 1735-1768.
- Tänavsuu-Milkeviciene, K., Sarg, J.F., Feng, J., Huang, S. & Bartov, Y. 2012. Sequence stratigraphy, climate, and organic-richness: Green River Formation, Lake Uinta, Colorado. In: AAPG (ed.) *AAPG Annual Convention and Exhibition*. AAPG, Long Beach, California.
- Tominaga, M. & Sager, W.W. 2010. Revised Pacific M-anomaly geomagnetic polarity timescale. *Geophysical Journal International*, **182**, 203-232.
- Townsend, W.N. 1973. An introduction to the scientific study of the soil. Edward Arnold Ltd., 299 pp.
- Townson, W.G. 1971. Facies analysis of the Portland Beds. PhD, University of Oxford, 575 pp.
- Townson, W.G. 1975. Lithostratigraphy and deposition of the type Portlandian. *Journal of the Geological Society*, **131**, 619-638.
- Townson, W.G. & Wimbledon, W.A. 1979. The Portlandian strata of the Bas Boulonnais, France. *Proceedings of the Geologists' Association*, **90**, 81-91.
- Trebitz, A.S. 2006. Characterizing seiche and tide-driven daily water level fluctuations affecting coastal ecosystems of the Great Lakes. *Journal of Great Lakes Research*, **32**, 102-116.
- Trudgill, B.D. 2002. Structural controls on drainage development in the Canyonlands grabens of southeast Utah. *AAPG Bulletin*, **86**, 1095-1112.
- Tucker, M. 2003. Sedimentary rocks in the field. Third Edition ed. John Wiley & Sons, 234 pp.
- Tucker, M. & Wright, P. 1990. Carbonate Sedimentology. Blackwell Science, 482 pp.
- Uchman, A. & Álvaro, J.J. 2000. Non-marine invertebrate trace fossils from the Tertiary Calatayud-Teruel Basin, NE Spain. *Revista Española de Paleontología*, **15**, 203-218.

- Underhill, J.R. 1998. Development, evolution and petroleum geology of the Wessex Basin. Geological Society of London, 420 pp.
- Underhill, J.R. 2002. Evidence for structural controls on the deposition of the Late Jurassic-Early Cretaceous Purbeck limestone group, Dorset, southern England. *In: Milner, A.R. & Batten, D.J. (eds.) Life and environments in Purbeck times.* Palaeontological Association, London, Special Papers in Palaeontology, **68**, 21-40.
- Underhill, J.R. & Paterson, S. 1998. Genesis of tectonic inversion structures: seismic evidence for the development of key structures along the Purbeck–Isle of Wight Disturbance. *Journal of the Geological Society*, **155**, 975-992.
- Underhill, J.R. & Stoneley, R. 1998. Introduction to the development, evolution and petroleum geology of the Wessex Basin. *In: Underhill, J.R. (ed.) The development, evolution and petroleum geology of the Wessex Basin.* Geological Society, London, Special Publications, **133**, 1-18.
- Vail, P. 1987. Seismic stratigraphy interpretation using sequence stratigraphy: Part 1: Seismic stratigraphy interpretation procedure. *In: Bally, A.W. (ed.) Atlas of Seismic Stratigraphy.* AAPG, **27**, 1-10.
- Vail, P., Hardenbol, J. & Todd, R. 1984. Jurassic unconformities, chronostratigraphy, and sea-level changes from seismic stratigraphy and biostratigraphy.
- Vakhrameev, V.A. 1970. Range and paleoecology of Mesozoic conifers, the Cheirolepidiaceae. *Paleontological Journal*, **4**, 12-24.
- Van Wagoner, J.C. 1995. Overview of sequence stratigraphy of foreland basin deposits: terminology, summary of papers, and glossary of sequence stratigraphy. *In: Van Wagoner, J.C. & Bertram, G.T. (eds.) Sequence stratigraphy of foreland basin deposits,* American Association of Petroleum Geologists Memoir, **64**, 9-21.
- Vasconcelos, C. & McKenzie, J.A. 1997. Microbial mediation of modern dolomite precipitation and diagenesis under anoxic conditions (Lagoa Vermelha, Rio de Janeiro, Brazil). *Journal of Sedimentary Research*, **67**, 378-390.
- Veeken, P.C.H. 2008. Seismic Stratigraphy, basin analysis and reservoir characterisation, Amsterdam, 509 pp.
- Virtualtourist.com 2011. Rottnest Island. <http://members.virtualtourist.com/m/pb/1c8a45/>
- Vogwill, R. 2012. Does water chemistry control structure of microbial assemblages and depositional products? *Symposium on research and conservation: south west Western Australia's microbialites*, Kensington, Western Australia.
- Vologdin, A.G. 1962. The oldest algae of the USSR. Publishing House of the USSR Academy of Sciences, Moscow, 656 pp.
- Walcott, C.D. 1914. Cambrian Geology and Paleontology: Dikelocephalus and Other Genera of the Dikelocephalinae. *Smithsonian Misc. Coll.*, **57**, 345-411.
- Walker, R.G. 1979. Facies models. Geological Association of Canada, Ontario, Canada, 211 pp.
- Walter, M.R. 1976. Stromatolites. Elsevier, 790 pp.
- Ward, W.C., Folk, R.L. & Wilson, J.L. 1970. Blackening of eolianite and caliche adjacent to saline lakes, Isla Mujeres, Quintana Roo, Mexico. *Journal of Sedimentary Petrology*, **40**, 548-555.

- Warren, J.K. 2006. *Evaporites: sediments, resources and hydrocarbons*. Springer, 1035 pp.
- Webster, T. 1826. IV—Observations on the Purbeck and Portland Beds. *Transactions of the Geological Society of London*, **1**, 37-44.
- Wentworth, C.K. 1922. A scale of grade and class terms for clastic sediments. *The Journal of Geology*, **30**, 377-392.
- Wernicke, B. 1985. Uniform-sense normal simple shear of the continental lithosphere. *Canadian Journal of Earth Sciences*, **22**, 108-125.
- West, I.M. 1960. On the occurrence of celestine in the Caps and Broken Beds at Durlston Head, Dorset. *Proceedings of the Geologists' Association*, **71**, 391-401.
- West, I.M. 1961. Lower Purbeck beds of Swindon facies in Dorset. *Nature*, **190**, 526.
- West, I.M. 1964. Deformation of the incompetent beds in the Purbeck Anticline. *Geological Magazine*, **101**, 373-373.
- West, I.M. 1973. Vanished evaporites - significance of strontium minerals. *Journal of Sedimentary Research*, **43**, 278-279.
- West, I.M. 1975. Evaporites and associated sediments of the basal Purbeck Formation (Upper Jurassic) of Dorset. *Proceedings of the Geologists' Association*, **86**, 205-225.
- West, I.M. 1979. Sedimentary environments and diagenesis of Purbeck strata (Upper Jurassic-Lower Cretaceous) of Dorset UK. PhD, Southampton University, 181 pp.
- West, I.M. 1992. Contribution on Purbeck Group. In: Cope, J.C.W., Ingham, J.K. & Rawson, P.F. (eds.) *Atlas of Palaeogeography and Lithofacies*. Geological Society of London, London, 124-126.
- West, I.M. 2013a. Purbeck Formation - Facies and Palaeoenvironments. <http://www.southampton.ac.uk/~imw/purbfac.htm>
- West, I.M. 2013b. The Purbeck Formation of Southern England; Sedimentology of Evaporites: Geology of the Wessex Coast. <http://www.southampton.ac.uk/~imw/Purbeck-evaporites.htm>
- West, I.M. 2013c. Ringstead Bay to White Nothe: Geology of the Wessex Coast (Jurassic Coast, Dorset and East Devon World Heritage Site). <http://www.southampton.ac.uk/~imw/Ringstead-White-Nothe.htm>.
- West, I.M. 2016. Geology of the Wessex Coast (including the UNESCO World Heritage Jurassic Coast and the Isle of Wight and part of East Devon). <http://www.southampton.ac.uk/~imw/index.htm>
- West, I.M., Barton, D. & Codd, J. 2013. Ridgeway Railway Cutting and Weymouth Relief Road Cuttings, Dorset, UK. <http://www.southampton.ac.uk/~imw/Ridgeway-Railway-Cutting.htm>
- Westhead, R.K. & Mather, A.E. 1996. An updated lithostratigraphy for the Purbeck Limestone Group in the Dorset type-area. *Proceedings of the Geologists' Association*, **107**, 117-128.
- Wilkinson, B.H., Pope, B.N. & Owen, R.M. 1980. Nearshore ooid formation in a modern temperate region marl lake. *The Journal of Geology*, **88**, 697-704.
- Wilson, J.L. 1967. Cyclic and reciprocal sedimentation in Virgilian strata of southern New Mexico. *Bulletin of the Geological Society of America*, **78**, 805-818.

- Wilson, M.E.J., Bosence, D.W.J. & Limbong, A. 2000. Tertiary syntectonic carbonate platform development in Indonesia. *Sedimentology*, **47**, 395-419.
- Wimbledon, W.A. & Hunt, C.O. 1983. The Portland-Purbeck junction (Portlandian-Berriasian) in the Weald, and correlation of latest Jurassic-early Cretaceous rocks in southern England. *Geological Magazine*, **120**, 267-280.
- Wimbledon, W.A.P. 2008. The Jurassic-Cretaceous boundary: an age-old correlative enigma. *Episodes*, **31**, 423-428.
- Withjack, M.O., Schlische, R.W. & Olsen, P.E. 2002. Rift-basin structure and its influence on sedimentary systems. In: R., R. & M., A.G. (eds.) *Sedimentation in continental rifts*. SEPM Special Publication, Tulsa, Oklahoma, USA, **73**, 57-81.
- Wolf, K.H. 1965. 'Grain-diminution' of algal colonies to micrite. *Journal of Sedimentary Research*, **35**, 420-427.
- Wood, M.W. & Shaw, H.F. 1976. The geochemistry of celestites from the Yate area near Bristol (UK). *Chemical Geology*, **17**, 179-193.
- Woodruff, S.L., House, W.A., Callow, M.E. & Leadbeater, B.S.C. 1999. The Effects of a Developing Biofilm on Chemical Changes across the Sediment-Water Interface in a Freshwater Environment. *International review of hydrobiology*, **84**, 509-532.
- Woodward, H.B. 1895. The Jurassic Rocks of Britain vol. 5. HM Stationery Office, London, 499 pp.
- Woodward, J.M.D. 1729. An attempt towards a natural history of the fossils of England: in a catalogue of the English fossils in the collection of J. Woodward. Longman, London, 637 pp.
- Wray, J.L. 1977. Calcareous algae. Elsevier, 185 pp.
- Wright, D.T. 1999. The role of sulphate-reducing bacteria and cyanobacteria in dolomite formation in distal ephemeral lakes of the Coorong region, South Australia. *Sedimentary Geology*, **126**, 147-157.
- Wright, D.T. & Wacey, D. 2005. Precipitation of dolomite using sulphate-reducing bacteria from the Coorong Region, South Australia: significance and implications. *Sedimentology*, **52**, 987-1008.
- Wright, V.P. 1990. Lacustrine carbonates. In: Tucker, M. & Wright, P. (eds.) *Carbonate Sedimentology*. Blackwell Science, 164-190.
- Wright, V.P. & Wright, J.M. 1985. A stromatolite built by a *Phormidium*-like alga from the Lower Carboniferous of South Wales. In: Toomey, D.F. & Nitecki, M.H. (eds.) *Paleoalgology: contemporary research and applications*. Springer-Verlag, 40-54.
- Ziegler, P.A. 1981. Evolution of sedimentary basins in north-west Europe. In: L.V., I. & G.P., H. (eds.) *Petroleum geology of the continental shelf of North-West Europe*. Heyden, London, 3-39.
- Ziegler, P.A. 1982. Geological Atlas of Western and Central Europe, Elsevier, Amsterdam, 130 pp.
- Ziegler, P.A., Cloetingh, S. & van Wees, J.-D. 1995. Dynamics of intra-plate compressional deformation: the Alpine foreland and other examples. *Tectonophysics*, **252**, 7-59.

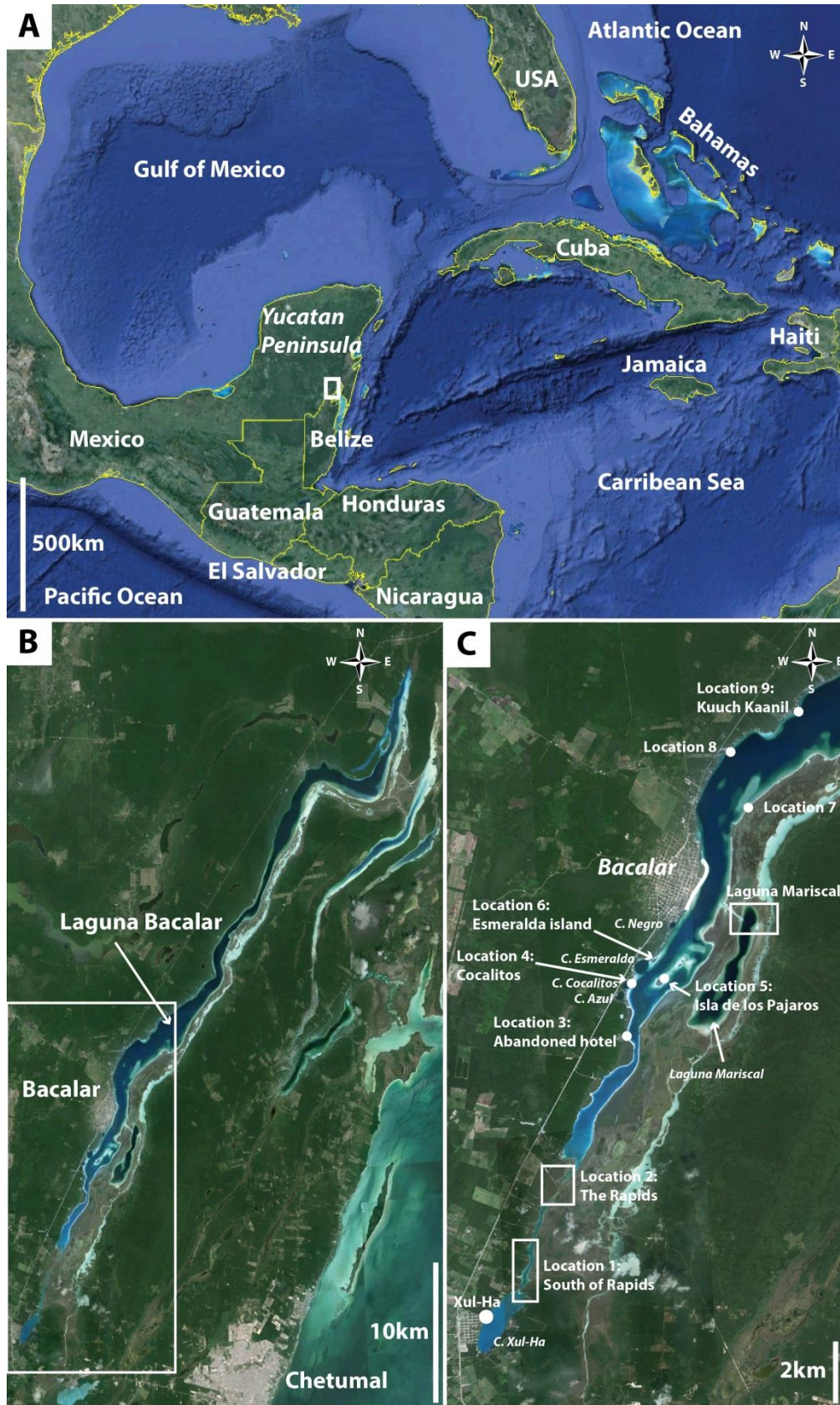
## Appendix 1

Modern analogue: Laguna  
Bacalar, Yucatan Peninsula,  
Quintana Roo, Mexico  
(jointly written with  
Estanislao Kozlowski).



## 1. Introduction

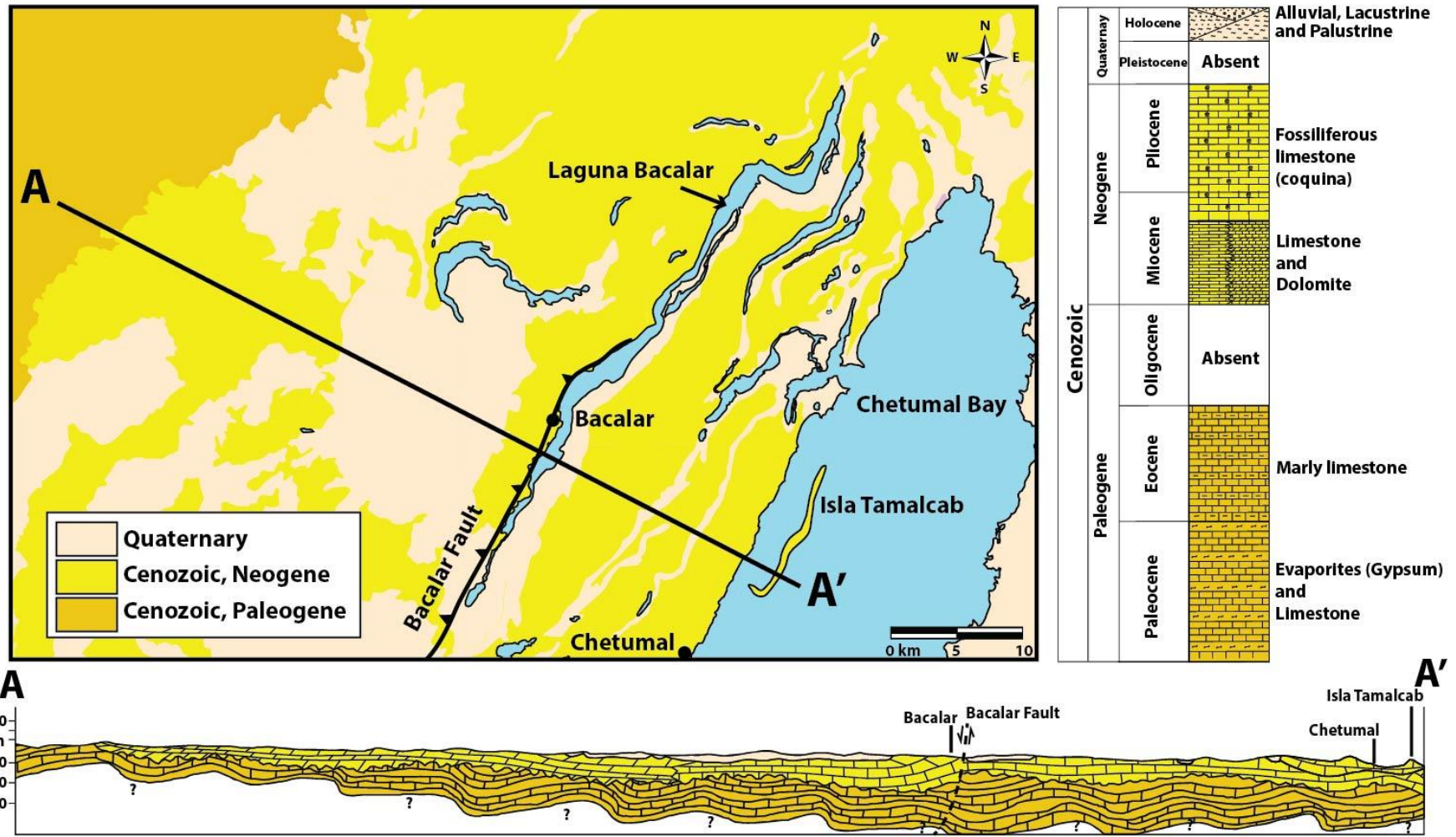
The Laguna Bacalar is a freshwater lake groundwater fed via cenotes about 50 km long and 2 km across at its widest, situated about 1.5 m above sea level with an area of about 3.1 km<sup>2</sup> (Fig. 1B; Castro-Contreras *et al.*, 2014). This lake is located in the south-east of the Yucatan Peninsula in Quintana Roo region in Mexico (Fig. 1). A one week trip was undertaken by the author and Estanislao Kozlowski in March 2015 during which a study of marginal thrombolitic deposits and associated facies was undertaken to characterise the controls on the mounds distribution and the relationship with the inter-mound facies in the Purbeck limestones. During this trip 10 locations were visited mainly on the south-western shore of the lake (Fig. 1C). This appendix aims to 1) describe the different morphologies of the microbial deposits; and 2) to define the controls on the microbial growth and microbial mound shapes, sizes and distribution in this lake. Ultimately these deposits are used as possible modern day lacustrine analogue to better characterise the Purbeck microbial mounds of the Skull, Hard and Soft Cap beds.



**Figure 1** Location maps of the Laguna Bacalar (maps © 2016 GoogleEarth.). A – Regional map that locates Laguna Bacalar in the south-east of the Yucatan Peninsula in Mexico. B – Close-up view of Laguna Bacalar showing the narrow lake. C – Close-up view that locates the places visited during the trip in March 2015.

## 2. Geological context

Laguna Bacalar is located in a lowland carbonate region composed of limestones, dolomites and evaporites that constitute the most extensive karstic area of the North American continent (Marshall, 2006; Perez *et al.*, 2011). The southern part of the Yucatan Peninsula consists of a carbonate platform deposited from the Cretaceous to the Holocene (Perry *et al.*, 2002; Castro-Contreras *et al.*, 2014). Figure 2 shows the surface as well as the main tectonic settings in the south-east of the Yucatan Peninsula around Laguna Bacalar. This lake is located in a faulted basin, bounded to the west by the northern extension of the normal Rio Hondo Fault, the Bacalar Fault (Fig. 2; Kenkmann and Schönian, 2006; Gischler, 2011). Although the tectonic events that led to the origin of such basins are still debated, Lara (1993) demonstrated that distinct tectonic events over the Late Cretaceous to Pliocene during the formation of the Yucatan Basin were responsible for the formation of these faulted basins.



**Figure 2** Geological map, lithostratigraphy and a NW-SE cross-section illustrating the tectonic settings of the south-east region of the Yucatan Peninsula and around the Laguna Bacalar (modified after Lopez *et al.*, 2005).

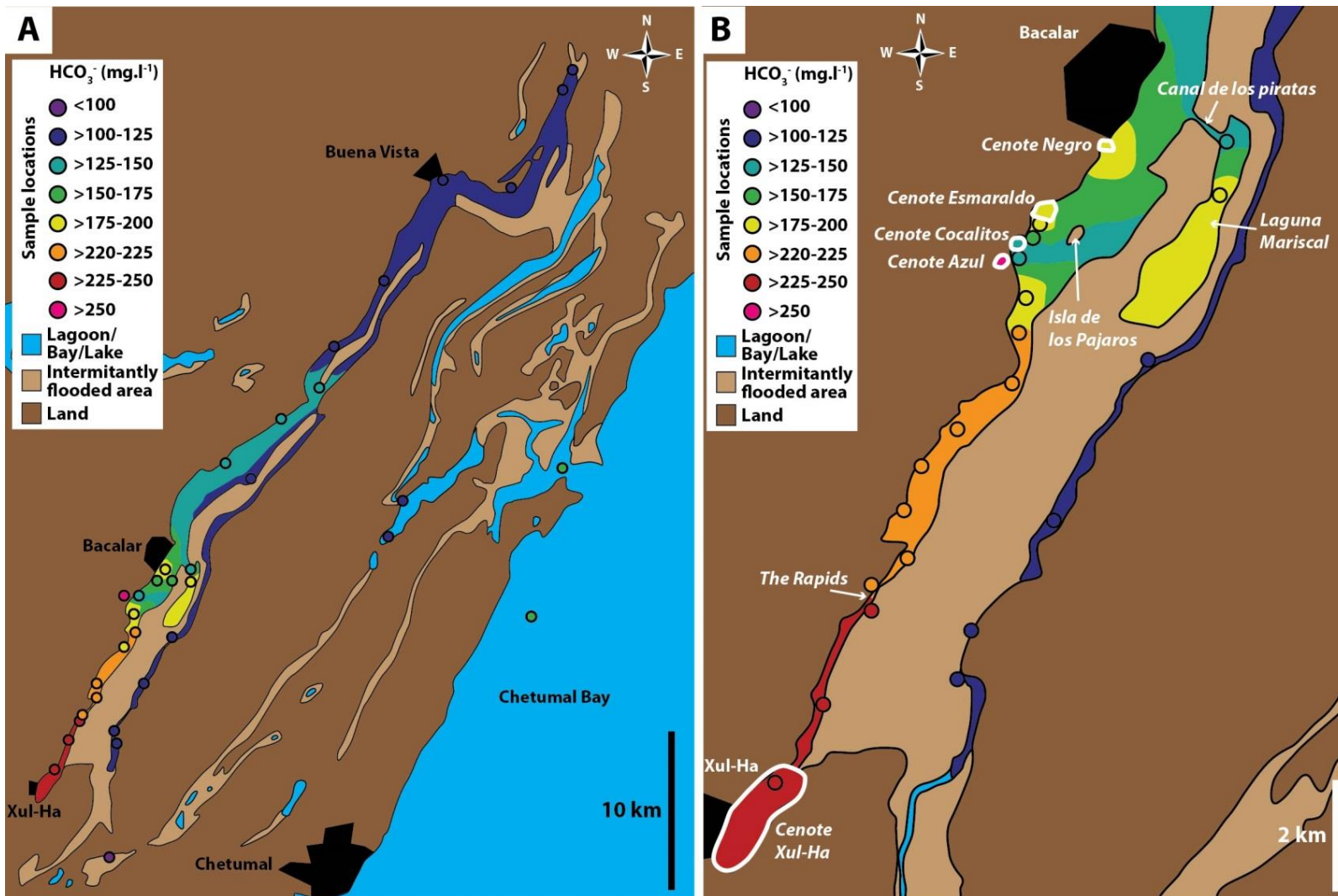
### 3. Lake settings

#### 3.1. Climate, hydrology and water chemistry

The Yucatan Peninsula is located between the Tropic of Cancer and the equator, and in a humid tropical climate zone (Perez *et al.*, 2011). This region has an annual average temperature of 26°C (Perez *et al.*, 2011) and the southern part of the Yucatan Peninsula has a precipitation of more than 3,200 mm per year (Perez *et al.*, 2011).

Despite the high precipitation the water flows in the southern part of the Yucatan Peninsula, where Laguna Bacalar is located, consist mainly of groundwater circulation through an extensive karstic system with large submerged caves and cenotes (Schmitter-Soto *et al.*, 2002; Perry *et al.*, 2003; Suárez-Morales, 2003; Alcocer and Bernal-Brooks, 2010; Perez *et al.*, 2011).

Laguna Bacalar is a freshwater lake and one of the numerous waterbodies that form on the Yucatan Peninsula. This lake is groundwater fed via five cenotes with the main water input via Xul-Ha Cenote to the south (Fig. 3) and four subsidiary cenotes, Azul (although disconnected from the surface circulation), Esmeraldo, Cocalitos and Negro located near the fault trace on the western shore of the lake (Fig. 3). Due to groundwaters flowing through the karstified carbonate rocks, the Laguna Bacalar waters show greater concentrations in carbonate ions (hydrogen-carbonate) than in marine environments even though they have slightly lower calcium concentrations than marine waters (Gischler *et al.*, 2011). Figure 3 show concentrations of carbonate ions measured by Gischler *et al.* in 2008 (Fig. 3A) and 2011 (Fig. 3B) across the lake. They found that the concentrations vary between 104 and 300 mg.l<sup>-1</sup> and Castro-Contreras *et al.* (2014) determined that the pH varies between 7.7 and 8.2. They also determined that concentrations are higher close to the cenotes (Fig. 3) with the highest values in the Cenote Xul-Ha (to the south of the lake) between 200 and 250 mg.l<sup>-1</sup> and in Cenote Azul (south of Bacalar town) with more than 250 mg.l<sup>-1</sup> (Fig. 3); and the lowest concentrations far from the Cenotes in the north of the lake with 110 mg.l<sup>-1</sup> and in the Laguna Mariscal (to the east of Laguna Bacalar) with 104 mg.l<sup>-1</sup> (Fig.3). In addition they found that the concentrations decrease both northwards and eastwards away from the cenotes (Fig. 3).



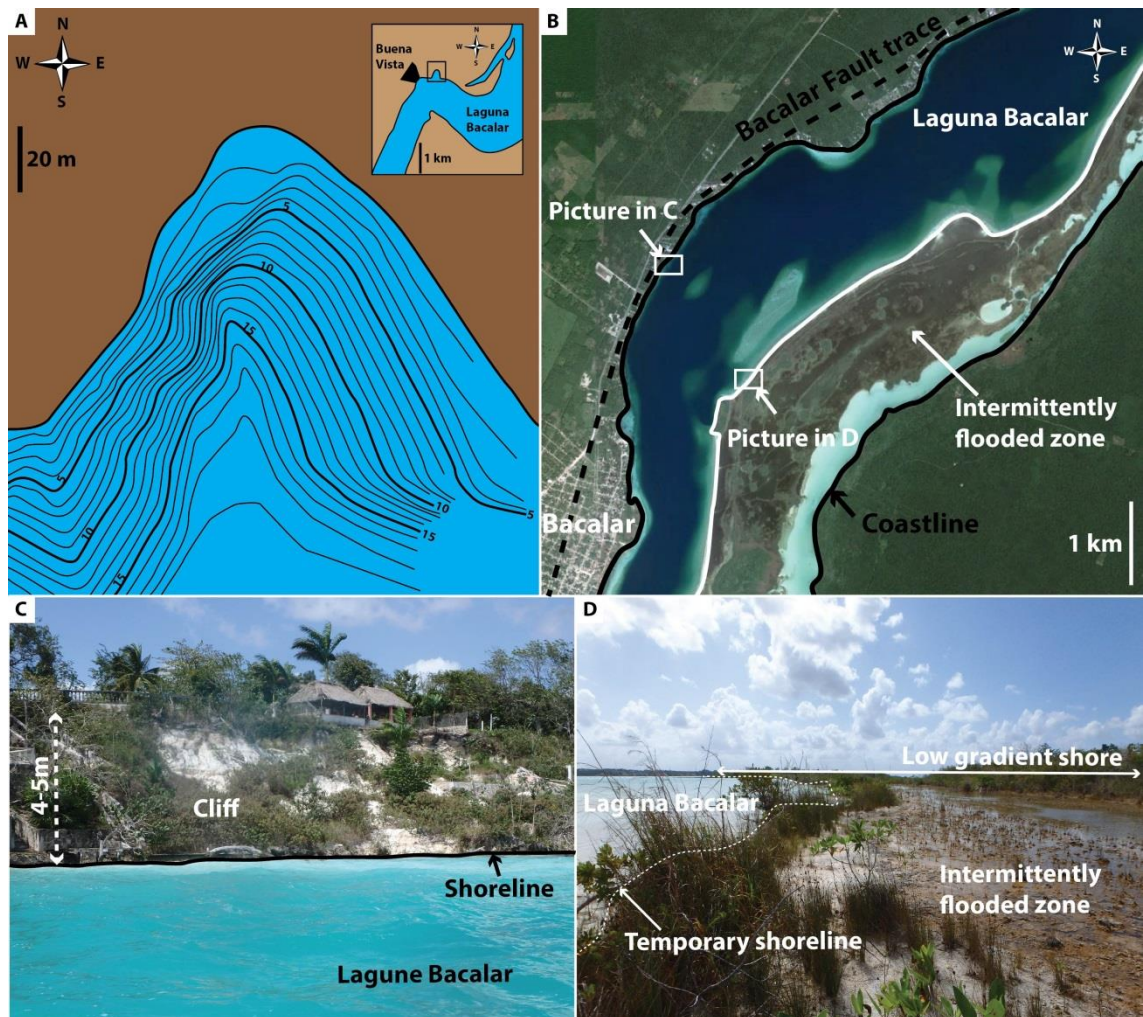
**Figure 3** Maps of Laguna Bacalar with concentrations of carbonate ions. A – Redrawn after Gishler *et al.*, 2008. B – Redrawn after Gishler *et al.*, 2011.

### 3.2. Bathymetry, lake floor topography and currents

Very few works are published on the bathymetry of the Laguna Bacalar as it has never been fully recorded and differences exist between different authors, with accounts maximum depths of 15 to 20 m by Carillo and Pereira (2003); 15 m by Gischler *et al.* (2008); and 20 m by Gischler *et al.* (2011). Gischler *et al.* (2011) added that according to local fishermen, the depth can reach down to 90 m in the cenotes. Sermanat (2008) is the only work available where a small portion of the bathymetry of the lake was recorded (Fig. 4). The survey is located to the north of the lake east of Buena Vista town and shows that the lake floor topography tends to be steepest on the western shore (Fig. 4).

This tendency can also be seen on satellite images (Fig. 4) where the eastern margins appear to be with a low gradient as indicated with the occurrence of intermittently flooded zones and the light blue colours of the water (Fig. 4); and the western margins appear to be steeper as indicated with the predominantly dark blue colours of the waters (Fig. 4). These features were also observed during the 2015 trip where the western shore has cliffs while the eastern shores have a lower gradient (Fig. 4C-D). These are thought to be due to tectonics as the Bacalar Fault trace is located onland to the west of the lake (Fig. 2) and this may well have shaped the topography of the shores and the lake floor.

Very few data are published concerning water current energy and direction. Gischler *et al.* (2008, 2011) are the only authors who noticed that there is strong current in the south of the lake with a northerly direction, particularly strong in The Rapids and in the Canal de los piratas. This northerly current direction was also noticed during the 2015 trip and in addition to was observed that wind appears to control current of at least superficial waters. The prevailing winds in the southern part of the Yucatan Peninsula are low intensity and blow from the E-SE to the W-NW (Sermanat, 2008). However this region is usually affected by tropical storms or cyclonic winds between August and November originated from the Caribbean Sea (Sermanat, 2008). This was experienced by the authors during a small storm during which a strong wind blew in a westerly direction and created superficial waves in this direction.



**Figure 4** Bathymetry and lake floor topography of Laguna Bacalar. A – Bathymetric survey in the northern part of the lake east of Buena Vista town that shows the steep gradient on the western margins (redrawn after Sermanat, 2008). B – Satellite image of Laguna Bacalar north of Bacalar town that shows the eastern low gradient shores and margins and western steep gradient margins (map © 2016 GoogleEarth). C – Picture of the western shore that shows the steep gradient (cliffs). Location in B. D – Picture of the eastern shore that shows the low gradient. Location in B.

### 3.3. Faunas and floras

The Laguna Bacalar and its shores harbour numerous species of animals and plants. Typical tropical forests are found on the terrestrial areas (*i.e.* never submerged) composed of more than 50 species of evergreen and low deciduous trees and plants (Sermanat, 2008). In the intermittently flooded areas are also found typical vegetation of this type of environments with more than 30 species of trees and plants (Sermanat, 2008) with a predominance of mangrove trees that can be very found locally in great quantity. In the lake waters are found about 5 species of freshwater algae that grow on the lake floor as well as about 70 species of epilithic diatoms (Sermanat, 2008; Siqueiros-Beltrones, 2013). On the shallow margins grows only one freshwater plant *Eleocharis cellulosa* that can be temporary emerged (Sermanat, 2008).



Concerning terrestrial animals, about 8 species of reptiles mainly iguanas and snakes, 45 species of birds and 15 species of mammals such as armadillos, badgers, rodents, foxes... are found around Laguna Bacalar (Sermanat, 2008). In terms of aquatic animals about 10 species of molluscs with predominantly *Pomacea* sp. gastropods and *Dreissena* sp. black-striped mussels and only one species of fish cichlid is found (Gamboa-Pérez and Schmitter-Soto, 1999; LaBuhn *et al.*, 2012). In these freshwaters are also found 5 families of bacteria including *Staphylococcus*, *Escherichia* and *Salmonella* genders with and 2 divisions of fungi, *Mastigomycota* and *Amastigomycota* (Carrillo and Pereira, 2003). In addition, as mentioned previously and described in more details in the next section, in this lake grow thrombolitic mounds that are bioconstructions due to calcification of microbial filaments (Golubic, 1976). Gischler *et al.* (2011) have undertaken a detailed study of the microbial filaments found in the microbialites of the Laguna Bacalar and they have described three types of microbial mats. The filamentous *Calothrix* and *Homeothrix* which are the most abundant in this lake; the coccoid *Scizothrix* or *Scytonema* with two species *Entophysalis* and *Gloeotheca*; and the filamentous *Leptolyngbya* mats (Gischler *et al.*, 2008, 2011).

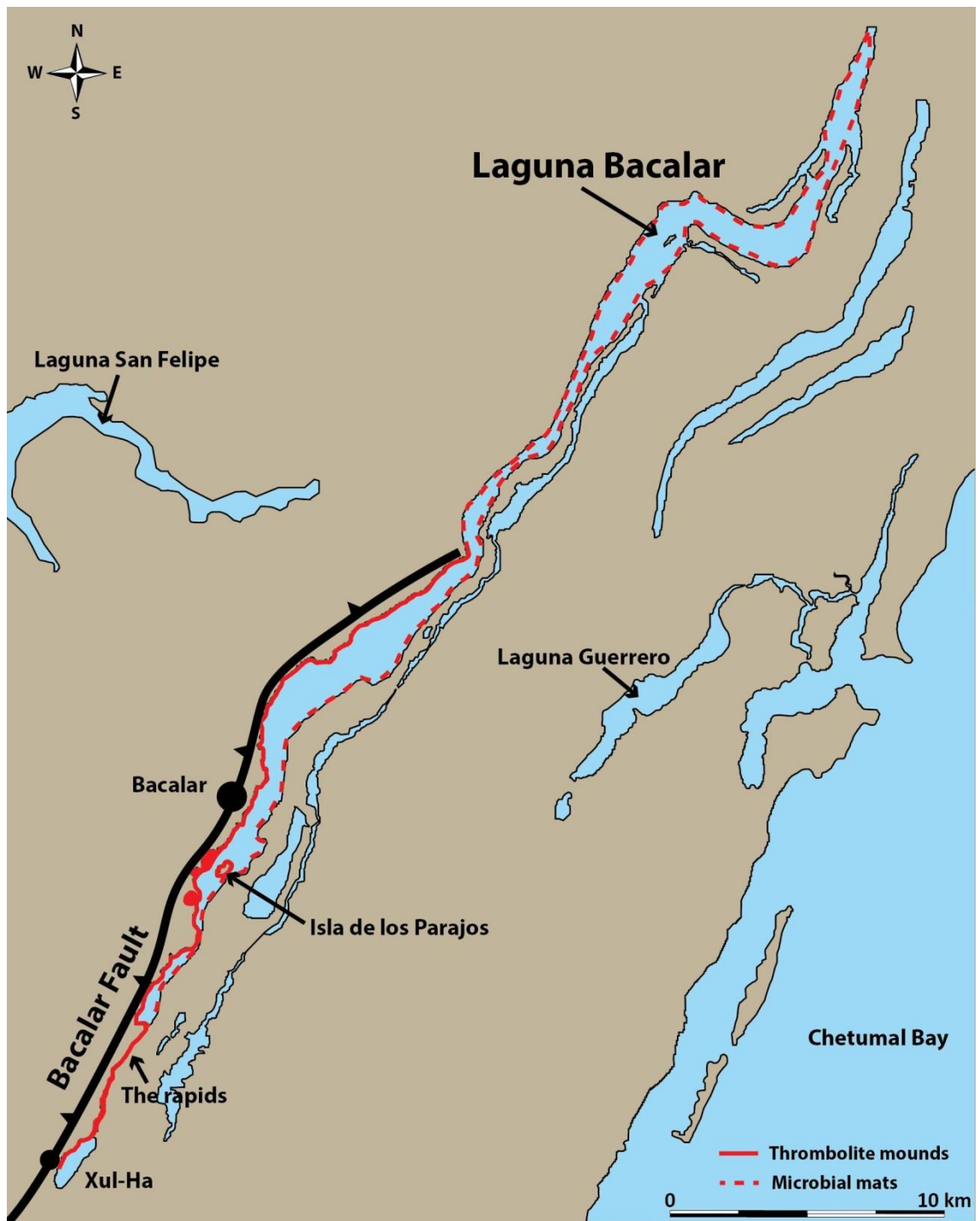
### 3.4. Sediments

The sediments in Laguna Bacalar are of two main types, microbial deposits that form mounded structures, crusts and oncolites and inter-mound facies (Gischler *et al.*, 2011).

The microbial deposits show most commonly clotted internal microfabric that classify them as thrombolites (as per Burne and Moore's, 1993, classification); and laminated microfabrics that classify them as stromatolites (as per Burne and Moore's, 1993, classification) can also be found (Gischler *et al.*, 2008, 2011; Castro-Contreras *et al.*, 2014). These microbialites are made of calcified microbial filaments that form tubes of low magnesium calcite (Gischler *et al.*, 2008), mainly for filaments of *Calothrix*, *Homeothrix* and *Leptolyngbya* (Gischler *et al.*, 2008). These authors also noticed that at the microscale the mats are made of a dense texture (mud?) that is often associated with mollusc fragments and diatom tests; and that at macroscale they found that the black mussels are very commonly encrusting the microbialites and can be locally densely packed. Castro-Contreras *et al.* (2014) showed that these mussels have little or no impact on the microbial growth that is mainly driven by the supersaturation of the waters with regard to calcium carbonate and the photosynthetic activity of the cyanobacteria. Sizes and morphologies of the mounded structures and crusts are detailed in the next section and mainly based on the 2015 visit. Gischler *et al.* (2008) determined

radiometric ages of these microbialites and found that they range between  $9,135 \pm 190$  and  $6,790 \pm 150$  cal yr BP (calibrated year before present) which give them early Holocene ages. However they show a hard water effect that is a common problem in radiometric dating in calcareous environment. In the Laguna Bacalar the waters feeding the lake are highly concentrated in carbonate due to the dissolution of Neogene and Pleistocene limestones that tends to reduce the dated ages. As a consequence Gischler *et al.* (2008) think that the microbialites of the Laguna Bacalar started to form in the Late Holocene and that the living part consists only of the surface microbial mats between up to 1 cm thick. The distribution of the microbialites is presented in figure 5 and is based on observations during the 2015 trip, by Gischler *et al.* (2008, 2011) and by Castro-Contreras (2014). The main conclusions are that microbialites preferentially grow in the southern part of the lake with a predominance of the western coast (Fig. 5). This distribution is closely linked with the locations of the cenotes and the carbonate concentrations that are much higher in the south than in the north.

Surprisingly very few studies described the lake sediments (other than microbialites) either found in the margins surrounding the microbialites (the inter-mound facies) or in the deepest part of the lake. Gischler *et al.* (2008) remains the only study that briefly described carbonate silt-sand with abundant mollusc shells (apple snail and black mussels) in the inter-mound sediments; and silt to mud carbonate sediments in the deepest part of the lake. The 2015 trip showed that marginal inter-mound sediment to be a coarse-grained texture with peloids, mollusc shells and microbial intraclasts.



**Figure 5** Distribution map of the microbial deposits in the Laguna Bacalar. Data compiled from Gischler *et al.* (2008, 2011), Castro-Contreras *et al.* (2014) and the 2015 trip.

## 4. Microbial deposits

### 4.1. Environmental controls on microbial growth

The distribution and morphology of microbial deposits are a function of intrinsic and extrinsic processes. The microbialite growth interacts with the surroundings, modifying the existing conditions, adding complexity to the depositional system. The main environmental controls on the appearance and occurrence of microbialites in Laguna Bacalar appear to be:

- Water depth
- Topography
- Energy
- Carbonate concentration

Figure 5 shows that microbialites are located along the lake shore. The maximum depth where these deposits were found vary according to the lake sector. In the south, in the rapids area, microbialites and oncoids were encountered down to 2 metres depth. In the northern part, their distribution is often concentrated above 1m depth. Gischler *et al.* (2008) recognised the importance of photosynthetic benthic communities in the precipitation on Bacalar carbonate deposits, therefore the correspondence between water depth and microbial sites can be partially explained with this process.

Lake bottom topography has also been identified by Gischler *et al.* (2008, 2011) as a key element in controlling the morphology of these microbialites (Gischler *et al.*, 2011, Fig. 3). Steep versus gentle slopes are often a function of the antecedent topography and the growing carbonates. Around the cenotes (sinkholes), vertical walls naturally occur due to the dissolution and collapse of the carbonate rock bottom. In the rapids area, fast-flowing water produced a narrow channel with steep edges. In other parts, the progradation of the shoreline due to coalescing mounds produce steep slopes. Areas of gentle slopes evolve where the initial topography and the growing potential of the carbonate system are not sufficient to produce substantial relief. In all cases, water depth is going to play a major role on the space available for mounds to grow.

Energy in Laguna Bacalar is a function of wind intensity (with the corresponding wind generated waves) and currents due to the inflow of groundwater from sinkholes into the lake. The balance between erosion, sediment transport and trapping and binding of particles by the microbial mat is going to control the development of microbialites in addition to the concentration of carbonate ions. The stress patterns generated by moving water are a function

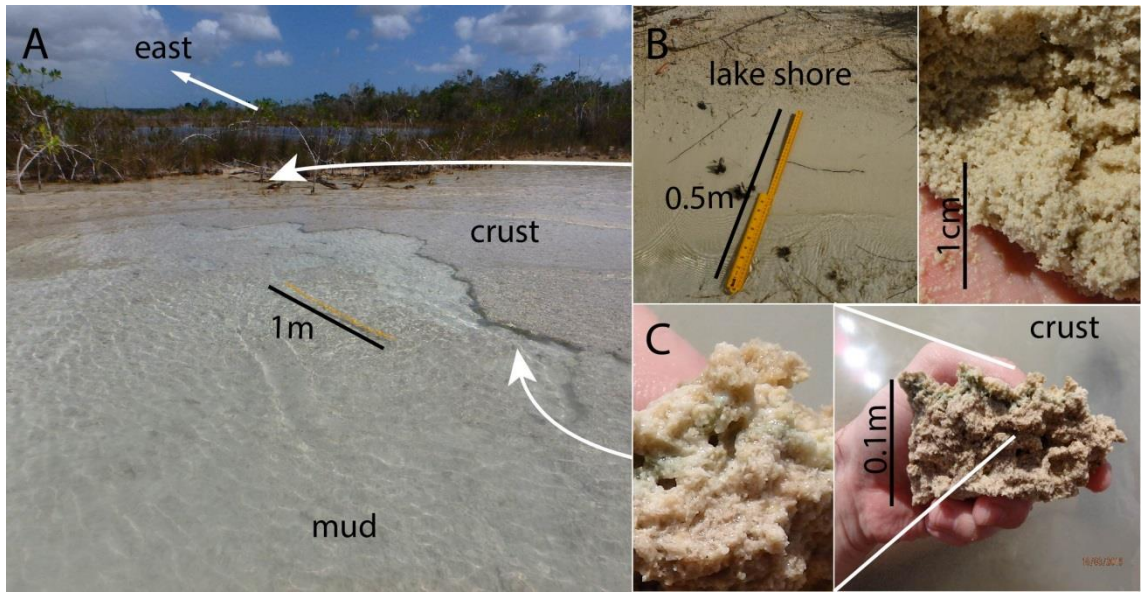
of the water depth and bathymetric features. Shore orientation regarding the westerly prevailing wind direction or northerly current direction is also important.

The carbonate concentration map (Fig. 3) shows the direct link between water chemistry and the appearance of microbialites. In Bacalar, microbial mounds occur in areas where  $\text{HCO}_3^-$  is over  $175 \text{ mg.l}^{-1}$  although less conspicuous microbial facies appear in areas of lower concentration. No microbialites were found at a  $\text{HCO}_3^-$  concentration below  $100 \text{ mg.l}^{-1}$ . It is clear the the different environmental parameters described above tend to add up, giving rise to a number of combinations of suitable environments for microbialite growth. This produces a variety of microbial morphologies, some of which are characteristics to a certain type of environment, while others can exist under different conditions.

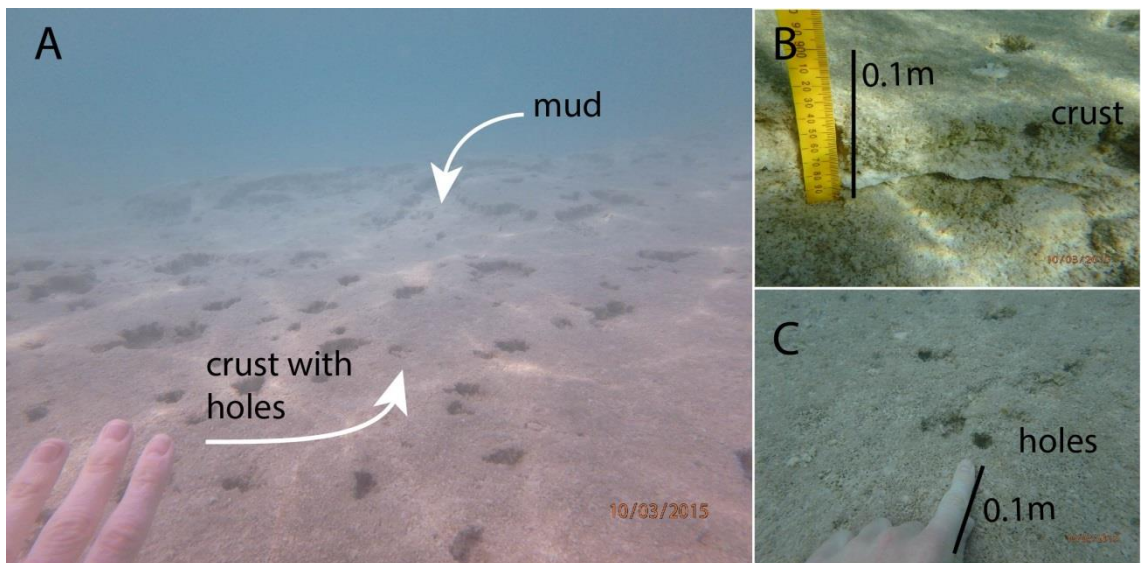
## **4.2. Microbial deposit morphologies**

### **4.2.1. Flat microbial crusts**

Two distinct types of microbial deposits are found in Laguna Bacalar: mounds and crusts (Gischler *et al.*, 2011). Crusts are mainly located in the eastern and northern part of the lake. In this area, carbonate concentration is lower due to the distance to the sink holes and the lake margins offers protection to wind-induced waves. The crusts consist of a semi-indurated layer sitting on soft, muddy sediment. They are most extensively developed in shallow, flat areas, down to a depth of 1 metre. The crust transitions into deeper, diatomaceous mud dominated areas (Fig. 7). In this deeper setting crusts commonly have cm-scale deep holes (Fig. 7). The thickness of the crust is about 10 cm, although the active microbial mat is located in the top centimetre. As recognised by Gischler *et al.* (2011), a yellow-orange sublayer serves as protection from UV light to the green photosynthetic layer (Fig. 6). Texturally, the can be classified as a thrombolite, with irregular cavities interfering with the layering.



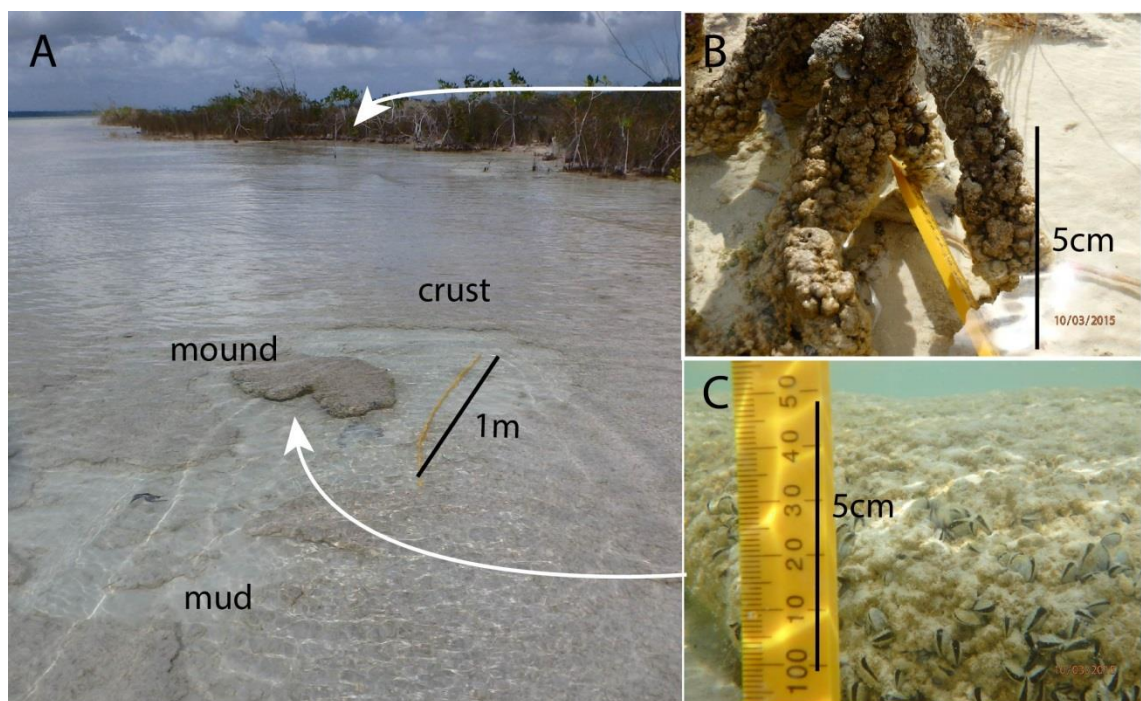
**Figure 6** Crust-type microbialites from the north-east coast of Laguna Bacalar (Location 7 in figure 1). A – The protected location allows the semi-indurated crust to develop from the coast to a depth of 1 m. B – On the shore, as patches, water saturated muddy diatomaceous carbonate sediment fails to support the weight of a standing person. C – The crust can be broken and the top centimetre contains green algae and microbial communities forming the active mat.



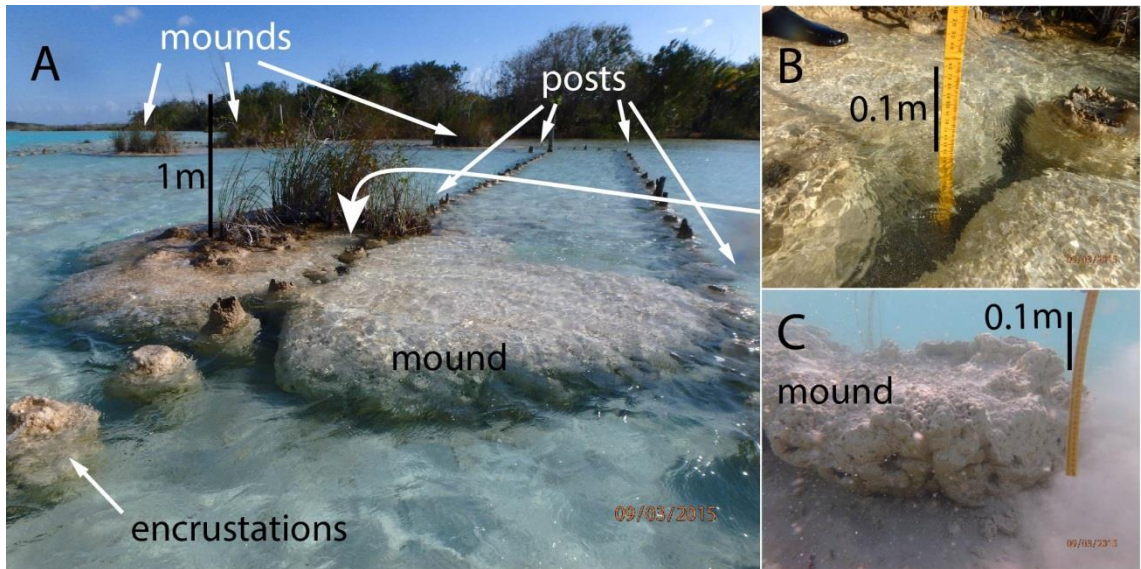
**Figure 7** Crust-type microbialites from the north-east coast of Laguna Bacalar (Location 7 in figure 1). Underwater view of the crust at approximately 1 m depth. The deposit is softer than the one closer to the shore, and often exhibits "burrows" (holes filled with muddy sediment).

#### 4.2.2. Encrustations

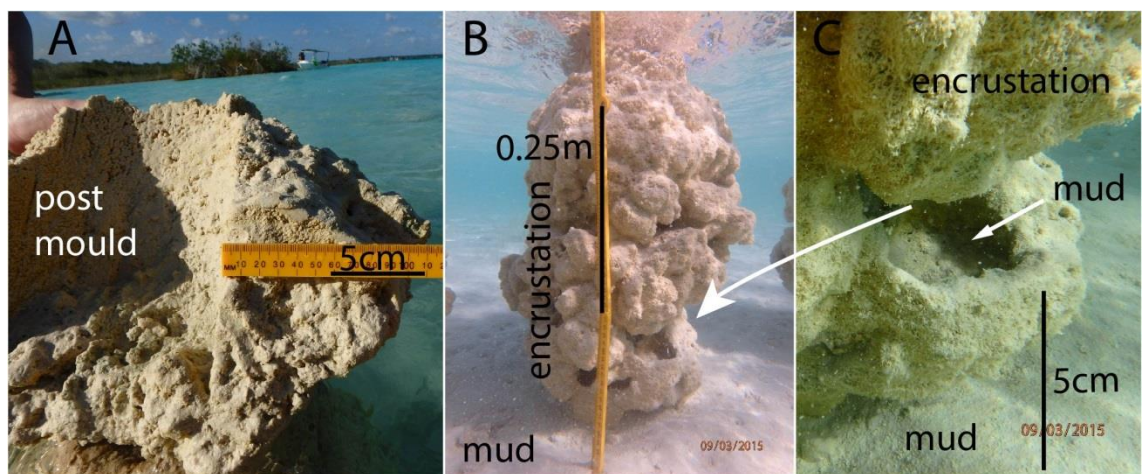
A common feature observed in Laguna Bacalar is the encrustation of tree trunks, roots and branches by microbialites (Figs. 8B, 9 and 10E). This feature has been observed in a variety of environments and at different scales. The encrustation can be developed in contact with the substrate, or above it, always surrounding the vegetation. In many cases, the encrustations evolve to form mounds (Fig. 11A-B). Mangrove trees, often spanning numerous roots to the substrate, contribute to create metre-scale structures formed by the coalescence of smaller units.



**Figure 8** Crust-type microbialites from the north-east coast of Laguna Bacalar (Location 7 in figure 1) and associated microbial facies. A and C: a 10-20 cm high mound developed near the lake shore. Close inspection shows that is covered by mytiloid bivalves of the genus *Dreissena* (Gischler *et al.*, 2008). B: occasionally, microbialites develop around mangrove trees, with a typical outer botryoidal texture enhanced by the occurrence of mussels.



**Figure 9** Encrusted microbialites from the abandoned hotel, west coast of Laguna Bacalar (Location 3 in figure 1). Twenty five years ago, posts were laid to serve as a pier. A – Large mounds around vegetation grow in a shallow lake margins. The flat shallow area is mainly covered by fine mud. In the distance, intense blue marks the deepening of the lake. Cracks developed when the mound was drilled to insert the posts. B – Inset of the crack shown in A, where microbialites were not able to fully fill the gap. Possible causes are discussed in the text. C – Lateral view of the mound. In this area, bivalves do not cover the mounds surface, a highly porous thrombolitic texture dominates. The fine mud from the lake bottom is easily disturbed.



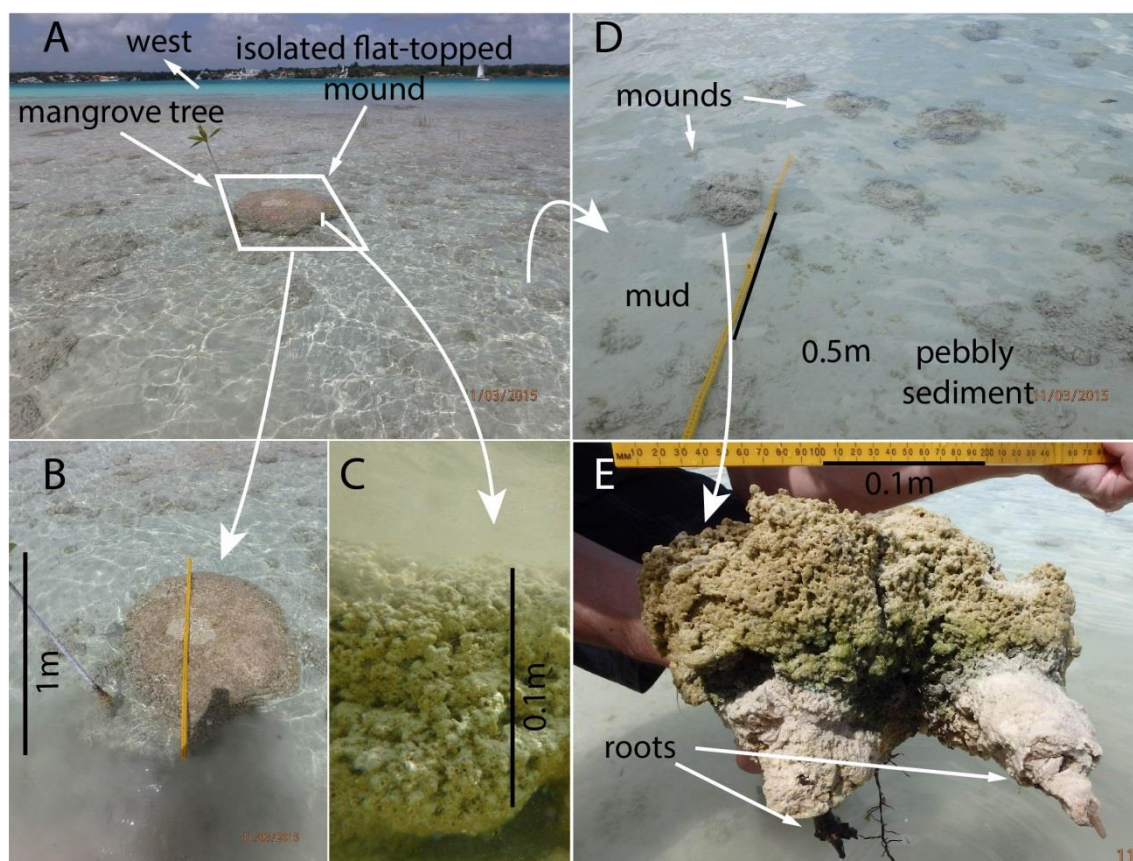
**Figure 10** Encrusted microbialites from the abandoned hotel, west coast of Laguna Bacalar (Location 3 in figure 1). Twenty five year-old posts are now covered by microbialites. A – A maximum encrustation thickness of 25 cm in some posts evidence a growth rate of 1 cm per year. Internally, encrustations show high porosity and a thrombolitic texture. B – Underwater view of the encrustation around a post, showing typical protrusions. Note that growth is lower in the top, probably due to seasonal lake-level variations. C – Close view, with algae covering the surface. Holes within the encrustation are partially filled with mud, as part of a large-scale trapping and binding.



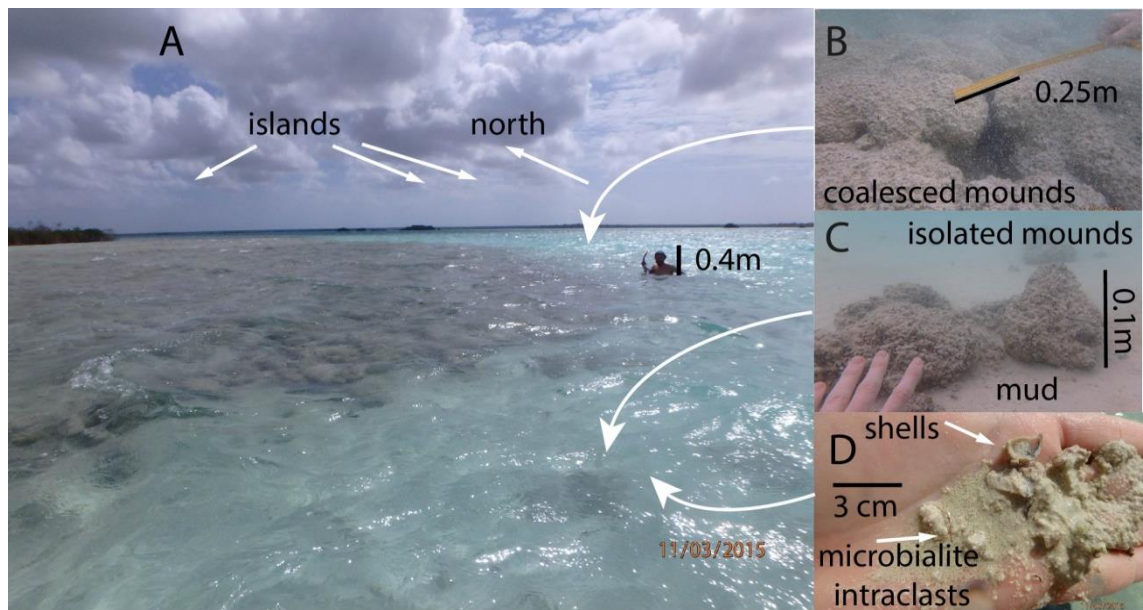
### 4.2.3. Low relief mounds

The distinction between low relief and tall mounds is useful since the vertical development of microbialites is linked to the environmental conditions. In areas where the water depth is not enough for tall microbial structures to develop, or where the conditions are not appropriate for a fast and consistent growth of microbialites, low relief mounds are often the dominant feature. For the purpose of this work, low relief mounds are defined as being generally less than 50 cm high. They can appear isolated, at all depths investigated. They may also coalesce, forming a continuous topographic feature.

Typically, mounds can grow up to lake level, therefore low relief mounds often occur on shallow areas (Figs. 8 and 11), where height is controlled by the accommodation. However, low relief mounds were also observed in deeper settings (Fig. 12), either coalesced or isolated.



**Figure 11** Low relief mounds from the western part of Isla de los Pajaros, Laguna Bacalar (Location 5 in figure 1). A – Low relief, individual and coalesced mounds develop in a shallow area (less than 20 cm. depth). B – Close view of a flat-topped mound, the centre of the structures is deeper than the edge and exhibits erosional features. C – Underwater picture of the lateral of the flat-topped mound, showing the typical thrombolitic texture. D – Small isolated mounds, abundant mud and pebbly sediment derived from the microbialites. E – Some mounds are located over roots, remnants of old trees.

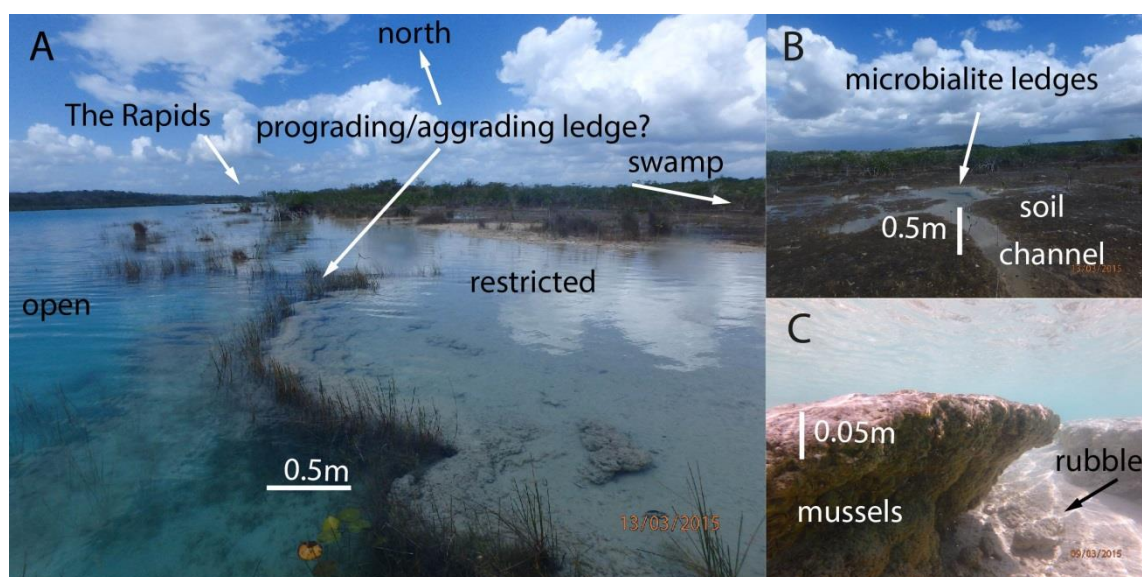


**Figure 12** Low relief mounds from the southern part of Esmeralda Island, western Laguna Bacalar (Location 6 in figure 1). A – Closely spaced mounds, permanently under water, form a microbially-dominated platform that quickly deepens to a mud dominated area. B – Close view of the coalesced mounds. Depth ranges from 20 cm to 1 metre. C – Isolated mounds typically occur in the deeper region, and are surrounded by mud or a microbial crust. D – Components of the inter-mound sediment from the deep area: mud, shells and microbialite intraclasts.

#### 4.2.4. Tall mounds

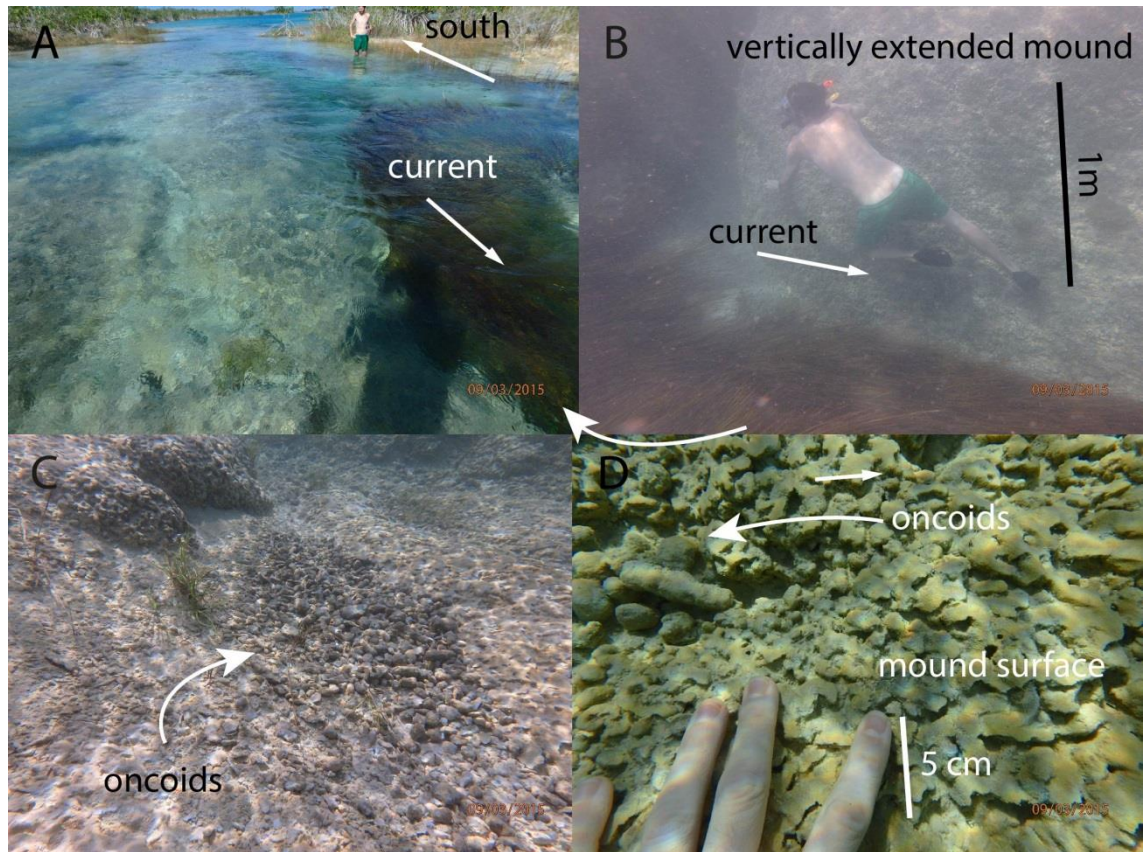
Under the "tall mounds" category are included microbial structures that managed to grow to heights of over 1 m. In the field, there are three types of structures, located in specific areas and with particular characteristics:

- Microbialites forming steep edges and even exhibiting ledges (Fig. 13). These are located in the southern part of the lake, near cenotes. These mounds typically form a continuous belt of coalesced, rounded structures that build out into the lake. They produce an important hydraulic separation between the open lake area to the front and the calm, shallow, partially disconnected area in the back. The back area is dominated by mud deposition over older microbialites. However, small mounds and incrustations are also common. As the microbial activity shifts towards the outer region, relict structures such as gaps or bridges between coalesced microbial heads are left behind. As the shore progrades, soils develop over these structures. In the front of these structures, rounded microbial head of several metres of diameter can form ledges. Water depth in the open lake area can reach over 2 metres.



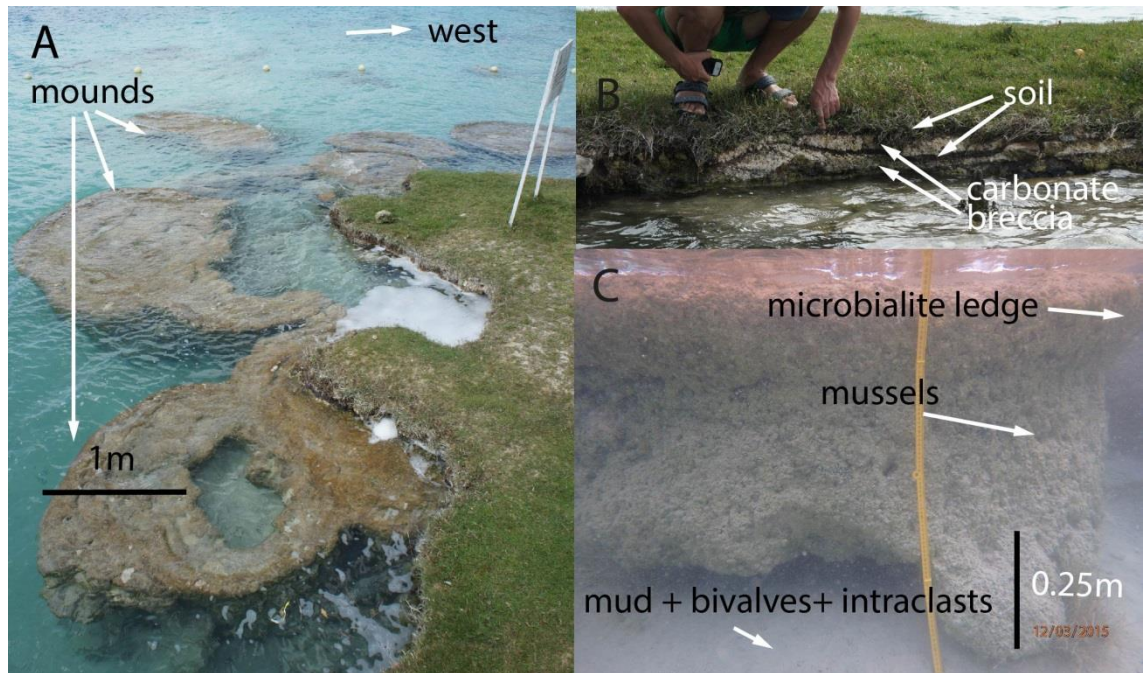
**Figure 13** Tall mounds near the Xul-Ha cenote (Location 1 in figure 1). A – Typical microbialite morphology found near the Rapids area. The semi-circular pan-shape mounds of metre to decametre in diameter coalesce to form an elongated barrier that separates the open lake to a restricted, low energy proximal area. B – In the back, soil develops over ancient mounds, showing the progradation of the system towards the west. C – The microbialites are covered by mussels. The ledges are prone to break, producing rubble towards the deep sector.

- Microbialites with smoother shapes (Fig. 14). These are located in the Rapids area. The hydraulic regime prevents the development of delicate ledges, more rounded shapes dominate. Microbialites developed in this region exhibit a hard, smooth surface. Mud deposition is restricted to locations where the current velocity falls significantly. Therefore, incorporation of particles to the microbialite structure is reduced to mussel shells.



**Figure 14** Tall mounds from the Rapids, southern Laguna Bacalar (Location 2 in figure 1). A – General view of the Rapids area, with depths of over two metres. The current is generated by a potential difference between the Xul-Ha cenote and the Laguna Bacalar. B – Tall mounds of over two metres high form the edge of the stream. C and D – In places of high current velocity ( $>0.5 \text{ m.s}^{-1}$ ), the surface of the microbialites is smooth and hard, and oncoids are common in the channel bottom.

- Microbialites in specific sites along the western coast of Laguna Bacalar are thought to be dead (Fig. 15). These large structures are interpreted as older microbial structures exposed as the western coast of the lake erodes. The spectacular rounded flat-topped mounds rise over 1 metre above the surrounding sediment. They are found south of Bacalar Town, in the Cocalitos beach club and in the north, in Kuuch Kaanil.



**Figure 15** Tall mounds from Cocalitos Beach Club (Location 4 in figure 1). The main structures are about 1000 yrs. old (Gischler *et al.*, 2008) and are being exposed as the lake shore retreats. A – The mounds, similar to those observed near the rapids, for well-indurated semi-circular structures with ledges. B – Detail of the soil and carbonate breccia covering the microbialite. C – Underwater view of the mound. The walls are covered by mussels. The lake bottom consists of unconsolidated sediment composed by mud, valves and microbialite intraclasts.

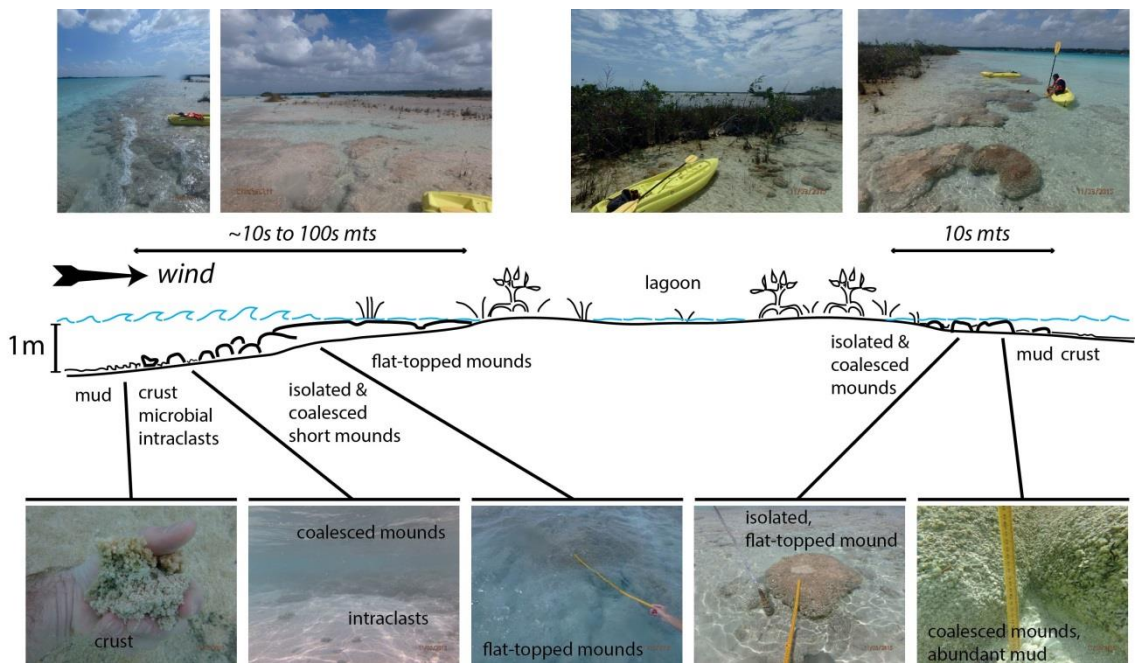
### 4.3. Microbial deposits distribution

#### 4.3.1. Windward and leeward deposition

Small islands offer adequate setting for studying differences in deposition due to energy differences, since transitions between environments occur rapidly. Regional characteristics, such as water chemistry, are expected to remain fairly constant. Therefore, changes in the deposition can be correlated to wind-driven waves. Figure 16 shows the differences between microbialites on both sides of the Isla de los Pajaros (Bird's Island). Although on both sides we can find the main types of deposits described in the previous section, there are some differences on the characteristics and abundance of the microbialite types.

The westerly dominant wind direction, implies that the leeward side is located in the western coast of the island. The beach profile shows a gentle slope. Low energy allows mud deposition throughout the coast. Low relief mounds mainly develop in the shallow area, either as individual or coalesced structures. However, the continuous mass extends only for a few meters from the coast towards the deeper area. Microbial crust develops are weakly developed. Microbial intraclasts are smaller and rarer than the ones observed in the windward area.

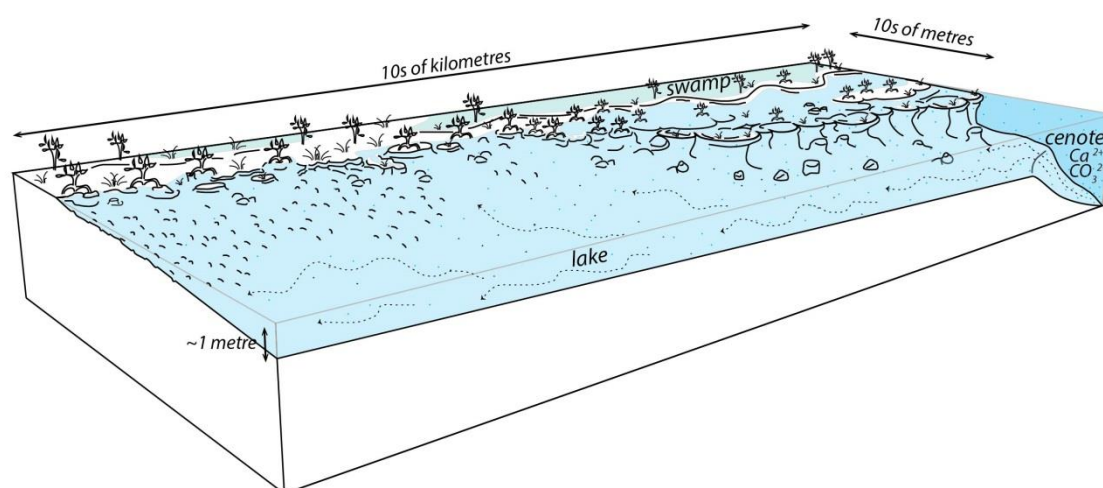
Towards the east, high energy associated to the windward side of the island seems to increase overall carbonate production. An extensive micro-platform appears to prograde towards deeper settings. A flat-topped microbial system occupies the internal area and quickly changes to coalesced and individual mounds reaching depths under 0.5 m. Large intraclasts (or irregular mounds) of several decimetres long are found lying over the muddy and/or crusty bottom.



**Figure 16** Cartoon showing the difference between windward and leeward microbial deposits. Based on Isla de los Pajaros and other associated islands. Top pictures, general views of the windward (left), internal and leeward (right) areas. Centre: sketch showing the location and characteristics of the deposits. Bottom pictures: Close look at some of the microbialites and associated facies. Low relief mounds and large intraclasts in deep settings appear exclusively on the windward area.

### 4.3.2. Bathymetry, microbial types and concentrations

Earlier models for Bacalar microbialites suggest a link between the slope and type of microbialites (Gischler *et al.*, 2011). Ledge type structures were considered to develop on near vertical coasts, and as the slope decreases, it evolves to mound type microbialites. Flat shallow bathymetries are dominated by crusts. Based on observations of depositional trends around the southern Laguna Bacalar, a new depositional model is proposed (Fig. 17). The microbial types are not just a response to the bathymetric profile, but they contribute to build the different slopes. The other two main forces controlling the type of microbialites are dissolved carbonate concentration in water and energy. The effect of high and low energy conditions on mound morphologies was explained in section 4.3.1. (Fig. 16).



**Figure 17** Proposed model illustrating the relationship between carbonate concentration in water, bathymetry and microbial types. Progradation of flat-topped microbial mounds are typical of areas with high dissolved carbonate concentration. Microbial crusts dominate in shallow, flat areas away from the source of dissolved carbonate.

The new model (Fig. 17) explains the effect of carbonate concentration on microbial growth, suggesting that when water with high dissolved  $\text{CaCO}_3$  concentration reaches low depths, microbialites start developing. Under the right hydrological conditions, microbialites fill the available space and generate a steep prograding front. In this environment, ledge-type structures can develop, and they seem to play an important role on the progradation process. Protrusions are seen to break down, generating rubble that serves as inception points of new mounds in deeper settings. If the carbonate concentration in water decreases, the potential growth of microbialites is lowered and crusts are the main morphology. This can be explained because the microbial system is not growing fast enough to generate a synoptic relief above the lake bottom. Slow aggradation dominates over progradation.

## 5. Conclusion

The 2015 visit enabled the authors to experience growth and accumulation of present day microbialites and to confirm the occurrence and distribution of microbial deposits mainly located to the south and to the western margins of the lake as observed by previous authors (Gischler *et al.*, 2008, 2011). This trip also helped to identify and describe four main types of microbial deposits, with flat microbial crusts, encrustations are found on all the margins and exclusive to the eastern margins and to the north; and low relief and tall thrombolitic mounds are exclusive to the western margins and the south areas. Field observation also helped to characterise depositional controls on the microbial growth and morphology distributions. The concentration of carbonate ions appear to be very important as mounds are bigger and denser to the south and on the western margins adjacent to the cenotes. In addition the wind-driven current is also of importance as illustrated with the difference of mound morphologies on the windward side with bigger and more indurated mounds than on the leeward side.

## 6. Reference list

- Alcocer, J. & Bernal-Brooks, F.W. 2002. Spatial and temporal heterogeneity of physical and chemical variables for an endorheic, shallow water body: Lake Pátzcuaro, México. *Archiv für Hydrobiologie*, **155**, 239-253.
- Burne, R.V. & Moore, L.S. 1993. Microatoll microbialites of Lake Clifton, Western Australia: Morphological analogues of *Cryptozoön proliferum* Hall, the first formally-named stromatolite. *Facies*, **29**, 149-168.
- Carrillo, R.A.A. & Pereira, C.A. 2003. Caracterización microbiológica preliminar del sistema Lagunar Bacalar. Congreso Internacional de Ciencias Ambientales, Facultad de Química de la Universidad Autónoma de Querétaro.
- Castro-Contreras, S.I., Gingras, M.K., Pecoits, E., Aubet, N.R., Petrash, D., Castro-Contreras, S.M., Dick, G., Planavsky, N. & Konhauser, K.O. 2014. Textural and geochemical features of freshwater microbialites from Laguna Bacalar, Quintana Roo, Mexico. *Palaios*, **29**, 192-209.
- Gamboa-Pérez, H.C. & Schmitter-Soto, J.J. 1999. Distribution of cichlid fishes in the littoral of Lake Bacalar, Yucatan Peninsula. *Environmental Biology of Fishes*, **54**, 35-43.
- Gischler, E., Gibson, M.A. & Oschmann, W. 2008. Giant Holocene Freshwater Microbialites, Laguna Bacalar, Quintana Roo, Mexico. *Sedimentology*, **55**, 1293-1309.
- Gischler, E., Golubić, S., Gibson, M.A., Oschmann, W. & Hudson, J.H. 2011. Microbial mats and microbialites in the freshwater Laguna Bacalar, Yucatan Peninsula, Mexico. In: Reitner, J., Quéric, N.-V. & Arp, G. (eds.) *Advances in Stromatolite Geobiology*. Springer-Verlag, 187-205.



- Golubić, S. 1976. Organisms that Build Stromatolites. In: Walter, E. (ed.) *Stromatolites*. Elsevier, Amsterdam, *Developments in Sedimentology*, 113-126.
- Kenkmann, T. & Schönián, F. 2006. Ries and Chicxulub: Impact craters on Earth provide insights for Martian ejecta blankets. *Meteoritics & Planetary Science*, **41**, 1587-1603.
- LaBuhn, S., Burrows, C., Groff, C., Neureuther, N., Schaal, S., Volk, J. & Flores, A. 2012. Chemistry and Preliminary Coliform Microbial Communities in Laguna Bacalar, Yucatan Peninsula, Mexico. *International Stromatolite Symposium Proceedings*.
- Lara, M.E. 1993. Divergent wrench faulting in the Belize southern lagoon: implications for Tertiary Caribbean plate movements and Quaternary reef distribution. *AAPG Bulletin*, **77**, 1041-1063.
- Lopez, Z.L., Lugo, F.A. & Pita, M.R.S. 2005. Chetumal E16-4-7. *Carta Geológico-Minera*.
- Marshall, J.S. 2006. Geomorphology and physiographic provinces of Central America. In: Alvarado, B. (ed.) *Central America geology, resources and hazard*. Taylor and Francis Group, London, 75-122.
- Pérez, L., Bugja, R., Lorenschat, J., Brenner, M., Curtis, J., Hoelzmann, P., Islebe, G., Scharf, B. & Schwalb, A. 2011. Aquatic ecosystems of the Yucatan peninsula (Mexico), Belize, and Guatemala. *Hydrobiologia*, **661**, 407-433.
- Perry, E., Velazquez-Oliman, G. & Marin, L. 2002. The hydrogeochemistry of the karst aquifer system of the northern Yucatan Peninsula, Mexico. *International Geology Review*, **44**, 191-221.
- Perry, E., Velazquez-Oliman, G. & Socki, R.A. 2003. Hydrogeology of the Yucatán Peninsula. The lowland Maya area. In: Pompa, A.G. & Fedick, S. (eds.) *The lowland Maya area*. The Halworth Press, Inc., New York, 115-138.
- Schmitter-Soto, J.J., Comín, F.A., Escobar-Briones, E., Herrera-Silveira, J., Alcocer, J., Suárez-Morales, E., Elías-Gutiérrez, M., Díaz-Arce, V., Marín, L.E. & Steinich, B. 2002. Hydrogeochemical and biological characteristics of cenotes in the Yucatan Peninsula (SE Mexico). *Hydrobiologia*, **467**, 215-228.
- Sermanat. 2008. *Manifestación de impacto ambiental. Secretaría de medio ambiente y recursion naturales*. Report.
- Siqueiros-Beltrones, D.A., Argumedo-Hernández, U. & Hernández-Almeida, O.U. 2013. Diagnosis prospectiva sobre la diversidad de diatomeas epilíticas en la laguna Bacalar, Quintana Roo, México. *Revista mexicana de biodiversidad*, **84**, 865-875.
- Suárez-Morales, E. 2003. Historical biogeography and distribution of the freshwater calanoid copepods (Crustacea: Copepoda) of the Yucatan Peninsula, Mexico. *Journal of Biogeography*, **30**, 1851-1859.

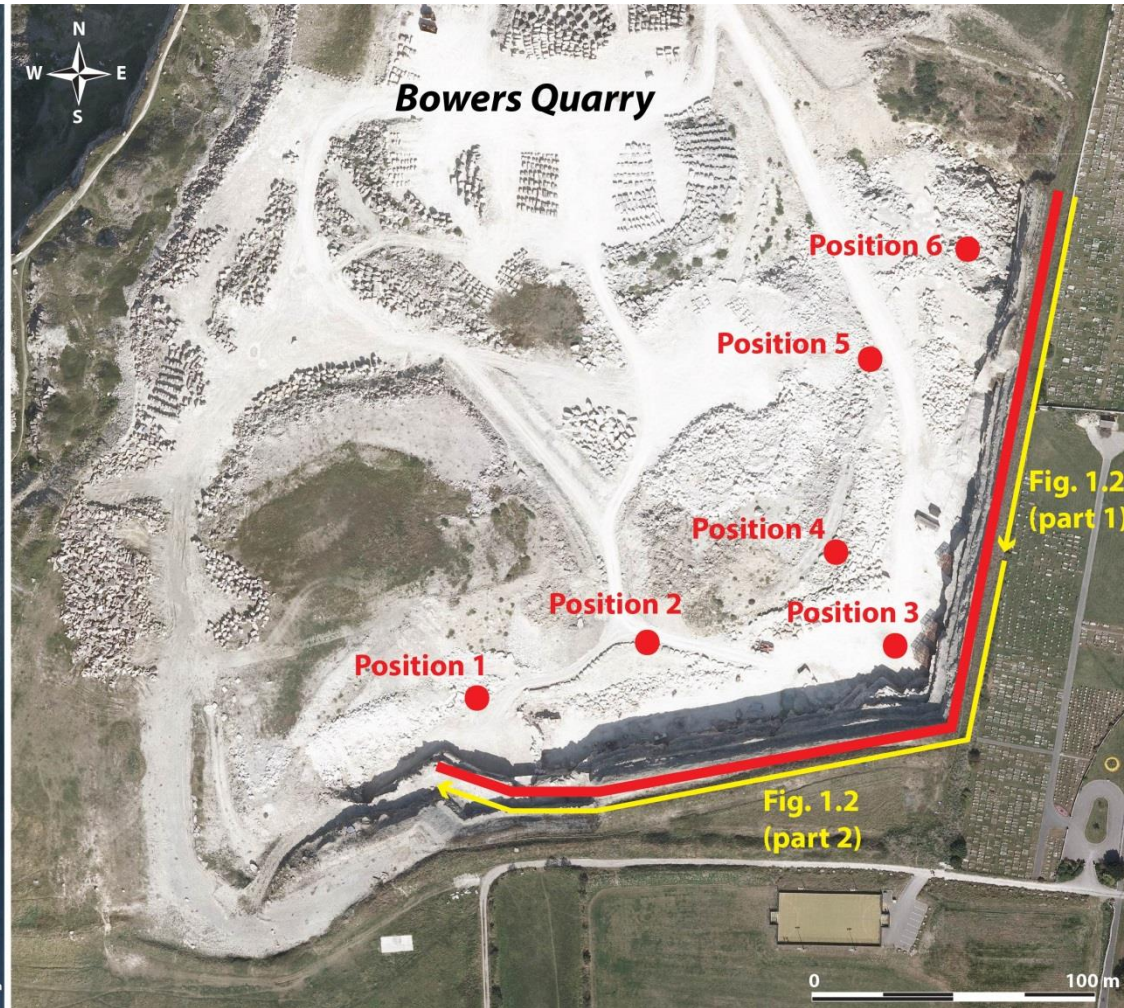
# Appendix 2

## Imaging techniques

- 2.1. Lidar dataset**
- 2.2. Hyperspectral imaging**
- 2.3. Ground penetrated radar (GPR)**

## **Appendix 2.1. Lidar dataset**

- 1 – Bowers Quarry**
- 2 – Coombefield Quarry**
- 3 – Freshwater Bay**
- 4 – God Nore**
- 5 – King Barrow Quarries**
- 6 – Sand Holes**
- 7 – South West Bowers**
- 8 – Analyses on orientation of quarry faces**



**1 – Bowers Quarry**

**Figure 1.1** Location map of Bowers Quarry, scans positions and cliff areas scanned (red plain line). Yellow arrows indicate direction of presentation of scans in figure 1.2. Maps © 2016 GoogleEarth.

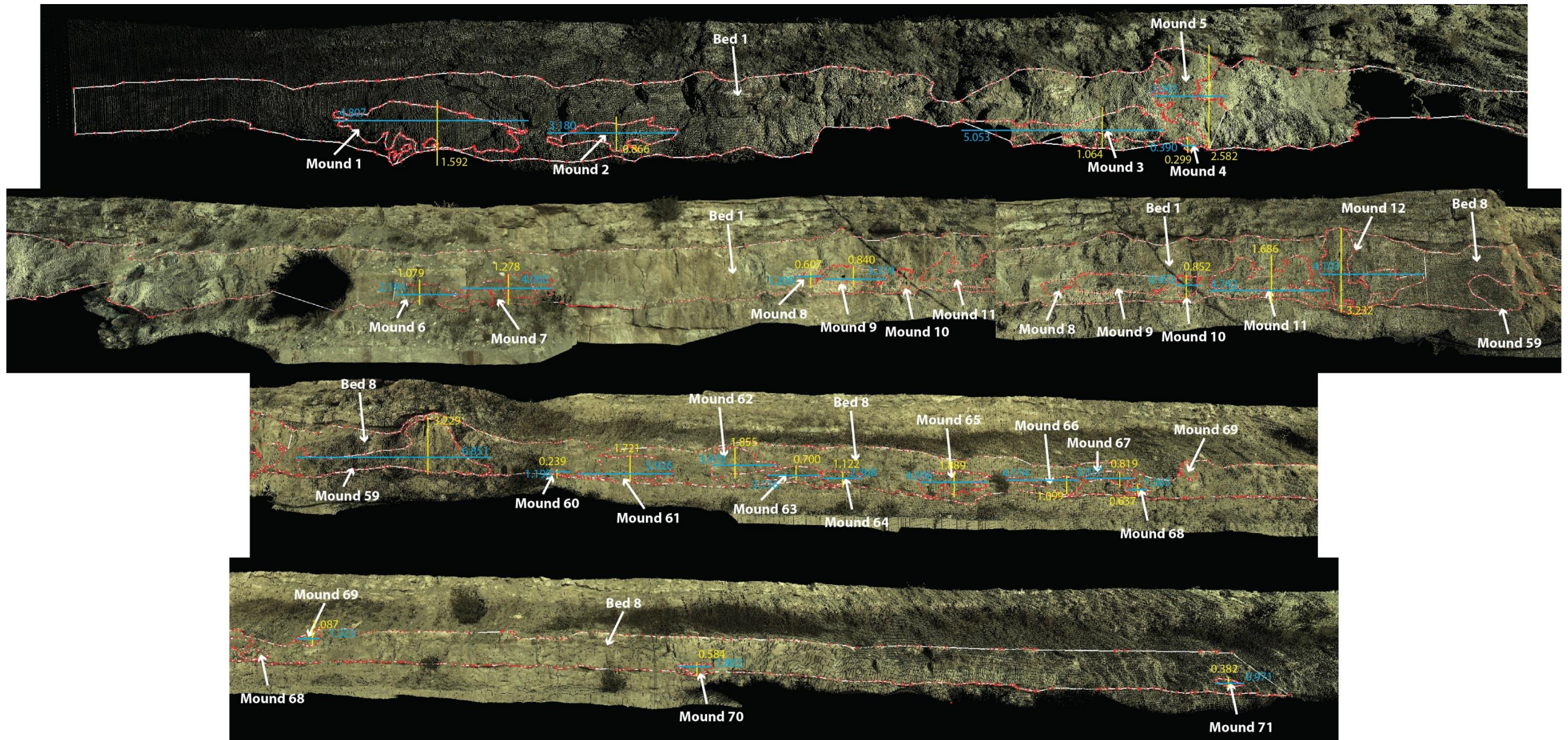


Figure 1.2 Lidar scans interpreted with height (yellow) and width (blue) measurements in meter (part 1).

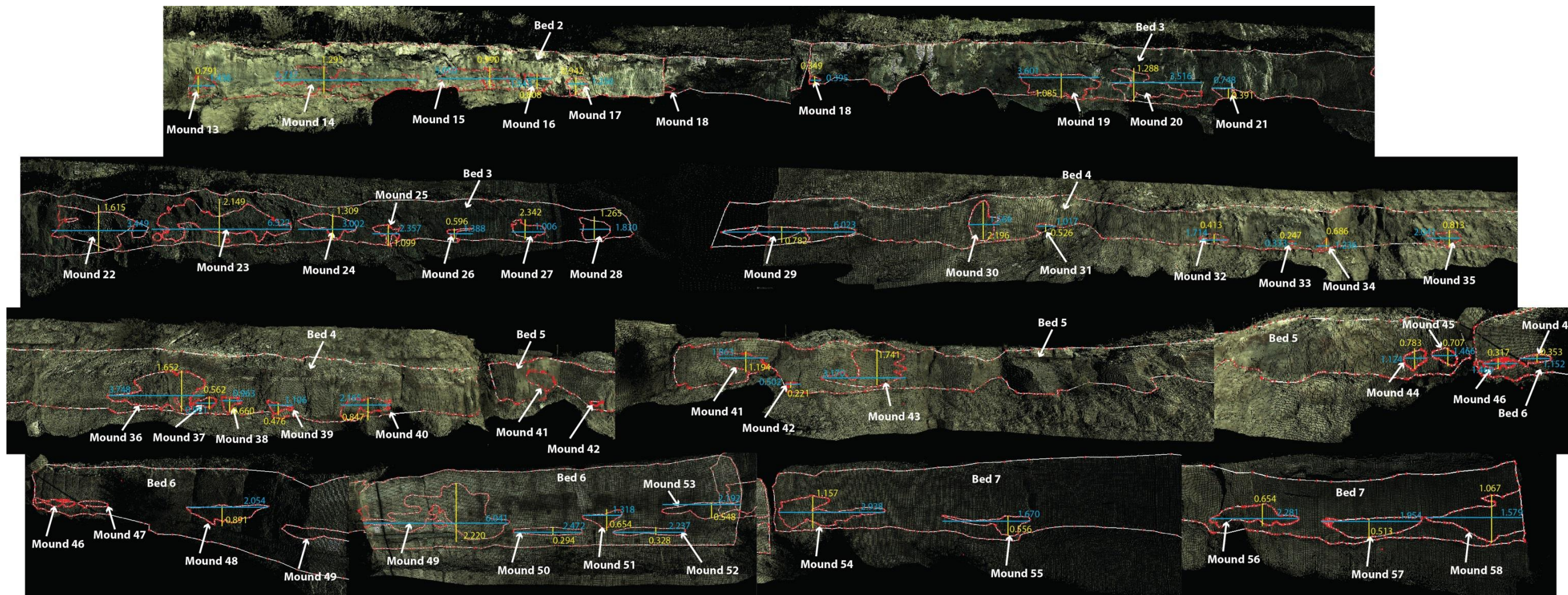
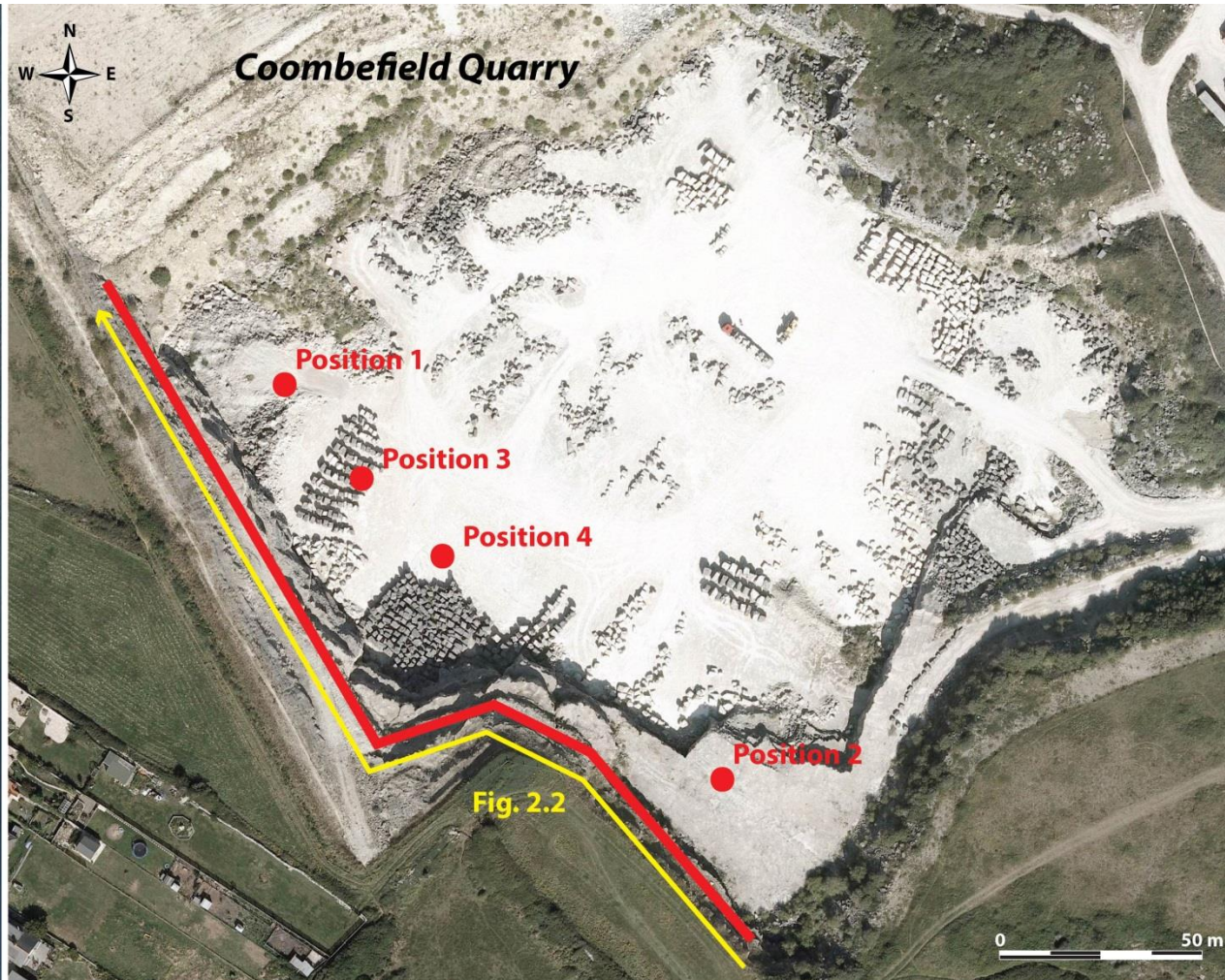


Figure 1.2 (continued) Lidar scans interpreted with height (yellow) and width (blue) measurements in meter (part 2).

Bowers Quarry						
Hard Cap						
	Orientation of face	Areas (m <sup>2</sup> )	vA (m)	Perimeter (m)	Width (m)	Height (m)
Mound 1	NNE-SSW	3.86343406	1.965562021	16.799	4.807	1.592
Mound 2	NNE-SSW	1.3152	1.146821695	8.714	3.18	0.866
Mound 3	NNE-SSW	2.34712	1.532031331	12.233	5.053	1.064
Mound 4	NNE-SSW	0.0774072	0.278221494	1.101	0.39	0.299
Mound 5	NNE-SSW	2.76931	1.664124394	10.334	2.043	2.582
Mound 6	NNE-SSW	1.21077	1.100349944	7.229	2.103	1.079
Mound 7	NNE-SSW	2.84933	1.687995853	14.033	4.06	1.278
Mound 8	NNE-SSW	0.424323	0.651400798	3.439	1.209	0.607
Mound 9	NNE-SSW	2.25941	1.503133394	8.39	3.319	0.84
Mound 10	NNE-SSW	0.587859	0.766719636	3.594	0.953	0.852
Mound 11	NNE-SSW	4.53666	2.129943661	17.764	4.742	1.686
Mound 12	NNE-SSW	5.41201	2.326372713	17.168	4.103	3.232
Mound 13	NE-SW	0.570694	0.755442916	3.748	1.436	0.791
Mound 14	NNE-SSW	4.93719	2.221978848	18.815	6.737	1.295
Mound 15	NNE-SSW	3.3968	1.843040965	13.712	5.05	0.99
Mound 16	NNE-SSW	0.853479	0.923839272	4.131	1.545	0.808
Mound 17	NNE-SSW	0.801946	0.895514377	3.665	1.256	0.942
Mound 18	ENE-WSW	0.10577	0.325223	1.307	0.395	0.349
Mound 19	ENE-WSW	3.04576	1.745210589	10.341	3.601	1.085
Mound 20	ENE-WSW	2.14649	1.465090441	12.432	3.516	1.288
Mound 21	ENE-WSW	0.232735	0.48242616	2.307	0.748	0.391
Mound 22	ENE-WSW	3.74599	1.935456019	13.205	3.449	1.615
Mound 23	ENE-WSW	6.58526	2.566176144	22.115	6.522	2.149
Mound 24	ENE-WSW	2.36023	1.536304006	7.781	3.002	1.309
Mound 25	ENE-WSW	1.25285	1.119307822	7.324	2.357	1.099
Mound 26	ENE-WSW	0.355295	0.596066271	4.055	1.388	0.596
Mound 27	ENE-WSW	1.47286	1.213614436	6.279	1.006	2.342
Mound 28	ENE-WSW	1.93629	1.391506378	5.773	1.83	1.265
Mound 29	ENE-WSW	3.00112	1.732374094	14.424	6.023	0.782
Mound 30	ENE-WSW	2.40659	1.551318794	6.472	1.569	2.196
Mound 31	ENE-WSW	0.343388	0.585993174	2.534	1.017	0.526
Mound 32	ENE-WSW	0.466019	0.682655843	4.11	1.714	0.413
Mound 33	ENE-WSW	0.0477622	0.218545647	0.859	0.333	0.247
Mound 34	ENE-WSW	0.576937	0.759563691	3.262	1.236	0.686
Mound 35	ENE-WSW	1.32742	1.152137145	5.423	2.041	0.813
Mound 36	ENE-WSW	4.06513	2.016216754	12.332	3.748	1.652
Mound 37	ENE-WSW	0.307131	0.554194009	2.586	0.951	0.562
Mound 38	ENE-WSW	0.3748	0.612209115	2.89	0.963	0.66
Mound 39	ENE-WSW	0.2777234	0.526994687	2.905	1.106	0.476
Mound 40	ENE-WSW	1.29988	1.1401228	6.989	2.165	0.847
Mound 41	ENE-WSW	1.21276	1.101253831	5.308	1.863	1.194
Mound 42	NNW-SSE	0.0763135	0.276248982	1.468	0.502	0.221
Mound 43	ENE-WSW	3.16309	1.778507802	10.8	3.17	1.741
Mound 44	NNE-SSW	0.48031	0.69304401	2.94	1.124	0.783
Mound 45	NNE-SSW	0.573232	0.757120862	3.437	1.466	0.707
Mound 46	NNW-SSE	0.323407	0.568688843	4.982	1.46	0.317
Mound 47	ENE-WSW	0.225467	0.474833655	2.622	1.152	0.353
Mound 48	ENE-WSW	0.794026	0.891081366	5.309	2.054	0.891
Mound 49	ENE-WSW	5.77994	2.404150578	21.197	6.041	2.22
Mound 50	ENE-WSW	0.556822	0.746205066	5.185	2.472	0.294
Mound 51	ENE-WSW	0.410018	0.640326479	3.201	1.318	0.654
Mound 52	ENE-WSW	0.5022	0.708660709	4.727	2.237	0.328
Mound 53	ENE-WSW	0.700936	0.837219207	5.007	2.192	0.548
Mound 54	NW-SE	1.84009	1.356499171	9.6	1.157	2.938
Mound 55	NW-SE	0.396547	0.629719779	4.23	1.67	0.556
Mound 56	NW-SE	1.21739	1.103353978	7.229	2.281	0.654
Mound 57	NW-SE	0.721155	0.849208455	5.039	1.954	0.513
Mound 58	NW-SE	0.928481	0.963577189	5.194	1.579	1.067
Mound 59	WNW-ESE	10.859	3.295299683	21.488	6.851	3.229
Mound 60	NNE-SSW	0.235879	0.485673759	2.63	1.19	0.239
Mound 61	NNE-SSW	5.96716	2.442777108	14.959	5.926	1.721
Mound 62	NNE-SSW	4.66042	2.158800593	10.471	3.97	1.855
Mound 63	NNE-SSW	1.85452	1.361807622	7.323	3.176	0.7
Mound 64	NNE-SSW	1.51817	1.232140414	5.866	2.368	1.122
Mound 65	NNE-SSW	4.82882	2.197457622	13.512	4.598	1.889
Mound 66	NNE-SSW	2.25124	1.500413276	9.145	4.114	1.099
Mound 67	NNE-SSW	1.45046	1.204350447	6.943	3.017	0.819
Mound 68	NNE-SSW	0.72791	0.853176418	3.661	1.565	0.637
Mound 69	NNE-SSW	0.925613	0.962087834	3.693	1.323	1.087
Mound 70	NNE-SSW	0.679404	0.824259668	4.166	1.802	0.584
Mound 71	NNE-SSW	0.268169	0.517850364	2.238	0.971	0.382
Bed 1		199.034		165.647		
Bed 2		59.6651		59.7		
Bed 3		145.772		128.695		
Bed 4		157.691		148.876		
Bed 5		56.7378		69.758		
Bed 6		63.1651		51.168		
Bed 7		30.5843		36.169		
Bed 8		221.089		220.608		
	<b>Total Mound</b>	<b>132.08</b>				
	<b>Total Bed</b>	<b>933.74</b>				
	<b>Total Intermound</b>	<b>801.66</b>				
	<b>% Mound</b>	<b>0.14</b>				
	<b>% Intermound</b>	<b>0.86</b>				

**Figure 1.3** Measurements performed on mound and inter-mound areas in the Hard Cap at Bowers Quarry. Measurements in red indicate partially imaged mounds.



2 – Coombefield Quarry

Figure 2.1 Location map of Coombefield Quarry, scans positions and cliff areas scanned (red plain line). Yellow arrows indicate direction of presentation of scans in figure 2.2. Maps © 2016 GoogleEarth.



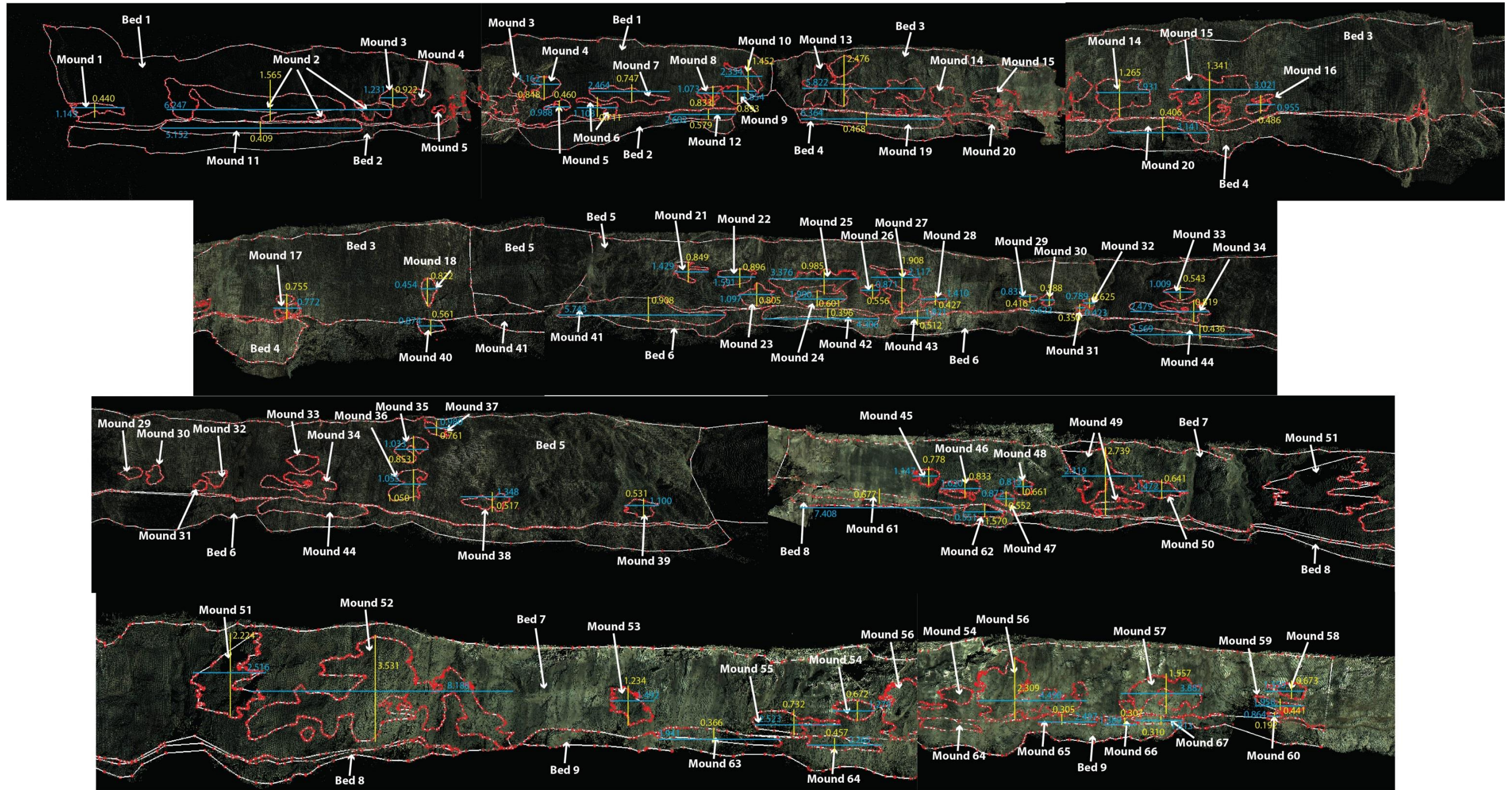
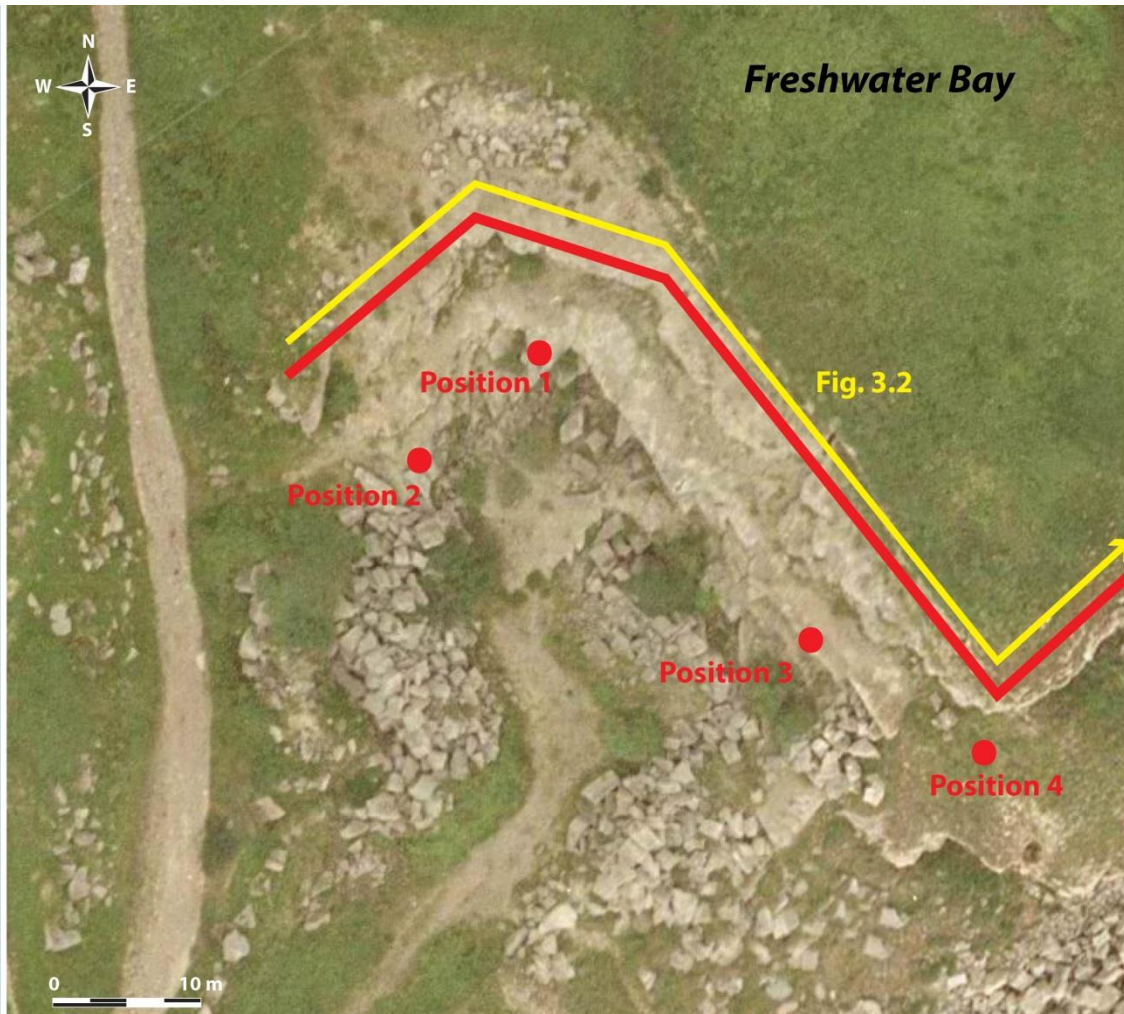
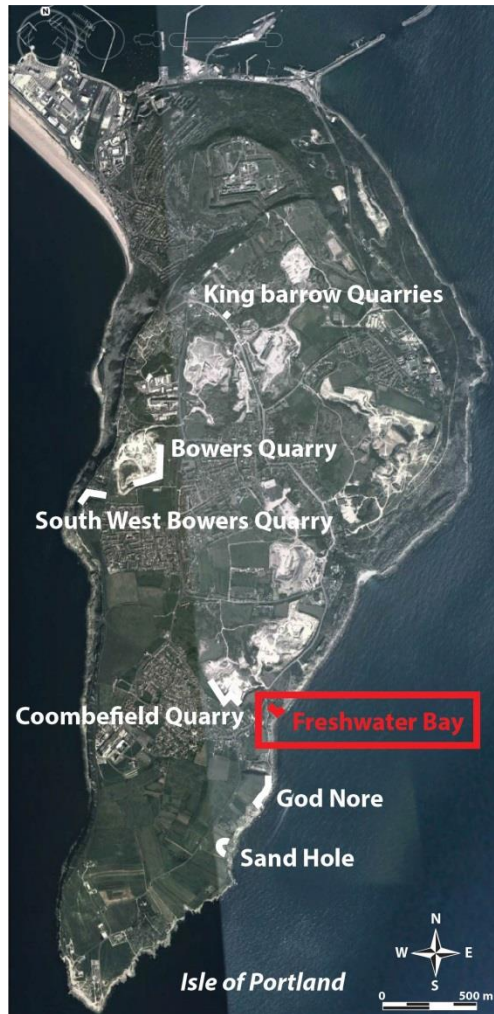


Figure 2.2 Lidar scans interpreted with height (yellow) and width (blue) measurements in meter.

Coombefield Quarry														
Hard Cap					Skull Cap									
	Orientation of face	Areas (m <sup>2</sup> )	∇A (m)	Perimeter (m)	Width (m)	Height (m)		Orientation of face	Areas (m <sup>2</sup> )	∇A (m)	Perimeter (m)	Width (m)	Height (m)	
Mound 1	N-S	0.264372	0.514171178	2.867	1.145	0.44		Mound 11	N-S	2.39023	1.546036869	11.648	5.152	0.409
Mound 2	N-S	3.85078	1.962340439	15.766	6.247	1.565		Mound 12	NE-SW	1.34386	1.159249757	7.019	2.602	0.579
Mound 3	NNW-SSE	0.732506	0.855865644	3.627	1.231	0.922		Mound 19	N-S	3.30369	1.817605568	13.871	6.364	0.468
Mound 4	NNW-SSE	0.665708	0.815909309	3.829	1.162	0.848		Mound 20	NW-SE	1.22947	1.108814682	7.903	3.141	0.406
Mound 5	NW-SE	0.249693	0.499692906	2.796	0.988	0.46		Mound 40	NW-SE	0.37022	0.608457065	3.103	0.874	0.561
Mound 6	NW-SE	0.251185	0.501183599	3.377	1.103	0.711		Mound 41	NW-SE	3.44507	1.856089976	13.295	5.743	0.908
Mound 7	NW-SE	0.98687	0.993413308	6.472	2.464	0.747		Mound 42	NW-SE	1.99576	1.412713701	10.292	4.306	0.396
Mound 8	NE-SW	0.460301	0.678454862	4.84	1.073	0.833		Mound 43	NW-SE	0.903145	0.950339413	4.946	1.821	0.512
Mound 9	NE-SW	1.03631	1.017993124	4.697	1.854	0.893		Mound 44	NW-SE	1.53257	1.237970113	8.616	3.569	0.436
Mound 10	NE-SW	1.27093	1.127355312	6.631	2.334	1.452		Mound 61	NW-SE	3.82816	1.956568425	18.189	7.408	0.677
Mound 13	N-S	6.84804	2.616876	30.723	5.822	2.476		Mound 62	NW-SE	0.688362	0.82967584	3.737	0.551	0.609
Mound 14	NW-SE	1.49172	1.221359898	6.327	1.931	1.265		Mound 63	NW-SE	1.43664	1.198599182	8.754	3.941	0.366
Mound 15	NW-SE	2.231732	1.493891964	13.386	3.021	1.341		Mound 64	NW-SE	0.736133	0.857981935	5.062	2.265	0.457
Mound 16	NW-SE	0.307386	0.554424025	3.913	0.955	0.486		Mound 65	NW-SE	0.761446	0.872608732	5.687	2.497	0.305
Mound 17	NE-SW	0.293763	0.541999077	3.812	0.772	0.755		Mound 66	NW-SE	0.320567	0.566186365	3.133	1.389	0.307
Mound 18	NE-SW	0.262176	0.512031249	2.083	0.454	0.822		Mound 67	NW-SE	0.553155	0.743743908	4.183	1.813	0.31
Mound 21	NW-SE	0.513711	0.716736353	5.935	1.429	0.849		Bed 2		12.6991		38.899		
Mound 22	NW-SE	0.836013	0.914337465	4.497	1.591	0.896		Bed 4		15.3914		38.636		
Mound 23	NW-SE	0.572946	0.756931965	3.899	1.097	0.805		Bed 6		27.9385		80.115		
Mound 24	NW-SE	0.873013	0.934351647	4.927	1.99	0.601		Bed 8		14.7795		64.431		
Mound 25	NW-SE	1.88082	1.371429911	10.475	3.376	0.985		Bed 9		19.5994		54.02		
Mound 26	NW-SE	0.30918	0.556039567	2.505	0.871	0.556								
Mound 27	NW-SE	1.98117	1.407540408	11.056	2.117	1.908								
Mound 28	NW-SE	0.422349	0.649883836	3.849	1.41	0.427		<b>Total Mound</b>		<b>24.84</b>				
Mound 29	NNW-SSE	0.214806	0.463471682	2.018	0.831	0.416		<b>Total Bed</b>		<b>90.41</b>				
Mound 30	NW-SE	0.241587	0.491515005	2.219	0.622	0.588		<b>Total Inter-mound</b>		<b>65.57</b>				
Mound 31	NW-SE	0.0999931	0.316216856	1.275	0.423	0.35								
Mound 32	NW-SE	0.271263	0.520829147	2.391	0.789	0.625		<b>% Mound</b>		<b>0.27</b>				
Mound 33	NW-SE	0.374445	0.611919112	2.571	1.009	0.543		<b>% Inter-mound</b>		<b>0.73</b>				
Mound 34	NW-SE	1.28393	1.13310635	10.187	2.479	0.819								
Mound 35	NW-SE	0.488099	0.698640823	3.865	1.033	0.853								
Mound 36	NW-SE	0.690571	0.831006017	4.476	1.055	1.05								
Mound 37	NW-SE	0.463422	0.680751056	2.899	0.98	0.761								
Mound 38	NW-SE	0.388312	0.623146853	3.714	1.348	0.517								
Mound 39	NW-SE	0.332753	0.576847467	2.996	1.1	0.531								
Mound 45	NW-SE	0.537715	0.733290529	4.384	1.147	0.778								
Mound 46	NW-SE	0.870477	0.932993569	6.737	1.62	0.833								
Mound 47	NW-SE	0.329282	0.573830986	2.607	0.872	0.552								
Mound 48	NW-SE	0.432767	0.657850287	2.61	0.813	0.661								
Mound 49	NW-SE	3.60941	1.89984473	17.462	2.319	2.739								
Mound 50	NW-SE	0.60269	0.776331115	3.937	1.472	0.641								
Mound 51	NE-SW	2.93528	1.713265887	13.138	2.516	2.224								
Mound 52	NW-SE	10.2944	3.208488741	39.695	8.188	3.531								
Mound 53	NW-SE	0.946146	0.972700365	6.005	1.492	1.234								
Mound 54	NW-SE	0.570309	0.755188056	3.33	1.279	0.672								
Mound 55	NW-SE	1.02893	1.014361868	6.347	2.523	0.732								
Mound 56	NW-SE	4.88043	2.209169527	20.2	4.49	2.309								
Mound 57	NW-SE	3.55276	1.884876654	11.453	3.887	1.557								
Mound 58	NW-SE	0.564764	0.751507818	3.954	1.35	0.673								
Mound 59	NW-SE	0.62873	0.792924965	5.529	1.958	0.441								
Mound 60	NW-SE	0.113697	0.337189857	1.8	0.864	0.192								
Bed 1		59.6933		51.596										
Bed 3		69.1295		58.515										
Bed 5		112.27523		92.888										
Bed 7		190.51		136.811										
	<b>Total Mound</b>	<b>65.34</b>												
	<b>Total Bed</b>	<b>431.61</b>												
	<b>Total Inter-mound</b>	<b>366.27</b>												
	<b>% Mound</b>	<b>0.15</b>												
	<b>% Inter-mound</b>	<b>0.85</b>												

**Figure 2.3** Measurements performed on mound and inter-mound areas in the Hard Cap (left) and Skull Cap (right) at Coombefield Quarry. Measurements in red indicate partially imaged mounds.



3 – Freshwater Bay

Figure 3.1 Location map of Freshwater Bay, scans positions and cliff areas scanned (red plain line). Yellow arrows indicate direction of presentation of scans in figure 3.2. Maps © 2016 GoogleEarth.

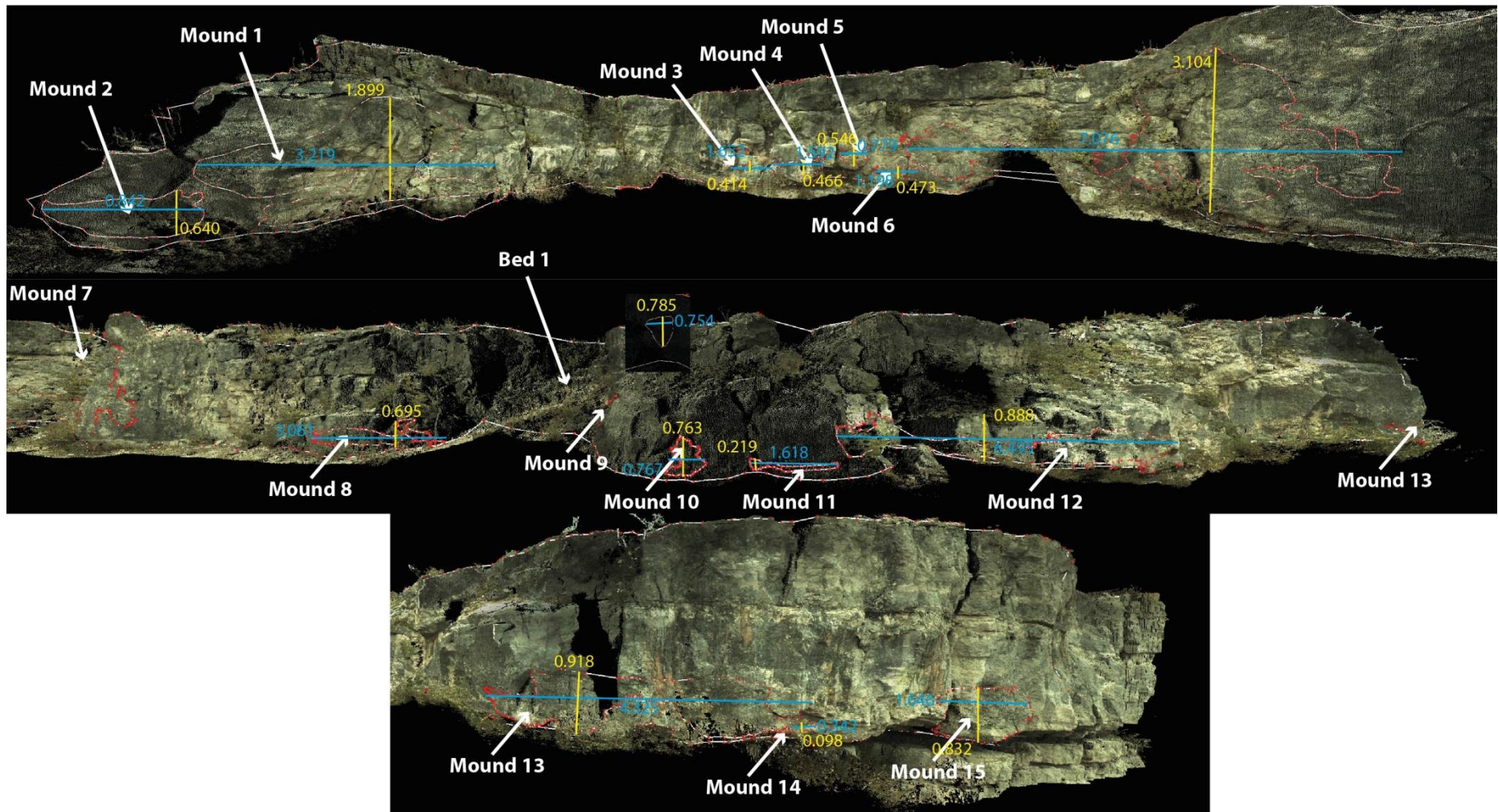
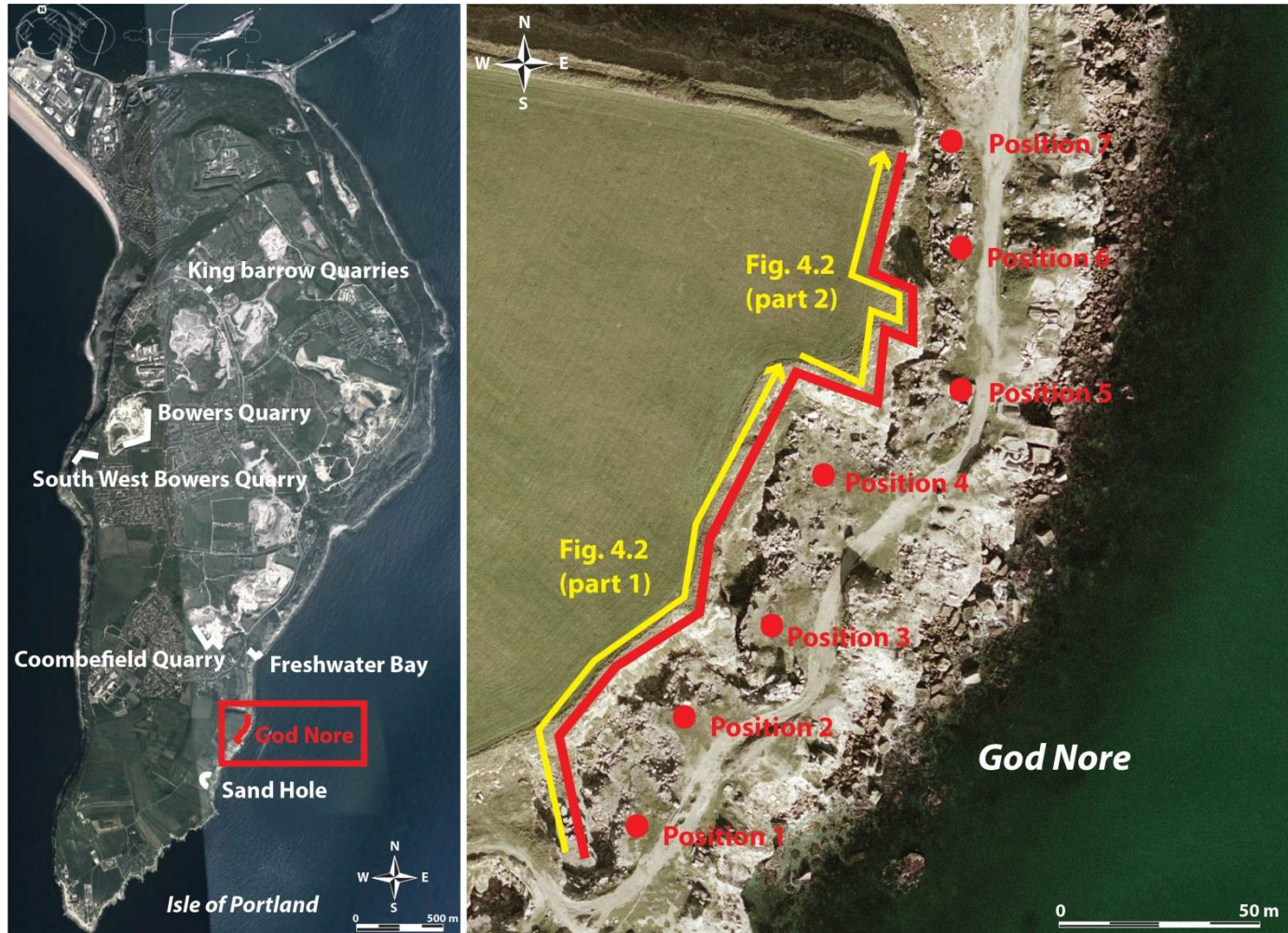


Figure 3.2 Lidar scans interpreted with height (yellow) and width (blue) measurements in meter.

Freshwater Bay						
Hard Cap						
	Orientation of face	Areas (m <sup>2</sup> )	VA (m)	Perimeter (m)	Width (m)	Height (m)
Mound 1	NE-SW	3.6834	1.919218591	13.320	3.219	1.899
Mound 2	NE-SW	0.357946	0.598285885	2.799	0.842	0.64
Mound 3	WNW-ESE	0.371357	0.609390679	4.793	1.652	0.414
Mound 4	WNW-ESE	0.750741	0.866453115	5.021	1.592	0.466
Mound 5	WNW-ESE	0.361707	0.601420818	2.402	0.779	0.546
Mound 6	WNW-ESE	0.337742	0.581155745	3.096	1.198	0.473
Mound 7	WNW-ESE & NW-SE	13.5549	3.681697978	30.741	7.076	3.104
Mound 8	NW-SE	0.969898	0.984833996	10.126	3.061	0.695
Mound 9	NE-SW	0.408678	0.639279282	2.585	0.754	0.785
Mound 10	NNW-SSE	0.304647	0.551948367	3.114	0.767	0.763
Mound 11	NNW-SSE	0.171879	0.414582923	3.772	1.618	0.219
Mound 12	NNW-SSE	3.4233	1.850216204	19.814	6.495	0.888
Mound 13	NW-SE	2.45724	1.567558611	13.121	4.325	0.918
Mound 14	NW-SE	0.0333362	0.182582036	0.917	0.342	0.098
Mound 15	NE-SW	1.08577	1.042002879	5.100	1.646	0.832
Bed 1		233.851		163.428		
	<b>Total Mound</b>	<b>28.27</b>				
	<b>Total Bed</b>	<b>233.85</b>				
	<b>Total Intermound</b>	<b>205.58</b>				
	<b>% Mound</b>	<b>0.12</b>				
	<b>% Intermound</b>	<b>0.88</b>				

**Figure 3.3** Measurements performed on mound and inter-mound areas in the Hard Cap at Freshwater Bay.



4 – God Nore

Figure 4.1 Location map of God Nore, scans positions and cliff areas scanned (red plain line). Yellow arrows indicate direction of presentation of scans in figure 4.2. Maps © 2016 GoogleEarth.

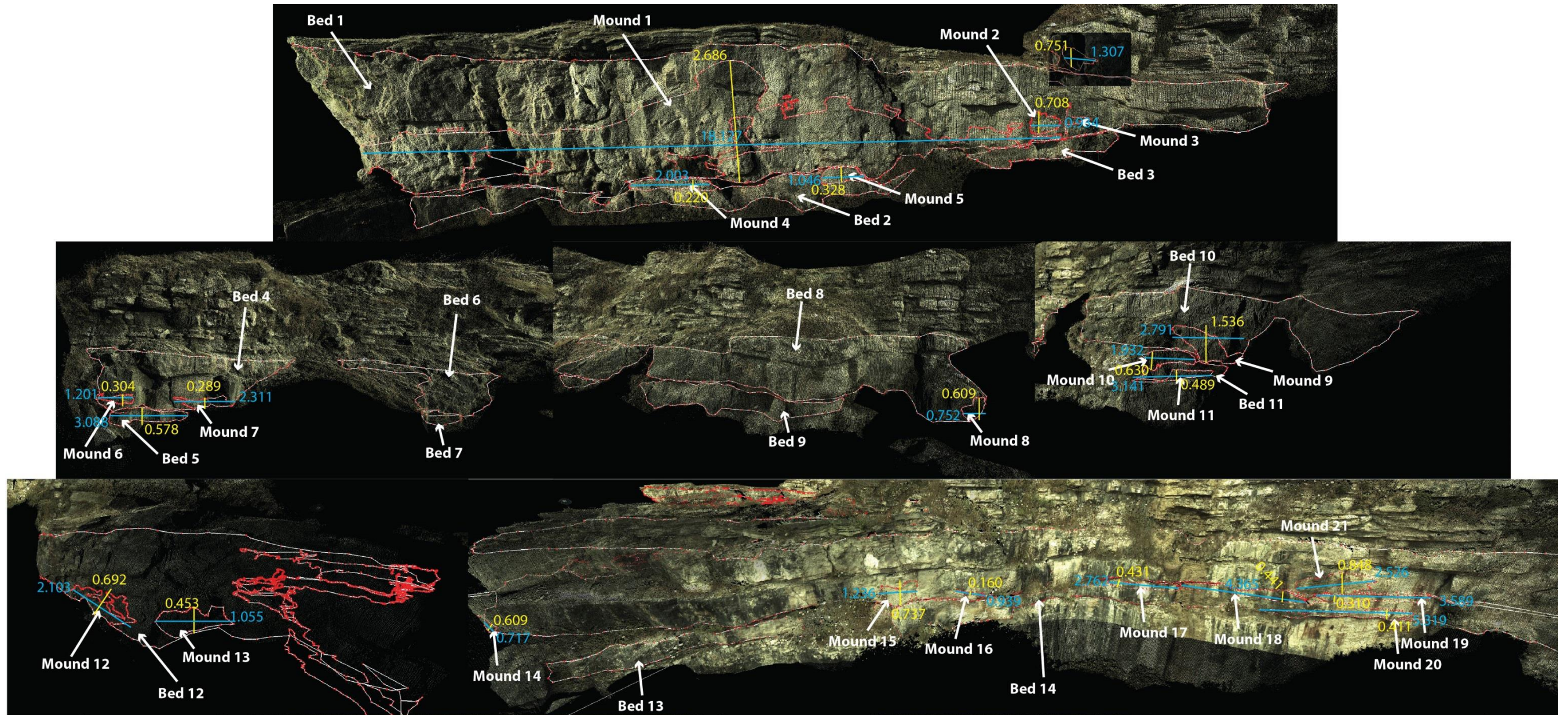


Figure 4.2 Lidar scans interpreted with height (yellow) and width (blue) measurements in meter (part 1).

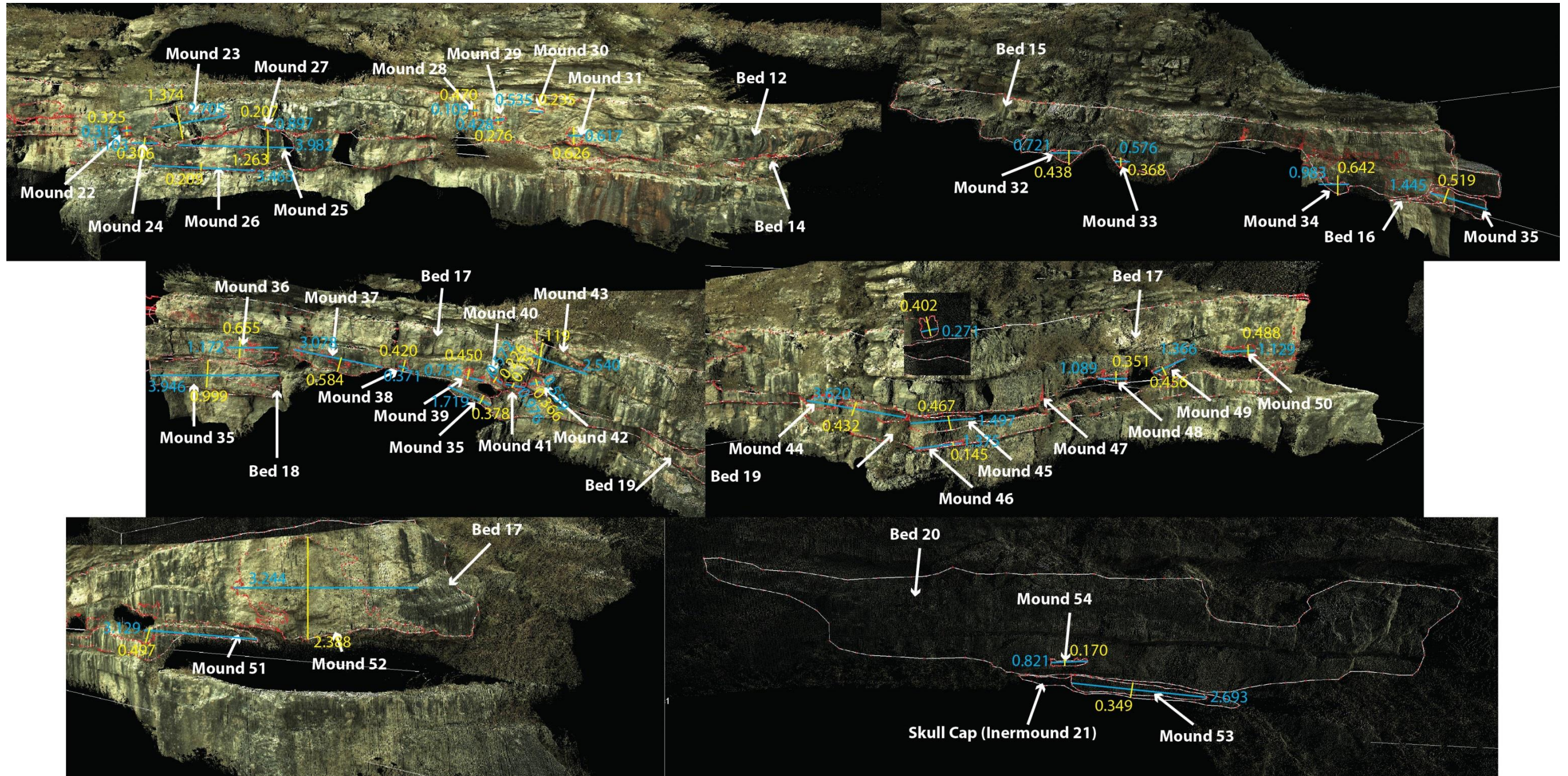


Figure 4.2 (continued) Lidar scans interpreted with height (yellow) and width (blue) measurements in meter (part 2).







5 – King Barrow Quarries

Figure 5.1 Location map of King Barrow Quarries, scans positions and cliff areas scanned (red plain line and surface). Yellow arrows indicate direction of presentation of scans in figure 5.2. Maps © 2016 GoogleEarth.

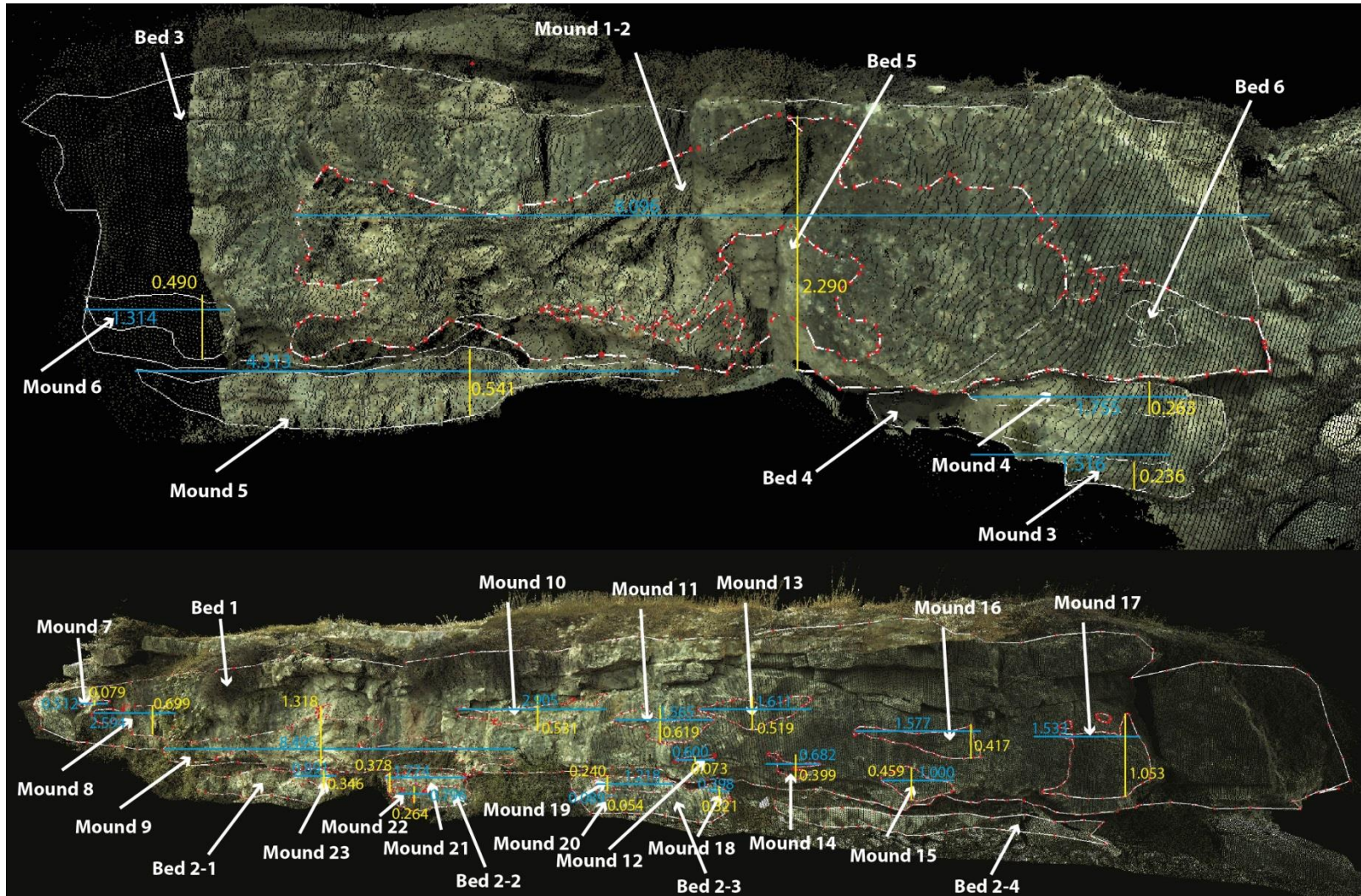
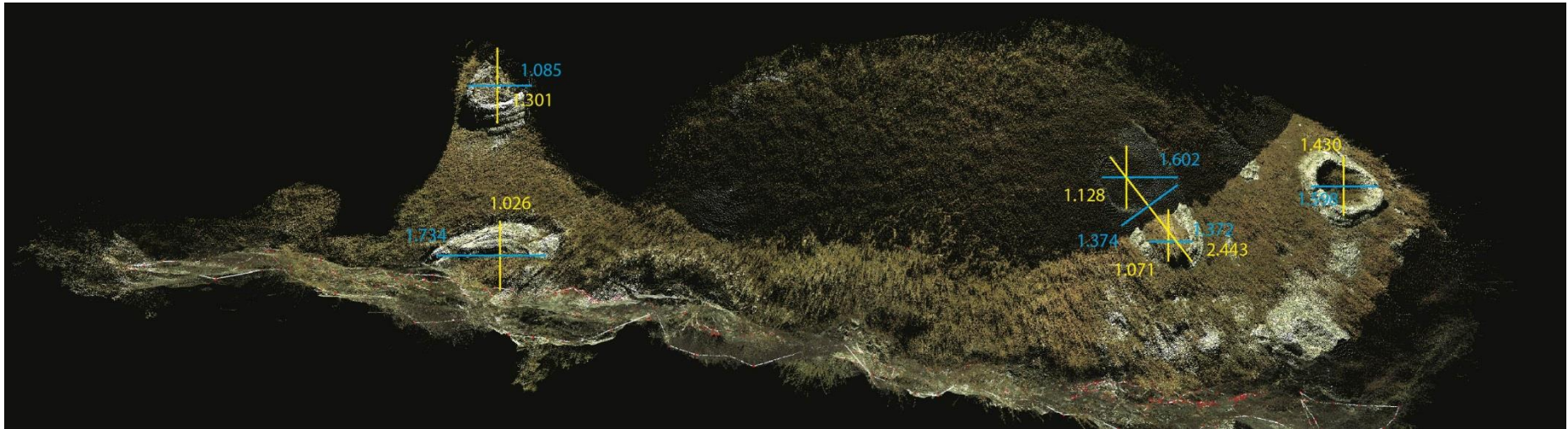


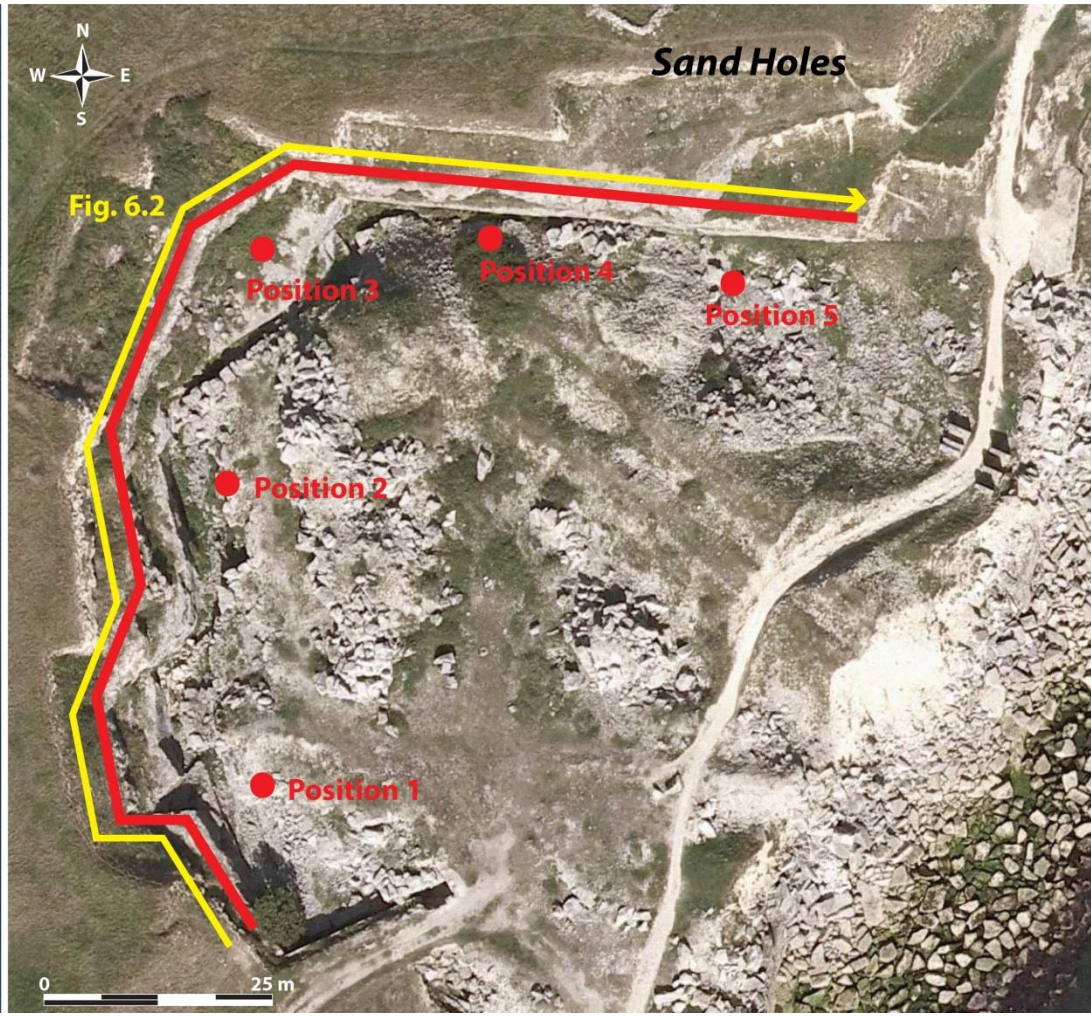
Figure 5.2 Lidar scans interpreted with height (yellow) and width (blue) measurements in meter.



**Figure 5.2 (continued)** Lidar scans interpreted with height (yellow) and width (blue) measurements in meter.

King Barrow Quarries													
Hard Cap							Skull Cap						
	Orientation of face	Areas (m <sup>2</sup> )	vA (m)	Perimeter (m)	Width (m)	Height (m)		Orientation of face	Areas (m <sup>2</sup> )	vA (m)	Perimeter (m)	Width (m)	Height (m)
Mound 1-2 combined	NE-SW	12.5676	3.545081099	25.089	8.096	2.29	Mound 3	NE-SW	0.239266	0.489148239	3.732	1.516	0.236
Mound 6	NE-SW	0.406982	0.637951409	3.372	1.314	0.49	Mound 4	NE-SW	0.432041	0.657298258	4.194	1.755	0.265
Mound 7	NW-SE	0.0579005	0.240625227	1.445	0.512	0.079	Mound 5	NE-SW	1.75276	1.323918426	9.802	4.313	0.541
Mound 8	NW-SE	1.57376	1.254495915	7.048	2.594	0.699	Mound 18	NW-SE	0.0538571	0.232071325	0.973	0.398	0.321
Mound 9	NW-SE	4.31034	2.076135834	21.65	8.495	1.308	Mound 19	NW-SE	0.263723	0.513539677	2.813	1.218	0.24
Mound 10	NW-SE	0.846075	0.919823353	7.4	2.905	0.531	Mound 20	NW-SE	0.00414201	0.064358449	0.253	0.089	0.054
Mound 11	NW-SE	0.501056	0.707853092	3.999	1.565	0.619	Mound 21	NW-SE	0.364386	0.603643935	4.23	1.774	0.378
Mound 12	NW-SE	0.0412915	0.2032031	1.327	0.6	0.073	Mound 22	NW-SE	0.0379522	0.194813244	1.307	0.796	0.264
Mound 13	NW-SE	0.431645	0.656996956	3.793	1.611	0.519	Mound 23	NW-SE	0.251668	0.501665227	2.381	0.891	0.346
Mound 14	NW-SE	0.0947135	0.307755585	2.189	0.682	0.399	Bed 2-1		1.74663		8.124		
Mound 15	NW-SE	0.293652	0.541896669	2.416	1	0.459	Bed 2-2		0.996239		4.648		
Mound 16	NW-SE	0.397736	0.630663143	3.991	1.577	0.417	Bed 2-3		1.32146		6.266		
Mound 17	NW-SE	0.969782	0.984775101	6.525	1.533	1.053	Bed 2-4		1.20165		10.12		
Bed 1		48.0276		53.894			Bed 4		2.16276		8.569		
Bed 3		23.4112		27.868									
Bed 5		1.57242		10.726									
Bed 6		0.101427		1.778									
	<b>Total Mound</b>	<b>20.82</b>						<b>Total Mound</b>	<b>3.40</b>				
	<b>Total Bed</b>	<b>71.44</b>						<b>Total Bed</b>	<b>9.18</b>				
	<b>Total Intermound</b>	<b>50.62</b>						<b>Total Intermound</b>	<b>5.78</b>				
	<b>% Mound</b>	<b>0.29</b>						<b>% Mound</b>	<b>0.37</b>				
	<b>% Intermound</b>	<b>0.71</b>						<b>% Intermound</b>	<b>0.63</b>				

**Figure 5.3** Measurements performed on mound and inter-mound areas in the Hard Cap (left) and Skull Cap (right) at King Barrow Quarries. Measurements in red indicate partially imaged mounds.



6 – Sand Holes

Figure 6.1 Location map of Sand Holes, scans positions and cliff areas scanned (red plain line). Yellow arrows indicate direction of presentation of scans in figure 6.2. Maps © 2016 GoogleEarth.

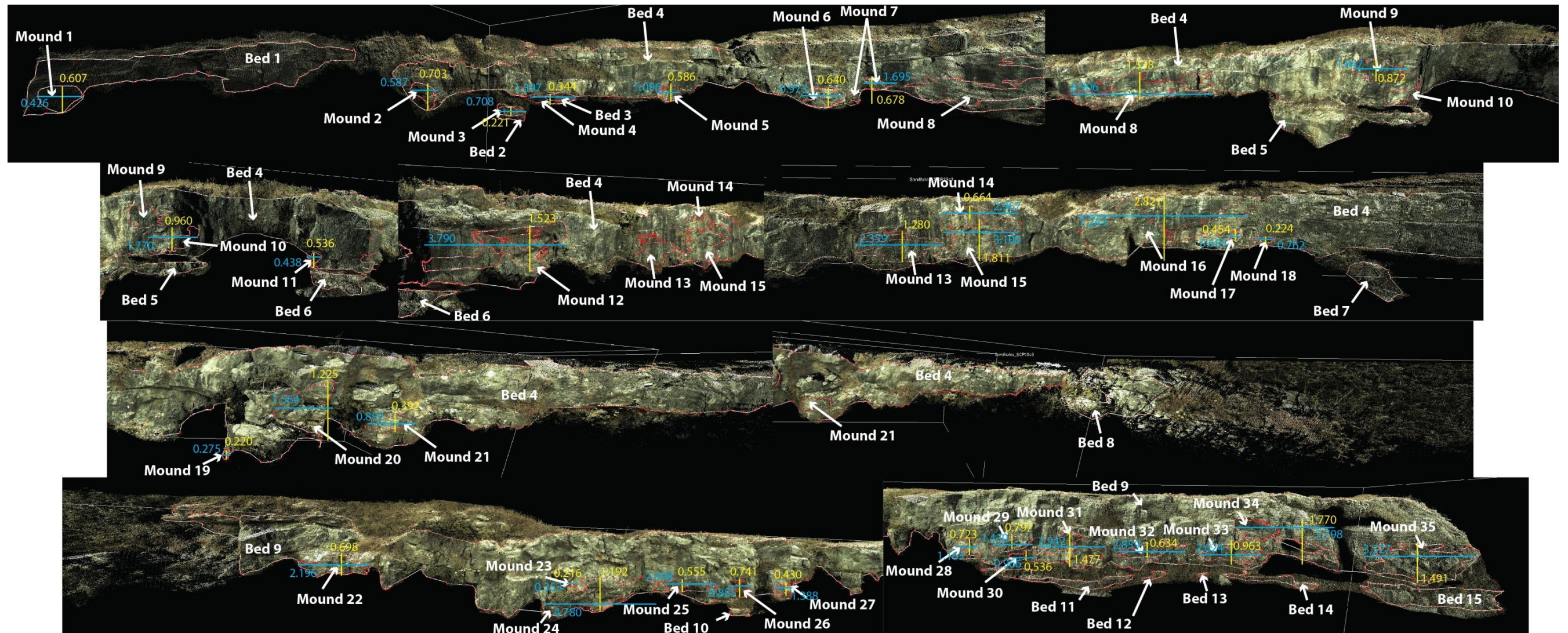
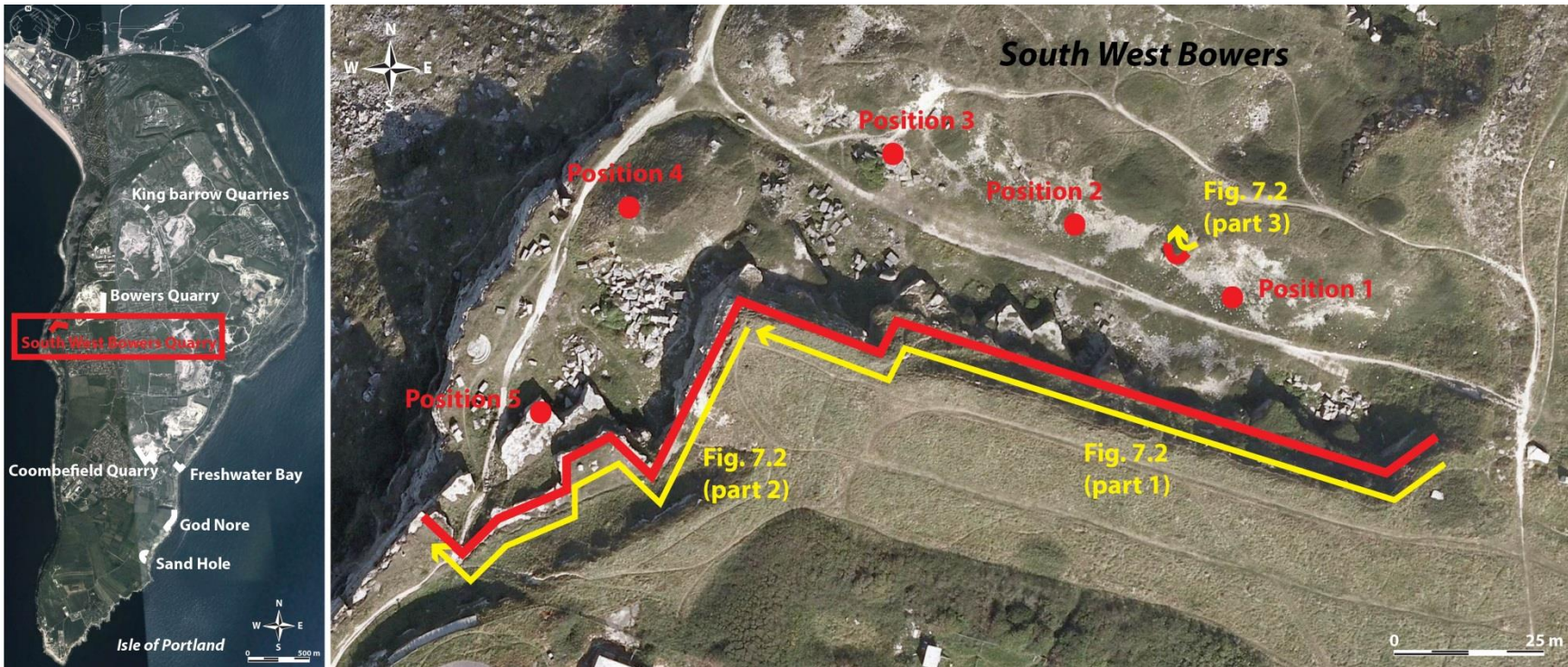


Figure 6.2 Lidar scans interpreted with height (yellow) and width (blue) measurements in meter.

Sand Holes													
Hard Cap						Skull Cap							
	Orientation of face	Areas (m <sup>2</sup> )	VA (m)	Perimeter (m)	Width (m)	Height (m)	Orientation of face	Areas (m <sup>2</sup> )	VA (m)	Perimeter (m)	Width (m)	Height (m)	
Mound 1	NNW-SSE	0.195967	0.442681601	1.864	0.426	0.607	Mound 3	NW-SE	0.153721	0.392072697	1.938	0.708	0.221
Mound 2	NW-SE	0.252475	0.502468905	2.348	0.587	0.703	Mound 4	NW-SE	0.213748	0.462328887	3.61	1.397	0.344
Mound 5	NW-SE	0.395944	0.629240812	3.142	1.096	0.586	Bed 2		0.294772		2.404		
Mound 6	NNW-SSE	0.361845	0.601535535	4.015	0.973	0.64	Bed 3		0.338752		3.957		
Mound 7	NNW-SSE	0.417118	0.645846731	4.129	1.695	0.678	Bed 5		6.08768		18.885		
Mound 8	NNW-SSE	5.75599	2.399164438	25.194	6.906	1.538	Bed 6		0.809635		5.314		
Mound 9	N-S	1.05307	1.02619199	6.157	1.847	0.872	Bed 7		0.809366		3.662		
Mound 10	NNW-SSE	0.833462	0.9129414	6.558	1.77	0.96	Bed 10		0.27375		2.967		
Mound 11	NE-SW	0.135782	0.368486092	2.125	0.438	0.536	Bed 11		1.67033		14.451		
Mound 12	NW-SE	2.650788	1.628124074	13.528	3.79	1.523	Bed 12		0.167544		2.728		
Mound 13	NNW-SSE	1.53978	1.240878721	10.039	2.359	1.28	Bed 13		0.0301759		0.959		
Mound 14	NNW-SSE	0.664925	0.815429335	7.228	2.967	0.664	Bed 14		0.686753		8.598		
Mound 15	NNW-SSE	2.64617	1.626705259	10.371	3.1	1.811	Bed 15		2.70628		10.665		
Mound 16	NNE-SSW	8.37955	2.894745239	23.816	7.243	2.821							
Mound 17	NNE-SSW	0.175456	0.418874683	2.053	0.693	0.454							
Mound 18	NNE-SSW	0.125972	0.354925344	1.933	0.762	0.224							
Mound 19	NNE-SSW	0.0462307	0.215013255	0.844	0.275	0.22							
Mound 20	NNE-SSW	1.18621	1.089132682	5.326	1.564	1.225							
Mound 21	NNE-SSW	0.261438	0.511310082	2.665	0.892	0.392							
Mound 22	WNW-ESE	0.933482	0.966168722	6.409	2.196	0.698							
Mound 23	WNW-ESE	0.0473179	0.21752678	1.013	0.353	0.216							
Mound 24	WNW-ESE	3.31423	1.820502678	13.808	4.78	1.192							
Mound 25	WNW-ESE	0.714154	0.845076328	5.805	2.098	0.555							
Mound 26	WNW-ESE	0.438758	0.662388104	4.372	0.885	0.741							
Mound 27	WNW-ESE	0.450341	0.671074512	3.883	1.388	0.43							
Mound 28	WNW-ESE	0.57896	0.760894211	3.615	1.163	0.723							
Mound 29	WNW-ESE	0.784684	0.88582391	4.235	1.43	0.797							
Mound 30	WNW-ESE	0.419421	0.647627208	3.208	0.966	0.536							
Mound 31	WNW-ESE	1.90924	1.38175251	10.566	2.942	1.477							
Mound 32	WNW-ESE	0.748547	0.865186107	8.21	2.859	0.634							
Mound 33	WNW-ESE	1.37182	1.171247199	7.927	2.624	0.963							
Mound 34	WNW-ESE	2.13556	1.461355535	13.88	3.798	1.77							
Mound 35	WNW-ESE	3.2796	1.810966593	12.575	3.327	1.491							
Bed 1		4.90684		16.561									
Bed 4		162.183		202.211									
Bed 8		2.16284		8.146									
Bed 9		132.144		128.575									
	<b>Total Mound</b>	<b>44.20</b>											
	<b>Total Bed</b>	<b>301.40</b>											
	<b>Total Intermound</b>	<b>257.19</b>											
	<b>% Mound</b>	<b>0.15</b>											
	<b>% Intermound</b>	<b>0.85</b>											
	<b>Total Mound</b>	<b>0.37</b>											
	<b>Total Bed</b>	<b>13.88</b>											
	<b>Total Intermound</b>	<b>13.51</b>											
	<b>% Mound</b>	<b>0.03</b>											
	<b>% Intermound</b>	<b>0.97</b>											

**Figure 6.3** Measurements performed on mound and inter-mound areas in the Hard Cap (left) and Skull Cap (right) at Sand Holes. Measurements in red indicate partially imaged mounds.





7 – South West Bowers

**Figure 7.1** Location map of South West Bowers, scans positions and cliff areas scanned (red plain line). Yellow arrows indicate direction of presentation of scans in figure 7.2. Maps © 2016 GoogleEarth.

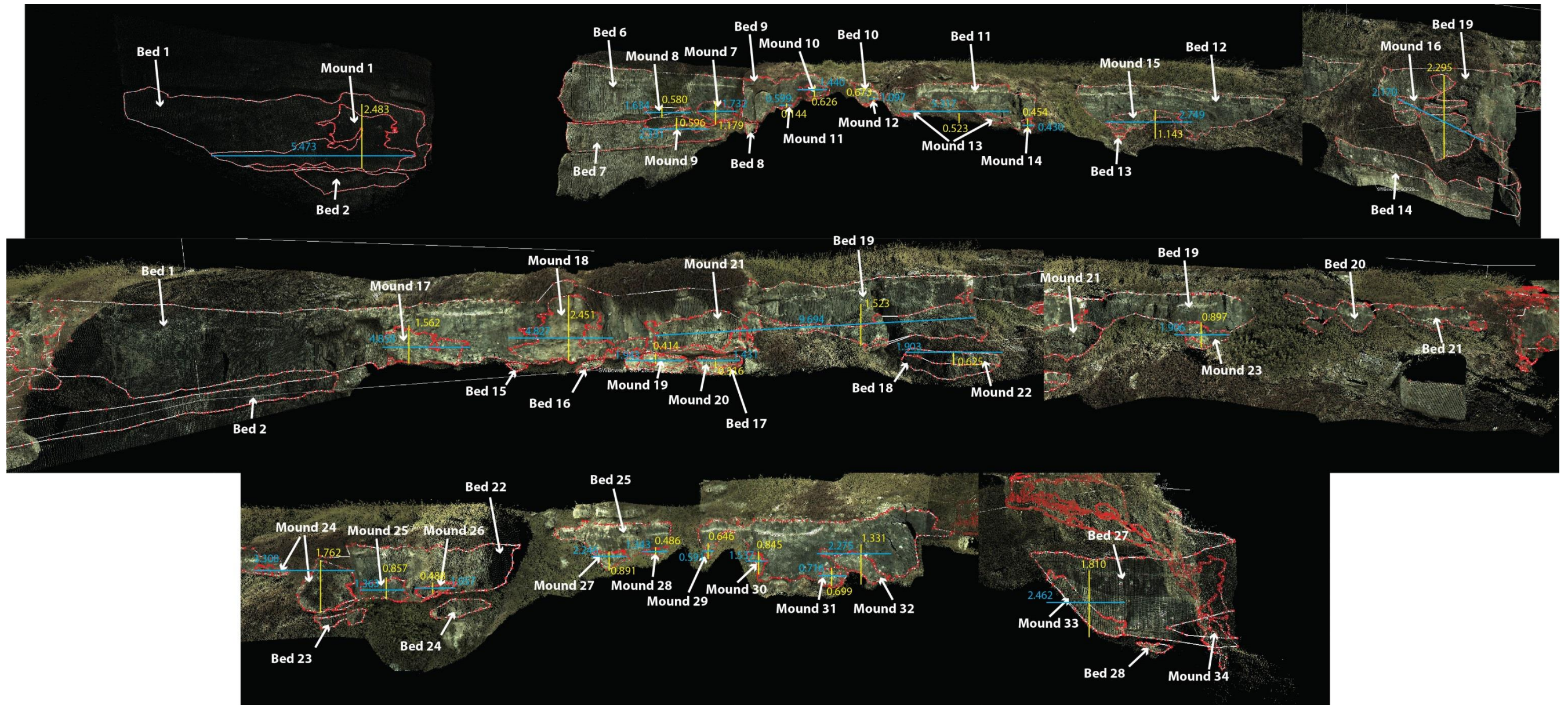


Figure 7.2 Lidar scans interpreted with height (yellow) and width (blue) measurements in meter (part 1).

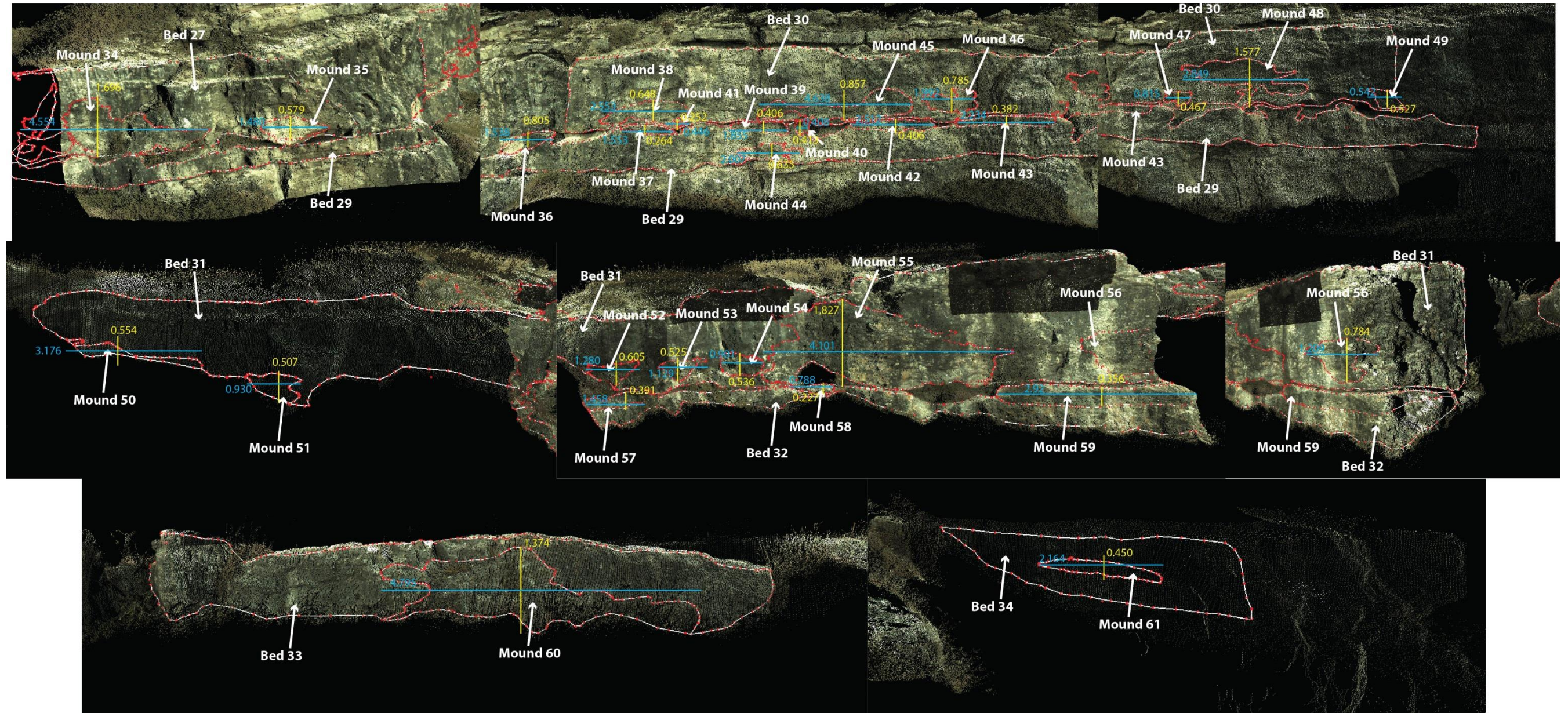


Figure 7.2 (continued) Lidar scans interpreted with height (yellow) and width (blue) measurements in meter (part 2).

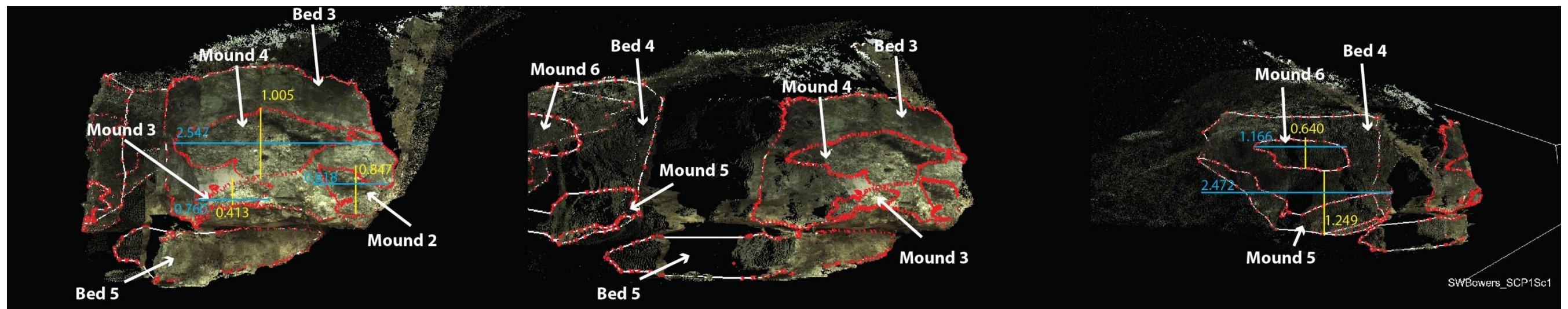
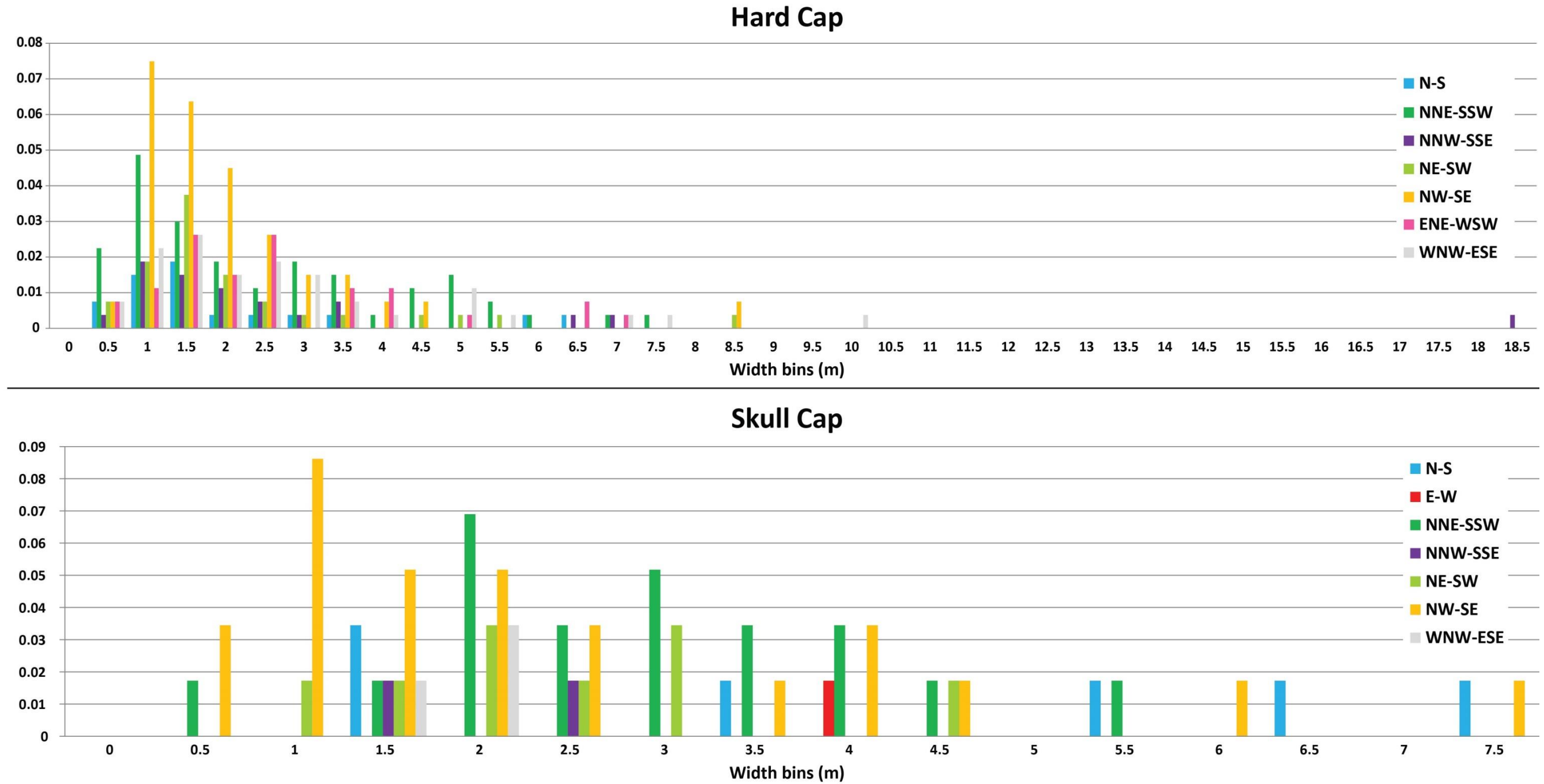


Figure 7.2 (continued) Lidar scans interpreted with height (yellow) and width (blue) measurements in meter (part 3)

South West Bowers													
Hard Cap						Skull Cap							
	Orientation of face	Areas (m <sup>2</sup> )	VA (m)	Perimeter (m)	Width (m)	Height (m)	Orientation of face	Areas (m <sup>2</sup> )	VA (m)	Perimeter (m)	Width (m)	Height (m)	
Mound 1	NE-SW	6.18965	2.487900721	23.002	5.473	2.483	Mound 9	NE-SW	0.601095	0.775303167	5.785	2.331	0.596
Mound 2	NW-SE	0.45662	0.675736635	3.439	0.818	0.847	Mound 19	WNW-ESE	0.640759	0.800474234	5.129	1.943	0.414
Mound 3	NW-SE	0.29589	0.543957719	3.299	0.76	0.413	Mound 20	WNW-ESE	0.404957	0.636362318	3.434	1.431	0.316
Mound 4	NW-SE	1.47266	1.213532035	7.241	2.547	1.005	Mound 22	WNW-ESE	0.607757	0.779587712	4.829	1.903	0.625
Mound 5	NW-SE	1.25756	1.121409827	8.428	2.472	1.249	Mound 36	NNE-SSW	0.553179	0.743760042	3.75	1.538	0.805
Mound 6	NW-SE	0.523073	0.723237859	3.288	1.166	0.64	Mound 37	NNE-SSW	0.291843	0.540224953	3.236	1.553	0.264
Mound 7	NE-SW	1.23308	1.110441354	5.137	1.732	1.179	Mound 39	NNE-SSW	0.534365	0.731002736	4.257	1.855	0.406
Mound 8	NE-SW	0.448562	0.669747714	3.848	1.634	0.58	Mound 40	NNE-SSW	0.127929	0.357671637	1.393	0.408	0.413
Mound 10	WNW-ESE	0.553806	0.744181429	4.248	1.44	0.626	Mound 42	NNE-SSW	0.676855	0.822711979	5.501	2.512	0.406
Mound 11	WNW-ESE	0.0580464	0.240928205	1.456	0.599	0.144	Mound 43	NNE-SSW	0.591174	0.768878404	5.31	2.234	0.382
Mound 12	WNW-ESE	0.120754	0.347496763	2.675	1.097	0.673	Mound 44	NNE-SSW	0.725221	0.851599084	5.408	2.007	0.635
Mound 13	WNW-ESE	0.533722	0.730562797	5.362	5.317	0.523	Mound 57	NE-SW	0.364641	0.603855115	3.341	1.458	0.391
Mound 14	WNW-ESE	0.193366	0.439734011	2.2	0.43	0.454	Mound 58	NE-SW	0.143175	0.378384725	1.891	0.788	0.227
Mound 15	WNW-ESE	1.45512	1.206283549	9.254	2.749	1.143	Mound 59	NE-SW	0.990599	0.9952884	8.225	2.92	0.356
Mound 16	NNW-SSE	3.07563	1.753747416	17.025	2.17	2.295	Bed 2		2.23821		8.95		
Mound 17	WNW-ESE	5.09678	2.257604926	14.391	4.858	1.562	Bed 5		2.16416		8.995		
Mound 18	WNW-ESE	5.70702	2.388937002	20.23	4.827	2.451	Bed 7		4.94122		14.337		
Mound 21	WNW-ESE	7.43842	2.727346696	30.035	9.694	1.523	Bed 8		0.345536		2.463		
Mound 23	WNW-ESE	0.915414	0.9567727	5.095	1.906	0.897	Bed 13		0.0523128		0.998		
Mound 24	WNW-ESE	1.86675	1.366290599	8.582	3.308	1.762	Bed 14		6.65852		26.878		
Mound 25	NE-SW	0.774583	0.880103971	3.979	1.363	0.857	Bed 15		0.124919		1.719		
Mound 26	NE-SW	0.324959	0.570051752	2.793	1.057	0.488	Bed 16		0.245366		2.49		
Mound 27	WNW-ESE	1.17425	1.083628165	6.196	2.246	0.891	Bed 17		1.70186		9.161		
Mound 28	WNW-ESE	0.358784	0.59898581	3.436	1.343	0.486	Bed 18		1.21106		5.452		
Mound 29	WNW-ESE	0.212535	0.461015184	2.148	0.591	0.646	Bed 23		0.409824		3.577		
Mound 30	WNW-ESE	0.675764	0.82204866	4.896	1.537	0.845	Bed 24		0.902565		4.301		
Mound 31	WNW-ESE	0.403836	0.63548092	2.499	0.716	0.699	Bed 28		0.175273		2.174		
Mound 32	WNW-ESE	1.06887	1.033861693	6.079	2.275	1.331	Bed 29		34.1624		79.122		
Mound 33	N-S	1.6997	1.303725431	7.34	2.462	1.81	Bed 32		5.33678		27.288		
Mound 34	N-S & NE-SW	4.68944	2.165511487	17.752	4.554	1.696							
Mound 35	NNE-SSW	0.564377	0.751250291	3.519	1.48	0.579	<b>Total Mound</b>	<b>7.25</b>					
Mound 38	NNE-SSW	1.15547	1.074927905	5.787	2.553	0.648	<b>Total Bed</b>	<b>60.67</b>					
Mound 41	NNE-SSW	0.0433117	0.208114632	1.062	0.446	0.252	<b>Total Intermound</b>	<b>53.42</b>					
Mound 45	NNE-SSW	2.16072	1.469938774	10.854	4.638	0.857							
Mound 46	NNE-SSW	0.925777	0.962173061	5.674	1.992	0.785	<b>% Mound</b>	<b>0.12</b>					
Mound 47	NNE-SSW	0.268511	0.51818047	2.424	0.815	0.467	<b>% Intermound</b>	<b>0.88</b>					
Mound 48	NNE-SSW	1.67373	1.293727174	10.101	2.849	1.577							
Mound 49	NNE-SSW	0.21502	0.463702491	2.141	0.542	0.527							
Mound 50	NW-SE	0.638326	0.798953065	8.295	3.176	0.554							
Mound 51	NW-SE	0.372411	0.610254865	2.907	0.93	0.507							
Mound 52	NE-SW	0.408479	0.639123619	3.411	1.28	0.605							
Mound 53	NE-SW	0.34609	0.588294144	3.117	1.129	0.525							
Mound 54	NE-SW	0.3935	0.627295784	2.663	0.901	0.536							
Mound 55	NE-SW	4.89373	2.21217766	13.963	4.101	1.827							
Mound 56	NE-SW	0.633445	0.795892581	4.132	1.209	0.784							
Mound 60	ENE-WSW	3.36948	1.835614339	14.039	4.795	1.374							
Mound 61	NNW-SSE	0.647743	0.804824826	4.817	2.164	0.45							
Bed 1		16.6547		22.496									
Bed 3		6.34493		11.62									
Bed 4		5.03705		10.358									
Bed 6		13.2272		18.636									
Bed 9		7.02092		14.99									
Bed 10		1.38032		5.348									
Bed 11		10.3674		22.083									
Bed 12		10.5536		18.184									
Bed 19		80.2864		89.962									
Bed 20		2.7583		14.367									
Bed 21		2.76206		10.959									
Bed 22		14.7423		21.165									
Bed 25		8.4934		16.765									
Bed 26		20.0035		30.985									
Bed 27		26.221		31.294									
Bed 30		41.8967		47.05									
Bed 31		39.8748		51.966									
Bed 33		11.084		22.769									
Bed 34		7.73049		14.03									
<b>Total Mound</b>		<b>68.98</b>											
<b>Total Bed</b>		<b>326.44</b>											
<b>Total Intermound</b>		<b>257.45</b>											
<b>% Mound</b>		<b>0.21</b>											
<b>% Intermound</b>		<b>0.79</b>											

**Figure 7.3** Measurements performed on mound and inter-mound areas in the Hard Cap (left) and Skull Cap (right) at South West Bowers. Measurements in red indicate partially imaged mounds.

## 8 – Analyses on orientation of quarry faces



**Figure 8.1** Histograms of widths of the mounds in either the Skull or the Hard Cap mounds, depending on the orientations of the quarry faces they are exposed. The main goal was to determine if there is a preferred direction of elongation of the mounds. However it appears that there are no such elongations.

## Appendix 2.2. Hyperspectral imaging

Hyperspectral imaging is a remote sensing application based on imaging spectrometry that measures the reflectance of rocks (ratio between the reflected and the incident light of a sample; Gaffrey, 1985; Kurz *et al.*, 2012). The source of radiation is commonly the sunlight and the reflectance is usually recorded in the visible and nearly infrared (0.3 to 2.55  $\mu\text{m}$  in wavelength) portion of the electromagnetic spectrum (Gaffrey, 1985; van der Meer and de Jong, 2002). The reflectance is a function of the wavelength, the chemical composition (mineralogy) of the rock and physical parameters such as grain size, sorting, surface roundness, porosity and mineral impurities (Kurz *et al.*, 2012, 2013). Minerals absorb and reflect part of the spectrum of light differently and in a unique manner for each mineral which are possible to measure with a spectral imaging device (Kurz *et al.*, 2012). The absorption that characterises each mineral is due to vibrational processes of the ions that either release or catch photons to compensate the energy gain or the loss on their external layers (Gaffrey, 1985; van der Meer and de Jong, 2002). Although hyperspectral imaging requires an large amount of post-processing, this technique can measure a wider portion of the electromagnetic spectrum in a continuum than with conventional imaging techniques that record only red, green and blue (*i.e.* RGB; Hunt, 1980; Goetz *et al.*, 1985; Clark *et al.*, 1990; Kurz *et al.*, 2012, 2013).

This technique was chosen to try to quantify automatically the quantity of microbial mounds (considered as pure calcite) versus the inter-mound facies (containing impurities such as quartz grains). In this project 5 samples were scanned in laboratory conditions in Bergen University (Norway) by Tobias Kurz and John Howell. The samples are named by a letter A, B, C, D and E and the way up is marked by an arrow (Figs. 1, 2 and 3). Sample A corresponds to SWB2 (South West Bowers, Isle of Portland) and is characterised by the Intraclastic peloidal packstone-grainstone facies (inter-mound) facies; sample B corresponds to SWB3 (South West Bowers, Isle of Portland) and is characterised by the Thrombolite sub-facies (microbial mound facies); and C, D and E correspond to GN6 (God Nore, Isle of Portland) respectively characterised by the inter-mound facies, the mound sub-facies and the marked transition between microbial mound and inter-mound facies. These samples were scanned on three sides, a rough surface (fresh break, Fig. 1), a plane surface (saw surface, Fig. 2) and the top surface (Fig. 3).

The following paragraphs are from the report sent together with the images and graphs by Tobias Kurz.

All images show the same results. The spectral properties of all 5 samples are quite similar and show the diagnostic absorption bands of carbonate ions at 2.33 nm, 2.14 nm, 1.99 nm and 1.87 nm (Figs. 1, 2 and 3). The broad absorption between 1400-1550 nm and between 1800-2050 nm is caused by the atmosphere mainly due to water vapour.

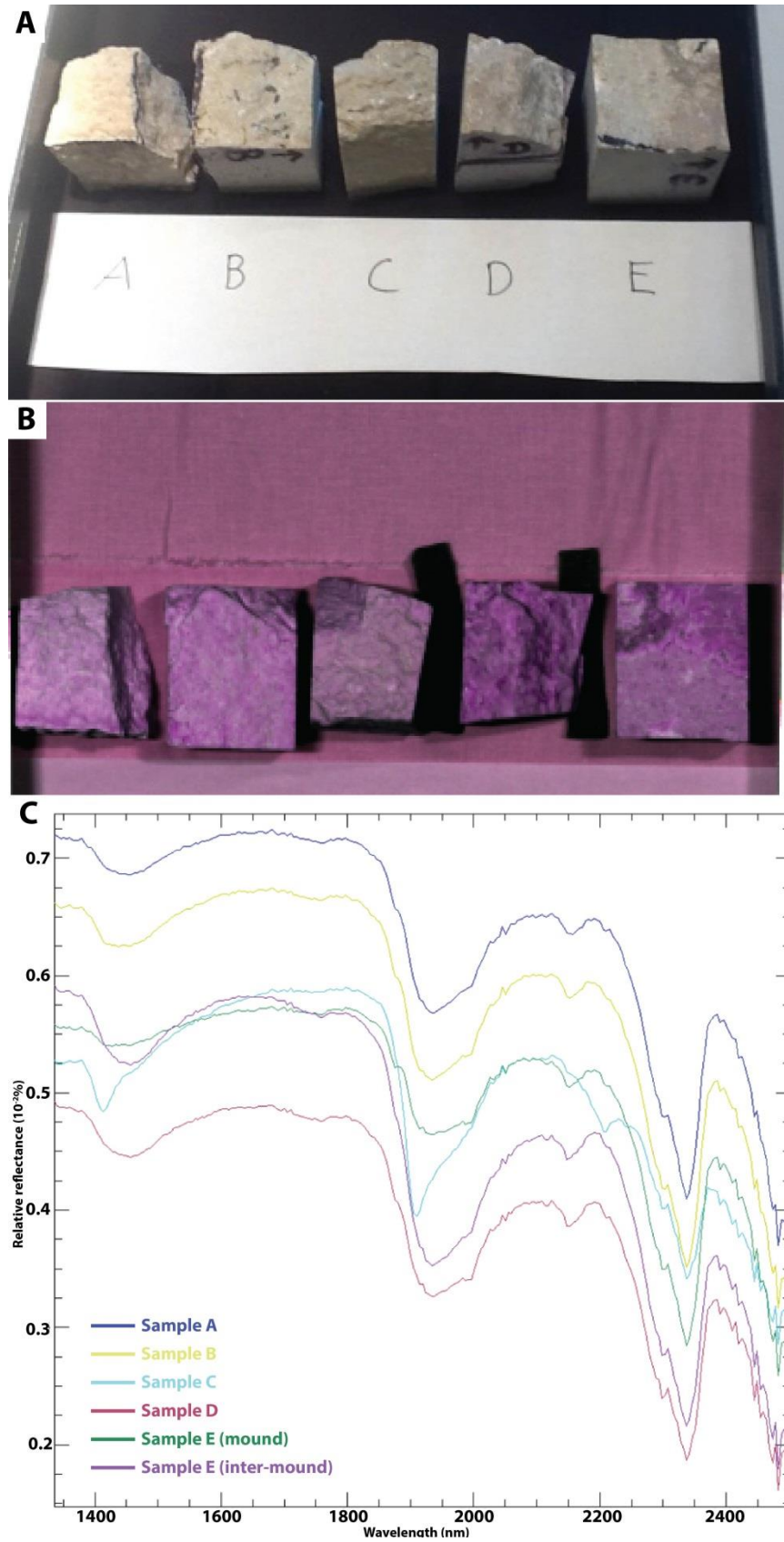
Some spectra show very weak absorption at 2200 nm, 1900 nm and 1400 nm. The absorption bands at 2200 nm and 1400 nm are typical for hydroxyl bearing material whereas the 1900 nm band indicates the presence of water within a mineral. These spectral properties might indicate the present of hydroxyl and/or water bearing clays although with very low concentration.

In the image of the fresh break surface (Fig. 1), the spectra of sample C (coloured in cyan) show pronounced absorption at 2200 nm, 1400 nm and less pronounced absorption at 1900 nm. This indicates probably the presence of a significant amount of clay. However this observation was not confirmed by scanning the same sample from two other sides. This can either mean that the sample consists of very heterogeneous material or the fresh break surface has been coated during sample preparation.

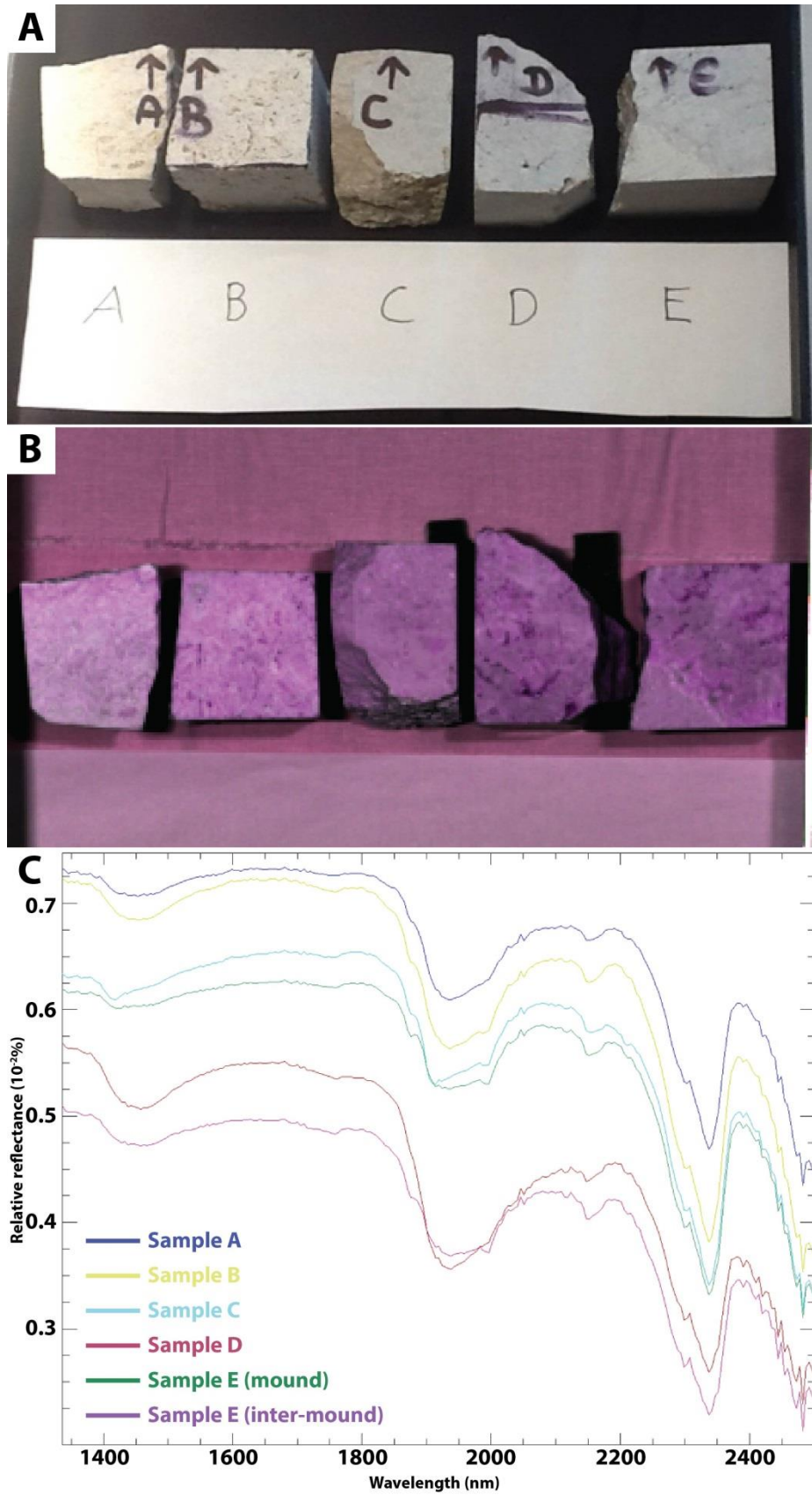
Beside the analysis and interpretation of the spectra absorption features, some image classifications were tested (not shown in the report). However, the classification images could not differentiate between the microbial mound and the inter-mound facies but this classification is not clear enough to be used in the field. The sample C was however noticeable in the classification images. It seems that sample C is somehow different although with weak evidence.

In conclusion, all samples consist of nearly pure calcium carbonate. Some sample spectra indicate a very low concentration of impurities (most likely some clay minerals). It seems that the microbial mound and the inter-mound facies differ in texture but do not show significant differences in mineral / material composition. Therefore a separation between both facies using hyperspectral imaging did not seem possible and was not pursued further.

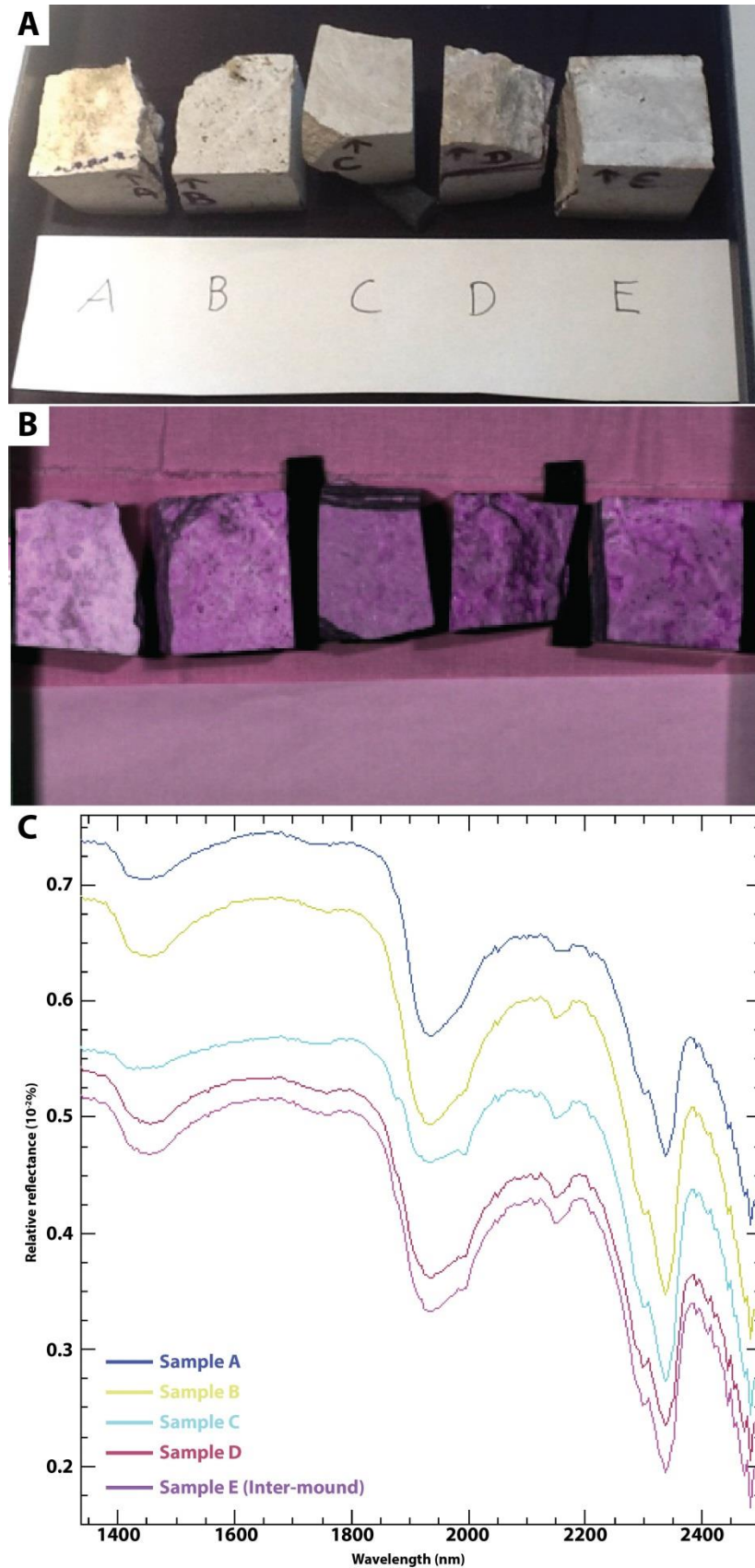




**Figure 1** Fresh break surface scans. A – Picture of the samples. B – Hyperspectral image. C – Spectral curves. Note that Sample C shows, beside the carbonate absorption feature, pronounced absorption bands at 2200nm, 1900 nm and 1425 nm, absorption bands at 2200 nm, 1900 nm and 1400 nm that indicates presence of hydroxyl and/or water bearing minerals.



**Figure 2** Saw surface scans. A – Picture of the samples. B – Hyperspectral image. C – Spectral curves.



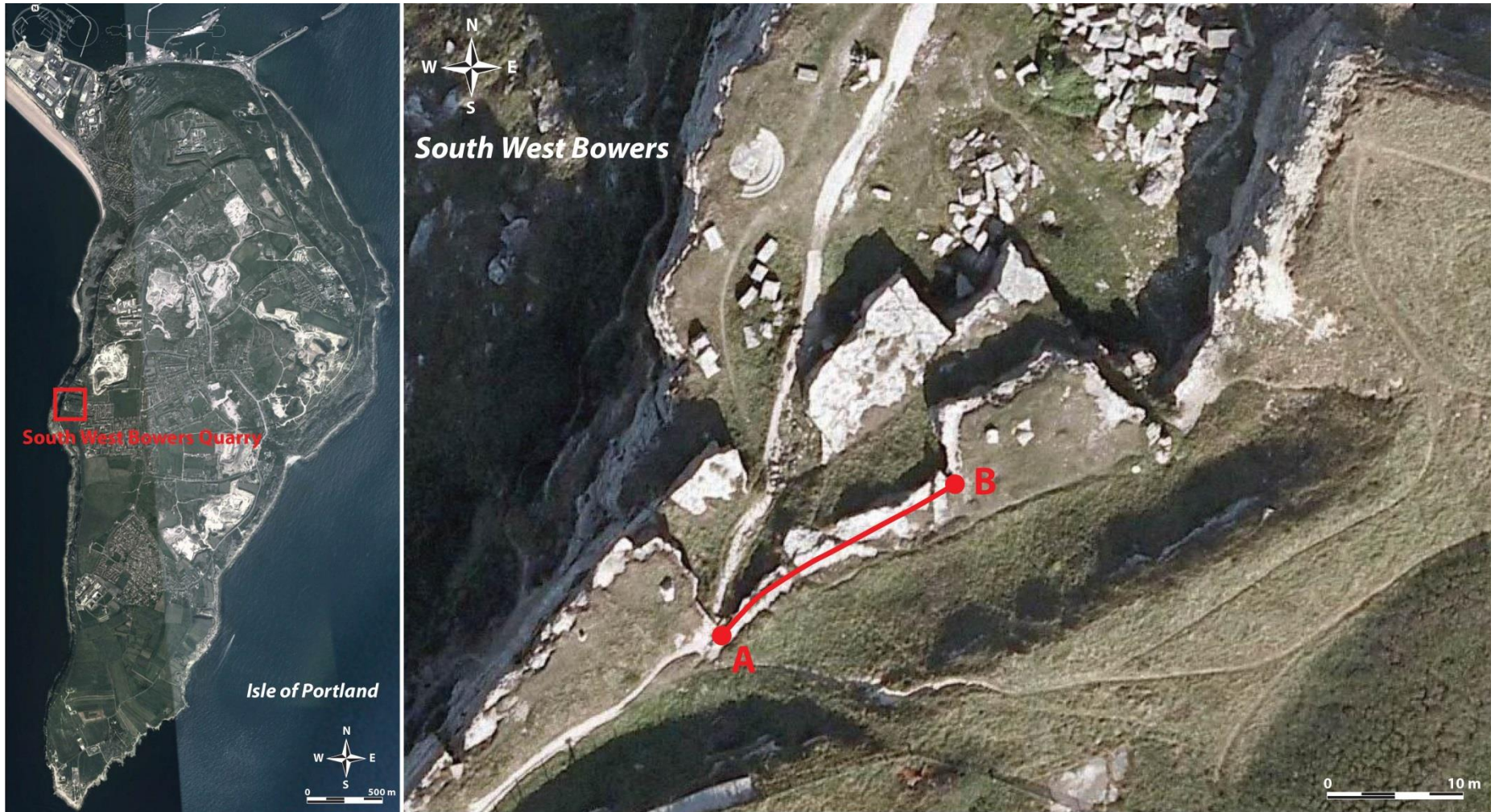
**Figure 3** Top surface scans. A – Picture of the samples. B – Hyperspectral image. C – Spectral curves.

## Appendix 2.3. Ground penetrated radar (GPR)

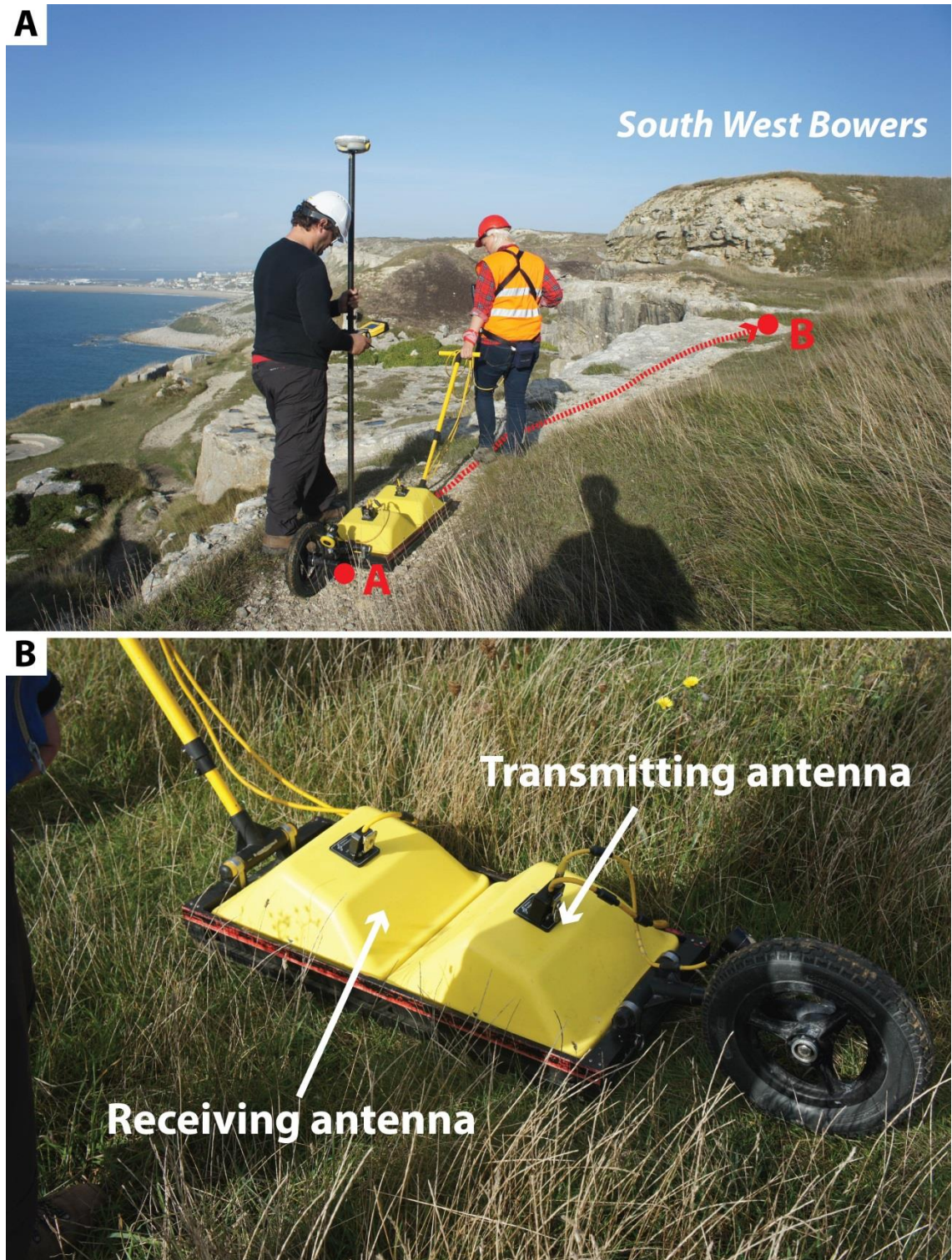
Ground penetrating radar (GPR) is based on propagation and reflection of electromagnetic waves in the sub-surface (Barker *et al.*, 2007). The velocity of propagation is controlled by the relative permittivity contrasts between layers that depend on the ability of the layers to store and propagate electromagnetic wave energy (Barker *et al.*, 2007). The recorded signal corresponds to electromagnetic waves refracted to the surface due to these permittivity contrasts between layers (Barker *et al.*, 2007). The GPR system is typically made of a transmitting antenna that generates electromagnetic waves and a receiving antenna that records reflected waves (Barker *et al.*, 2007). An important characteristic of electromagnetic waves is that their attenuation is dependent of the magnetic permeability (ability of a layer to be magnetised) and the electrical conductivity (ability of electrons to move when an electrical field is applied) of layers (Barker *et al.*, 2007). The magnetic permeability value is commonly equal to 1 for most rock and soils and will not be the main factor influencing the attenuation (Barker *et al.*, 2007). The electrical conductivity mainly depends on the water saturation of rocks or soils and the conductivity will be high when the water saturation is high (Barker *et al.*, 2007). As a consequence the attenuation of the electromagnetic waves is greatest when the conductivity and the water saturation are high (Barker *et al.*, 2007). Barker *et al.* (2007) stated that commonly is GPR studies of clay soils show high conductivity resulting in significant attenuation of the encountered electromagnetic waves.

In this project two profiles were attempted to be acquired and only one was actually recorded. Both were performed at South West Bowers disused quarry on the western side of the Isle of Portland (Fig. 1). The surveys were done in collaboration with Dr. Julien Moreau and Trine Hansen from the University of Copenhagen (Denmark) using 250 MHz antennae of the PulseEKKO system of Sensors & Software Inc. (Mississauga, ON, Canada, Fig. 2). The first survey was undertaken directly on top of a modern soil therefore, because of the high conductivity of soils as described above, the electromagnetic waves were attenuated within the soil and no profiles could be recorded. The second survey was done on top of the rock surface of the Hard Cap bed (Figs. 1 and 2) and the sub-surface could be imaged (Fig. 3). This space profile is about 19.5 m long for a maximum depth of clear image between 3 m (on the left) and 4.5 m (on the right, Fig. 3). No waves were reflected beyond these depths probably due to the Lower Dirt Bed paleosol that would be expected to have increased conductivity and a maximum attenuation and accompanied loss of image (Fig. 3).

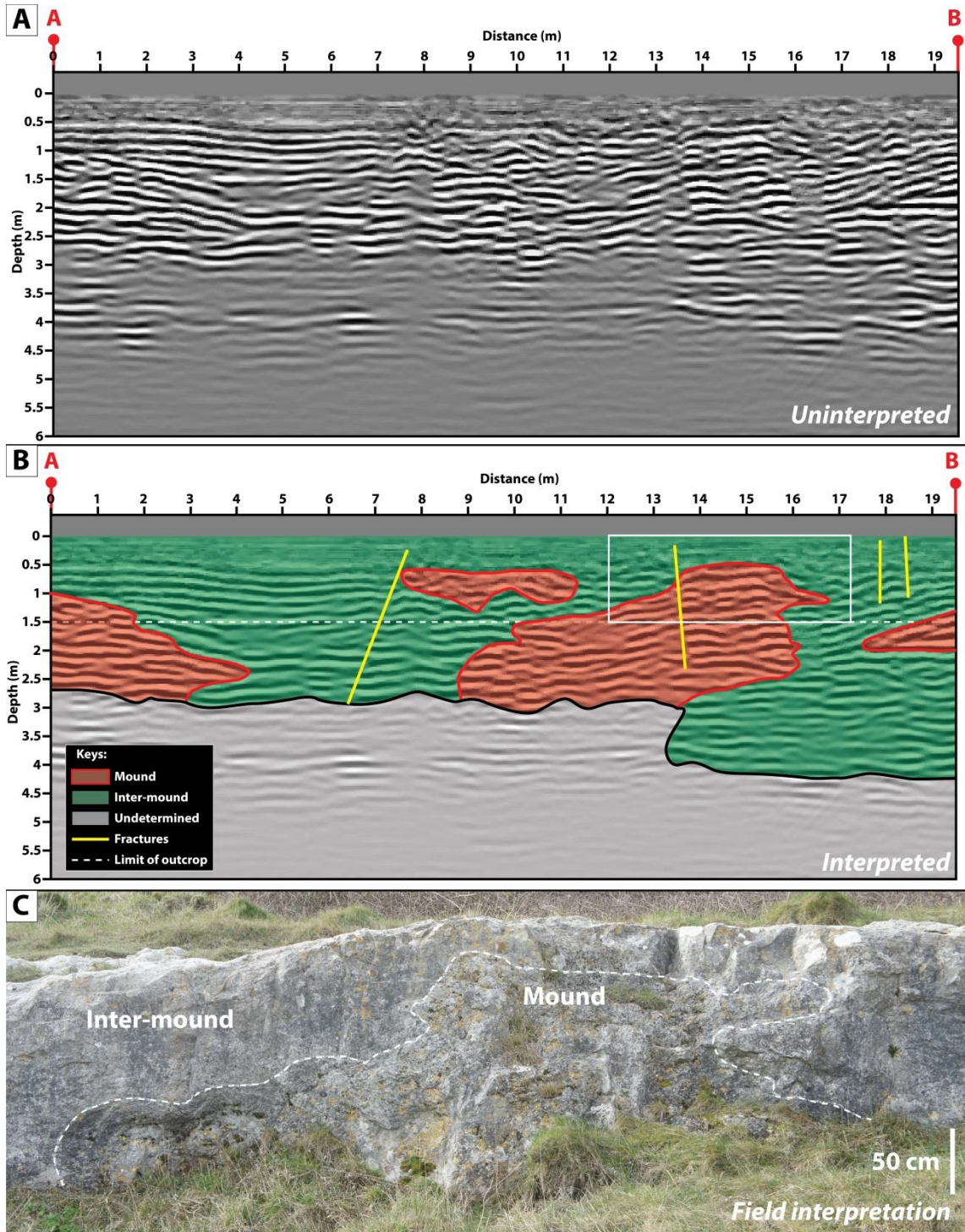
Although the survey is very good quality and detailed mounds and inter-mound facies (Fig. 3), outcrop conditions good enough to record high quality surveys are met in few locations along the Dorset coast, it was decided to not proceed further with GPR surveys.



**Figure 1** Location map and path followed for acquisition of the profile (shown in figure 3). Maps © 2016 GoogleEarth.



**Figure 2** GPR used in this study. A – Acquisition in South West Bowers by Dr. Julien Moreau (left) with the GPS unit and Trine Hansen (right) pulling the GPR unit. Note the path followed as per figure 1. B – Detail of the equipment used.



**Figure 3** GPR profile acquired at South West Bowers from point A to point B of figure 1. A – Uninterpreted profile. B – Interpreted profile. Note the white square locates the image in C. C – Interpretation from the field for comparison with GPR profile interpreted. Note the matching interdigitation to the right.



# Appendix 3

## Sedimentary logs

## 1. Sedimentary logs

1 – Legend

2 – Broadcroft Quarry

3 – Chalbury

4 – Coombefield Quarry

5 – Dungy Head

6 – Durlston Head

7 – Fishermen’s Ledge

8 – Fossil Forest

9 – God Nore

10 – Hell’s Bottom

11 – King Barrow Quarries

12 – Lawnsheds Quarry

13 – Mupe Bay

14 – Penn’s Weare

15 – Perryfield Quarry

16 – Portesham Quarry

17 – Portland Bill

18 – Poxwell Quarry

19 – South West Bowers

20 – Swanworth Quarry

21 – Tout Quarry

22 – West Lulworth Cove

23 – Worbarrow Bay


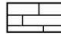

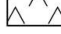
**Stratigraphy:**

**HCB: Hard Cockle Bed**  
**CF: Cypris Freestone**  
**SC: Soft Cap**  
**GDB: Great Dirt Bed**  
**HC: Hard Cap**  
**LDB: Lower Dirt Bed**  
**SkC: Skull Cap**  
**BDB: Basal Dirt Bed**  
**TB: Transition Bed**  
**PG: Portland Group**

**Textures in log:**

**M: Mudstone**  
**W: Wackestone**  
**F: Floatstone**  
**P: Packstone**  
**G: Grainstone**  
**R: Rudstone**  
**B: Boundstone**  
**C: Crystalline**








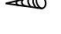
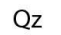







**Lithologies:**

 **Paleosol**  
 **Limestone**  
 **Laminations**  
 **Evaporites**



**Facies:**

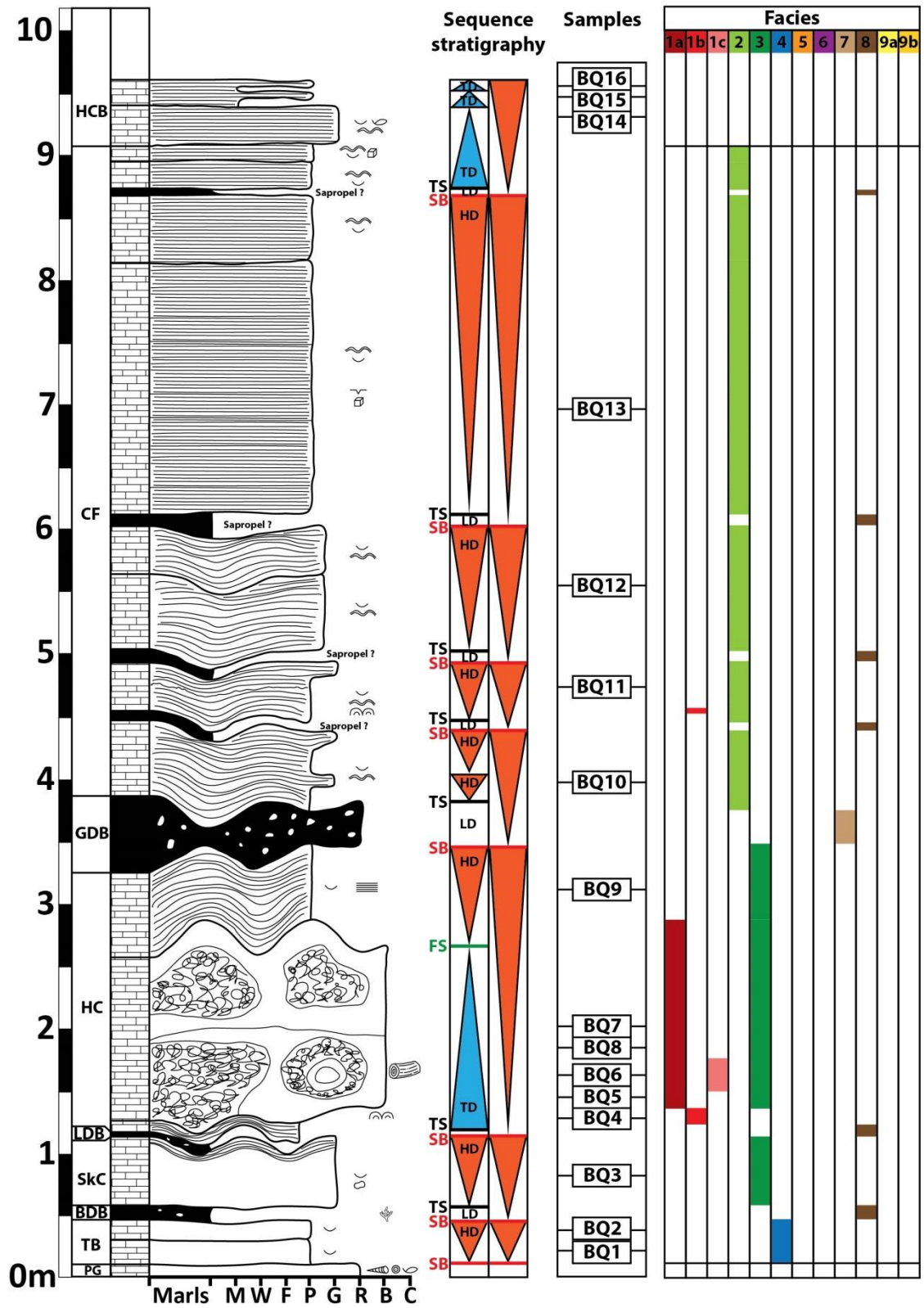
**1a: Thrombolite**  
**1b: Stromatolite**  
**1c: Burrowed peloidal packstone**  
**2: Intraclastic peloidal packstone-grainstone**  
**3: Cross-bedded peloidal packstone-grainstone**  
**4: Wackestone to fine grainstone**  
**5: Gypsiferous peloidal packstone**  
**6: Calcareous sandstone**  
**7: Conglomerate**  
**8: Carbonaceous marl**  
**9a: Evaporite vuggy**  
**9b: Evaporite breccia**

**Log components:**

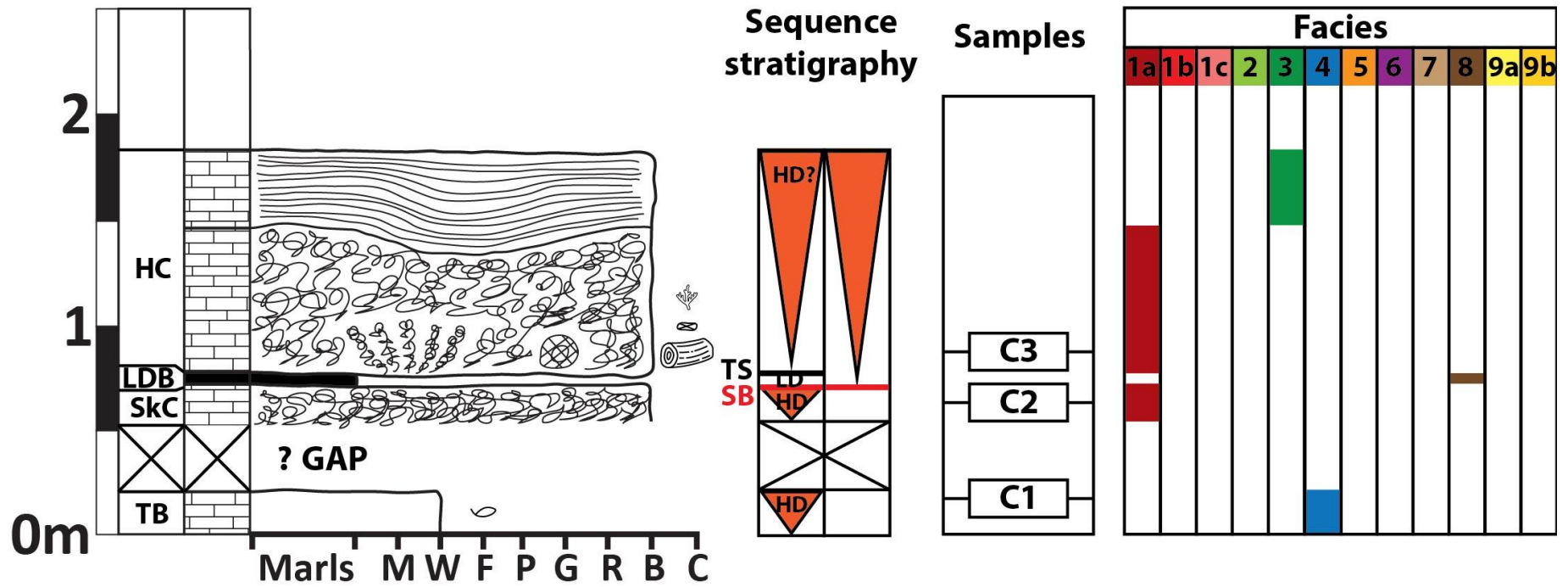
 **Mudcrack**  
 **Herring bone cross-stratification**  
 **Cross-lamination**  
 **Planar lamination**  
 **Wavy-bedding**  
 **Ostracod**  
 **Bivalve**  
 **Gastropod**  
 **Fish bone**  
 **Intraclast**  
 **Quartz grain**  
 **Ooid**  
 **Stromatolite**  
 **Evaporite pseudomorph**  
 **Log**  
 **Stump**  
 **Wood remain**  
 **Chert nodule**  
 **Cherty bed**  
 **Thrombolites**  
 **Micro-karstic surface**

**Sequence stratigraphy:**

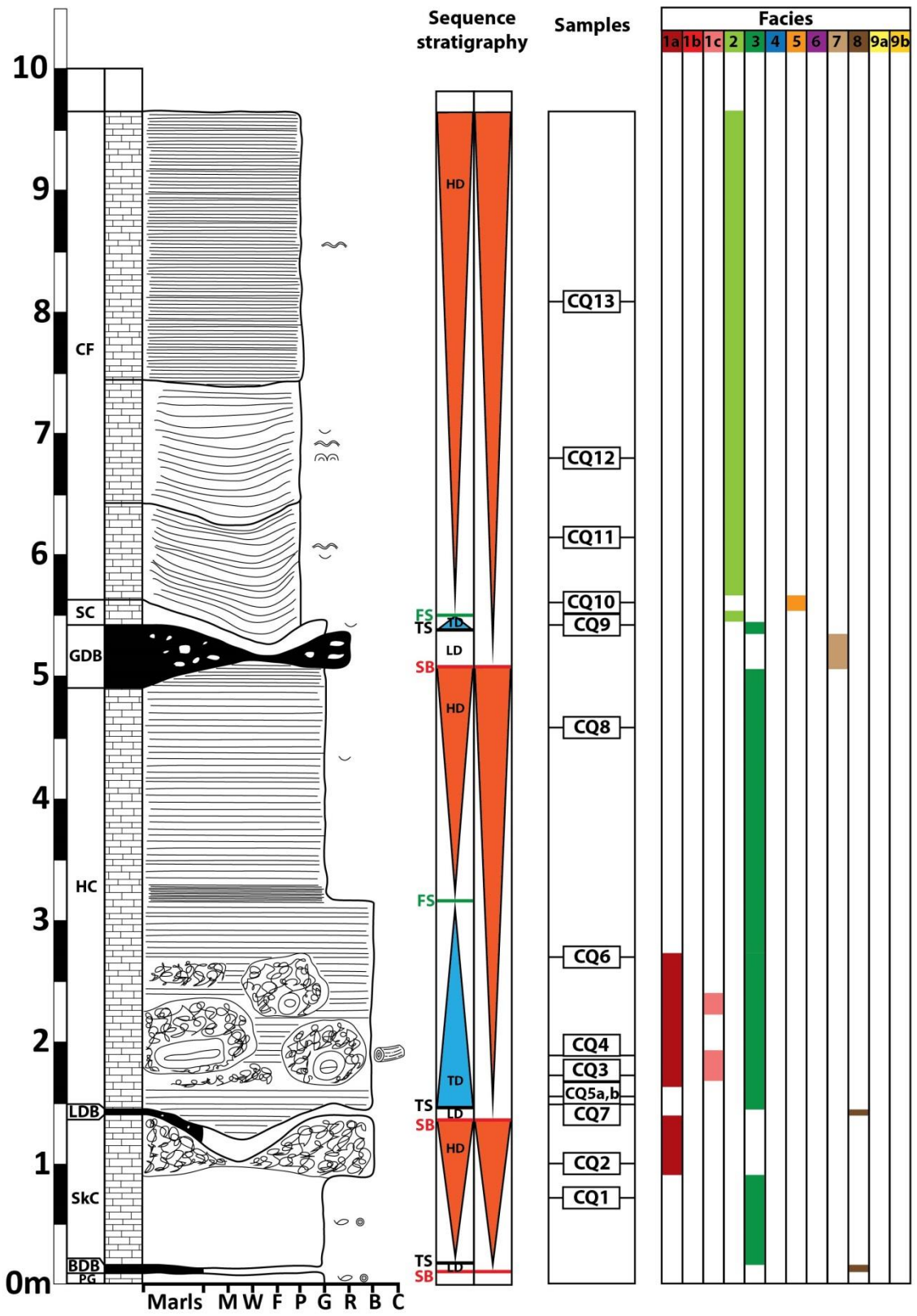
**TD: Transgressive deposits**  
**LD: Lowstand deposits**  
**HD: Highstand deposits**  
**FS: Flooding surface**  
**FSZ: Flooding surface zone**  
**TS: Transgressive surface**  
**SB: Sequence boundary**  
 **Shallowing upward trend**  
 **Deepening upward trend**



2 – Broacraft Quarry

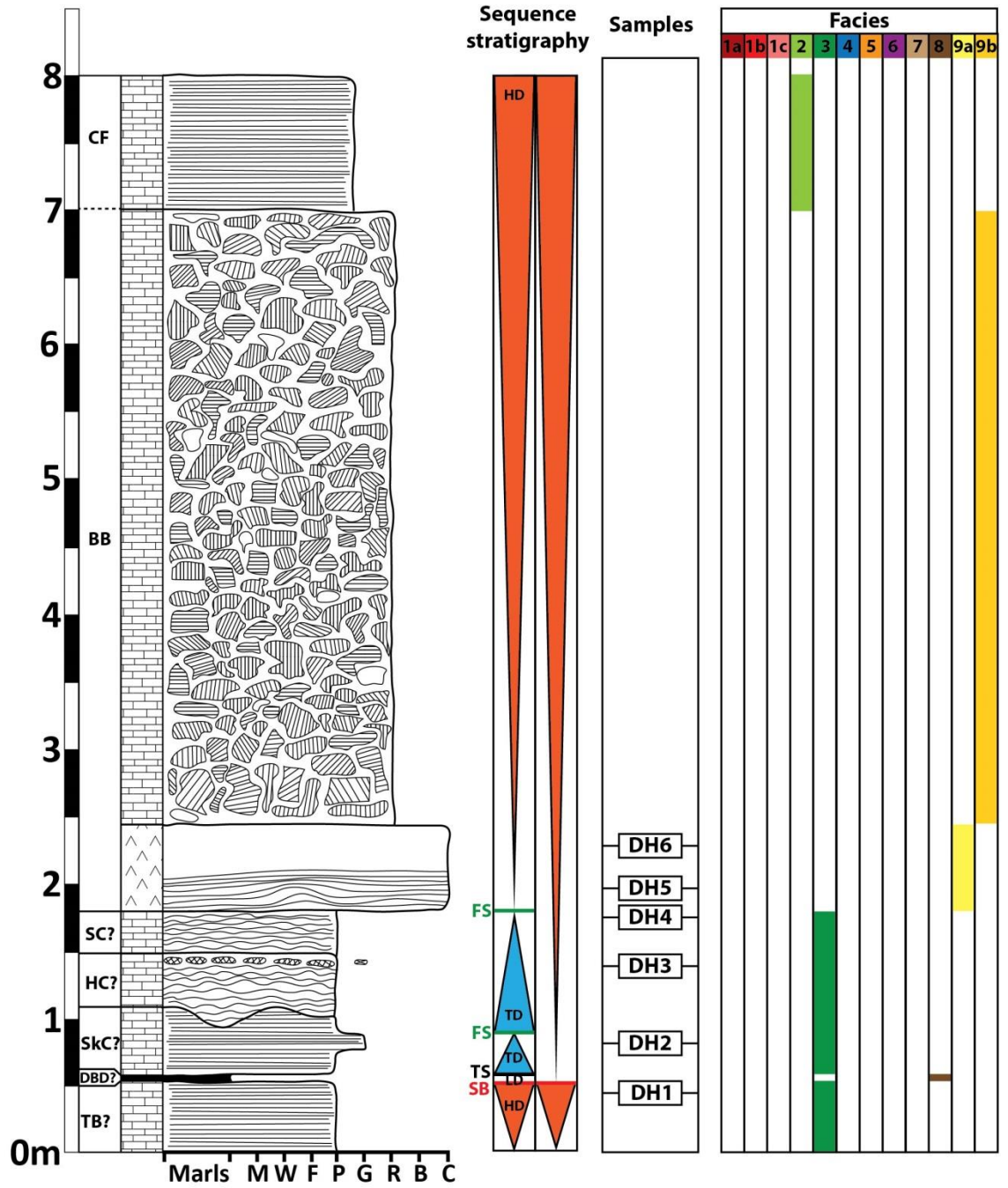


3 - Chalbury



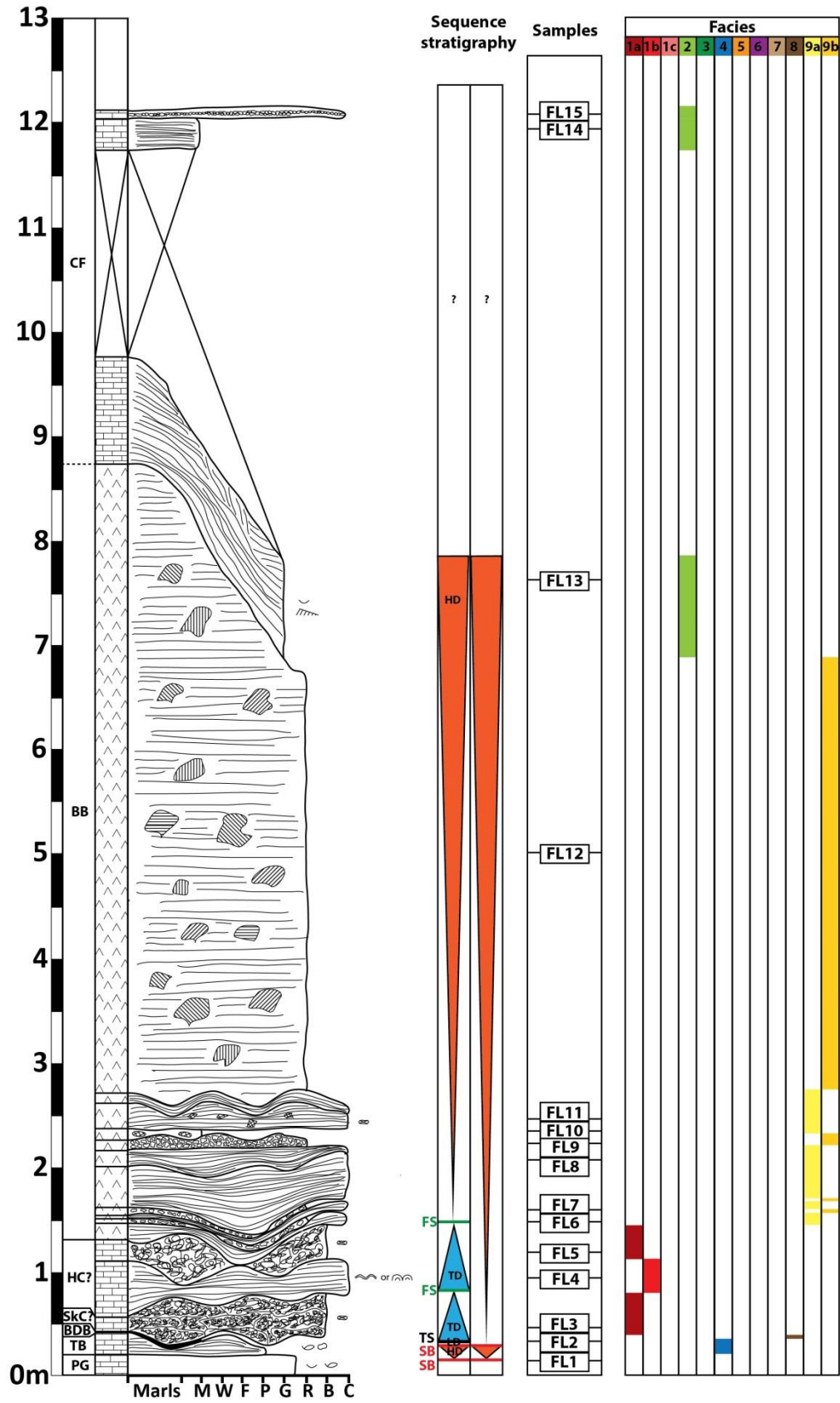
4 – Coombe Field Quarry



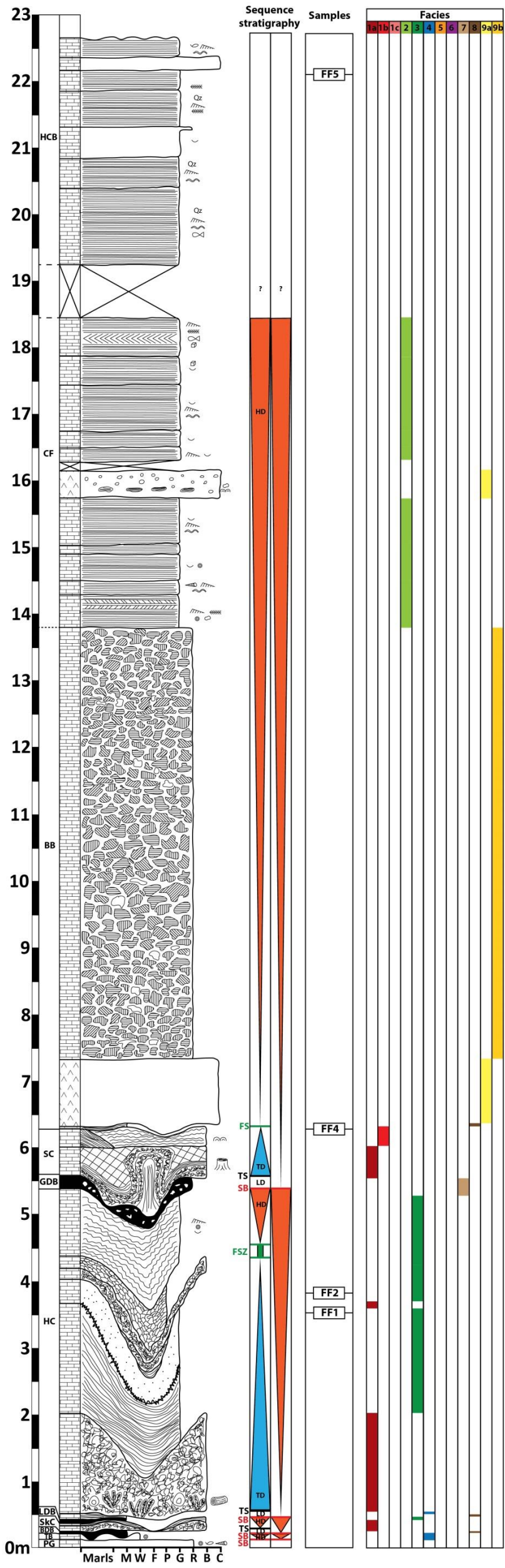


6 – Durlston Head

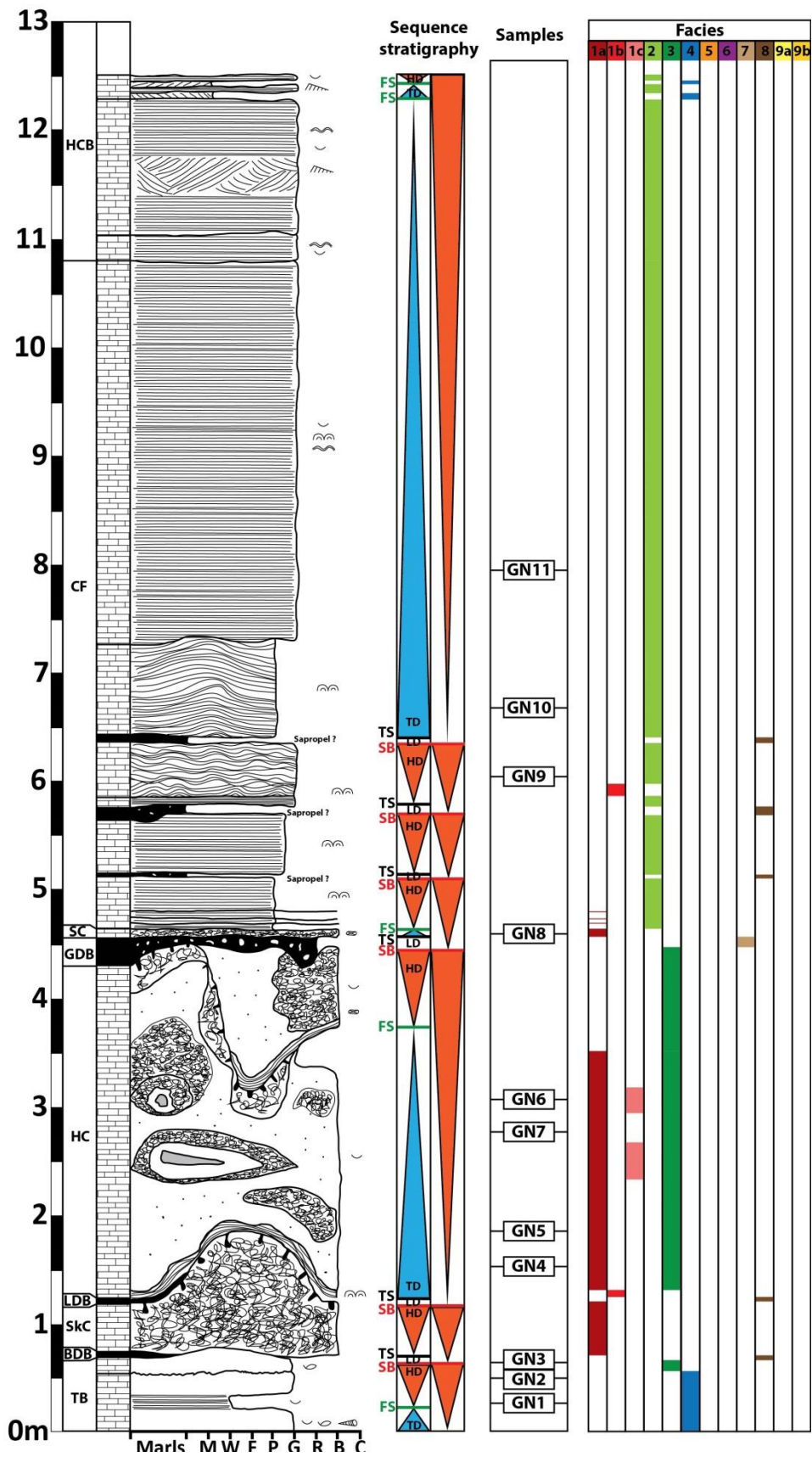




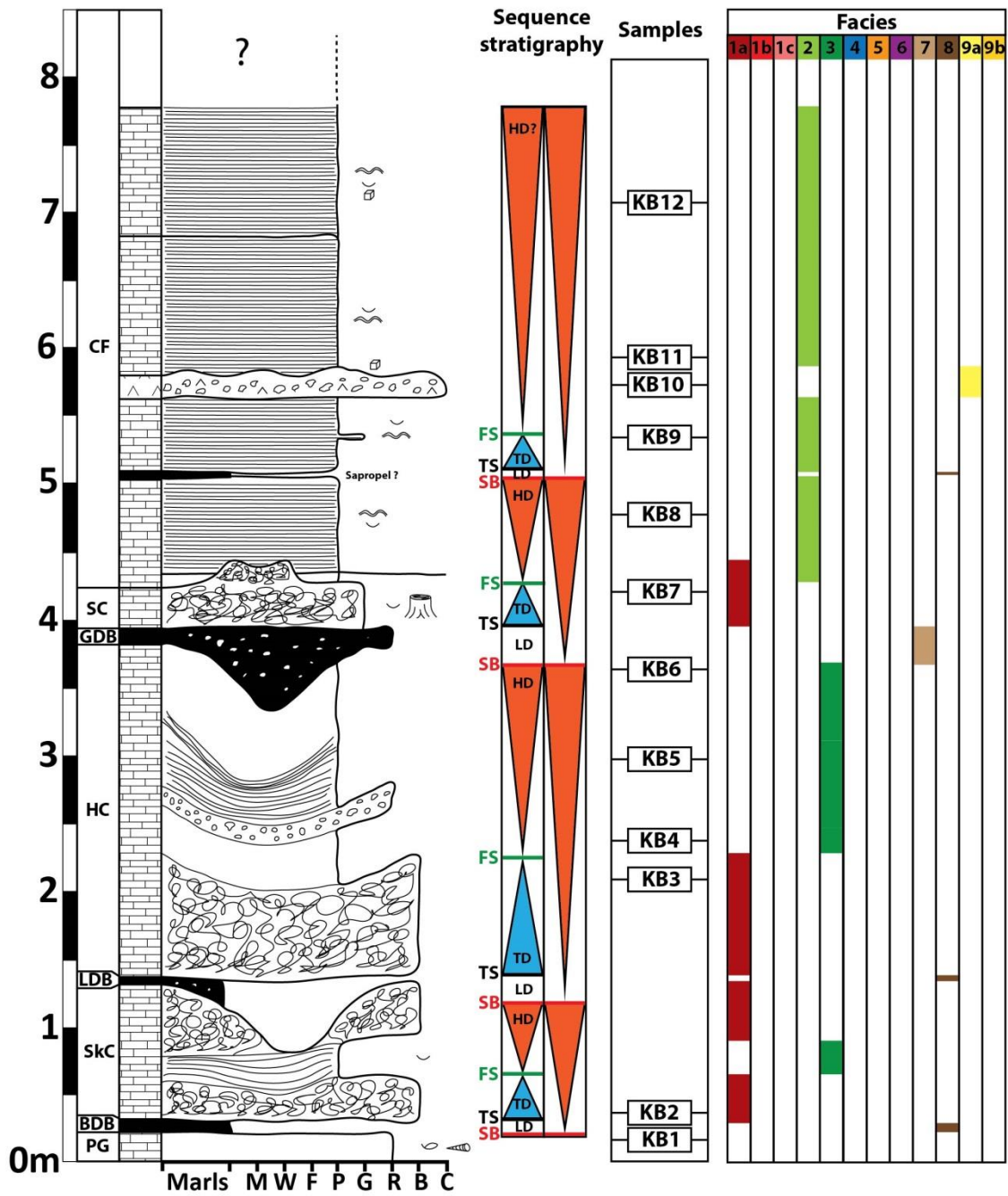
7 – Fishermen's Ledge



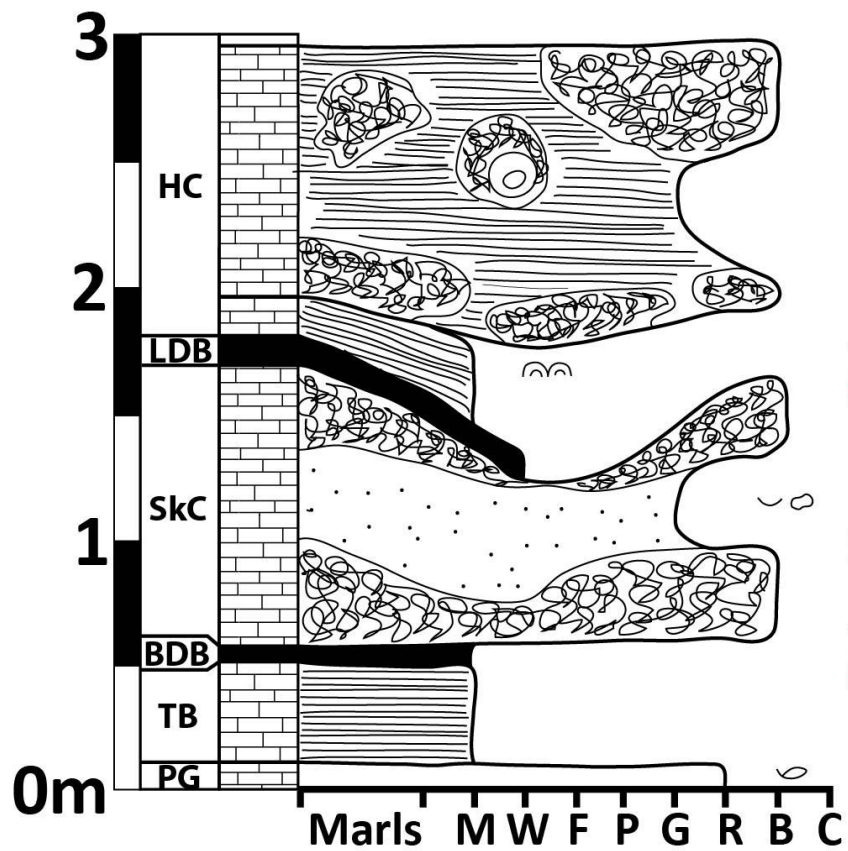
8 – Fossil Forest



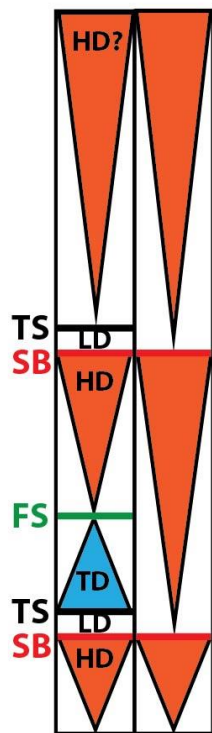




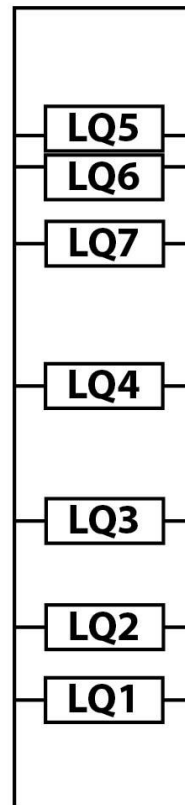
11 – King Barrow Quarries



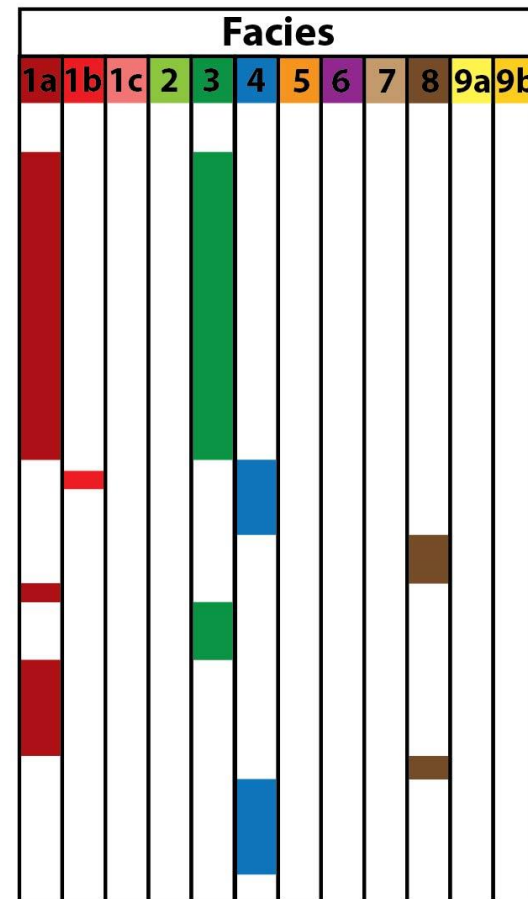
Sequence stratigraphy



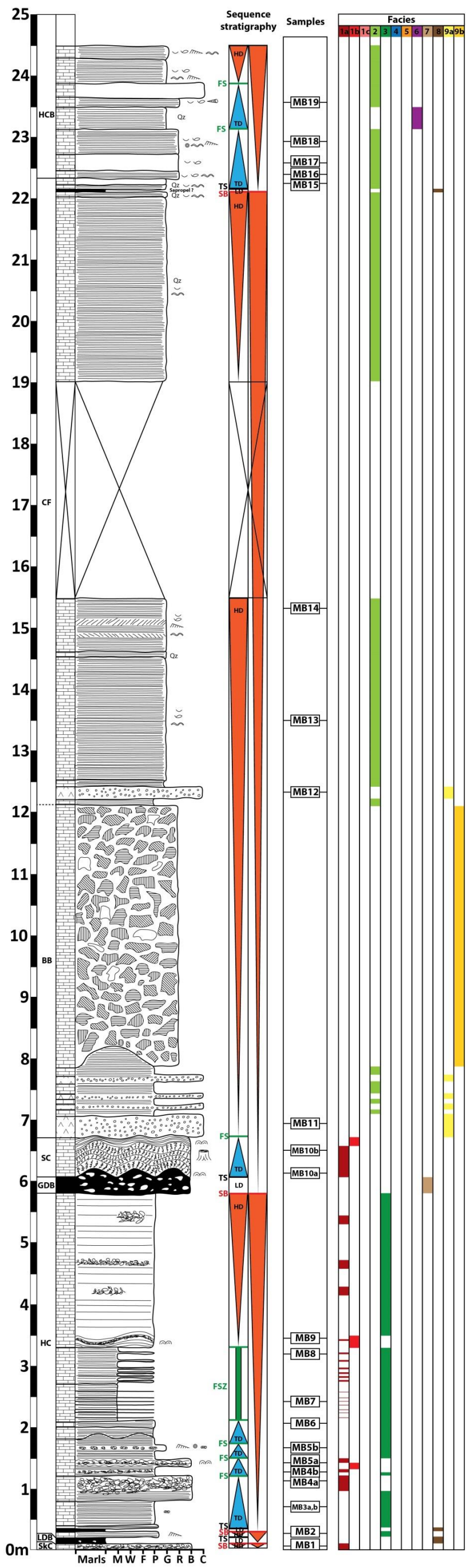
Samples



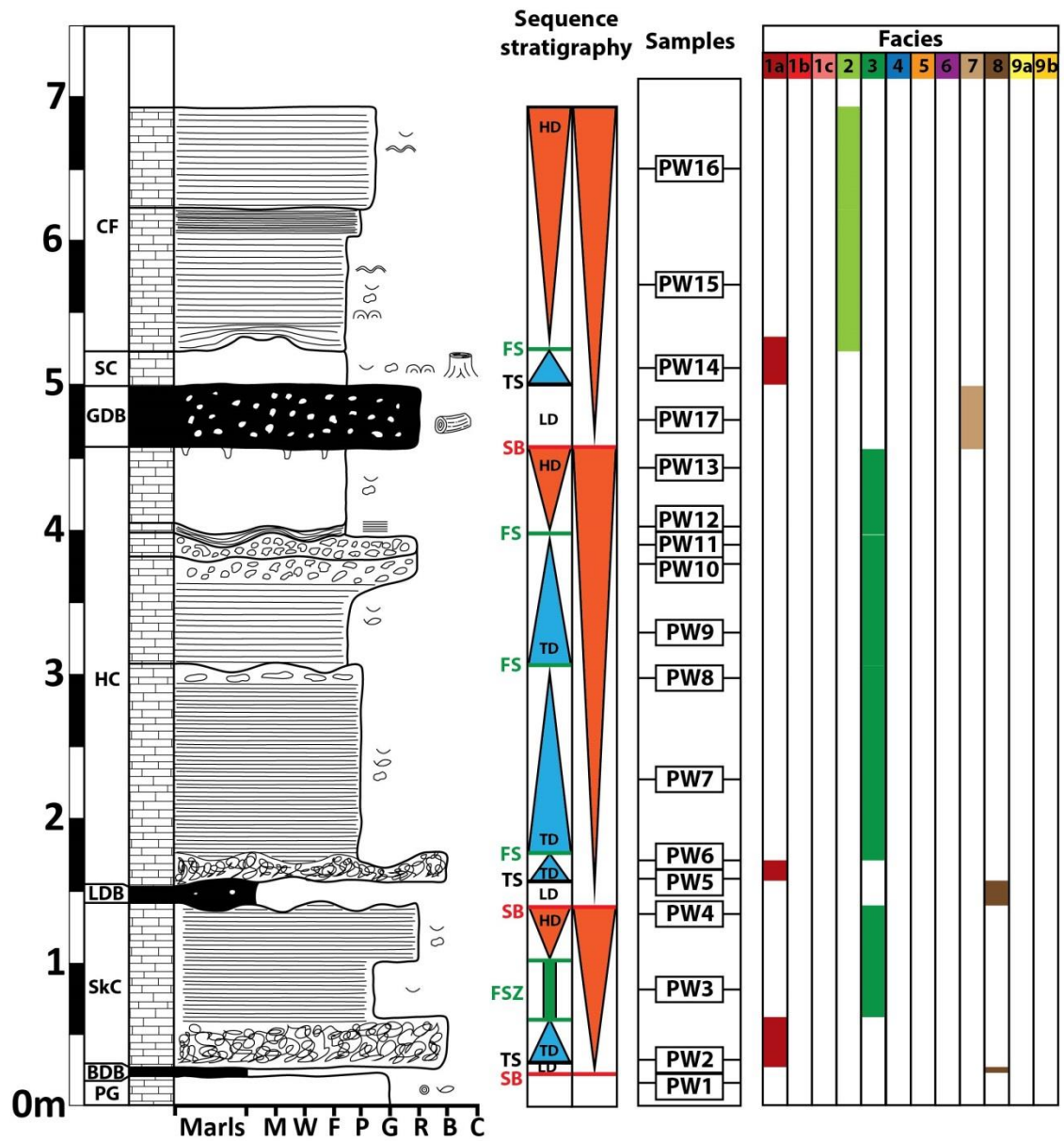
Facies



12 – Lawnsheds Quarry

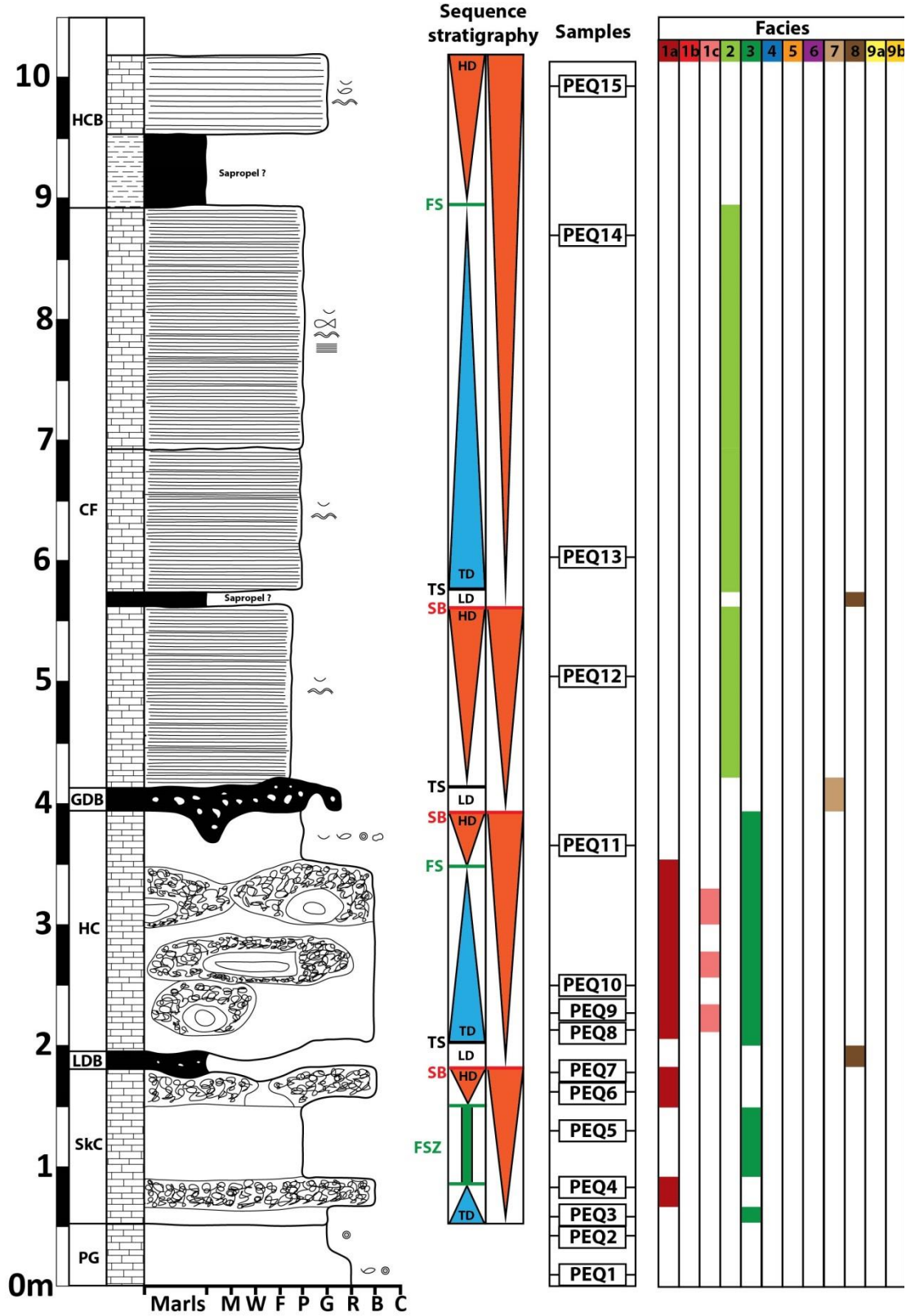


13 – Mupe Bay

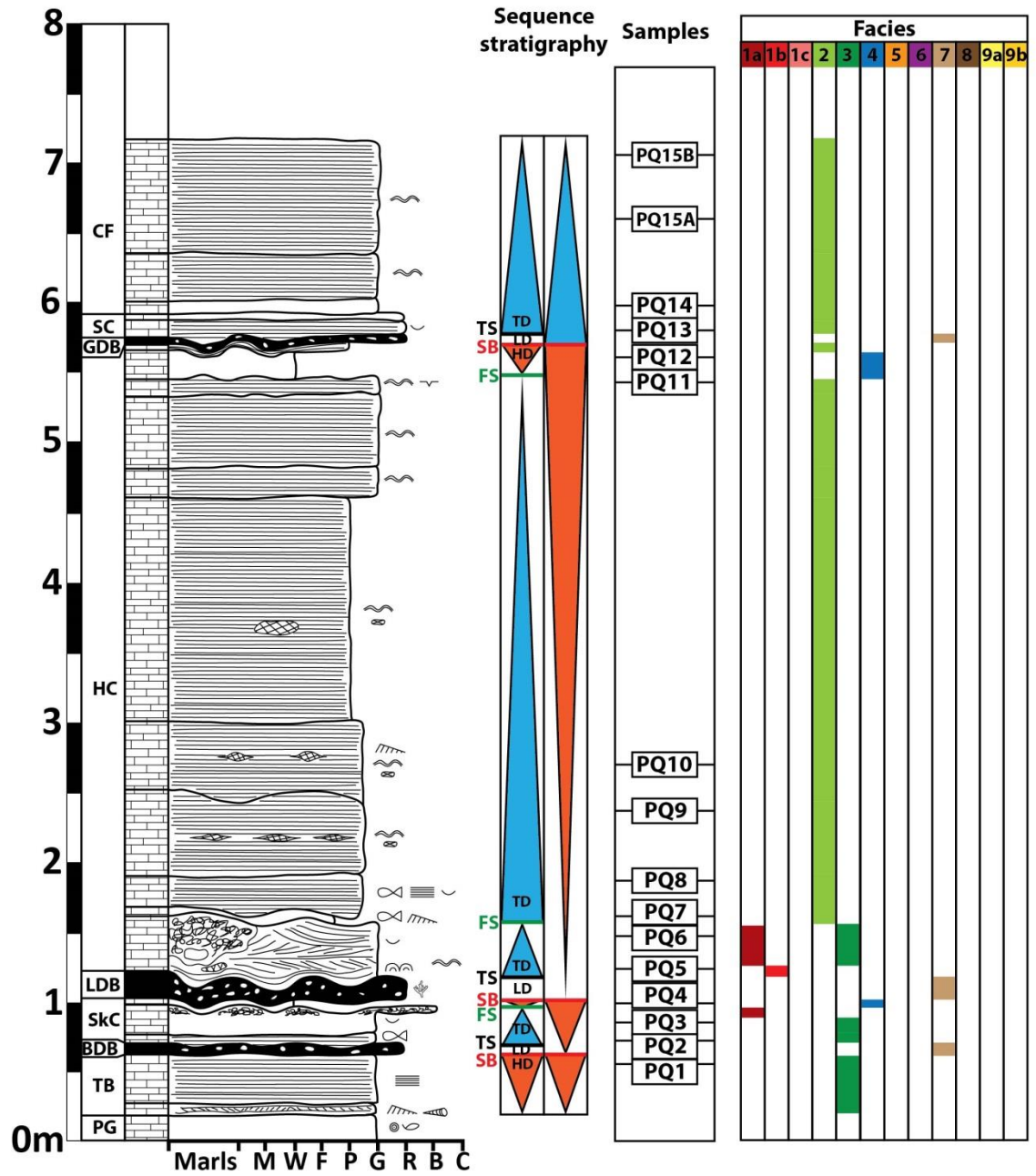


14 – Penn's Weare

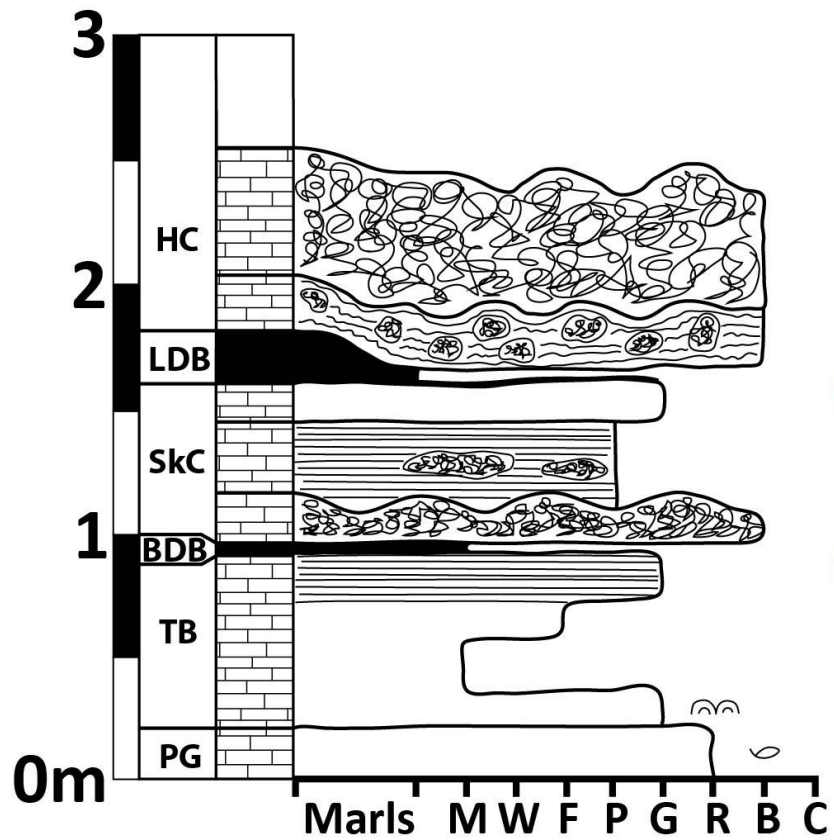




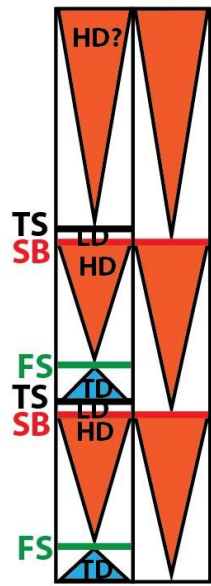
15 – Perryfield Quarry



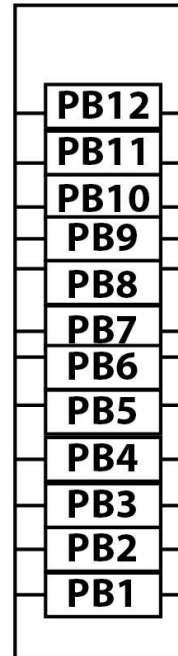
16 – Portesham Quarry



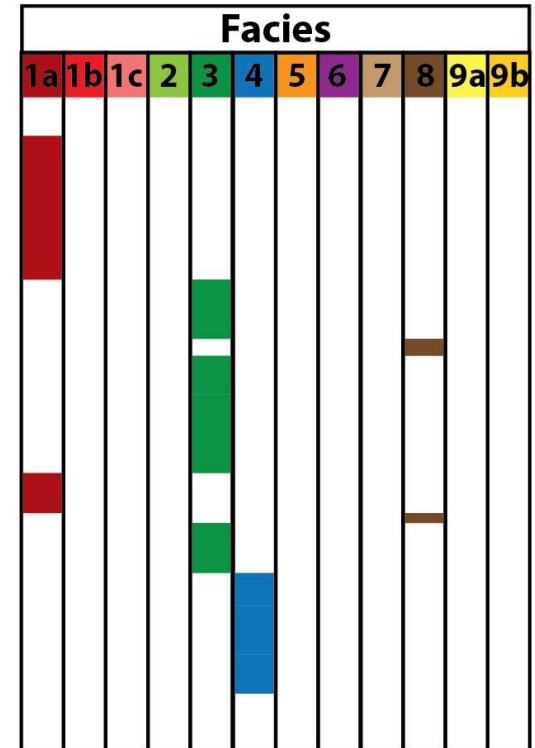
### Sequence stratigraphy

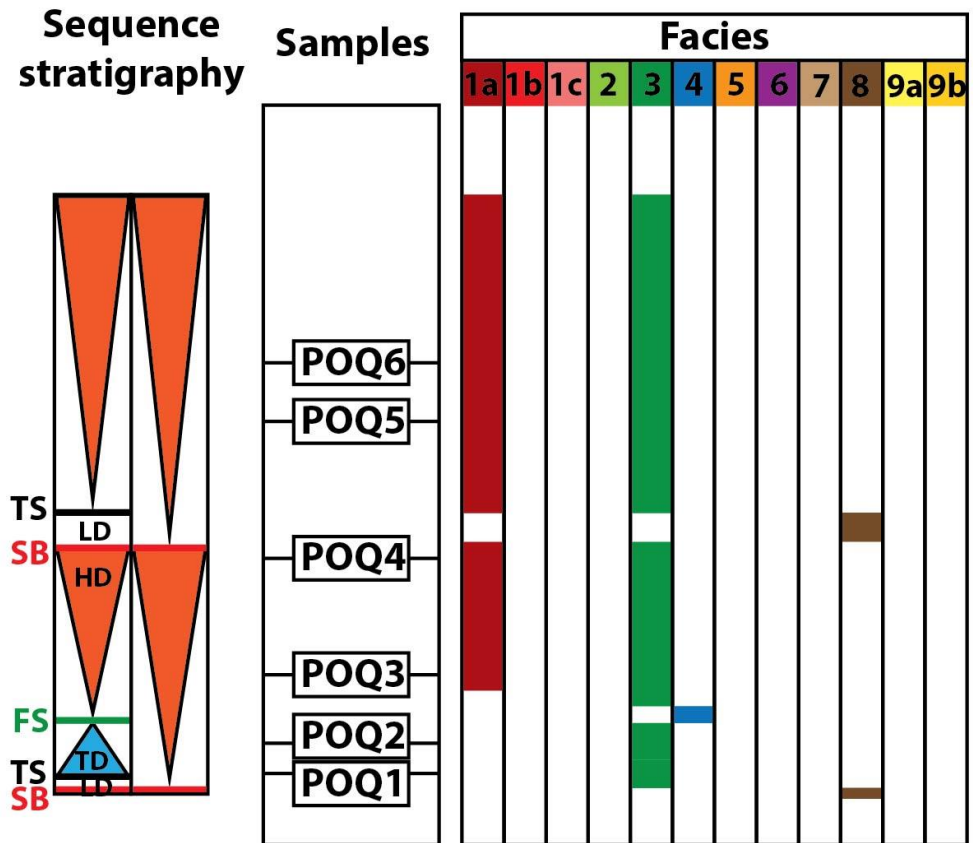
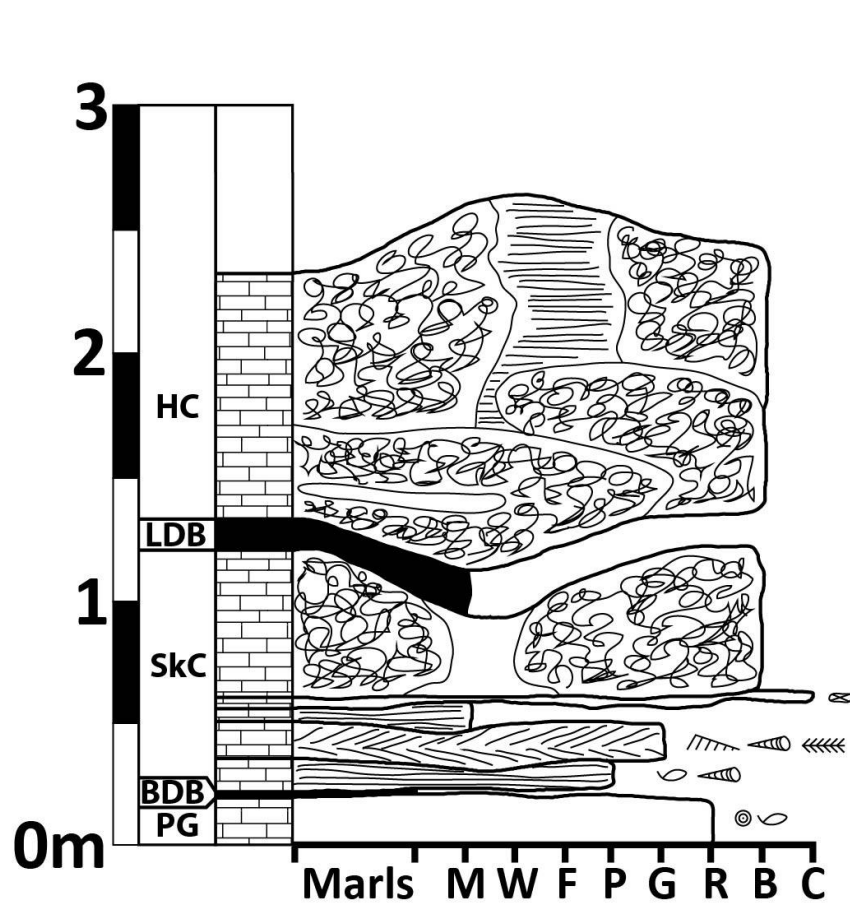


### Samples

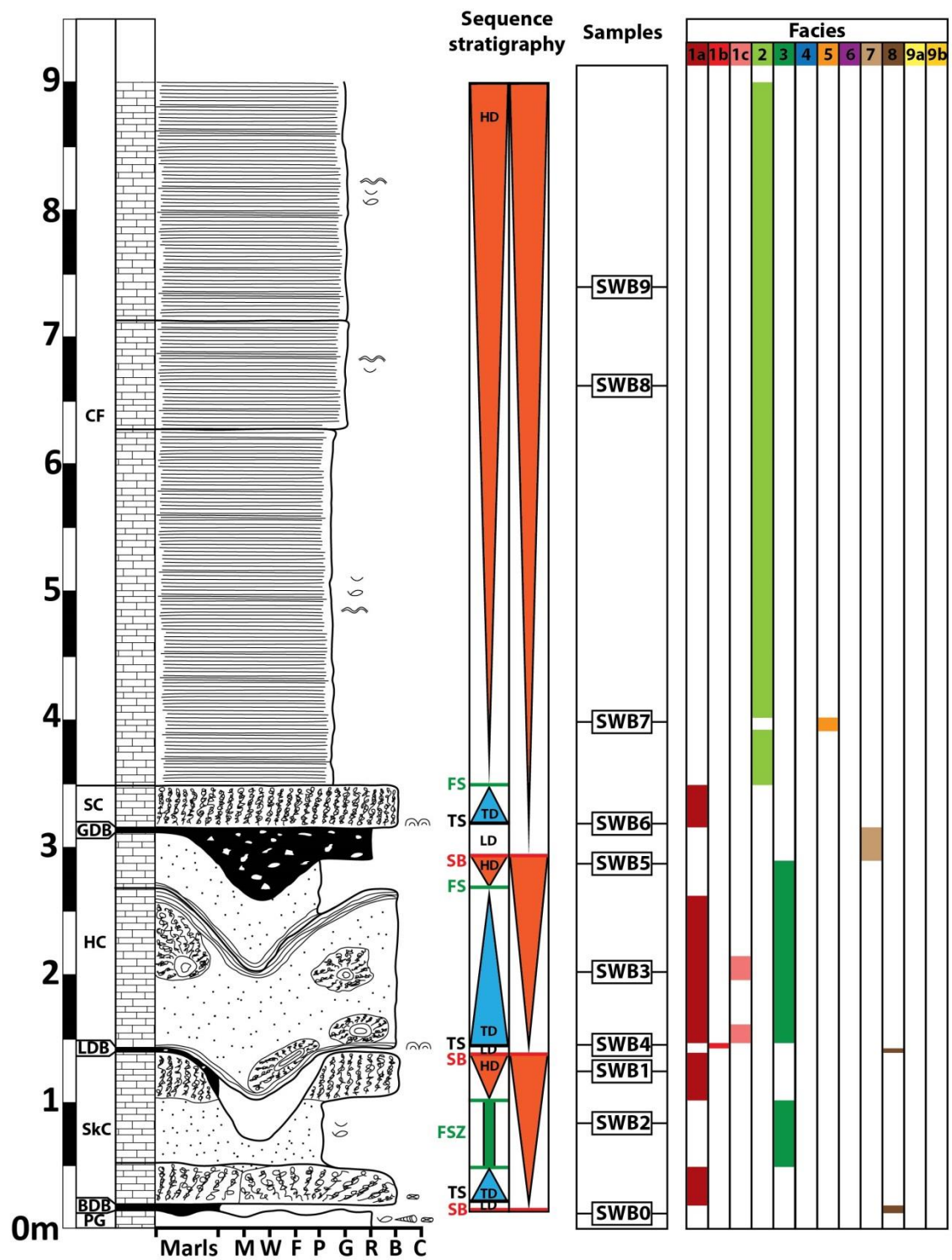


### Facies

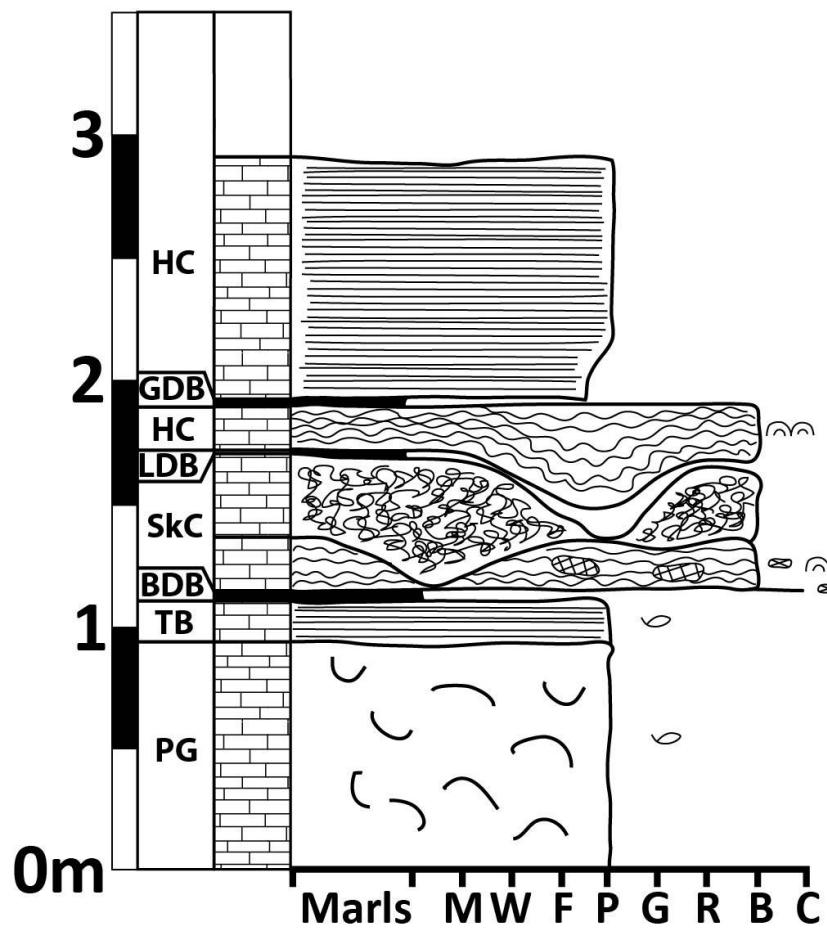




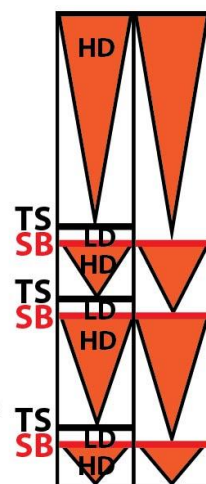
18 – Poxwell Quarry



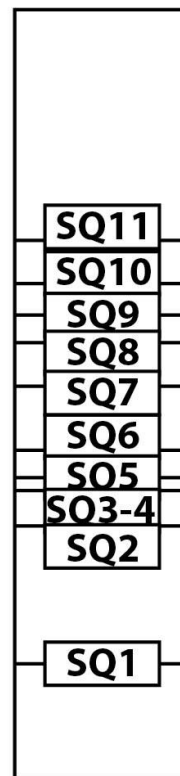
19 – South West Bowers



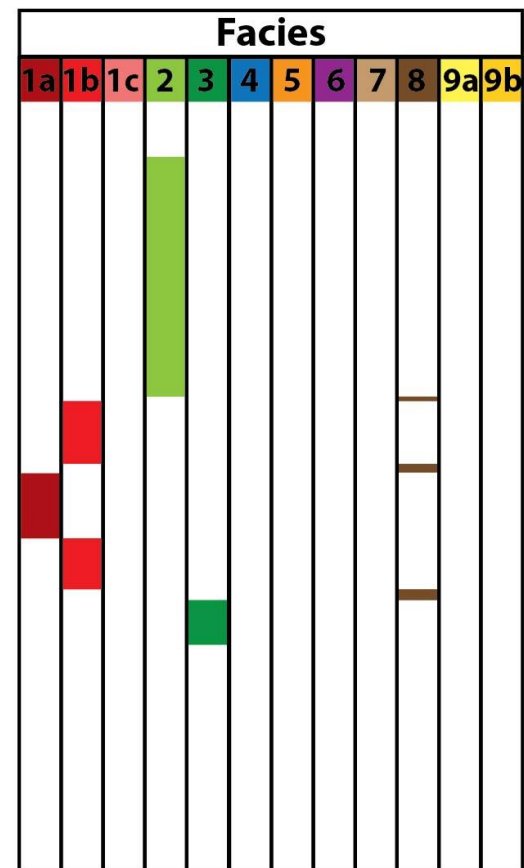
Sequence stratigraphy



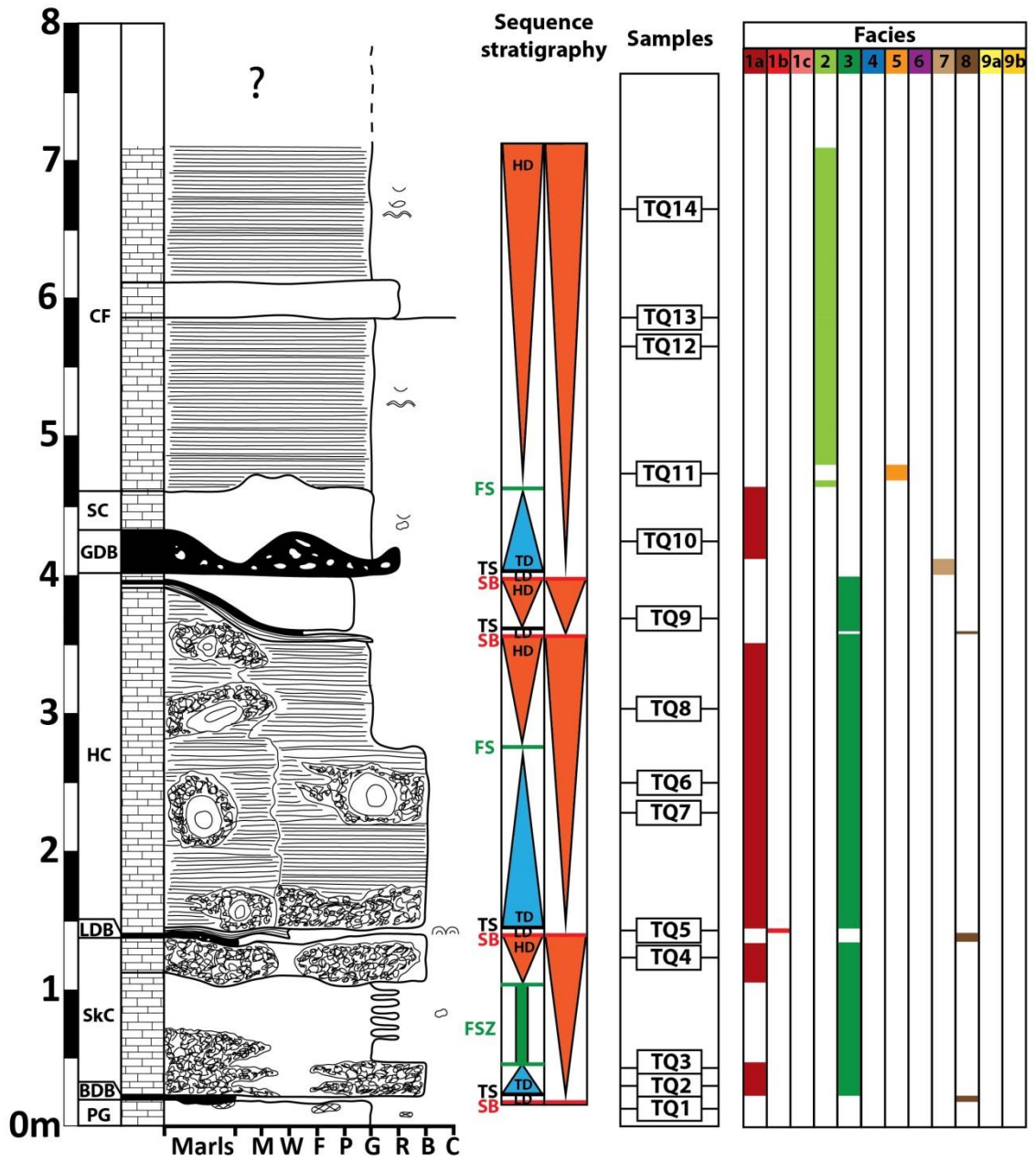
Samples



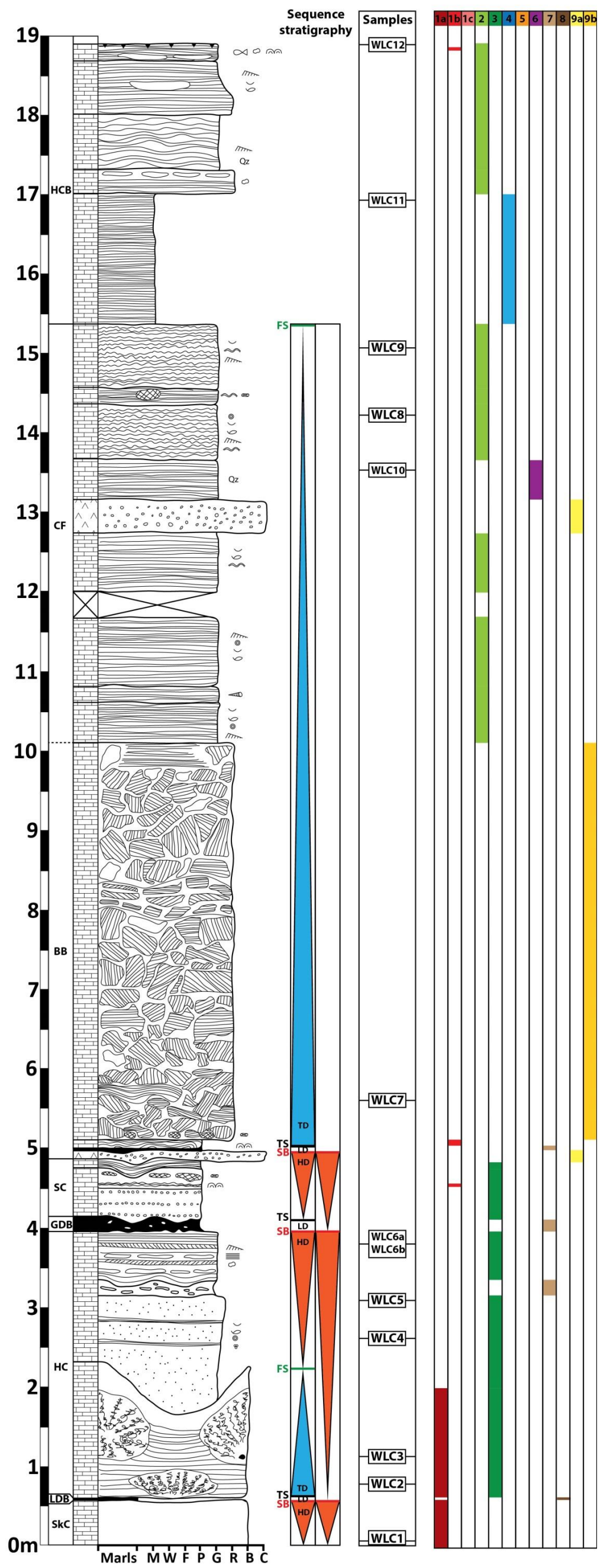
Facies



20 – Swanworth Quarry



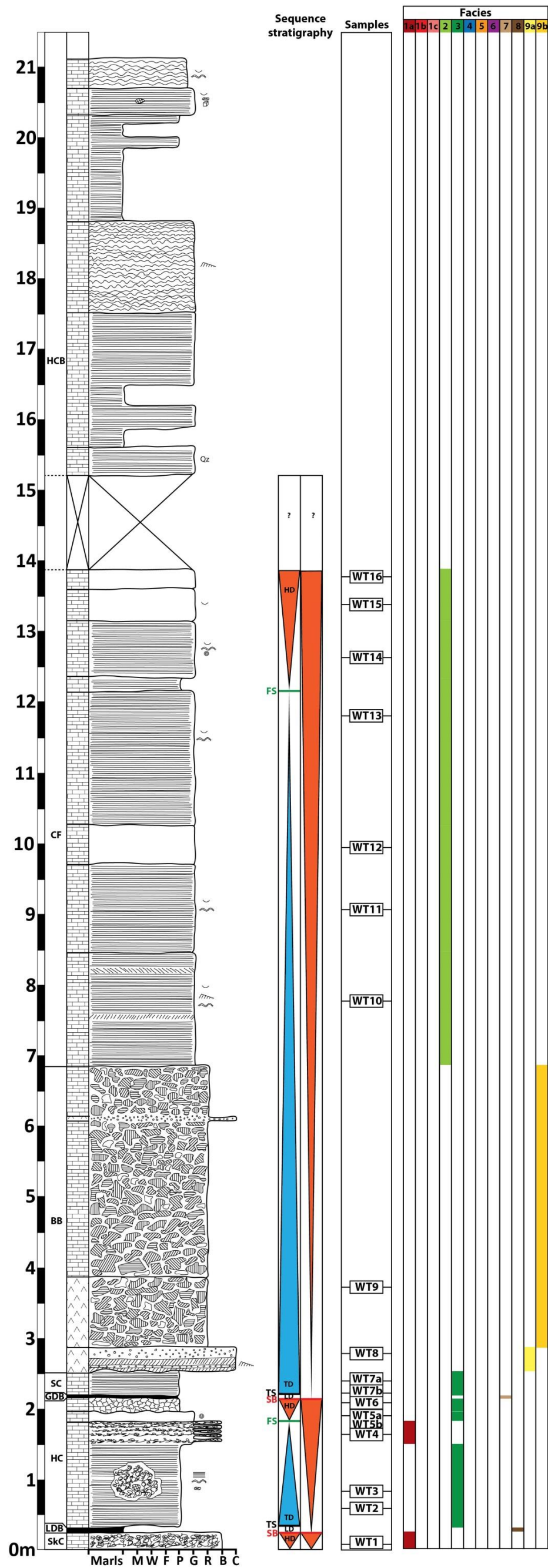
21 – Tout Quarry



22 – West Lulworth Cove



23 – Worbarrow Bay



## 2. Facies transition analysis

The first step consists in counting each transition between each facies from the recorded logs and this is listed in a matrix. This matrix is read from the left to the right, the facies listed in the left column are overlain by the facies on the top row. The number in the corresponding box shows the number of transitions counted from all the sedimentary logs. Several counting methods are possible (Walker, 1979; Davis, 2002); either the facies thickness is counted at regular intervals or transitions between facies can be counted for each bed (usually used to identify cyclicity or sequencing in the stratigraphical column; Davis, 2002) or for each facies change (Walker, 1979; Davis, 2002). In this study the recording was done each time a new facies was encountered in the log and recorded in the “transition matrix”. This counting method results in a better representativeness of facies transitions and their relationships, the main aim of this exercise. The second step was to convert this transition matrix into a matrix of probabilities, showing which transitions are more likely to occur. The third step consists in the construction of another matrix of probabilities with the assumption that facies transitions are randomly organised (Walker, 1979). The probabilities in this matrix results simply from this equation:

$$r_{ij} \frac{n_j}{N - n_i}$$

where  $r_{ij}$  is the random probability of transition from facies  $i$  to facies  $j$ ,  $n_i$  is the number of occurrence of facies  $i$  and  $n_j$  the number of occurrence of facies  $j$  and  $N$  the total number of occurrence of all facies (Walker, 1979). The fourth step consisted in the calculation of the difference matrix, simply subtracting the random probabilities to the calculated probabilities (Walker, 1979). The resulting matrix shows plus and minus figures for each facies transition where values close to 0 indicate that transitions are random, high positive numbers where transitions are much common than if random and high negative if they are less common than if facies transitions were random (Walker, 1979). These differences of probabilities were used to create the facies relationship diagram. This diagram illustrates which transitions of facies are more likely to occur if facies are not random according to the difference of probability values (Walker, 1979). Walker (1979) showed that to determine which value (*i.e.* which transitions are more probable) in the difference matrix will be taken into account some trial-and-error tests are necessary. In this study the minimum value taken into account in the construction of the facies relationship diagram was +0.050 because after some trial-and-error tests all the difference values greater than +0.050 are more representative of the transitions observed in the sedimentary logs.

Number of transition matrix													
	1a	1b	1c	2	3	4	5	6	7	8	9a	9b	Totals
1a	0	4	15	10	58	1	0	0	8	5	1	0	102
1b	7	0	0	2	4	1	0	0	0	2	1	1	18
1c	15	0	0	0	0	0	0	0	0	0	0	0	15
2	4	3	0	0	0	9	2	3	4	7	8	1	41
3	52	2	0	1	0	2	1	0	19	5	2	0	84
4	3	1	0	8	2	0	0	0	3	3	1	0	21
5	0	0	0	2	1	0	0	0	0	0	0	0	3
6	0	0	0	3	0	1	0	0	0	0	0	0	4
7	10	6	1	6	9	2	0	0	0	0	0	0	34
8	11	2	4	5	5	1	0	0	0	0	1	0	29
9a	0	0	0	8	0	0	0	1	0	1	0	8	18
9b	0	0	0	6	0	0	0	0	0	0	4	0	10

Probability matrix													
	1a	1b	1c	2	3	4	5	6	7	8	9a	9b	
1a	0	0.039	0.147	0.098	0.569	0.010	0	0	0.078	0.049	0.010	0	
1b	0.389	0	0	0.111	0.222	0.056	0	0	0	0.111	0.056	0.056	
1c	1	0	0	0	0	0	0	0	0	0	0	0	
2	0.098	0.073	0	0	0	0.220	0.049	0.073	0.098	0.171	0.195	0.024	
3	0.619	0.024	0	0.012	0	0.024	0.012	0	0.226	0.060	0.024	0	
4	0.143	0.048	0	0.381	0.095	0	0	0	0.143	0.143	0.048	0	
5	0	0	0	0.667	0.333	0	0	0	0	0	0	0	
6	0	0	0	0.750	0	0.250	0	0	0	0	0	0	
7	0.294	0.176	0.029	0.176	0.265	0.059	0	0	0	0	0	0	
8	0.379	0.069	0.138	0.172	0.172	0.034	0	0	0	0	0.034	0	
9a	0	0	0	0.444	0	0	0	0.056	0	0.056	0	0.444	
9b	0	0	0	0.600	0	0	0	0	0	0	0.400	0	

Probability matrix for random sequence													
	1a	1b	1c	2	3	4	5	6	7	8	9a	9b	
1a	0	0.056	0.079	0.184	0.279	0.079	0.010	0.013	0.115	0.095	0.059	0.033	
1b	0.269	0	0.061	0.142	0.216	0.061	0.008	0.010	0.089	0.074	0.046	0.025	
1c	0.274	0.044	0	0.145	0.220	0.062	0.008	0.010	0.090	0.075	0.047	0.026	
2	0.299	0.048	0.068	0	0.239	0.068	0.008	0.011	0.099	0.082	0.051	0.028	
3	0.325	0.052	0.074	0.172	0	0.074	0.009	0.012	0.107	0.089	0.055	0.031	
4	0.274	0.044	0.062	0.145	0.220	0	0.008	0.010	0.090	0.075	0.047	0.026	
5	0.260	0.042	0.059	0.137	0.208	0.059	0	0.010	0.086	0.071	0.044	0.025	
6	0.260	0.042	0.059	0.138	0.209	0.059	0.007	0	0.086	0.071	0.044	0.025	
7	0.282	0.045	0.064	0.149	0.226	0.064	0.008	0.011	0	0.077	0.048	0.027	
8	0.277	0.045	0.063	0.147	0.223	0.063	0.008	0.010	0.092	0	0.047	0.026	
9a	0.270	0.043	0.061	0.142	0.216	0.061	0.008	0.010	0.089	0.074	0	0.025	
9b	0.264	0.042	0.060	0.140	0.212	0.060	0.007	0.010	0.087	0.072	0.045	0	

Facies occurrence													
	1a	1b	1c	2	3	4	5	6	7	8	9a	9b	Total
106	17	24	56	85	24	3	4	35	29	18	10		411

Observed minus random													
	1a	1b	1c	2	3	4	5	6	7	8	9a	9b	
1a	0.000	-0.017	0.068	-0.086	0.290	-0.069	-0.010	-0.013	-0.036	-0.046	-0.049	-0.033	
1b	0.120	0.000	-0.061	-0.031	0.006	-0.005	-0.008	-0.010	-0.089	0.038	0.010	0.030	
1c	0.726	-0.044	0.000	-0.145	-0.220	-0.062	-0.008	-0.010	-0.090	-0.075	-0.047	-0.026	
2	-0.201	0.025	-0.068	0.000	-0.239	0.152	0.040	0.062	-0.001	0.089	0.144	-0.004	
3	0.294	-0.028	-0.074	-0.160	0.000	-0.050	0.003	-0.012	0.119	-0.029	-0.031	-0.031	
4	-0.131	0.004	-0.062	0.236	-0.124	0.000	-0.008	-0.010	0.052	0.068	0.001	-0.026	
5	-0.260	-0.042	-0.059	0.529	0.125	-0.059	0.000	-0.010	-0.086	-0.071	-0.044	-0.025	
6	-0.260	-0.042	-0.059	0.612	-0.209	0.191	-0.007	0.000	-0.086	-0.071	-0.044	-0.025	
7	0.012	0.131	-0.034	0.028	0.039	-0.005	-0.008	-0.011	0.000	-0.077	-0.048	-0.027	
8	0.102	0.024	0.075	0.026	-0.050	-0.028	-0.008	-0.010	-0.092	0.000	-0.013	-0.026	
9a	-0.270	-0.043	-0.061	0.302	-0.216	-0.061	-0.008	0.045	-0.089	-0.018	0.000	0.419	
9b	-0.264	-0.042	-0.060	0.460	-0.212	-0.060	-0.007	-0.010	-0.087	-0.072	0.355	0.000	

Figure 2.1 Matrices realised for the facies transition analysis.

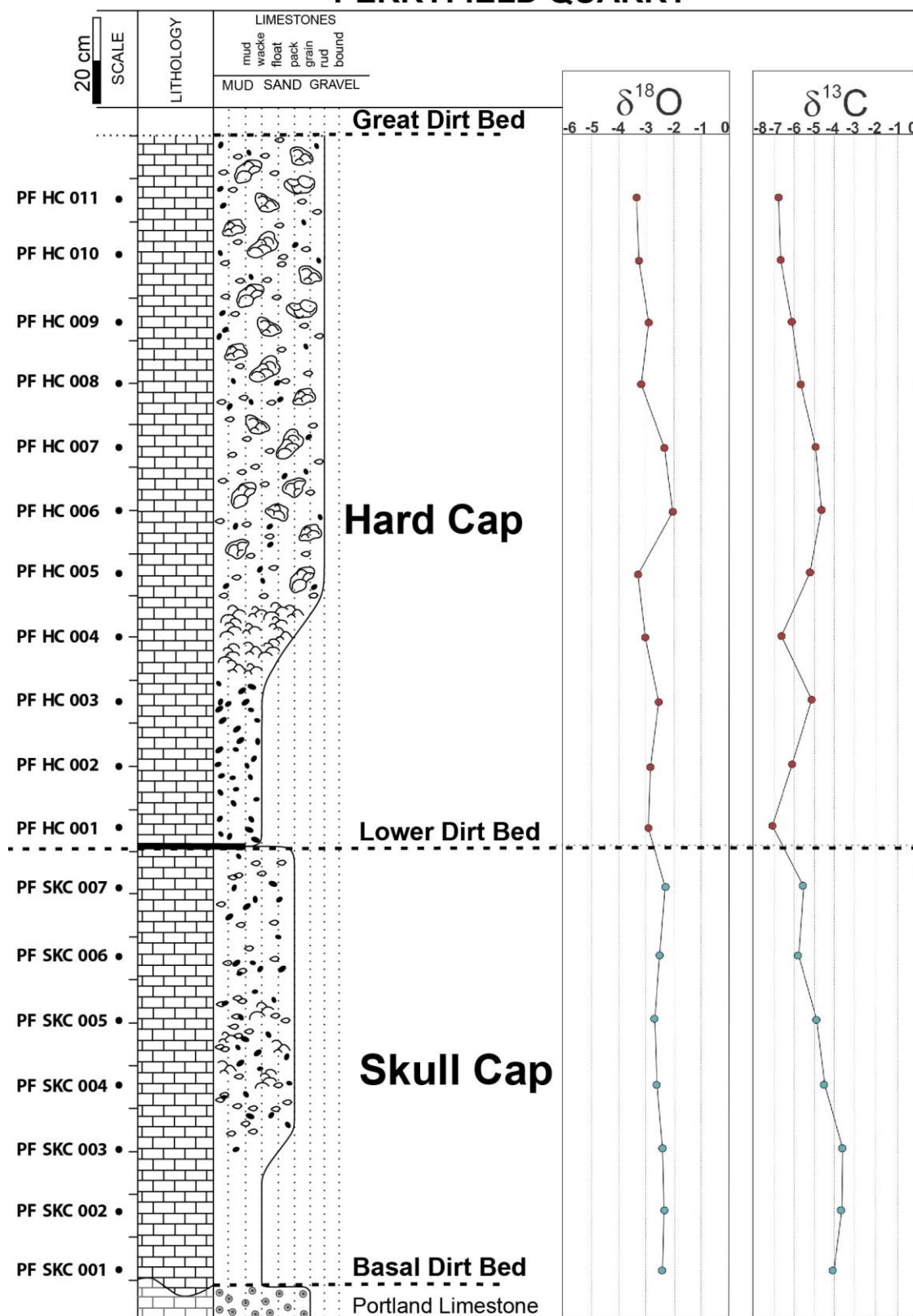
### 3. Stable isotope (carbon and oxygen) data

Skull Cap					Hard Cap				
Samples	$\delta^{18}\text{O}$ (‰)	$\sigma$ (‰)	$\delta^{13}\text{C}$ (‰)	$\sigma$ (‰)	Samples	$\delta^{18}\text{O}$ (‰)	$\sigma$ (‰)	$\delta^{13}\text{C}$ (‰)	$\sigma$ (‰)
PF SKC 001	-2.43	0.02	-4.09	0.01	PF HC 001	-2.95	0.05	-7.04	0.01
PF SKC 002	-2.36	0.09	-3.70	0.02	PF HC 002	-2.85	0.04	-6.12	0.02
PF SKC 003	-2.42	0.06	-3.65	0.01	PF HC 003	-2.56	0.06	-5.15	0.01
PF SKC 004	-2.63	0.01	-4.53	0.03	PF HC 004	-3.05	0.09	-6.61	0.00
PF SKC 005	-2.72	0.04	-4.90	0.03	PF HC 005	-3.30	0.09	-5.21	0.03
PF SKC 006	-2.53	0.02	-5.80	0.03	PF HC 006	-2.04	0.01	-4.63	0.00
PF SKC 007	-2.32	0.02	-5.53	0.01	PF HC 007	-2.35	0.09	-4.95	0.04
					PF HC 008	-3.19	0.07	-5.66	0.07
BC SKC 001	-0.98	0.02	-3.56	0.00	PF HC 009	-2.91	0.05	-6.11	0.01
BC SKC 002	-2.65	0.04	-3.72	0.02	PF HC 010	-3.27	0.03	-6.62	0.02
BC SKC 003	-2.83	0.09	-3.41	0.00	PF HC 011	-3.34	0.01	-6.75	0.04
BC SKC 004	-2.29	0.08	-3.36	0.02					
BC SKC 005	-2.27	0.02	-3.29	0.03	BC HC 001	-2.66	0.08	-4.87	0.02
BC SKC 006	-0.77	0.05	-3.59	0.03	BC HC 002	-3.31	0.03	-4.91	0.04
BC SKC 007	-0.82	0.04	-3.87	0.01	BC HC 003	-3.12	0.04	-5.16	0.02
BC SKC 008	-0.74	0.10	-4.14	0.02	BC HC 004	-3.39	0.02	-5.42	0.00
BC SKC 009	-0.72	0.09	-4.77	0.01	BC HC 005	-2.42	0.03	-4.00	0.04
					BC HC 006	-2.82	0.07	-4.48	0.02
SB SKC 001	-0.77	0.03	-3.91	0.00	BC HC 007	-2.91	0.08	-4.98	0.02
SB SKC 002	-1.88	0.04	-3.77	0.01	BC HC 008	-3.21	0.04	-4.95	0.02
SB SKC 003	-2.12	0.00	-2.71	0.00	BC HC 009	-2.47	0.05	-5.56	0.00
SB SKC 004	-1.61	0.01	-2.88	0.02	BC HC 010	-2.40	0.01	-4.80	0.02
SB SKC 005	-1.35	0.00	-2.84	0.02	BC HC 011	-2.58	0.05	-5.28	0.00
SB SKC 006	-1.04	0.01	-3.12	0.00	BC HC 012	-3.04	0.00	-6.76	0.03
SB SKC 007	-1.23	0.01	-3.07	0.02	BC HC 013	-3.25	0.01	-6.84	0.02
SB SKC 008	-1.55	0.05	-3.59	0.02	BC HC 014	-3.56	0.04	-7.14	0.03
SB SKC 009	-1.82	0.05	-4.63	0.01	BC HC 015	-2.47	0.06	-7.20	0.01
SB SKC 010	-1.58	0.04	-4.07	0.04					
SB SKC 011	-1.65	0.05	-4.01	0.02	SB HC 001	-0.75	0.01	-6.33	0.01
SB SKC 012	-1.95	0.01	-3.95	0.00	SB HC 002	-2.40	0.03	-5.82	0.03
					SB HC 003	-2.98	0.09	-6.15	0.01
					SB HC 004	-3.38	0.07	-6.30	0.01
					SB HC 005	-3.17	0.01	-6.24	0.00
					SB HC 006	-3.46	0.03	-5.75	0.00
					SB HC 008	-2.28	0.07	-5.34	0.02
					SB HC 009	-3.12	0.07	-6.27	0.04
					SB HC 010	-2.94	0.07	-4.86	0.01
					SB HC 011	-2.55	0.03	-6.41	0.00
					SB HC 012	-2.96	0.02	-7.07	0.05
					SB HC 013	-3.36	0.01	-7.05	0.01
					SB HC 014	-4.28	0.05	-6.98	0.01
					SB HC 015	-3.63	0.00	-7.05	0.02
					SB HC 016	-2.41	0.08	-7.05	0.00

Keys:  
PF: Perryfield Quarry  
BC: Broadcroft Quarry  
SB: Bowers Quarry  
SKC: Skull Cap  
HC: Hard Cap  
 $\sigma$ : standard deviation

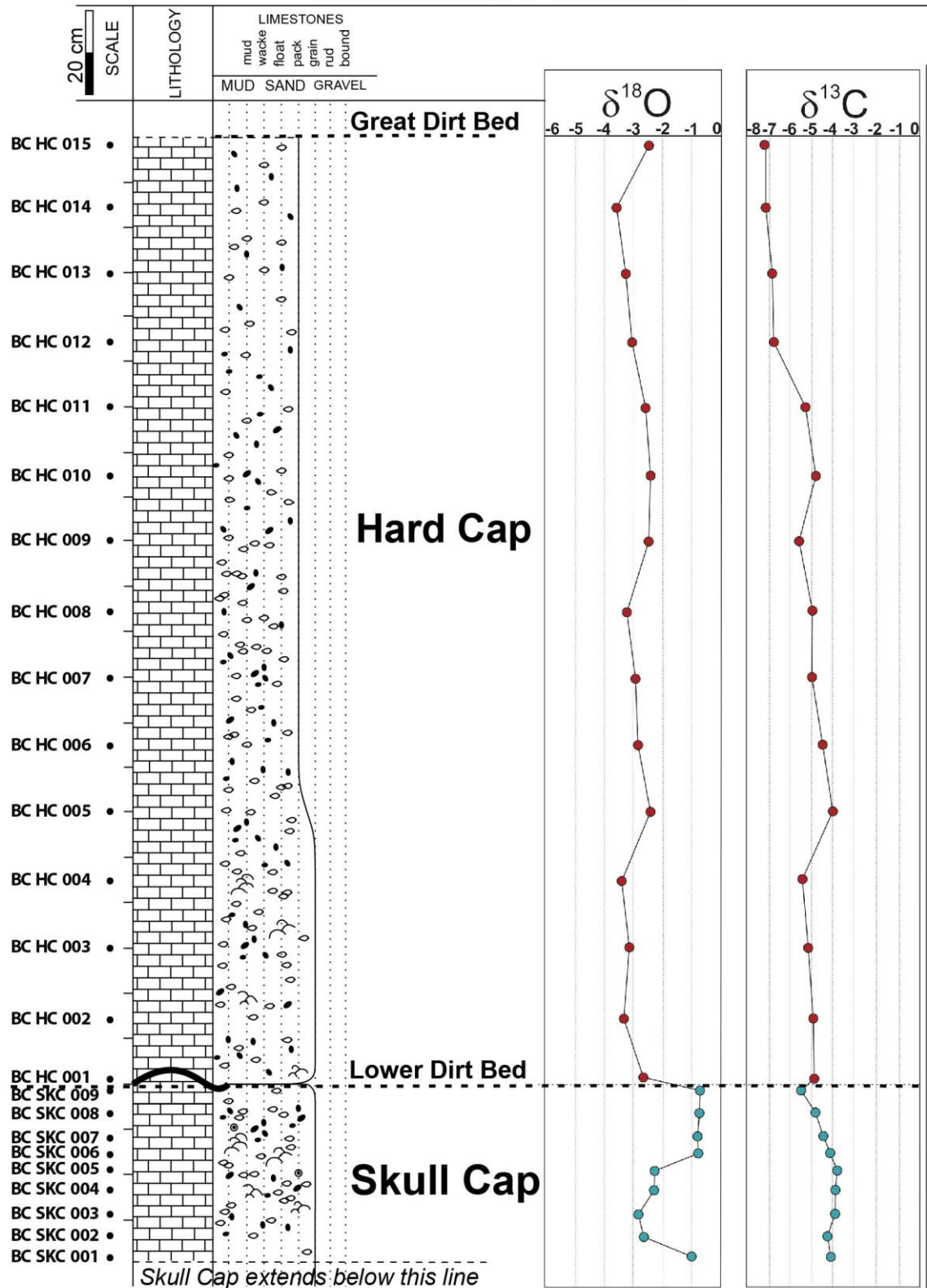
**Figure 3.1** Stable isotope values and standard deviations. Note that sample numbers are increasing up section (1 at the bottom of the bed and the greatest numbers at the top). Data recorded by Dharmarajah, 2015.

# PERRYFIELD QUARRY



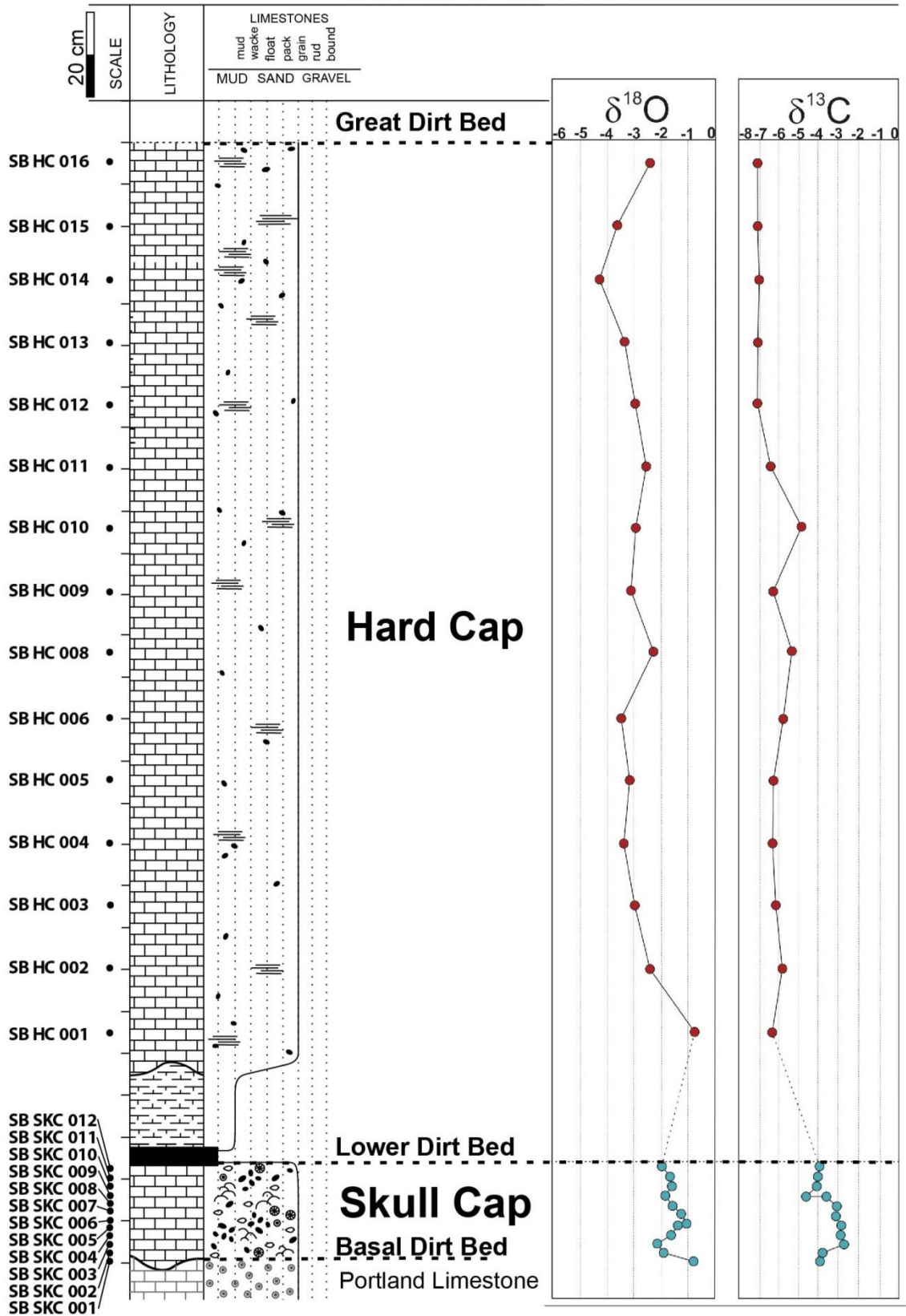
**Figure 3.2** Sedimentary log from Perryfield Quarry with locations of samples on the left and the evolution of  $\delta^{13}\text{C}$  and  $\delta^{18}\text{O}$  on the right.  $\delta^{13}\text{C}$  and  $\delta^{18}\text{O}$  are ‰. Modified after Dharmarajah, 2015.

# BRODCROFT QUARRY



**Figure 3.3** Sedimentary log from Brodcroft Quarry with locations of samples on the left and the evolution of  $\delta^{13}\text{C}$  and  $\delta^{18}\text{O}$  on the right.  $\delta^{13}\text{C}$  and  $\delta^{18}\text{O}$  are ‰. Modified after Dharmarajah, 2015.

# BOWERS QUARRY



**Figure 3.4** Sedimentary log from Bowers Quarry with locations of samples on the left and the evolution of  $\delta^{13}\text{C}$  and  $\delta^{18}\text{O}$  on the right.  $\delta^{13}\text{C}$  and  $\delta^{18}\text{O}$  are ‰. Modified after Dharmarajah, 2015.

## Reference list

Davis, J.C. 2002. Statistics and data analysis in geology. Third Edition ed. John Wiley & Sons, 638 pp.

Dharmarajah, V. 2015. Sequences and layering in lacustrine carbonates; Purbeck Limestone, Wessex Basin. MSc, Royal Holloway University of London. 86 pp.

Walker, R.G. 1979. Facies models. Geological Association of Canada, Ontario, Canada, 211 pp.